Shore Power
at Royal Roos

A flexible approach to Shore to Ship power infrastructure

by

Morten Haas

TUDelft

Abstract

For the delivery of Shore to Ship power, the 'status quo' of shore power delivered just from the grid results in the overcapacity of power installation, these resources need to be more optimally utilized. This research investigates what configuration of electrical components to deliver shore power to vessels is the most cost-effective at the quay-side of Royal Roos. This thesis ends with the answers to the research questions that guided the research, and thereby help explain under which conditions an implementation for shore power supply is more cost-effective than another.

Acknowledgements

I give my thanks to my supervisor Dr. Zian Qin and company supervisor Fulko Roos for helping me during my research.

Contents

Part I

Introduction

Background

The large scale dependency of human civilization on fossil fuels has resulted in a devastating increase of CO_2 in the atmosphere in the pursuit of continued economic growth. The CO_2 already present in the atmosphere and the projected future of more CO_2 emissions will result in global warming levels that according to the Intergovernmental Panel on Climate Change (IPCC) will have devastating consequences for all life on this planet [79]. Governments and corporations around the world have promised to dedicate themselves to lowering their carbon emissions, but to little effect as yearly global carbon emissions have reached a record high in 2023 at *36.8 billion tonnes, up 1.1%* from 2022 [3]. The maritime shipping industry is a large contributor to global emissions directly through the act of transportation and also indirectly through the facilitation of trade. There is no 'silver bullet' solution to solving the pollution of the environment and the global warming caused by CO_2 emissions, there are, however, solutions to mitigate the emissions caused by vessels as they are docked in port.

Shore to ship power or 'cold ironing' has been proposed since the early 2000's to reduce or remove the harmful emission from a diesel generator of a vessel when it is docked [97]. The fuel these vessels use results in high amounts of toxic air pollution [97], which makes it quite dangerous to the neighbourhoods surrounding ports if these vessels need to keep running their diesel generators while at port. To solve this problem several ports around the world including Rotterdam, Gothenburg, Los Angeles and more have implemented Shore to Ship power infrastructure at container vessel terminals and/or cruise ship terminals [70]. This is augmented by the IMO [61] mandating reductions in emissions in and around ports, which has resulted in large vessels being mandated to use Shore to Ship power instead of running on their diesel generators when at port from 2030 onwards [65].

Motivation

It is expected that legislation mandating that all vessels at port need to use Shore to Ship power will be forthcoming in the future (stated as 2030 [65]). Anticipating this means that energy infrastructure needs to be greatly expanded to support this. So far all focus has been on the largest vessels that cause the most pollution when they are at port. However, in the future smaller vessels with smaller power loads will also be expected to use Shore to Ship power when docked.

Royal Roos is a maritime company located in the Merwehaven in the port of Rotterdam. They are interested in taking up the task of being a leader in providing Shore to Ship power to smaller vessels that will dock at their quay-side and sharing their experience with other terminal owners.
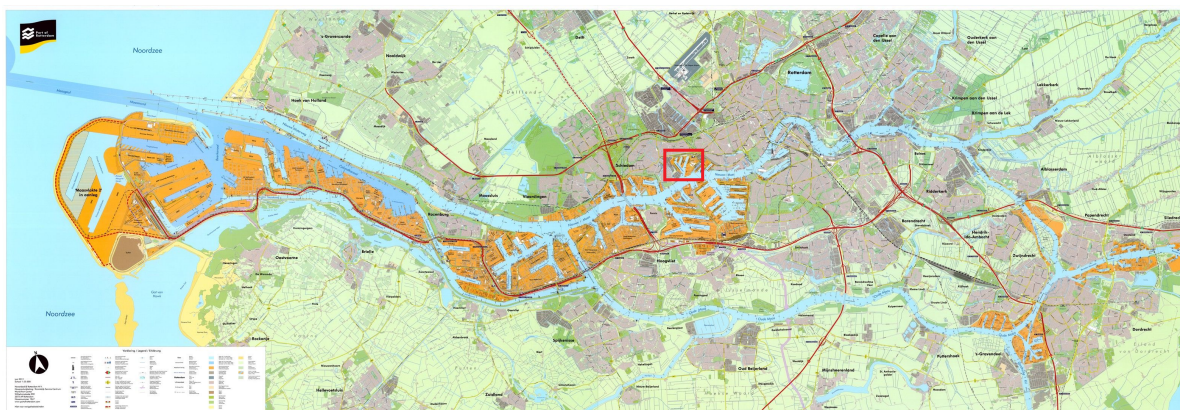

Figure 1: Map of the Port of Rotterdam with a highlighted Merwehaven, based on [26]

Figure 2: Map of the Merwehaven with the quay-side of Royal Roos being highlighted, based on [60]

Problem Statement

This section will introduce the problem definition that will guide this thesis. It stems from the need to have more insight in how to make Shore to Ship power more cost-effective. Royal Roos already has pre-existing shore power infrastructure and they wish to expand this infrastructure, so that they are able to service vessels with a higher power demand. The problem statement of this thesis is:

For the delivery of Shore to Ship power, the 'status quo' of shore power delivered just from the grid results in the overcapacity of power installation, these resources need to be more optimally utilized.

In order to investigate this problem, the status quo will be compared to other configurations that are possible for the delivery of Shore to Ship power. The configurations for shore power investigated in this research are:

1. Status quo power directly and only from the grid, or status quo
2. Shore power from the grid + alternative power supply, or Basic APS shore power configuration
3. Shore power from the grid + high energy capacity energy storage, or HE ESS shore power configuration
4. Shore power from the grid + high power & low energy capacity energy storage, or HP ESS shore power configuration
5. Shore power from the grid + high energy capacity energy storage + alternative power supply, or HE APS shore power configuration
6. Shore power from the grid + high power & low energy capacity energy storage + alternative power supply, or HP APS shore power configuration
7. Shore power from the grid + high energy capacity energy storage + high power & low energy capacity energy storage, or Hybrid ESS shore power configuration
8. Shore power from the grid + high energy capacity energy storage + high power & low energy capacity energy storage + alternative power supply, or Hybrid ESS APS shore power configuration

The full system that is possible is displayed in Figure 3, the other configurations are a subset of the full system from Figure 3. The different configurations will be more explained in Section 1.5.
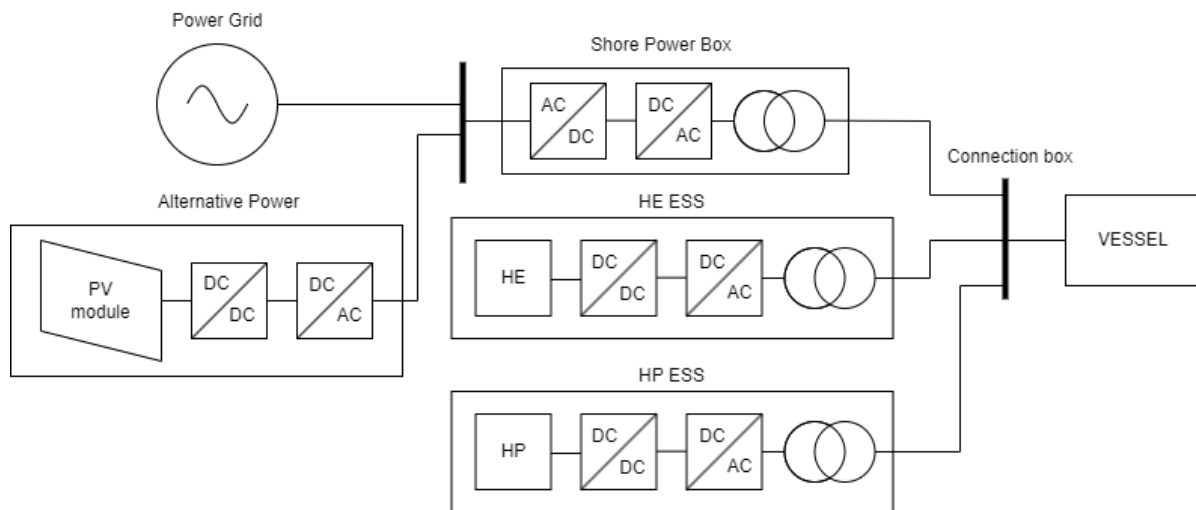
Figure 3: The full possible system

Research Question

This section presents the research questions that will be answered in Chapter 5, they follow from the problem statement introduced in the previous section. The main research question that will be answered throughout this thesis and the sub research questions are:

What is the most cost effective method and configuration to deliver shore power to vessels at the quay-side of Royal Roos?

1. What effect does adding HE ESS have on the cost-effectiveness of supplying shore power?
2. What effect does adding HP ESS have on the cost-effectiveness of supplying shore power?
3. What effect does adding Alternative Power Supply have on the cost-effectiveness of supplying shore power?
4. What effect do different ratios of hotel load versus peak power demand of the vessel have on the sizing and type of the energy storage systems?
5. How do different docking scenarios for vessels affect the different configurations?
6. How do the different configurations differ in capital cost and operational cost in comparison to the 'status quo'?

Thesis outline

This section presents the outline of the thesis that will provide answers to the research questions. Figure 4 shows the general outline. The literature review was done to get an understanding of shore power, so the problem could be formulated. To provide an overview of the energy storage systems that can be used in conjunction with Shore to Ship power. To investigate how alternative power production can be utilized and how these components can be effectively configured together.

Through scenario building and interviewing stakeholders in the form of vessel owners and manufacturers of energy storage system data could be collected. Data such as the component characteristics of energy storage systems but also the measurement data of vessel power profiles as they are docked. By reviewing different optimization strategies and algorithms, an optimization algorithm can be build that will use the collected data to perform cost analysis of different scenarios and configurations. These results will then be analysed and compared so that the research questions of the thesis will be answered.
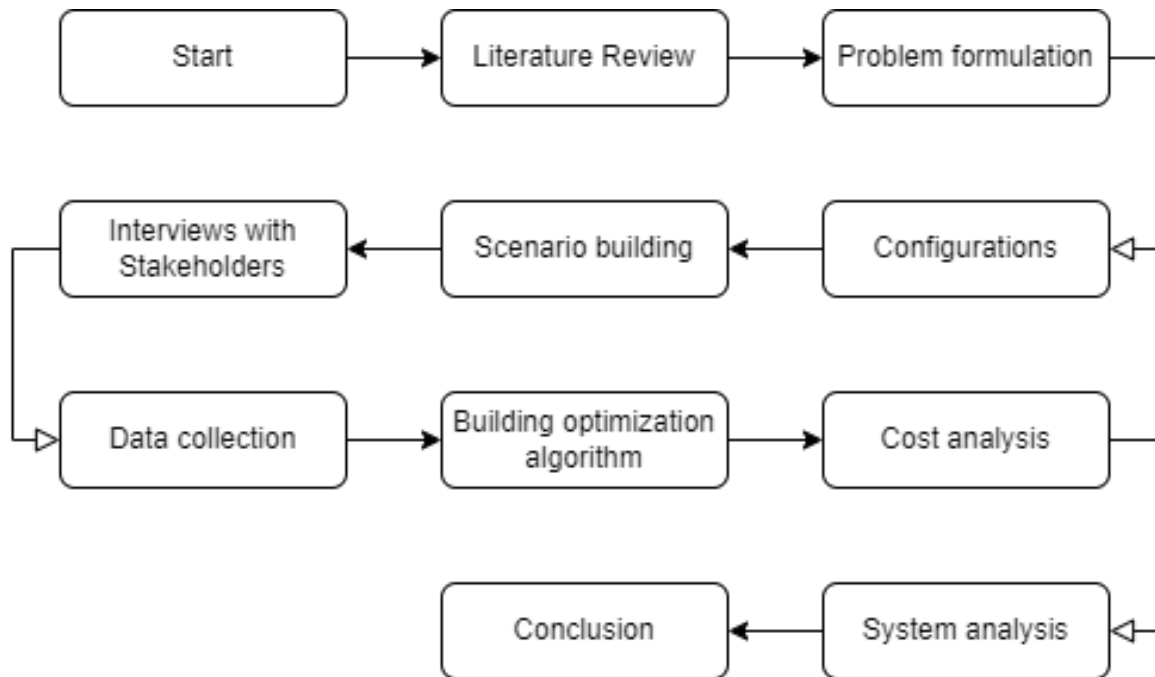
Figure 4: Flowchart of thesis research structure

Limitations

The limitations of the work carried out are presented in this section. These include:

- The research is focused on the cost-effectiveness of supplying shore power, so any other uses or purpose that the shore power system can be used for is not considered.
- The research is focused on the cost-effectiveness of supplying shore power at the quay-side of Royal Roos by Royal Roos, any other terminal or point of view is not considered. And the types of vessels and why they come is limited to what happens at the quay-side of Royal Roos.
- This research uses cost based optimization to do analysis. Any other variable that could be optimized for, like CO_2, is ignored.

Summary

This chapter introduced this master thesis research project. The background and motivation sections provide the context for the problem statement and research questions. This is followed by the outline of the thesis. Finally, the limitations of the research are addressed.

Part II

Analysis of the system

Full background & literature review of shore power and HESS

This chapter provides information on how Shore to Ship power supply functions. This is followed by a section covering how energy storage systems can enhance the stability and cost-effectiveness of the utility grid when they are integrated with renewable energy sources. Then every type of energy storage is introduced and several examples are given which are investigated for their use case in shore power applications. Furthermore, the advantages of hybrid energy storage systems are investigated and this is used to categorise the energy storage systems for the research. Which leads to the different forms of alternative power supply that will be considered and how these function. This is then used to establish all the different configurations possible according to the guidelines introduced before.

1.1. Shore to ship power systems

Shore to ship power supply is the supply of electrical power to ships at berth. This is required if ships want to use electricity without having to run their engines to power generators on board. Vessels often keep their engines running even when operations at port are done, to keep emergency systems functioning.

The first port to install shore power was Goteborg in the year 2000 [45]. Since then many more ports have installed shore power, with 65 ports having declared they have shore power facilities in 2023 [20]. So, clearly the potential and utility of shore to ship power facilities are being seen by port authorities. This increase has been possible through large scale feasibility studies like [86], which highlights barriers to implementation. Barriers like: legislation, ownership, grid capacity and costs of infrastructure. By identifying these interconnected barriers, ports can more easily find where their efforts should be directed. These efforts are bolstered and pushed forward by not only port authorities, but also national governments and international organizations such as the International Maritime Organization (IMO) and the European Union (EU) [61] [27].

Many governments have declared their commitment to net-zero carbon emissions and many ports are a not insignificant source of emissions, especially locally [70] [98]. The Port of Rotterdam has resolved to implement shore power, and mandated that by 2030 at least 90% of the offshore, ferries, cruise, roll-on-roll-off ships and container ships that berth in Rotterdam must use shore power [64].
The EU Emissions Trading Scheme (ETS) includes 100% of emission when vessels are within EU ports [25], this trading scheme will be implemented in 2024. This will cause more vessel owners to consider retrofitting their vessels for using onshore power supply. To enable global standards for onshore power supply the IMO has agreed to interim guidelines for safe operation of onshore power supply service for sea and ocean going vessels [61]. These vessels can reach far greater sizes and have more capabilities, and therefore have a bigger power demand, than inland shipping vessels. Sea-going vessels, albeit of generally smaller variety, are the type of vessels that Royal Roos wishes to service with shore power at their quay-side. So, these vessels are what the research will focus on.

1.1.1. Shore power configuration and implementation

A barrier to widespread shore power implementation is the non-standardization of voltage and frequency levels that vessels operate on. About 3 quarters of sea-going vessels have 60 Hz and the remaining quarter use 50 Hz [47], [95]. While voltage levels range from 380 V to 11 kV, where most ships use lower voltage ranges (380 V - 460 V) [47].

Large vessels such as cruise ships, bulk carriers or container ships require higher voltages, either 6.6 kV or 11 kV [47]. This variability makes the implementation of shore power supply difficult. Shore to ship power supply facilities need a solution for this variability in both frequency and voltage level. This solution comes in the form of power electronics that convert the frequency and voltage to the required levels for the vessel at berth. In theory this could also be done by variable frequency transformers [54], however these are much more expensive due to the large coils required at such a low frequency.

Power electronic converters enable reliable power transfer despite the variability in the power demand of vessels. Figure 1.1 shows a basic diagram of a shore power system being connected to a vessel's power grid. An unfortunate side-effect of power electronics is that they lower the inertia of both the supply of power to the vessel and also the inertia of the electricity grid [95]. This can be mitigated through virtual inertia emulation methods. This functionality is created through additional feedback that allow for control schemes that simulate the behavioural response of a synchronous generator to disturbances, which increases the inertia and therefore the stability of the power system [21] [56].
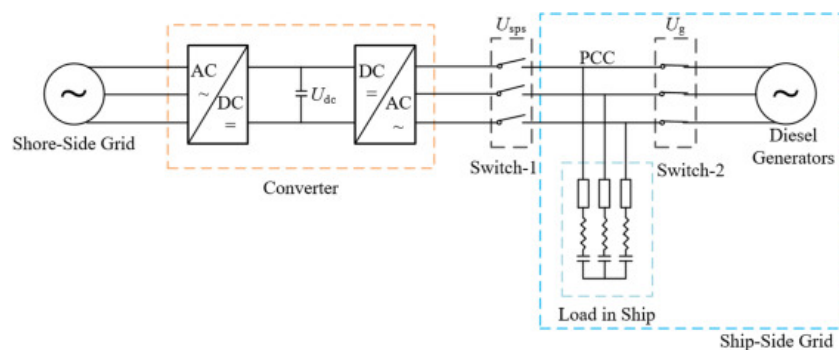

Figure 1.1: Shore-to-ship circuit model from [95]

Control strategies for shore power
Conventionally, ship to shore synchronization strategies are used [72], because these are more simple to implement. This means that the vessel is synchronized to the phase of the shore side power grid. However, given that in the future there will be a greater utilization of power electronic converters, [72] argues that a shore to ship synchronization strategy (instead of ship to shore synchronization) can provide smoother load transfer. That this would involve more measurement and control equipment on board of the vessel is a drawback for wide-spread implementation.

[95] proposes a V/f control strategy based on pre-synchronous control which is then switched to droop control after grid connection. This achieves less distortion upon connection between shore side grid and ship side grid than without pre-synchronisation control[95]. Meanwhile, [49] proposes pre-synchronization control based on virtual synchronous generator control model to allow for greater renewable energy penetration. Virtual synchronous generator models allow for inertia adaptive control strategies which help with stabilizing weak grids[49].

On the vessel, the synchronous generator ensures stability on board [50]. [50] further investigates causes and effects of short circuit faults while a vessel is connected to a shore power supply system. These load disturbances can be mitigated by hybrid energy storage [50]. Significant energy optimization is possible when modeling ship to shore systems as a whole, because this allows for reducing net

reactive power in the supply network to zero [39]. This is why [39] proposes a model for complete port power supply networks.

More effective energy optimization is possible by integrating hybrid energy production with the scheduling of vessels at call in a port [87]. Furthermore, as shown by [50] better stability of port electricity grids when supplying shore power requires energy storage systems. Which is why the following section will introduce them.

1.2. Energy Storage Systems

As the world integrates more Renewable Energy Sources (RES) intro existing electricity infrastructure, to be less reliant on fossil fuel electricity production, the intermittent nature of RES causes more and more issues for the reliability of the electricity grid. This has caused greater emphasis on research and development of Energy Storage Systems (ESS) so that ESS may offset the variability of RES [55] [59] [91]. The ability for ESS to store electricity, generally in some other form of energy, for some time period allows for far greater reliability of power. By being able to store electricity that is generated at a opportune time and release it when electricity generation is less opportune or when demand for electricity increases, ESS are able to mitigate the shortcomings of RES. So far, the complexity and cost of production of large scale ESS has been a barrier to widespread and large-scale adoption. However, the energy transition towards RES demands greater integration with ESS in the electricity grid, so such barriers have to be overcome.

The increase in demand has resulted in far more research into both old and new ESS technologies [55]. ESS can be classified into 4 [59] or 5 [91] main categories depending on definition and categorization. In this report the 5 categories shown in Figure 1.2 are used. Each type of ESS has its own advantages and disadvantages and use cases. Additionally, these different types of ESS such as for example Battery Energy Storage Systems (BESS) have many different implementations that vary wildly in their characteristics. These too will be covered in detail.
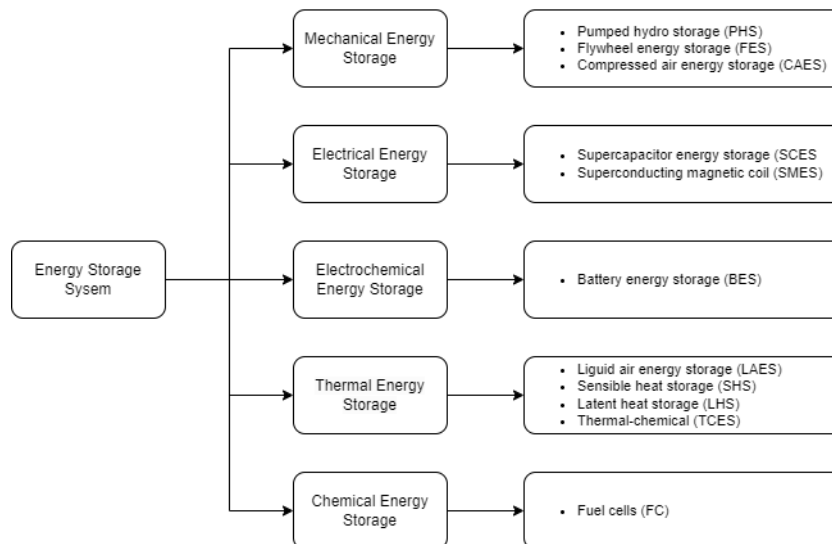
Figure 1.2: Energy Storage Systems classification

1.2.1. Mechanical Energy Storage

Mechanical energy storage transforms electrical energy into different forms of mechanical energy depending on the type of storage. There are three different ways to store mechanical energy. Through kinetic energy, gravitational energy or pressure. The types of ESS that result from these are flywheel energy storage, pumped hydro storage and compressed air energy storage respectively [55]. These

will be covered in this section.

Flywheel Energy Storage

The oldest form of mechanical energy storage, Flywheel Energy Storage (FES) was invented in 1883 [55]. A FES stores its energy mechanically be spinning a cylinder at rapid speed and connecting the shaft to an electric machine, which acts as either a motor or generator depending on whether the FES stores or releases energy. Figure 1.3 shows the basic construction of a FES, with an electric machine connected to the external grid that powers the flywheel itself. The amount of energy stored is determined by the speed of rotation, it is stored as rotational kinetic energy and then released as electrical energy again [59] [91] [55]. The release of energy lowers the speed until a minimum speed is reached, upon which the FES needs to be charged by accelerating the rotor again.

There are two types of FES, split between low speed rotation (up to 6000 rpm) and high speed rotation (over 10000 rpm). This difference is determined by the difference in material of the rotor. Low speed FES use steel as a rotor, and the rotational stress of steel limits the FES to this lower speed. Because of this lower speed, low speed FES can get away with using mechanical bearings, without too much losses [8]. High speed FES use newer composite materials, which can sustain higher rotational speeds. But this makes magnetic bearings necessary, as these remove mechanical friction losses of the rotor which would limit the rotational speed [8]. The bearings can either be active or passive, where the former consists of magnetic coils and a feedback system, while the latter uses permanent magnets [8].

All FES are characterized by fast charging and discharging cycles, high efficiency, high power density, low operational costs, long lifespan and high number of life cycles. Their disadvantages are high investment costs, high self-discharge, especially for low speed FES with mechanical bearings, and they also have low energy density. Where high speed FES also have higher costs compared to low speed FES [8]. These characteristics make them ideal for high power, short and cyclic bursts of energy charging and discharging. Low speed FES has found more use in Uninterruptible Power Supplies (UPS), regenerative braking (in vehicles, trains or vessels) and grid frequency stabilization. While high speed FES has found use in aircraft and spacecraft applications [8]. Although, high speed FES has also found use in grid stabilization and smoothing of power quality [8].

As FES already facilitate power smoothing, it is an already proven ESS suited to mitigating the unpredictable nature of RES and allow for more reliable generation [8]. Therefore, FES will be considered in the research going forward.
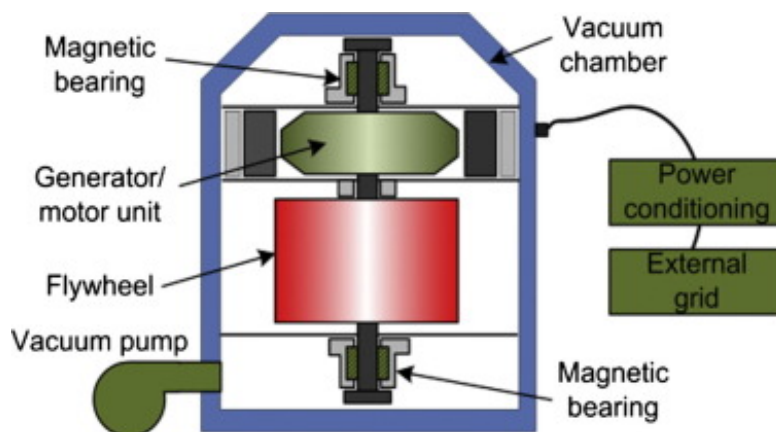

Figure 1.3: Description of flywheel energy storage system [51]

Pumped Hydro Energy Storage

Pumped hydro energy storage (PHS) is the most widely implemented mechanical energy storage system. This is due to the large energy storage capacity of PHS. Which can also be stored for long periods

of time. PHS is a simple design using the gravitational energy of the water in a higher reservoir. Figure 1.4 shows a basic depiction of a PHS system. It consists of at least two different water reservoirs, one of which is higher in elevation than the other. The higher reservoir acts as the storage and the PHS is charged when water from the lower reservoir is pumped up towards the higher reservoir using surplus electricity. This electricity is then discharged when the water flows back down and spins a turbine as it does so [59] [91] [55].

At present the largest ESS are PHS, which range up to several GW [51]. However, they are very geographically sensitive, as they rely on the presence of both large volumes of water and water reservoirs that are separated by a difference in elevation. This means that further PHS installation is difficult, because finding suitable locations is very hard. Most places where PHS can be constructed have already seen such development or there are significant environment, social or economic pressures to stop the construction of PHS [14].

The advantages of PHS are: very high maturity, low self-discharge, large storage capacity, long life-time and long life cycle spans. The disadvantages are: geographical restriction, low energy density resulting in large footprint which is cause for serious environmental concerns [5].

Currently PHS is used as large scale ESS with black start capability to support the electricity grid when supply falters. Making it capable of supporting RES and allowing for peak shaving in future energy grids[55] [14]. However, its geographical restrictions make it unsuitable for a port city like Rotterdam.
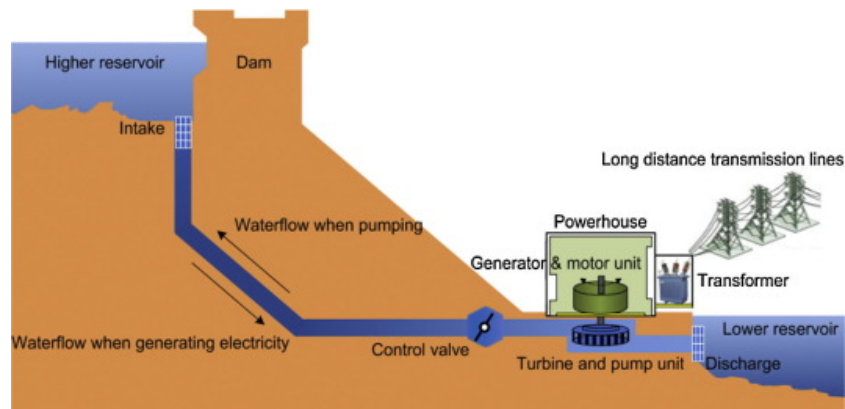

Figure 1.4: Pumped hydroelectric storage schematic layout [51]

Compressed Air Energy Storage
Compressed air energy storage (CAES) is the youngest form of mechanical energy storage [55]. It is also more complex than the other forms of mechanical energy storage. Figure 1.5 shows the basic layout of CAES. The technology is based on gas turbines and is therefore mature even though its first use was quite recent [5]. The basic principle is an electric machine, powered by the grid, driving air compressors which store air in storage volumes. When electricity needs to be discharged again, this air is then routed through turbines which spin the electric machine, which now acts as a generator, releasing the stored energy. Any enclosed volume can function as storage, but fabricating it is far too expensive compared to using depleted mines or gas fields. The large investment costs mean that all currently operating CAES facilities have large operating capacities and rated power [59] [91] [55] [83].

The advantages of CAES are its technological maturity and the large capacity which can be stored for long periods because of the low self-discharge. The main drawback is the huge amount of space needed for air reservoirs, due to its low energy density which results in location dependency of the facilities. This means there are high investment and operation costs [83]. CAES is currently used for peak-shaving, just like PHS [83] [14] and also for integration with RES to resolve their intermittency [83]. However, the geographical difficulties presented by the need for underground caverns, means
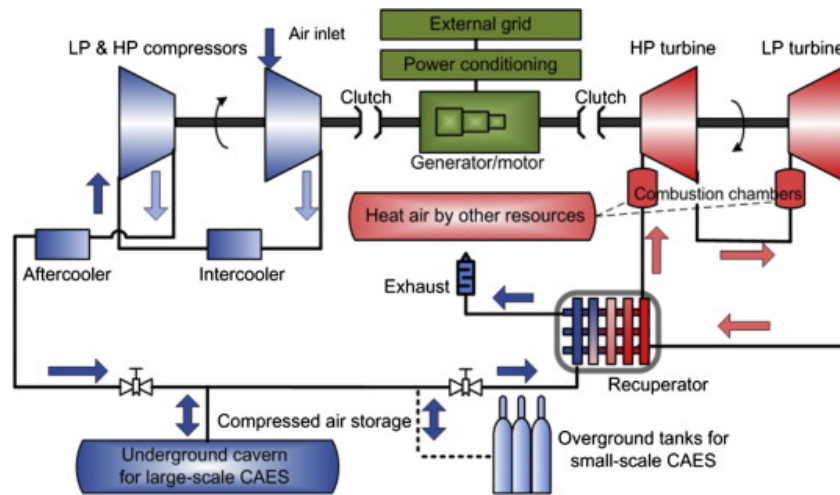
that it is unsuitable for this research.

Figure 1.5: Schematic overview of compressed air energy storage system [51]

1.2.2. Electrical Energy Storage

Electrical energy storage functions by storing energy in the form of charge as electrostatic energy or in the form of magnetic fields created by electric current. This means the energy remains as electrical energy without converting it into another form of energy. The basic, passive electrical components that are based on these forms of energy storage are capacitors and inductors. To make them more effective in high power storage applications these basic structures become supercapacitor energy storage and superconducting magnetic energy storage respectively. Because these ESS do not convert from one form of energy to another, but instead remain in the electrical domain, they have very low response times and high power densities [22].

Supercapacitor Energy Storage

A 'normal' capacitor consists of two electrical conductors separated by a layer of dielectric material. The energy is stored in the dielectric material in an electrostatic field. Capacitors can be used for storing small quantities of electrical energy and conducting alternating current. Capacitors have a high power density and low energy density, with high self-discharge losses. This allows them to be used in smoothing the output of power supplies [51].

Supercapacitors (SC) are a type of capacitor called electric double-layer capacitor or ultracapacitor. SC combine some of the characteristics of capacitors and batteries by using an electrolyte and a porous membrane separator, which is then sandwiched by two electrodes as shown in Figure 1.6. The energy is stored as ions that are collected near the electrodes. This space charge zone between the two interfaces is called the electrical double layer (EDL) that gives SC their official name [66].

The properties of SC include a high power density and low energy density, which is in between those of batteries and capacitors [51]. So, SC have a higher power density than batteries, but a lower power density than regular capacitors. While, SC energy density is better than regular capacitors, but worse than that of batteries. SC have fast charge and discharge, high self-discharge, long life span and cycle life with high efficiency. SC also have a high capital cost [66]. SC can be classified according to their construction. They can be made into a flat, a cylindrical or a rectangular container. The normal operating process is as described above, using the EDL principle, but some SC called pseudocapacitors utilize reversible Faradaic redox reactions for charge [66]. Finally, hybrid supercapacitors replaces one of the electrodes with a lithium-insertion electrode [66].

Pseudocapacitors have a higher energy density, higher capacitance and lower cost compared to EDL capacitors. However, pseudocapacitors also have lower power density and a shorter life cycle. Hybrid SC are a middle ground in between pseudocapacitors and EDL capacitors [66]. SC of all types are used in similar applications. SC can be found in communication hardware or cell phones, in UPS, power-quality enhancers, power tools and regenerative braking in vehicles [66] [55]. SC can also act as stabilizers for wind power and photovoltaic power in hybrid energy storage applications [66]. SC are therefore applicable to this research.
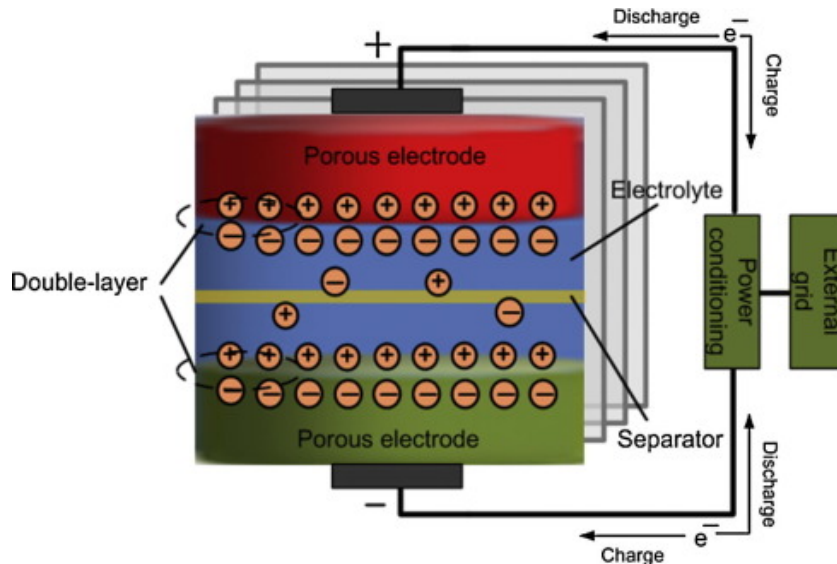

Figure 1.6: Schematic diagram of a supercapacitor energy storage system [51]

Superconducting Magnetic Energy Storage
Superconducting magnetic energy storage (SMES) is constructed from three different parts. As shown in Figure 1.7 SMES contains a superconducting magnetic coil, a cooling unit and a power regulator and converter. SMES stores energy by converting AC current from an external grid into DC current, which generates a magnetic field in the coil. This coil is made of special superconducting material (often an Niobium - Titanium alloy), which means that its resistance approaches zero when it is cooled below its superconducting critical temperature. Because the cooling unit cryogenically cools the coil, the electrical energy can be stored without any resistive heating losses, resulting in very high cycling efficiencies [51] [91] [55] [4].

SMES can be divided into two categories: high temperature superconductors (HTS) coils operating at about 70 $^\circ K$ and low temperature superconducting (LTS) coils operating at around 7 $^\circ K$ [51] [22]. LTS technology is more mature and commercially available compared to HTS technology. While research into HTS can result in more cost effective SMES by reducing the costs for the cooling unit [91].

The advantages of SMES are fast response speed, high power density, high efficiency, high cycle life and long lifespan. SMES is further known for being able to completely discharge in less than a minute. The disadvantages of SMES include high capital cost, high self-discharge rate, high temperature sensitivity to operation and the generated magnetic fields affect their environment [91] [4].

SMES are currently used in power systems to improve power quality by balancing fluctuating loads, voltages and frequencies. SMES is also used in power systems to improve the power system stability by reducing system oscillation and improving voltage stability [55]. LTS systems of up to 10MW have been deployed in Japan for the purpose of providing voltage compensation of critical industrial loads [4]. Because of the high capital cost further use has been limited, but the development of HTS systems promises greater adoption because of cost reduction and the expanding need for power quality

smoothing for RES [4]. However, SMES will never have large installed capacity, as it would need an estimated 16 km of loop per 100 MWh installed [4].

Since, SMES are already deployed for improving fluctuating power quality, they are also suitable for improving the power quality of RES in the future. However, they are currently still very niche and also very expensive. So, SMES is not considered for this research.
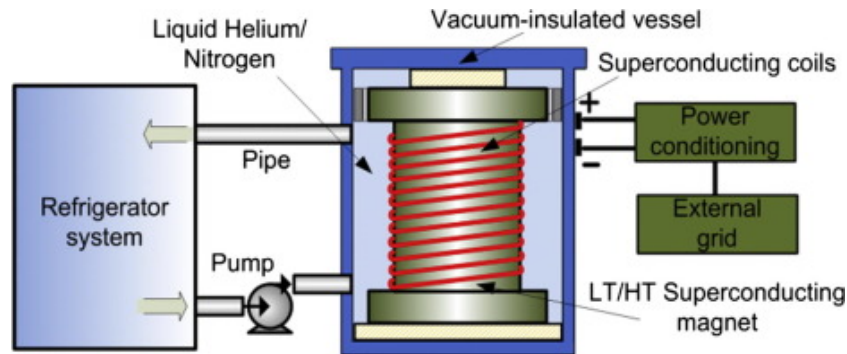

Figure 1.7: Schematic diagram of a superconducting magnetic energy storage system [51]

1.2.3. Electrochemical Energy Storage

Electrochemical energy storage converts electrical energy into chemical energy or vice versa. This is done between the electrolyte and the electrode of the battery though an electrochemical redox reaction [41]. Electrochemical energy storage is also known as battery energy storage, because depending on definition it is the only form of electrochemical energy storage.

Battery Energy Storage

Battery Energy Storage (BES) is the most common energy storage device available world wide. It is also one of the oldest forms of energy storage system, as the lead-acid battery was invented in 1859 [55]. Since then many more types of BES have been invented. These are generally divided into 2 different types: primary and secondary. Primary BES are single use, once the chemical has been used up, the battery stops functioning. Secondary BES on the other hand are rechargeable, granting them much greater usability and lifespan [55]. In this research only rechargeable batteries are considered, as non-rechargeable batteries serve no real purpose in renewable power systems.

BES consists of one or more cells, these can be linked in series or parallel to increase either the output voltage or the output current of the battery. The cells consist of three basic components: an anode, a cathode and an electrolyte. This electrolyte allows for the transport of electrons between the anode and cathode. The electrons flow from the anode to the cathode through the electrolyte when the battery is charging, and the electrons flow from the cathode to the anode when the battery is discharging. Figure 1.8 shows the basic structure and operation of a rechargeable BES system.

There are six sub-categories for batteries:

- Lithium-based
- Nickel-based
- Sodium-based
- Lead-acid
- Redox flow
- Hybrid flow

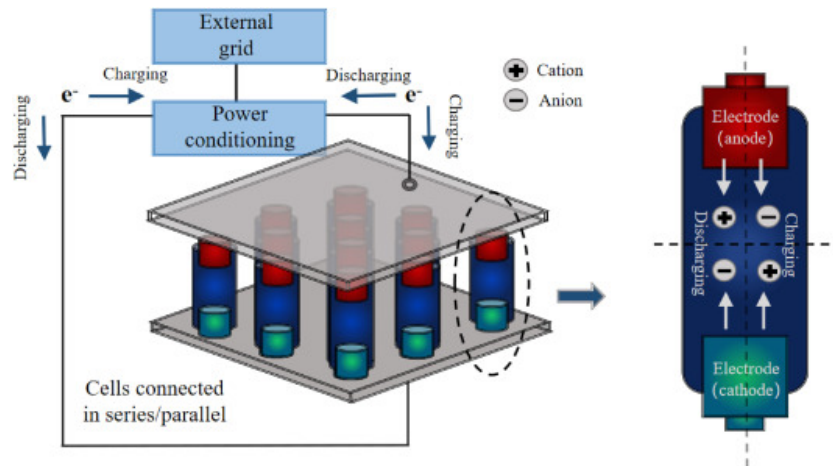Every sub-category also has different implementations [82].

Figure 1.8: Schematic diagram of Battery Energy Storage System operation from [51]

Lithium-based BES

Lithium-based batteries have found wide spread usage in portable electric devices like phones and laptops. This is because lithium-based batteries have high energy density, high power density and high discharge depth or DOD. Whereas their daily self-discharge of 1% - 5% is not very significant for these applications [59]. Lithium-based batteries are further characterized by high efficiency of over 90%, high number of cycles at around 10000 and a long lifetime of around 10 years. They do have a high sensitivity to temperature and the degradation, efficiency and self-discharge increase with temperature.

The main drawback of lithium-based BES are the high cost of lithium, its scarcity and the environmentally damaging refining and extraction process for the manufacturing of the batteries [82]. Because of its versatility, its high energy and power density, a lot of research has been put into Li-ion batteries to improve their performance. This has made them viable in electric vehicles, for example. There is also much emphasis on the use of Li-ion batteries as ESS for grid based energy storage [82]. This drive for better and more sustainable Li-ion batteries has resulted in a lot of different cathode materials for Li-ion being developed. Each with their own advantages. These different types of Li-ion batteries are:

- LCO
- LFP
- LMO
- NMC
- NCA
- LTO

LCO or lithium cobalt oxide batteries are one of the more mature Li-ion batteries as they dominate consumer electronics. However, because of the use of the very rare and expensive element cobalt, they are seen as unsuitable for grid ESS applications[84]. LFP or lithium iron phosphate batteries are seen as a suitable ESS for grid applications, because it does not rely on cobalt and it has high stability and power capacity [82]. LFP is already installed for large scale energy storage at Smart Grid East Flevoland at a capacity of 48 MWh [73], showcasing its applicability for large scale energy storage. LMO or lithium manganese oxide have not seen widespread usage in consumer electronics, this is because of its low charge and discharge rate. However, as stated in [96] newly researched and developed LMO-Hydrogen BES has the potential to overcome this limitation with a 50C discharge rate according to lab tests. This technology is not yet mature however, so it remains to be seen if these results can be replicated outside of a lab setting. But it does show promise for future grid ESS usage.

NMC or lithium nickel manganese cobalt oxide batteries have a high lifetime, energy density and are cost competitive [82]. NMC has already seen large scale energy storage applications, as a 7.5 MWh NMC battery has been installed at Smart Grid East Flevoland [74]. However, citing the expense and scarcity of cobalt GIGA storage have not continued installing NMC batteries [73]. NCA or nickel cobalt

aluminium oxide batteries are a mature implementation of Li-ion batteries that have been utilized as an alternative BES for electric vehicle applications [81]. This technology still uses cobalt, so these are also not recommended for future RES grid storage. LTO or lithium titanate oxide batteries are a newly developed type of Li-ion battery. They are suitable for high power applications such as electric vehicles with fast charging. Their high power capability has given them an edge over other Li-ion battery technologies, but their high cost and relatively low maturity means that LTO batteries are used in hybrid energy storage systems as the high power component [57]. From these cathode materials, LFP, NMC and LTO have proven to be the most suitable for hybrid installations, because of their load leveling applications [82] and they will be considered in the research going forward.

Nickel-based BES
Nickel-based batteries are known for their high energy density at low cost. However, their low depth of discharge limits them to stationary applications. They are used for example in Uninterruptible Power Supplies (UPS) [59] [91] [82]. There are several Nickel-based batteries with different anode materials:

- Ni-Cd
- Ni-Fe
- Ni-MH
- Ni-Zn
- Ni-H_2

Ni-Cd or nickel cadmium batteries are by far the most utilized nickel-based BES, they are characterized by a higher cycle life of over 2000 compared to the other nickel-based batteries. Ni-Cd batteries also experience a memory effect, which can significantly reduce the rated capacity of the battery [91]. Most importantly however, the toxicity of cadmium means that this battery technology has uncertain future prospects [59]. Furthermore, the sale of nickel-cadmium batteries for handheld power tools is already banned in the EU [63]. Compared to Ni-Cd, Ni-Fe or nickel iron batteries are not toxic and also have a higher efficiency than Ni-Cd batteries. On the other hand, Ni-Fe batteries do suffer from low specific power, short life time and high cost making them unsuitable for large scale ESS [91]. Ni-MH or nickel-metal hydride batteries have similar applicability to Ni-Cd, without suffering from the memory effect. Ni-MH batteries also do not use toxic materials [91]. Unfortunately, it does use rare earth metals which are very limited [82]. This makes them less suitable for large scale energy storage to support RES power production.

Ni-Zn or nickel zink batteries are very similar to Ni-Fe, with the same advantages in no-toxic materials and high efficiency. But Ni-Zn also has the same drawbacks as Ni-Fe, in that they suffer from low specific power, short life time and cycle life, not to mention high cost [91]. Meaning these too are not suitable for large scale ESS applications. Finally, Ni-H_2 or nickel hydrogen batteries have a high rated capacity and long life cycle compared to the other nickel-based BES. On the other hand, because of their high self-discharge, low energy density and high price they have not seen large scale usage, yet [91]. This means that no nickel-based BES is suitable for large scale grid supporting ESS applications and they will not be considered in this research.

Sodium-based BES
Na-based BES is capable of large scale energy storage. Na-based batteries are also capable of high power applications. Na-based batteries do suffer from high operating temperatures [82]. The Na-based batteries discussed here are:

- Na-S
- Na-ion
- $NaNiCl_2$

Na-S or sodium sulfur batteries have high power capability, high energy density and requiring high operating temperatures [59]. They have high rated capacity, high efficiency and long life time. But the drawbacks include high corrosion and high operating cost due to the high temperature [91]. However, an improved room-temperature version is being developed and still faces challenges for implementation [93]. So, Na-S batteries will not be included for this research. Na-S batteries are suitable for large

scale energy storage for supporting grid operations.

Na-ion batteries have emerged as a potential rival to Li-ion batteries, with similar performance but cheaper as sodium is abundant [55]. The future prospects of Na-ion batteries for replacing Li-ion batteries as favored medium of large scale energy storage are assessed in [92]. There are commercial Na-ion batteries available so they are considered for this research. $NaNiCl_2$ or sodium nickel chloride batteries have a lower power density compared to Na-S batteries [82]. They do have better energy density, lower corrosion and better safety compared to Na-S batteries. $NaNiCl_2$ like Na-S requires a high operating temperature, which is a major drawback here too [91]. This means $NaNiCl_2$ also has high operating costs. And unfortunately, they are also not commercially available like Na-S batteries. Of the Na-based BES, Na-ion will be considered for this research.

Lead-acid BES
Lead-acid batteries are the oldest form of electrochemical energy storage [55]. This age combined with their uncomplicated construction results in lead-acid batteries being among the most mature ESS in the world. They have seen usage in many different energy storage applications, but are currently most commonly found as ESS in cars (both gasoline and electric) and as auxiliary power in UPS or renewable energy storage [91].

There are two main types of lead-acid batteries, the older flooded lead-acid (FLA) variant and the newer valve-regulated lead-acid (VRLA) battery. The main difference being that VRLA batteries are "sealed with a pressure regulating valve, which prevents air from entering the cells" [55]. Both types of lead-acid battery are characterized by: low daily self-discharge rate, high cycle efficiency, high reliability and safety and low energy capital cost. Their disadvantages are: low cycle life and low energy density [91]. This can be remedied by increasing the temperature, this increases efficiency and energy density, but also decreases the life span [59]. The main advantage of VRLA are its high specific power, allowing for fast charging and its lower maintenance costs. This has caused them to be used in electric vehicles [91] and also for stationary long term energy storage [82].
Unfortunately, for this research cycle life is quite important. So, no lead-acid based BES are considered for this research.

Redox flow BES
Redox flow batteries are a type of flow battery. The other type, hybrid flow, will be covered in the next section. With redox flow BES all electroactive materials are dissolved in liquid electrolyte stored separately from the cell [5]. Figure 1.9 shows the general working of a redox flow battery (RFB), where the two different electrolytes are pumped through the battery and kept separate by an exchange membrane. This membrane allows for electrons to flow from one electrode to the other. The energy density of the RFB depends on the concentration and volume of the electrolyte. While the power density is determined by the size of the electrodes and the number of batteries [91]. RFB have a high efficiency, long life cycle, long lifetime and low self-discharge making them useful for long-term and large scale energy storage. There are primarily 2 types of mature RFB in use: vanadium RFB and polysulfide bromine flow battery (PSB) [55].

Vanadium RFB is the most mature flow battery technology. Currently, there is a 100MW and 400MWh ESS using vanadium RFB technology connected to the electricity grid in Dalian, China. With plans to expand it to a 200MW and 800MWh [77]. This is clear proof of vanadium RFB being capable of large scale energy storage to support the grid with peak-shaving capability. Vanadium RFB is characterized by fast response time, long cycle life, high efficiency (85%), being capable of deep discharge and also fast charge or discharge [91]. The disadvantages of vanadium RFB are its low energy density, resulting in large (and stationary) area allocation, which combined with the high price of vanadium, means the capital expense is a large barrier to wider implementation [55].

Polysulfide bromine flow battery or PSB is another promising redox flow battery technology. It is characterized by no self-discharge [55], fast response time and easier to source materials compared to vanadium RFB. It is disadvantaged by the lower efficiency compared to vanadium RFB and higher operations and preparations costs due to the toxic bromine gas [55], [91]. Most unfortunate of all, there
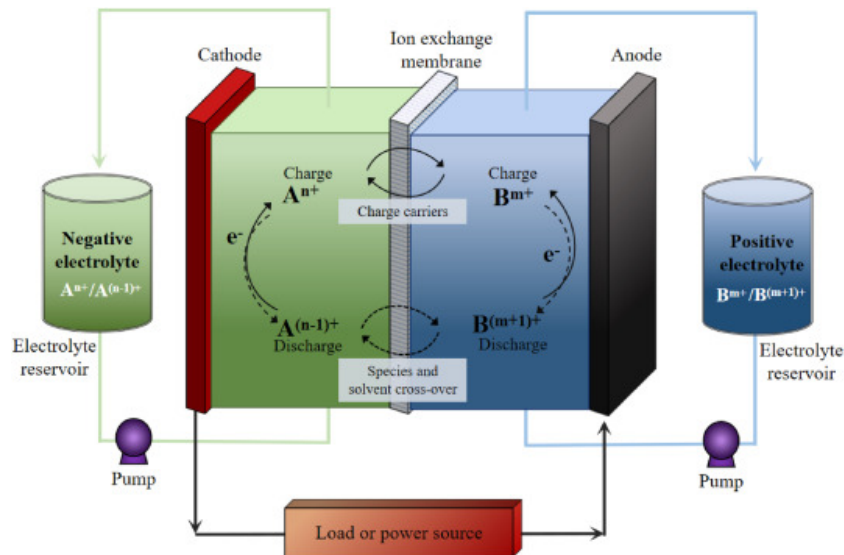
Figure 1.9: Schematic depiction of a Redox Flow Battery [91]

has been no large scale proven commercial ESS. In 2002, a 15 MW and 100 MWh PSB was supposed to be installed in the UK. However, the commissioning was stopped before being completed [55]. So, PSB does have the potential and in the lab it seems to be cost-effective, but this has not been proven [91]. Of the two types or RFB, neither will be considered for this research. Even though Vanadium RFB has proven applicability, the area requirements for a decent size RFB system is too large, due to the storage tanks.

Hybrid flow BES
The distinction between hybrid flow batteries and redox flow batteries is that in hybrid flow batteries electroactive materials are not just stored in liquid solutions external to the cell. One material is stored in the cell, while the other is a liquid stored in an external tank that is pumped into the battery cell [5].

The only mature hybrid flow BES is the zinc bromine (ZnBr) flow battery. The advantages of ZnBr batteries include: low self-discharge rate, high energy density, long lifespan and deep discharge capability [91]. Its disadvantages are: corrosive materials, lower cycle efficiency compared to vanadium RFB and a narrow temperature range [91]. There have been a few large scale 1 MW/ 4 MWh prototypes in 1991 [48] and more recently commercial utility-scale of up to 1 MW are being developed [55]. Here too, the are requirement is too high for this particular use-case. Therefore, ZnBr flow batteries will not be included in the research.

1.2.4. Thermal Energy Storage
Thermal energy storage (TES) works by storing excess electricity as heat energy in a storage medium. TES consist of two groups: low-temperature TES that stores excess electricity by cooling materials and high-temperature TES that stores excess electricity by heating materials. The main type of low-temperature TES is liquid air energy storage (LAES). While high-temperature TES consists of sensible heat storage (SHS), latent heat storage (LHS) and thermal chemical heat storage (TCES) [51].

Liquid air energy storage
Liquid air energy storage or LAES is based on CAES technology. As shown in Figure 1.10 LAES introduces an extra step into the CAES process, after compression of the air it is also cooled until liquefaction. This reduces the storage volume for the now liquid air, which greatly reduces the area footprint of the plant and removes the location dependency that is inherent to CAES [17]. This puts LAES in the league of other large capacity storage ESS like CAES and PHS. LAES has similar advantages such as: high maturity, long lifespan and high number of cycle life. LAES has higher energy density than

both CAES and PHS, but has lower roundtrip efficiencies [17].

There already is a grid-scale LAES of 5MW / 15MWh being operated in the UK as the sole currently operational, industrial LAES facility [17]. It will be joined by even larger 50MW / 250MWh LAES facilities, in the UK and in the US [17]. However, according to [17], LAES no matter the size, can only achieve profitability if they include waste heat recovery and hybridizing the plant with short term and high power ESS, due to the slow response time of LAES. This means that LAES has potential in future energy system only when it is deeply integrated with other ESS and energy production systems. Which is not the case for shore power supply facilities. So, LAES will not be considered for this research.
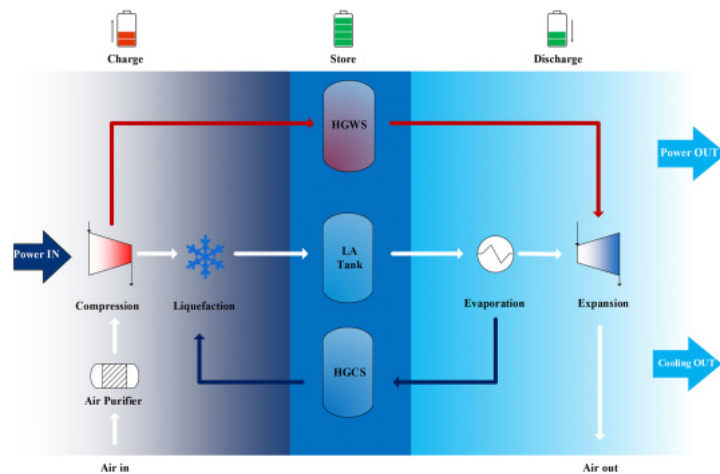
Figure 1.10: Schematic depiction of a liquid air energy storage system [17]

Sensible heat storage
In sensible heat storage (SHS) systems the heat energy is stored in a solid or liquid without changing the phase of the material. The capacity of SHS depends mainly on the specific heat of the medium and the temperature range that is used. SHS is the simplest and most widely used TES [55]. [91] shows that many different medium materials are possible. For liquid SHS, the most common choice for low temperature systems is water as it has a high specific heat and low cost. For higher temperatures, materials such as heat transfer oil, molten nitrate, liquid sodium and concrete are used. Solid SHS uses different kinds of rocks and metals. The choice is very important as it has a big impact on the number of cycles, the temperature range and the application of the system [91].

SHS is generally characterized by relatively low capital cost, low self-discharge rate and has good energy density and specific energy depending on the choice of medium. SHS also has a low cycling efficiency and the life span can vary wildly [51] [22].
The technology is quite mature, but it is most applicable in industrial or residential areas, where they can act as seasonal storage [22]. And is therefore unsuitable for this research.
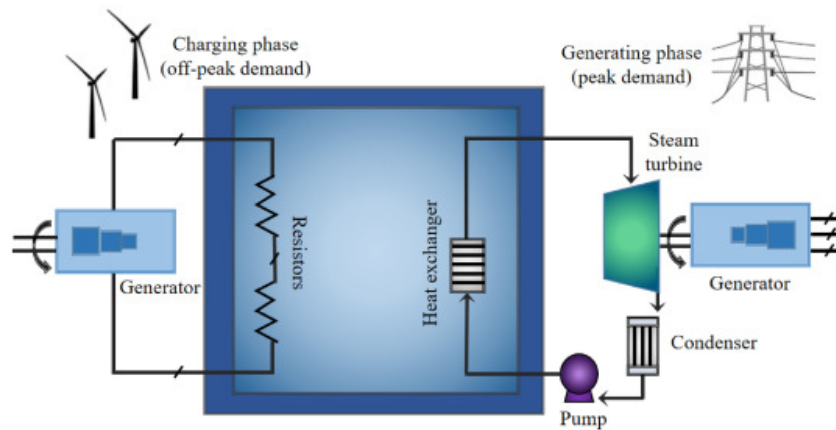
Figure 1.11: Sensible heat storage system [91]

Latent heat storage

Latent heat storage (LHS) differs from sensible heat storage by heating media past phase change temperatures. This utilizes the heat absorbed or released when the medium undergoes a phase change (usually from solid to liquid or vice versa). Figure 1.12 shows a basic LHS system. The media for LHS are also known as Phase Change Materials or PCM, on account of their useful phase changing properties [67]. PCM can be organic, inorganic or a mixture. Common PCM are wax, alcohols, fatty acids, glycols and salt hydrates [67]. The PCM exchange heat energy through metal matrix structures which are connected to steam turbines[59].

Because LHS utilizes the additional energy of a phase change it is far more energy dense than SHS. This results in smaller footprints, which is one of the biggest drawbacks of SHS systems. Furthermore, LHS has greater cycling efficiency [67]. The main drawback of LHS compared to SHS is the cost, LHS systems are far more costly than SHS systems. The higher cost of LHS has been a barrier to the commercialization that SHS systems have seen. Future cost reduction has been predicted, but so far not enough practical evidence for this economic viability has been demonstrated [67]. Which means LHS is not applicable for this research.
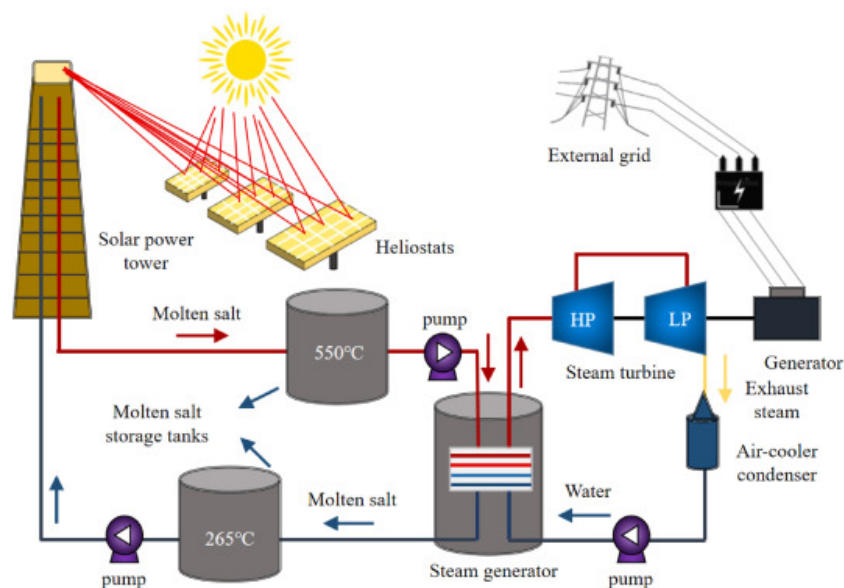

Figure 1.12: Latent heat storage system [91]

Thermal chemical

Thermal chemical heat energy storage (TCES) uses a reversible chemical reaction to store or release heat. TCES reactions include multipurpose chemical reactions, hydrate reactions and photochemical reactions. The basic principle is a material is heated, which results in a chemical reaction where two or more new materials are created. This is the storing of energy. Then the chemical reaction is reversed, which returns the original material. This releases the heat energy again [91].

Because the heat is stored chemically, there is very low self-discharge and also the energy density is very high. Unfortunately, because of poor heat exchange, the cycling efficiency is very low. Furthermore, the only TCES systems are lab-based and small scale, so a lot of research and testing is needed to see its viability. Therefore, TCES is not considered for this research.

1.2.5. Chemical Energy Storage

Chemical Energy Storage is the most used form of energy storage. This is because coal, gas, diesel and other fossil fuel based products are, in actuality, chemical compounds being created over geologic time periods. These chemicals are also non-renewable and the cause of the climate crisis. However, it is possible to renewably store energy in the form of hydrogen and then convert that back into electricity.

Hydrogen Energy Storage

The oldest type of ESS is the hydrogen Fuel Cell (FC), invented in 1839 [55]. Hydrogen Energy Storage (HES) consists of two chemical reactions. The first is electrolysis which generates hydrogen from water and electricity. This hydrogen can be stored or electrolysis can be reversed by a fuel cell which converts the hydrogen back into water and electricity [59]. Figure 1.13 shows the basic principle of a hydrogen energy storage system.

The working principle of an electrolyzer is simple. An electrolysis reaction is created by putting two electrodes in an electrolyte solution and applying sufficiently high voltage between the electrodes. To generate hydrogen gas the electrolyte solution has to be water [89]. Fuel cells reverse this process. Fuel cells are similar to batteries, in batteries the fuel is kept inside of the device. Where in fuel cells the fuel is provided from an external source [91]. In fuel cells the hydrogen gas is oxidized into H+ protons and electrons at the anode. Where the electrons flow to the cathode through the electrodes and power the external circuit and the H+ protons flow through the electrolyte to the cathode. At the cathode the electrons and H+ protons combine with oxygen to create water [55].
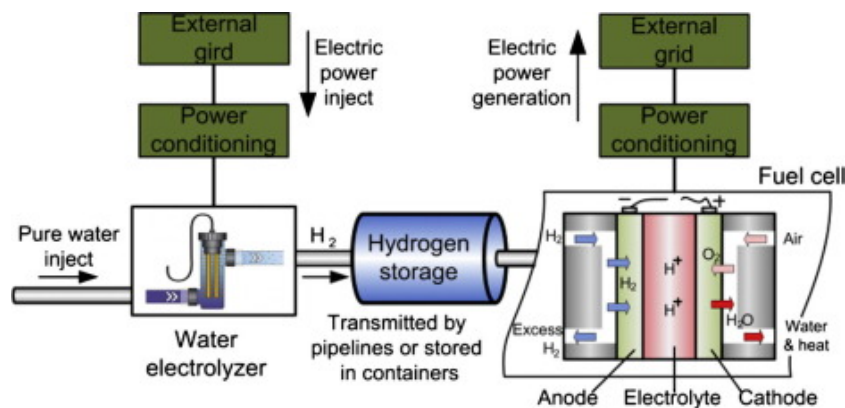

Figure 1.13: Hydrogen Energy Storage system [51]

Hydrogen has seen a rapid rise in interest in recent years for all sorts of energy applications. In the transportation sector vehicles, planes and ships powered by fuel cells using hydrogen is seen as the sustainable alternative for fossil fuel powered transportation. Further applications include heating and cooling alternatives, long term energy storage and backup power or simply power generation [43]. This widespread field of application has resulted in hydrogen being conceived of as a central part of a future

100% renewable energy systems [18]. Where, apart from hydrogen being used in HES, it is also used in combination with carbon capture to create carbon neutral synthetic electricity-based fuels (e-fuels) like e-methanol and e-methane. Or hydrogen gas is combined with nitrogen to create e-ammonia. These e-fuels are then used as carbon neutral fuel alternatives for their fossil fuel based contemporaries in industry, agriculture and transportation [18].

Because hydrogen has become such a crucial gas for the energy transition. The projected future demand of it has increased phenomenally, which places a lot of pressure on the efficient production of hydrogen gas by renewable powered electrolyzers and the efficient storage of hydrogen [43]. The storage of hydrogen is a particular challenge, because hydrogen gas has a very low volume energy density. Making distributed storage very difficult, because of the large footprint [80]. This has meant that a lot of research has been put into making three different types of storage as cost-effective as possible [43]:

- compressed hydrogen storage, which offers better volume energy density, but the high pressure storage vessels are still very bulky
- liquid hydrogen storage, which offers better energy density than compressed hydrogen storage, but requires cryogenic cooling
- solid state storage, which offers the best volumetric energy density, but is heavier and is still reaching maturity

The main limitation to HES is the high capital cost and the low system efficiencies, usually less than 50% [59] [43]. Because hydrogen is seen as a future energy carrier, even though the capital cost is high, there will be a rise in large scale production of hydrogen, large scale storage of hydrogen and also power generation using hydrogen [43] [18]. Where each step of the HES is separated and externalized. So renewable or 'green' hydrogen production using electrolyzers is done at large scale production facilities. Which are separate from large scale storage and transportation facilities to different end-users. And finally, the power generation using the hydrogen is distributed. The hydrogen is then used for direct marine or aircraft propulsion, turned into e-fuels or power production for the grid [43].

However, these large scale hydrogen production facilities do not exist yet and a complete but smaller HES system on-site would still be too large of a footprint. So, HES is not considered for this research.

1.3. Hybrid Energy Storage System

An energy storage systems does not need to be homogeneous, two or more types of energy storage can be combined into what is known as a Hybrid Energy Storage System (HESS). If monotype ESS are used, then sacrifices need to be made for either high power applications or high energy applications. This is because ESS are limited by either power density or energy density [11]. This means that by combining multiple ESS, it is possible to take advantage of their traits in such a way that high power and high energy applications can be combined in one system [42]. Although in theory more than two types of ESS can be used, it is more common to use just two types, to keep complexity down. Where one type of energy storage is used for its high power density for high power demand, fast response and transient behaviour. And the other type of energy storage is used for its high energy density for high capacity storage, with characteristics of low self-discharge and low energy specific costs [16].

[6] shows how this combination of high power and high capacity, LTO and NMC batteries respectively, can decrease the cost and size of the BES for marine propulsion. Similar results have been shown by [38] for HESS applications in aircraft. [90] shows how a HESS can improve the overall cost, weight and performance over a monotype BES for an electric vehicle. While, [37] shows how a HESS can improve the reliability of a microgrid when used with optimal control strategies. And [88] shows how HESS can help improve general power systems stability, while also optimizing for economic viability. The following subsections will go into more detail about HESS structure, working principle and use cases.

1.3.1. HESS topology

HESS can be configured in multiple ways. Through a direct DC link, a single bi-directional DC/DC converter to the dc link for one ESS, or separate bi-directional DC/DC converters [16]. Where a simple DC link is called a passive configuration, a single bi-directional DC/DC converter is called a semi-active configuration and separate bi-directional DC/DC converters is called an active configuration [11].

A passive configuration of a HESS is shown in Figure 1.14. This is the simplest topology that can be used [16]. It does require that the voltage of the different ESS are matched in order for it to function [11]. Even though it is the cheapest option, it does experience a number of drawbacks. There is no control over which ESS responds when, because there is no possibility for power flow control or energy management. This results in the high power storage system being used ineffectively and the high energy storage system experiencing greater degradation [11] [16].
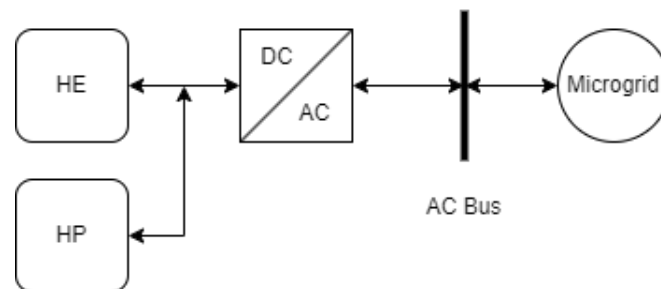
Figure 1.14: Passive interconnection configuration of HESS based on [11], where HE is the high energy storage system and HP is the high power storage system

A semi-passive configuration of a HESS is shown in Figure 1.15. In this topology either ESS can be controlled through the DC/DC converter but not both. If the high energy storage is connected to the converter, it will be protected against fast load fluctuations and peak power delivery, however the DC bus voltage will fluctuate quite heavily [16]. If the high power storage is connected to the converter, the power exchange from the high power storage can be controlled. In both implementations the high power storage handles the power fluctuations [11]. A semi-passive configuration offers greater flexibility to the system, however the high energy storage needs to be oversized if it is connected to the converter or the converter should be oversized when it is connected to the high power storage [11].
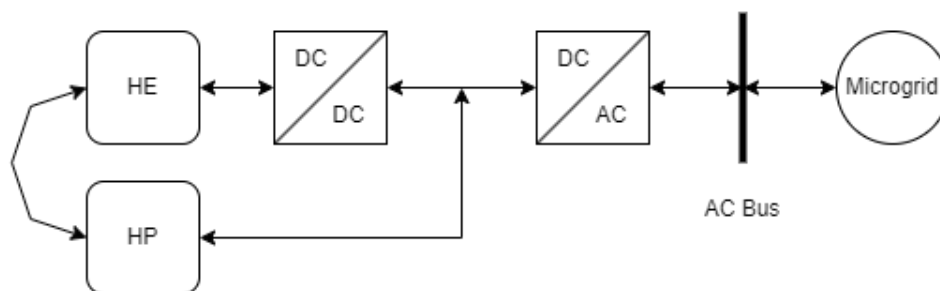

Figure 1.15: Semi-passive interconnection configuration of HESS based on [11], where HE is the high energy storage system and HP is the high power storage system

An active configuration of a HESS is shown in Figure 1.16. Here full controllability of power flow and energy management is possible, which makes it possible to use much more optimized control strategies. In Figure 1.16 a parallel configuration is shown, however a serial topology is also possible. Series configuration is more expensive and more difficult to control [16]. An active configuration is more expensive than the other two HESS configurations. However, an active configuration keeps the DC bus voltage stable and increases fault tolerance, because the ESS are decoupled from the DC bus [11]. Furthermore, the decoupled control of either ESS means it is the most widely utilized configuration for
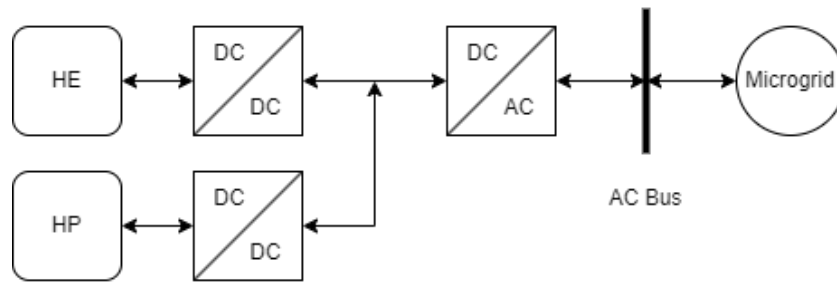
HESS in power systems [11].

Figure 1.16: Active interconnection configuration of HESS based on [11], where HE is the high energy storage system and HP is the high power storage system

1.3.2. HESS control strategies

There are three general categories for grouping different HESS control strategies. A filter based approach to the controller, a rule based approach to the controller and an optimization based controller [53]. Filter based and rule based control strategies are also known as non-optimized control strategies, as they use pre-optimization.

Filter based control strategies are the most frequently used control strategies for HESS applications [53]. Here the power transfer is divided into high frequency and low frequency components. This is most commonly done by a low pass filter. The high frequency components consist of the overshoots, load fluctuations or the fluctuations in power generation. These high frequency components are handled by the high power storage. The low frequency component can be seen as the more average power demand which is handled by the high energy storage. This means that the cut off frequency of the low pass filter has a significant affect on the sizing of either ESS [53]. Therefore, the optimization of the cut off frequency has a lot of influence on the cost-effectiveness of the HESS. [76] shows an approach to optimize the cut off frequency for life cycles between a battery and a flywheel. [53] shows how to choose the cut off frequency based on the difference in energy density between a battery and a flywheel.

In rule based control strategies a sequence of rules are devised by either mathematical models or system expertise [11]. The optimization objective is reached by sequentially going through the rules, a little like going through a series of 'else if' statements. A simple version is the 'thermostat' concept. This strategy consists of only using the high energy storage when the lower SOC-threshold of the high power storage is reached [16]. Another approach is shown in [1], where the lowest possible fuel cost is reached by the optimal utilization of a battery and supercapacitor HESS.

Optimization based controllers are the most broad in terms of implementation. They can be categorized as global and real-time algorithms [16]. The main advantage of optimization based control strategies is the minimization of the total cost-function, because these strategies do whole system optimizations. This is the approach that will be taken in this report and it will be elaborated on later.

1.3.3. HESS combinations

HESS by their hybrid nature combine different ESS, which results in a lot of different potential combinations. Typical implementations include SC/battery, SMES/battery, FC/battery, FC/SC, flywheel/battery, battery/battery, battery/CAES and flywheel/FC according to [42]. For this research the high power storage and the high energy storage are separated and a technology is considered as either one or the other. The list of high energy capacity energy storage is:

- LFP
- NMC
- Na-ion

And the list of high power capacity energy storage is:

- LTO
- SC
- FESS

Therefore, the basic configurations consist of FESS/battery, SC/battery, or battery/battery implementations of HESS. These are what [42] considers to be short-term optimal HESS combinations. Which makes sense as seasonal storage is not the goal of this research. Instead it is more focused on load-leveling and short term peak-shaving capabilities for shore power delivery.

1.4. Alternative power supply

The status quo of shore power supply using only power from the grid is the simplest way to service ships with shore power. However, this puts ever increasing burdens on the electricity grid, as vessels have large and also fluctuating power demands. One way to mitigate this congestion is by integrating energy storage systems with the shore power supply facility. Another way to mitigate the congestion is with local or even on site power production. This local power generation can in theory include small scale diesel generators, however this would be uneconomical compared to the power taken from the electricity grid. Not to mention that this would not be renewable and displace the pollution from the vessel to the shore. So, instead only renewable, non-polluting power generation is considered.

The structures that localize and distribute power generation to the place of consumption are known as microgrids. These microgrids are distributed power supply systems that control power production, the load that consumes the power and energy storage devices [94]. The distributed nature of microgrids has become a necessity due to the increasing complexity that renewable (and also decentralized) energy production penetrating the centralized power grid has brought. The traditional power grid has become ever more interconnected to increase its reliability, however without distributed power generation the possibility of blackouts still persists [94]. By distributing power generation, lower transmission losses and decrease congestion in power transmission can be realised. This results in improvement of the performance, lowers the total necessary capacity and increases the reliability of the power grid [94]. However, this does increase the complexity of the utility grid, making it less controllable from a central system administrators point of view.

With the development of power electronics, the controllability of decentralized power systems has increased [12]. This is where the concept of small, independent and decentralized systems as microgrids has emerged [94]. Microgrids can be islanded or grid-connected depending on the location and requirements [22]. The basic depiction of a microgrid is shown in Figure 1.17. The variability of renewable energy production makes the decentralized and local control that microgrids provide necessary [12]. This is why the quay-side at Royal Roos will be considered as a microgrid. The alternative forms of power supply that are considered in this report are: wind power based power production and photovoltaic based power production.
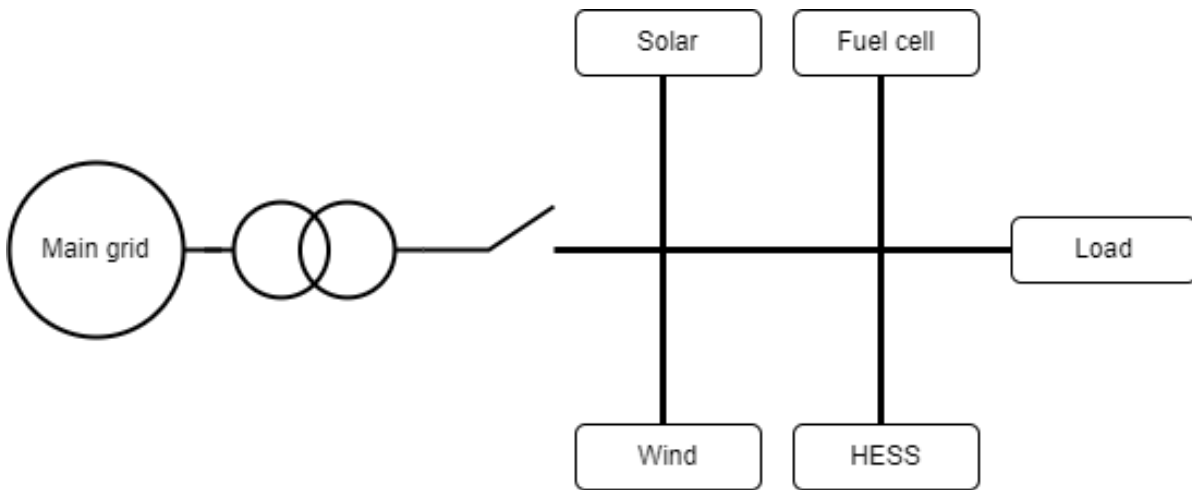
Figure 1.17: A basic diagram of a microgrid including grid connection, multiple sources of power production, a HESS and a load

1.4.1. Wind power production

Wind power production functions by extracting the kinetic energy of a mass or air as it passes within the rotor blades of the rotational axis of a wind turbine. This axis can be vertical or horizontal [85]. Wind energy is really a form of solar energy, the uneven heating of the Earth's surface cause temperature differentials in the air. This temperature difference and also the rotation of the Earth creates air streams or wind. The total power of the wind is expressed by the equation:

$$P_w = \frac{1}{2}\rho A v^3 \tag{1.1}$$

where ρ is the density of air, A is a particular area the wind passes through and v is the wind velocity. In order for the wind turbine to extract energy from the wind, it needs to interfere with the wind in to form of rotor blades. The kinetic energy of the wind is decreased and this energy is transferred to the rotor blades, which makes them rotate. The decrease in kinetic energy means the wind slows down. For full extraction the wind should be stopped, but this means the rotor blades can not rotate anymore either. The optimal balance between fully stopping the wind and not at all is called the Betz limit, which states that the maximum theoretical efficiency of a wind turbine is 59.3%. However, due to power losses realistic efficiencies of wind turbines vary between 15% and 50% [85].

Clearly, from the equation of the wind power, the amount of power generated by a wind turbine increases with the wind speed and the length of the rotor blades that trace out the area through which the air moves. This has lead to the development of ever taller towers for the turbines, as higher wind speeds are found higher up in the sky. And this has also lead to longer rotor blades to increase the effective area of the wind turbine [9].

Site viability

Site assessment for wind power viability is very important to the cost-effectiveness of the wind turbine. By measuring the frequency of occurrence of particular wind speeds at a site, an assessment can be made to the potential wind power generation possible there. This can then be combined with the beneficial power curve characteristics of a wind turbine to calculate the expected power generation [24]. Figure 1.18 shows an example of such a power curve and wind speed distribution.

According to [32], the North Sea has great potential for offshore wind, which is already partially being realised. Furthermore, the Netherlands as a country also has great onshore wind power potential, though a lot of that potential already has been utilized [32]. Wind turbine sites are quite heavily regulated, because of environmental concern for animal life and human habitation. All EU countries including the Netherlands have regulations for the spacing between wind turbine towers [28]. The spacing is partially based on operational effectiveness, so wind turbines do not negatively affect each others performance.

However, wind turbines also emit significant amounts of noise when operating, which negatively affects wild and human life [24]. The regulations in the Netherlands for offshore wind turbines is solely based on noise pollution, this affects the spacing and the sizing as bigger rotor blades create more noise [28]. Onshore wind turbines have stricter regulations as hub height is also regulated be provincial or city authorities [58]. This means permits need to be given, and when the wind turbine would intrude upon a envisioned skyline such permits do not get approval [58].

This means that on site wind power generation for Royal Roos is very unlikely, as significant power generation requires large tower hubs which would not be approved by the municipality of Rotterdam. So, wind power is not considered for further analysis.
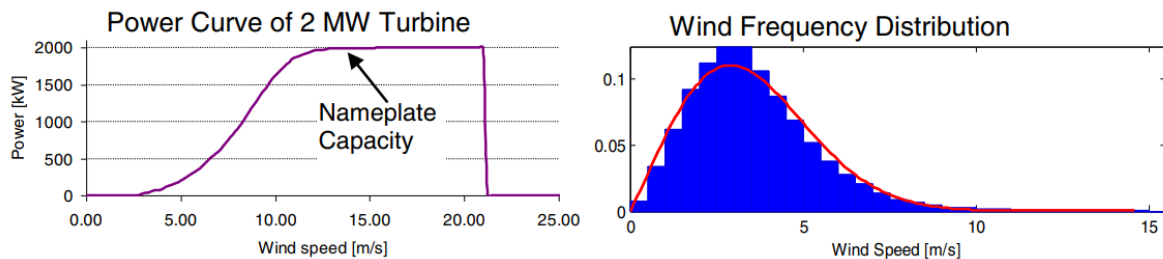
Figure 1.18: Example wind turbine power curve (left) and example wind frequency distribution (right) from [24]

1.4.2. Photovoltaic power production

Solar or photovoltaic (PV) power production directly converts solar irradiance into electrical current inside of a solar cell. Which means it uses the most abundant form of energy that can be accessed on Earth. Solar cells are made of (at least) 2 different materials and use the photovoltaic effect. The photovoltaic effect creates a potential difference across these 2 materials when light hits the surface of the solar cell. With an electrical connection between the two layers, the potential difference is resolved in the form of direct current, which can be used to power appliances [71]. Figure 1.19 shows a schematic depiction of a solar cell generating electrical current.
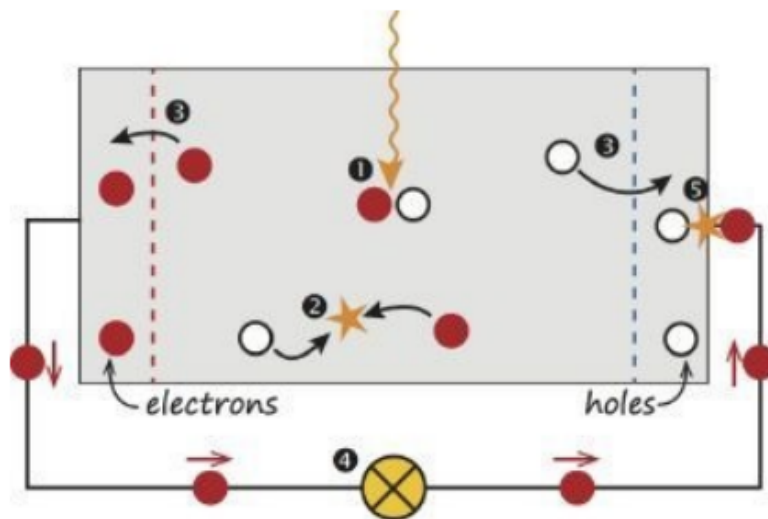
Figure 1.19: Schematic diagram of solar cell generating electricity [71]

Types of solar cells and applications

The expansion of PV power production over the last 2 decades and the pressure to achieve greater

maturity of the technology has resulted in a lot of research [46]. This research has resulted in several 'generations' of photovoltaic solar cells. The first generation ist the most conventional and commercial. First generation solar cells are crystalline silicon solar cells, made from polysilicon or monocrystalline silicon. The second generation or thin film solar cells, are made from amorphous silicon and are also commercial. The third, and so far final, generation are also thin film solar cells that are still emerging and have far higher efficiencies. Third generation solar cells are not commercial yet [13] [31].

As mentioned above, first generation solar cells are by far the most utilized type of solar cell. This is due in no small part because of the vast amount of funding crystalline silicon solar cell production has gotten in China. Most (crystalline solar cell) PV modules are made in China [71]. Figure 1.20 shows a depiction of a single mono-crystalline solar cell. The lattice structure visible in Figure 1.20 is quite thick, which is why thin film solar cells are being developed. So far crystalline silicon solar cells do remain dominant in PV technology. They are cheapest to manufacture on a large scale and have a proven and reliable efficiency of around 20% in commercial and industrial applications. And lab tests have resulted in efficiencies of up to 26% [40]. PV modules based on crystalline silicon solar cells are used in applications ranging from off grid power production to residential power production for personal use to large scale solar farms for renewable energy generation [46].

Second generation solar cells have been developed because of the expense of pure crystalline silicon necessary for first generation solar cells. Second generation solar cells are considered 'thin film' solar cells, meaning that the amount of silicon necessary is vastly reduced from around 230 μm [71] to 1 μm [31]. The most mature form of thin film solar cells are amorphous silicon (a-Si) solar cells [13] [31]. The efficiency of a-Si solar cells is poorer than that of crystalline solar cells at around 11% [40]. They have found a niche, however, in powering pocket calculators and they are also used to power remote facilities and homes [31]. Because a-Si solar cells can be made into transparent modules [31], they can be used in building integrated PV applications [13]. These applications include photovoltaic glazing laminated onto windows or walls [13].

Third generation solar cells are multi-junction solar cells that increase cell efficiency to 40% [31]. So far, they have not been commercialized, but the research is very promising and some of the technologies are close to commercial prototype fabrication [31].
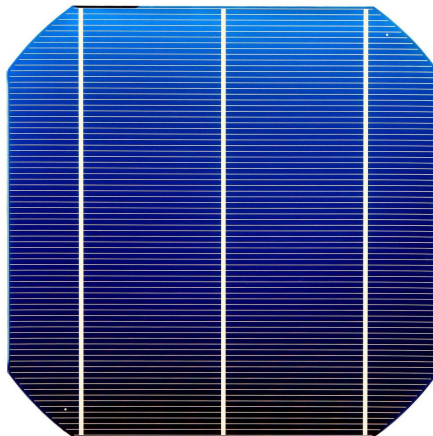

Figure 1.20: Image of a single mono-crystalline solar cell [23]

Solar potential

The potential for solar power production is almost limitless as a renewable energy source. As the Earth's surface receives an amount of solar irradiation in a single day is greater than the total energy consumption of the entire world for a full year [10]. According to [46], certain 'black dot' areas, shown in Figure 1.21, could provide the entire worlds energy demand by themselves. Though this potential is theoretical in nature, it still indicates the viability of solar power as a RES.

Figure 1.21 also shows that geographical location has a large influence on power production potential of solar power. This does not mean, however, that only in regions relatively close the equator that solar power is a viable RES. As shown by [99] even in more northern countries like Germany, almost all household electricity demand can be met by local PV generation (placed on rooftops) if it is combined with energy storage. [99] also shows that oversizing of PV production does not result in a greater share of RES of the total energy demand, due to mismatch in timing of power demand and power production, which makes integration with ESS necessary for residential solar power production.
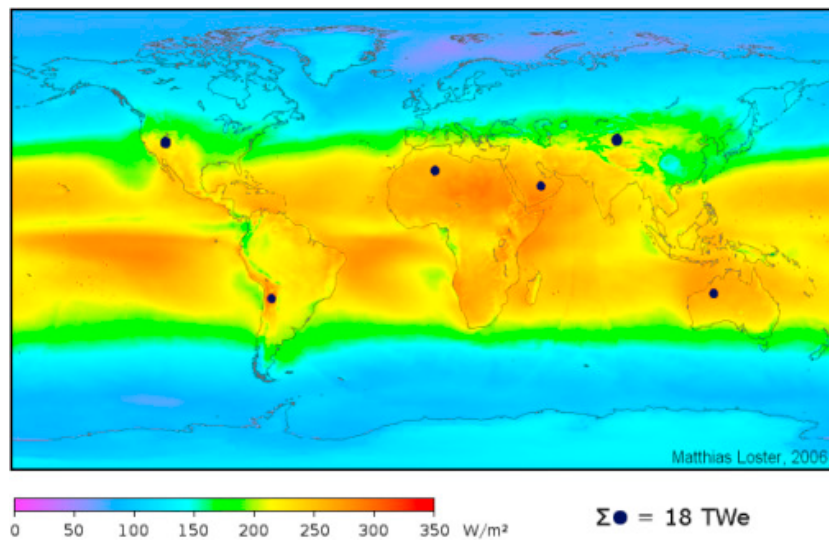
Figure 1.21: Annual average solar irradiance distribution over the surface of the Earth [46]

The irregularity of sunlight, because of day and night cycles and also cloud covers, results in unpredictability of power generation. This creates problems for large solar farm integration with the utility grid, where stability and reliability of power production is vital [68]. The intermittency of solar irradiation causes harmonics because of the power electronics converters that are used to transform the DC voltage output of a solar cell into AC voltage. The role of power electronics in solar power generation will be explored later.

Among renewable energy sources, solar power production has certain advantages. One such advantage that solar power production has over wind power production is lower environmental impacts. Solar power uses about 10 times less land than wind power for the same level of power production [78]. This is not to say that solar power has no environmental impact. In the lifetime of a PV module, the part that has the largest impact is the manufacturing. The extraction of materials necessary to fabricate a PV module and the fabrication process itself have very significant environmental impacts [78]. The recyclability or the biodegradability of solar panels is quite low currently. However, there is research being done to be able to recover raw materials and use polymeric materials that are biodegradable in PV modules [78].

Array construction

The voltage of individual solar cells is quite low, usually around 1 volt for crystalline silicon solar cells. Even if they are increased in size, the voltage output of the cell will not increase, instead the current will [71]. So, in order to increase the output voltage, solar cells are connected in series. This is what

a PV module is. Solar cells can also be connected in parallel to increase the current, however this is usually not done because that would increase resistive losses [71] and a higher output voltage is more desirable.

PV modules can then be used standalone or connected with other pv modules in series or parallel in a PV array. The specific configuration would depend on the application and the installation site. Figure 1.22 shows a full PV system, this includes both a DC/DC converter and an inverter. Both are necessary, because a PV array does not necessarily operate at its maximum power point (MPP), so a DC/DC converter is used to find and keep the PV array operating at its MPP [71]. Since, a solar cell generates DC voltage, an inverter is needed to connect it to the utility grid or a local microgrid. These power electronic converters are not trivial to the cost of the PV system. The converters and mounting system are now a greater share of capital investment than the PV module itself [71].
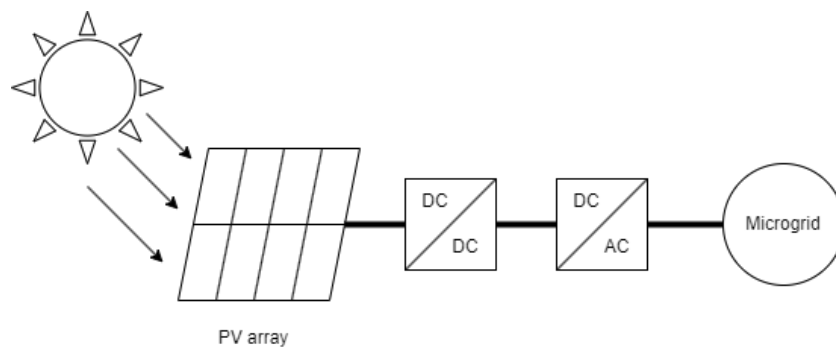
Figure 1.22: Schematic of a PV array under irradiation, with a DC/DC converter and an inverter connection to a microgrid

1.5. The possible configurations

Now that the literature review has been covered, let's return to the problem statement and the different configurations that will be investigated. To re-iterate, the different configurations are:

1. The status quo of shore power from the grid only
2. Shore power + PV, or Basic PV shore power configuration
3. Shore power + HE ESS, or HE ESS shore power configuration
4. Shore power + HP ESS, or HP ESS shore power configuration
5. Shore power + HE ESS + PV, HE PV shore power configuration
6. Shore power + HP ESS + PV, HP PV shore power configuration
7. Shore power + HE ESS + HP ESS, Hybrid ESS shore power configuration
8. Shore power + HE ESS + HP ESS + PV, Hybrid ESS PV shore power configuration

Where the status quo, as covered in section 1.1, is the delivery of shore power by converting the grid power through an AC/AC power electronics connection to synchronise with the vessel using the right frequency and voltage. Configuration 2 is used as a baseline for including PV. Also, this is the current infrastructure at Royal Roos.

The next two configurations are explained by section 1.2. Where, as covered in section 1.3, the high energy storage is any of the following:

- LFP
- NMC
- Na-ion

and the high power storage is any of the following:

- LTO

- SC
- FESS

This means that both configuration 3 and configuration 4 have 3 different possible optimal solutions. Configuration 5 and configuration 6 include the alternative power production in the form of solar power as explained by section 1.4.

Configuration 7 is explained by section 1.3 and finally, configuration 8 includes the full system.
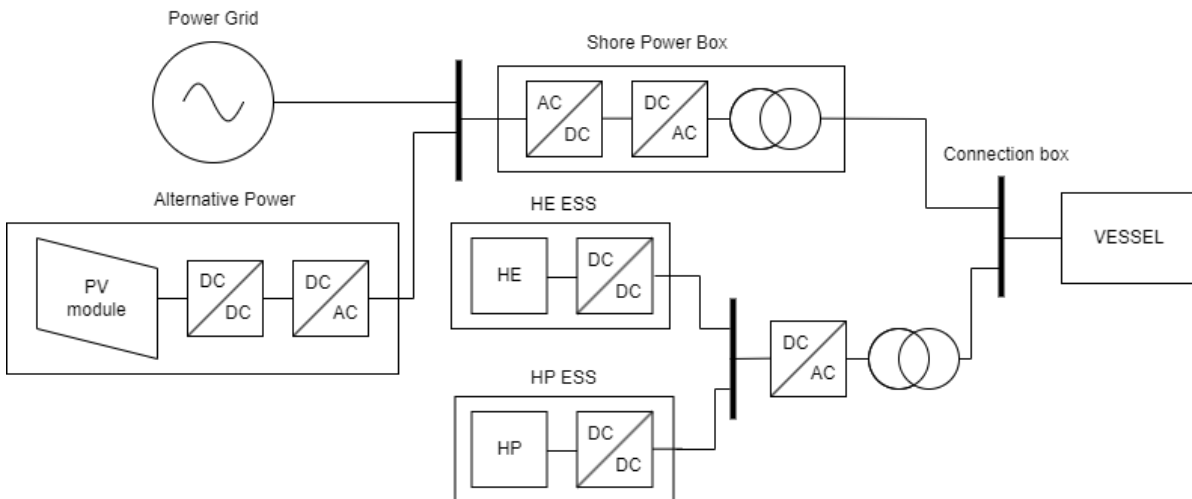

Figure 1.23: Full system diagram example

1.6. Summary

This chapter covered the background literature review for this research. Section 1.1 explains what shore power entails and why it is being promoted as a (partial) solution to port emissions. Section 1.2 covers every form of energy storage and its relevance to this research. Section 1.3 explains the benefits of combining different types of energy storage and what is necessary to integrate multiple forms of energy storage with each other. Section 1.4 explains the utility of different renewable energy sources as alternative power production and their use case for this research. Sections 1.5 compiles all the energy storage systems and renewable energy sources that are relevant for this research.

2

Vessel power estimation

This chapter explores how to create vessel power profiles. In order to perform analysis, it is necessary to utilize vessel power profiles, where the data contains the power demand of the vessel over time. Ideally, such data is acquired through the logging of detailed high frequency sampled power measurements of a vessel. However, vessels are quite reluctant to either to do such measurements or to hand over this data. So, other means of acquiring data need to be used and then this data should be used to construct a vessel power profile artificially.

2.1. Power Load balance

Vessels commonly track the requirements for their generators by balancing them against the total nominal demand of each appliance on board. This is done through what is called an 'Electrical Load Balance'. An example of an Electrical Load Balance is shown in Appendix A. An Electrical Load Balance also lists what type of operations the vessel should handle, ie. Transit or Harbour operations and if the appliance is applicable it is added to the subtotal of that category.

Additionally, vessels have what is called a 'Hotel Load', this is the nominal load that is required by the vessel to keep the 'Hotel' running when at port. The Hotel Load contains basic emergency appliances, large appliances like pumps and compressors but also lighting and cooking equipment. The Hotel Load is used as the value that the shore power should be able to supply to the vessel. The Hotel Load is constructed from the Electrical Load Balance, and it is a subset of the Harbour operations column specifically. Luckily, vessels are more willing to provide the Hotel Load, so this calculation does not need to be done and the value given can simply be used.

The Hotel Load does not include the service cranes that vessels commonly have. Which means that if the crew would like to use their crane to haul cargo, repair equipment or provisions on to or off of the vessel, they then need to return to using the generator to do that. Vessels generally want to avoid this as it is a lot of hassle to go back and forth on using their generator. This results in a reluctance to utilize shore power. So, it is important to include the use of the crane into the vessel power profile as well as the Hotel Load.

2.2. Relevant vessels

Now that the parameters for the power profile are determined, it is necessary to consider which vessel(s) should be included in the research. Firstly, the quay-side at Royal Roos is not used for offloading cargo. Instead the quay-side is used by vessels that wish to do maintenance, repairs or upgrades and it is used for mobilisations. These vessels can still be considerable large transport vessels, as the quay-side is 250 meters long, but this does limit the range of vessels that should be considered.

2.2.1. Selection of vessels

The vessels that commonly do dock at Royal Roos fall into two general categories: smaller vessels like tugs that are used in the harbour itself or larger vessels that come to do maintenance or repairs. This last category contains general cargo vessels, container cargo vessels and ocean going tug support vessels. The latter category is of greater interest for this research as shore power infrastructure to service these vessels is currently not adequate at Royal Roos.

To keep this research focused one vessel in particular is used: The Kolga or the Bylgia. These are sister ocean going anchor handling tug support vessels and would require the same infrastructure for shore power. Figure 2.1 shows these vessels. Another reason why these vessels will be used in particular is that accurate nominal power values for its hotel load and crane load are known, because Royal Roos is already investigating how to implement shore to ship power specifically for either of these vessels. Secondly, the hotel load is higher than the present shore power facilities can handle. So, investigating the optimal configuration and sizing for this vessel makes sense as it is beneficial to the company.

The nominal power values of the Kolga or the Bylgia are shown in table 2.1.

	P_{nom}
Hotel load	450 [kW]
Crane load	200 [kW]

Table 2.1: The nominal load of the Kolga or Bylgia

Figure 2.1: Image of the Kolga and the Bylgia

2.3. Building of power profiles

Using the selected vessel and its Hotel Load and Crane Load it is possible to artificially construct a power profile that approximates a real power profile. At least to the extent that analysis can be done. There are a number of elements that the power profile depends on. Evidently the values for hotel load and crane load, but also the length of time that the vessel uses shore power, the number of times the crane is used and more. These will be covered one at time.

An assumption is made regarding the Hotel Load, which is that it is fairly constant. In other words the large appliances are always in use, but the personal electricity use of the crew is changing. The magnitude of the change is put at 1 percent of the hotel load. This results in a power profile shown in Figure 2.2. The length of time is determined by how long the vessel is expected to stay in the scenario,

while the power demand is scaled to the Hotel Load of the vessel, in this case it is 450 kW.
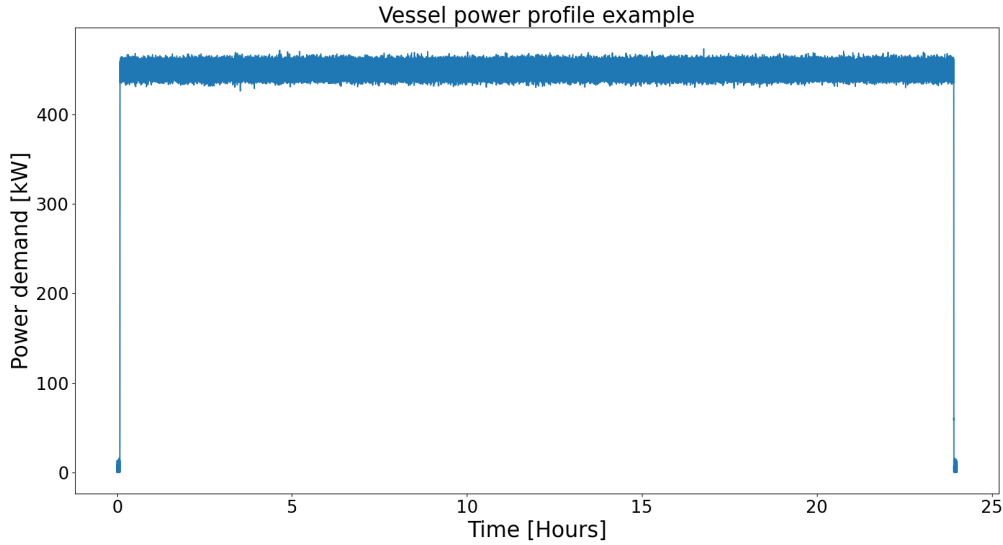
Figure 2.2: An example of the nominal Hotel Load of the Kolga or the Bylgia being used to create a fairly constant power profile, where the length is 24 hours.

The next step is creating the crane power profile based on a nominal power value. Unfortunately, here too assumptions have to be made. There is no universal way to operate a crane and the power profile depends heavily on what type of crane is used, what kind of load is lifted and how heavy the load is.

So firstly, the crane is all electric which means that when the load is lowered, the crane acts as a flywheel and the gravitational energy of the load is returned to the grid with some losses. Secondly, because the vessels use cranes to lift or lower equipment or containers instead of loose bulk at a terminal, the operation is more gentle and careful so it takes longer. In this case the length is 3 minutes as advised by my company supervisor. Thirdly, the harshest operational profile is chosen, so the transition from lift to swing to lowering is instant and the maximum load is always lifted.

Figure 2.3 shows this power profile, 40 kW was chosen as base value and power profile will be scaled to the proper nominal value when creating the full power profile of a vessel. The following equation is used for that:

$$P_{set,new}[1:N] = P_{set}[1:N] * \frac{P_{actual}}{P_{base}}$$

(2.1)

Where N is final sample in the series. This only changes the magnitude but not the overall behaviour of the crane.

With both of the separate power profiles, the power profile for the Hotel Load and the power profile of the crane, the full power profile of the vessel can be constructed. Here too choices need to be made. After all, the amount of crane uses and how they are clustered makes quite a difference. This ultimately depends on what kind of operation needs to be simulated, ie. loading and unloading cargo or repairs/maintenance where equipment is hauled on or off the vessel at random throughout the day. Later on the differences will be discussed and their effect.

The power profile also needs downtime where the quay-side is empty. As the quay-side is not always occupied. This ensures that there is time for ESS to be charged while there is no vessel and then be discharged as needed when a vessel is present. Therefore a downtime of equal to the length of the stay of vessel was chosen. So, a 50 percent occupation rate is assumed.
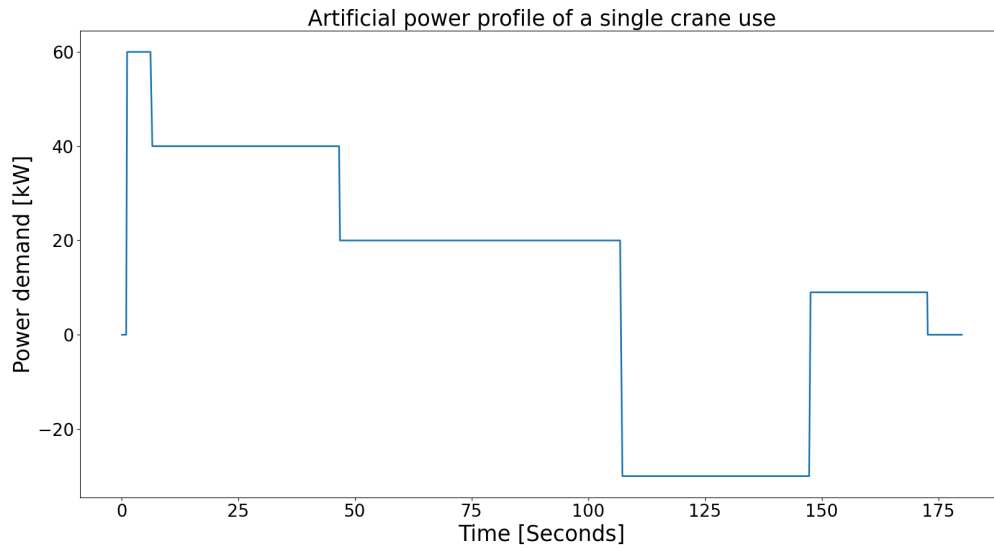
Figure 2.3: The artificial crane power profile, with a nominal crane power of 40 kW and a length of 180 seconds (3 minutes). It starts with an overshoot and then settles to the nominal power as the maximum load is lifted, followed by a slow and careful swing and then lowering the load slowly. The crane then returns unloaded to its starting position.

Finally, in order to model the power profile accurately a high sampling rate should be chosen. However, due to the long simulation time of multiple days or even longer, this high sampling rate would result in very long run time for calculations. Through an experimental method, a sampling rate of 10 Hz was chosen as a good balance between accuracy and runtime. Figure 2.4 shows an example of such a power profile where this is all combined.
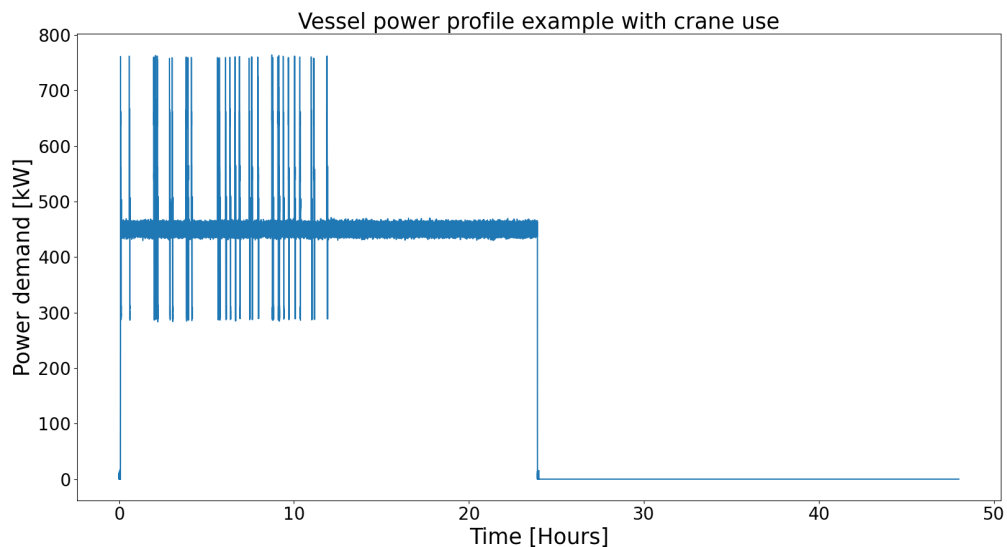
Figure 2.4: An example of a vessel power profile for the Kolga or Bylgia, with a length of 24 hours + 24 hours of an empty quay-side. The crane is used at random throughout the working day, meaning for only 12 hours.

2.4. Different possible power profiles

As mentioned in 2.3 there are different possible scenarios for using the crane and for the length of stay of the vessel. The amount of crane use and its distribution has a great effect on the sizing of ESS necessary and so does the amount of days the vessel uses shore power. In order to resolve this, it is better to handle each of these independently so their effect on can be studied separately from each other.

2.5. PV power profile

Solar power can also be included in the shore power configuration as an alternative power supply. This can add cost-effectiveness as the electricity generated from local PV panels is free, however it is more intermittent and less reliable than electricity supplied by the grid. This is simply due to the fact that clouds can severely dampen the amount of irradiance that a PV array receives, not to mention that no solar power is possible during the night.

Since the optimization algorithm will create an optimal solution for the specific weather data that is used as input, it is better to use more average data that excludes the sudden drops in irradiance due to clouds. The weather data that will be used is from PVGIS [62] and contains the irradiance data for Rotterdam for the year 2020. However, that weather data will not be literally used as an input, instead an 'average summer day' and an 'average winter day' will be constructed from this data and these will be used for the research.

This irradiance data is then normalized by dividing it by 1000 W/m^2 as that is standard test conditions. And the power rating of the PV array will be based on standard test conditions. This creates a per unit profile of an average summer day and average winter day as shown in Figure 2.5. This per unit profile can then be multiplied by the optimal nominal power, whatever that may be, of the PV array to create the power profile of the PV array.
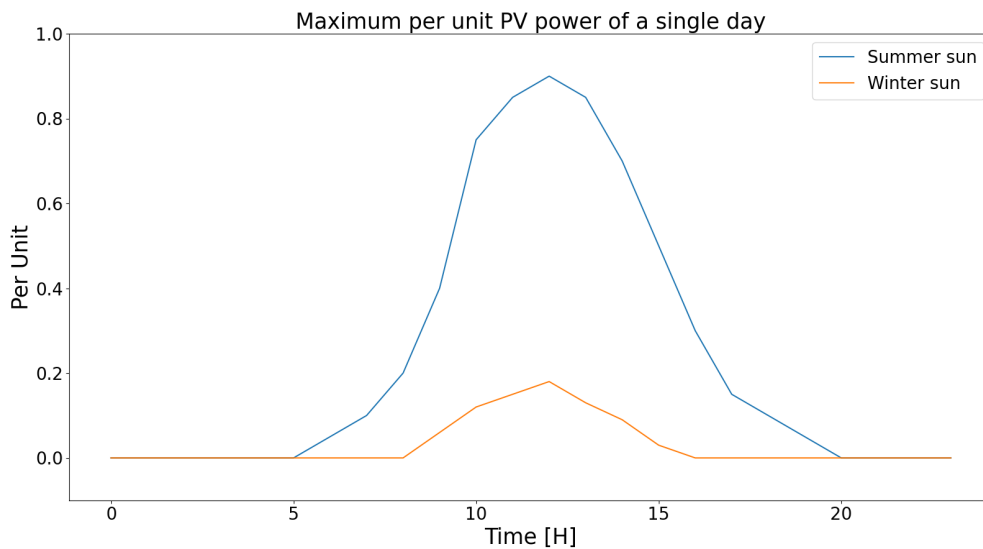
Figure 2.5: The per unit maximum output power according to solar conditions of an average summer day in Rotterdam or the solar conditions of an average winter day in Rotterdam. The base of the PV array is the rated power for the PV array determined by the research.

The final step that is to map the per unit profile of the PV to the same timescale as the vessel power profile. Since the PV data has a single data point per hour and the vessel power profile has sampling frequency of 10 Hz, this means upsampling the PV data a lot. This results in the data point for a specific hour being held constant with the sampling frequency of the vessel power profile. Figure 2.6 shows

what that looks like for the vessel power profile shown in Figure 2.4. Where the upsampling during the supply of shore power results in a stepped PV power profile, while the downtime can remain downsampled at a single data point per hour.
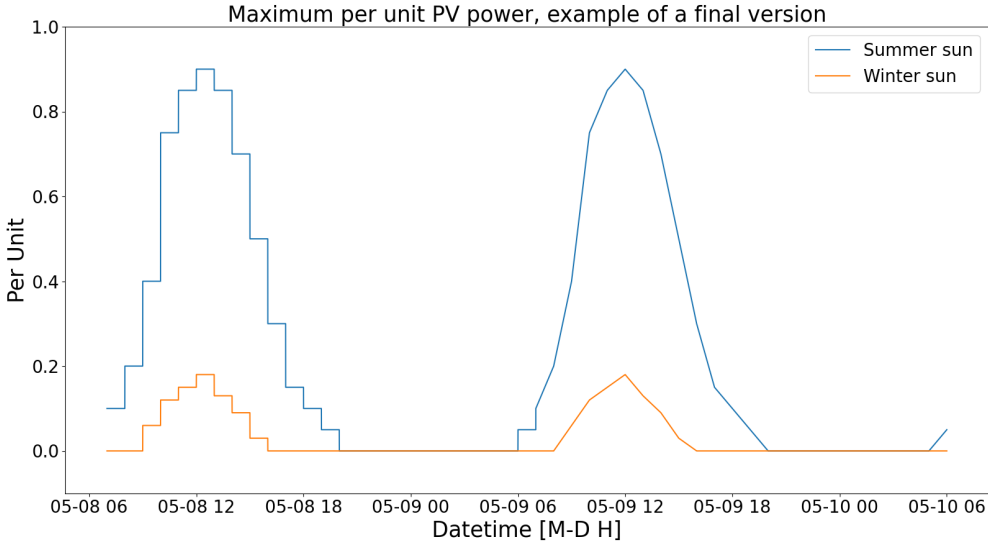
Figure 2.6: Example of a maximum per unit PV power profile to be used in the research, where there is a single day of shore power supply to a vessel and a single day of downtime.

2.6. Summary

This chapter covers how the vessel power profile is constructed that is used as an input for the optimization in this research. This vessel power profile is based on nominal power values for the Hotel load and the crane load, specifically that of the Kolga or the Bylgia. The vessel power profile can be constructed in many different ways depending on what type of analysis is needed, so multiple scenarios will be constructed to investigate the effect of these different parameters that influence the vessel power profile. This will be covered in the next chapter. Finally, this chapter explained how the power profile for the solar power is constructed.

3

Optimization Problem

This chapter focuses on what optimization is, why it is necessary for this research and how it is implemented. Then the chapter concludes with the considerations that were taken and how these lead to the scenarios for supplying shore power. These different scenarios are necessary for doing more in depth analysis.

3.1. Introduction to optimization

Optimization is the process by which an optimal solution, either a maximum or a minimum, to a problem is found. It is a mathematical computation where an objective is reached by taking into account the restrictions upon it. An optimization problem needs 3 parts: the objective function 'f(x)', which defines the mathematical function that has to be minimized or maximized for the optimal solution; the decision variables 'x', these consist of the range defined by the constraints that the objective function is able to use; and the constraints 'g(x)', these define the region for the decision variables to take values from for finding the optimal solution. Equation 3.1 shows the mathematical formulation of a general optimization problem.

$$
\begin{aligned}
Obj.\ function \quad &:- \quad min./max. \quad && f(x_i) \\
Decision\ variables \quad &:- \quad x_i \quad && i \in [1,2,3,4,5] \\
s.t\ Constraints \quad &:- \quad g_j(x_i) \leq 0 \quad && i \in [1,2] \\
s.t\ Bounds \quad &:- \quad x_i \geq 0 \quad && i \in [1,2,3,4,5]
\end{aligned}
\tag{3.1}
$$

Optimization problems fall into 4 major types [44]. Figure 3.1 graphically illustrates them, but in short there is:

- Linear Programming (LP)
- Non-Linear Programming (NLP)
- Mixed-Integer Linear Programming (MILP)
- Mixed-Integer Non-Linear Programming (MINLP)

A LP optimization problem is defined by linear objective functions and linear constraints. Conversely, a NLP optimization problem consists of non-linear objective function and/or non-linear constraints. For both these types of optimization problems the step towards their mixed-integer versions changes the way decision variables are defined. For both MILP and MINLP (some) decision variables are restricted to being integers instead of continuous real variables. MILP is further characterized by the same linear objective functions and linear constraints as LP is. The same is true for MINLP for non-linear objective functions and non-linear constraints with respect to NLP. There are numerous different ways such optimization problems can be solved. Genetic Algorithm (GA) and Particle Swarm Optimization (PSO) being popular techniques to solve optimization problems [7].

For this research the PyPSA python package [19] is used, which is used for MILP optimization problems for Power Systems Analysis. It can calculate linear optimal power flow with least-cost optimization of power generation and energy storage. This last part is especially vital for this research as the sizing of the energy storage according to capex costs is quite simple, but optimal power flow according to operational expenses is significantly more difficult.
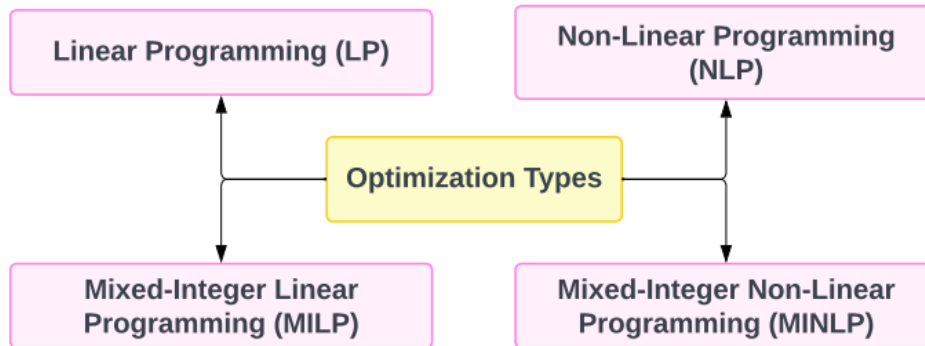
Figure 3.1: The types of optimization problems, figure from [2]

3.2. Practical considerations

In this section the considerations that were taken into account for this research. They are:

1. This research is about reaching the most cost-effective solution for (just) supplying shore power.
2. Once a vessel has docked, all power demand will be taken care of by the shore power system. The engine will not be utilized once connected.
3. On the vessel side, it is assumed that all necessary infrastructure for receiving shore power is present.
4. Average efficiencies for electrical components are assumed.
5. The nominal Hotel Load (as mentioned in Section 2.3) is assumed to be almost constant when constructing the vessel power profile.
6. Every crane use is identical to each other and can be simply added to the baseline power profile constructed from the Hotel Load.
7. Each crane use degrades the ESS lifetime.
8. The limit to the grid connection is 1.7 MW as that is the rating of the transformer at Royal Roos.
9. The grid connection does not experience congestion.
10. Vessels come for maintenance, repairs or installing new equipment. This lasts from 1 day up to a week or more.
11. Prices for components are based on linearly scaling factors, these factors are based on informal quotes from different companies.
12. All electrical components are modelled as PyPSA objects.
13. The differences between types of ESS was considered more important than the differences a different manufacturer creates for a single type of ESS. So, only one manufacturer per type of ESS was considered for this research.
14. The grid is modelled as a single point of generation.
15. The shore power converter is uni-directional as is legally required, because the vessel is classified as solely a consumer [35]).
16. The PV power is modelled using either high irradiance days or low irradiance days.
17. The PV does not supply surplus power to the grid for a profit, because the electricity price goes negative if there is a lot of solar generation in the surrounding area.
18. The cables that connect to the vessel are always 100 meters in length.
19. Electricity prices are based on the contracts that Royal Roos has with either Stedin or BCI Energy Commodities.

3.3. Implementation

The optimization done for this research was done using the python package for Power Systems Analysis or PyPSA. This python package was developed for large scale power system analysis like what is depicted in Figure 3.2. In such systems there is a lot of inter-connectivity and different types of power generation combined with cities being depicted as a single load, where the timescale uses hours as unit. The simulation time is then multiple years. In this research the timescale is instead at a 100 ms, while still doing long term simulations of several days or longer. And the power system is quite simple as depicted in Figure 1.23. This results in a incredible amount of detail and number of computations necessary even for such a small system. Resulting in long run times, requiring simplifications that will be explained later.

Every component is implemented using inbuilt PyPSA objects, the important ones for this research are:

- The grid or the solar power modelled as a Generator
- Power electronic conversion and connections, like the shore power converter and cables, modelled as Links
- All energy storage systems with fixed power and energy ratios are implemented as Storage Units
- All energy storage systems with independent power and energy are implemented as a Store and a Link

Each of these objects has its own inbuilt constraints, while PyPSA has inbuilt Objective functions that can be used and modified according to the optimization problem. These will be covered henceforth.
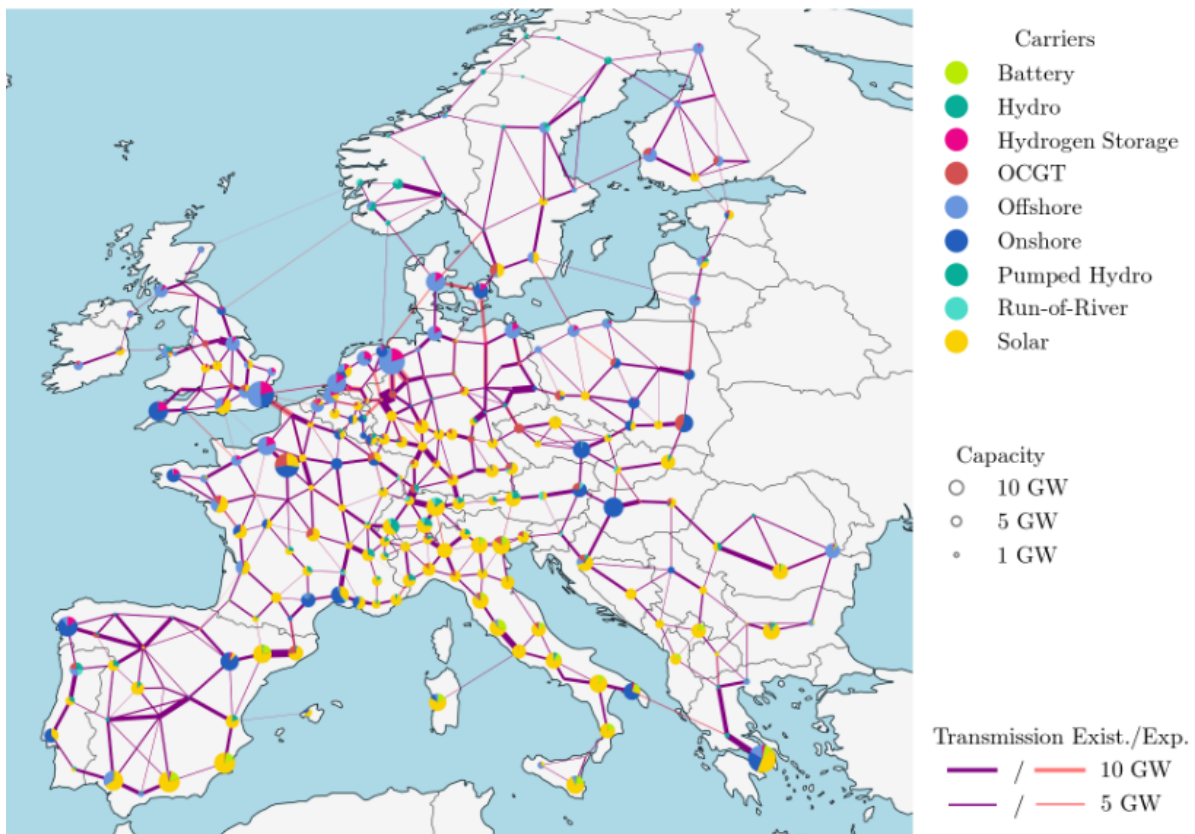
Figure 3.2: Graphical depiction of power lines, power generation and energy storage from the PyPSA-Eur project, from [29]

3.3.1. Objective function

PyPSA has its own inbuilt standard objective function for the minimization of costs, and also for the minimization of CO_2 emissions. For this research, as the vessel is not supposed to run its engines,

only the minimization of costs is of interest. The inbuilt objective function for costs:

$$min \left(\sum_{n,s} c_{n,s} \bar{g}_{n,s} + \sum_{n,s} c_{n,s} \bar{h}_{n,s} + \sum_{l} c_{l} F_{l} + \right.$$
$$\left. \sum_{t} w_{t} \left[\sum_{n,s} o_{n,s,t} g_{n,s,t} + \sum_{n,s} o_{n,s,t} h_{n,s,t} \right] + \sum_{t} [suc_{n,s,t} + sdc_{n,s,t}] \right)$$

(3.2)

Where,
$c_{n,s}$ is the capital cost of component s connected to bus n per 1 kW of capacity
c_{l} is the cost of branch l
$\bar{g}_{n,s}$ is the nominal power of generator s at bus n
$\bar{h}_{n,s}$ is the nominal power of storage unit s at bus n
F_{l} is the capacity of branch l
w_{t} is the weighting of time t in the objective function
$o_{n,s,t}$ is the marginal cost of 1 kWh for component s at bus n at time t
$g_{n,s,t}$ is the dispatch of generator s at bus n at time t
$h_{n,s,t}$ is the dispatch of storage unit s at bus n at time t
$suc_{n,s,t}$ is the start-up cost if generator s at bus n started at time t
$sdc_{n,s,t}$ is the shut-down cost if generator s at bus n shut down at time t

However, this version is used for large scale power systems and is not very useful for this research. So, the objective function for costs optimization is modified into this:

$$min \left(\sum_{n,s} c_{n,s} \bar{g}_{n,s} + \sum_{n,s} c_{n,s} \bar{h}_{n,s} + \sum_{n,s} c_{n,s} \bar{e}_{n,s} + \sum_{n,m,s} c_{n,m,s} \bar{l}_{n,m,s} + \right.$$
$$\left. \sum_{t} w_{t} \left[\sum_{n,s} o_{n,s,t} g_{n,s,t} + \sum_{n,s} o_{n,s,t} h_{n,s,t} + \sum_{n,s} o_{n,s,t} e_{n,s,t} \right] \right)$$

(3.3)

Where,
$c_{n,s}$ is the capital cost of component s connected to bus n per 1 kW or 1 kWh of capacity
$c_{n,m,s}$ is the capital cost of link s connected between bus n and bus m per 1 kW of capacity
$\bar{g}_{n,s}$ is the nominal power of generator s at bus n
$\bar{h}_{n,s}$ is the nominal power of storage unit s at bus n
$\bar{e}_{n,s}$ is the nominal energy capacity of store s at bus n
$\bar{l}_{n,m,s}$ is the nominal power capacity of link s between bus n and bus m
w_{t} is the weighting of time t in the objective function
$o_{n,s,t}$ is the marginal cost of 1 kWh for component s at bus n at time t
$g_{n,s,t}$ is the dispatch of generator s at bus n at time t
$h_{n,s,t}$ is the dispatch of storage unit s at bus n at time t
$e_{n,s,t}$ is the dispatch of store s at bus n at time t

3.3.2. Decision variables
There are two types of decision variables in this optimization problem. The first type of decision variable concerns the sizing of each component, in other words their nominal capacity. This is governed in the objective function by the cost relation between capex cost and nominal capacity (of either energy or power). While the other type of decision variable concerns the optimal power flow in order to satisfy the power demand of the vessel after the nominal capacity of each component is established.

3.3.3. Constraints
The constraints are split into four parts.
Time dependent generator constraints:

$$\tilde{g}_{n,s,t} * \bar{g}_{n,s} \leq g_{n,s,t} \leq \bar{g}_{n,s,t} * \bar{g}_{n,s}$$

(3.4)

Time dependent energy storage with fixed power and energy ratio constraints:

$$0 \le h_{n,s,t} \le \bar{h}_{n,s}$$
$$0 \le f_{n,s,t} \le \bar{h}_{n,s}$$
$$0 \le soc_{n,s,t} \le r_{n,s}\bar{h}_{n,s}$$
$$soc_{n,s,t} = \eta^{w_t}_{stand;n,s} soc_{n,s,t-1} + \eta_{store;n,s} w_t f_{n,s,t} - \frac{1}{\eta_{dispatch;n,s}} w_t h_{n,s,t}$$
$$soc_{n,s,t=-1} = soc_{n,s,t=|T|-1}$$

(3.5)

Time dependent energy storage with independent power and energy ratio constraints:

$$-\bar{l}_{n,s} \le h_{n,s,t} \le \bar{l}_{n,s}$$
$$\tilde{e}_{n,s} \le soc_{n,s,t} \le \bar{e}_{n,s}$$
$$soc_{n,s,t} = \eta^{w_t}_{stand;n,s} soc_{n,s,t-1} - w_t h_{n,s,t}$$
$$soc_{n,s,t=-1} = soc_{n,s,t=|T|-1}$$

(3.6)

Time independent link constraints:

$$\tilde{l}_{n,s} \le l_{n,s,t} \le \bar{l}_{n,s}$$

(3.7)

3.3.4. The docking scenarios

There are a number of limitations to this optimization algorithm, namely that there is a high focus on capex over opex and this is partially due to the way the model optimizes for that first. But secondly, the long run time means that simulation length should be kept short. So, every vessel stay is simulated separately and small variations are used to infer what the effect would be for long term simulations.

The different investigations are:

- What effect does the length of time that the vessel stays have on the sizing of HE ESS? This is investigated by multiple simulations where the length that the vessel stays is increased. From 1 day to however many is necessary to do analysis.
- What effect does sustained crane use have on HP ESS sizing? This is investigated by different simulations where the amount of crane use is increased from one to the other. The crane use is clustered, as that is a harsher on the sizing.
- How does the amount of P_{nom} of the vessel's crane affect the HP ESS sizing? This is investigated through simulating different sizes of the crane.
- What effect does adding PV power to the status quo, HE configuration or HP configurations have on these shore power configurations? This is investigated by adding different sizes of PV array to the shore power configurations and comparing the results to the shore power configurations without PV power.

By simulating these different scenarios the effect of adding energy storage and alternative power supplies in different configuration can have for shore power infrastructure.

3.4. Summary

This chapter covers what optimization is and how an optimization algorithm was implemented for this research. The considerations that have been taken into account for building the optimization algorithm are covered and finally the docking scenarios are introduced.

4

Cost analysis

Since this research is based on cost-optimization it is very important that the prices that are used are realistic. This chapter covers the validity of the prices of the different components that make up the shore power configurations. The prices are as of June 3rd, 2024.

4.1. Site analysis

First, let's cover what is already present at the quay-side of Royal Roos. The company has a contract with Stedin for a grid connection rated for about 1700 kW. Furthermore, at present they do not experience grid congestion issues. So, there is no time-dependent limitation on the amount of power that they are able to supply. There are already shore power facilities at Royal Roos. These include a shore power converter shown in Figure 4.1 and a shore power connection box shown in Figure 4.2.

Figure 4.1: Picture of the shore power converter owned by Royal Roos

Apart from their shore power facilities Royal Roos also has solar panels located on the roof. The full system is displayed in Figure 4.3. The PV power can be used for supplying shore power, by the building itself or supplied back to the grid. But in this research it is assumed that all available shore power is used for supplying shore power only. The power consumption of the building is at most in few 10's of kW. Although this is really peak demand, and it is in general lower. While, the hotel load of the

Figure 4.2: Picture of the shore power connection box owned by Royal Roos

vessel is 450 kW. So, with the focus of this research being on supplying shore power specifically, the contribution of the power consumption of the building is ignored. The PV power is only used for supplying shore power and not as a means of supplying power to the grid, because the price of electricity goes negative when a lot of PV power is available in the wider area. This means the company would have to pay in order to supply power to the grid, so instead the PV power is used locally or it is discarded.
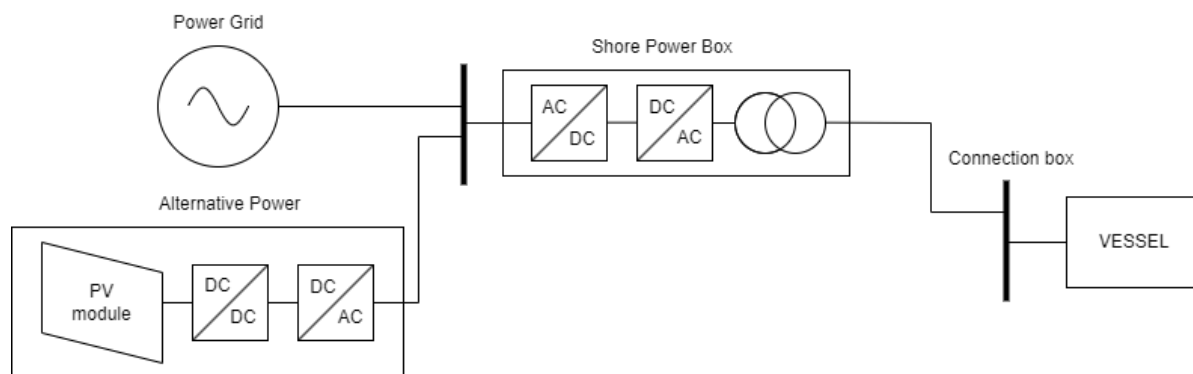
Figure 4.3: Diagram of the shore power facilities at Royal Roos at present

The optimization algorithm requires a linearization of the price per kW capacity of each component of the system. The prices used in this research are shown in Table 4.1.

Table 4.1: The prices for the different parts was calculated by consulting Royal Roos

Name of part	Power rating	Full price	Linear price/power relation
Shore power converter + connection box	280 [kW]	290,100 [euro]	1,035.71 [euro/kW]
PV array + converters	320 [kW]	568,000 [euro]	1,775.00 [euro/kW]

4.2. Electricity prices

Another part of the cost analysis is the price that is to be paid for the grid connection and electric energy. The prices for the grid connection come from Stedin, which is the grid operator in Rotterdam. While the electricity price comes from BCI Energy Commodities. Table 4.2 shows the prices from Stedin, which is only concerned with instantaneous power demand. The transformer for the grid connection is paid for once upon connection, and then continuously rented every month. A fixed price per month is paid for transport and contracted kW, this price is fixed within a range. The category for Royal Roos is a range between 151 kW - 1500 kW. The upper bound is larger than the peak demand allowed by the vessel so the higher ranges do not need to be taken into account.

Table 4.2 shows a contracted kW and peak over contracted kW tab. What this means is that a certain amount of instantaneous power is reserved from Stedin by Royal Roos in their contract. If the peak demand through their grid connection is above this amount, then a higher fee is paid per kW for the amount of kW over the contracted level. So, in other words the contracted kW should always be larger than the peak kW demand otherwise a higher price is paid needlessly.

	Paid Once	Paid Monthly
Connection	26928.5 [euro]	94.8303 [euro]
Transport	-	36.75 [euro]
Contracted kW	-	1.917 [euro/kW]
Peak over contracted kW	-	2.8524 [euro/kW]

Table 4.2: Stedin official electricity prices as of 2024 [33]

The electricity price per kWh consists of the electricity price, an energy tax and the transaction tax rate as shown by Table 4.3.

	per kWh
Electricity price	0.1018×(1+BTW) [euro/kWh]
Energy tax	0.1088×(1+BTW) [euro/kWh]
Total	0.2548 [euro/kWh]

Table 4.3: BCI Energy Commodities electricity prices as of 2023, BTW is tax rate of 21% as of 2024, prices calculated by consulting Royal Roos

4.3. ESS

The final part of the cost analysis are the different Energy Storage Systems that will be considered and the power electronic converters that are required for the ESS to interface with the rest of the electrical system.
First, let's consider the power electronic converters. There are two kinds that are necessary, one that converts the DC of the battery or the supercapacitor to ac or the other that is needed for the flywheel to output the AC power to the AC bus.

This first converter is depicted in Figure 4.4, while the other is shown in Figure 4.5. The converter shown in Figure 4.4 is priced at 580 euro/kW, this price was calculated by consulting the company ELINSA. While the price for the converter shown in Figure 4.5 is already integrated into the price shown in Table 4.5 and was calculated by consulting the company QuinteQ.

4.3.1. ESS comparison

The different ESS and their characteristics are shown in Table 4.4 and Table 4.5. The table covers the manufacturer, capex, opex, energy capacity per module, power capacity per module, self-discharge rate and lifetime of each type of ESS, split into two groups. Either High Energy capacity ESS or High power capacity ESS. The main difference between the two types can be found when comparing the
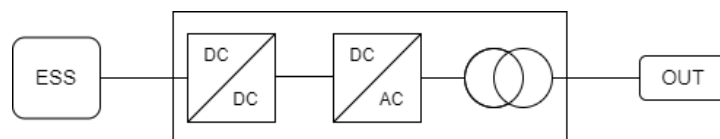
Figure 4.4: Diagram of power electronics used to interface ESS with the AC grid of the larger system
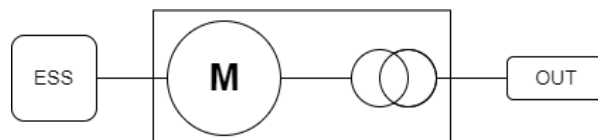
Figure 4.5: Diagram of the motor and transformer necessary for the FESS to connect to the larger system

number of lifecycles the ESS is capable of, as shown in Tables 4.4 & 4.5. Where HE ESS are only capable of a couple 1000 cycles, HP ESS are capable of 10,000s of cycles or more. This is important, as the use of the crane will thus degrade the lifetime and performance of the ESS. Meaning that if HE ESS are used to peak-shave the load of the crane then they will need to be replaced more quickly. So, even though on paper the LFP battery is the cheapest option, according to Tables 4.4 & 4.5. This is not true when the full life time of the system is considered. The results will show the full effect of this, but for now the two types of ESS will be considered for different purposes.

Table 4.4: HE ESS characteristics used in this research. The prices are calculated by consulting GWL group for the LFP battery, Shenzhen Westart Technology for the NMC battery and Acculon Energy for the Na-ion battery.

	LFP [34]	NMC [69]	Na-ion [36]
manufacturer	ELERIX	Westart	Acculon Energy
capex [euro/kW]	175 + 580	212 + 580	370 + 580
opex [euro/kWh]	-	-	-
e mod [kWh]	0.352	0.111	1.728
p mod [kW]	0.352 (1C)	0.222 (2C)	3.456 (2C)
self-discharge	3% per month	3% per month	5% per month
life cycle	3000 [#N] / 15 [yrs]	1000 [#N] / 3 [yrs]	5000 [#N] / 15 [yrs]

Table 4.5: HP ESS characteristics, *calculated with e mod=5 kWh and p mod=150 kW. The prices are calculated by consulting Toshiba for the LTO battery, AEP international for the supercapacitor and QuinteQ for the flywheel.

	LTO [30]	SC [15]	FESS [75]
manufacturer	Toshiba	Maxwell	QuinteQ
capex [euro/kW]	248 + 580	337 + 580	1000*
opex [euro/kWh]	-	-	1500 [euro/yr]
e mod [kWh]	0.052	0.053	5
p mod [kW]	0.52 (10C)	3.4 (64C)	50
self-discharge	4% per month	0.5% per second	0.1% per hour
life cycle	40,000 [#N] / 25 [yrs]	1,000,000 [#N] / 10 [yrs]	infinite [#N] / 30 [yrs]

4.4. Summary

This chapter covers the different prices that were used as inputs for the optimization algorithm discussed in Chapter 3. The contents of this chapter as well as the contents of Chapter 2 are used by the optimization algorithm to create the results shown in the next chapter.

$$5$$

Results

This chapter covers the results of the optimization algorithm for the different docking scenarios discussed in Section 3.3.4.

5.1. Length of vessel stay

The benefit of HE ESS for supplying shore power is investigated through changing the length that a vessel needs to be supplied with shore power. Figure 5.1 shows the shore power system that is investigated here.
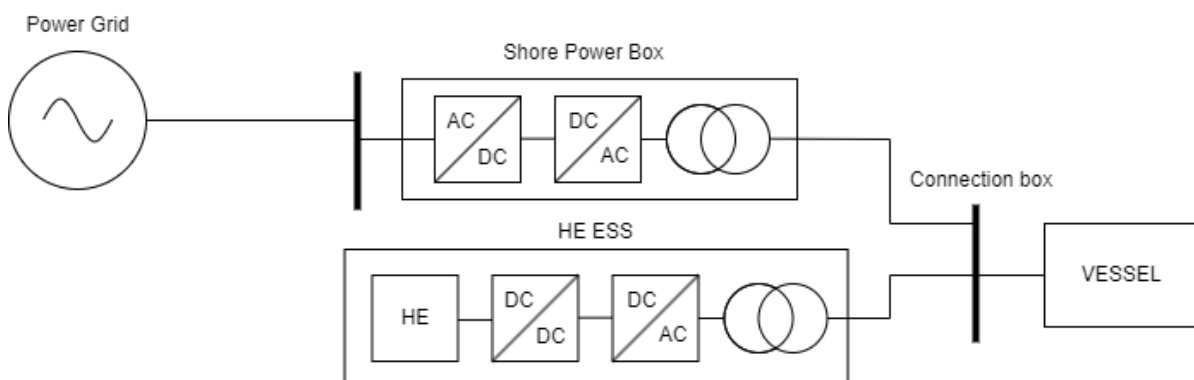
Figure 5.1: Diagram of the configuration of the shore power system that includes HE ESS

5.1.1. With crane use

The vessel power profile shown in Figure 5.2 was used to investigate the cost-effective optimal solution for the configuration given in Figure 5.1. This vessel power profile includes the use of the vessel's crane, to show the effect that crane use has on an optimal solution involving HE ESS.

Tables 5.1 - 5.4 show the calculated results from the optimization algorithm for the scenario shown in Figure 5.2. Where Table 5.1 covers the sizing of the shore power converter and Table 5.2 covers the sizing of the different ESS. In other words, the optimal solution for the configuration using LFP as HE ESS includes a 495.7 kW size shore power converter and a LFP battery of 337.92 kW / 337.92 kWh. While the optimal solution for the configuration using NMC as HE ESS includes a 497.56 kW size shore power converter and a NMC battery of 336.11 kW / 168.05 kWh. Similarly, the Na-ion version includes a 498.5 kW size shore power converter and a Na-ion battery of 335.2 kW / 167.6 kWh. Compared to this the status quo configuration optimal solution for this vessel power profile only utilizes a shore power converter but it is 851.4 kW instead.
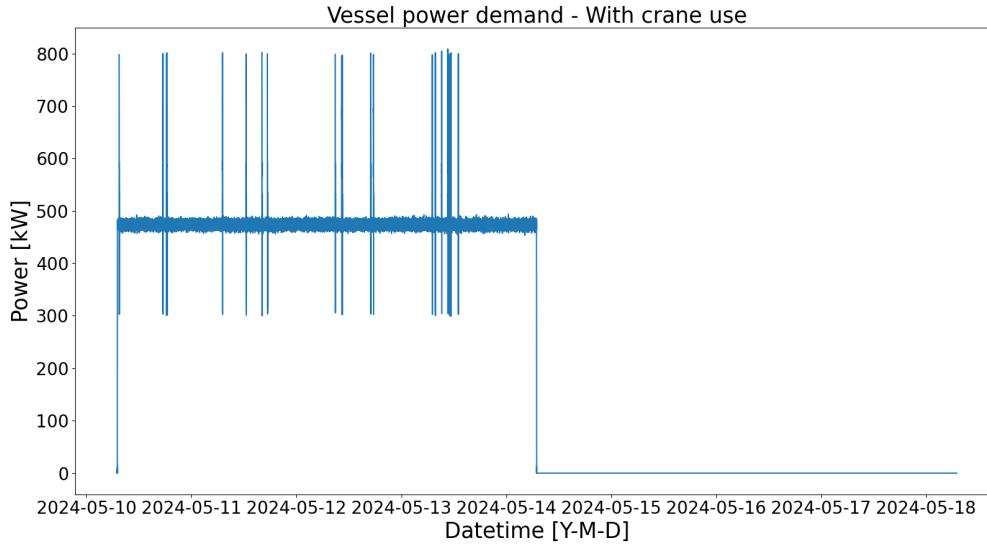
Figure 5.2: Figure of a vessel power profile, meaning power use of time. The crane use is included and dispersed over the 4 days that vessel is docked and requires shore power. After those 4 days there is 4 days of downtime, where the quay-side is unoccupied. The x-axis is in datetime, meaning it is fixed to a particular date and time.

Table 5.1: Table of the P_{nom} of the shore power converter for versions of the HE ESS shore power configuration for the vessel power profile shown in Figure 5.2.

	Status quo	LFP	NMC	Na
4 days	851.4 [kW]	495.7 [kW]	497.56 [kW]	498.5 [kW]

Table 5.2: Table of nominal power & energy capacity of the different ESS implementations of the HE ESS shore power configuration. The results are optimized for the vessel power profile shown in Figure 5.2.

	LFP	NMC	Na
4 days	337.92 [kW] & 337.92 [kWh]	336.11 [kW] & 168.05 [kWh]	335.23 [kW] & 167.6 [kWh]

Clearly, a significantly sized battery system should be included according to the optimal solution and Tables 5.3 and 5.4 detail why. Table 5.3 shows the total capex of system needed for each version, while Table 5.4 shows the opex of the system needed for each version for the 4 day vessel power profile. The opex shown in Table 5.4 is almost the same for each version, which makes sense as the same amount of electricity is used whether ESS is included or not. On the other hand the capital investment required to supply shore power to the power profile shown in Figure 5.2 differs significantly for the different versions. As Table 5.3 shows, the status quo configuration is the most expensive, while the HE ESS configuration using a LFP battery is the cheapest option. This was also shown in Table 4.4, where LFP was the cheapest per kW of battery.

Table 5.3: Table of the CAPEX of the whole shore power system for different versions of the HE ESS shore power configuration. Where the results are optimized for Figure 5.2.

	Status quo	LFP	NMC	Na
4 days	1,161,601 [euro]	935,155 [euro]	941,440 [euro]	994,668 [euro]

Figure 5.3 shows power output of the ESS, specifically for the LFP version and Figure 5.4 shows the corresponding grid power supply. The figures for the other two HE versions are given in the appendix (cite), but they are very similar. As shown by Figure 5.3 the ESS 'handles' the crane uses and the noise of other small appliances, thereby keeping the power demand from the grid very stable as shown in Figure 5.4. However, this also means that the cycling of the battery is increased as shown in Figure

Table 5.4: Table of the OPEX of whole shore power system for different versions of the HE ESS shore power configuration. Where the results are optimized for Figure 5.2.

	Status quo	LFP	NMC	Na
4 days	12193 [euro]	12198 [euro]	12197 [euro]	12196 [euro]

5.5 due to the battery being used to keep the power supply of the grid to a particular threshold. This additional cycling decreases the lifetime.

If it is assumed that such a cycle produced by a crane use is enough to degrade the battery in the same way as specified in Table 4.4, then a LFP battery could only support 3000 crane uses before it needs to be replaced. Similarly, for a NMC battery it would take 1000 crane uses or 5000 crane uses for a Na-ion battery until the battery would need to be replaced. How long this would take depends on how much a crane is used by a vessel, but if an average of 50 crane uses is assumed per month then it would take a LFP battery only about 5 years before it would need to be replaced. While a NMC battery would last less than 2 years, not to mention that it would need to be replaced after 3 years regardless. A Na-ion battery would last a little longer at about 8 years, but it is also the most the most expensive option out of the three HE options.

This issue will be revisited in section .... when crane use is investigated for HP ESS. For now, crane use is excluded from the vessel power profile for HE.
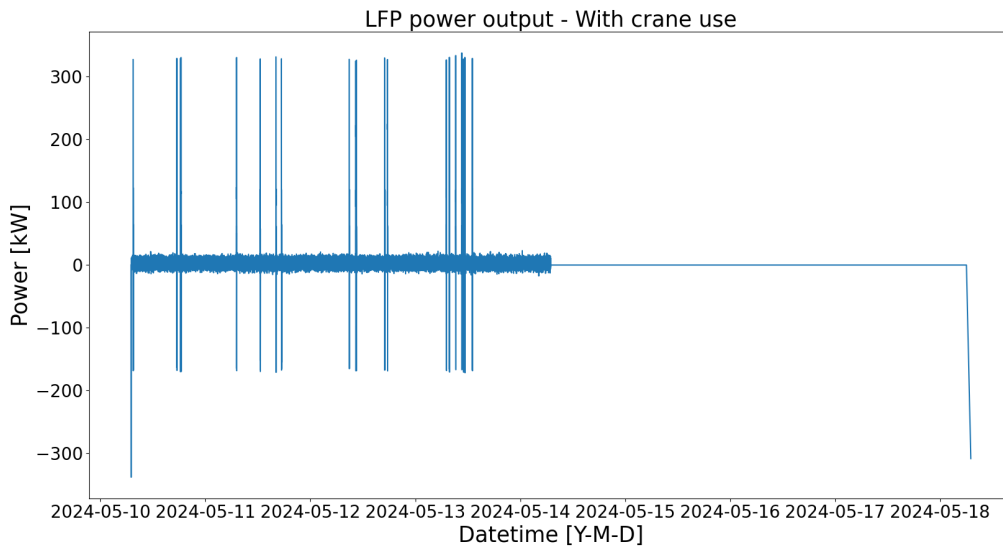
Figure 5.3: Figure of the output power of a LFP battery over time for the optimal solution of providing shore power to the power profile from Figure 5.2.

Grid power supply - LFP version - With crane use
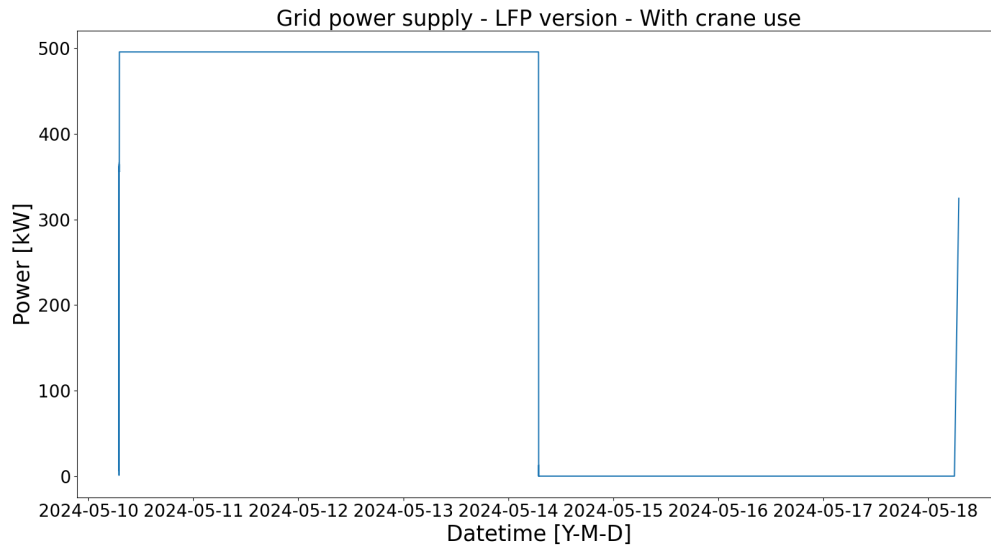
Figure 5.4: Figure of the grid power supply for the shore power configuration of Figure 5.1 where the HE ESS is LFP and the vessel power demand is shown in Figure 5.2.

Zoomed in SOC of LFP on crane use
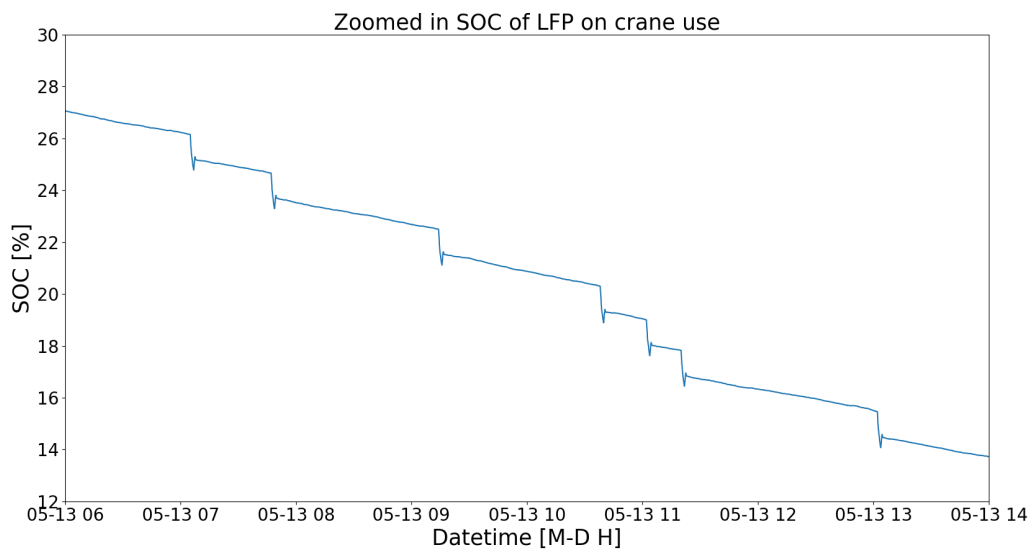
Figure 5.5: Figure of the SOC over time of the LFP battery, zoomed in on the cycles produced by the crane use.

5.1.2. Without crane use

This section covers the use of HE ESS for vessel power profiles where crane use is excluded. It investigates the effect the length of time a vessel stays has on the optimal sizing of HE ESS. Figure 5.6 and Figure 5.7 show two examples of vessel power profiles, others are included in the appendix (cite). Figure 5.6 shows the power profile for a vessel that docks for a single day and Figure 5.7 shows the power profile for a vessel that docks for 4 days, both include an equal amount of downtime.
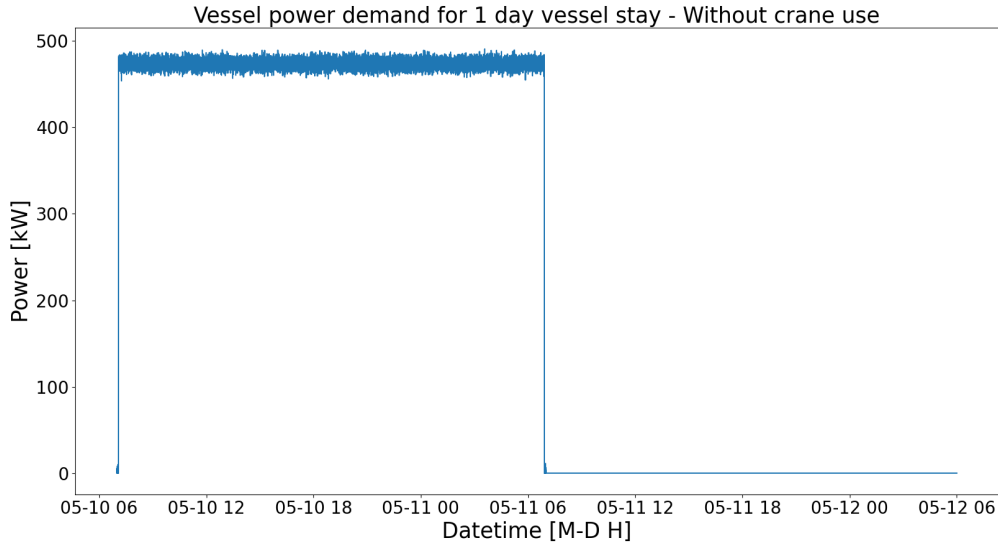
Figure 5.6: Figure of vessel power profile without a crane. Where the vessel requires shore power for a single day, followed by 1 day of downtime. The x-axis is in datetime, meaning it specifies a particular date and time for each instant
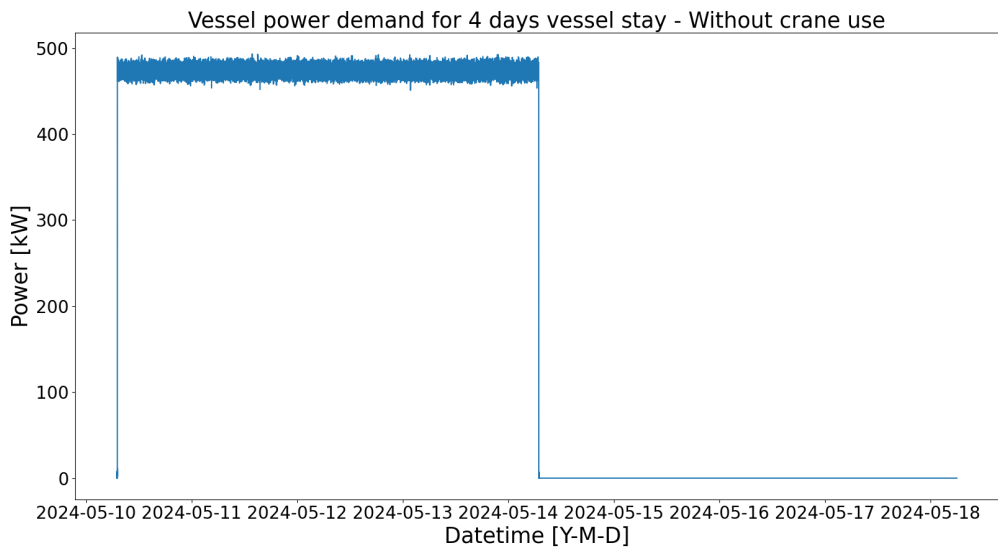
Figure 5.7: Figure of vessel power profile without a crane. Where the vessel requires shore power for 4 days, followed by 4 days of downtime. The x-axis is in datetime, meaning it specifies a particular date and time for each instant

Tables 5.5 - 5.8 cover the optimization results for vessel power profiles ranging from 1 day to 4 days of vessel shore power demand. Table 5.5 shows that each version of the configuration, the amount of days that a vessel docks has effectively zero effect on the sizing of shore power converter. Likewise, Table 5.6 shows that the amount of days, ranging between 1 and 4, has little to no effect on the sizing of the ESS. Further, Table 5.6 shows that the sizing of ESS for all versions, be that LFP, NMC or Na-ion based, is very small compared to the size of ESS in Table 5.2. The lower significance of ESS for a vessel power profile with no crane use is further corroborated by Tables 5.7 and 5.8. Even though all 3 HE versions have lower optimal costs than their respective status quo optimal cost, the difference is quite small. Table 5.7 shows the LFP version is the cheapest version of the configuration with HE ESS, just like Table 5.3. However, even though all 3 HE versions have lower optimal costs than the optimal status quo solution, the difference is not that big. This is shown more clearly in Table 5.9, where LFP

also edges out NMC as the cheapest version. Finally, Table 5.8 shows that, as expected, the opex rises linearly with the amount of time the vessel stays and requires shore power. And that like Table 5.4 there is little to no difference between each version from an opex perspective.

Table 5.5: Table of the P_{nom} of the shore power converter for each version of the HE ESS shore power configuration. The results are optimized for vessel power profiles without crane use, where the vessels stays from 1 day though 4 days.

	Status quo	LFP	NMC	Na
1 day	518.8 [kW]	497.8 [kW]	498.2 [kW]	498.2 [kW]
2 days	520.5 [kW]	498.2 [kW]	498.4 [kW]	498.4 [kW]
3 days	519.4 [kW]	498.3 [kW]	498.5 [kW]	498.4 [kW]
4 days	519.1 [kW]	498.4 [kW]	498.5 [kW]	498.5 [kW]

Table 5.6: Table of nominal power & energy capacity of the different ESS implementations of the HE ESS shore power configuration. The results are optimized for vessel power profiles without crane use, where the vessels stay from 1 through 4 days.

	LFP	NMC	Na
1 day	17.95 [kW] & 17.95 [kWh]	17.54 [kW] & 8.77 [kWh]	20.74 [kW] & 10.37 [kWh]
2 days	20.06 [kW] & 20.06 [kWh]	17.76 [kW] & 8.88 [kWh]	20.74 [kW] & 10.37 [kWh]
3 days	20.06 [kW] & 20.06 [kWh]	19.31 [kW] & 9.66 [kWh]	20.74 [kW] & 10.37 [kWh]
4 days	19.71 [kW] & 19.71 [kWh]	18.87 [kW] & 9.44 [kWh]	20.74 [kW] & 10.37 [kWh]

Table 5.7: Table of the CAPEX of the whole shore power system for different versions of the HE ESS shore power configuration. The results are optimized for a vessel power profile without crane use from 1 through 4 days.

	Status quo	LFP	NMC	Na
1 day	691,999 [euro]	677,984 [euro]	678,380 [euro]	684,274 [euro]
2 days	694,354 [euro]	680,117 [euro]	678,789 [euro]	684,471 [euro]
3 days	692,747 [euro]	680,221 [euro]	680,120 [euro]	684,516 [euro]
4 days	692,421 [euro]	680,042 [euro]	679,768 [euro]	684,589 [euro]

Table 5.8: Table of the OPEX of the whole shore power system for different versions of the HE ESS shore power configuration. The results are optimized for a vessel power profile without crane use from 1 through 4 days.

	Status quo	LFP	NMC	Na
1 day	3028 [euro]	3029 [euro]	3029 [euro]	3029 [euro]
2 days	6078 [euro]	6079 [euro]	6079 [euro]	6079 [euro]
3 days	9127 [euro]	9128 [euro]	9129 [euro]	9128 [euro]
4 days	12,177 [euro]	12,179 [euro]	12,178 [euro]	12,178 [euro]

Table 5.9: Table showing the total CAPEX decrease for each version using HE compared to the status quo optimal solution from Table 5.7

	LFP	NMC	Na
1 day	-2.03%	-1.97%	-1.12%
2 days	-2.05%	-2.24%	-1.41%
3 days	-1.81%	-1.82%	-1.19%
4 days	-1.79%	-1.83%	-1.13%
average	-1.92%	-1.97%	-1.21%

The reason why HE ESS has so little effect on the total cost of the sytem can be more easily explained using Figures 5.8 - 5.12. Where Figure 5.8 shows the power supply from the grid and Figure 5.9 the power output of a ESS, corresponding to the same optimal solulion for LFP HE ESS configuration for a

single day of shore power for a vessel with another day of downtime. Figure 5.8 and Figure 5.9 together fulfill the power demand from Figure 5.6. Likewise, for the combination of Figure 5.10 and Figure 5.11 for the power demand of Figure 5.7. These figures serve as examples, but similar figures for the NMC version and Na-ion version can be found in the appendix.

From both Figure 5.9 and Figure 5.11 it is clear that the ESS is tasked with keeping the grid power supply constant by getting rid of all the fluctuations. These fluctuations are very small in terms of energy and do not really degrade or affect the battery. From Figure 5.12 it is clear that the average power output of the ESS is larger than 0 as the ESS does fully discharge at the end of the vessel stay. However, this average is a very low amount of power that is scaled to last the entire vessel stay.

So, the HE ESS is only tasked with keeping the fluctuating power demand of the vessel more constant for the grid in the optimal cost-effective solution.
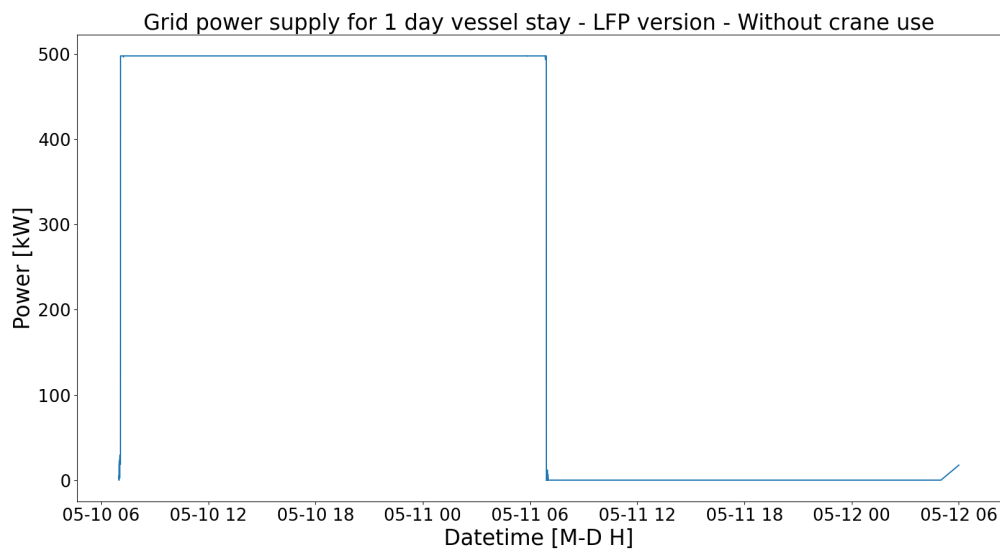
Figure 5.8: Figure depicting the grid power supply required for 1 day of supplying shore power and 1 day of downtime. This shore power configuration includes a LFP battery as the HE ESS.
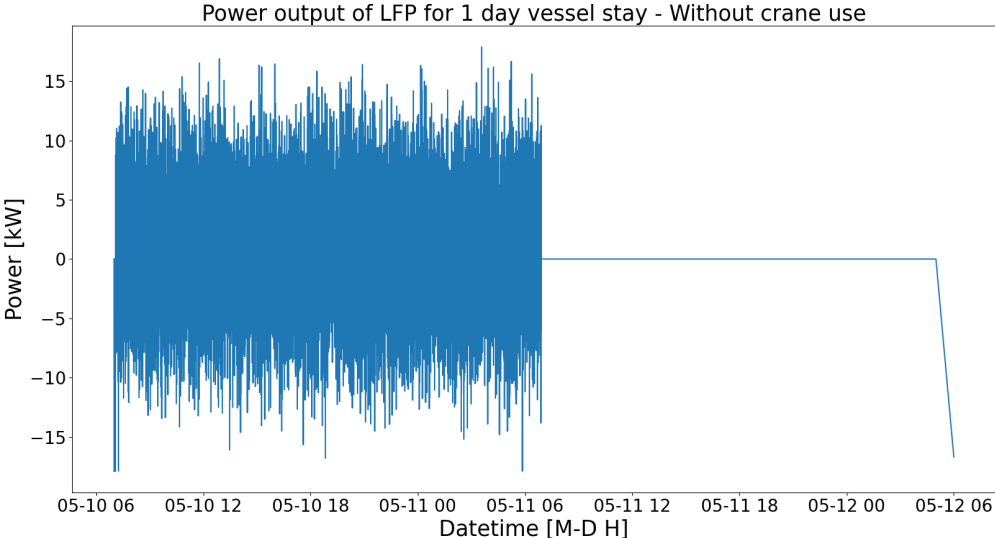
Figure 5.9: Figure of the power output of the LFP battery as the HE ESS in the shore power configuration for 1 day of supplying shore power and 1 day of downtime.
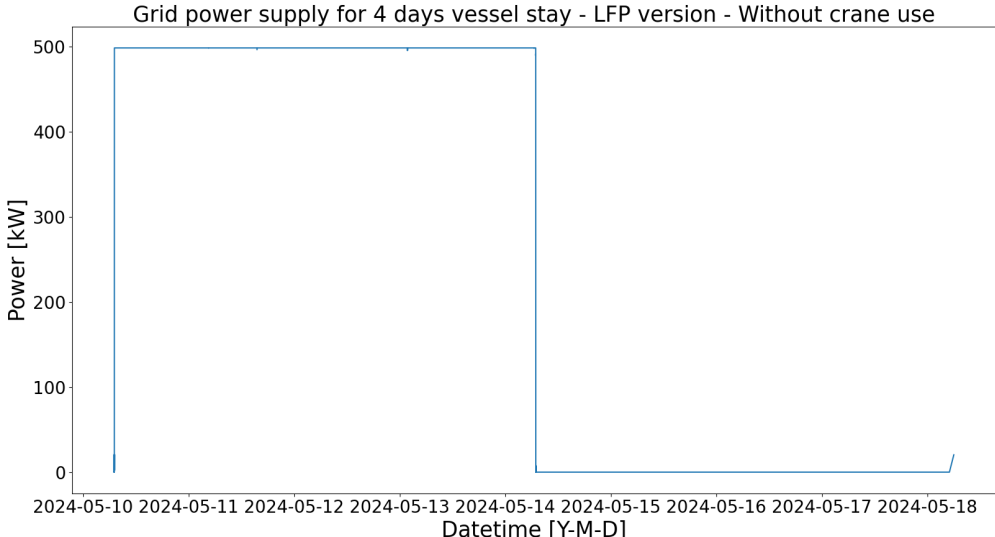
Figure 5.10: Figure depicting the grid power supply required for 4 days of supplying shore power and 4 days of downtime. This shore power configuration includes a LFP battery as the HE ESS.
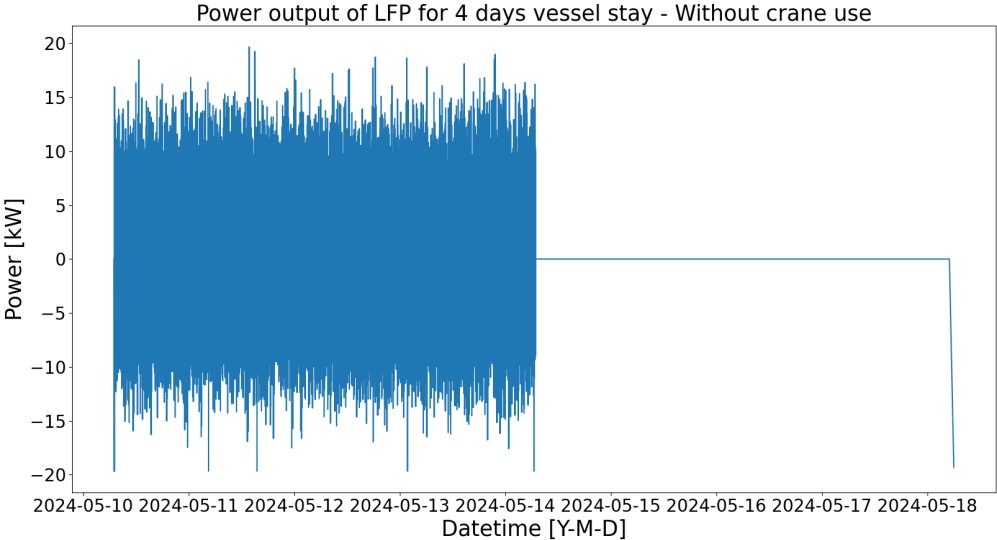
Figure 5.11: Figure of the power output of the LFP battery as the HE ESS in the shore power configuration for 4 days of supplying shore power and 4 days of downtime.
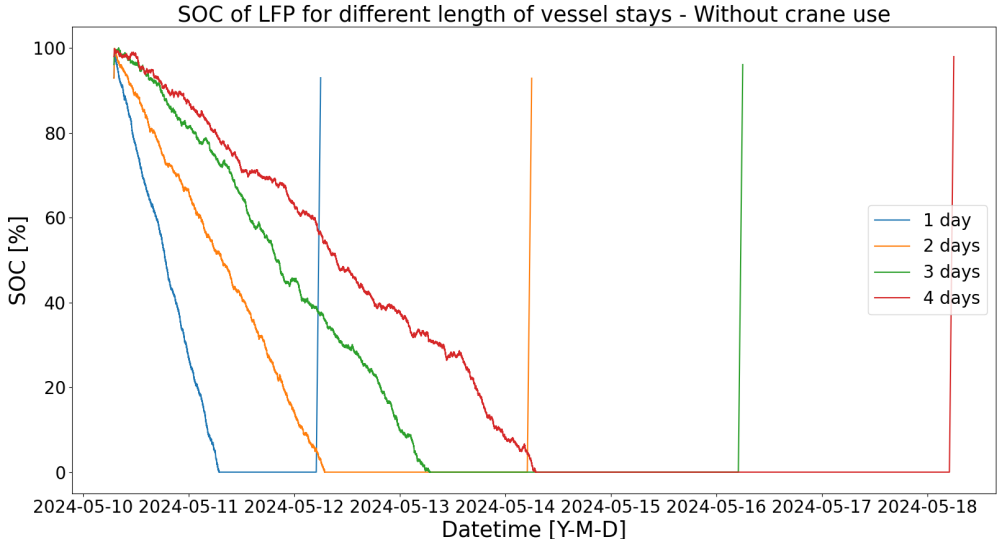
Figure 5.12: Figure of the SOC of the LFP battery in the HE ESS shore power configuration over time. It includes the SOC for different amount of days of supplying shore power to vessels without the use of a crane.

5.2. Amount of crane use

HP ESS configurations for shore power are used for mitigating the effect the use of a crane has on the sizing of the rest of the shore power system. Figure 5.13 shows the configuration to be investigated in this section.
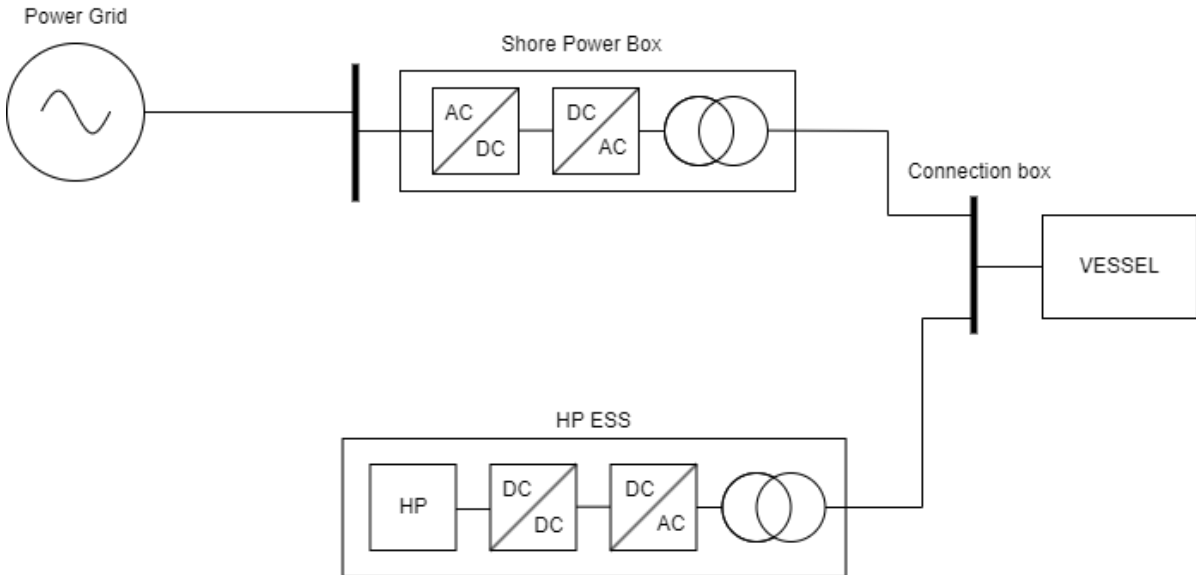
Figure 5.13: Diagram of HP ESS configuration shore power system

The effect that the amount of crane uses on the system is tested by increasing the amount of crane uses several simulation in a row. All of the crane uses are on after the other, in order to create the worst case scenario for the HP ESS. Figures 5.14 and 5.15 show the vessel power profile for 4 days of required shore power and 30 crane uses. Figure 5.14 shows the power profile in full, while Figure 5.15 shows the zoomed in power profile of the crane uses. Figure 5.16 and Figure 5.17 are similar but instead of 30 consecutive crane uses, here there are 50 consecutive crane uses. Figures 5.18 and 5.19 repeat this trend, but then for 100 crane uses. Figures 5.14, 5.16 and 5.18 are the vessel power profiles used for the optimal solution gives below. While, Figure 5.14 has about 90 minutes of continuous crane use, Figure 5.18 contains 300 minutes or 5 hours of continuous crane use. This is chosen as the upper limit, as there is no human crane operator that can keep working that long without stop or taking a mandated break. So, any more consecutive crane uses would simply not be realistic.
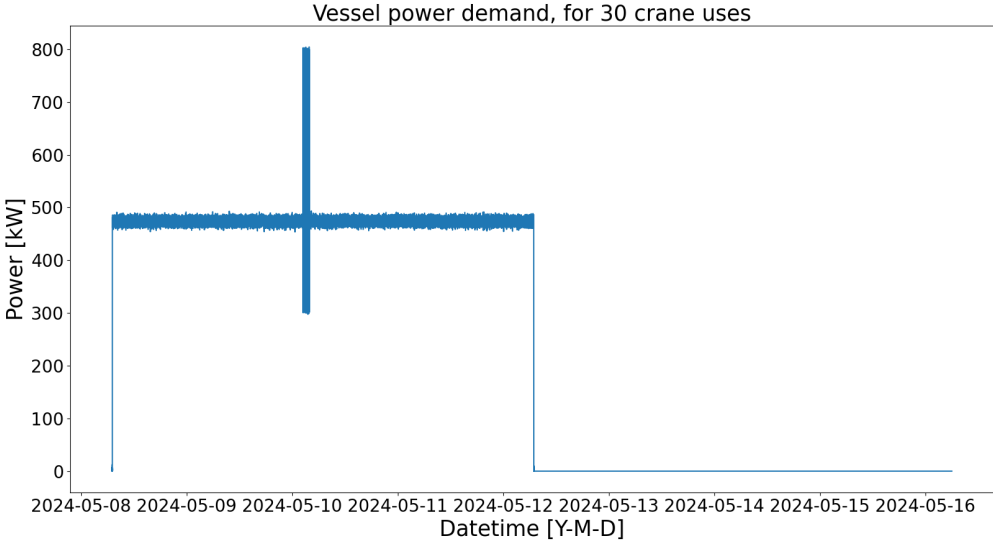
Figure 5.14: Figure of a vessel power profile that includes 30 consecutive crane uses. The vessel docks for 4 days and then 4 days of downtime follow. The x-axis is in datetime, so each data point is bound to a date and time.
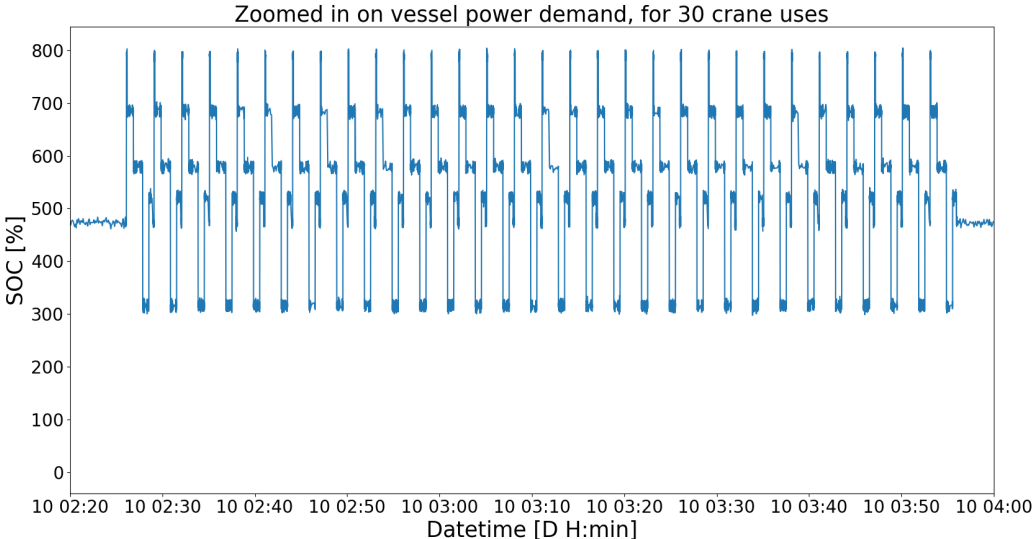
Figure 5.15: Figure of a zoomed in vessel power profile on the 30 consecutive crane uses. The x-axis is in datetime, so each data point is bound to a date and time.
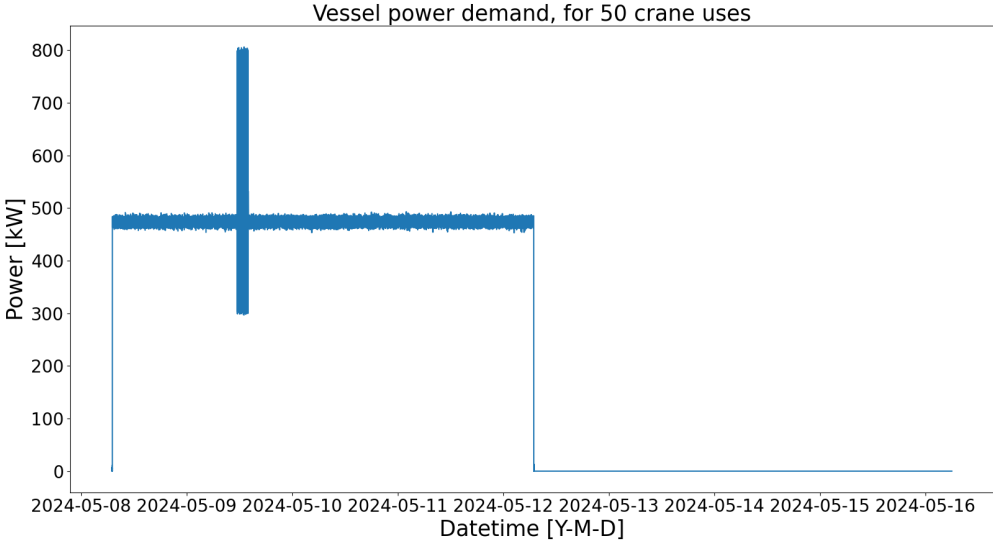
Figure 5.16: Figure of a vessel power profile that includes 50 consecutive crane uses. The vessel docks for 4 days and then 4 days of downtime follow. The x-axis is in datetime, so each data point is bound to a date and time.
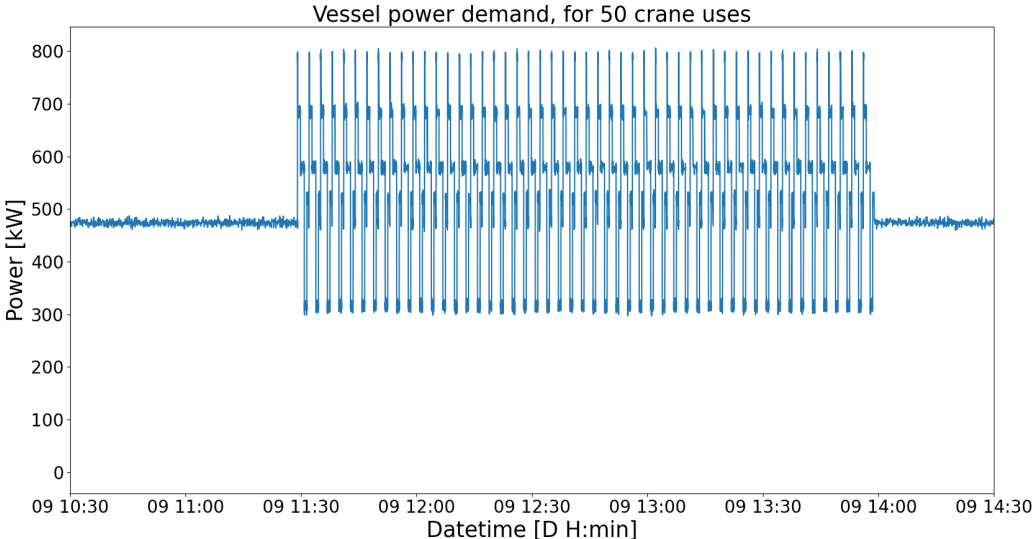
Figure 5.17: Figure of a zoomed in vessel power profile on the 50 consecutive crane uses. The x-axis is in datetime, so each data point is bound to a date and time.
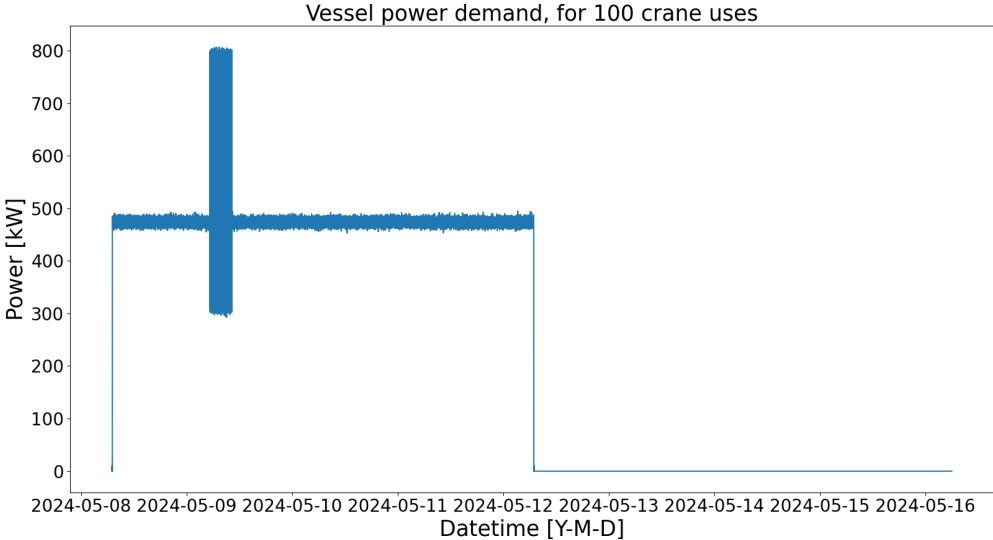
Figure 5.18: Figure of a vessel power profile that includes 100 consecutive crane uses. The vessel docks for 4 days and then 4 days of downtime follow. The x-axis is in datetime, so each data point is bound to a date and time.
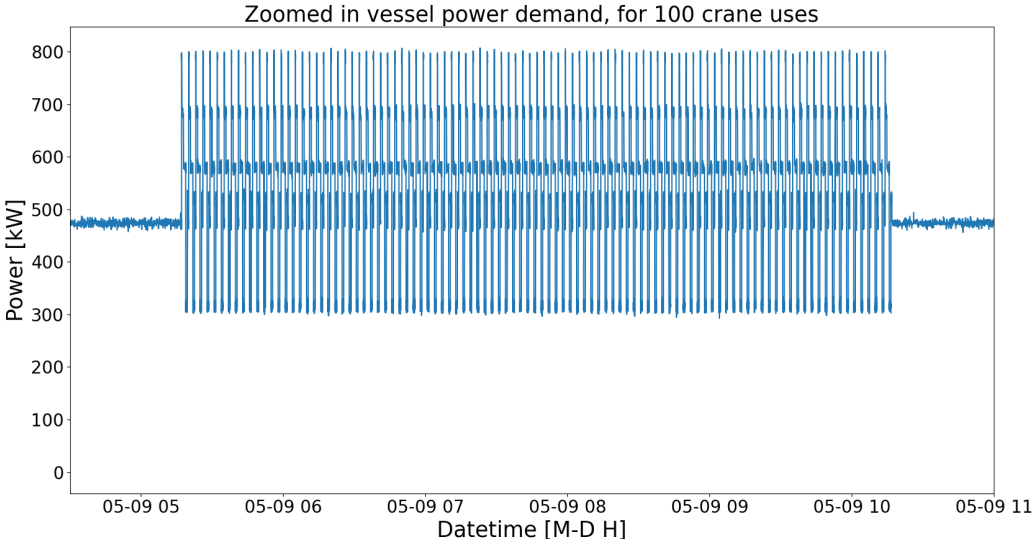
Figure 5.19: Figure of a zoomed in vessel power profile on the 100 consecutive crane uses. The x-axis is in datetime, so each data point is bound to a date and time.

The optimal results for the LTO, SC and FESS versions of the HP ESS shore power configuration are shown in Tables 5.10 - 5.13. Table 5.10 shows how the sizing of the shore power converter is affected by an increasing number of crane uses. The amount of crane uses has barely any effect on the status quo solution, the SC version and the FESS version of the HP ESS configuration. However, the LTO version is affected, here the shore power converter increases in capacity. This trend is repeated in Table 5.11, where the size of the LTO ESS decreases with ever more consecutive crane uses. This will be elaborated on later.

Tables 5.12 and 5.13 show the capex and opex respectively of the optimal solutions for the different versions. Clearly, Table 5.12 shows that the HP ESS shore power configuration have lower optimal costs than the status quo optimal solution and that this remains true even as crane uses increase. Table 5.13 shows that once again the opex does not differ much between the different version. And as expected if there are more crane uses than the opex increases a little bit.

From Table 5.14 it is clear that the FESS version of the HP ESS shore power configuration results in the biggest cost reduction compared to the status quo solution, followed by the LTO version and then the SC version. Although, the relative cost reduction for LTO decreases as the consecutive number of crane uses that needs to be optimized for increases. Keeping in line with the observations from Tables 5.10 and 5.11.

Table 5.10: Table of the P_{nom} of the shore power converter with increasing amount of crane uses, columns correspond to different ESS or the optimal status quo implementation.

	Status quo	LTO version	SC version	FESS version
30 uses	846.8 [kW]	547.0 [kW]	567.7 [kW]	563.8 [kW]
50 uses	848.5 [kW]	554.6 [kW]	566.0 [kW]	564.4 [kW]
100 uses	849.4 [kW]	560.4 [kW]	566.6 [kW]	565.1 [kW]

Table 5.11: Table of the nominal power & energy capacity of the HP ESS with increasing amount of crane uses

	LTO	SC	FESS
30 uses	284.96 [kW] & 28.496 [kWh]	265.2 [kW] & 4.134 [kWh]	300.0 [kW] & 5.0 [kWh]
50 uses	279.24 [kW] & 27.924 [kWh]	268.6 [kW] & 4.187 [kWh]	300.0 [kW] & 5.0 [kWh]
100 uses	274.56 [kW] & 27.456 [kWh]	268.6 [kW] & 4.187 [kWh]	300.0 [kW] & 5.0 [kWh]

Table 5.12: Total CAPEX of the whole shore power system for different versions of the HP ESS shore power configuration. The results are optimized for different amount of consecutive crane uses.

	Status quo	LTO version	SC version	FESS version
30 uses	1,155,197 [euro]	977,129 [euro]	1,019,337 [euro]	931,204 [euro]
50 uses	1,157,579 [euro]	982,907 [euro]	1,020,266 [euro]	932,033 [euro]
100 uses	1,158,770 [euro]	987,025 [euro]	1,021,168 [euro]	932,993 [euro]

Table 5.13: Total OPEX of the whole shore power system for different versions of the HP ESS shore power configuration. The results are optimized for different amount of consecutive crane uses.

	Status quo	LTO version	SC version	FESS version
30 uses	12,203 [euro]	12,204 [euro]	12,204 [euro]	12,203 [euro]
50 uses	12,218 [euro]	12,220 [euro]	12,221 [euro]	12,219 [euro]
100 uses	12,262 [euro]	12,265 [euro]	12,266 [euro]	12,262 [euro]

Table 5.14: Table showing the total CAPEX decrease for each version using HP compared to the status quo optimal solution from Table 5.12

	LTO	SC	Na
30 uses	-15.41%	-11.76%	-19.39%
50 uses	-15.09%	-11.86%	-19.48%
100 uses	-14.82%	-11.87%	-19.48%
average	-15.11%	-11.83%	-19.45%

The reason for the different behaviour from optimization that is found for the LTO version compared to the other HP ESS version is explained using Figures 5.20 - 5.26. These are zoomed in on the crane uses, using the LTO versions of the figures as examples. The full versions of the plots, as well as the other versions can be found in the appendix. However, these results are very similar and so these examples can be used to draw conclusions.

Figures 5.20 and 5.21 go together to fulfil the power demand found in Figure 5.15. Likewise, Figures 5.22 and 5.23 go together to fulfil the power demand found in Figure 5.18. Figure 5.21 and Figure 5.23 show that the ESS, in this case LTO, is only concerned with stabilizing the power demand of the crane and nothing else. This is corroborated in Figure 5.20 for Figure 5.21 and in Figure 5.22 for Figure 5.23 respectively. As the grid supplies the power for the constant power demand and when the crane will be used the grid will start charging the ESS and keep that power constant throughout the usage of the crane. This is true for all the HP ESS versions.

However, what differs for the LTO version is that this upper threshold for the maximum grid power is increased as the number of consecutive crane uses is increased. So that a smaller part of the power demand is taken care of by the LTO ESS and instead being supplied from the grid. Thereby decreasing the energy capacity required from the ESS. This is not the case for the SC and FESS versions as these can be charged up much more quickly on account of their lower energy capacity as shown by Figure 5.25. Meaning that it is much easier to keep continuously recharging the ESS while it is in use.

Figures 5.24 and 5.26 show the SOC over time of either the 30 crane use version or the 100 crane use version respectively. They show that all ESS are charged just before the crane uses and are perfectly discharged afterwards. This is also why Figure 5.20 and Figure 5.22 show a drop in power supply from the grid. The optimization algorithm knows the vessel power profile used as input and therefore knows when the final crane use is and so it doesn't recharge (partially or otherwise) the ESS at this final crane use. So, instead the grid power supply drops to absorb the power drop of the crane.
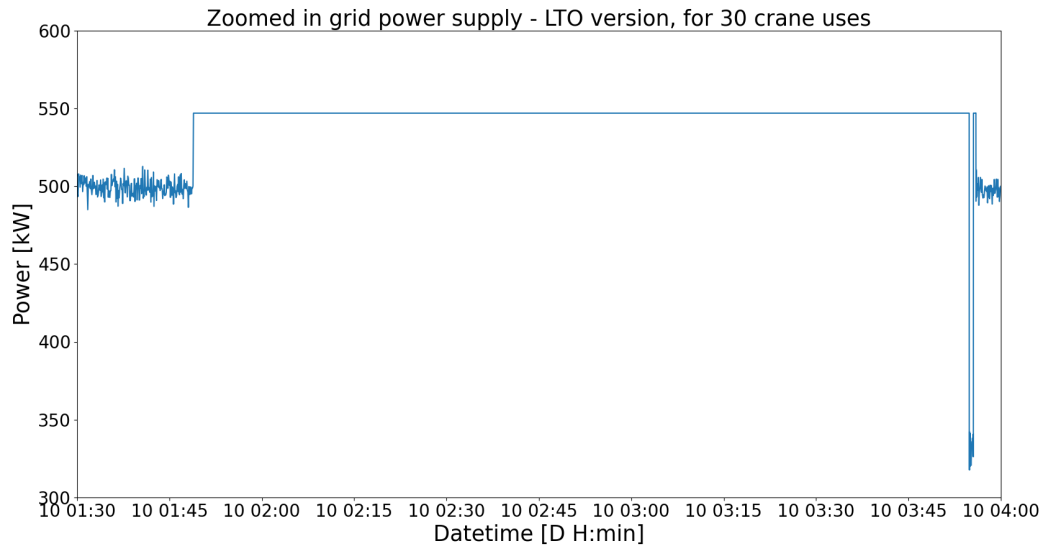
Figure 5.20: Figure of the grid power supply to the shore power system. It is zoomed in on the part where the crane is in use. This result is from the HP ESS shore power configuration that includes and LTO battery. The grid supplies power to the vessel power profile found in Figure 5.14.
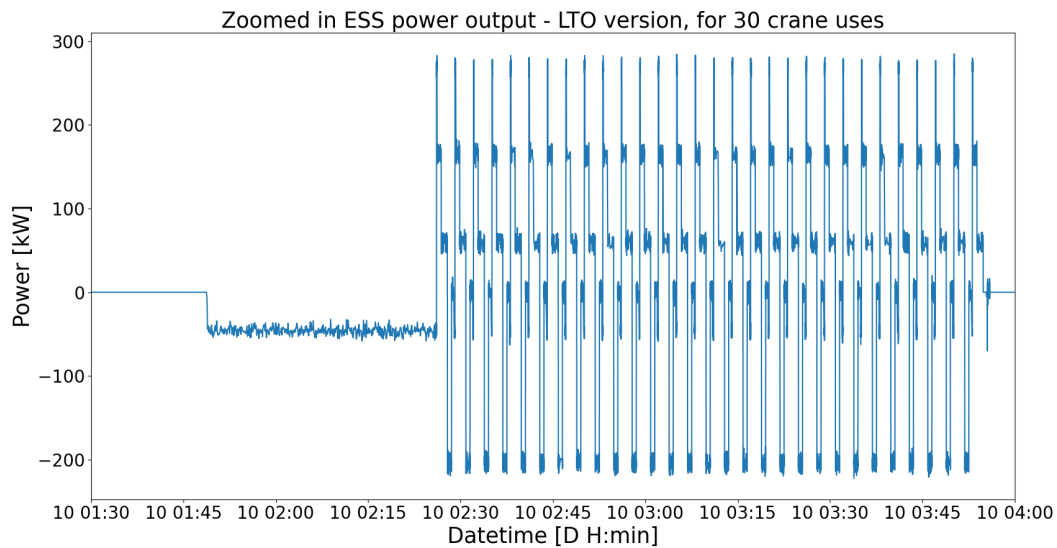
Figure 5.21: Figure of the power output of the LTO battery included in this version of the HP ESS shore power configuration. It is the zoomed in on the part where the crane is in use. The ESS is used for the vessel power profile found in Figure 5.14.
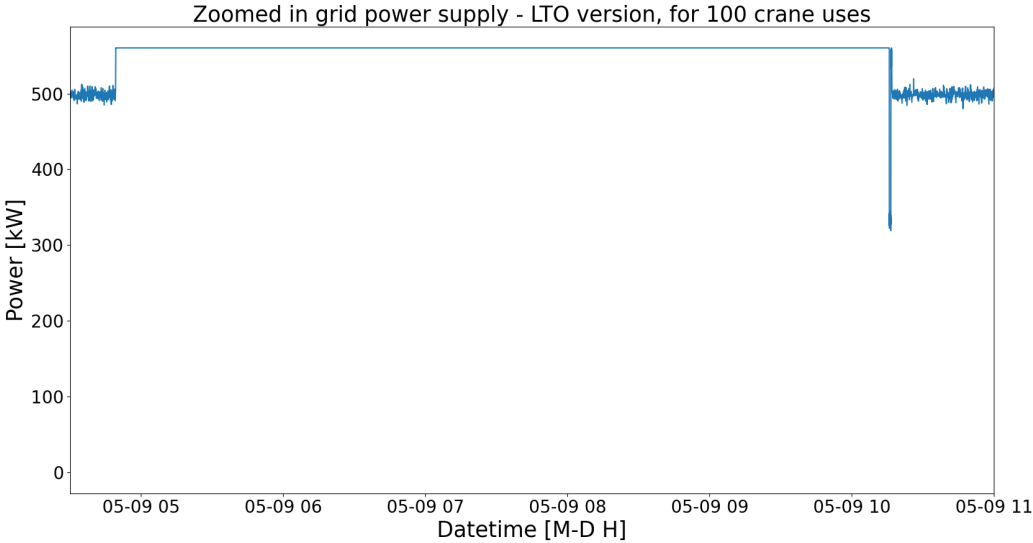
Figure 5.22: Figure of the grid power supply to the shore power system. It is zoomed in on the part where the crane is in use. This result is from the HP ESS shore power configuration that includes and LTO battery. The grid supplies power to the vessel power profile found in Figure 5.18.
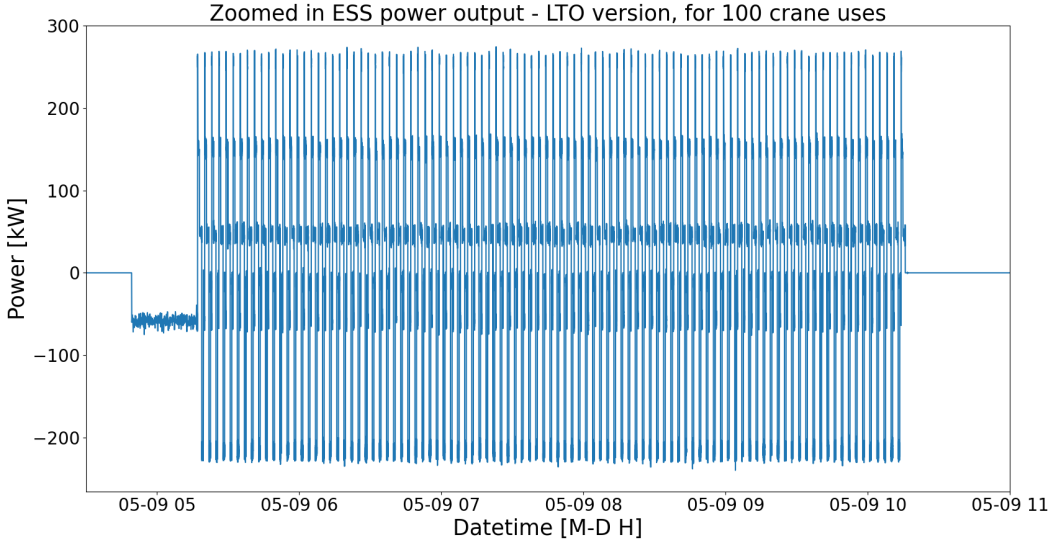
Figure 5.23: Figure of the power output of the LTO battery included in this version of the HP ESS shore power configuration. It is the zoomed in on the part where the crane is in use. It is the zoomed in on the part where the crane is in use. The ESS is used for the vessel power profile found in Figure 5.18.
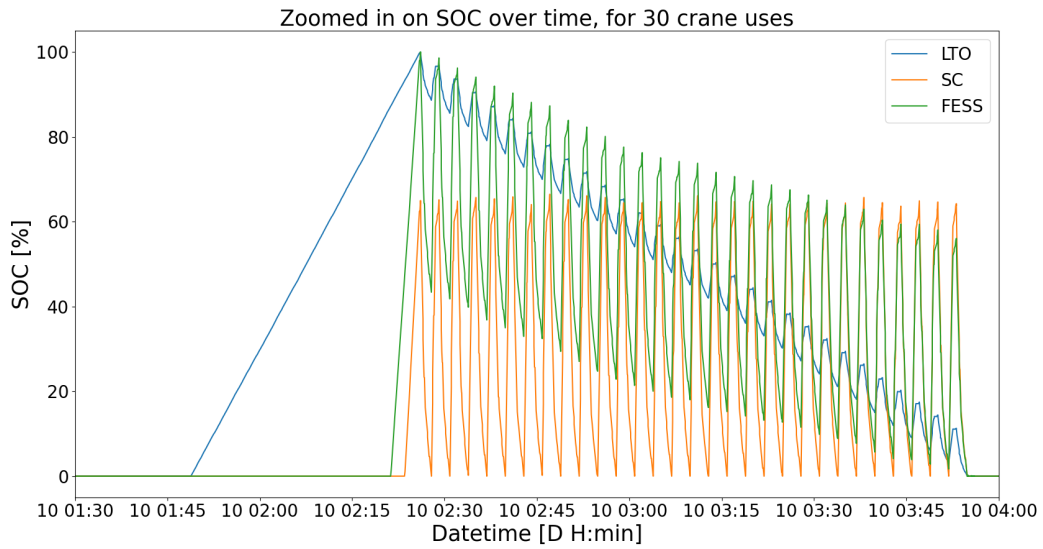
Figure 5.24: Figure of the SOC of all 3 HP ESS versions. It is zoomed in on the part where the crane is used. This figure corresponds to the vessel power profile of Figure 5.14.
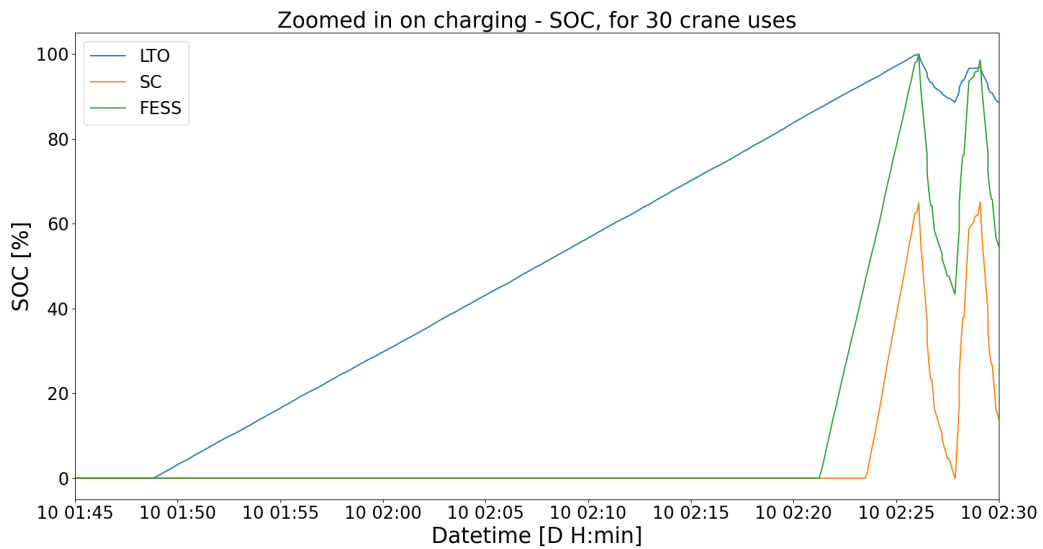
Figure 5.25: Figure of the SOC of all 3 HP ESS versions. It is zoomed in on the very start that the ESS are used, to display the length of time needed to charge the ESS. This figure corresponds to the vessel power profile of Figure 5.14, however this start up behaviour is no different than for the vessel power profiles of Figures 5.16 and 5.18.
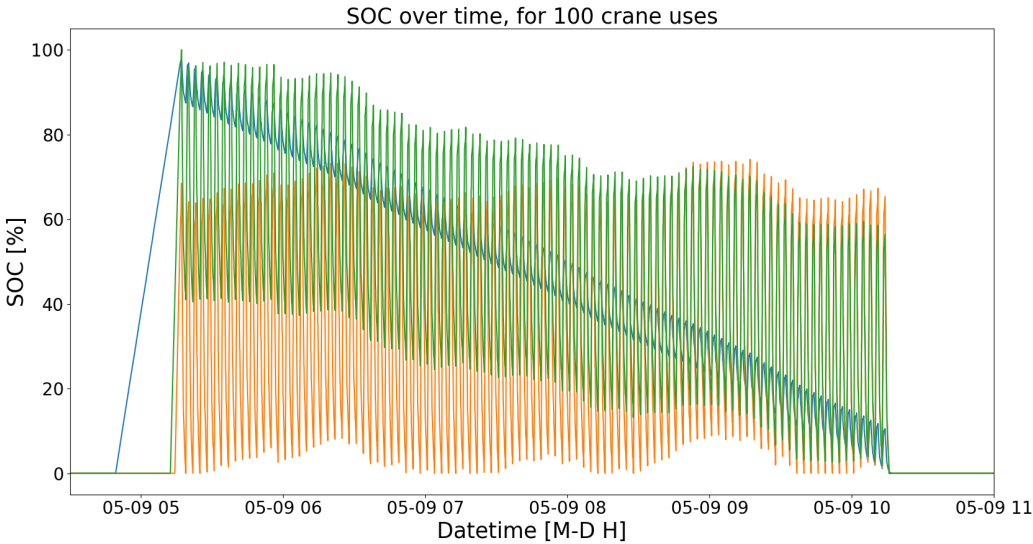
Figure 5.26: Figure of the SOC of all 3 HP ESS versions. It is zoomed in on the part where the crane is used. This figure corresponds to the vessel power profile of Figure 5.18.

5.3. Amount of P_{nom} of crane

This section continues the investigation into the optimal HP ESS shore power configuration. In this section the nominal power of the crane is increased in steps, in order to investigate at what point this solution becomes a benefit. Figure 5.27 and Figure 5.28 show examples of power profiles where the nominal power of the crane is lower than that shown in Section 5.2. The other vessel power profiles used in this section can be found in the appendix and are for 40 kW, 60 kW and 80 kW nominal power of the crane.
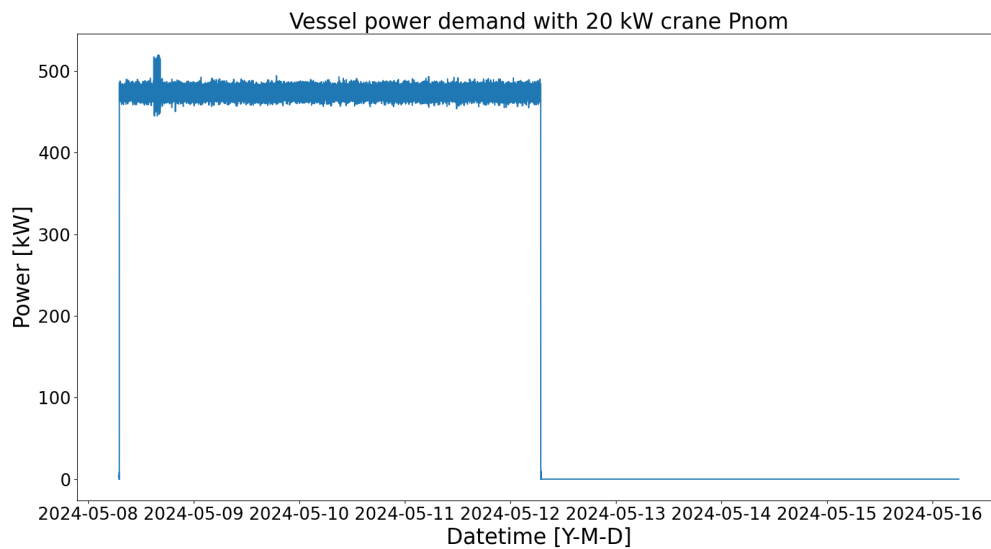
Figure 5.27: Figure of a vessel power profile that includes consecutive crane uses of a crane with 20 kW nominal power. There are 30 crane uses total. The vessel requires shore power for 4 days and this is followed by 4 days of downtime. The x-axis is in datetime, so each data point is mapped to a date and time.
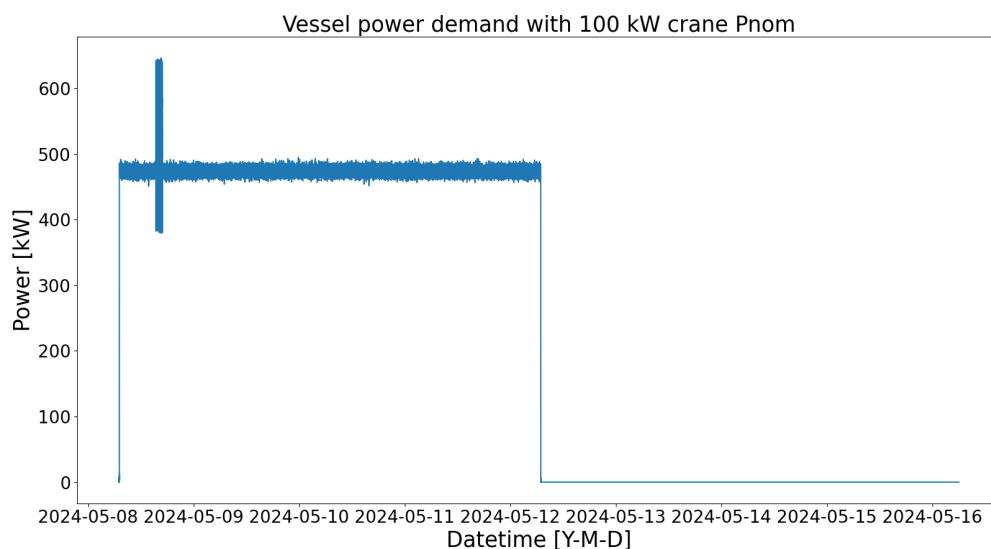
Figure 5.28: Figure of a vessel power profile that includes consecutive crane uses of a crane with 100 kW nominal power. There are 30 crane uses total. The vessel requires shore power for 4 days and this is followed by 4 days of downtime. The x-axis is in datetime, so each data point is mapped to a date and time.

The optimization results can be found in Tables 5.15 - 5.18. Table 5.16 shows the clearest how FESS is not suitable for lower P_{nom} of the crane. This is due to the fact that it is less modular than either LTO batteries or supercapacitors. Table 5.15 shows how the capacity of the shore power converter also increases as the crane P_{nom} increases, not just the capacity of the HP ESS. This means that more of the crane power demand is taken up by the grid power supply, like what happens to the optimal solution in Section 5.2 as the number of consecutive crane uses increases.

Tables 5.17 and 5.18 show the costs of the optimal solutions. Table 5.18 shows the opex of the different versions and once again it does not really differ between the different versions and it only increases a little bit as the nominal power of the crane increases. Table 5.19 is the more legible version of Table 5.17. It shows the relative advantage of including HP ESS increases for every ESS version as the P_{nom} of the crane increases. LTO reduces costs more than SC or FESS at lower P_{nom} of the crane. FESS only becomes more cost-effective than the status quo version around 80 kW P_{nom} of the crane, but by 200 kW P_{nom} of the crane FESS has become the most cost-effective version for delivering shore power.

Table 5.15: Table of the P_{nom} of the shore power converter for each version of the HP ESS shore power configuration. The results are optimized for different P_{nom} of the crane.

P_{nom} of crane	Basic	LTO	SC	FESS
20 kW	547.1 [kW]	502.8 [kW]	505.5 [kW]	547.1 [kW]
40 kW	583.8 [kW]	507.7 [kW]	512.4 [kW]	583.8 [kW]
60 kW	613.3 [kW]	513.7 [kW]	520.3 [kW]	613.3 [kW]
80 kW	649.4 [kW]	518.1 [kW]	527.7 [kW]	523.5 [kW]
100 kW	680.3 [kW]	524.3 [kW]	534.1 [kW]	531.3 [kW]
200 kW	846.8 [kW]	547.0 [kW]	567.7 [kW]	563.8 [kW]

Table 5.16: Table of nominal power & energy capacity of the different ESS implementations of the HP ESS shore power configuration. The results are optimized for different P_{nom} of the crane.

P_{nom} of crane	LTO	SC	FESS
20 kW	42.12 [kW] & 4.212 [kWh]	40.8 [kW] & 0.636 [kWh]	0.0 [kW] & 0.0 [kWh]
40 kW	72.28 [kW] & 7.228 [kWh]	68.0 [kW] & 1.060 [kWh]	0.0 [kW] & 0.0 [kWh]
60 kW	94.64 [kW] & 9.464 [kWh]	88.4 [kW] & 1.378 [kWh]	0.0 [kW] & 0.0 [kWh]
80 kW	124.8 [kW] & 12.48 [kWh]	115.6 [kW] & 1.802 [kWh]	150 [kW] & 5.0 [kWh]
100 kW	148.2 [kW] & 14.82 [kWh]	139.4 [kW] & 2.173 [kWh]	150 [kW] & 5.0 [kWh]
200 kW	285.0 [kW] & 28.50 [kWh]	265.2 [kW] & 4.13 [kWh]	300 [kW] & 5.0 [kWh]

Table 5.17: Table of the CAPEX of the whole shore power system for different versions of the HP ESS shore power configuration. The results are optimized for different P_{nom} of the crane.

P_{nom} of crane	Basic	LTO	SC	FESS
20 kW	731,985 [euro]	705,764 [euro]	712,814 [euro]	731,985 [euro]
40 kW	783,775 [euro]	738,778 [euro]	749,212 [euro]	783,775 [euro]
60 kW	825,449 [euro]	766,533 [euro]	780,162 [euro]	825,449 [euro]
80 kW	876,357 [euro]	798,817 [euro]	817,136 [euro]	852,445 [euro]
100 kW	919,989 [euro]	827,730 [euro]	849,337 [euro]	864,143 [euro]
200 kW	1,155,198 [euro]	977,129 [euro]	1,019,338 [euro]	931,204 [euro]

Table 5.18: Table of the OPEX of the whole shore power system for different versions of the HP ESS shore power configuration. The results are optimized for different P_{nom} of the crane.

P_{nom} of crane	Basic	LTO	SC	FESS
20 kW	12,179 [euro]	12,180 [euro]	12,179 [euro]	12,179 [euro]
40 kW	12,181 [euro]	12,181 [euro]	12,182 [euro]	12,181 [euro]
60 kW	12,185 [euro]	12,185 [euro]	12,185 [euro]	12,185 [euro]
80 kW	12,187 [euro]	12,187 [euro]	12,187 [euro]	12,187 [euro]
100 kW	12,191 [euro]	12,191 [euro]	12,192 [euro]	12,191 [euro]
200 kW	12,203 [euro]	12,204 [euro]	12,204 [euro]	12,203 [euro]

Table 5.19: Table showing the total CAPEX decrease for each version using HP compared to the status quo optimal solution from Table 5.17.

	LTO	SC	FESS
20 kW	-3.58%	-2.62%	0%
40 kW	-5.73%	-4.41%	0%
60 kW	-7.14%	-5.49%	0%
80 kW	-8.85%	-6.76%	-2.73%
100 kW	-10.03%	-7.68%	-6.07%
200 kW	-15.41%	-11.76%	-19.39%

Further elaboration on the fact that as the nominal power of the crane increases the shore power converter also increases is given through Figures 5.29 - 5.32. The figures for the other versions and the other P_{nom} of the crane can be found in the appendix.
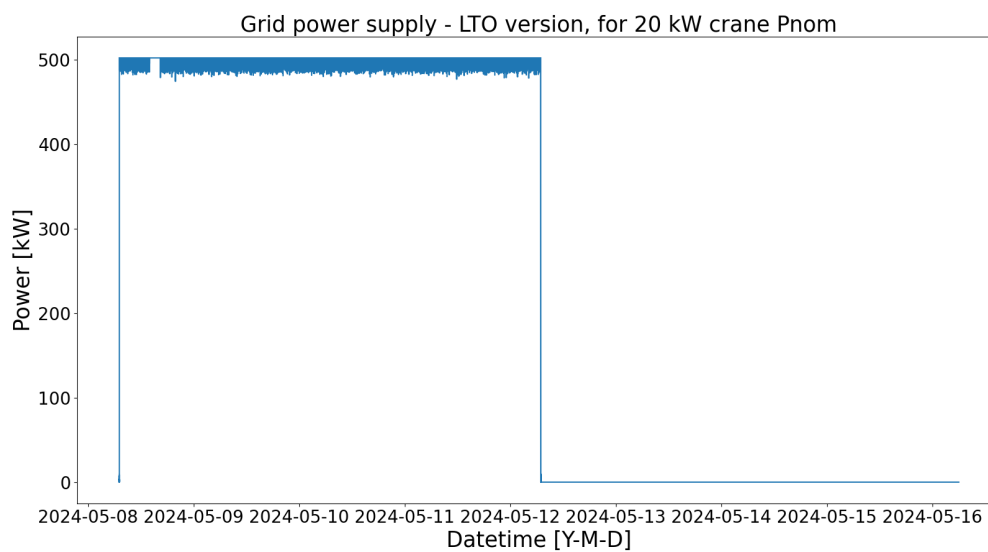
Figure 5.29: Figure of the grid power supply when the vessel uses a crane with 20 kW of nominal power. This figure corresponds to the vessel power profile of Figure 5.27 with a LTO battery for the HP ESS shore power configuration.
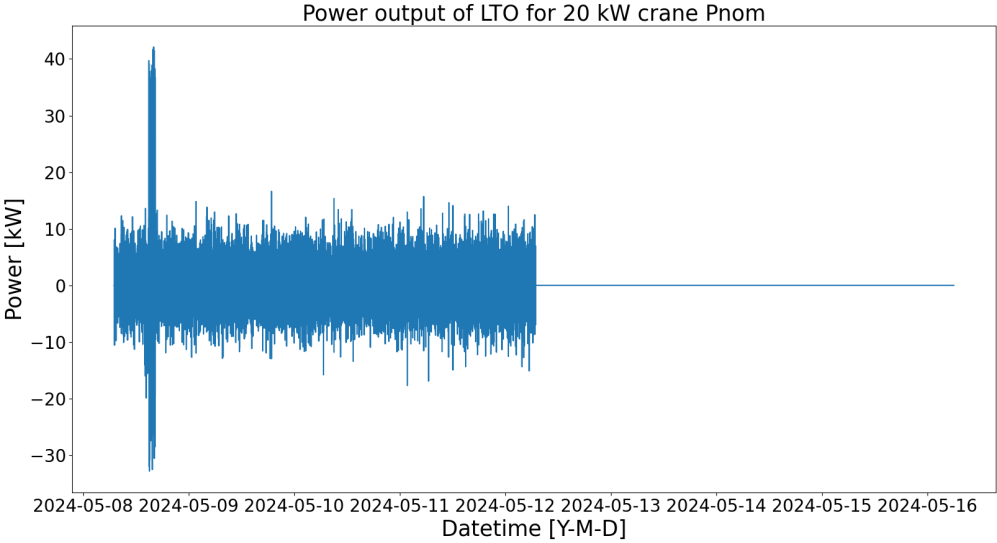
Figure 5.30: Figure of the LTO battery power output corresponding to Figure 5.27. The peak of the crane use is higher than 20 kW because of the overshoot. The ESS is also used to stabilize the fluctuations of the vessel power demand.
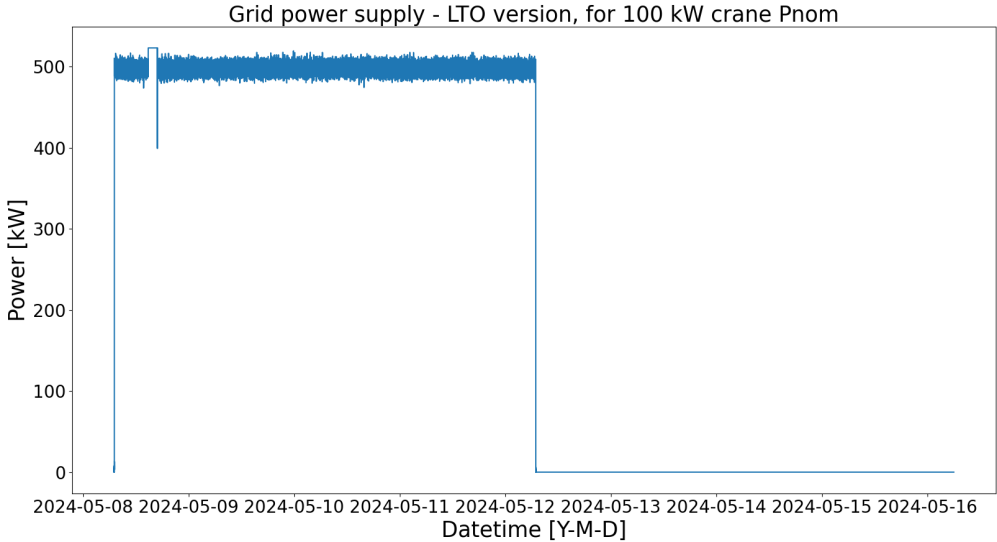
Figure 5.31: Figure of the grid power supply when the vessel uses a crane with 20 kW of nominal power. This figure corresponds to the vessel power profile of Figure 5.27 with a LTO battery for the HP ESS shore power configuration.
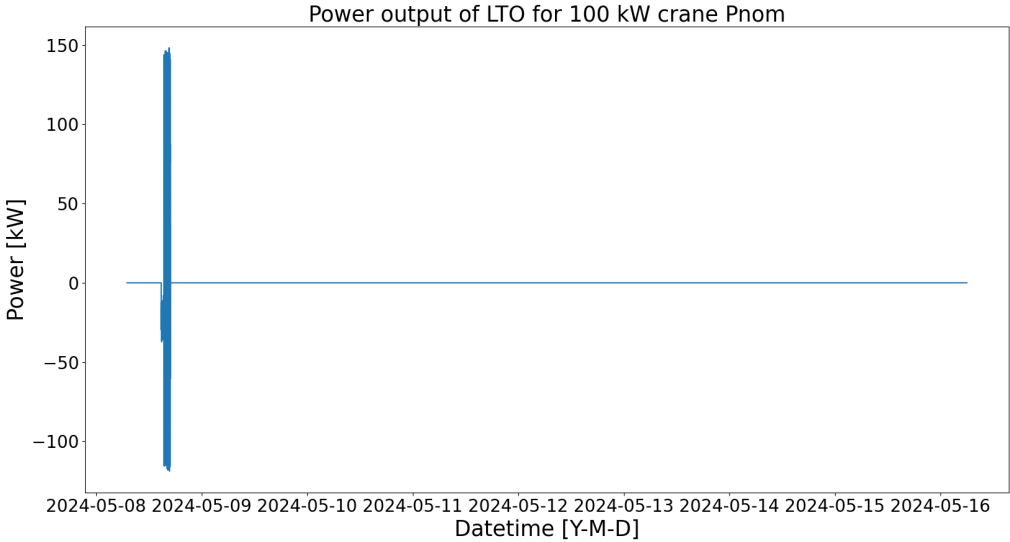
Figure 5.32: Figure of the LTO battery power output corresponding to Figure 5.28. The peak of the crane use is higher than 100 kW because of the overshoot. The ESS is no longer used to stabilize the fluctuations of the vessel power demand.

5.4. PV

The inclusion of alternative power production creates more possibilities for the analysis. Therefore different shore power configurations are investigated in this section. Section 5.4.1 uses the configuration shown in Figure 5.33 to calculate the opex savings that solar power enables. Section 5.4.2 uses the configuration shown in Figure 5.34 to investigate the effect that the addition of PV power has on the HE ESS sizing for long term vessel stay. And finally Section 5.4.4 uses the configuration from Figure 5.35 to investigate the effect that adding PV power has on the HP ESS sizing for crane uses.

The investigation is done by forcing the optimization algorithm to implement several sizes of PV array. This is done because the opex savings from solar power do not offset the additional capital investment in the short simulation time of a few days. The different sizes for PV array are:

- 300 kW, smaller than the Hotel load
- 500 kW, about the same as the Hotel Load
- 700 kW, bigger than the Hotel load
- 1000 kW, double the Hotel load
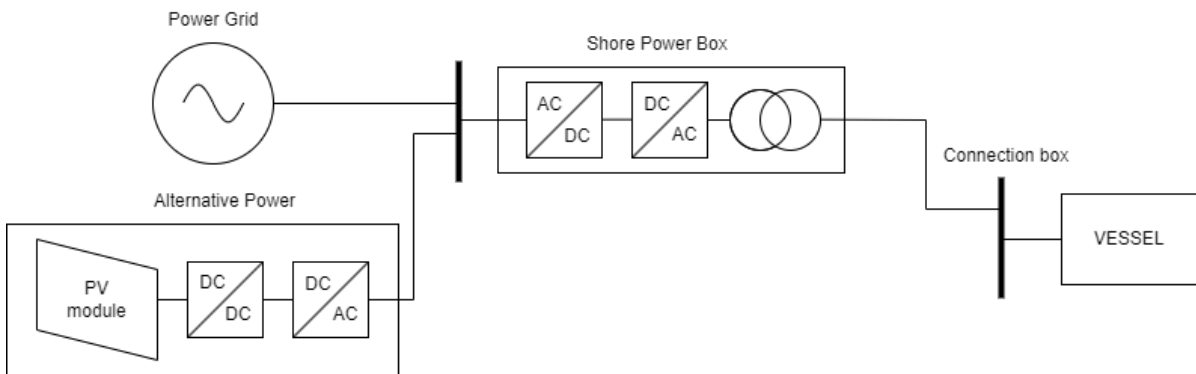
Figure 5.33: Diagram of a basic PV configuration shore power system
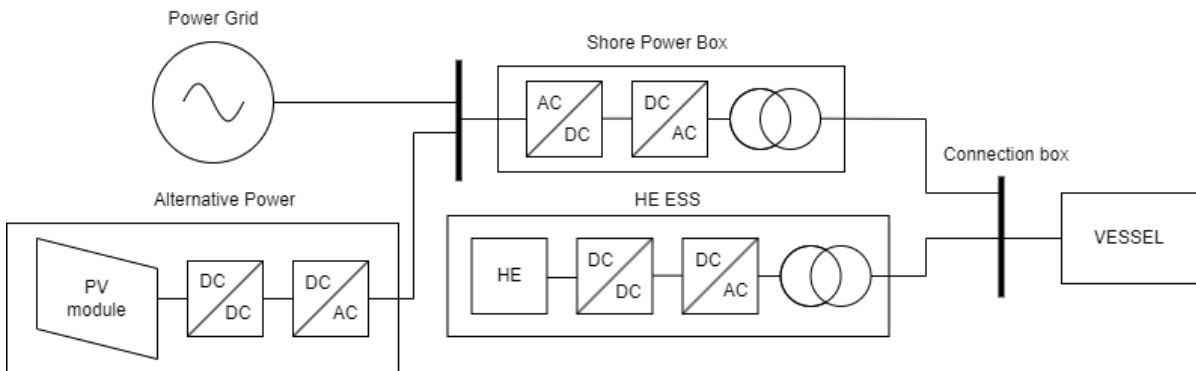
Figure 5.34: Diagram of the shore power configuration with both HE ESS and PV
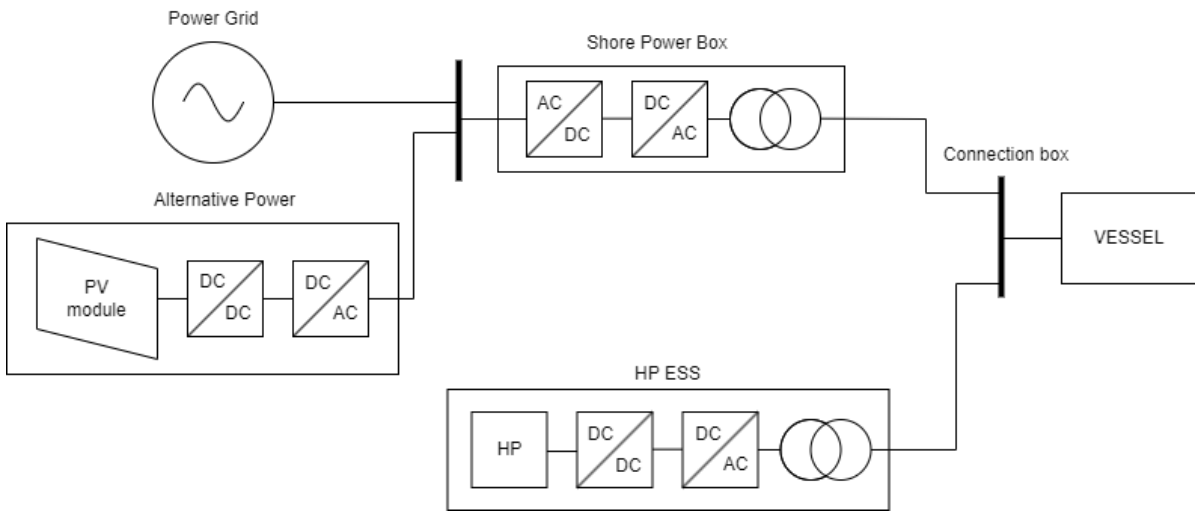
Figure 5.35: Diagram of the shore power configuration with both HP ESS and PV

5.4.1. OPEX

The length of time needed for the PV array to break even depends on the amount of opex that is reduced by the PV array and the capex of the PV array itself. The vessel power profile used is shown in Figure 5.36, it does not include crane uses as that makes the simulation simpler and crane uses do not add significant additional operational expenses. It is only for a single day, because multiple days would simply be a linear continuation of the estimation made for a single day. The configuration shown in Figure 5.33 will be compared to results from the optimal status quo solution for the vessel power profile of Figure 5.36.
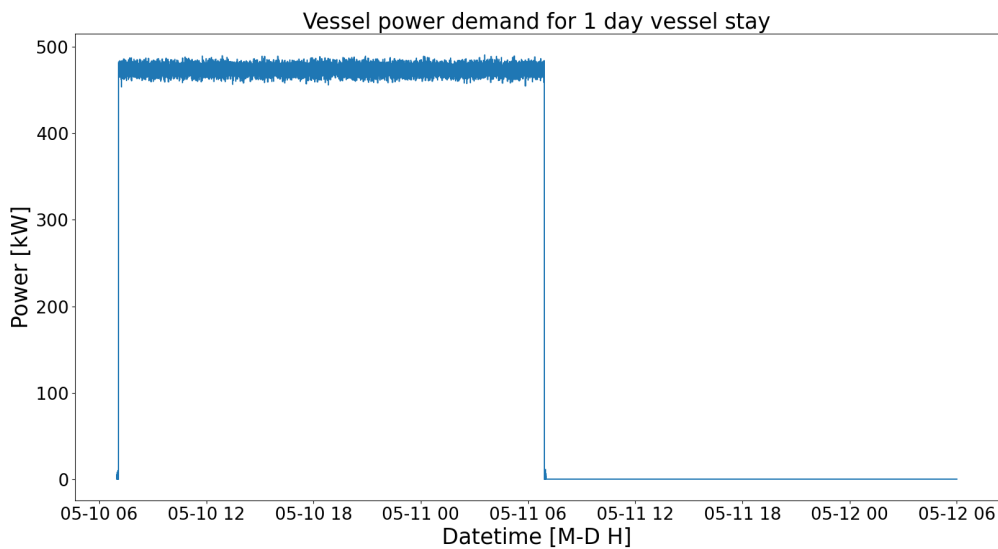
Figure 5.36: Figure of the vessel power profile used to estimate the break even point for PV as alternative power supply. The power demand of the vessel does not include crane uses, it is a single day of shore power use followed by a day of downtime. The x-axis is in datetime meaning that every data point is mapped to a particular date and time.

Table 5.20 shows the OPEX results of the simulations as well as the CAPEX of the corresponding PV array. Table 5.21 shows the cost reduction in OPEX compared to the status quo directly. As expected as the PV array increases in size, there is greater reduction in OPEX as well as greater CAPEX of the PV array.

Table 5.20: Table showing the operational expenses of the status quo, and the basic PV configuration for different sizes of the PV array. The OPEX of a single day is shown for a 'summer' day and a 'winter' day as well as the cost of the PV array for that particular size.

	Summer day OPEX	Winter day OPEX	PV array CAPEX
Basic	2502.65 [euro]	2502.65 [euro]	-
300 kW	2130.61 [euro]	2454.64 [euro]	532,500.0 [euro]
500 kW	1882.64 [euro]	2422.63 [euro]	887,500.0 [euro]
700 kW	1708.40 [euro]	2390.62 [euro]	1,242,500.0 [euro]
1000 kW	1591.14 [euro]	2342.60 [euro]	1,775,000.0 [euro]

Table 5.21: Table of the cost reduction in OPEX that is achieved per size of PV array compared to the status quo optimal solution, for both an average 'summer' day and an average 'winter' day.

	Summer day OPEX reduction	Winter day OPEX reduction
300 kW	-372.04 [euro]	-48.01 [euro]
500 kW	-620.01 [euro]	-80.02 [euro]
700 kW	-794.25 [euro]	-112.03 [euro]
1000 kW	-911.51 [euro]	-160.05 [euro]

Once the reduction of opex is calculated, the next step is estimating how many of these average 'summer' days and average 'winter' days are there in a year on average. This is done by using the solar irradiance data for Rotterdam for the year 2020 from PVGIS [62]. The amount of solar irradiance of a day is summed and then normalized by dividing by 1000 W/m^2. This is done for every single day of that year. These days are then compared to Figure 2.5 and categorized as either a 'summer' day, a 'winter' day or a no irradiance day.

The total irradiance of the summation of 'summer' days and 'winter' days is then compared to the original data, to ensure that the newly created data stays representative of the original. This results in 214 average 'summer' days, 123 average 'winter' days and 29 days of too little sunlight. The sum of this irradiance is 1356.08 compared to the total irradiance of the original data, normalized by dividing by 1000 W/m^2, of 1356.37.

The equation to calculate the amount of cost reduction per year is:

$$OPEX\_reduction/year = (214*summer\_day\_reduction+123*winter\_day\_reduction)*occupation\_ratio$$
(5.1)

and the equation for the break even point is:

$$\#\_of\_years = \frac{PV\_CAPEX}{OPEX\_reduction/year}$$
(5.2)

Therefore the final unknown is the occupation ratio, which is changed from 0.1 to 0.5 to see the effect on the number of years it takes to break even. Table 5.22 shows the results. Clearly, the payback time is heavily dependent on the occupation ratio, which is the ratio of the amount of time a vessel is being supplied with shore power out of the whole year, as it can take around 50 years for the PV array to break even or around 10 years. Furthermore, Table 5.22 shows that the PV array should be sized at no more than the Hotel load of the vessel in order to achieve the lowest payback time.

Table 5.22: Table of the number of years it takes for a PV array to pay back its own investment cost. The occupation ratio can be between 0 and 1.

Occupation ratio	300 kW PV array	500 kW PV array	700 kW PV array	1000 kW PV array
0.1	62.3 [yr]	62.3 [yr]	67.6 [yr]	82.7 [yr]
0.2	31.1 [yr]	31.1 [yr]	33.8 [yr]	41.3 [yr]
0.3	20.8 [yr]	20.8 [yr]	22.5 [yr]	27.6 [yr]
0.4	15.6 [yr]	15.6 [yr]	16.9 [yr]	20.7 [yr]
0.5	12.4 [yr]	12.4 [yr]	13.5 [yr]	16.5 [yr]

5.4.2. HE PV

This section presents the influence of PV on the sizing of HE ESS when it is used as shown in the configuration from Figure 5.34. The comparison to the sizing of HE ESS of Section 5.1.2 is done by using the same vessel power profiles to optimize for. So, for each vessel power profile (1 day, 2 days, 3 days or 4 days of supplying shore power) there are 4 simulations for each HE ESS. Since this section is only interested in the sizing of the ESS, the results shown in Tables 5.23 - 5.26 only show the size of the ESS.

It is clear from Tables 5.23 - 5.26 that the size of the PV array has no influence on the sizing of HE ESS. In fact, the size of the ESS is the exact same found in Section 5.1.2 when comparing the same length of vessel stay. This is because the vessel power profile that is used as input for the optimization is the same, so the optimal size of the ESS is the same as well.

Table 5.23: Table of the nominal power & energy capacity of the different HE ESS. These results are for the different sizes of the PV array for a 1 day vessel stay power profile.

PV array	LFP	NMC	Na
0 kW	17.95 [kW] & 17.95 [kWh]	17.54 [kW] & 8.77 [kWh]	20.74 [kW] & 10.37 [kWh]
300 kW	17.95 [kW] & 17.95 [kWh]	17.54 [kW] & 8.77 [kWh]	20.74 [kW] & 10.37 [kWh]
500 kW	17.95 [kW] & 17.95 [kWh]	17.54 [kW] & 8.77 [kWh]	20.74 [kW] & 10.37 [kWh]
700 kW	17.95 [kW] & 17.95 [kWh]	17.54 [kW] & 8.77 [kWh]	20.74 [kW] & 10.37 [kWh]
1000 kW	17.95 [kW] & 17.95 [kWh]	17.54 [kW] & 8.77 [kWh]	20.74 [kW] & 10.37 [kWh]

Table 5.24: Table of the nominal power & energy capacity of the different HE ESS. These results are for the different sizes of the PV array for a 2 days vessel stay power profile.

PV array	LFP	NMC	Na
0 kW	20.06 [kW] & 20.06 [kWh]	17.76 [kW] & 8.88 [kWh]	20.74 [kW] & 10.37 [kWh]
300 kW	20.06 [kW] & 20.06 [kWh]	17.76 [kW] & 8.88 [kWh]	20.74 [kW] & 10.37 [kWh]
500 kW	20.06 [kW] & 20.06 [kWh]	17.76 [kW] & 8.88 [kWh]	20.74 [kW] & 10.37 [kWh]
700 kW	20.06 [kW] & 20.06 [kWh]	17.76 [kW] & 8.88 [kWh]	20.74 [kW] & 10.37 [kWh]
1000 kW	20.06 [kW] & 20.06 [kWh]	17.76 [kW] & 8.88 [kWh]	20.74 [kW] & 10.37 [kWh]

Table 5.25: Table of the nominal power & energy capacity of the different HE ESS. These results are for the different sizes of the PV array for a 3 days vessel stay power profile.

PV array	LFP	NMC	Na
0 kW	20.06 [kW] & 20.06 [kWh]	19.31 [kW] & 9.66 [kWh]	20.74 [kW] & 10.37 [kWh]
300 kW	20.06 [kW] & 20.06 [kWh]	19.31 [kW] & 9.66 [kWh]	20.74 [kW] & 10.37 [kWh]
500 kW	20.06 [kW] & 20.06 [kWh]	19.31 [kW] & 9.66 [kWh]	20.74 [kW] & 10.37 [kWh]
700 kW	20.06 [kW] & 20.06 [kWh]	19.31 [kW] & 9.66 [kWh]	20.74 [kW] & 10.37 [kWh]
1000 kW	20.06 [kW] & 20.06 [kWh]	19.31 [kW] & 9.66 [kWh]	20.74 [kW] & 10.37 [kWh]

Table 5.26: Table of the nominal power & energy capacity of the different HE ESS. These results are for the different sizes of the PV array for a 4 days vessel stay power profile.

PV array	LFP	NMC	Na
0 kW	19.71 [kW] & 19.71 [kWh]	18.87 [kW] & 9.44 [kWh]	20.74 [kW] & 10.37 [kWh]
300 kW	19.71 [kW] & 19.71 [kWh]	18.87 [kW] & 9.44 [kWh]	20.74 [kW] & 10.37 [kWh]
500 kW	19.71 [kW] & 19.71 [kWh]	18.87 [kW] & 9.44 [kWh]	20.74 [kW] & 10.37 [kWh]
700 kW	19.71 [kW] & 19.71 [kWh]	18.87 [kW] & 9.44 [kWh]	20.74 [kW] & 10.37 [kWh]
1000 kW	19.71 [kW] & 19.71 [kWh]	18.87 [kW] & 9.44 [kWh]	20.74 [kW] & 10.37 [kWh]

Figure 5.37 and Figure 5.38 show that the ESS, LFP in this case, is used for the small energy fluctuations in the vessel power demand. The only difference the larger PV array makes is that the ESS in Figure 5.37 requires a little extra power during the downtime so that it is fully charged by the end of the simulation. Figure 5.39 and Figure 5.40 further corroborate the fact that the ESS is only used to stabilize the power demand of the vessel. Sizing the ESS any larger is simply not economical, even with 2 times the amount of PV generation as required by the Hotel load of the vessel, the night leaves no power generation and so all other components need to be sized accordingly. Which means that the only thing the PV array adds is lower opex.

Figure 5.41 proves that the size of PV array has not effect on the way the HE ESS should be optimally used for supplying shore power. All the different plots perfectly overlap, except for the 300 kW PV array as it too small to charge the ESS to full in the very early morning. So, it charges the battery a little bit beforehand.

These plots are used as examples, and they are very similar to the ones for the other lengths of vessel stay or for the other HE ESS (NMC and Na-ion). All these plots can be found in the appendix.
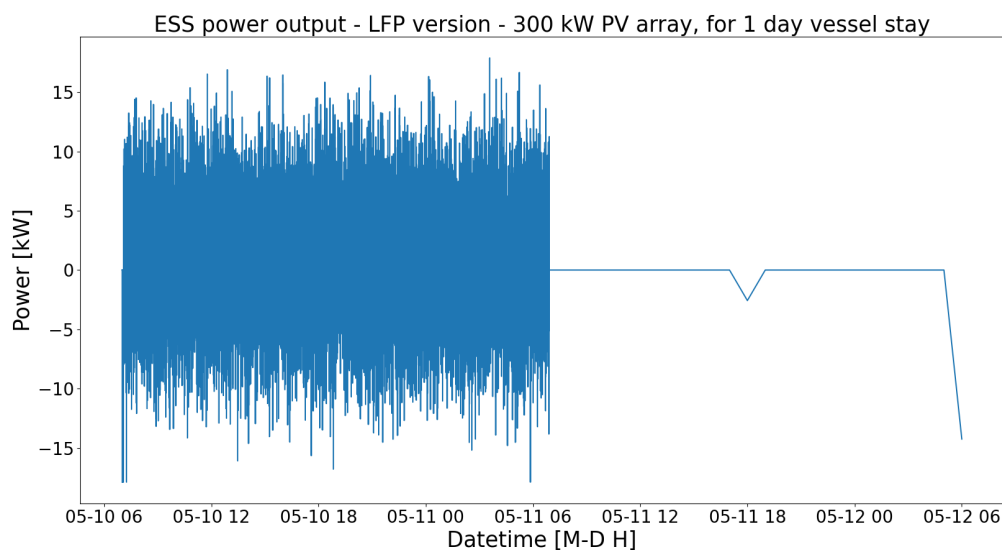
Figure 5.37: Figure of the power output of the LFP battery in the HE PV shore power configuration. This is part of the optimal solution for supplying shore power to the vessel power demand of Figure 5.6, where the configuration includes a 300 kW PV array.
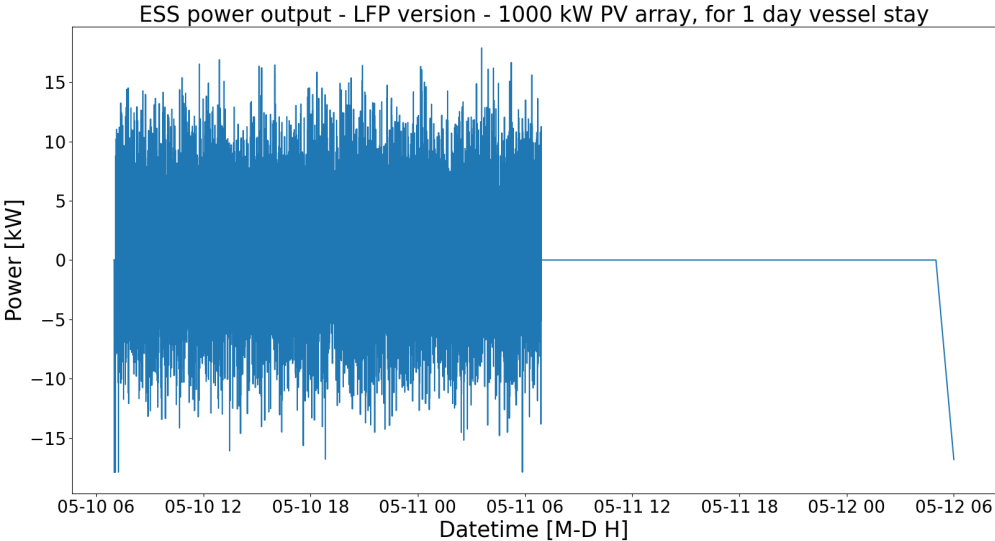
Figure 5.38: Figure of the power output of the LFP battery in the HE PV shore power configuration. This is part of the optimal solution for supplying shore power to the vessel power demand of Figure 5.6, where the configuration includes a 1000 kW PV array.
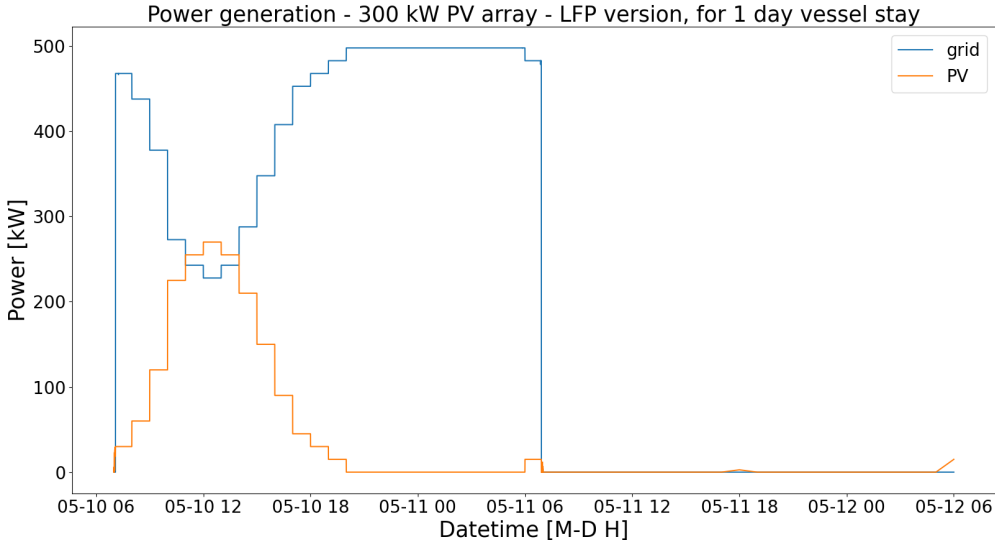
Figure 5.39: Figure of the power generation, either from the grid or from onsite PV. Supplying power to the vessel power demand of Figure 5.6. The PV array is 300 kW for the LFP version of the HE PV shore power configuration.
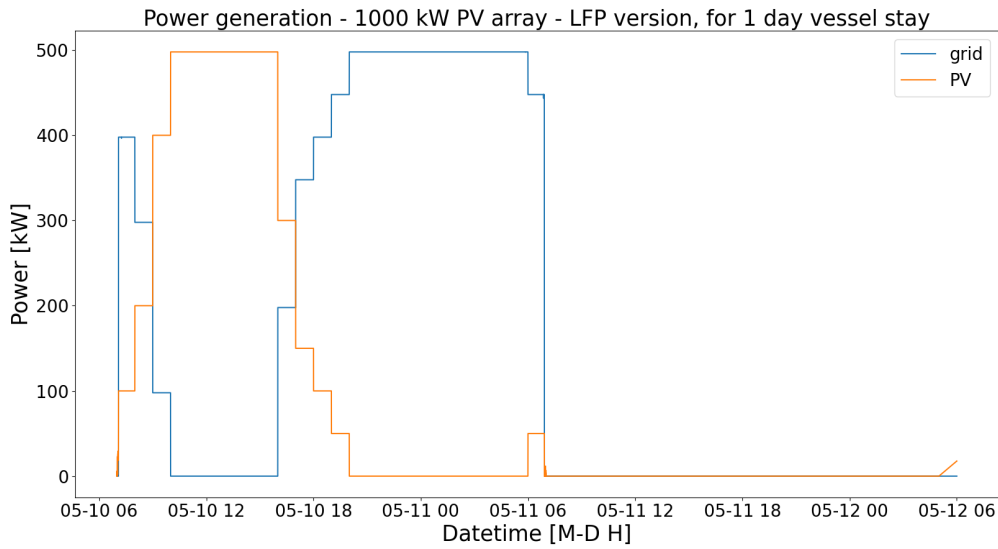
Figure 5.40: Figure of the power generation, either from the grid or from onsite PV. Supplying power to the vessel power demand of Figure 5.6. The PV array is 1000 kW for the LFP version of the HE PV shore power configuration.
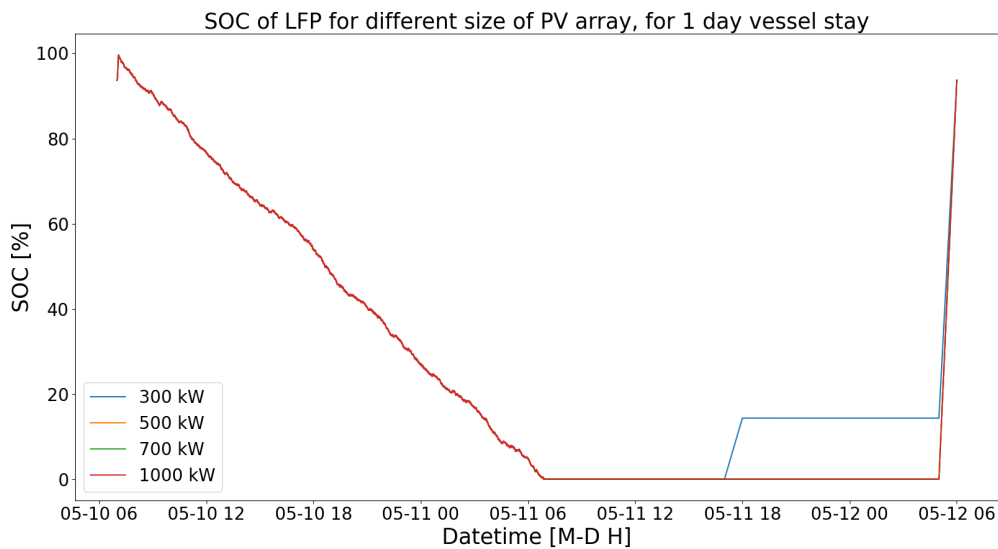
Figure 5.41: Figure of the SOC over time of the LFP battery implemented in the HE PV shore power configuration. Where the vessel power profile does not include the use of a crane and requires a single day of shore power followed by a day of downtime. The different PV array sizes perfectly overlap during the supply of shore power, while the 300 kW PV array is too small to fully charge the LFP battery in the early morning.

5.4.3. Alternative HE PV

Even though there is surplus solar power generation with a 1000 kW size PV array, all that power still needs to go through the shore power converter in order to charge the ESS. So, if the bus the PV array is connected to changes to a bus on the vessel side of the shore power converter then this might result in different sizing of the HE ESS. Figure 5.42 shows the electrical diagram of this alternative HE PV shore power configuration.
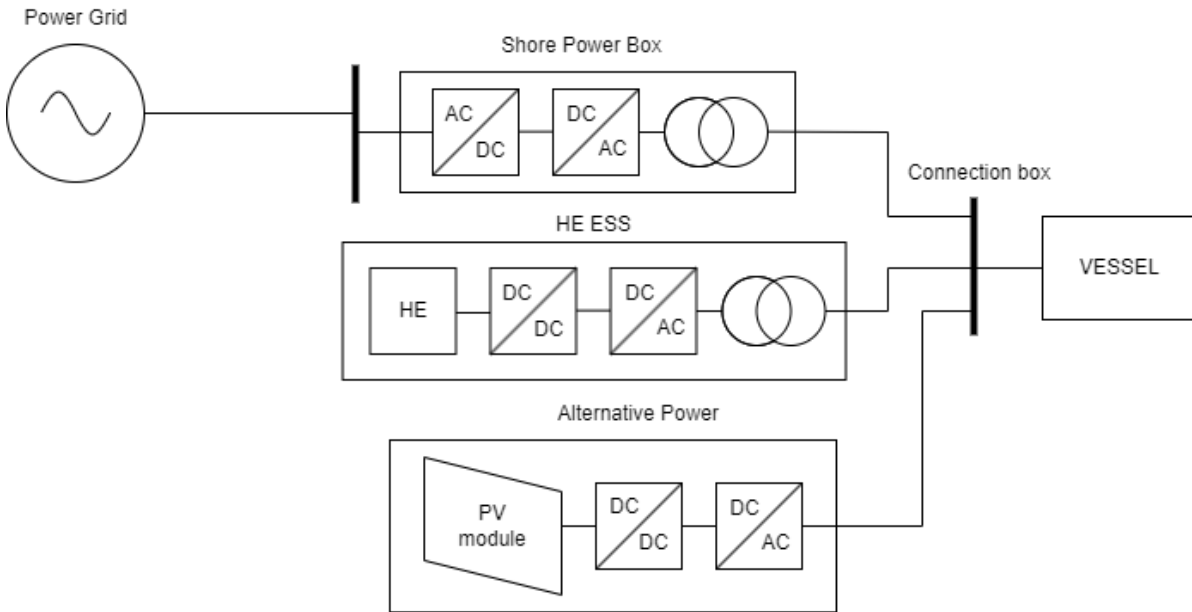
Figure 5.42: Diagram of the HE PV shore power configuration where the PV array is connected to the shore power connection box instead of the main switchboard.

The vessel power profile used is the same one found in Figure 5.6 and the results can be found in Tables 5.27 - 5.32. Although the results are not identical to the results from Section 5.4.2, they are not significantly different. Table 5.27, Table 5.29 and Table 5.31 show that the sizing of the ESS in each case is very similar to the results of Section 5.1.2. Table 5.28, Table 5.30 and Table 5.32 show that there is an improvement in terms of cost reduction for both capex and opex, but it is very a small difference.

Table 5.27: Table of the results from the alternative HE PV shore power configuration. LFP is the HE ESS used in this implementation. The results are optimized for the vessel power profile of Figure 5.6.

PV array size	shore power converter size	ESS size	CAPEX	OPEX
300 kW	496.6 [kW]	19.0 [kW] & 19.0 [kWh]	1,208,695 [euro]	2549 [euro]
500 kW	496.6 [kW]	19.0 [kW] & 19.0 [kWh]	1,563,695 [euro]	2234 [euro]
700 kW	496.6 [kW]	19.0 [kW] & 19.0 [kWh]	1,918,695 [euro]	2038 [euro]
1000 kW	496.6 [kW]	19.0 [kW] & 19.0 [kWh]	2,451,195 [euro]	1897 [euro]

Table 5.28: Cost reduction for alternative HE PV shore power configuration with LFP compared to the 'regular' HE PV shore power configuration with LFP. Both corresponding to the vessel power demand from Figure 5.6.

	CAPEX	OPEX
300 kW	-0.12%	-0.97%
500 kW	-0.09%	-1.72%
700 kW	-0.07%	-1.26%
1000 kW	-0.06%	-1.3%

Table 5.29: Table of the results from the alternative HE PV shore power configuration. NMC is the HE ESS used in this implementation. The results are optimized for the vessel power profile of Figure 5.6.

PV array size	shore power converter size	ESS size	CAPEX	OPEX
300 kW	497.6 [kW]	18.2 [kW] & 9.1 [kWh]	1,209,968 [euro]	2552 [euro]
500 kW	497.6 [kW]	18.2 [kW] & 9.1 [kWh]	1,564,968 [euro]	2236 [euro]
700 kW	497.6 [kW]	18.2 [kW] & 9.1 [kWh]	1,919,968 [euro]	2043 [euro]
1000 kW	497.6 [kW]	18.2 [kW] & 9.1 [kWh]	2,452,468 [euro]	1902 [euro]

Table 5.30: Cost reduction for alternative HE PV shore power configuration with NMC compared to the 'regular' HE PV shore power configuration with NMC. Both corresponding to the vessel power demand from Figure 5.6.

	CAPEX cost reduction	OPEX cost reduction
300 kW	-0.08%	-0.93%
500 kW	-0.06%	-1.76%
700 kW	-0.05%	-1.11%
1000 kW	-0.04%	-1.14%

Table 5.31: Table of the results from the alternative HE PV shore power configuration. Na-ion is the HE ESS used in this implementation. The results are optimized for the vessel power profile of Figure 5.6.

PV array size	shore power converter size	ESS size	CAPEX	OPEX
300 kW	497.9 [kW]	20.7 [kW] & 10.4 [kWh]	1,215,715 [euro]	2552 [euro]
500 kW	497.9 [kW]	20.7 [kW] & 10.4 [kWh]	1,570,715 [euro]	2236 [euro]
700 kW	497.9 [kW]	20.7 [kW] & 10.4 [kWh]	1,925,715 [euro]	2043 [euro]
1000 kW	497.9 [kW]	20.7 [kW] & 10.4 [kWh]	2,458,215 [euro]	1902 [euro]

Table 5.32: Cost reduction for alternative HE PV shore power configuration with Na-ion compared to the 'regular' HE PV shore power configuration with Na-ion. Both corresponding to the vessel power demand from Figure 5.6.

	CAPEX cost reduction	OPEX cost reduction
300 kW	-0.03%	-0.93%
500 kW	-0.03%	-1.76%
700 kW	-0.02%	-1.11%
1000 kW	-0.02%	-1.14%

Figures 5.43 and 5.44 together fulfil the power demand of Figure 5.8, the same for Figures 5.45 and 5.46. The plots are a little different compared to those in Secton 5.4.2, instead of the ESS being used to remove the fluctuations in power demand of the vessel the entire time that the vessel requires shore power, the ESS is used here during the night only. As the solar power does not pass through the shore power converter it becomes easier to reduce the power required from the grid. And the ESS has losses, even if they are very small, so the fluctuations are taken care of by the grid and only when the solar generation stops is the ESS required.

Because there is over abundant solar generation in Figures 5.45 and 5.46 the HE ESS is charged at different moments with the free solar power and then discharged to lower the opex a little bit. Figure 5.47 shows the SOC over time of the LFP ESS with different sizes of PV array. The figures for the NMC HE ESS and Na-ion HE ESS versions can be found in the appendix.
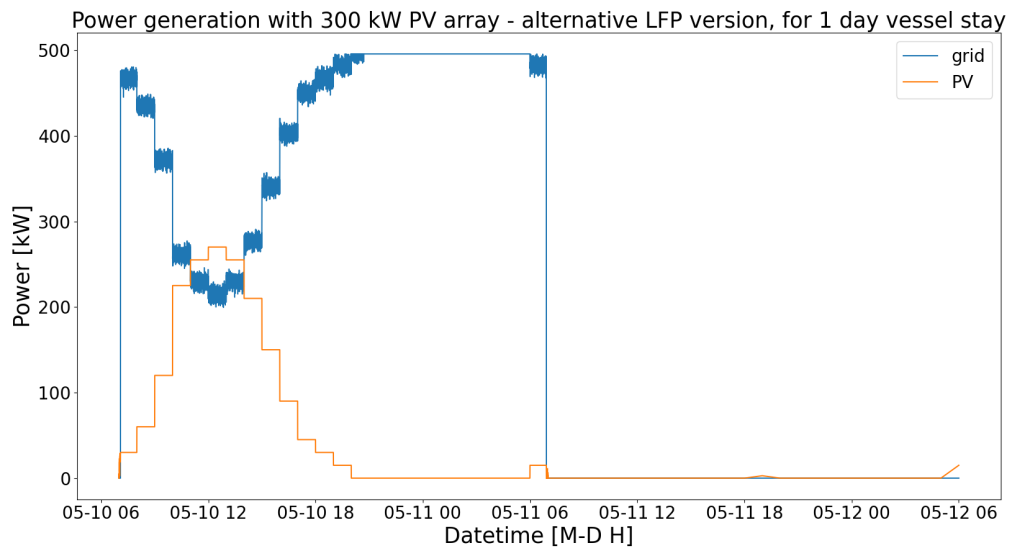
Figure 5.43: Figure of the power generation with a 300 kW PV array. The power is supplied to the vessel power profile of Figure 5.6. The alternative HE PV shore power configuration is used where LFP is the HE ESS.
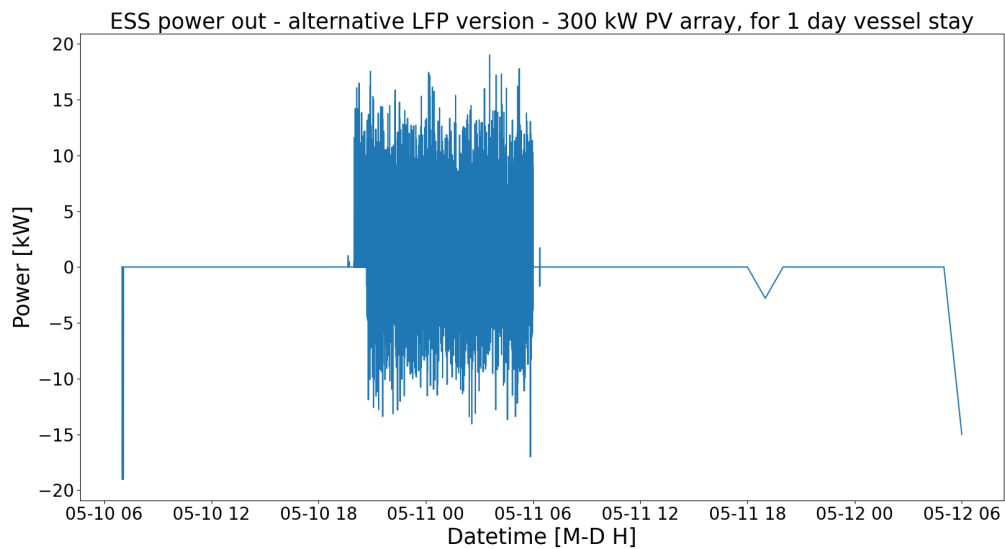
Figure 5.44: Figure of the power output from the HE ESS in the alternative HE PV shore power configuration supplying shore power to the vessel power demand of Figure 5.6. LFP is HE ESS used in this implementation with 300 kW PV array.
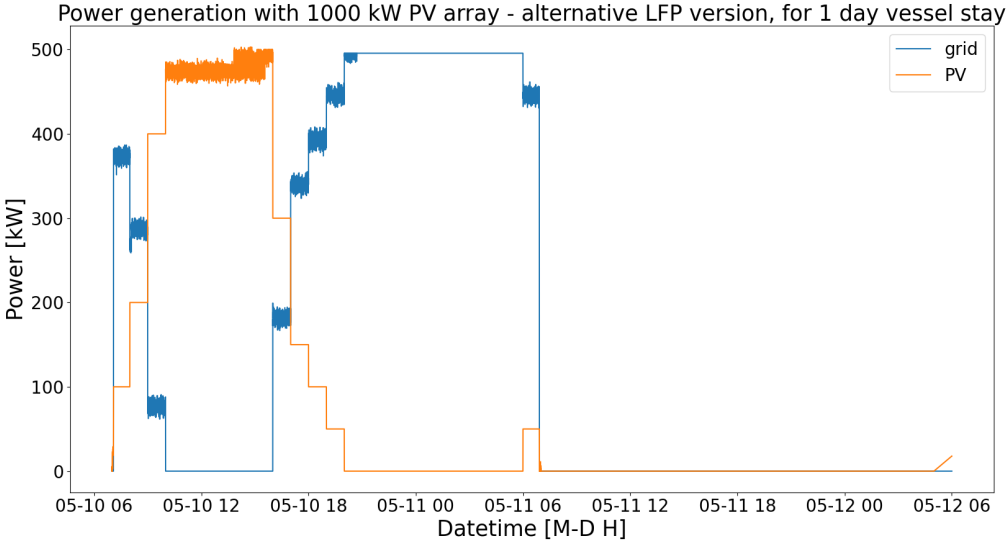
Figure 5.45: Figure of the power generation with a 1000 kW PV array. The power is supplied to the vessel power profile of Figure 5.6. The alternative HE PV shore power configuration is used where LFP is the HE ESS.
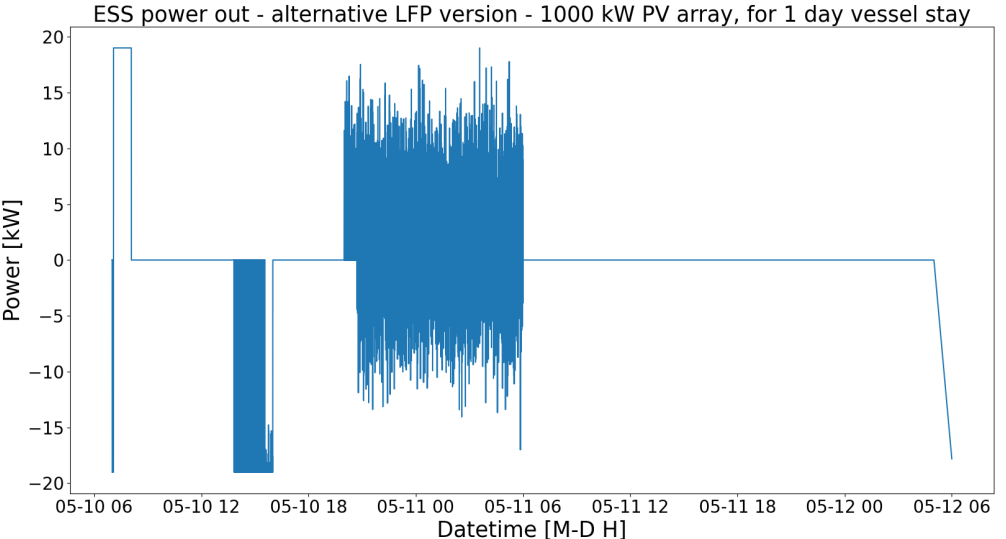
Figure 5.46: Figure of the power output from the HE ESS in the alternative HE PV shore power configuration supplying shore power to the vessel power demand of Figure 5.6. LFP is HE ESS used in this implementation with 1000 kW PV array.
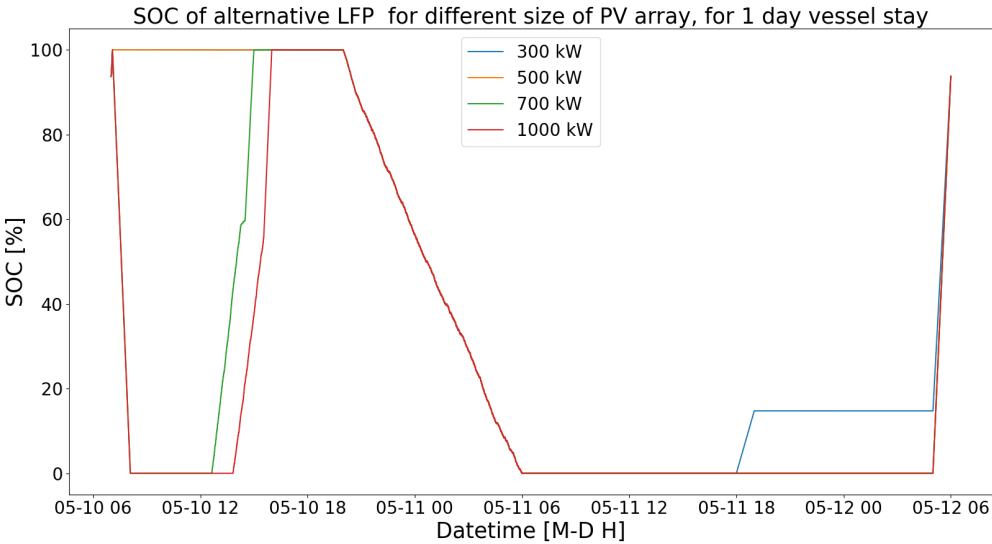
Figure 5.47: SOC of the ESS used in the alternative HE PV shore power configurations. The ESS is LFP for different sizes of PV array.

5.4.4. HP PV

The final shore power configuration that uses alternative power supply is investigated in this section. The configuration is shown in Figure 5.35. The vessel power profile used is shown in Figure 5.48.
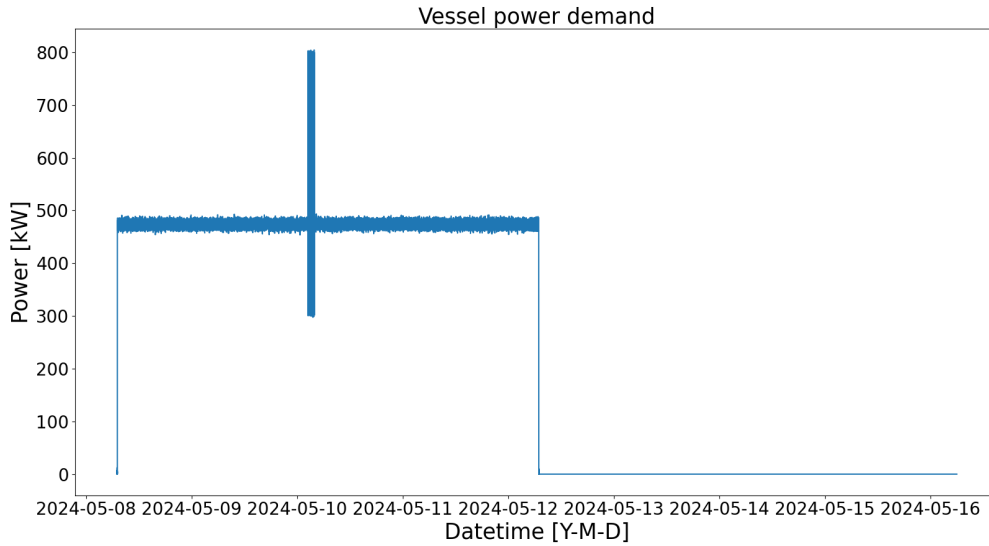
Figure 5.48: Figure of the vessel power demand used for the HP PV shore power configuration. It is 4 days of required shore power supply followed by 4 days of downtime. 30 consecutive crane uses are included. The x-axis is in datetime meaning every data point is fixed to a specific date and time.

The results for the optimization are shown in Tables 5.33 - 5.36. Table 5.33 shows that the size of the PV array has no influence on the size of the shore power converter of the system, just like what was shown in Section 5.4.2 for the HE ESS. Similarly, the sizing of the ESS is unaffected by the size of PV array as shown by Table 5.34. The only difference the PV array makes is an increase of capex of the system as shown by Table 5.35 and a decrease of opex of the system as shown by Table 5.36. But other than that there is no influence on any other component.

Table 5.33: Table of the P_{nom} of shore power converter for each version of the HP PV shore power configuration. The results include optimizations for the power profile of Figure 5.48 for different sizes of PV array.

PV array	Status quo	LTO	SC	FESS
0 kW	846.8 [kW]	547.0 [kW]	567.7 [kW]	563.8 kW
300 kW	-	547.0 [kW]	567.7 [kW]	563.8 [kW]
500 kW	-	547.0 [kW]	567.7 [kW]	563.8 [kW]
700 kW	-	547.0 [kW]	567.7 [kW]	563.8 [kW]
1000 kW	-	547.0 [kW]	567.7 [kW]	563.8 [kW]

Table 5.34: Table of the nominal power & energy capacity of the ESS implementations of the HP PV shore power configuration. The results include optimizations for the power profile of Figure 5.48 for different sizes of PV array.

PV array	LTO	SC	FESS
0 kW	285.0 [kW] & 28.5 [kWh]	265.2 [kW] & 4.1 [kWh]	300 [kW] & 5.0 [kWh]
300 kW	285.0 [kW] & 28.5 [kWh]	265.2 [kW] & 4.1 [kWh]	300 [kW] & 5.0 [kWh]
500 kW	285.0 [kW] & 28.5 [kWh]	265.2 [kW] & 4.1 [kWh]	300 [kW] & 5.0 [kWh]
700 kW	285.0 [kW] & 28.5 [kWh]	265.2 [kW] & 4.1 [kWh]	300 [kW] & 5.0 [kWh]
1000 kW	285.0 [kW] & 28.5 [kWh]	265.2 [kW] & 4.1 [kWh]	300 [kW] & 5.0 [kWh]

Table 5.35: Total CAPEX of the whole shore power system for different versions of the HP PV shore power configuration. The results include optimizations for the power profile of Figure 5.48 for different sizes of PV array.

PV array	Status quo	LTO	SC	FESS
0 kW	1,155,197 [euro]	977,129 [euro]	1,019,337 [euro]	931,204 [euro]
300 kW	-	1,510,484 [euro]	1,546,533 [euro]	1,464,204 [euro]
500 kW	-	1,865,484 [euro]	1,901,533 [euro]	1,819,204 [euro]
700 kW	-	2,220,484 [euro]	2,256,533 [euro]	2,174,204 [euro]
1000 kW	-	2,752,984 [euro]	2,789,033 [euro]	2,706,704 [euro]

Table 5.36: Total OPEX of the whole shore power system for different versions of the HP PV shore power configuration. The results include optimizations for the power profile of Figure 5.48 for different sizes of PV array.

PV array	Status quo	LTO	SC	FESS
0 kW	12203 [euro]	12204 [euro]	12202 [euro]	12202 [euro]
300 kW	-	10393 [euro]	10400 [euro]	10398 [euro]
500 kW	-	9191 [euro]	9198 [euro]	9196 [euro]
700 kW	-	8316 [euro]	8349 [euro]	8346 [euro]
1000 kW	-	7744 [euro]	7778 [euro]	7773 [euro]

Figure 5.49 and Figure 5.50 together fulfil the power demand of Figure 5.48. Likewise for Figure 5.51 and Figure 5.52. These are examples of the FESS implementation, the figures for LTO, SC and for the other sizes of PV array are included in the appendix. Figure 5.53 shows the SOC over time for FESS for the different implementations of the HP PV shore power configuration.

From Figures 5.49 and 5.50 it is clear that if the solar generation is lower than the generation required for the Hotel load of the vessel, then the HP ESS is only used for the crane power demand. While, Figures 5.51 and 5.52 show that if the solar generation is overabundant compared to the load required, then the HP ESS is also used to lower the opex during the day a little by discharging during the moment that PV power dips below what is required by the vessel power demand.
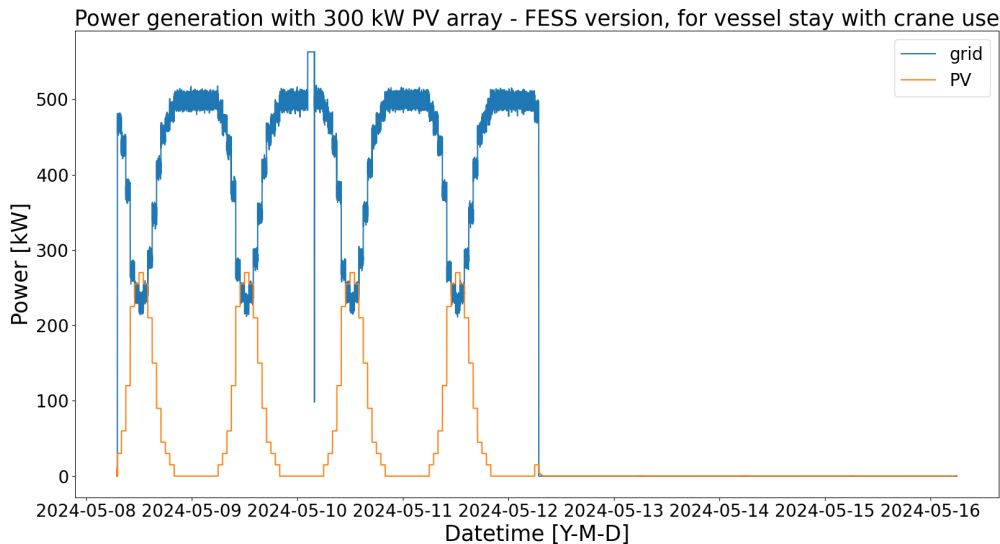
Figure 5.49: Figure of the power generation, including the grid power and a 300 kW PV array. The power is supplied to the vessel power demand of Figure 5.48.
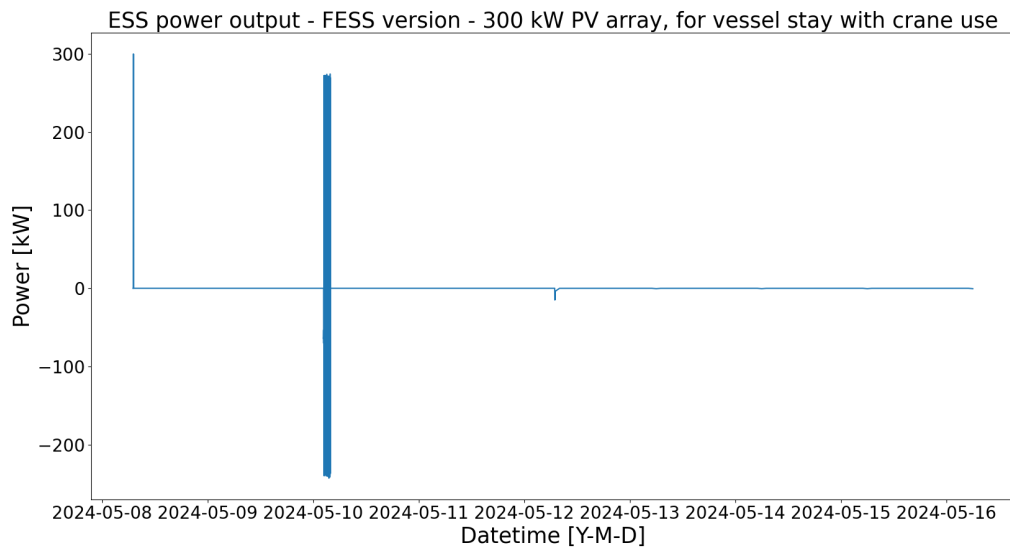
Figure 5.50: Figure of the power output of the FESS in the HP PV shore power configuration for the power demand of Figure 5.48. A 300 kW PV array is included in the configuration.
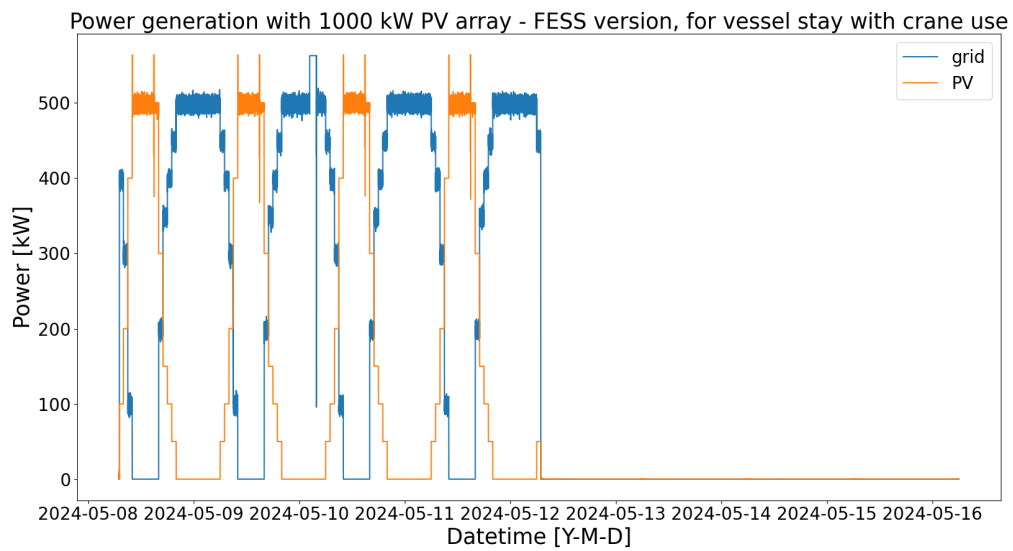
Figure 5.51: Figure of the power generation, including the grid power and a 1000 kW PV array. The power is supplied to the vessel power demand of Figure 5.48.
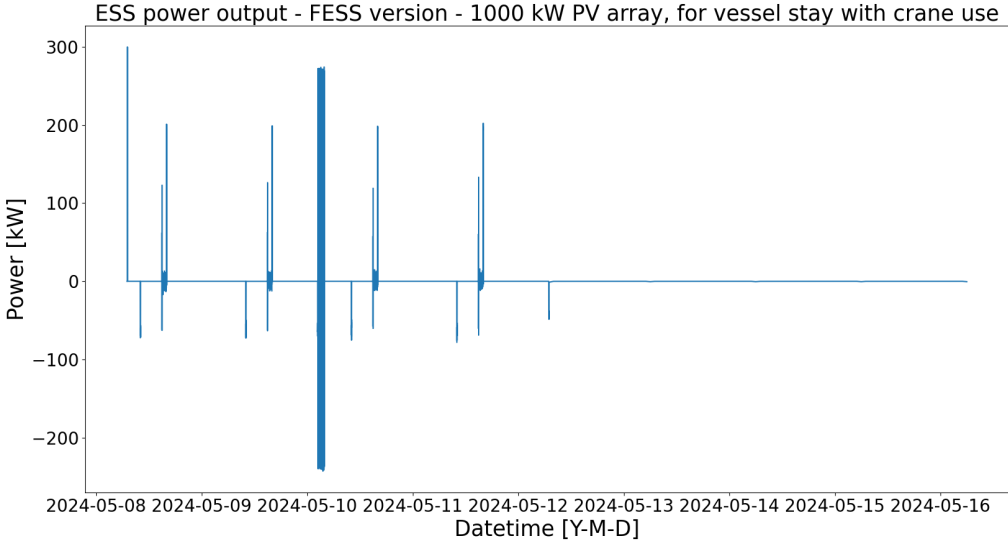
Figure 5.52: Figure of the power output of the FESS in the HP PV shore power configuration for the power demand of Figure 5.48. A 1000 kW PV array is included in the configuration.
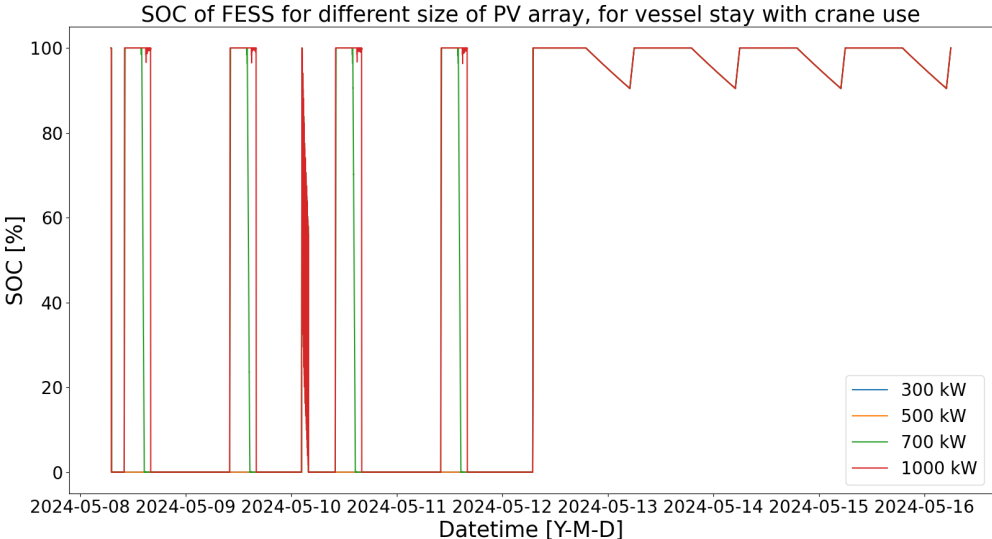
Figure 5.53: Figure of the SOC of the FESS in the HP PV shore power configuration. The SOC is differentiated according to the different sizes of PV array.

5.5. Validation

It is crucial that all the results so far are true optimal results. So, this section clarifies whether HE ESS should not be used for crane uses, by doing a cost analysis compared to Section 4.3 to check whether the split between HE and HP is necessary. And then the validity of the optimal solutions so far is tested.

5.5.1. HE vs HP

To test the validity of separating the HE ESS from the HP ESS, both the HE shore power configuration and the HP shore power configuration are used to optimize for the vessel power profile shown in Figure 5.54. Where 30 consecutive crane uses are included.
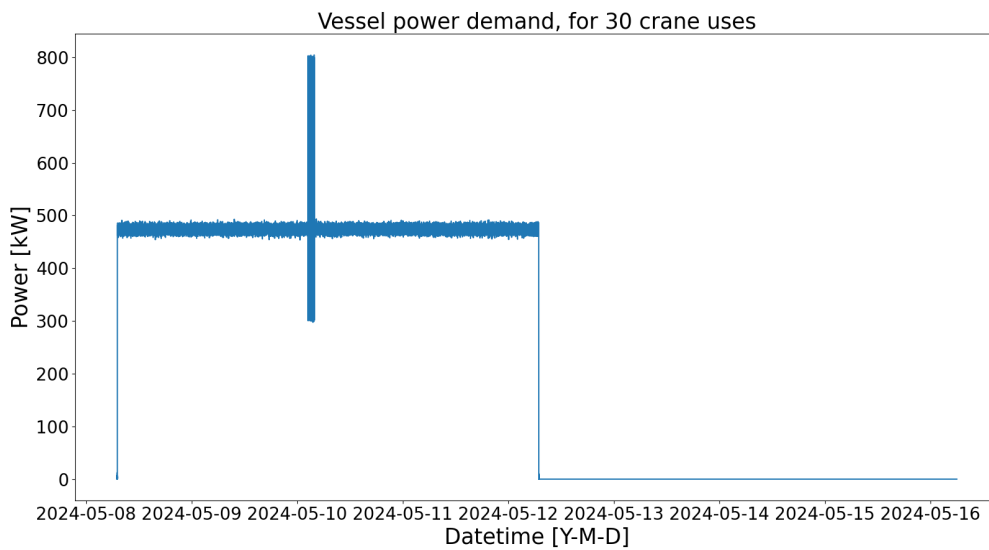
Figure 5.54: Figure of a vessel power profile for 4 days of shore power and 4 days of downtime. The power demand includes 30 consecutive crane uses. The x-axis is in datetime so each data point is fixed to a particular date and time.

The full results can be found in Table 5.37, it covers the shore power converter size, ESS size and most importantly the costs as those determine the optimal solution. FESS remains the best option when a crane is included, however the next most cost-effective options are with LFP and then NMC. Followed by LTO, then Na-ion and finally SC. This does not include the additional costs due to degradation of the ESS over the lifetime of the shore power system. According to Table 4.4 the NMC battery needs to be replaced every 3 years and even sooner according to the degradation from crane uses. This means an additional 71,253.2 [euro] every 3 years. So, over 15 years of use that is an additional 285,012.8 [euro]. Similarly, due to degradation the LFP battery will need to be replaced about every 5 years as mentioned in Section 5.1.1, which adds 59,132.5 [euro] every time or 118,265 [euro] over 15 years of use. The Na-ion battery would need to be replaced once after about 8 years in a 15 year times span of use, resulting in an additional 124,024 [euro]. Finally, the SC also has a short lifetime. Even though it can take an near infinite number of uses it is less able to withstand the degradation due to time. It will need to be replaced after about 10 years, costing an additional 89,372 [euro]. LTO and FESS both have the life time and life cycle to still be operational after 15 years without replacement. Although, FESS will need some maintenance every year.

Table 5.38 shows the final CAPEX for 15 years of the different shore power configurations using a single ESS, either HE or HP. It also includes the relative cost reduction in CAPEX still achieved over that lifetime compared to the optimal status quo solution. Here, the NMC version is not longer even a better option than the status quo and Na-ion or SC do not improve the cost-effectiveness by much. The LFP version remains a decent option, while FESS and LTO are the most cost-effective options for

supplying shore power to a vessel with crane use.

Table 5.37: Table with the optimal results for all ESS for the vessel power profile of Figure 5.54.

	shore power converter size	ESS size	CAPEX	OPEX
LFP	495.7 [kW]	337.9 [kW] & 337.9 [kWh]	935,155 [euro]	12204 [euro
NMC	497.6 [kW]	336.1 [kW] & 168.1 [kWh]	941,440 [euro]	12203 [euro]
Na	498.5 [kW]	335.2 [kW] & 167.6 [kWh]	994,668 [euro]	12205 [euro]
LTO	547.0 [kW]	285.0 [kW] & 28.5 [kWh]	977,129 [euro]	12204 [euro]
SC	567.7 [kW]	265.2 [kW] & 4.1 [kWh]	1,019,337 [euro]	12204 [euro]
FESS	563.8 [kW]	300.0 [kW] & 5.0 [kWh]	931,024 [euro]	12205 [euro]

Table 5.38: Table of the true CAPEX over 15 years of each shore power configuration using either just HE ESS or just HP ESS. The table also includes the cost reduction relative to the status quo.

	15 year CAPEX	relative cost reduction
Status quo	1,155,197 [euro]	-
LFP	1,053,420 [euro]	-8.81%
NMC	1,226,454 [euro]	+6.17%
Na	1,118,692 [euro]	-3.16%
LTO	977,129 [euro]	-15.41%
SC	1,108,709 [euro]	-4.02%
FESS	953,524 [euro]	-17.46%

5.5.2. Optimization algorithm

To check whether the results so far were really the optimal results, the ESS included in a shore power configuration is forced to be either a bit smaller or larger than the optimal solution presented before. Only a couple tests were done as test samples instead of checking every result. Table 5.39 shows that the optimal result for the LFP version of the HE ESS shore power configuration given in Section 5.1.2 is indeed the optimal result for that implementation for a vessel power profile of a single day with no crane use.

Table 5.40 shows that the optimal result for the FESS version of the HP ESS shore power configuration given in Section 5.2 is indeed the optimal result for that implementation for a vessel power profile of 4 days and 4 days of downtime where 30 consecutive crane uses are included.

And finally Table 5.41 shows that the optimal result for the LFP version of the HE PV shore power configuration with a 300 kW PV array given in Section 5.4.2 is indeed the optimal result for that implementation for a vessel power profile of a single day with no crane use.

Table 5.39: Table showing 2 less optimal results and the optimal solution for the HE ESS shore power configuration for a vessel power profile without crane use. For the less optimal solutions the capacity of the LFP battery was forced either lower or higher than the optimal solution from Section 5.1.2

LFP power capacity	CAPEX
15.0 [kW]	681,566 [euro]
17.95 [kW]	677,984 [euro]
20.0 [kW]	678,450 [euro]

Table 5.40: Table showing 2 less optimal results and the optimal solution for the HP ESS shore power configuration for a vessel power profile with 30 consecutive crane uses. For the less optimal solutions the capacity of the FESS was forced either lower or higher than the optimal solution from Section 5.2

FESS power capacity	CAPEX
250.0 [kW]	960,818 [euro]
300.0 [kW]	913,204 [euro]
350.0 [kW]	937,204 [euro]

Table 5.41: Table showing 2 less optimal results and the optimal solution for the HE PV shore power configuration with 300 kW PV array for a vessel power profile without crane use. For the less optimal solutions the capacity of the LFP battery was forced either lower or higher than the optimal solution from Section 5.4.2

LFP power capacity	CAPEX
15.0 [kW]	1,211.009 [euro]
17.95 [kW]	1,210,126 [euro]
20.0 [kW]	1,210,824 [euro]

5.6. Summary

This chapter covers the results of this research. Covering the non-existing effect that the length of time a vessel stays has on the sizing of the HE ESS, once the vessel stays for 1 day or longer. Followed by the effect that an increasing number of crane uses has on the sizing of the HP ESS, or the P_{nom} of the crane at which the FESS becomes more cost-effective than the LTO battery implementation. Finally, this chapter covers the length of time it takes for the PV array to become cost-effective. And this chapter explains how PV power does not affect the sizing of any of the other components of the shore power system. PV power only lowers the OPEX of the system by supplying free electricity during the day.

Part III

Conclusion

This chapter aims to conclude the thesis set out by the research question(s) formulated in the Introduction. The conclusion is based on the results presented in Chapter 5. The conclusion is followed by recommendations about future work in Section 6.2.

6.1. Conclusion

The CO_2 emissions of vessels in ports needs to be lowered according to the IMO and the municipalities of many these ports. Methods for lowering these emissions include: cleaner or alternative fuels, full electric vessels, lowering the vessel's speed and shore power. This thesis aimed to investigate the cost-effectiveness of different configurations for supplying shore power. Therefore, the main research question can be answered.

"What is the most cost-effective method and configuration to deliver shore power to vessels at the quay-side of Royal Roos"

This thesis developed an optimization algorithm based on cost optimization to answer this question. This includes multiple shore power configurations and multiple docking scenarios to investigate these shore power configurations. The results for this shore power configurations were compared to the status quo for shore power supply, and the different versions of each configuration were also compared against each other to draw conclusions. The sub-questions of this thesis assist in answering the main research question and explaining the conclusions.

1: - *"What effect does adding HE ESS have on the cost-effectiveness of supplying shore power?"*

The split between HE ESS and HP ESS based on the number of cycles the ESS can withstand is validated by Section 5.5. So, if this split is enforced as is done Section 5.1.2, where the HE ESS can only be used for long term energy storage, then the lowered costs only amount to 1-2 percent compared to the status quo. Furthermore, the ESS is charged and discharged with highly fluctuating and low energy pulses. These power fluctuations can be more easily and cheaply taken care of by adding capacitors to the DC-bus of the shore power converter. This optimal behaviour does not change in the range of time for the vessel to stay that is investigated in this research. Which means that adding HE ESS to the shore power configuration has little effect on the cost-effectiveness of supplying shore power to vessels, under the conditions and considerations discussed in Section 3.2. This is why the Hybrid ESS shore power configuration and Hybrid ESS PV shore power configuration were not researched in this thesis.

2: - *"What effect does adding HP ESS have on the cost-effectiveness of supplying shore power?"*

The effect of adding HP ESS to the shore power system is investigated in Section 5.2 and Section 5.3. From both these sections it is clear that adding HP ESS to the shore power system, when there is ship's crane that needs to be used, reduces the cost of the whole system significantly. Even if the crane needs to be used very consistently and frequently the sizing of the ESS does not need to change. All three versions: LTO, SC and FESS reduce the costs of the systems, but Section 5.5 makes clear that SC is a less optimal implementation compared to LTO or FESS. Where, the FESS implementation is the most cost-effective version. Especially, if the crane is big (200 kW or more) and needs to lift heavy loads (so full power demand).

3: - *"What effect does adding Alternative Power Supply have on the cost-effectiveness of supplying shore power?"*

The effect that alternative power supply in the form of solar power has on shore power supply is discussed in Section 5.4. It is clear that the addition of a PV array has no influence on the sizing of any of the other components of the shore power system, when utilized according to the considerations from Section 3.2. Neither HE ESS nor HP ESS is affected by the addition of a PV array no matter the size. Nor does it matter if the PV array is connected on the grid side or the inverter side of the shore power

converter. This does not mean that the optimal solutions is completely unaffected by the addition of a PV array. The optimal power flow does change as there is free power available when the sun is out and this means that the ESS might be charged at different times, compared to the shore power configuration without PV, to take advantage of this free electricity as shown by Figure 5.53. It is clear from Section 5.4.1 that the cost-effectiveness of PV heavily depends on the occupation rate of the quay-side by vessels with a hotel load that is at least as high or more as the amount of power the PV array is able to produce. In fact, as Table 5.22 shows, at around an occupation rate of 25% or lower the time it takes for the PV array to break even is over 20 years. The lifetime of most PV panels is around 20 years, so if an occupation rate higher than 25% can not be guaranteed then the addition of PV power for the supply of shore power is not cost-effective.

4: - *"What effect do different ratios of hotel load versus peak power demand of the vessel have on the sizing and type of the ESS?"*

The peak power demand of a vessel is achieved by the crane power demand on top of the hotel load of the vessel. The different ratios between hotel load and peak power demand have been investigated by increasing the P_{nom} of the crane in Section 5.3. As Section 5.3 shows, the lower that the ratio between hotel load and peak power demand becomes, the greater the cost reduction is possible by implementing a HP ESS shore power configuration over the status quo. Furthermore, the higher the P_{nom} of the crane, the more that the FESS version overtakes the LTO version in cost-effectiveness. This is because the FESS can be optimized for nominal power independently of energy capacity. So, while the cost for a single flywheel module is high, the cost of scaling the electric motor-generator that interfaces between the flywheel and the rest of the system is quite low. This means that it is not cost-effective to implement the FESS with lower crane $P_{[}nom]$, instead the LTO version is more cost-effective. However, if the crane P_{nom} is lower, then the benefit of the HP ESS shore power configuration over the status quo configuration is also smaller.

5: - *"How do different docking scenarios for vessels affect the different shore power configurations?"*

The length of time that a vessel stay beyond 1 day has little influence on the HE ESS shore power configuration, as shown in Section 5.1.2. Similarly, for the HP ESS shore power configuration, that is only used to peak shave the power demand of the crane uses, the length of time that a vessel stays is irrelevant to the sizing of the HP ESS. Section 5.4 shows that this is true whether PV is added to the shore power configuration or not. The amount of consecutive crane uses is largely irrelevant for the SC and FESS versions of the HP ESS shore power configuration according to Section 5.2. This is not the case for the LTO version of the HP ESS shore power configuration, but even more so for the HE ESS if they were used for peak-shaving of the crane power demand. The HE ESS optimal solution would behave similarly to the LTO optimal solution in Section 5.2, where the more crane uses there are the smaller the ESS is sized and the larger the shore power converter is sized. Furthermore, the degradation of the HE ESS would also quickly increase with the greater amount of crane uses. The length of time estimated in Section 5.5 before the ESS needs to be replaced is based on an average of 50 crane uses per month. If this number increases beyond that, then the HE ESS needs to be replaced even more frequently, making the HE ESS shore power configuration no longer cost-effective at all.

6: - *"How do the different shore power configurations differ in capital cost and operational cost in comparison to the 'status quo'?"*

As Table 5.38 shows the addition of any ESS except NMC always lowers the CAPEX compared to the status quo. So, both the HE ESS shore power configuration and the HP ESS shore power configuration lower the capital investment cost compared to the status quo. These two shore power configuration do not lower the operational cost as is shown throughout Chapter 5. The addition of ESS instead increases the operational cost, however this increase is very marginal and is negligible compared to the decrease in CAPEX.

Shore power configurations that include PV power increase the capital cost significantly compared to the status quo as shown by Table 5.35, due to the CAPEX of the added PV array. The addition of

PV power does lower the operational cost of the shore power system as shown by Table 5.36. This relationship with increased CAPEX and decreased OPEX holds for every shore power configuration with PV power. It holds for the Basic PV configuration of Section 5.4.1, the HE PV configuration of Section 5.4.2 and also the HP PV configuration of Section 5.4.4.

6.1.1. Recommended configuration and implementation

The most promising shore power configuration is the HP ESS shore power configuration, shown in Figure 6.55. So long as there is a crane aboard the vessel and the crane needs to be used, then it is better to implement the HP ESS shore power configuration over the status quo. If the crane does not need to be used much and is still small, it would still be possible to switch to a HE ESS shore power configuration using LFP. However, if the crane does not to be used a lot, then it is better to implement the HP ESS shore power configuration with LTO. If the P_{nom} is about 200 kW or more it is better to switch to the FESS version of the HP ESS shore power configuration.
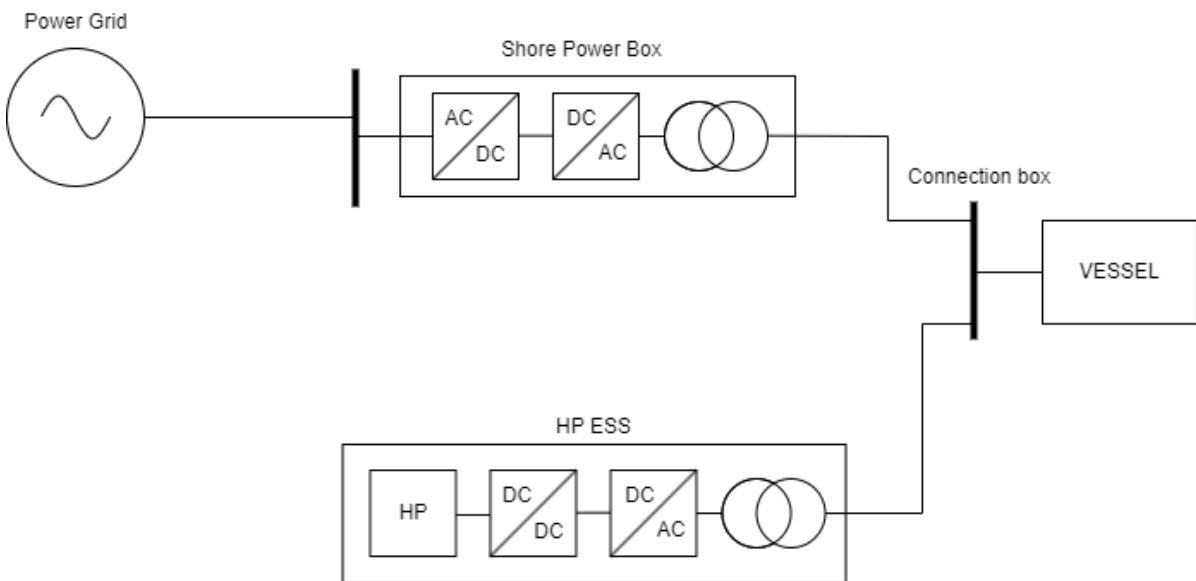
Figure 6.55: Diagram of the HP ESS shore power configuration

The addition of PV power turning this configuration in the HP PV shore power configuration shown in Figure 6.56 is viable if sufficient time of the year is spent supplying shore power to a vessel. If the occupation rate is not above 25% then the PV power will never be a profitable addition to the shore power system. Simply, because supplying power back to the grid at times of high solar irradiation will lead to losses as the electricity price will be negative. This does not mean other load can not be supplied with power by the PV array. Bi-lateral agreements can be made with businesses locally that take power if there is no vessel that requires shore power. This is outside the research of this thesis, but this would also increase the viability of including PV power into the shore power system, by essentially subsidizing some of the capital cost of the PV array.
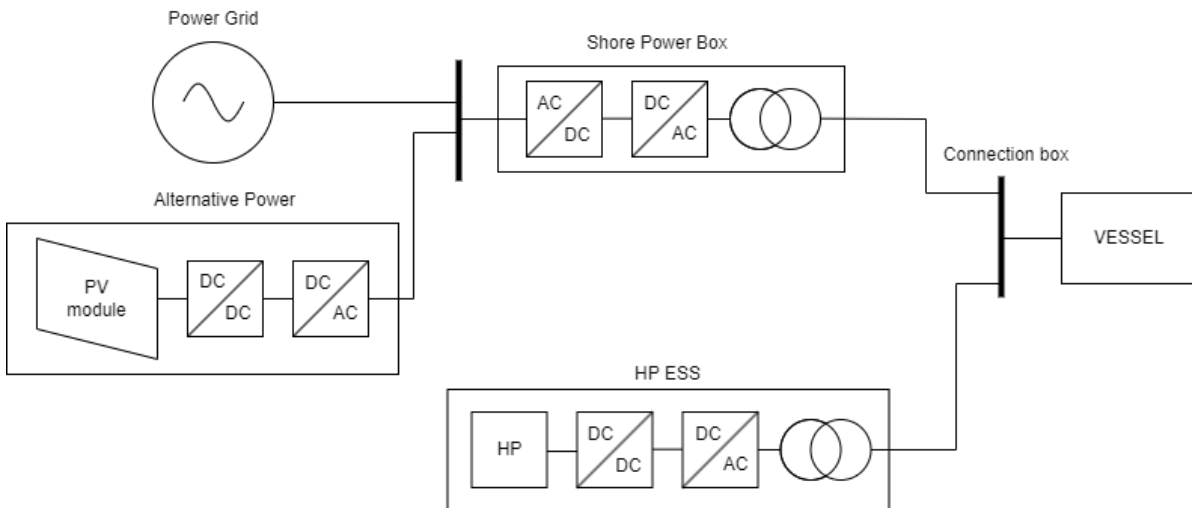
Figure 6.56: Diagram of the HP PV shore power configuration

6.2. Recommendations for future research and work

This research is not all encompassing in terms of shore power supply possibilities and it is also limited in many ways by the considerations that had to be made in Section 3.2. This section explores the challenges that limited the research and then I, as the author, give my advice on how to overcome some of the challenges and I recommend further areas of study to improve the accuracy and viability of this research.

6.2.1. Challenges & Limitations

The main challenge faced by this research was the way data had to be used for the optimization. There is essentially two types of input data required by the optimization tool that was created for this research.

- The vessel power profile
- The cost of the different components of the shore power system

Neither of these is that accurate in this research.

The vessel power profile used in this research was created from nominal power values of the hotel load and crane load of a specific vessel. This was then used to construct a vessel power profile. It would have been much preferable if the a vessel power profile was simply available to be used, however no such data is currently available. As this thesis is being written MARIN [52] is conducting research to measure the power profile of each appliance on board a vessel and constructing the complete power profile of vessel. Once this research is published, and especially once this data is available or other data like it becomes publicly available this research can be done again. Using this data would remove a lot of the abstraction necessary in this thesis, the shore power scenarios could become much more varied and realistic. Meaning that this research can be repeated in a few years and it could completely invalidate the conclusions drawn in this thesis.

The costs that were used to calculate the optimal cost-effectiveness of the shore power configurations is based on the supposed linear relation of power capacity and cost of each component. No such relation is true. Furthermore, the price for a component can fluctuate very wildly. Not to mention that a battery manufacturer might give out a 20% discount through negotiations. So, the validity of final prices from the various optimal solutions is in doubt, not because the calculations made to reach them were faulty. But instead the baseline assumption of this fixed linear relationship between power capacity and cost is in doubt. To check this, it is necessary to go around several component manufacturers, for each component of the shore power system, and ask them for a quote on a component of the size calculated by the optimization model. Then go into negotiations to get the best price and then compare to the

original optimal solutions and use these new prices to calibrate the model more effectively.

Furthermore, the optimization method itself can also be called into question. Whether the optimization algorithm finds either a local or global optimum is not completely certain. The optimization algorithm is able to find the global optimum, instead of just a local optimum, within the dataset and problem definition that it is given. However, these results still need to be judged and interpreted by someone with expertise regarding the research. This is because the way a dataset is used and how the problem is defined greatly influences the result that is optimized for. Which means that the optimal result that is calculated can not be a real solution for the real world problem that the optimization problem is based on. This is why so many different simulations were done, where the vessel power profile changed slightly. Because comparison between these results allows for more concrete analysis and more nuanced conclusions. In order to remedy the uncertainty regarding results of this optimization algorithm, it is necessary to do an in depth comparison to other optimization techniques. If this problem were repeated with other optimization techniques a better understanding could be reached, with less uncertainty regarding the results.

Finally, the distinction between HE ESS and HP ESS in this research is based on the assumption that a single crane use degrades the lifetime of an ESS the same amount as a full charge and discharge of the ESS. This is likely not true, but it would degrade the ESS to some extent. So, to find out how much crane uses would degrade an ESS, if that ESS is used to peak shave the power demand of that crane, experimental testing would need to be done. Which is research separate from supplying shore power, but it would be very relevant to the validity of the methodology of this research.

6.2.2. Further recommendations

HE ESS seems as a rather lack luster addition to shore power systems according to this thesis. However, that is not always necessarily so. It is instead the outcome of the consideration and boundaries of the research presented in Section 3.2. If a vessel stays for a day or longer then HE ESS does not add any benefit to the shore power system, but not every terminal is a terminal where repairs are done. At a container terminal a vessel might only stay for a few hours to unload some of the cargo before it leaves again. These vessels need to keep transporting cargo continuously to make enough money. So an interesting area of further research would be to investigate the types of operations done at various (different types of) terminals and research how the optimal shore power configuration might change for that terminal compared to the optimal solution found in this thesis.

PV power (or any other form of alternative power supply) also does not seem that feasible, because of the requirement for a guarantee of power demand necessary to make it viable. However, this due to the fact that the grid connection at Royal Roos is sufficiently sized to accommodate any vessel that requires shore power. 1700 kW is sufficient power even for larger vessel than discussed in this thesis. Furthermore, the area of the grid that Royal Roos is connected to does not currently experience grid congestion in terms of demand, instead solar power production is overabundant. But this is not the case everywhere, and it could also change for Royal Roos in the future. In a scenario where the amount of grid power is available is not sufficient for shore power, either because the grid connection is limited in capacity or because time-dependent grid congestion is present, the addition of PV power to the shore power system might become a necessity. So a further area of research would be under which conditions does PV power become a requirement for shore power supply instead of a possible detriment. This also includes HE ESS to make the PV power more reliable by helping with long term peak-shaving.

6.2.3. Optimization tool improvement

As mentioned, it would be a good idea to re-do this research once accurate data of a vessel power profile becomes available. The optimization tool that was made for this research would need to be modified only very slightly to use this data. So that does not pose significant difficulty.

The tool should be able to use reactive power measurements as well as active power measurements, but it has only been tested using active power, so that is still a grey area. Additionally, the optimization

tool would be improved with better calibration for the prices of the different components.

The current implementation of the optimization tool, does not take into account the physical limitations of the different ESS, like response time or the lifetime. Instead the only differentiation between HE ESS and HP ESS, for the optimization tool, is the cost per kW and the associated kWh of energy. This is partially because of the simulation time being only a couple days so far, but this can be improved to make better optimization that is based on the true CAPEX over the lifetime of the system and the response time of the ESS.

Other than that, improvement would come in terms of usability. Right now the optimization tool has no user interface other than a python editor. So, a graphical user interface would make the tool more accessible to others, although creating other shore power configurations than those used in this research would still require a familiarity with python and the PYPSA python package.

References

[1] Mahmoud S. Abdelrahman, Hossam Hussein, and Osama A. Mohammed. "Rule-Based Power and Energy Management System For Shipboard Microgrid With HESS To Mitigate Propulsion and Pulsed Load Fluctuations". In: *2023 IEEE Green Technologies Conference (GreenTech)*. 2023, pp. 224–228. DOI: `10.1109/GreenTech56823.2023.10173813`.

[2] A Abhyankar. *Feasibility of Bipolar DC Grids on Ships*. 2023.

[3] Kate Abnett. *Global CO2 emissions from fossil fuels to hit record high in 2023-report*. 2023. URL: `https://www.reuters.com/business/environment/global-co2-emissions-fossil-fuels-hit-record-high-2023-report-2023-12-05/` (visited on 01/04/2024).

[4] Bukola Babatunde Adetokun, Oghenewvogaga Oghorada, and Sufyan Ja'afar Abubakar. "Superconducting magnetic energy storage systems: Prospects and challenges for renewable energy applications". In: *Journal of Energy Storage* 55 (2022), p. 105663. ISSN: 2352-152X. DOI: `https://doi.org/10.1016/j.est.2022.105663`. URL: `https://www.sciencedirect.com/science/article/pii/S2352152X22016516`.

[5] International Renewable Energy Agency. "Electricity Storage and Renewables: Costs and Markets to 2030". In: *IRENA (2017)* (2017). URL: `https://www.irena.org/-/media/Files/IRENA/Agency/Publication/2017/Oct/IRENA_Electricity_Storage_Costs_2017.pdf?rev=a264707cb8034a52b6f6123d5f1b1148`.

[6] Mohsen Akbarzadeh, Jasper De Smet, and Jeroen Stuyts. "Battery Hybrid Energy Storage Systems for Full-Electric Marine Applications". In: *Processes* 10.11 (2022). ISSN: 2227-9717. DOI: `10.3390/pr10112418`. URL: `https://www.mdpi.com/2227-9717/10/11/2418`.

[7] Satyajith Amaran et al. "Simulation optimization: a review of algorithms and applications". In: *Annals of Operations Research* 240.1 (May 2016), pp. 351–380. ISSN: 1572-9338. DOI: `10.1007/s10479-015-2019-x`. URL: `https://doi.org/10.1007/s10479-015-2019-x`.

[8] A.A. Khodadoost Arani et al. "Review of Flywheel Energy Storage Systems structures and applications in power systems and microgrids". In: *Renewable and Sustainable Energy Reviews* 69 (2017), pp. 9–18. ISSN: 1364-0321. DOI: `https://doi.org/10.1016/j.rser.2016.11.166`. URL: `https://www.sciencedirect.com/science/article/pii/S1364032116309054`.

[9] Muhammad Arshad and Brendan O'Kelly. "Global status of wind power generation: theory, practice, and challenges". In: *International Journal of Green Energy* 16.14 (2019), pp. 1073–1090. DOI: `10.1080/15435075.2019.1597369`. URL: `https://doi.org/10.1080/15435075.2019.1597369`.

[10] Muhammad Ashraf et al. "Recent Trends in Sustainable Solar Energy Conversion Technologies: Mechanisms, Prospects, and Challenges". In: *Energy & Fuels* 37.9 (2023), pp. 6283–6301. DOI: `10.1021/acs.energyfuels.2c04077`. URL: `https://doi.org/10.1021/acs.energyfuels.2c04077`.

[11] Thanikanti Sudhakar Babu et al. "A Comprehensive Review of Hybrid Energy Storage Systems: Converter Topologies, Control Strategies and Future Prospects". In: *IEEE Access* 8 (2020), pp. 148702–148721. DOI: `10.1109/ACCESS.2020.3015919`.

[12] Faisal R. Badal et al. "A Survey on Control Issues in Renewable Energy Integration and Microgrid". In: *Protection and Control of Modern Power Systems* 4.1 (2019), pp. 1–27. DOI: `10.1186/s41601-019-0122-8`.

[13] Askari Mohammad Bagher, Mirzaei Mahmoud Abadi Vahid, and Mirhabibi Mohsen. "Types of solar cells and application". In: *American Journal of optics and Photonics* 3.5 (2015), pp. 94–113.

[14] Andrew Blakers et al. "A review of pumped hydro energy storage". In: *Progress in Energy* 3.2 (Mar. 2021), p. 022003. DOI: `10.1088/2516-1083/abeb5b`. URL: `https://dx.doi.org/10.1088/2516-1083/abeb5b`.

[15] *BMOD0165 P048 C08 Datasheet*. 300149-EN.9. Maxwell Technologies. URL: `https://maxwell.com/wp-content/uploads/2023/02/3001491-EN.9_DS_48V-165F-C0B-BMOD0165-P048_20230116.pdf`.

[16] Thilo Bocklisch. "Hybrid Energy Storage Systems for Renewable Energy Applications". In: *Energy Procedia* 73 (2015). 9th International Renewable Energy Storage Conference, IRES 2015, pp. 103–111. ISSN: 1876-6102. DOI: `https://doi.org/10.1016/j.egypro.2015.07.582`. URL: `https://www.sciencedirect.com/science/article/pii/S1876610215013508`.

[17] Emiliano Borri et al. "A review on liquid air energy storage: History, state of the art and recent developments". In: *Renewable and Sustainable Energy Reviews* 137 (2021), p. 110572. ISSN: 1364-0321. DOI: `https://doi.org/10.1016/j.rser.2020.110572`. URL: `https://www.sciencedirect.com/science/article/pii/S1364032120308571`.

[18] Christian Breyer and et al. "On the History and Future of 100% Renewable Energy Systems Research". In: *IEEE Access* 10 (2022). DOI: `10.1109/ACCESS.2022.3193402`.

[19] T. Brown, J. Hörsch, and D. Schlachtberger. "PyPSA: Python for Power System Analysis". In: *Journal of Open Research Software* 6.4 (1 2018). DOI: `10.5334/jors.188`. eprint: `1707.09913`. URL: `https://doi.org/10.5334/jors.188`.

[20] cenit, WPCAP, and Port de Barcelona. *POWER-TO-SHIP (P2S)/ONSHORE POWER SUPPLY (OPS) QUESTIONNAIRE RESULTS*. 2023. URL: `https://sustainableworldports.org/wp-content/uploads/On_shore_power_supply_summary-surveys_final.pdf`.

[21] Shimiao Chen et al. "Reviews On Inertia Emulation Technology With Power Electronics". In: *2020 IEEE Energy Conversion Congress and Exposition (ECCE)*. 2020, pp. 2101–2107. DOI: `10.1109/ECCE44975.2020.9236033`.

[22] Subhashree Choudhury. "Review of energy storage system technologies integration to microgrid: Types, control strategies, issues, and future prospects". In: *Journal of Energy Storage* 48 (2022), p. 103966. ISSN: 2352-152X. DOI: `https://doi.org/10.1016/j.est.2022.103966`. URL: `https://www.sciencedirect.com/science/article/pii/S2352152X22000147`.

[23] Animalia-life club. *Single Solar Panel*. 2019. URL: `https://animalia-life.club/qa/pictures/single-solar-panel` (visited on 02/12/2024).

[24] Charlotte Cockle et al. *WIND ENERGY ENGINEERING: A Handbook For Onshore And Offshore Wind Turbines, 2ND EDITION*. Elsevier Inc., 2023.

[25] European Comission. *Scope of the EU Emissions Trading System*. 2023. URL: `https://climate.ec.europa.eu/eu-action/eu-emissions-trading-system-eu-ets/scope-eu-emissions-trading-system_en` (visited on 01/16/2024).

[26] Commee. *Havenkaart Rotterdam*. 2017. URL: `https://www.commee.nl/stadsplattegronden/92-havenkaart-rotterdam-125000.html` (visited on 02/14/2024).

[27] European Commission. "REPORT FROM THE COMMISSION TO THE EUROPEAN PARLIAMENT AND THE COUNCIL". In: *2023 Report on Energy Subsidies in th EU* (2023), pp. 1–17.

[28] European Commission et al. *Wind potentials for EU and neighbouring countries – Input datasets for the JRC-EU-TIMES model*. Publications Office, 2018. DOI: `doi/10.2760/041705`.

[29] PyPSA Community. *PyPSA Website*. 2018. URL: `https://pypsa.org/#home` (visited on 05/30/2024).

[30] Toshiba Corporation. *High-power type cells | SCiB*. 2024. URL: `https://www.global.toshiba/ww/products-solutions/battery/scib/product/cell/high-power.html` (visited on 05/31/2024).

[31] Mugdha V Dambhare, Bhavana Butey, and SV Moharil. "Solar photovoltaic technology: A review of different types of solar cells and its future trends". In: *Journal of Physics: Conference Series*. Vol. 1913. 1. IOP Publishing. 2021, p. 012053.

[32] Marie-Alix Dupré la Tour. "Photovoltaic and wind energy potential in Europe – A systematic review". In: *Renewable and Sustainable Energy Reviews* 179 (2023), p. 113189. ISSN: 1364-0321. DOI: `https://doi.org/10.1016/j.rser.2023.113189`. URL: `https://www.sciencedirect.com/science/article/pii/S136403212300045X`.

[33] *Elektriciteit TARIEVEN 2024*. Aansluiting en transport voor grootverbruikers. STEDIN.

[34] *ELERIX EX-L110 High Power LFP Cell*. EX-L110. ELERIX. URL: `https://files.gwl.eu/inc/_doc/attach/StoItem/7872/ELERIX-EX-L110-QuickDatasheet.pdf`.

[35] EMSA. *Shore-Side Electricity (SSE)*. 2024. URL: `https://emsa.europa.eu/electrification/sse.html` (visited on 07/08/2024).

[36] Acculon Energy. *Sodium-ion*. 2024. URL: `https://acculonenergy.com/core-components/#sodium24` (visited on 05/31/2024).

[37] Ehsan Farrokhi, Hoda Ghoreishy, and Roya Ahmadi Ahangar. "Optimization-based power management for battery/supercapacitor hybrid energy storage system with load estimation capability in a DC microgrid". In: *International Journal of Electrical Power & Energy Systems* 155 (2024), p. 109665. ISSN: 0142-0615. DOI: `https://doi.org/10.1016/j.ijepes.2023.109665`. URL: `https://www.sciencedirect.com/science/article/pii/S0142061523007226`.

[38] Pengfei Gao et al. "Optimization of Hybrid Energy Storage System Sizing With Considering Energy Management Strategy for High-Power Pulsed Load in Aircraft". In: *IEEE TRANSACTIONS ON VEHICULAR TECHNOLOGY* (2023). DOI: `10.1109/TVT.2023.3228734`.

[39] Sergey German-Galkin and Dariusz Tarnapowicz. "Energy Optimization of the 'Shore to Ship' System—A Universal Power System for Ships at Berth in a Port". In: *Sensors* 20.14 (2020). ISSN: 1424-8220. DOI: `10.3390/s20143815`. URL: `https://www.mdpi.com/1424-8220/20/14/3815`.

[40] Martin A. Green et al. "Solar cell efficiency tables (Version 60)". In: *Progress in Photovoltaics: Research and Applications* 30.7 (2022), pp. 687–701. DOI: `https://doi.org/10.1002/pip.3595`. eprint: `https://onlinelibrary.wiley.com/doi/pdf/10.1002/pip.3595`. URL: `https://onlinelibrary.wiley.com/doi/abs/10.1002/pip.3595`.

[41] Otto Haas and Elton J. Cairns. "Electrochemical energy storage". In: *Physical Chemistry Annual Reports* (1999).

[42] Salman Hajiaghasi, Ahmad Salemnia, and Mohsen Hamzeh. "Hybrid energy storage system for microgrids applications: A review". In: *Journal of Energy Storage* 21 (2019), pp. 543–570. ISSN: 2352-152X. DOI: `https://doi.org/10.1016/j.est.2018.12.017`. URL: `https://www.sciencedirect.com/science/article/pii/S2352152X18305188`.

[43] Qusay Hassan et al. "Hydrogen energy future: Advancements in storage technologies and implications for sustainability". In: *Journal of Energy Storage* 72 (2023), p. 108404. ISSN: 2352-152X. DOI: `https://doi.org/10.1016/j.est.2023.108404`. URL: `https://www.sciencedirect.com/science/article/pii/S2352152X23018017`.

[44] Frederick S. Hillier and Gerald J. Lieberman. *Introductions To Operations Research*. McGraw-Hill Publishing Company, 1991.

[45] Alexander Innes and Jason Monios. "Identifying the unique challenges of installing cold ironing at small and medium ports – The case of aberdeen". In: *Transportation Research Part D: Transport and Environment* 62 (2018), pp. 298–313. ISSN: 1361-9209. DOI: `https://doi.org/10.1016/j.trd.2018.02.004`. URL: `https://www.sciencedirect.com/science/article/pii/S1361920917309124`.

[46] Ehsanul Kabir et al. "Solar energy: Potential and future prospects". In: *Renewable and Sustainable Energy Reviews* 82 (2018), pp. 894–900. ISSN: 1364-0321. DOI: `https://doi.org/10.1016/j.rser.2017.09.094`. URL: `https://www.sciencedirect.com/science/article/pii/S1364032117313485`.

[47] Jagdesh Kumar, Lauri Kumpulainen, and Kimmo Kauhaniemi. "Technical design aspects of harbour area grid for shore to ship power: State of the art and future solutions". In: *International Journal of Electrical Power & Energy Systems* 104 (2019), pp. 840–852. ISSN: 0142-0615. DOI: `https://doi.org/10.1016/j.ijepes.2018.07.051`. URL: `https://www.sciencedirect.com/science/article/pii/S0142061517325231`.

[48] X. Li et al. "Chapter 8 - Zinc-based flow batteries for medium- and large-scale energy storage". In: *Advances in Batteries for Medium and Large-Scale Energy Storage*. Ed. by Chris Menictas, Maria Skyllas-Kazacos, and Tuti Mariana Lim. Woodhead Publishing Series in Energy. Woodhead Publishing, 2015, pp. 293–315. ISBN: 978-1-78242-013-2. DOI: `https://doi.org/10.1016/B978-1-78242-013-2.00008-X`. URL: `https://www.sciencedirect.com/science/article/pii/B978178242013200008X`.

[49] Jiawen Liu et al. "Pre-synchronization Control of Port Shore Power Grid Connected Inverter Based on VSG". In: *2023 IEEE PELS Students and Young Professionals Symposium (SYPS)*. 2023, pp. 1–6. DOI: 10.1109/SYPS59767.2023.10268230.

[50] Jun Liu et al. "Study on Transient Stability of Ship-shore Alternating AC-DC Hybrid Power System". In: *2023 7th International Conference on Transportation Information and Safety (ICTIS)*. 2023, pp. 2393–2402. DOI: 10.1109/ICTIS60134.2023.10243861.

[51] Xing Luo et al. "Overview of current development in electrical energy storage technologies and the application potential in power system operation". In: *Applied Energy* 137 (2015), pp. 511–536. ISSN: 0306-2619. DOI: https://doi.org/10.1016/j.apenergy.2014.09.081. URL: https://www.sciencedirect.com/science/article/pii/S0306261914010290.

[52] MARIN. *Maritime Research Institue Netherlands*. 2024. URL: https://www.marin.nl/en (visited on 07/10/2024).

[53] S. Masoome Maroufi and Giovanni De Carne. "Optimal Design for Hybrid Energy Storage Systems Considering System Aging and Costs". In: *2023 IEEE 14th International Symposium on Power Electronics for Distributed Generation Systems (PEDG)*. 2023, pp. 496–500. DOI: 10.1109/PEDG56097.2023.10215260.

[54] A. Merkhouf, S. Upadhyay, and P. Doyon. "Variable frequency transformer - an overview". In: *2006 IEEE Power Engineering Society General Meeting*. 2006, 4 pp.-. DOI: 10.1109/PES.2006.1709639.

[55] J. Mitali, S. Dhinakaran, and A.A. Mohamad. "Energy storage systems: a review". In: *Energy Storage and Saving* 1.3 (2022), pp. 166–216. ISSN: 2772-6835. DOI: https://doi.org/10.1016/j.enss.2022.07.002. URL: https://www.sciencedirect.com/science/article/pii/S277268352200022X.

[56] Smita Mohanty, Anandarup Das, and Bhim Singh. "Virtual Inertia Control for CHB-STATCOM in a Power Electronics Dominated Grid". In: *IEEE Transactions on Industry Applications* 59.5 (2023), pp. 5517–5526. DOI: 10.1109/TIA.2023.3288855.

[57] Thomas Nemeth et al. "Lithium titanate oxide battery cells for high-power automotive applications – Electro-thermal properties, aging behavior and cost considerations". In: *Journal of Energy Storage* 31 (2020), p. 101656. ISSN: 2352-152X. DOI: https://doi.org/10.1016/j.est.2020.101656. URL: https://www.sciencedirect.com/science/article/pii/S2352152X20314936.

[58] RVO Netherlands Enterprise Agency. *Installing wind turbines*. 2023. URL: https://business.gov.nl/regulation/wind-turbines/ (visited on 02/08/2024).

[59] A.G. Olabi et al. "Critical review of energy storage systems". In: *Energy* 214 (2021), p. 118987. ISSN: 0360-5442. DOI: https://doi.org/10.1016/j.energy.2020.118987. URL: https://www.sciencedirect.com/science/article/pii/S0360544220320946.

[60] Vertrekhal Oranjelijn. *Kaart Vierhavengebied eo, 1993*. 2019. URL: http://vertrekhaloranjelijn.nl/historie/1993/367 (visited on 02/14/2024).

[61] International Maritime Organization. "ANY OTHER BUSINESS, Consolidated text draft interim guidelines on safe operation of onshore power supply (ONS) service in port for ships engaged on international voyages with draft modifications". In: *SUB-COMITTEE on SHIP SYSTEMS AND EQUIPMENT, 9th session, Agenda item 19* (2022), pp. 1–15.

[62] PVGIS. *Solar Energy Calculator and Mapping Tool*. 2024. URL: https://pvgis.com/ (visited on 06/21/2024).

[63] European Parliament Press Release. *MEPs ban cadmium from power tool batteries and mercury from button cells*. 2013. URL: https://www.europarl.europa.eu/news/en/press-room/20131004IPR21519/meps-ban-cadmium-from-power-tool-batteries-and-mercury-from-button-cells (visited on 02/15/2024).

[64] Port of Rotteram. *Research on shore-based power at terminals*. 2023. URL: https://www.portofrotterdam.com/en/port-future/energy-transition/ongoing-projects/shore-based-power-rotterdam/research-on-shore-based (visited on 01/16/2024).

[65] Port of Rotterdam. *Onderzoek aanleg walstroom bij terminals*. 2022. URL: `https://www.portofrotterdam.com/nl/haven-van-de-toekomst/energietransitie/lopende-projecten/walstroom-rotterdam/onderzoek-aanleg` (visited on 07/25/2024).

[66] Mustafa Ergin Şahin, Frede Blaabjerg, and Ariya Sangwongwanich. "A Comprehensive Review on Supercapacitor Applications and Developments". In: *Energies* 15.3 (2022). ISSN: 1996-1073. DOI: `10.3390/en15030674`. URL: `https://www.mdpi.com/1996-1073/15/3/674`.

[67] Luckywell Seyitini, Basim Belgasim, and Christopher Chintua Enweremadu. "Solid state sensible heat storage technology for industrial applications – A review". In: *Journal of Energy Storage* 62 (2023), p. 106919. ISSN: 2352-152X. DOI: `https://doi.org/10.1016/j.est.2023.106919`. URL: `https://www.sciencedirect.com/science/article/pii/S2352152X2300316X`.

[68] Md Shafiullah, Shakir D. Ahmed, and Fahad A. Al-Sulaiman. "Grid Integration Challenges and Solution Strategies for Solar PV Systems: A Review". In: *IEEE Access* 10 (2022), pp. 52233–52257. DOI: `10.1109/ACCESS.2022.3174555`.

[69] Ltd. Shenzhen Westart Technology Co. *Westart NMC lithium battery cell*. 2009. URL: `https://szwestart.com/westart-ncm-pouch-cell-ws-ncm30ah-37v.html` (visited on 05/31/2024).

[70] Sustainable Ships. *Overview of Ports' Sustainable & Shore Power Ambitions*. 2023. URL: `https://www.sustainable-ships.org/stories/2023/overview-rules-regulations-ports` (visited on 01/16/2024).

[71] Arno Smets et al. *Solar Energy - The physics and engineering of photovoltaic conversion, technologies and systems*. Feb. 2016. ISBN: 9781906860325.

[72] Robert Smolenski et al. "Ship-to-Shore Versus Shore-to-Ship Synchronization Strategy". In: *IEEE Transactions on Energy Conversion* 33.4 (2018), pp. 1787–1796. DOI: `10.1109/TEC.2018.2839702`.

[73] GIGA Storage. *The Buffalo Battery*. 2022. URL: `https://giga-storage.com/en/projects/buffalo/` (visited on 01/22/2024).

[74] GIGA Storage. *The Rhino Battery*. 2020. URL: `https://giga-storage.com/en/projects/rhino/` (visited on 01/22/2024).

[75] QuinteQ energy storage. *The Flywheel*. 2023. URL: `https://quinteqenergy.com/product/` (visited on 05/31/2024).

[76] Gayathri Nair Sudha and Nilanjan Senroy. "A Unified Approach to the Sizing and Control of Energy Storage Systems". In: *Electric Power Components and Systems* 45.7 (2017), pp. 693–704. DOI: `10.1080/15325008.2017.1292568`. URL: `https://doi.org/10.1080/15325008.2017.1292568`.

[77] Liu Tao. *World's Largest Flow Battery Energy Storage Station Connected to Grid*. 2022. URL: `http://english.dicp.cas.cn/news/rn/202210/t20221018_321685.html` (visited on 01/25/2024).

[78] Muhammad Tawalbeh et al. "Environmental impacts of solar photovoltaic systems: A critical review of recent progress and future outlook". In: *Science of The Total Environment* 759 (2021), p. 143528. ISSN: 0048-9697. DOI: `https://doi.org/10.1016/j.scitotenv.2020.143528`. URL: `https://www.sciencedirect.com/science/article/pii/S0048969720370595`.

[79] Core Writing Team. *Climate Change 2023 Synthesis Report, A report of the Intergovernmental Panel on Climate Change*. 2023.

[80] Muhammad R. Usman. "Hydrogen storage methods: Review and current status". In: *Renewable and Sustainable Energy Reviews* 167 (2022), p. 112743. ISSN: 1364-0321. DOI: `https://doi.org/10.1016/j.rser.2022.112743`. URL: `https://www.sciencedirect.com/science/article/pii/S1364032122006311`.

[81] Selvamani Vadivel et al. "High-Performance Li-Ion Batteries Using Nickel-Rich Lithium Nickel Cobalt Aluminium Oxide–Nanocarbon Core–Shell Cathode: In Operando X-ray Diffraction". In: *ACS Applied Materials & Interfaces* 11.34 (2019). PMID: 31369226, pp. 30719–30727. DOI: `10.1021/acsami.9b06553`. URL: `https://doi.org/10.1021/acsami.9b06553`.

[82] S.F.J. Van Kleef. *A techno-economic analysis of the implementation of grid-connected battery energy storage systems into shore power installations in the port of Rotterdam*. 2023.

[83] Jidai Wang et al. "Overview of Compressed Air Energy Storage and Technology Development". In: *Energies* 10.7 (2017). ISSN: 1996-1073. URL: https://www.mdpi.com/1996-1073/10/7/991.

[84] Kai Wang et al. "Recent advances and historical developments of high voltage lithium cobalt oxide materials for rechargeable Li-ion batteries". In: *Journal of Power Sources* 460 (2020), p. 228062. ISSN: 0378-7753. DOI: https://doi.org/10.1016/j.jpowsour.2020.228062. URL: https://www.sciencedirect.com/science/article/pii/S0378775320303657.

[85] Tabbi Wilberforce et al. "Wind turbine concepts for domestic wind power generation at low wind quality sites". In: *Journal of Cleaner Production* 394 (2023), p. 136137. ISSN: 0959-6526. DOI: https://doi.org/10.1016/j.jclepro.2023.136137. URL: https://www.sciencedirect.com/science/article/pii/S0959652623002950.

[86] R. Winkel et al. "Shore Side Electricity in Europe: Potential and environmental benefits". In: *Energy Policy* 88 (2016), pp. 584–593. ISSN: 0301-4215. DOI: https://doi.org/10.1016/j.enpol.2015.07.013. URL: https://www.sciencedirect.com/science/article/pii/S0301421515300240.

[87] Dunzhu Xia et al. "Shore Power Optimal Scheduling Based on Gridding of Hybrid Energy Supply System". In: *Sustainability* 14.23 (2022). ISSN: 2071-1050. DOI: 10.3390/su142316250. URL: https://www.mdpi.com/2071-1050/14/23/16250.

[88] Chenxuan Xu et al. "Economic Analysis of Li-Ion Battery – Supercapacitor Hybrid Energy Storage System Considering Multitype Frequency Response Benefits in Power Systems". In: *Energies* 16.18 (2023). ISSN: 1996-1073. DOI: 10.3390/en16186621. URL: https://www.mdpi.com/1996-1073/16/18/6621.

[89] Meiling Yue et al. "Hydrogen energy systems: A critical review of technologies, applications, trends and challenges". In: *Renewable and Sustainable Energy Reviews* 146 (2021), p. 111180. ISSN: 1364-0321. DOI: https://doi.org/10.1016/j.rser.2021.111180. URL: https://www.sciencedirect.com/science/article/pii/S1364032121004688.

[90] Lei Zhang et al. "Multiobjective Optimal Sizing of Hybrid Energy Storage System for Electric Vehicles". In: *IEEE Transactions on Vehicular Technology* 67.2 (2018), pp. 1027–1035. DOI: 10.1109/TVT.2017.2762368.

[91] Ziyu Zhang et al. "A review of technologies and applications on versatile energy storage systems". In: *Renewable and Sustainable Energy Reviews* 148 (2021), p. 111263. ISSN: 1364-0321. DOI: https://doi.org/10.1016/j.rser.2021.111263. URL: https://www.sciencedirect.com/science/article/pii/S1364032121005505.

[92] Lina Zhao et al. "Engineering of Sodium-Ion Batteries: Opportunities and Challenges". In: *Engineering* 24 (2023), pp. 172–183. ISSN: 2095-8099. DOI: https://doi.org/10.1016/j.eng.2021.08.032. URL: https://www.sciencedirect.com/science/article/pii/S2095809922003630.

[93] Lingfei Zhao et al. "A Critical Review on Room-Temperature Sodium-Sulfur Batteries: From Research Advances to Practical Perspectives". In: *Advanced Materials* n/a.n/a (), p. 2402337. DOI: https://doi.org/10.1002/adma.202402337. eprint: https://onlinelibrary.wiley.com/doi/pdf/10.1002/adma.202402337. URL: https://onlinelibrary.wiley.com/doi/abs/10.1002/adma.202402337.

[94] Xuesong Zhou, Tie Guo, and Youjie Ma. "An overview on microgrid technology". In: *2015 IEEE International Conference on Mechatronics and Automation (ICMA)*. 2015, pp. 76–81. DOI: 10.1109/ICMA.2015.7237460.

[95] Xiaoqiang Zhu et al. "Research on the control strategy of grid connection between shore power supply and ship power grid". In: *Energy Reports* 8 (2022). 2022 The 5th International Conference on Electrical Engineering and Green Energy, pp. 638–647. ISSN: 2352-4847. DOI: https://doi.org/10.1016/j.egyr.2022.08.164. URL: https://www.sciencedirect.com/science/article/pii/S2352484722016079.

[96] Zhengxin Zhu et al. "A High-Rate Lithium Manganese Oxide-Hydrogen Battery". In: *Nano Letters* 20.5 (2020). PMID: 32302150, pp. 3278–3283. DOI: `10.1021/acs.nanolett.0c00044`. URL: `https://doi.org/10.1021/acs.nanolett.0c00044`.

[97] Thalis P.V. Zis. "Prospects of cold ironing as an emissions reduction option". In: *Transportation Research Part A: Policy and Practice* 119 (2019), pp. 82–95. ISSN: 0965-8564. DOI: `https://doi.org/10.1016/j.tra.2018.11.003`. URL: `https://www.sciencedirect.com/science/article/pii/S0965856418303264`.

[98] Nick Zrinyi. *List of Countries with Net-Zero Commitments and Climate Accountability Legislation*. 2021. URL: `https://rosagalvez.ca/en/initiatives/climate-accountability/list-of-countries-with-net-zero-commitments-and-climate-accountability-legislation/` (visited on 01/16/2024).

[99] Henrik Zsiborács et al. "Exploring the Grid Electricity Saving Potentials of Using Hybrid PV Systems in European Countries: A Comparative Study". In: *IEEE Access* 11 (2023), pp. 90698–90714. DOI: `10.1109/ACCESS.2023.3307465`.

A
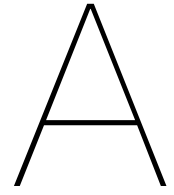
Appendix A

Ulstein SX121
Project U10687
Hull 300

Electrical Load Calculation
AUTRO/AUTR

APPR. BY		REVISIONS	DATE	SIGN	REV
DNV	OWNER				
		Updated values for emergency switchboard acc. to comments from DNV	04.04.13	TOB	2

Contents:

Explanation of the Electrical Load Calculation:

The abbreviation "L.F." means Load Factor, and is actual a factor made up of the power efficiency of a consumer and the utilization of the same consumer, i.e. the relationship between the size of e.g. an electrical motor and the power requirement.

The abbreviation "D.F." means Diversity Factor, and indicates the degree of probability of a consumer to run simultaneously with other consumers.

The abbreviation "U.F." means Utilisation Factor, and indicates the degree of utilisation of the consumers capasity.

Applicable Electrical Load Calculation is for DYNPOS-AUTRO. The 3-split configuration (DYNPOS AUTR) is for info only.

The following power sources/ generators are available:

6x2740kW   3x690V, 60Hz Main diesel generating set.
1x300kW   3x440V, 60Hz emergency diesel generator set.
1 x 800A   3x440V, 60Hz Shore connection.

Normal operation of switchboards:

1. 230V SWB to be fed by both 440/230V transformers and bus-tie breakers to be closed. Bus-tie breakers to be disconnected in case of short-circuit of 230V bus-bar.
2. 440V SWB to be fed by both 690/440V transformers and bus-tie breakers to be closed. Bus-tie breakers to be disconnected in case of short-circuit of 440V bus-bar.
3. 690V MSB to be fed by 6 pc diesel generator sets according to power demand and operation mode. Bus-tie breaker to be normally closed, but in heavy / critical maneouvering mode it preferably should be open. In DP operations, the bus-bars shall be divided by opening the main tie breakers, see configuration options described in building specification.
4. 440V ESB to be fed from 440V MSB in normal operation. Automatic start and connection of emergency generator and automatically disconnection of feeder from MSB in case of failure of main source of power.

Project: U10687
Ulstein SX121
IMRV

Ref. SFI	CONSUMER	No. off	Rated in kW	L.F.	TRANSIT 8,5 knots T=6,5m			TRANSIT 14,5 knots T=6,5m			DYNPOS EF@90°			OFFSHORE CRANE OPERATION			ROV OPERATION			WORST SINGLE FAILURE AUTRO EF@90°			WORST SINGLE FAILURE AUTR EF@90°			PIPE LAYING VLS OPERATION			HARBOUR			EMERGENCY		
					D.F.	No. in use	Load (KW)	D.F.	No. in use	Load (KW)	D.F.	No. in use	Load (KW)	D.F.	No. in use	Load (KW)	D.F.	No. in use	Load (KW)	D.F.	No. in use	Load (KW)	D.F.	No. in use	Load (KW)	D.F.	No. in use	Load (KW)	D.F.	No. in use	Load (KW)	D.F.	No. in use	Load (KW)
411	X-radar	1	2,5	0,85	0,5	1	1	0,5	1	1	0,5	1	1	0,5	1	1	0,5	1	1	0,5	1	1	0,5	1	1	0,5	1	1	0,1	1	0	1,0	1	2
427	Navigation lights	1	2,0	1,00	0,5	1	1	0,5	1	1	0,5	1	1	0,5	1	1	0,5	1	1	0,5	1	1	0,5	1	1	0,5	1	1	0,1	1	0	1,0	1	2
513	Watertight doors	23	0,5	0,85	0,1	1	0	0,1	1	0	0,1	1	0	0,1	1	0	0,1	1	0	0,1	1	0	0,1	1	0	0,1	1	0	0,1	1	0	1,0	23	11
665	Space Heater for Emergency Generator	1	3,0	1,00	1,0	1	3	1,0	1	3	1,0	1	3	1,0	1	3	1,0	1	3	1,0	1	3	1,0	1	3	1,0	1	3	1,0		0			0
811	Fire Alarm System	1	0,2	1,00	0,8	1	0	0,8	1	0	0,8	1	0	0,8	1	0	0,8	1	0	0,8	1	0	0,8	1	0	0,8	1	0	0,8	1	0	1,0	1	0
882	Battery Chargers for Emergency Generator	2	0,3	1,00	0,5	2	0	0,5	2	0	0,5	2	0	0,5	2	0	0,5	2	0	0,5	2	0	0,5	2	0	0,5	2	0	0,5	2	0	1,0	2	1
882	Battery Chargers for 24V system	4	2,9	1,00	0,5	0	0	0,5	0	0	0,5	0	0	0,5	0	0	0,5	0	0	0,5	0	0	0,5	0	0	0,5	0	0	0,5	0	0	1,0	4	12
891	Light In Machinery Spaces	1	6,0	1,00	1,0	1	6	1,0	1	6	1,0	1	6	1,0	1	6	1,0	1	6	1,0	1	6	1,0	1	6	1,0	1	6	1,0	1	6	1,0	1	6
892	Light in Accomodation	1	12,0	1,00	1,0	1	12	1,0	1	12	1,0	1	12	1,0	1	12	1,0	1	12	1,0	1	12	1,0	1	12	1,0	1	12	1,0	1	12	1,0	1	12
893	Floodlights on Deck	1	4,0	1,00	0,5	1	2	0,5	1	2	0,5	1	2	0,5	1	2	0,5	1	2	0,5	1	2	0,5	1	2	0,5	1	2	0,5	1	2	1,0	1	4
893	Lighting in Cargo Area	1	6,0	1,00	0,8	1	5	0,8	1	5	0,8	1	5	0,8	1	5	0,8	1	5	0,8	1	5	0,8	1	5	0,8	1	5	0,8	1	5	1,0	1	6
893	Lighting on Deck	1	1,5	1,00	0,5	1	1	0,5	1	1	0,5	1	1	0,5	1	1	0,5	1	1	0,5	1	1	0,5	1	1	0,5	1	1	0,5	1	1	1,0	1	2
412	Radio and navigation equipment	1	2,0	1,00	0,3	1	1	0,3	1	1	0,3	1	1	0,3	1	1	0,3	1	1	0,3	1	1	0,3	1	1	0,3	1	1	0,3	1	1	1,0	1	2
LOAD 230V ESB (kW)							**32**			**32**			**32**			**32**			**32**			**32**			**32**			**32**			**27**			**58**
440/230V TRANSFORMERS AND LOAD IN %	1	99	kVA				**48 %**			**48 %**			**48 %**			**48 %**			**48 %**			**48 %**			**48 %**			**48 %**			**42 %**			**79 %**

(Load in % is based on only one transformer in operation)

Average Power Factor of Consumers for Calculation of Transformer Load in %: 0,85

Addition load, transformers with 110% capasity of the load in kW: 1,1   8,415

Project: U10687
Ulstein SX121
IMRV

Ref. SFI	CONSUMER	No. off	Rated in kW	L.F.	TRANSIT 8,5 knots T=6,5m D.F.	No. in use	Load (KW)	TRANSIT 14,5 knots T=6,5m D.F.	No. in use	Load (KW)	DYNPOS 0 EF@90° D.F.	No. in use	Load (KW)	OFFSHORE CRANE OPERATION D.F.	No. in use	Load (KW)	ROV OPERATION D.F.	No. in use	Load (KW)	WORST SINGLE FAILURE AUTRO EF@90° D.F.	No. in use	Load (KW)	WORST SINGLE FAILURE AUTR EF@90° D.F.	No. in use	Load (KW)	PIPE LAYING VLS OPERATION D.F.	No. in use	Load (KW)	HARBOUR D.F.	No. in use	Load (KW)	EMERGENCY D.F.	No. in use	Load (KW)
	Emergency Transformer (from 230V ESB)	1	99kVA				32			32			32			32			32			32			32			32			27			58
574	Emergency Generator Room Fan	1	1,2	0,85																												1,0	1	1
574	Supply fan engine room	4	35,0	0,91																												1,0	2	64
731	Starting air compr.	2	7,8	0,86	0,3	1	2	0,3	1	2	0,3	1	2	0,3	1	2	0,3	1	2	0,4	1	3	0,4	1	3	0,4	1	3			0	1,0	1	7
813	Emergency fire pump	1	40,0	0,87																												1,0	1	35
	Smoke diving compressor	1	2,2	0,85																												1,0	1	2
817	Water mist system	2	30,0	0,88																												1,0	2	53
403	Steering gear pumps	1	45,0	0,89	0,4		0	0,4		0	0,4		0	0,7		0	0,7		0	0,5		0	0,5		0	0,5		0			0	1,0	1	40
803001	Bilge pump	1	12,0	0,85	0,1	1	1	0,1	1	1	0,1	0	0	0,1	0	0	0,1	0	0	0,1	0	0	0,1	0	0	0,1	1	1	0,1	1	1	1,0	1	10
	LOAD 440V ESB (kW)						**35**			**35**			**34**			**34**			**34**			**34**			**34**			**35**			**28**			**270**

Project: U10687
Ulstein SX121
IMRV

Ref. SFI	CONSUMER	No. off	Rated in kW	L.F.	TRANSIT 8,5 knots T=6,5m D.F.	No. in use	Load (KW)	TRANSIT 14,5 knots T=6,5m D.F.	No. in use	Load (KW)	DYNPOS 0 EF@90° D.F.	No. in use	Load (KW)	OFFSHORE CRANE OPERATION D.F.	No. in use	Load (KW)	ROV OPERATION D.F.	No. in use	Load (KW)	WORST SINGLE FAILURE AUTRO EF@90° D.F.	No. in use	Load (KW)	WORST SINGLE FAILURE AUTR EF@90° D.F.	No. in use	Load (KW)	PIPE LAYING VLS OPERATION D.F.	No. in use	Load (KW)	HARBOUR D.F.	No. in use	Load (KW)	EMERGENCY D.F.	No. in use	Load (KW)
42	Communication Equipment	1	3,0	1,00	0,5	1	2	0,5	1	2	0,5	1	2	0,5	1	2	0,5	1	2	0,5	1	1	0,5	1	1	0,5	1	2	0,1	1	0			0
404	Heating Generators, Thrusters etc.	1	4,0	1,00	0,2	3	2	0,1	3	1	0,0	0	0	0,0	0	0	0,0	0	0	0,1	1	0	0,1	1	0	0,1	0	0	1,0	4	16			0
427	Searchlight	3	2,0	1,00	0,1	1	0	0,1	0	0	0,1	1	0	0,5	1	1	0,5	1	1	0,5	2	2	0,5	2	2	0,5	2	2	0,1	0	0			0
515	Window Wipers	37	1,5	0,85	0,3	8	3	0,3	8	3	0,3	8	3	0,3	8	3	0,3	8	3	0,3	19	7	0,3	4	2	0,3	8	3	0,0	0	0			0
515	Heated Windows	22	2,9	1,00	0,7	7	14	0,7	7	14	0,7	7	14	0,7	10	20	0,7	10	20	0,7	11	23	0,7	11	23	0,3	0	0	0,3	0	0			0
541	Cabin Refrigerators, TV's etc.	1	15,0	0,86	0,3	1	4	0,3	1	4	0,3	1	4	0,3	1	4	0,3	1	4	0,3	1	2	0,3	1	2	0,3	1	4	0,3	1	4			0
584	Drinking Water Fountain	4	1,0	0,85	0,3	4	1	0,3	4	1	0,3	4	1	0,3	4	1	0,3	4	1	0,3	2	1	0,3	2	1	0,7	4	2	0,3	4	1			0
551	Galley & Laundry Equipment (558)	1	10,0	1,00	0,8	1	8	0,8	1	8	0,8	1	8	0,8	1	8	0,8	1	8	0,8	1	4	0,8	1	4	0,8	1	8	0,5	1	5			0
882	Battery Chargers for 24V system	4	2,9	1,00	0,5	4	6	0,5	4	6	0,5	4	6	0,5	4	6	0,5	4	6	0,5	2	3	0,5	2	3	0,5	4	6	0,5	4	6	1,0	0	0
882	UPS DP (Dynpos System)	5	3,0	1,00	0,2	1	1	0,2	1	1	1,0	2	6	0,2	2	1	0,2	2	1	0,5	3	4	0,5	1	2	0,5	1	2	0,1	1	0			0
891	Light In Machinery Spaces	1	12,0	1,00	1,0	1	12	1,0	1	12	1,0	1	12	1,0	1	12	1,0	1	12	1,0	1	6	1,0	1	6	1,0	1	12	1,0	1	12			0
892	Light in Accomodation	1	30,0	1,00	0,7	1	21	0,7	1	21	0,7	1	21	0,7	1	21	0,7	1	21	0,7	1	11	0,7	1	11	1,0	1	30	0,7	1	21			0
892	Panel Heaters Accomodation	20	2,0	1,00	0,7	12	17	0,7	12	17	0,7	12	17	0,7	12	17	0,7	12	17	0,7	10	14	0,7	10	14	0,8	12	19	0,7	12	17			0
893	Floodlights on Deck	16	0,8	1,00	0,2	4	1	0,2	4	1	0,2	4	1	0,8	16	10	0,8	16	10	0,5	8	3	0,5	8	3	0,5	16	6	0,2	16	3			0
893	Lighting in Cargo Area	10	0,8	1,00	0,8	4	3	0,8	4	3	0,8	4	3	0,8	10	6	0,8	10	6	0,8	5	3	0,8	5	3	0,8	10	6	0,8	10	6			0
893	Lighting on Deck	1	5,0	1,00	0,2	1	1	0,2	0	0	0,2	0	0	0,6	1	3	0,6	1	3	0,5	1	1	0,5	1	1	0,5	1	3	0,8	1	4			0
574002	Supply fan bow thruster room 1&2	2	2,0	0,85	0,4	0	0	0,4	0	0	0,4	2	1	0,4	2	1	0,4	2	1	0,4	1	1	0,4	1	1	0,4	1	1			0			0
576002	Supply fan propulsion room	3	0,2	0,85	1,0	2	0	1,0	2	0	1,0	2	0	1,0	2	0	1,0	2	0	1,0	1	0	1,0	1	0	1,0	2	0			0			0
LOAD 230V MSB (kW)							**95**			**93**			**99**			**117**			**117**			**84**			**76**			**106**			**95**			**0**

(Load in % is based on only one transformer in operation)

		No. off	Rated	L.F.																														
440/230V TRANSFORMERS LOAD IN %		2	198	kVA	1		67 %	1		65 %	1		69 %	1		80 %	1		80 %	1		60 %	1		55 %	1		73 %	1		66 %			0 %

Average Power Factor of Consumers for Calculation of Transformer Load in %: 0,85
Addition load, transformers with 110% capasity of the load in kW: 1,1 16,83

Project: U10687
Ulstein SX121
IMRV

Ref. SFI	CONSUMER	No. off	Rated in kW	L.F.	TRANSIT 8,5 knots T=6,5m D.F.	No. in use	Load (kW)	TRANSIT 14,5 knots T=6,5m D.F.	No. in use	Load (kW)	DYNPOS 0 EF@90° D.F.	No. in use	Load (kW)	OFFSHORE CRANE OPERATION D.F.	No. in use	Load (kW)	ROV OPERATION D.F.	No. in use	Load (kW)	WORST SINGLE FAILURE AUTRO EF@90° D.F.	No. in use	Load (kW)	WORST SINGLE FAILURE AUTR EF@90° D.F.	No. in use	Load (kW)	PIPE LAYING VLS OPERATION D.F.	No. in use	Load (kW)	HARBOUR D.F.	No. in use	Load (kW)	EMERGENCY D.F.	No. in use	Load (kW)
351006	MEG pumps	2	40,0	1,09																														0
403020	Steering gears	6	45,0	0,89	0,2	6	48	0,2	6	48	0,4	6	96	0,4	6	96	0,4	6	96	0,5	4	80	0,5	4	80	0,4	6	96			0			0
404031	Servo pumps tunnel thrusters	2	11,0	0,85			0			0	1,0	2	19	1,0	2	19	1,0	2	19	1,0	1	9	1,0	1	9	1,0	1	9			0			0
433047	Windlass/mooring hydr. pump unit	2	30,0	0,89																									0,5	2	27			0
433047	Capstan mooring hydr. pump unit	1	55,0	0,89																									0,5	1	24			0
501020	MOB boat davit	1	54,0	0,89																									0,1	1	5			0
551001	Galley & Laundry Equipment (558)	X	90,0	1,00	0,4	1	36	0,4	1	36	0,4	1	36	0,4	1	36	0,4	1	36	0,4	1	36	0,4	1	36	0,3	1	27	0,1	1	9			0
554001	PROVISION PLANT AGGR. 1&2.	2	13,0	0,85	0,7	1	8	0,7	1	8	0,7	1	8	0,7	1	8	0,7	1	8	0,7	1	4	0,7	1	4	0,7	1	8	0,7	1	8			0
561001	Personell lift	1	17,6	0,89	0,1	1	2	0,1	1	2	0,1	1	2	0,1	1	2	0,1	1	2	0,1	0	0	0,1	0	0	0,1	1	2	0,1	1	2			0
561001	Provision lift	1	2,0	0,87	0,1	0	0	0,1	0	0	0,1	0	0	0,1	0	0	0,1	0	0	0,1	0	0	0,1	0	0	0,1	0	0	0,3	1	1			0
571011	Div. small acc. exhaust fans	10	0,8	0,85	0,8	10	5	0,8	10	5	0,8	10	5	0,8	10	5	0,8	10	5	0,8	5	3	0,8	5	3	1,0	5	3	0,8	5	3			0
571020	Chilled water pumps HVAC	4	17,3	1,09	0,3	2	11	0,3	2	11	0,3	2	11	0,3	2	11	0,3	2	11	0,3	1	6	0,3	1	6	0,3	2	11	0,3	2	11			0
572011	Exhaust fan galley	1	2,6	0,85	1,0	1	2	1,0	1	2	1,0	1	2	1,0	1	2	1,0	1	2	1,0	1	2	1,0	1	2	1,0	1	2	1,0	1	2			0
572011	Supply fan galley	1	4,7	0,85	1,0	1	4	1,0	1	4	1,0	1	4	1,0	1	4	1,0	1	4	1,0	1	4	1,0	1	4	1,0	1	4	1,0	1	4			0
574002	Supply fan engine room	4	35,0	0,89	0,5	2	31	0,8	2	50	0,8	2	50	0,8	2	50	0,8	2	50	0,8	1	25	0,8	1	25	0,5	2	31	0,2	2	12			0
574004	Div. small deck/ store supply/ exhaust fans	10	0,6	0,85	1,0	10	5	1,0	10	5	1,0	10	5	1,0	10	5	1,0	10	5	1,0	5	3	1,0	5	3	1,0	5	3	1,0	5	3			0
577001	FW circ.pump, chilled water	4	17,3	0,85	1,0	2	29	1,0	2	29	1,0	4	59	1,0	4	59	1,0	4	59	1,0	1	15	1,0	3	44	1,0	4	59	1,0	2	29			0
581001	FW generator plant	1	8,3	0,85	0,2	1	1	0,2	1	1	0,2	1	1	0,2	1	1	0,2	1	1	0,2	1	1	0,2	1	1	0,2	1	1	0,2	1	1			0
581002	FW Hydrophore pump	2	8,6	0,85	0,4	1	3	0,4	1	3	0,4	1	3	0,4	1	3	0,4	1	3	0,4	1	3	0,4	1	3	0,4	1	3	0,4	1	3			0
581023	Hot water circ. pump sanitary syst.	2	0,4	0,85	1,0	1	0	1,0	1	0	1,0	1	0	1,0	1	0	1,0	1	0	1,0	1	0	1,0	1	0	1,0	1	0	1,0	1	0			0
582010	Sewage treatment plant	1	5,0	0,85	0,3	1	1	0,3	1	1	0,3	1	1	0,3	1	1	0,3	1	1	0,3	1	1	0,3	1	1	0,3	1	1	0,3	1	1			0
582017	Sewage discharge pump	1	3,6	0,85	0,1	0	0	0,1	0	0	0,1	0	0	0,1	0	0	0,1	0	0	0,1	0	0	0,1	0	0	0,1	0	0	0,1	1	1			0
648001	HW BOILER	1	40,0	1,00	0,1	1	4	0,1	1	4	0,1	1	4	0,1	1	4	0,1	1	4	0,0	1	1	0,0	1	1	0,1	1	4	0,1	1	4			0
701025	FO TRANSFER PUMP	2	4,3	0,85	0,2	1	1	0,2	1	1	0,2	1	1	0,2	1	1	0,2	1	1	0,2	1	1	0,2	1	1	0,2	1	1	0,2	0	0			0
701025	FO SUPPLY PUMP TO DECK	1	0,4	0,85	0,4	1	0	0,4	1	0	0,4	1	0	0,4	1	0	0,4	1	0	0,4	1	0	0,4	1	0	0,4	1	0	0,1	1	0			0
702010	FO separator and supply pump	4	5,0	0,85	0,4	2	2	0,4	2	2	0,4	2	3	0,4	2	3	0,4	2	3	0,4	1	2	0,4	1	2	0,4	1	2	0,4	0	2			0
703051	DO circ. pump to incinerator	1	0,2	0,85	0,4	1	0	0,4	1	0	0,4	1	0	0,4	1	0	0,4	1	0	0,4	1	0	0,4	1	0	0,4	1	0	0,4	1	0			0
711002	LO separator and supply pump	6	5,0	0,85	0,4	1	2	0,4	4	7	0,4	3	5	0,4	2	3	0,4	2	3	0,4	2	2	0,4	2	2	0,4	2	3	0,4	0	0			0
711003	LO TRANSFER PUMPS	2	1,6	0,85	0,2	2	1	0,2	2	1	0,2	2	1	0,2	4	1	0,2	4	1	0,2	4	1	0,2	4	1	0,2	4	1	0,1	1	0			0
714002	LO PRIMING PUMP MAIN ENGINES	6	6,6	0,85	1,0	5	28	1,0	4	22	1,0	0	0	1,0	0	0	1,0	0	0	0,4	0	0	0,4	0	0	0,4	2	2	1,0	6	34			0
722002	FW COOLING PUMPS FOR MAIN PROP.	6	8,6	0,85	0,5	3	11	0,5	3	11	0,5	3	11	0,5	3	11	0,5	3	11	0,5	2	7	0,5	2	7	0,5	3	11	0,5	0	0			0
722003	FW COOLING PUMPS FOR MISC.SYSTEMS AFT	2	40,0	0,85	0,5	1	17	0,5	1	17	0,5	1	17	0,5	1	17	0,5	1	17	0,5	0	0	0,5	0	0	0,5	1	17	0,5	1	17			0
722003	FW cooling pumps for misc.systems	8	40,0	0,85	0,5	2	34	0,5	2	34	0,5	4	68	0,5	4	68	0,5	4	68	0,5	2	34	0,5	3	51	0,5	4	68	0,5	1	17			0
722015	FW preheating, ME	6	18,0	1,00	0,6	4	43	0,6	2	22	0,6	0	0	0,6	0	0	0,6	0	0	0,6	0	0	0,6	0	0	0,6	1	11	0,6	6	65			0
731001	Starting air compr.	2	7,8	0,85	0,1	2	1	0,1	2	1	0,1	2	1	0,1	2	1	0,1	2	1	0,1	1	1	0,1	1	1	0,1	2	1	0,1	1	1			0
732001	Working air compressor	1	26,8	0,86	0,2	1	5	0,2	1	5	0,2	1	5	0,2	1	5	0,2	1	5	0,2	1	5	0,2	1	5	0,2	1	5			0			0
734017	INSTR.AIR DRYER	1	17,5	0,86	0,1	1	2	0,1	1	2	0,1	1	2	0,1	1	2	0,1	1	2	0,1	1	2	0,1	1	2	0,1	1	2			0			0
803001	BILGE PUMP	4	12,0	0,85	0,1	1	1	0,1	1	1	0,1	1	1	0,1	1	1	0,1	1	1	0,1	1	1	0,1	1	1	0,1	1	1	0,1	1	1			0
803002	BILGE water separator	1	8,6	0,85	0,1	1	1	0,1	1	1	0,1	1	1	0,1	1	1	0,1	1	1	0,1	1	1	0,1	1	1	0,1	1	1			0			0
803027	SLUDGE PUMP	1	3,0	0,85	0,4	1	1	0,4	1	1	0,4	1	1	0,4	1	1	0,4	1	1	0,4	1	1	0,4	1	1	0,4	1	1			0			0
813001	FIRE PUMP NO.1&2	2	40,0	0,86	0,1	0	0	0,1	0	0	0,1	0	0	0,1	0	0	0,1	0	0	0,1	1	3	0,1	1	3	0,1	0	0	0,1	0	0			0
	LOAD 440V ESB (kW)						35			35			34			34			34			34			34			35			28			270
	LOAD 230V MSB (kW)						95			93			99			117			117			84			76			106			95			0
	LOAD 440V MSB (kW)						470			464			554			572			572			364			403			529			407			270

| 2 | 1200 | KVA | | | 1 | | 56 % | 1 | | 56 % | 1 | | 64 % | 1 | | 66 % | 1 | | 66 % | 1 | | 46 % | 1 | | 50 % | 1 | | 62 % | 1 | | 50 % | | | |

(Load in % is based on only one transformer in operation)

690V/440V TRANSFORMERS LOAD IN %

Average Power Factor of Consumers for Calculation of Transformer Load in %: 0,85

Addition load, transformers with 110% capasity of the load in kW: 102

1,1

Project: U10687
Ulstein SX121
IMRV

Ref. SFI	CONSUMER	No. off	Rated in kW	L.F.	TRANSIT 8,5 knots T=6,5m U.F.	No. in use	Load (KW)	TRANSIT 14,5 knots T=6,5m U.F.	No. in use	Load (KW)	DYNPOS 0 EF@90° U.F.	No. in use	Load (KW)	OFFSHORE CRANE OPERATION U.F.	No. in use	Load (KW)	ROV OPERATION U.F.	No. in use	Load (KW)	WORST SINGLE FAILURE AUTRO EF@90° U.F.	No. in use	Load (KW)	WORST SINGLE FAILURE AUTR EF@90° U.F.	No. in use	Load (KW)	PIPE LAYING VLS OPERATION U.F.	No. in use	Load (KW)	HARBOUR U.F.	No. in use	Load (KW)	EMERGENCY U.F.	No. in use	Load (KW)
	690V / 440V Ships Transformer T7a (PS)						118			116			139			143			143			91			0			132			102			0
322001	250T Offshore crane - S1	1	930	0,93										0,6	1	519	0,5	1	432	0,3	0	0	0,3	0	0	0,3	1	259						0
405001	Anti-heeling pump 1/3	1	121,0	0,92										0,7	1	78	0,7	1	78	0,7	0	0	0,7	0	0	0,2	1	22						0
482001	Offshore equipment switchboard S1	1	2500	1,00										0,3	1	750	0,3	1	750	0,4	0	0	0,4	0	0	0,7	1	1750						0
571020	Chilled water cooling compr. 1/4 HVAC	1	182,0	0,94	0,6	1	103	0,6	1	103	0,6	1	103	0,6	1	103	0,6	1	103	0,6	1	103	0,6	0	0	0,6	1	103	0,6	1	103			0
571001	AC-1 Central unit aircondition plant (acc.)	1	61,0	1,09	0,5	1	33	0,5	1	33	0,5	1	33	0,5	1	33	0,5	1	33	0,5	0	0	0,5	0	0	0,5	1	33	0,5	1	33			0
571002	AC-2 Central unit aircondition plant (bridge)	1	12,8	1,09	0,5	1	7	0,5	1	7	0,5	1	7	0,5	1	7	0,5	1	7	0,5	0	0	0,5	0	0	0,5	1	7	0,5	1	7			0
571003	AC-3 Central unit aircondition plant (acc.)	1	57,0	1,09	0,5	1	31	0,5	1	31	0,5	1	31	0,5	1	31	0,5	1	31	0,5	0	0	0,5	0	0	0,5	1	31	0,5	1	31			0
721001	SW COOLING pumps ME 1+2	3	17,5	1,09	0,5	1	9	0,5	2	19	0,5	1	9	0,5	2	19	0,5	2	19	0,5	2	19	0,5	0	0	0,5	2	19						0
721002	SW cooling pumps MP1	2	8,6	1,09	0,5	1	5	0,5	1	5	0,5	1	5	0,5	1	5	0,5	1	5	0,5	1	5	0,5	0	0	0,5	1	5						0
721003	SW cooling pumps misc.equip	2	17,5	1,09	0,5	1	9	0,5	1	9	0,5	1	9	0,5	1	9	0,5	1	9	0,5	1	9	0,5	0	0	0,5	1	9						0
721003	SW cooling pumps misc.equip aft.	1	17,5	1,09	0,5	0	0	0,5	0	0	0,5	1	9	0,5	1	9	0,5	1	9	0,5	2	19	0,5	0	0	0,5	1	9						0
571005	Heating/cooling/defroster unit wheelhouse	1	12,8	0,87	0,5	1	6	0,5	1	6	0,5	1	6	0,5	1	6	0,5	1	6	0,5	1	3	0,5	0	0	0,5	1	6						0
	Sum for ship load excluding thrusters Port						**320**			**328**			**351**			**1712**			**1625**			**249**			**0**			**2386**			**275**			**0**
404	Bow thruster 1	1	2140	1,09							0,46	1	1080	0,46	1	1080	0,46	1	1080	1,00	1	2333	0,46	0	0	0,46	0	0			0			0
630	MP1	1	3000	1,09	0,12	1	345	0,85	1	2550	0,13	1	410	0,13	1	410	0,13	1	410	0,83	1	2721	0,13	0	0	0,13	1	410			0			0
	Sum thruster load Port						**345**			**2550**			**1490**			**1490**			**1490**			**5053**			**0**			**410**			**0**			**0**

Ref. SFI	CONSUMER	No. off	Rated in kW	L.F.	TRANSIT 8,5 knots T=6,5m U.F.	No. in use	Load (KW)	TRANSIT 14,5 knots T=6,5m U.F.	No. in use	Load (KW)	DYNPOS 0 EF@90° U.F.	No. in use	Load (KW)	OFFSHORE CRANE OPERATION U.F.	No. in use	Load (KW)	ROV OPERATION U.F.	No. in use	Load (KW)	WORST SINGLE FAILURE AUTRO EF@90° U.F.	No. in use	Load (KW)	WORST SINGLE FAILURE AUTR EF@90° U.F.	No. in use	Load (KW)	PIPE LAYING VLS OPERATION U.F.	No. in use	Load (KW)	HARBOUR U.F.	No. in use	Load (KW)	EMERGENCY U.F.	No. in use	Load (KW)
	690V/ 440V Ships Transformer T7b (PS)						118			116			139			143			143			91			101			132			102			0
721001	SW COOLING pumps ME 3	2	17,5	1,09	0,5	0	0	0,5	1	9	0,5	0	0	0,5	0	0	0,5	0	0	0,5	1	9	0,5	1	9	0,5	2	19			0			0
721002	SW cooling pumps MP2	2	8,6	1,09	0,5	1	5	0,5	1	5	0,5	1	5	0,5	1	5	0,5	1	5	0,5	1	5	0,5	1	5	0,5	1	5			0			0
721003	SW cooling pumps misc.equip	2	17,5	1,09	0,5	1	9	0,5	1	9	0,5	1	9	0,5	1	9	0,5	1	9	0,5	1	9	0,5	1	9	0,5	1	9			0			0
405001	Anti-heeling pump 2/3	1	121,0	0,92										0,7	1	78	0,7	1	78	0,7	0	0	0,7	0	0	0,2	0	0						0
571020	Chilled water cooling compr. 2/4 HVAC	1	182,0	0,94	0,6	0	0	0,6	0	0	0,6	1	103	0,6	1	103	0,6	1	103	0,6	0	0	0,6	1	103	0,6	1	103	0,6	1	103			0
331004	Deck Service crane	1	232,0	0,87										0,5	1	101	0,5	0	0										0,2	1	40			0
	Sum for ship load excluding thrusters Starboard						**132**			**140**			**255**			**439**			**338**			**115**			**227**			**268**			**245**			**0**
630	MP2	1	3000	1,09	0,12	1	345	0,85	1	2550	0,12	1	395	0,12	1	395	0,12	1	395	0,78	1	2565	0,22	1	714	0,12	1	395			0			0
	Sum thruster load Starboard						**345**			**2550**			**395**			**395**			**395**			**2565**			**714**			**395**			**0**			**0**

Project: U10687
Ulstein SX121
IMRV

Ref. SFI	CONSUMER	No. off	Rated in kW	L.F.	TRANSIT 8,5 knots T=6,5m			TRANSIT 14,5 knots T=6,5m			DYNPOS 0 EF@90°			OFFSHORE CRANE OPERATION			ROV OPERATION			WORST SINGLE FAILURE AUTRO EF@90°			WORST SINGLE FAILURE AUTR EF@90°			PIPE LAYING VLS OPERATION			HARBOUR			EMERGENCY		
					U.F.	No. in use	Load (KW)	U.F.	No. in use	Load (KW)	U.F.	No. in use	Load (KW)	U.F.	No. in use	Load (KW)	U.F.	No. in use	Load (KW)	U.F.	No. in use	Load (KW)	U.F.	No. in use	Load (KW)	U.F.	No. in use	Load (KW)	U.F.	No. in use	Load (KW)	U.F.	No. in use	Load (KW)
	690V / 440V Ships Transformer T8a (SB)						118			116			139			143			143			0			101			132			102			0
721001	SW COOLING pumps ME 4	2	17,5	1,09	0,5	0	0	0,5	1	9	0,5	1	9	0,5	1	9	0,5	1	9	0,5	0	0	0,5	1	9	0,5	1	9			0			0
721003	SW cooling pumps misc.equip	2	17,5	1,09	0,5	1	9	0,5	1	9	0,5	1	9	0,5	1	9	0,5	1	9	0,5	0	0	0,5	1	9	0,5	1	9			0			0
405001	Anti-heeling pump 3/3	1	121,0	0,92										0,7	1	78	0,7	0	0	0,7	0	0	0,7	0	0	0,2	0	0			0			0
571020	Chilled water cooling compr. 3/4 HVAC	1	182,0	0,94	0,6	0	0	0,6	0	0	0,6	1	103	0,6	1	103	0,6	1	103	0,6	0	0	0,6	1	103	0,6	1	103	0,6	1	103			0
322001	250T Offshore crane - S2	1	930	0,93										0,6	1	519	0,5	1	432	0,3	0	0	0,3	0	0	0,3	1	259						0
	Sum for ship load excluding thrusters Starboard						**127**			**135**			**260**			**861**			**697**			**0**			**222**			**513**			**204**			**0**
404	Bow thruster 2	1	2140	1,09							0,46	1	1080	0,46	1	1080	0,46	1	1080	0,46	0	0	0,89	1	2067	0,46	0	0			0			0
	Sum thruster load Starboard						**0**			**0**			**1080**			**1080**			**1080**			**0**			**2067**			**0**			**0**			**0**

Ref. SFI	CONSUMER	No. off	Rated in kW	L.F.	TRANSIT 8,5 knots T=6,5m U.F.	No. in use	Load (KW)	TRANSIT 14,5 knots T=6,5m U.F.	No. in use	Load (KW)	DYNPOS 0 EF@90° U.F.	No. in use	Load (KW)	OFFSHORE CRANE OPERATION U.F.	No. in use	Load (KW)	ROV OPERATION U.F.	No. in use	Load (KW)	WORST SINGLE FAILURE AUTRO EF@90° U.F.	No. in use	Load (KW)	WORST SINGLE FAILURE AUTR EF@90° U.F.	No. in use	Load (KW)	PIPE LAYING VLS OPERATION U.F.	No. in use	Load (KW)	HARBOUR U.F.	No. in use	Load (KW)	EMERGENCY U.F.	No. in use	Load (KW)
	690V/440V Ships Transformer T8b (SB)						118			116			139			143			143			0			101			132			102			0
721001	SW COOLING pumps ME 5+6	3	17,5	1,09	0,5	0	0	0,5	0	0	0,5	1	9	0,5	1	9	0,5	1	9	0,5	0	0	0,5	1	9	0,5	1	9			0			0
721002	SW cooling pumps MP3	2	8,6	1,09	0,5	1	5	0,5	1	5	0,5	1	5	0,5	1	5	0,5	1	5	0,5	0	0	0,5	1	5	0,5	2	9			0			0
721003	SW cooling pumps misc.equip	2	17,5	1,09	0,5	1	9	0,5	1	9	0,5	1	9	0,5	1	9	0,5	1	9	0,5	0	0	0,5	1	9	0,5	1	9			0			0
721003	SW cooling pumps misc.equip aft.	1	17,5	1,09	0,5	0	0	0,5	0	0	0,5	0	0	0,5	0	0	0,5	0	0	0,5	0	0	0,5	1	9	0,5	1	9			0			0
322001	250T Offshore crane - S3	1	930	0,93										0,6	1	519	0,5	1	432	0,5	0	0	0,5	0	0	0,5	1	432						0
404031	Servo pump retractable thruster	1	63,0	0,91			0			0	1,0	1	57	1,0	1	57	1,0	1	57	1,0	0	0	1,0	1	57	1,0	1	57			0			0
482001	Offshore equipment switchboard S2	1	2500	1,00										0,3	1	750	0,3	1	750	0,4	0	0	0,4	0	0	0,7	1	1750						0
571020	Chilled water cooling compr. 4/4 HVAC	1	182,0	0,94	0,6	1	103	0,6	1	103	0,6	1	103	0,6	1	103	0,6	1	103	0,6	0	0	0,6	1	103	0,6	1	103	0,6	1	103			0
	Sum for ship load excluding thrusters Starboard						234			233			322			1595			1509			0			294			2512			204			0
404	Retractable thruster	1	2000	1,09	0,12	1	345	0,85	1	2550	0,47	1	1016	0,47	1	1016	0,47	1	1016	0,47	0	0	0,90	1	1953	0,47	1	1016			0			0
630	MP3	1	3000	1,09							0,11	1	352	0,11	1	352	0,11	1	352	0,11	0	0	0,18	1	596	0,11	1	352			0			0
	Sum thruster load Starboard						345			2550			1368			1368			1368			0			2550			1368			0			0

Project: U10687
Ulstein SX121
IMRV

Consumer load (TOTAL LOAD 690V MSB)

Ref. SFI	CONSUMER	TRANSIT 8,5 knots T=6,5m Load (KW)	TRANSIT 14,5 knots T=6,5m Load (KW)	DYNPOS 0 EF@90° Load (KW)	OFFSHORE CRANE OPERATION Load (KW)	ROV OPERATION Load (KW)	WORST SINGLE FAILURE AUTRO EF@90° Load (KW)	PIPE LAYING VLS OPERATION Load (KW)	HARBOUR Load (KW)	EMERGENCY Load (KW)
	Ship load and operation systems MBB1	320	328	351	1712	1625	249	2386	275	
	Ship load and operation systems MBB2	132	140	255	439	338	115	268	245	
	Ship load and operation systems MBB3	127	135	260	861	697	0	513	204	
	Ship load and operation systems MBB4	234	233	322	1595	1509	0	2512	204	
	Main propulsion and thrusters MBB1	345	2550	1490	1490	1490	5053	410	0	
	Main propulsion and thrusters MBB2	345	2550	395	395	395	2565	395	0	
	Main propulsion and thrusters MBB3	0	0	1080	1080	1080	0	0	0	
	Main propulsion and thrusters MBB4	345	2550	1368	1368	1368	0	1368	0	
	TOTAL LOAD 690V MSB	1848	8486	5522	8940	8502	7981	7852	929	
	TOTAL LOAD 440V ESB (emergency operation)									270

ALTERNATOR SETS WORKING AND LOAD IN %.

MBB1+MBB2 in kW: 606
MBB3+MBB4 in kW: 582

Total power requirement minus ship load: 363 / 0 / 7737
Loss 10% : 774
Remaining generator capasity limited to: 6963

EMERGENCY GENERATOR — No. off 1, Rated 300 : 90 %

GENERATORS % LOAD — CLOSED BUS TIES

	Rated in kW	TRANSIT 8,5 knots	TRANSIT 14,5 knots	DYNPOS	OFFSHORE CRANE	ROV	WORST SINGLE FAILURE	PIPE LAYING VLS
GENERATOR SET 1 (Bus-bar connection)	2740	67 % MBB1	77 % MBB1	101 % MBB1	82 % MBB1	78 % MBB1	97 % MBB1	96 % MBB1
GENERATOR SET 2 (Bus-bar connection)	2740	0 % MBB1	77 % MBB1	101 % MBB1	82 % MBB1	78 % MBB1	97 % MBB1	96 % MBB1
GENERATOR SET 3 (Bus-bar connection)	2740	0 % MBB2	77 % MBB2	0 % MBB2	82 % MBB2	78 % MBB2	97 % MBB2	96 % MBB2
GENERATOR SET 4 (Bus-bar connection)	2740	0 % MBB3	77 % MBB3	0 % MBB3	82 % MBB3	78 % MBB3	0 % MBB3	0 % MBB3
GENERATOR SET 5 (Bus-bar connection)	2740	0 % MBB4	0 % MBB4	0 % MBB4	0 % MBB4	0 % MBB4	0 % MBB4	0 % MBB4
GENERATOR SET 6 (Bus-bar connection)	2740	0 % MBB4	0 % MBB4	0 % MBB4	0 % MBB4	0 % MBB4	0 % MBB4	0 % MBB4
Number of engines running		1	4	2	4	4	3	3

GENERATORS % LOAD — OPEN BUS TIES, 2-SPLIT

	Rated in kW	TRANSIT 8,5 knots	TRANSIT 14,5 knots	DYNPOS	OFFSHORE CRANE	ROV	WORST SINGLE FAILURE	PIPE LAYING VLS
GENERATOR SET 1 (Bus-bar connection)	2740	42 % MBB1	68 % MBB1	91 % MBB1	74 % MBB1	70 % MBB1	97 % MBB1	63 % MBB1
GENERATOR SET 2 (Bus-bar connection)	2740	0 % MBB1	68 % MBB1	0 % MBB1	74 % MBB1	70 % MBB1	97 % MBB1	63 % MBB1
GENERATOR SET 3 (Bus-bar connection)	2740	0 % MBB2	68 % MBB2	0 % MBB2	0 % MBB2	0 % MBB2	97 % MBB2	0 % MBB2
GENERATOR SET 4 (Bus-bar connection)	2740	26 % MBB3	53 % MBB3	55 % MBB3	90 % MBB3	85 % MBB3	#DIV/0! MBB3	80 % MBB3
GENERATOR SET 5 (Bus-bar connection)	2740	0 % MBB4	53 % MBB4	55 % MBB4	90 % MBB4	85 % MBB4	#DIV/0! MBB4	80 % MBB4
GENERATOR SET 6 (Bus-bar connection)	2740	0 % MBB4	0 % MBB4	0 % MBB4	0 % MBB4	0 % MBB4	#DIV/0! MBB4	0 % MBB4
Number of engines running		2	5	3	4	4	3	4

(AND)

Total installed generator capasity: **16440 kW**

POWER USED RELATIVE TO FULL AVAILABLE CAPACITY:

	TRANSIT 8,5	TRANSIT 14,5	DYNPOS	OFFSHORE CRANE	ROV	WSF	PIPE LAYING
	RGC 14592	RGC 7954	RGC 10918	RGC 7500	RGC 7938	RGC 239	RGC 8588
	67 %	77 %	91 %	90 %	85 %	97 %	80 %

DIESEL GENERATORS: 67 % | 77 % | 91 % | 90 % | 85 % | 97 % | 80 % | (HARBOUR) 34 %

Legend:
- Power plant utilisation according available power on main bars
- N/A situation
- WSF situation

CONSUMER — Load table

Ref. SFI	CONSUMER	TRANSIT 8,5 knots T=6,5m No. in use	Load (KW)	TRANSIT 14,5 knots T=6,5m No. in use	Load (KW)	DYNPOS 0 EF@90° No. in use	Load (KW)	OFFSHORE CRANE OPERATION No. in use	Load (KW)	ROV OPERATION No. in use	Load (KW)	WORST SINGLE FAILURE AUTR EF@90° No. in use	Load (KW)	PIPE LAYING VLS OPERATION No. in use	Load (KW)	HARBOUR No. in use	Load (KW)	EMERGENCY No. in use	Load (KW)
	Ship load and operation systems MBB1		320		328		351		1712		1625		0		2386		275		
	Ship load and operation systems MBB2		132		140		255		439		338		227		268		245		
	Ship load and operation systems MBB3		127		135		260		861		697		222		513		204		
	Ship load and operation systems MBB4		234		233		322		1595		1509		294		2512		204		
	Main propulsion and thrusters MBB1		345		2550		1490		1490		1490		0		410		0		
	Main propulsion and thrusters MBB2		345		2550		395		395		395		714		395		0		
	Main propulsion and thrusters MBB3		0		0		1080		1080		1080		2067		0		0		
	Main propulsion and thrusters MBB4		345		2550		1368		1368		1368		2550		1368		0		
	TOTAL LOAD 690V MSB		1848		8486		5522		8940		8502		6075		7852		929		
	TOTAL LOAD 440V ESB (emergency operation)																		270

ALTERNATOR SETS WORKING AND LOAD IN %.

MBB1+MBB2 in kW: 606 / 582
MBB3+MBB4 in kW: 7494

Total power requirement minus ship load: 227 / 516 / 10057 / 1006 / 9051
Loss 10%
Remaining generator capasity limited to 90%

	No. off	Rated in kW	
EMERGENCY GENERATOR	1	300	90 %

GENERATORS % LOAD — CLOSED BUS TIES

	Rated in kW	TRANSIT 8,5 knots	Load	TRANSIT 14,5 knots	Load	DYNPOS	Load	OFFSHORE CRANE	Load	ROV	Load	WORST SINGLE FAILURE	Load	PIPE LAYING VLS
GENERATOR SET 1 (Bus-bar connection)	2740	1 MBB1	67 %	1 MBB1	77 %	1 MBB1	101 %	1 MBB1	82 %	1 MBB1	78 %	0 MBB1	0 %	1 MBB1 96 %
GENERATOR SET 2 (Bus-bar connection)	2740	0 MBB1	0 %	1 MBB1	77 %	1 MBB1	101 %	1 MBB1	82 %	1 MBB1	78 %	0 MBB1	0 %	1 MBB1 96 %
GENERATOR SET 3 (Bus-bar connection)	2740	0 MBB2	0 %	1 MBB2	77 %	0 MBB2	0 %	1 MBB2	82 %	1 MBB2	78 %	1 MBB2	55 %	1 MBB2 96 %
GENERATOR SET 4 (Bus-bar connection)	2740	0 MBB3	0 %	1 MBB3	77 %	0 MBB3	0 %	1 MBB3	82 %	1 MBB3	78 %	1 MBB3	55 %	0 MBB3 0 %
GENERATOR SET 5 (Bus-bar connection)	2740	0 MBB4	0 %	0 MBB4	0 %	0 MBB4	0 %	0 MBB4	0 %	0 MBB4	0 %	1 MBB4	55 %	0 MBB4 0 %
GENERATOR SET 6 (Bus-bar connection)	2740	0 MBB4	0 %	0 MBB4	0 %	0 MBB4	0 %	0 MBB4	0 %	0 MBB4	0 %	1 MBB4	55 %	0 MBB4 0 %
Number of engines running		1		4		2		4		4		4		3

GENERATORS % LOAD — OPEN BUS TIES, 3-SPLIT

	Rated in kW	TRANSIT 8,5 knots	Load	TRANSIT 14,5 knots	Load	DYNPOS	Load	OFFSHORE CRANE	Load	ROV	Load	WORST SINGLE FAILURE	Load	PIPE LAYING VLS
GENERATOR SET 1 (Bus-bar connection)	2740	1 MBB1	24 %	1 MBB1	53 %	1 MBB1	67 %	1 MBB1	58 %	1 MBB1	57 %	0 MBB1	#DIV/0!	1 MBB1 51 %
GENERATOR SET 2 (Bus-bar connection)	2740	0 MBB1	0 %	1 MBB1	53 %	0 MBB1	0 %	1 MBB1	58 %	1 MBB1	57 %	0 MBB1	#DIV/0!	1 MBB1 51 %
AND														
GENERATOR SET 3 (Bus-bar connection)	2740	0 MBB2	0 %	1 MBB2	52 %	1 MBB2	73 %	1 MBB2	51 %	1 MBB2	92 %	1 MBB2	59 %	1 MBB2 43 %
GENERATOR SET 4 (Bus-bar connection)	2740	1 MBB3	22 %	1 MBB3	52 %	0 MBB3	0 %	1 MBB3	51 %	0 MBB3	0 %	1 MBB3	59 %	0 MBB3 0 %
AND														
GENERATOR SET 5 (Bus-bar connection)	2740	1 MBB4	21 %	1 MBB4	102 %	1 MBB4	62 %	1 MBB4	54 %	1 MBB4	52 %	1 MBB4	52 %	1 MBB4 71 %
GENERATOR SET 6 (Bus-bar connection)	2740	0 MBB4	0 %	0 MBB4	0 %	0 MBB4	0 %	1 MBB4	54 %	1 MBB4	52 %	1 MBB4	52 %	1 MBB4 71 %
Number of engines running		3		5		3		6		5		4		5

Total installed generator capasity: 16440 kW

POWER USED RELATIVE TO FULL AVAILABLE CAPACITY

	TRANSIT 8,5	TRANSIT 14,5	DYNPOS	OFFSHORE	ROV	WORST SINGLE	PIPE LAYING	HARBOUR
RGC	14592	7954	10918	7500	7938	4885	8588	
DIESEL GENERATORS	67 %	77 %	73 %	58 %	92 %	59 %	71 %	34 %

Legend:
Power plant utilisation according available power on main bars
N/A situation
WSF situation

A

Appendix B

A.1. Length of vessel stay with crane use
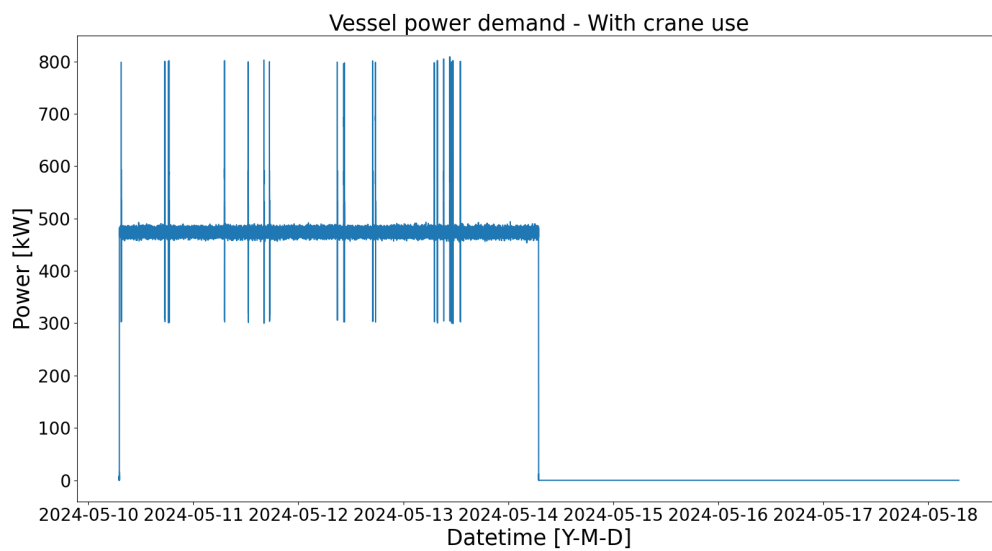
Figure A.1: Figure of a 4 day vessel power profile followed by 4 days of downtime. The vessel power profile includes 20 crane use dispersed among the 4 days. This vessel power profile was used for the HE ESS shore power configuration. The x-axis is in datetime meaning each data point is fixed to a date and time.
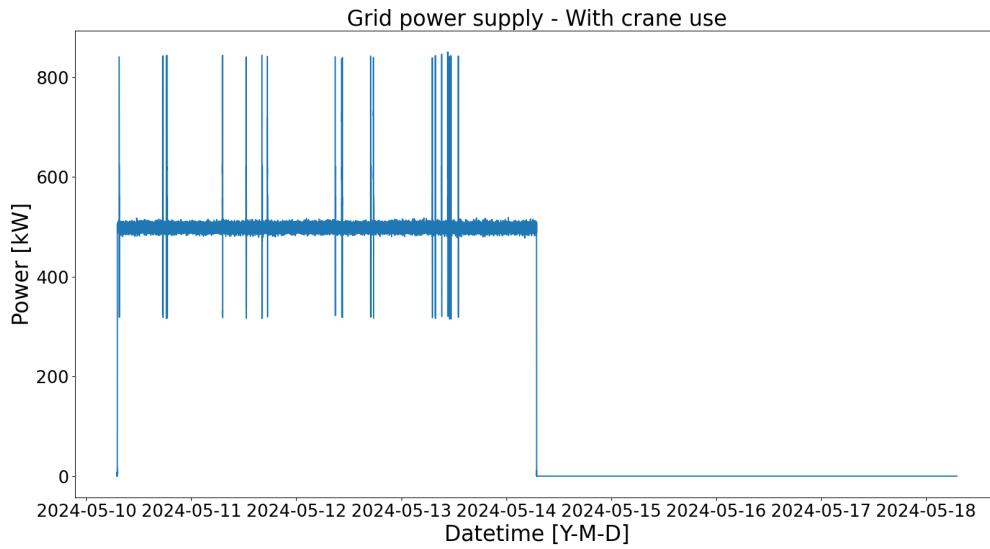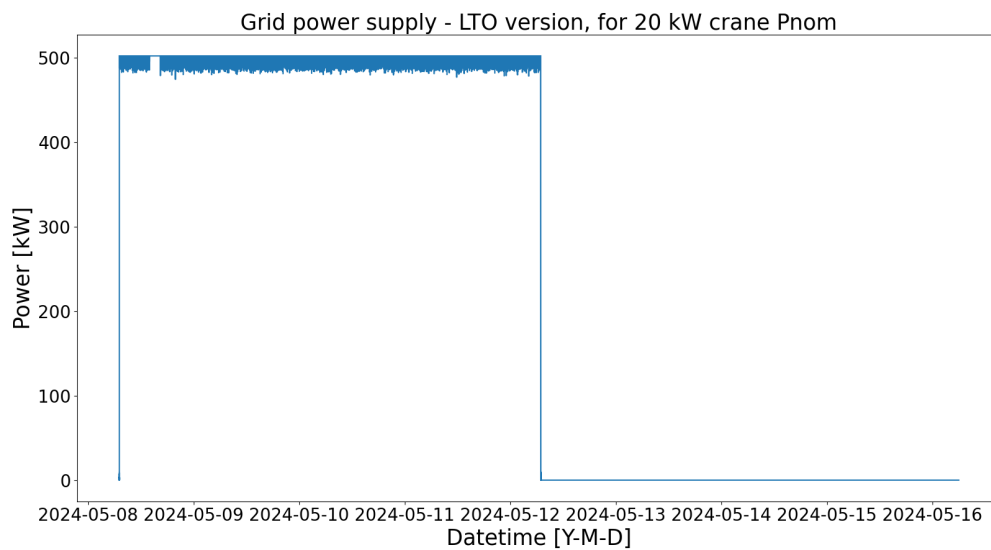
Figure A.2: Figure of the grid power supply by the status quo shore power configuration. The grid supplies the power that the power demand of Figure A.1 requires. This figure is used to compare to the different versions of the HE ESS shore power configuration.
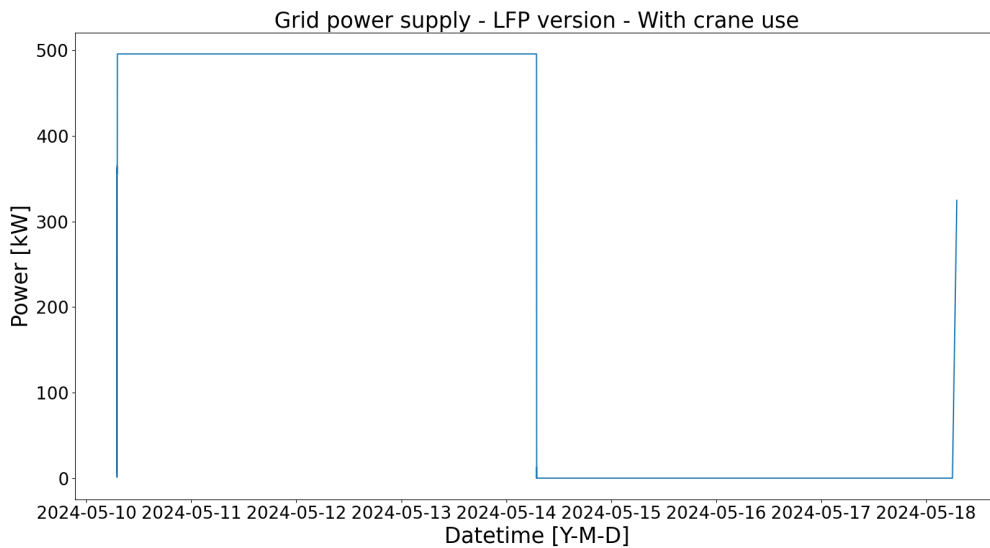
Figure A.3: Figure of the grid power supply by the LFP version of the HE ESS shore power configuration. The minor and major fluctuations in power demand of the vessel power profile of Figure A.1 are peak shaven by the LFP battery.
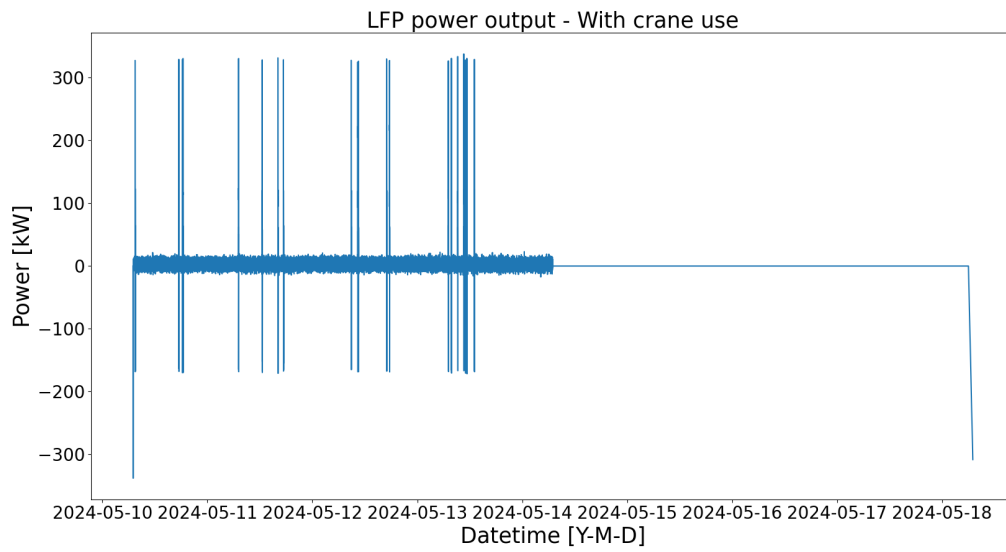
Figure A.4: Figure of the LFP battery power output of the LFP version of the HE ESS shore power configuration. The LFP battery peak shaves the minor and major fluctuations in power demand of the vessel power profile of Figure A.1.
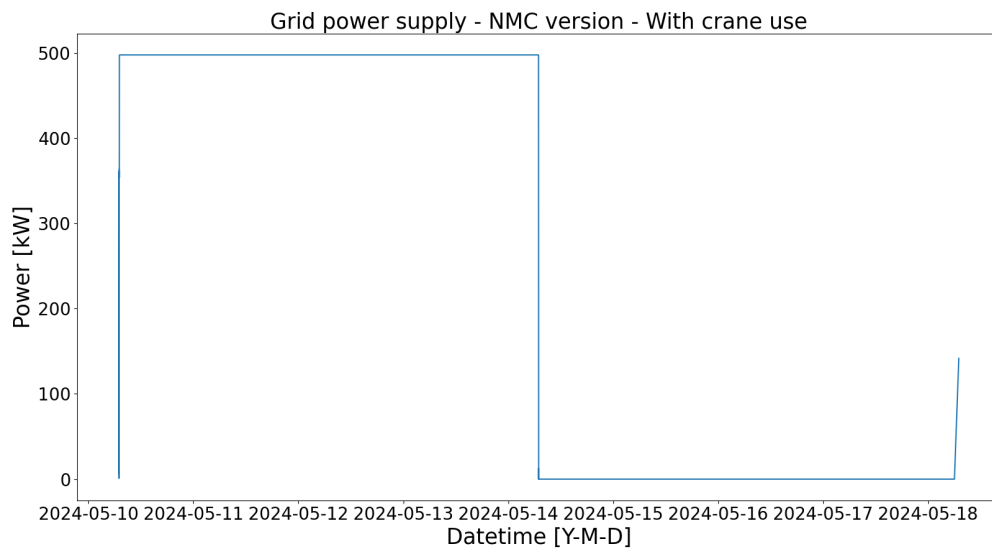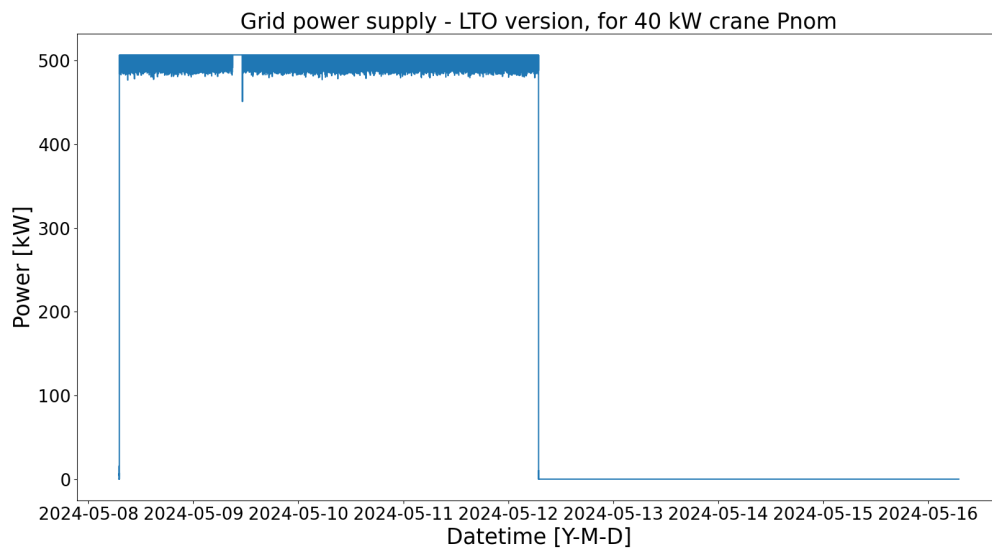

Figure A.5: Figure of the grid power supply by the NMC version of the HE ESS shore power configuration. The minor and major fluctuations in power demand of the vessel power profile of Figure A.1 are peak shaven by the NMC battery.
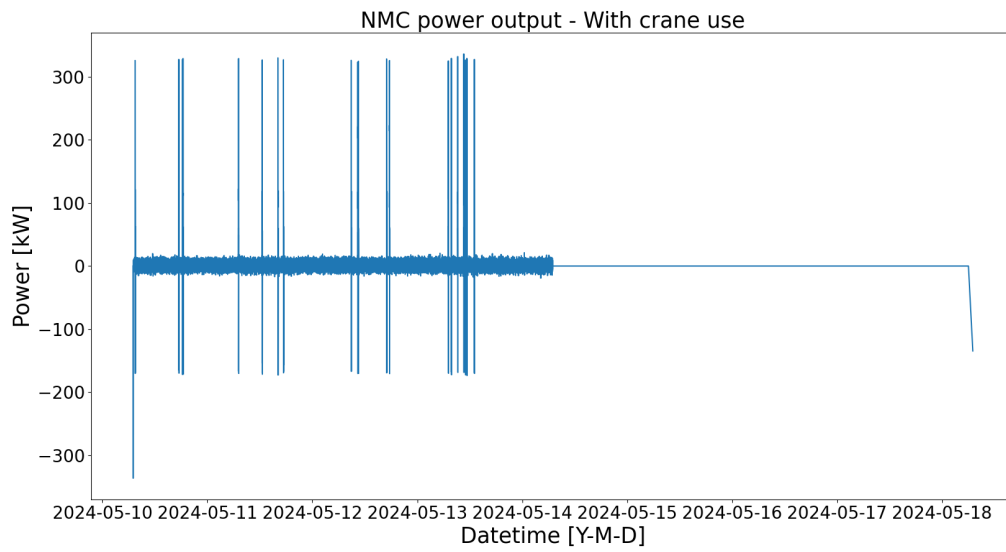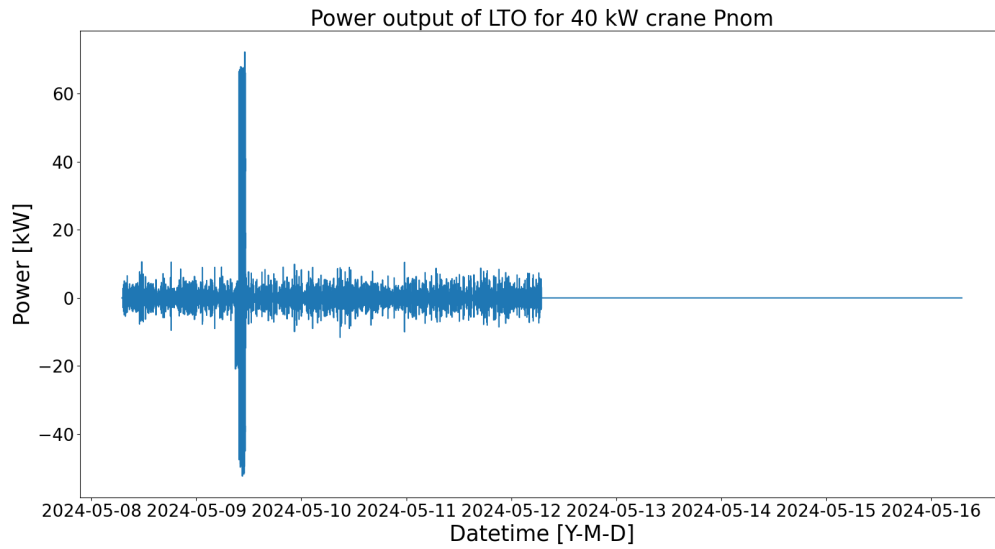
Figure A.6: Figure of the NMC battery power output of the NMC version of the HE ESS shore power configuration. The NMC battery peak shaves the minor and major fluctuations in power demand of the vessel power profile of Figure A.1.
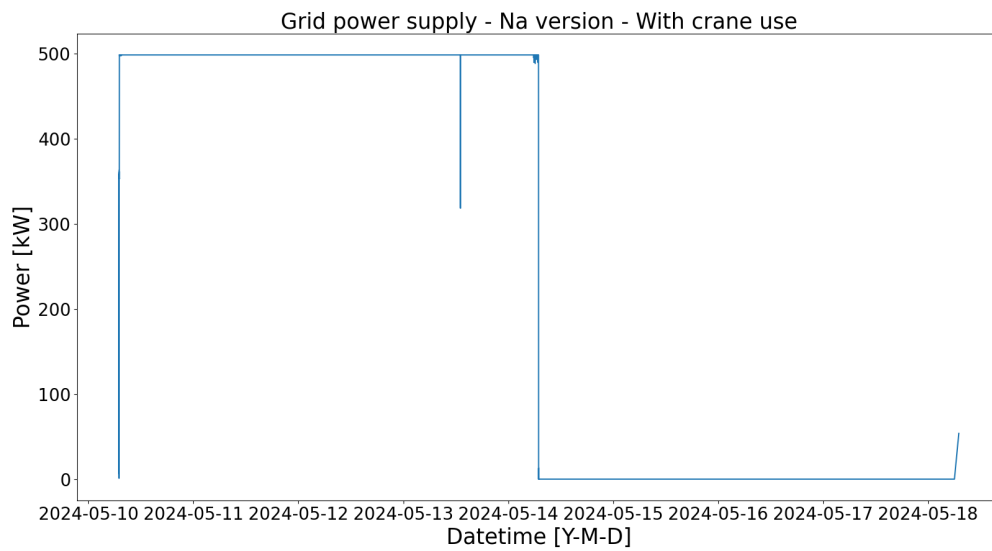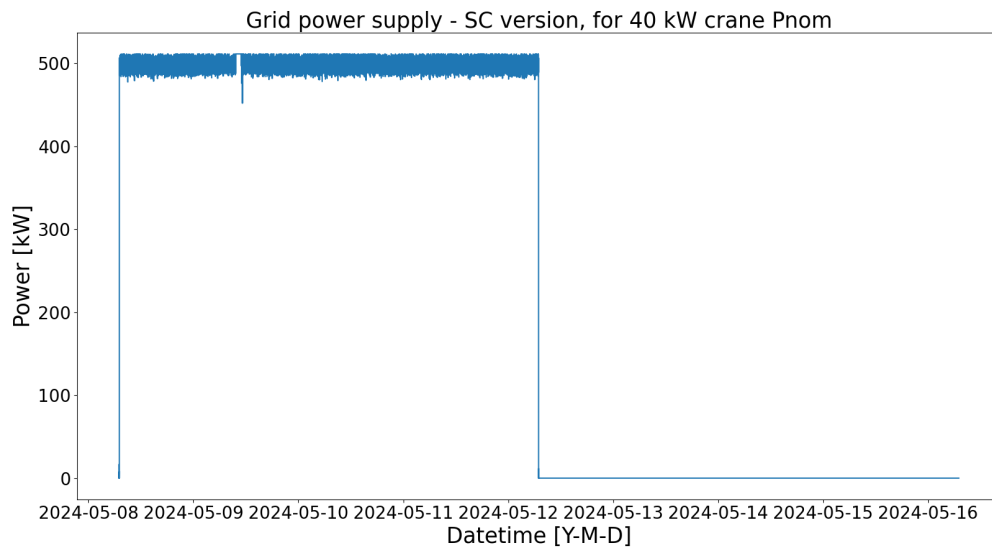

Figure A.7: Figure of the grid power supply by the Na-ion version of the HE ESS shore power configuration. The minor and major fluctuations in power demand of the vessel power profile of Figure A.1 are peak shaven by the Na-ion battery.
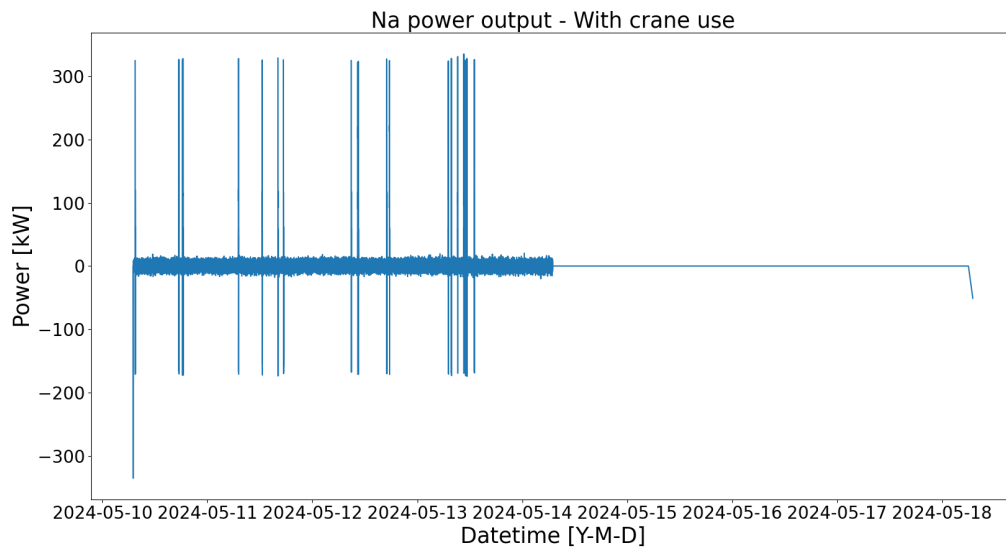
Figure A.8: Figure of the Na-ion battery power output of the Na-ion version of the HE ESS shore power configuration. The Na-ion battery peak shaves the minor and major fluctuations in power demand of the vessel power profile of Figure A.1.
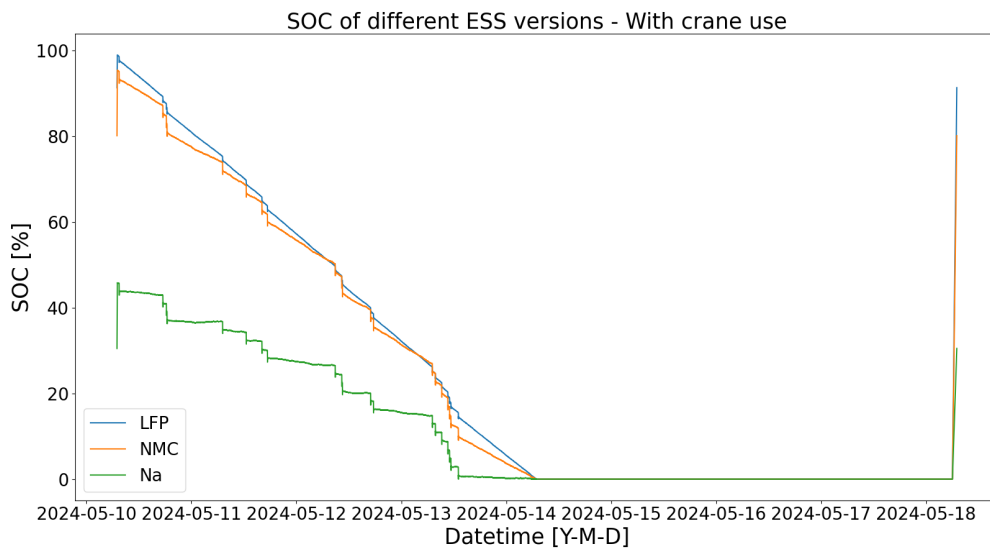
Figure A.9: Figure of the SOC of the different versions of the HE ESS shore power configuration. The ESS is continuously discharged but there are spikes in discharge when the crane is used.
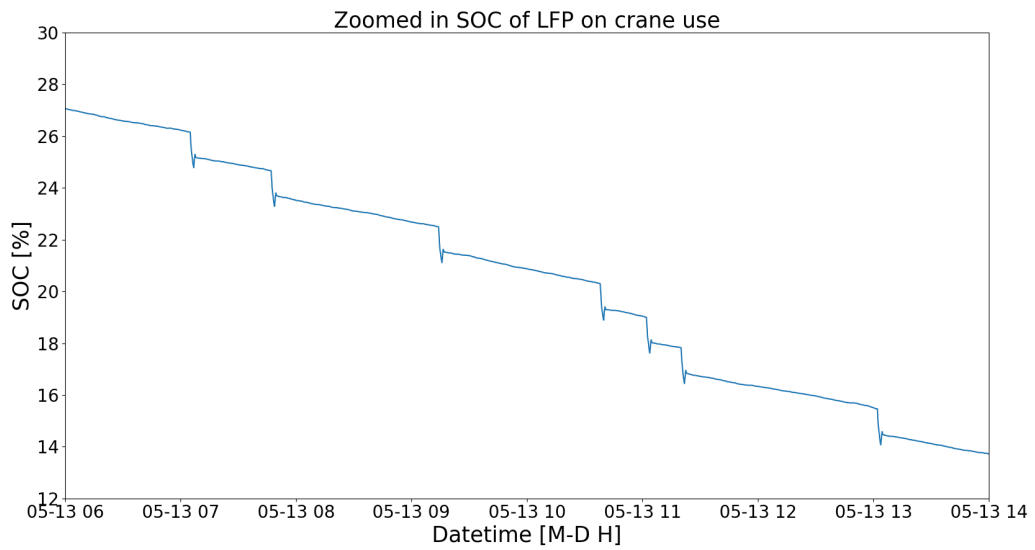
Figure A.10: Figure of the SOC of the LFP version of the HE ESS shore power configuration. The figure is zoomed in on a few crane uses to show that there is a small charge and discharge cycle per crane use.

A.2. Length of vessel stay without crane use
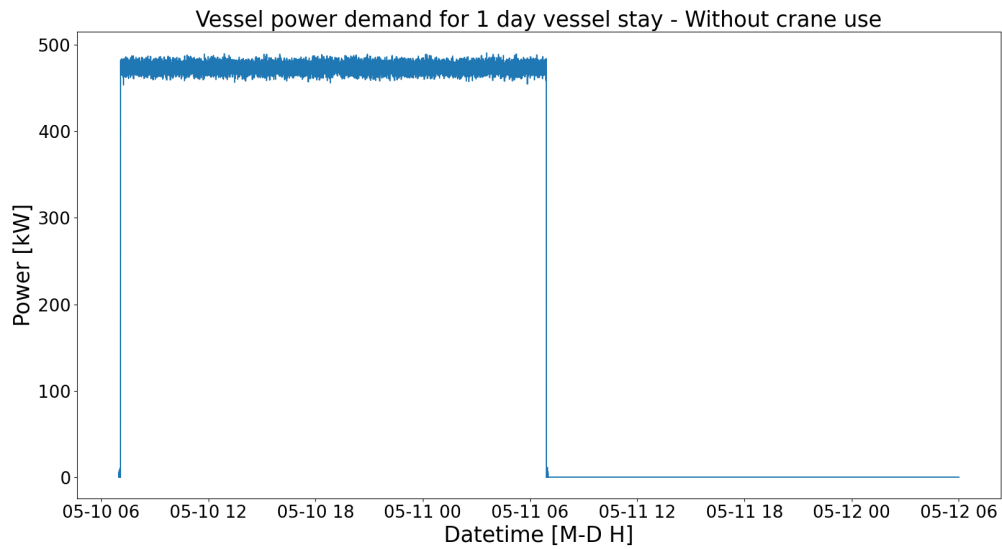
Figure A.11: Figure of a vessel power profile of 1 day followed by 1 day of downtime. The power profile does not include crane uses. The vessel power profile was used for the HE ESS shore power configuration. The x-axis is in datetime meaning each data point is fixed to a date and time.
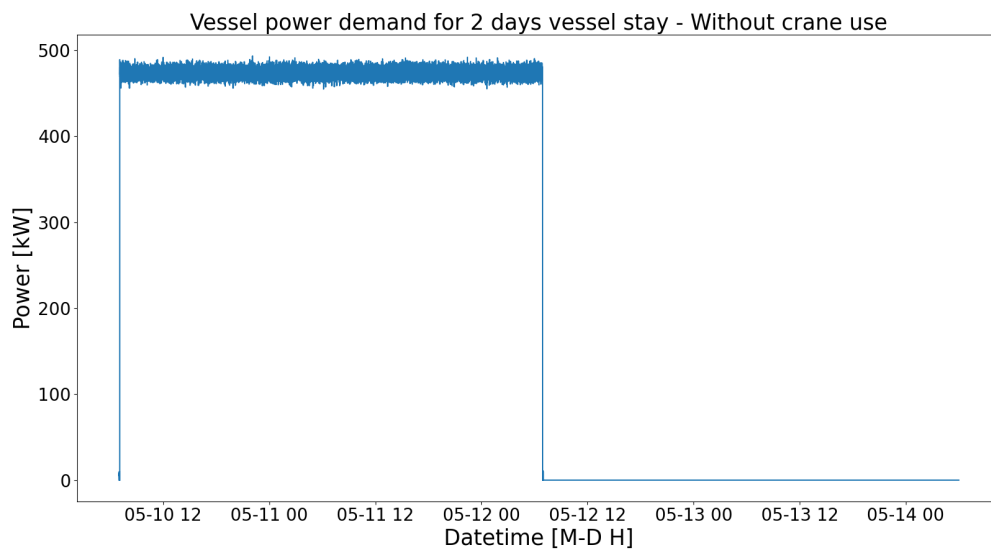
Figure A.12: Figure of a vessel power profile of 2 days followed by 2 days of downtime. The power profile does not include crane uses. The vessel power profile was used for the HE ESS shore power configuration. The x-axis is in datetime meaning each data point is fixed to a date and time.
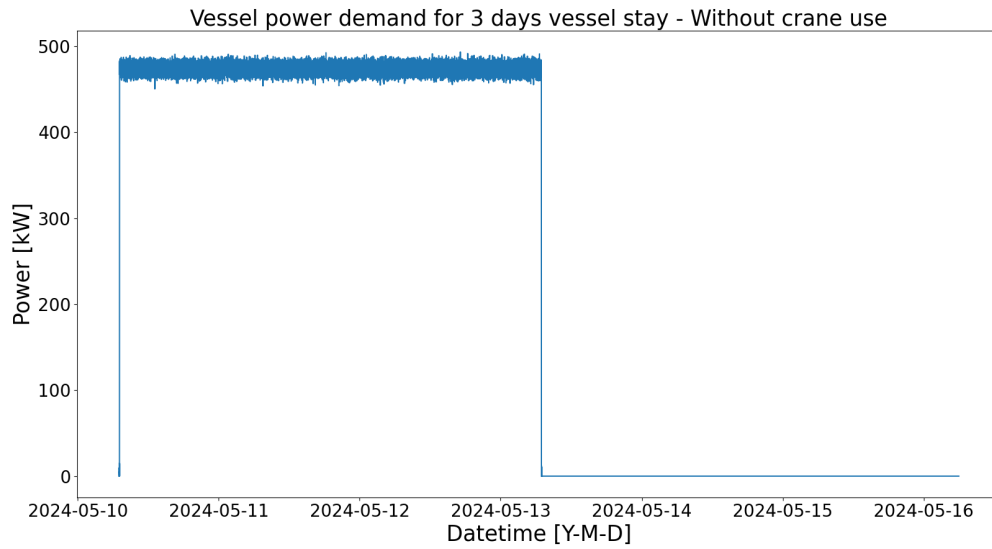
Figure A.13: Figure of a vessel power profile of 3 days followed by 3 days of downtime. The power profile does not include crane uses. The vessel power profile was used for the HE ESS shore power configuration. The x-axis is in datetime meaning each data point is fixed to a date and time.
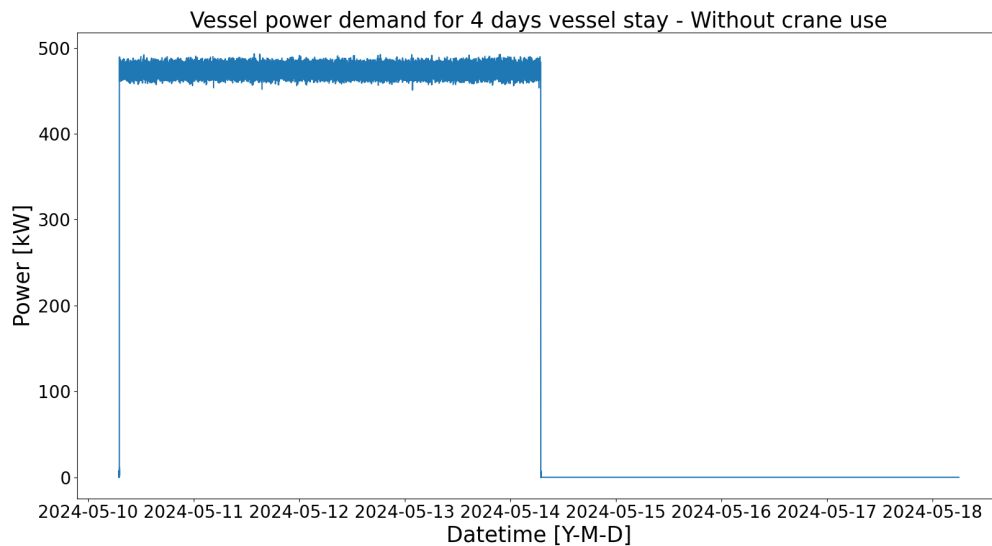
Figure A.14: Figure of a vessel power profile of 4 days followed by 4 days of downtime. The power profile does not include crane uses. The vessel power profile was used for the HE ESS shore power configuration. The x-axis is in datetime meaning each data point is fixed to a date and time.

A.2.1. LFP

Grid power supply for 1 day vessel stay - LFP version - Without crane use
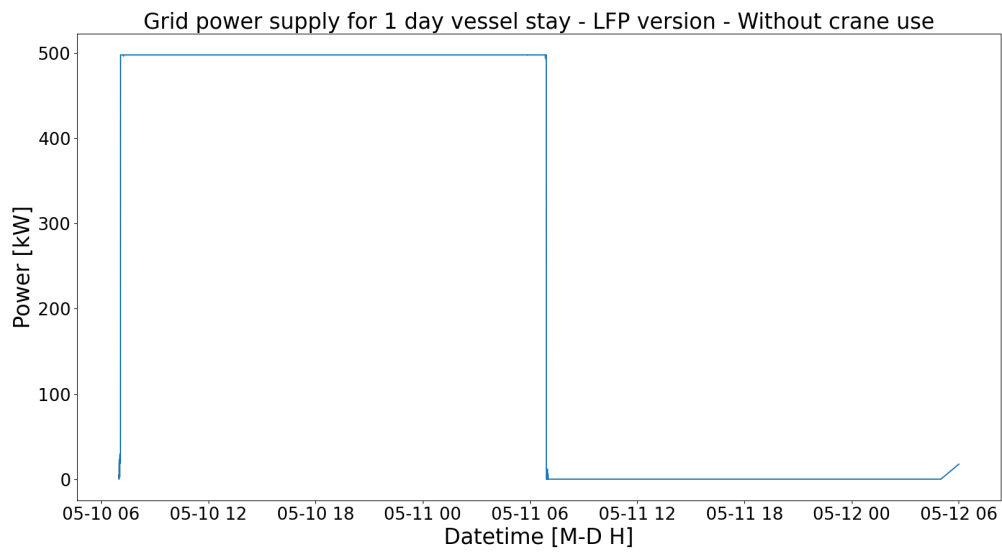
Figure A.15: Figure of the grid power supply by the LFP version of the HE ESS shore power configuration. The minor fluctuations in power demand of the vessel power profile of Figure A.11 are peak shaven by the LFP battery.

Power output of LFP for 1 day vessel stay - Without crane use
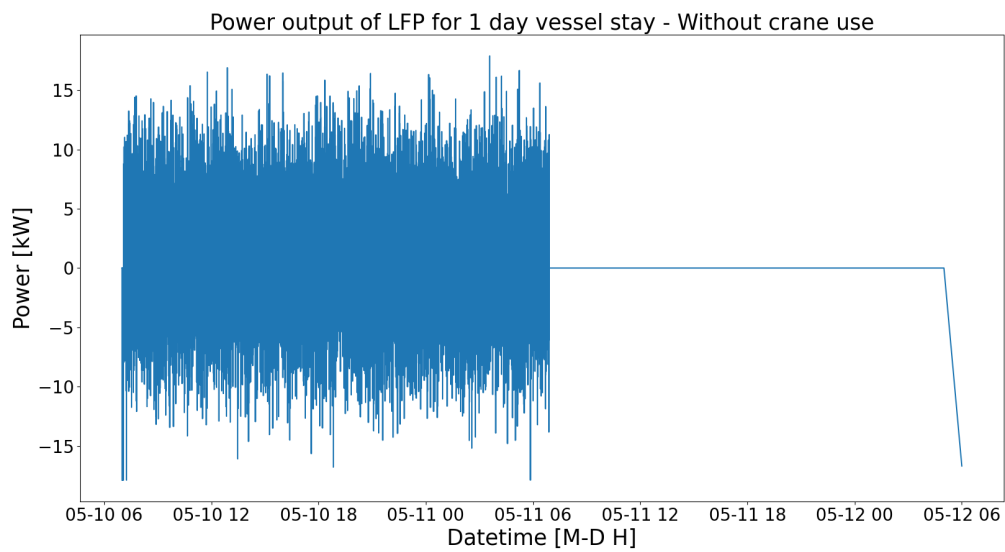
Figure A.16: Figure of the power output of the LFP battery by the LFP version of the HE ESS shore power configuration. The minor fluctuations in power demand of the vessel power profile of Figure A.11 are peak shaven by the LFP battery.
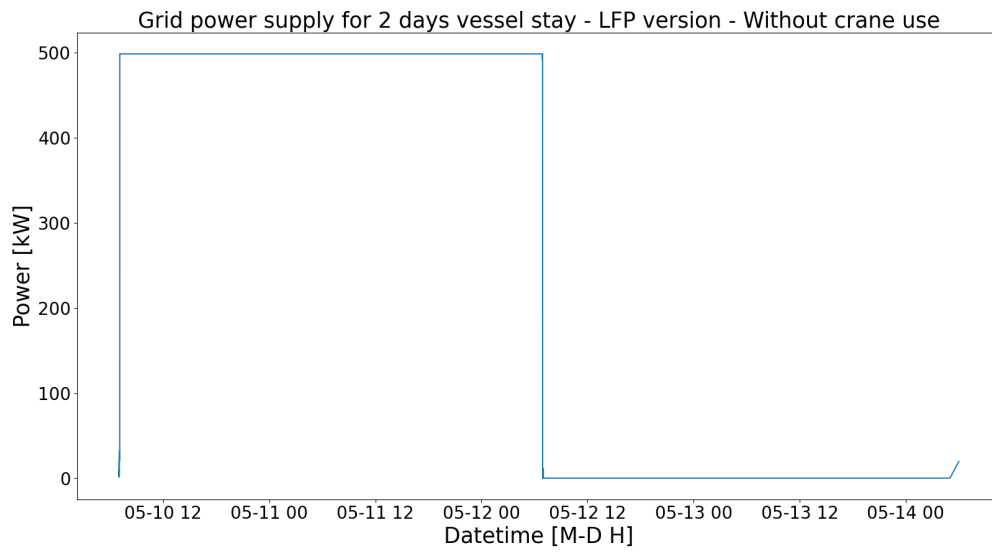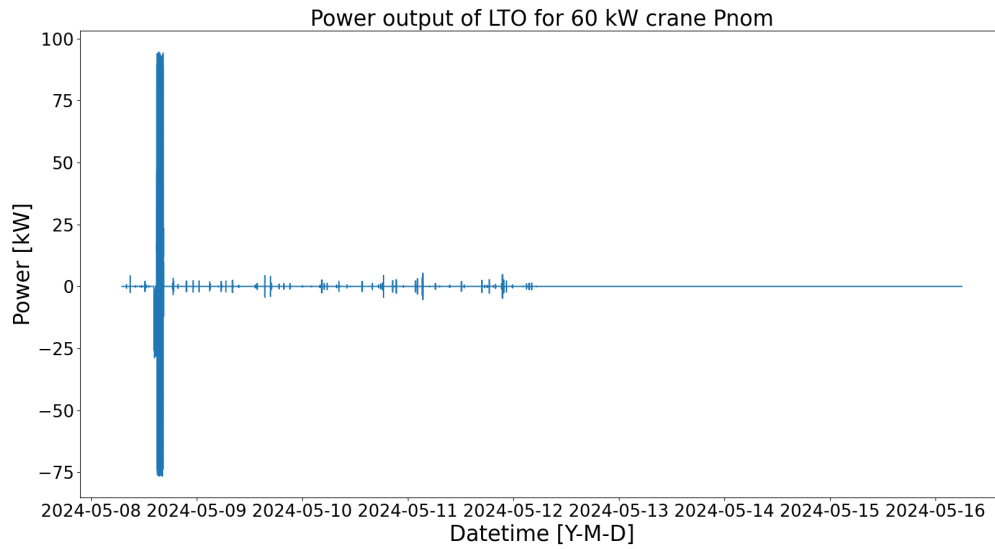
Figure A.17: Figure of the grid power supply by the LFP version of the HE ESS shore power configuration. The minor fluctuations in power demand of the vessel power profile of Figure A.12 are peak shaven by the LFP battery.
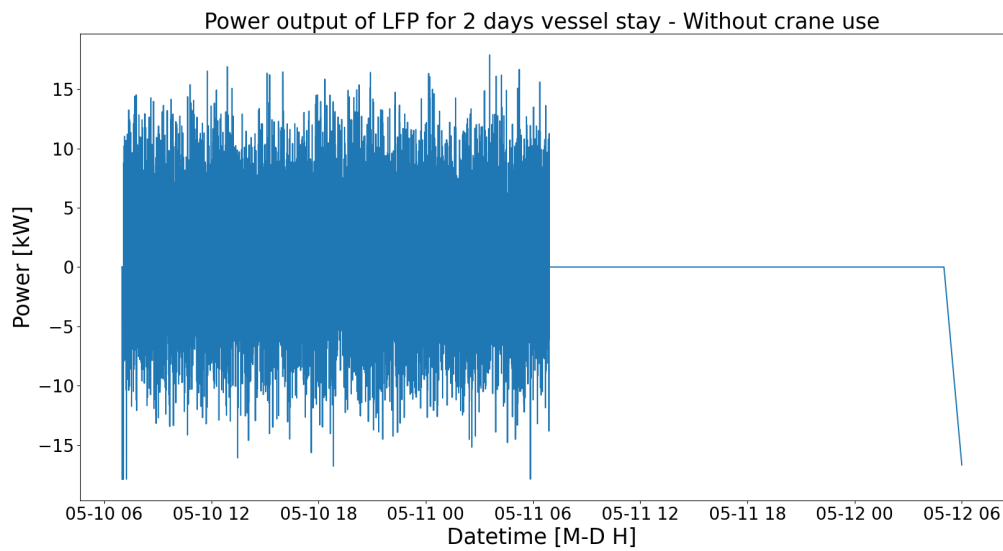
Figure A.18: Figure of the power output of the LFP battery by the LFP version of the HE ESS shore power configuration. The minor fluctuations in power demand of the vessel power profile of Figure A.12 are peak shaven by the LFP battery.
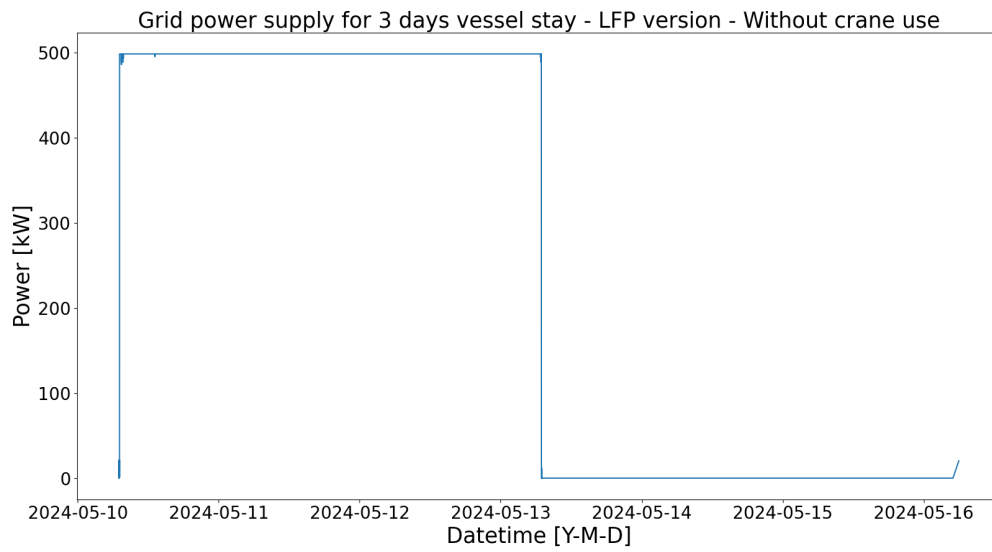
Figure A.19: Figure of the grid power supply by the LFP version of the HE ESS shore power configuration. The minor fluctuations in power demand of the vessel power profile of Figure A.13 are peak shaven by the LFP battery.
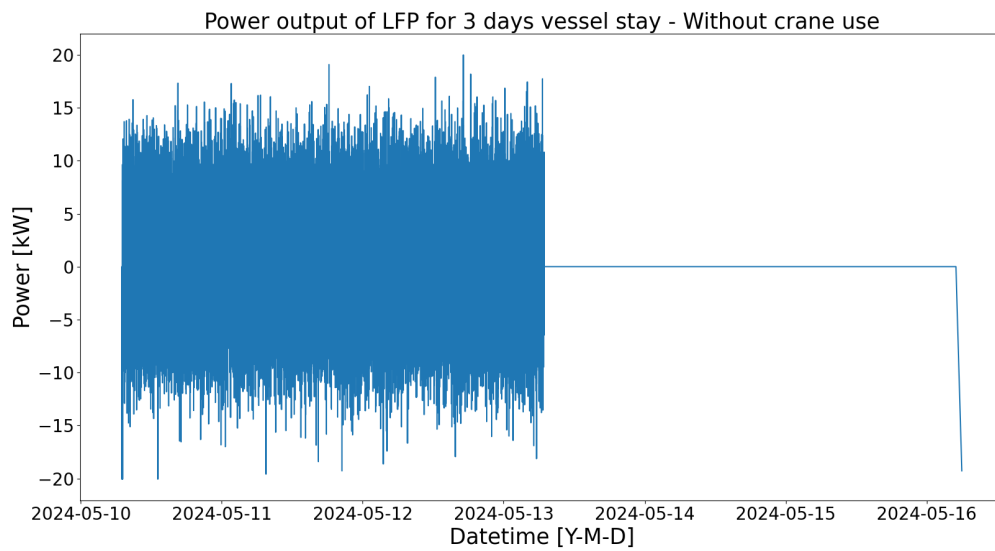
Figure A.20: Figure of the power output of the LFP battery by the LFP version of the HE ESS shore power configuration. The minor fluctuations in power demand of the vessel power profile of Figure A.13 are peak shaven by the LFP battery.
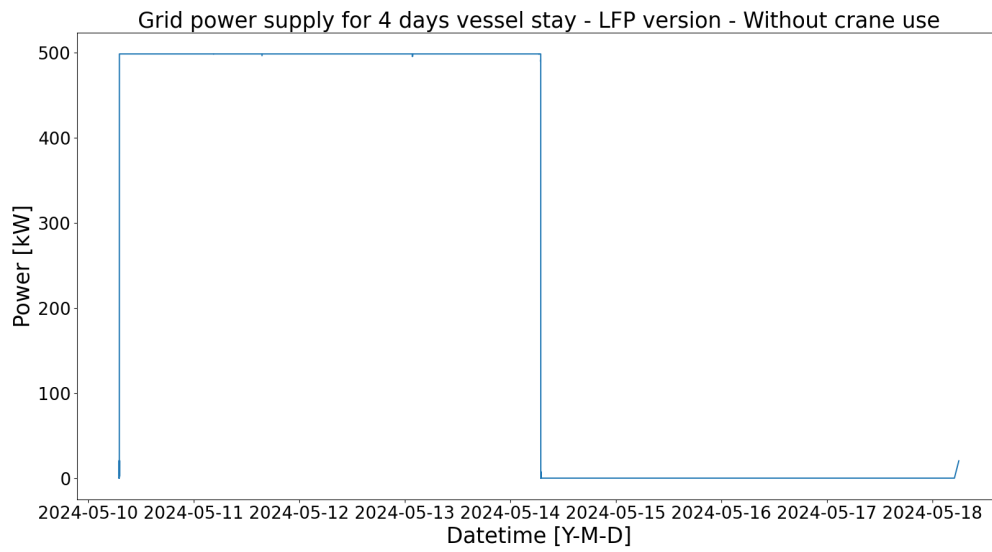
Figure A.21: Figure of the grid power supply by the LFP version of the HE ESS shore power configuration. The minor fluctuations in power demand of the vessel power profile of Figure A.14 are peak shaven by the LFP battery.
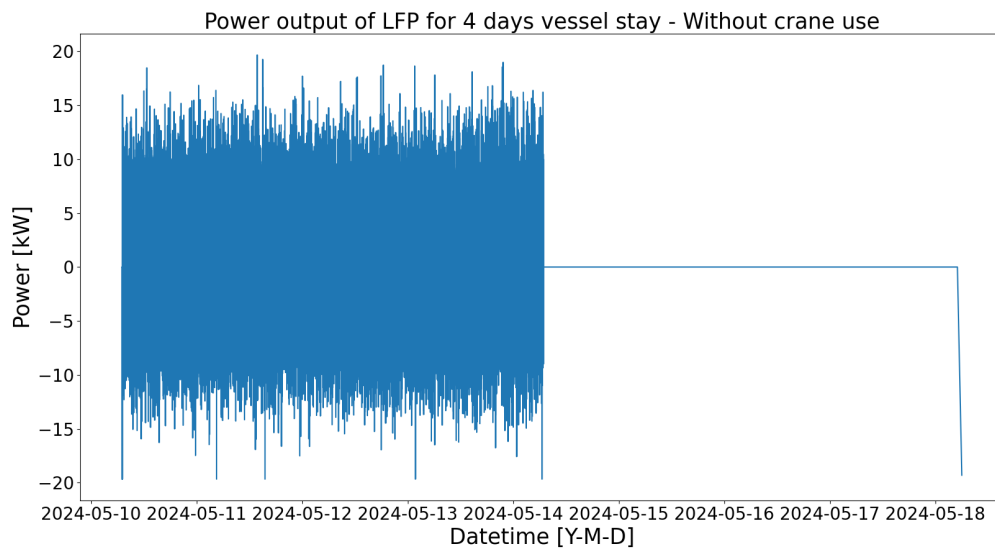
Figure A.22: Figure of the power output of the LFP battery by the LFP version of the HE ESS shore power configuration. The minor fluctuations in power demand of the vessel power profile of Figure A.14 are peak shaven by the LFP battery.
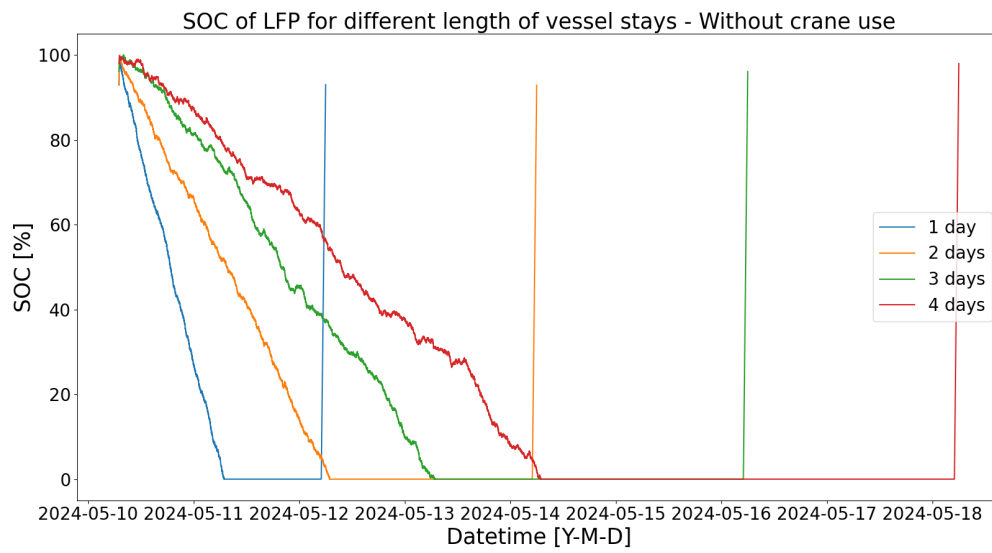
Figure A.23: Figure of the SOC of the LFP version of the HE ESS shore power configuration. The different plots correspond to different length of vessel stays that are simulated. All plots are charged up to full before the vessel connects and then slowly fully discharge until the vessel disconnects.

A.2.2. NMC
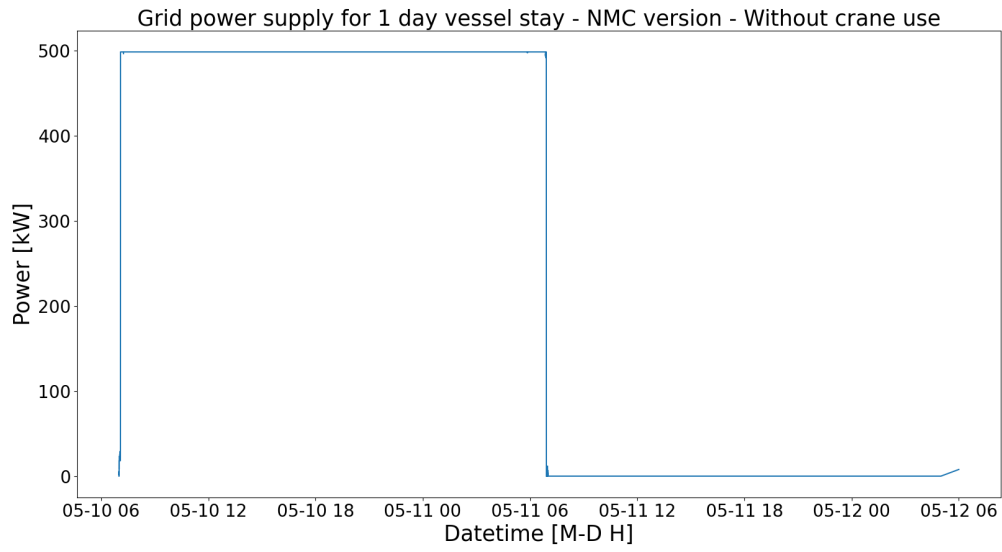
Figure A.24: Figure of the grid power supply by the NMC version of the HE ESS shore power configuration. The minor fluctuations in power demand of the vessel power profile of Figure A.11 are peak shaven by the NMC battery.
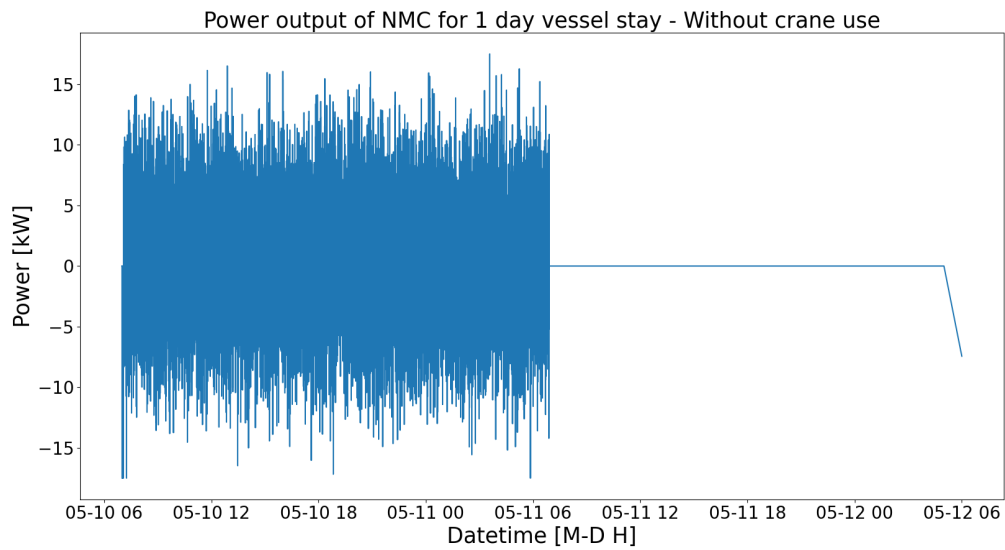
Figure A.25: Figure of the power output of the NMC battery by the NMC version of the HE ESS shore power configuration. The minor fluctuations in power demand of the vessel power profile of Figure A.11 are peak shaven by the NMC battery.
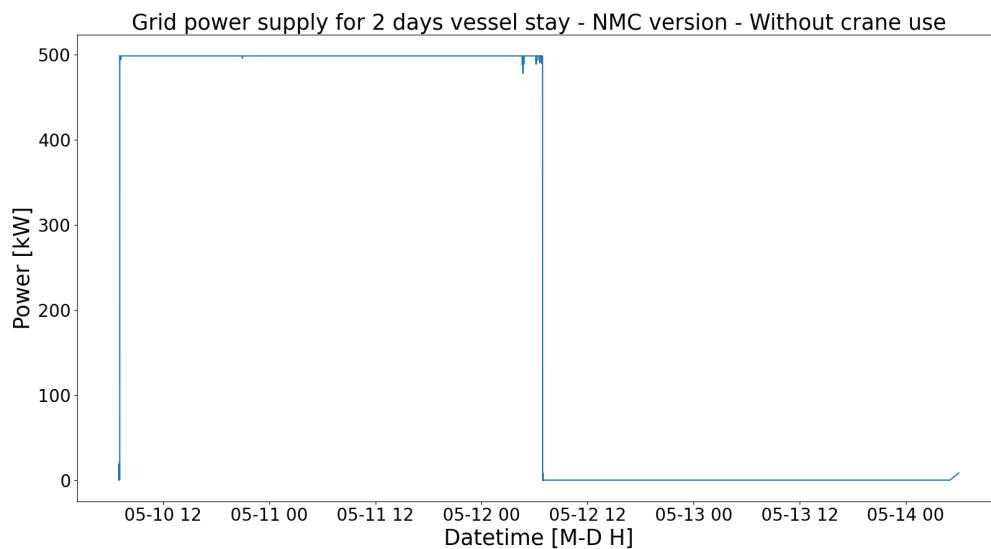
Figure A.26: Figure of the grid power supply by the NMC version of the HE ESS shore power configuration. The minor fluctuations in power demand of the vessel power profile of Figure A.12 are peak shaven by the NMC battery.
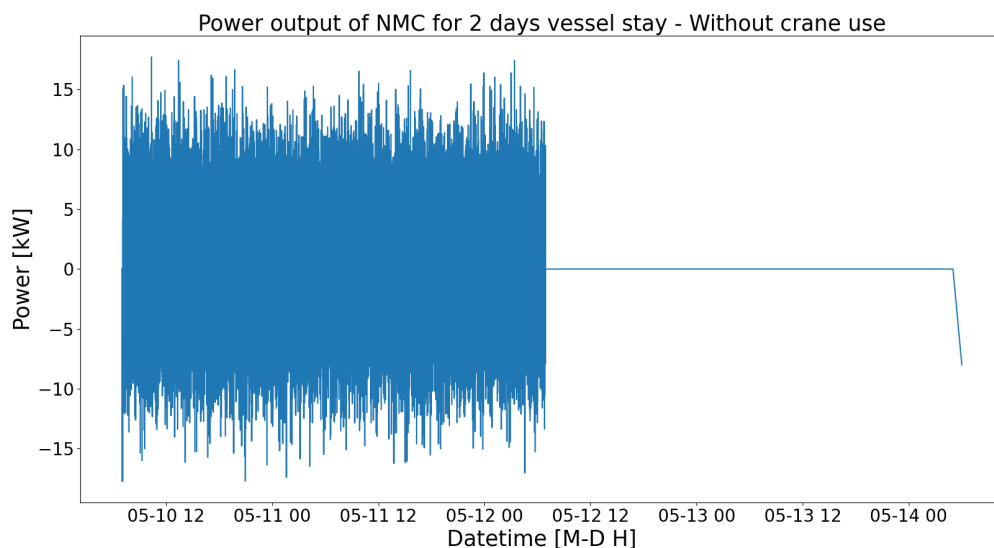
Figure A.27: Figure of the power output of the NMC battery by the NMC version of the HE ESS shore power configuration. The minor fluctuations in power demand of the vessel power profile of Figure A.12 are peak shaven by the NMC battery.
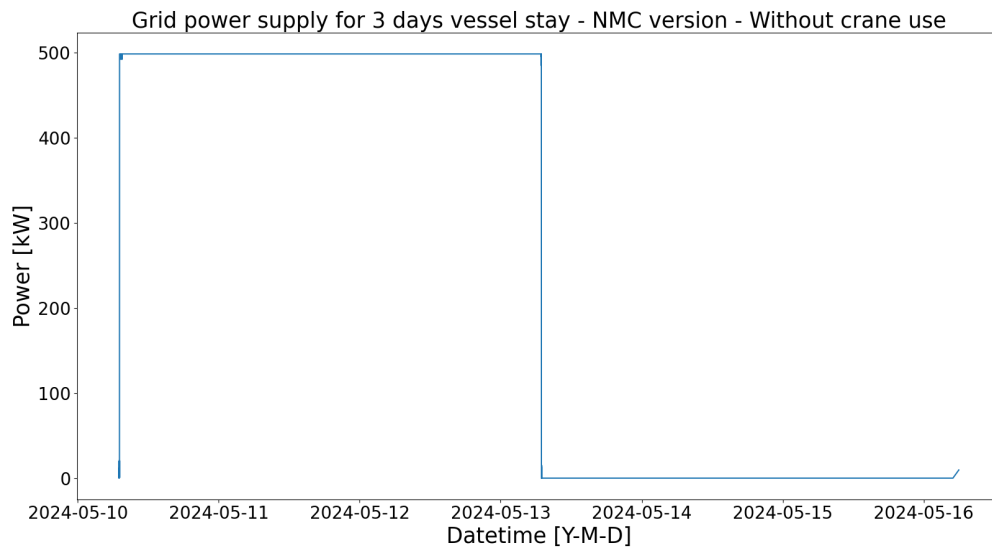
Figure A.28: Figure of the grid power supply by the NMC version of the HE ESS shore power configuration. The minor fluctuations in power demand of the vessel power profile of Figure A.13 are peak shaven by the NMC battery.
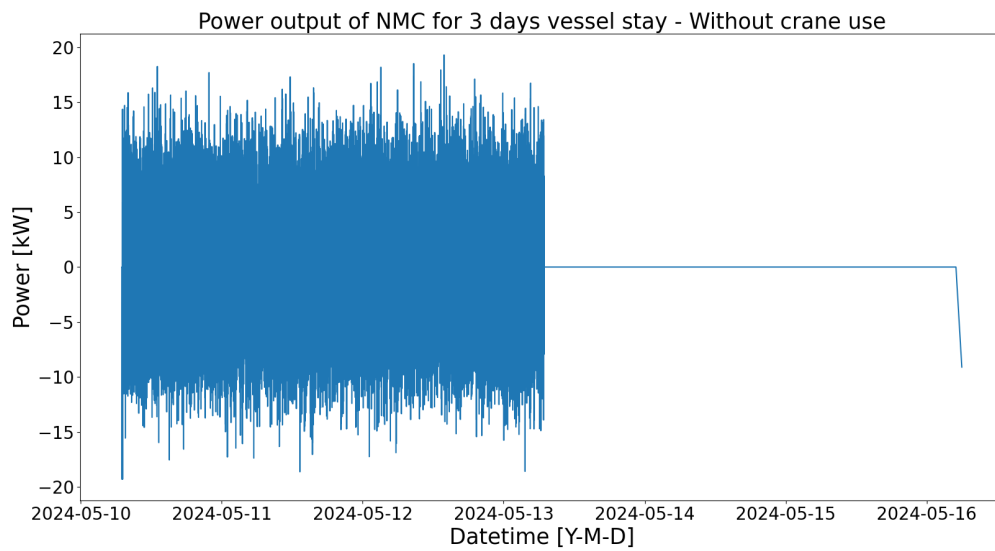
Figure A.29: Figure of the power output of the NMC battery by the NMC version of the HE ESS shore power configuration. The minor fluctuations in power demand of the vessel power profile of Figure A.13 are peak shaven by the NMC battery.
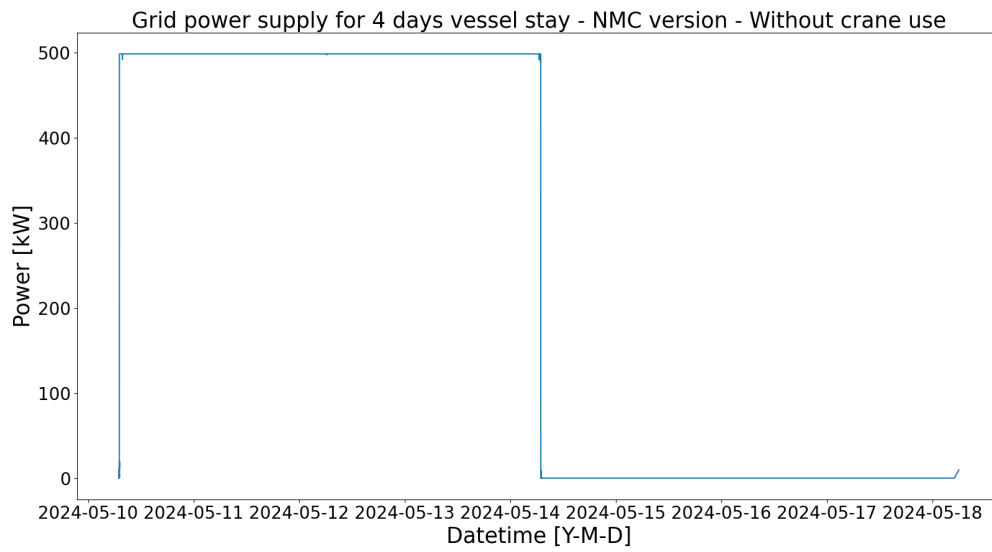
Figure A.30: Figure of the grid power supply by the NMC version of the HE ESS shore power configuration. The minor fluctuations in power demand of the vessel power profile of Figure A.14 are peak shaven by the NMC battery.
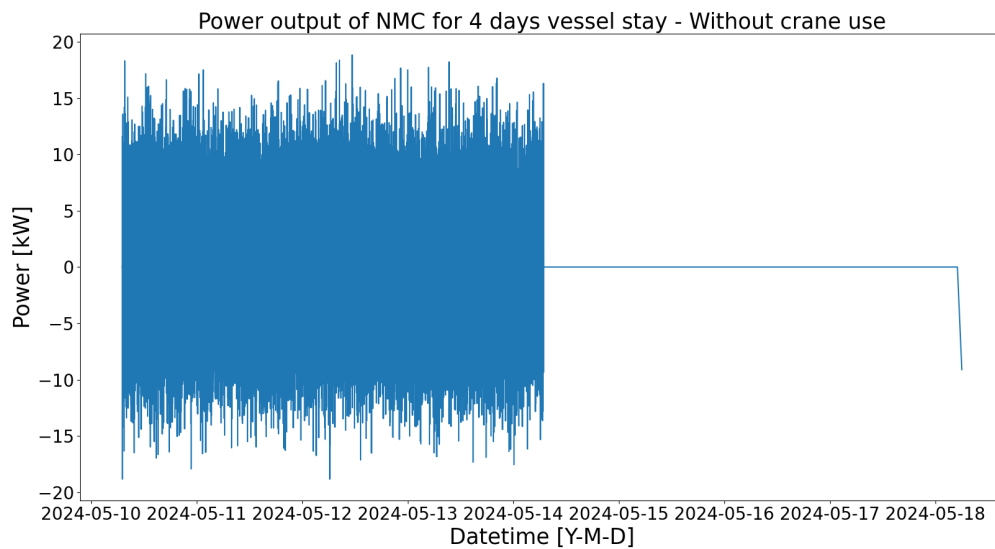
Figure A.31: Figure of the power output of the NMC battery by the NMC version of the HE ESS shore power configuration. The minor fluctuations in power demand of the vessel power profile of Figure A.14 are peak shaven by the NMC battery.
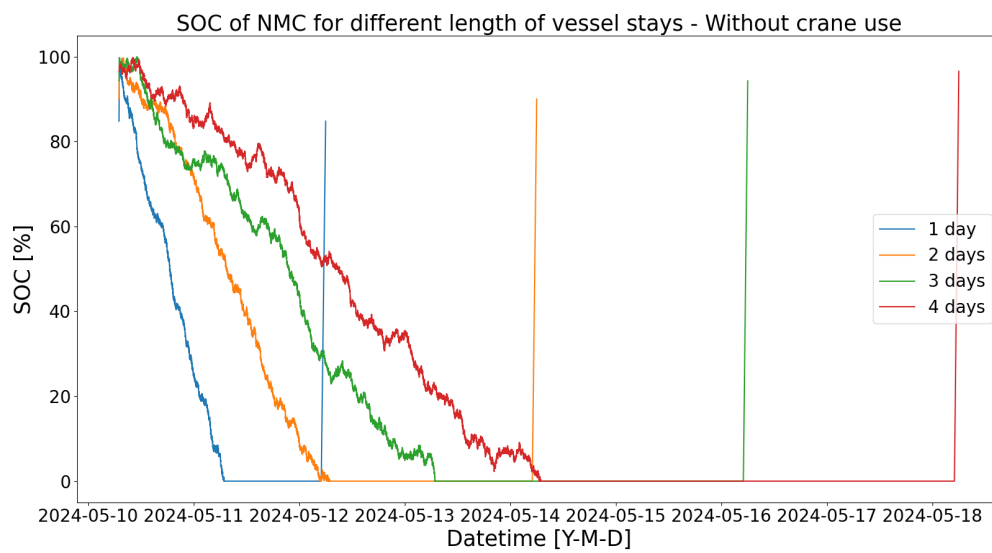
Figure A.32: Figure of the SOC of the NMC version of the HE ESS shore power configuration. The different plots correspond to different length of vessel stays that are simulated. All plots are charged up to full before the vessel connects and then slowly fully discharge until the vessel disconnects.

A.2.3. Na-ion
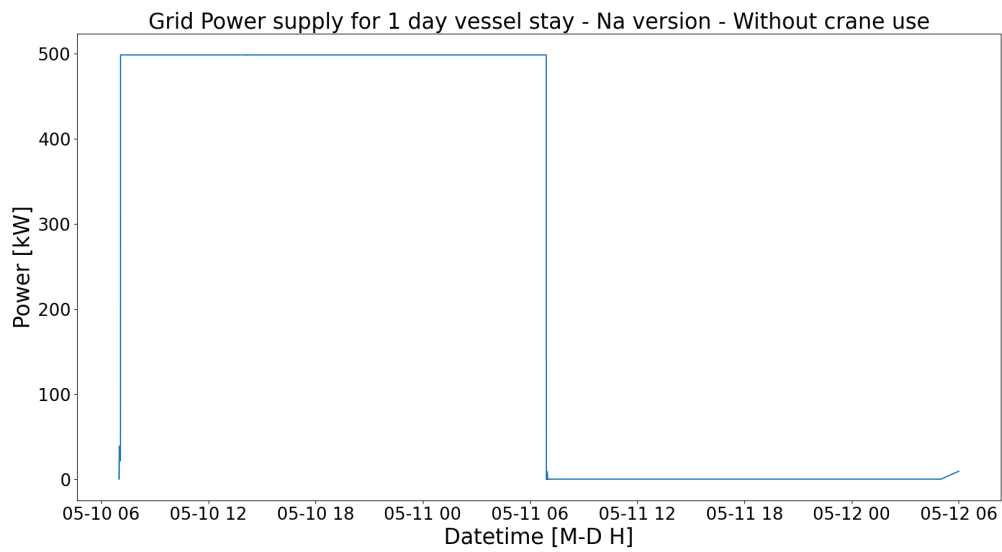
Figure A.33: Figure of the grid power supply by the Na version of the HE ESS shore power configuration. The minor fluctuations in power demand of the vessel power profile of Figure A.11 are peak shaven by the Na battery.
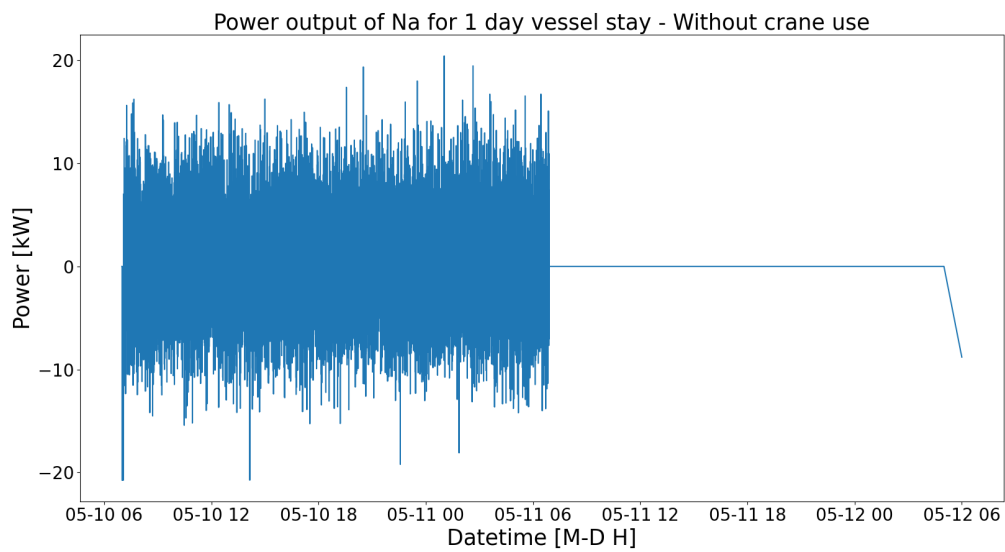
Figure A.34: Figure of the power output of the Na battery by the Na version of the HE ESS shore power configuration. The minor fluctuations in power demand of the vessel power profile of Figure A.11 are peak shaven by the Na battery.
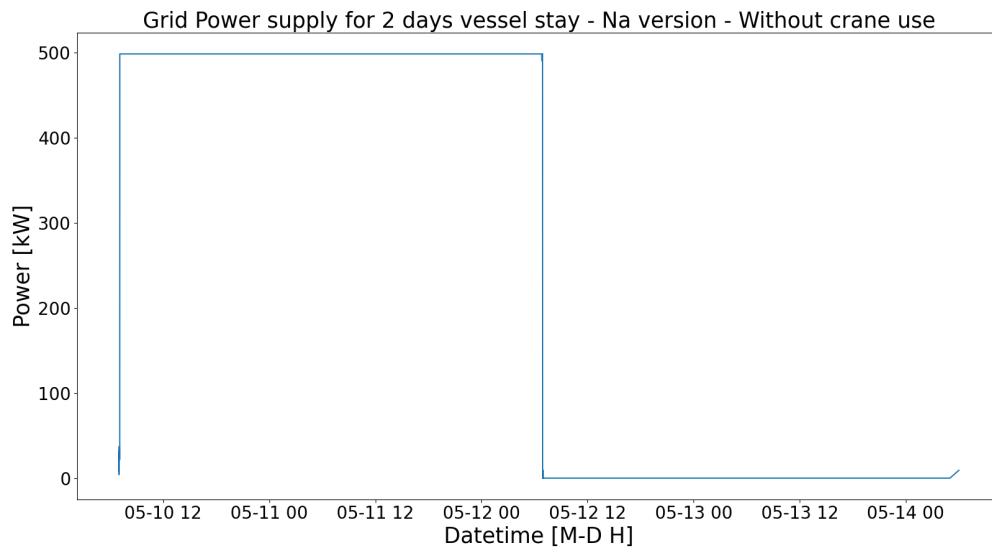
Figure A.35: Figure of the grid power supply by the Na version of the HE ESS shore power configuration. The minor fluctuations in power demand of the vessel power profile of Figure A.12 are peak shaven by the Na battery.
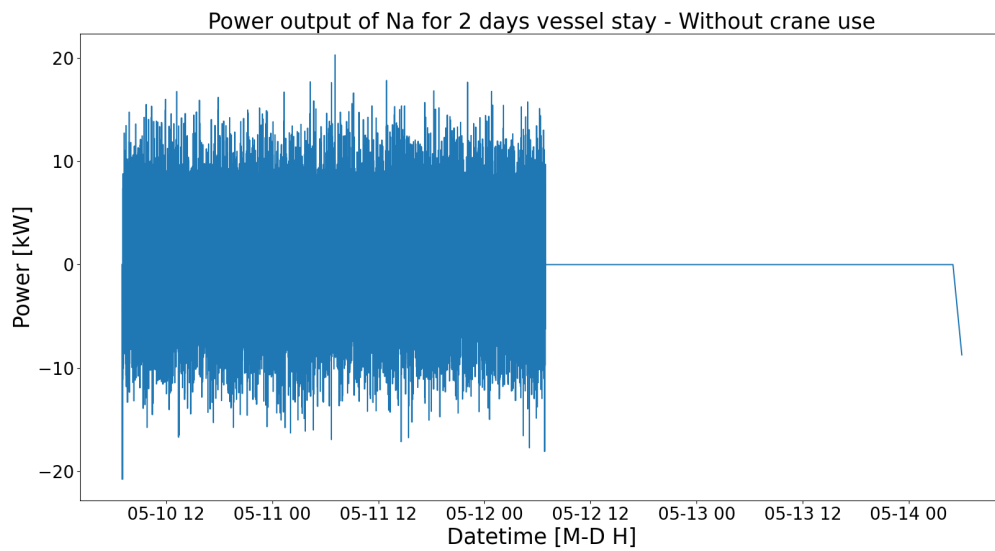
Figure A.36: Figure of the power output of the Na battery by the Na version of the HE ESS shore power configuration. The minor fluctuations in power demand of the vessel power profile of Figure A.12 are peak shaven by the Na battery.
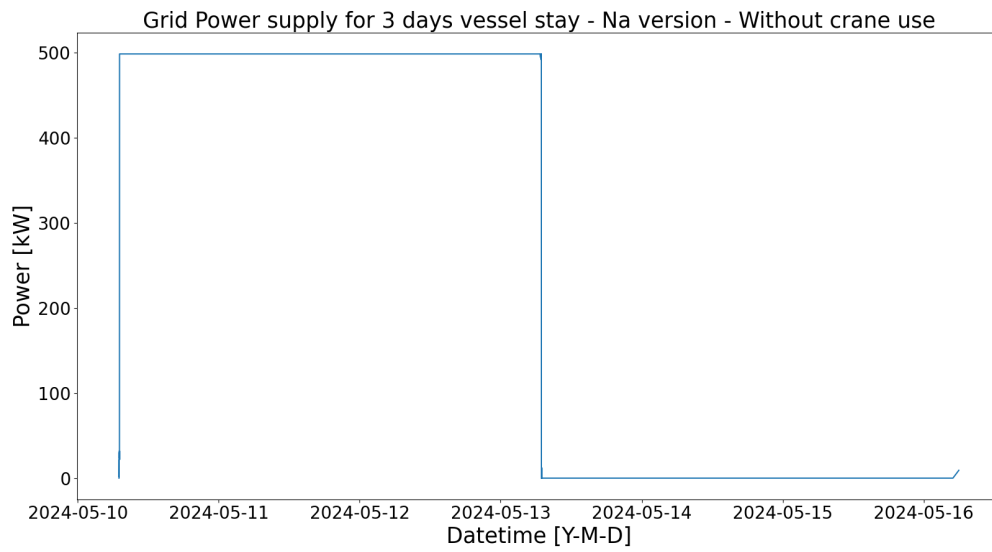
Figure A.37: Figure of the grid power supply by the Na version of the HE ESS shore power configuration. The minor fluctuations in power demand of the vessel power profile of Figure A.13 are peak shaven by the Na battery.
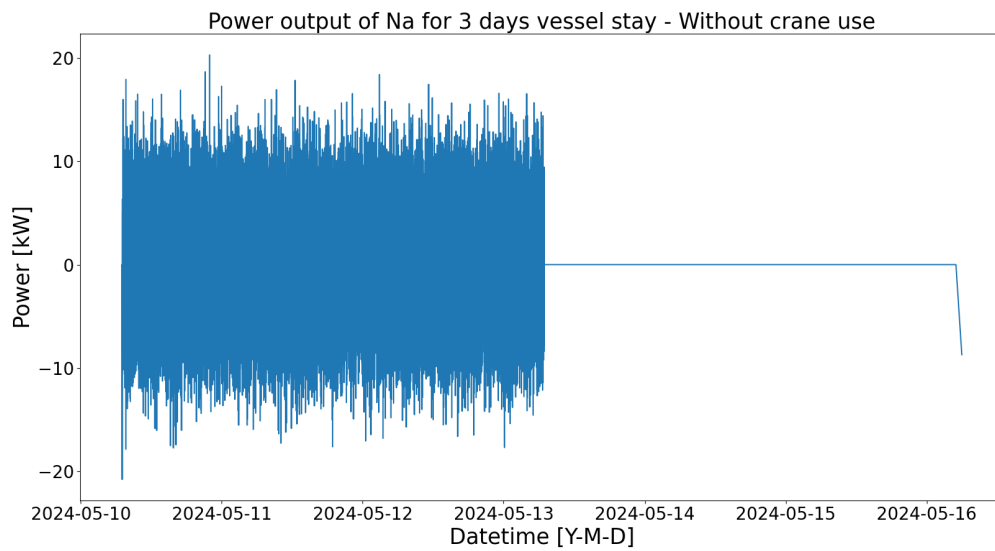
Figure A.38: Figure of the power output of the Na battery by the Na version of the HE ESS shore power configuration. The minor fluctuations in power demand of the vessel power profile of Figure A.13 are peak shaven by the Na battery.
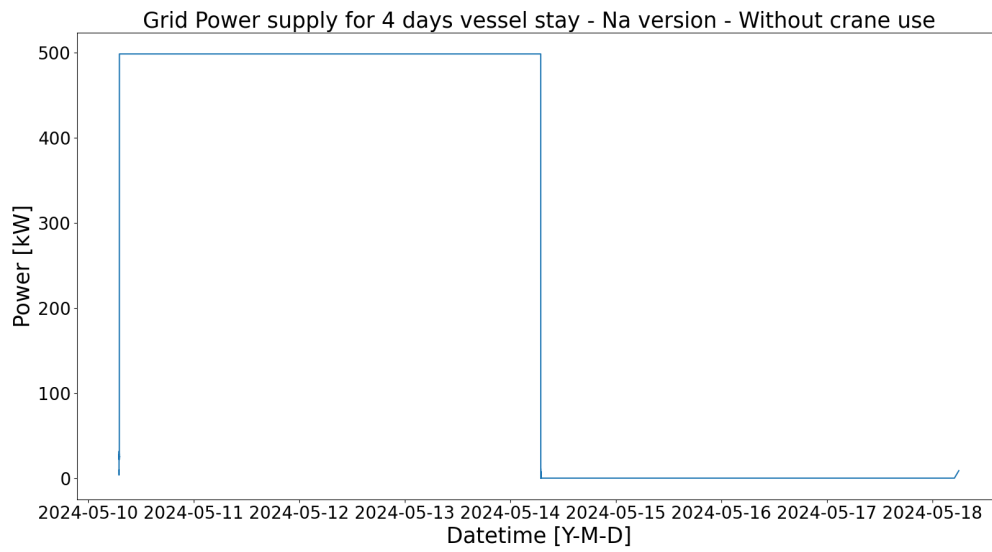
Figure A.39: Figure of the grid power supply by the Na version of the HE ESS shore power configuration. The minor fluctuations in power demand of the vessel power profile of Figure A.14 are peak shaven by the Na battery.
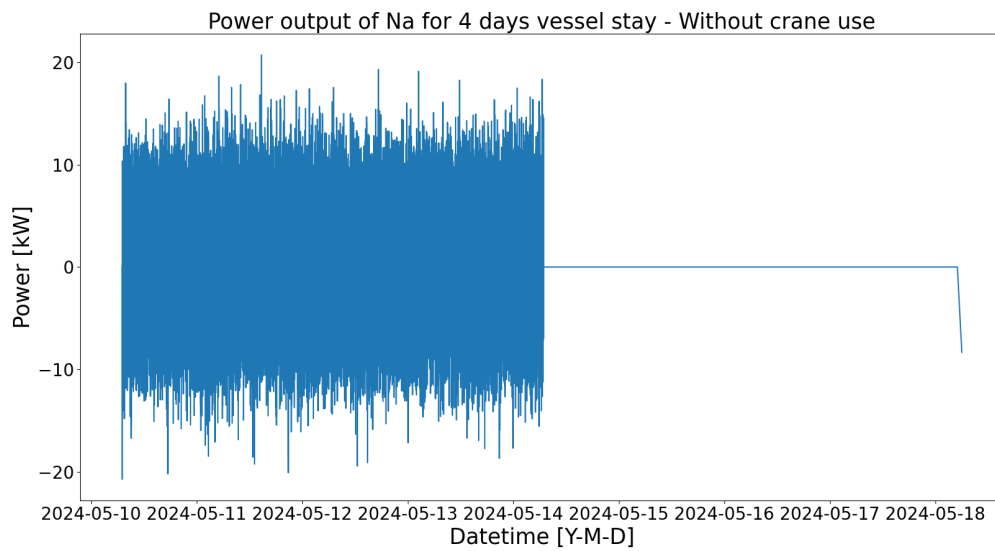
Figure A.40: Figure of the power output of the Na battery by the Na version of the HE ESS shore power configuration. The minor fluctuations in power demand of the vessel power profile of Figure A.14 are peak shaven by the Na battery.
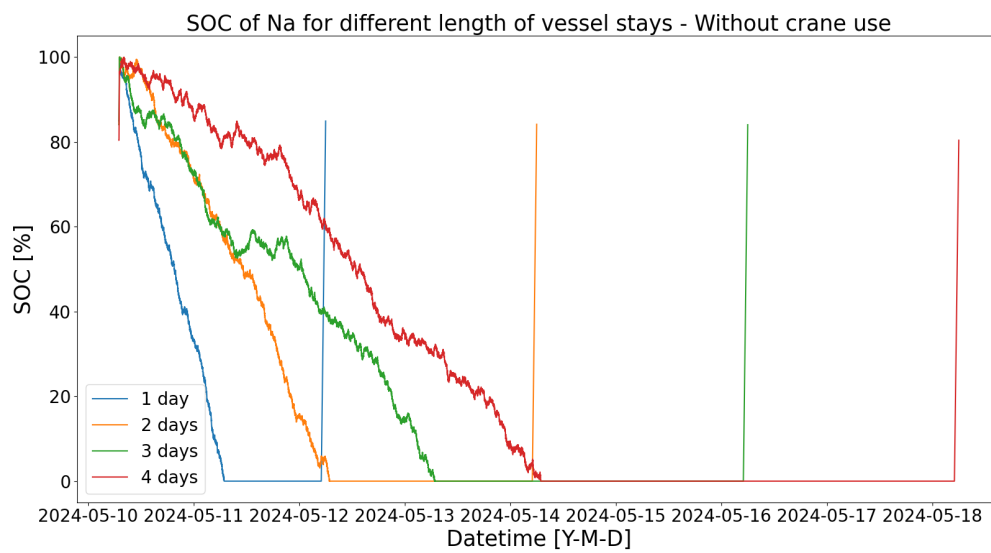
Figure A.41: Figure of the SOC of the Na version of the HE ESS shore power configuration. The different plots correspond to different length of vessel stays that are simulated. All plots are charged up to full before the vessel connects and then slowly fully discharge until the vessel disconnects.

A.3. Amount of crane uses
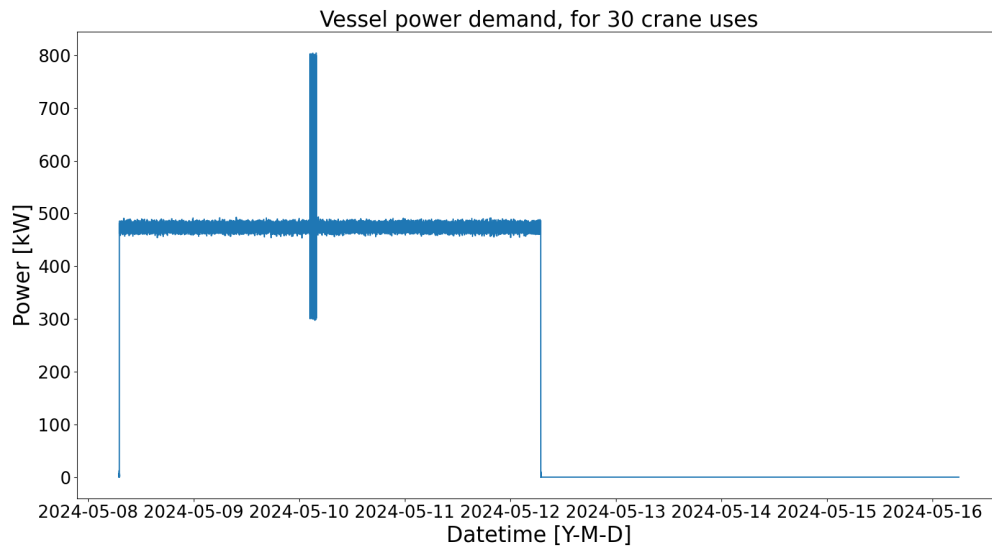
Figure A.42: Figure of a 4 day vessel power profile followed by 4 days of downtime. The vessel power profile includes 30 crane use that are fully clustered together. This vessel power profile was used for the HP ESS shore power configuration. The x-axis is in datetime meaning each data point is fixed to a date and time.
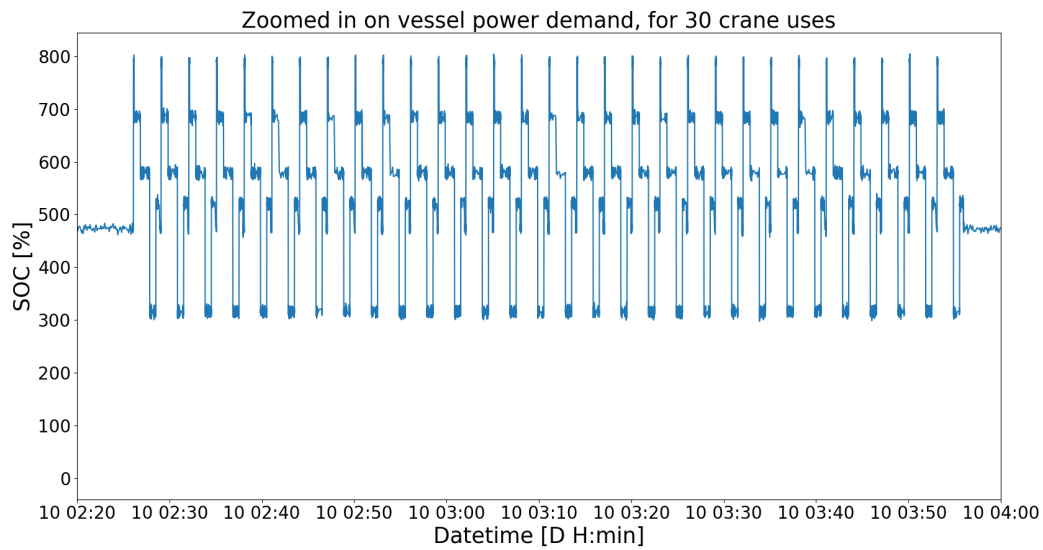
**Figure A.43:** Figure of the zoomed in version of Figure A.42. The figure is zoomed in on the 30 consecutive crane uses. This original vessel power profile was used for the HP ESS shore power configuration. The x-axis is in datetime meaning each data point is fixed to a date and time.
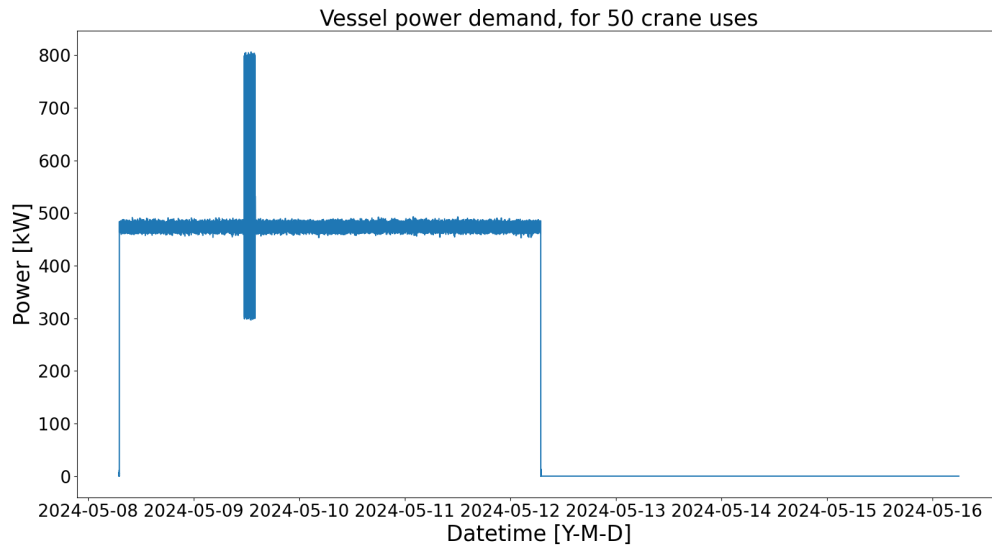
Figure A.44: Figure of a 4 day vessel power profile followed by 4 days of downtime. The vessel power profile includes 50 crane use that are fully clustered together. This vessel power profile was used for the HP ESS shore power configuration. The x-axis is in datetime meaning each data point is fixed to a date and time.
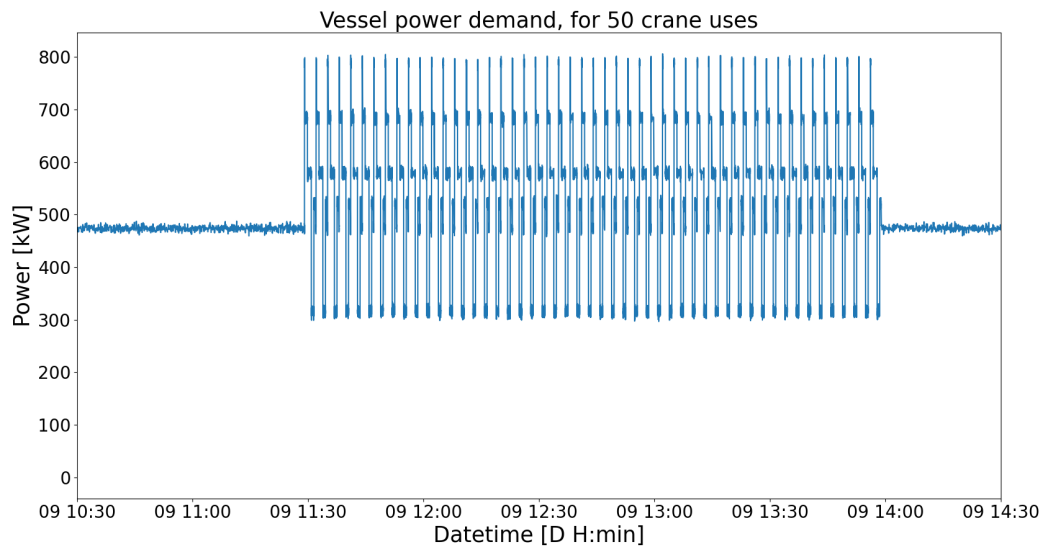
Figure A.45: Figure of the zoomed in version of Figure A.44. The figure is zoomed in on the 50 consecutive crane uses. This original vessel power profile was used for the HP ESS shore power configuration. The x-axis is in datetime meaning each data point is fixed to a date and time.
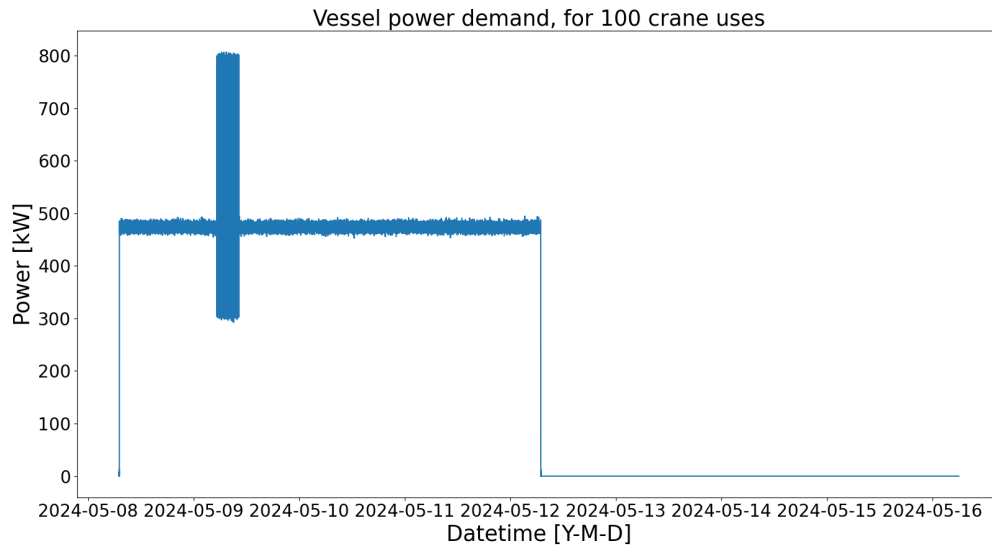
Figure A.46: Figure of a 4 day vessel power profile followed by 4 days of downtime. The vessel power profile includes 100 crane use that are fully clustered together. This vessel power profile was used for the HP ESS shore power configuration. The x-axis is in datetime meaning each data point is fixed to a date and time.
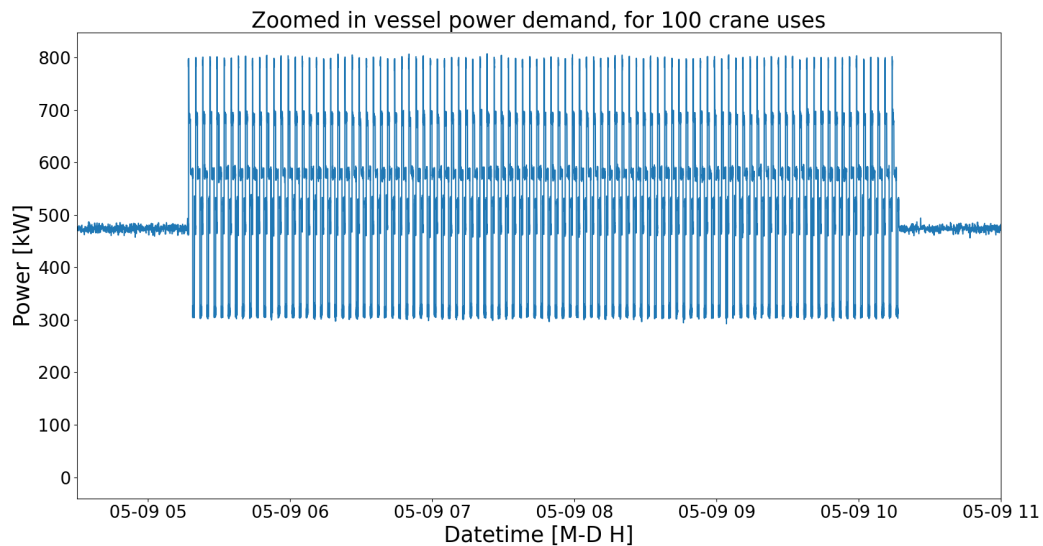
Figure A.47: Figure of the zoomed in version of Figure A.46. The figure is zoomed in on the 100 consecutive crane uses. This original vessel power profile was used for the HP ESS shore power configuration. The x-axis is in datetime meaning each data point is fixed to a date and time.

A.3.1. 30 crane uses
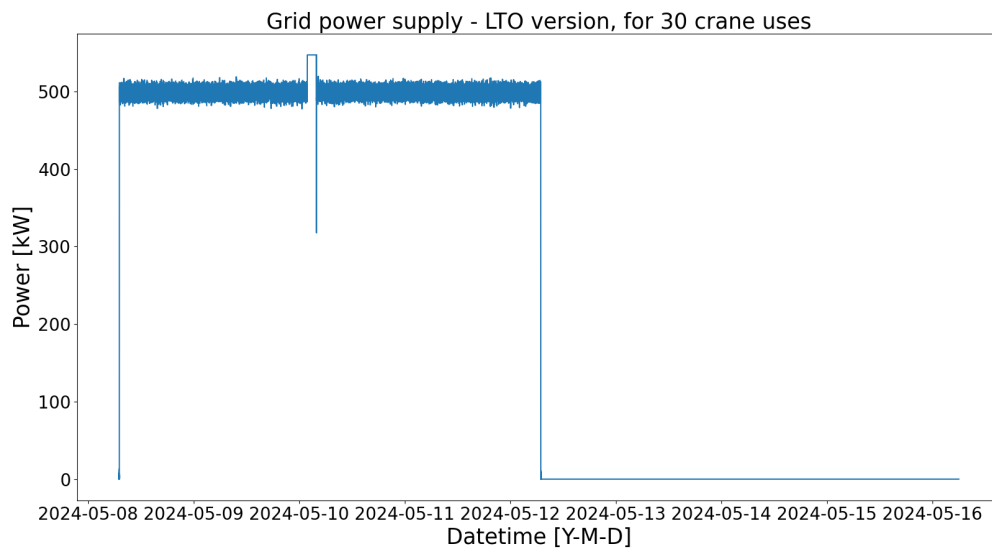
Figure A.48: Figure of the grid power supply by the LTO version of the HP ESS shore power configuration. The crane uses of the vessel power profile of Figure A.42 are peak shaven by the LTO battery.
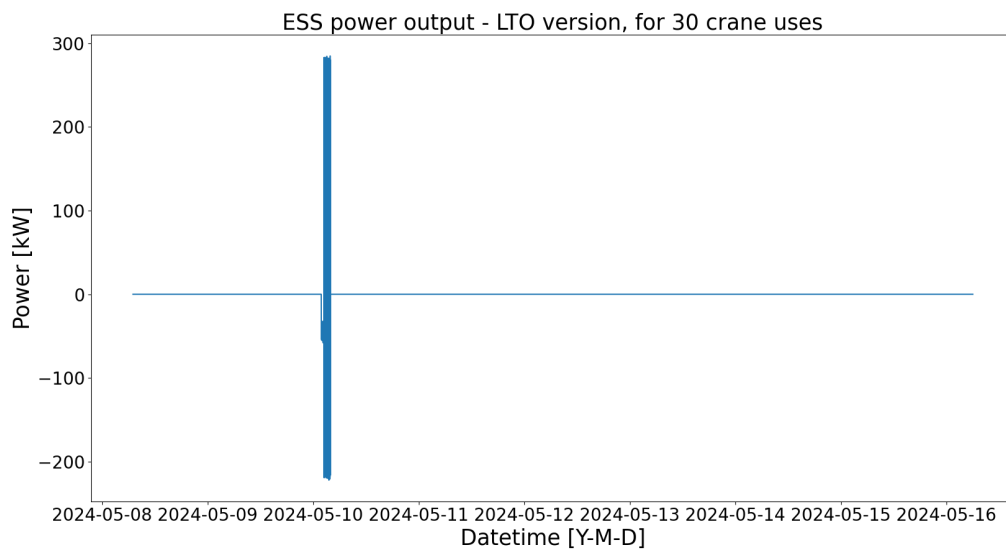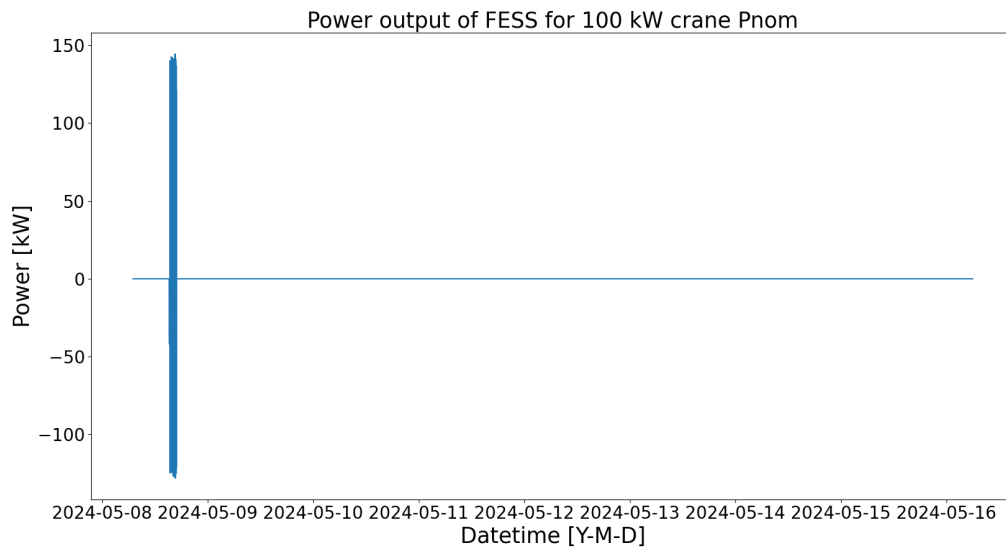

Figure A.49: Figure of the LTO battery power output of the LTO version of the HP ESS shore power configuration. The LTO battery peak shaves the crane uses of the vessel power profile of Figure A.42.
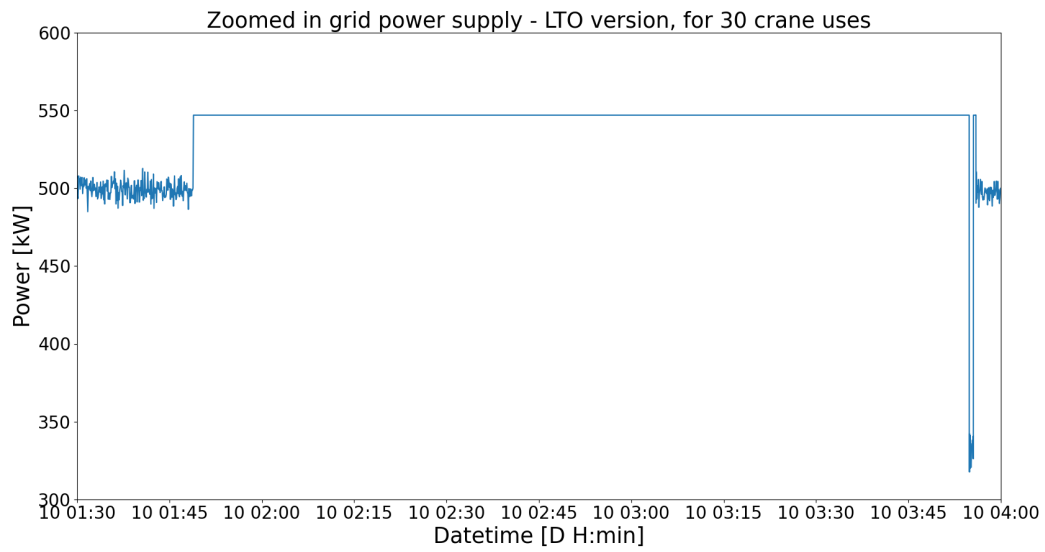
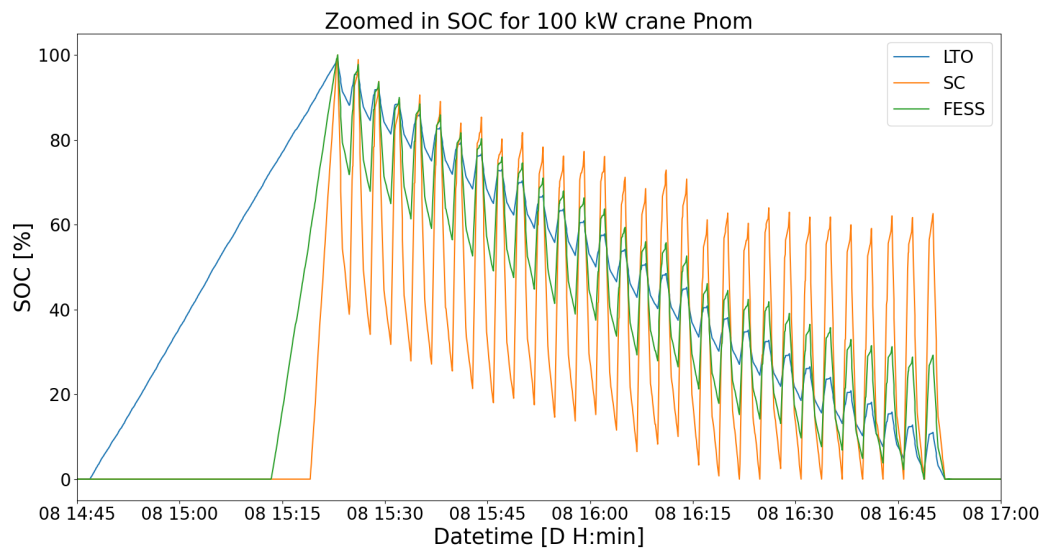**Figure A.50:** Figure of the grid power supply by the LTO version of the HP ESS shore power configuration, zoomed in on the crane uses. The crane uses of the vessel power profile of Figure A.42 are peak shaven by the LTO battery.
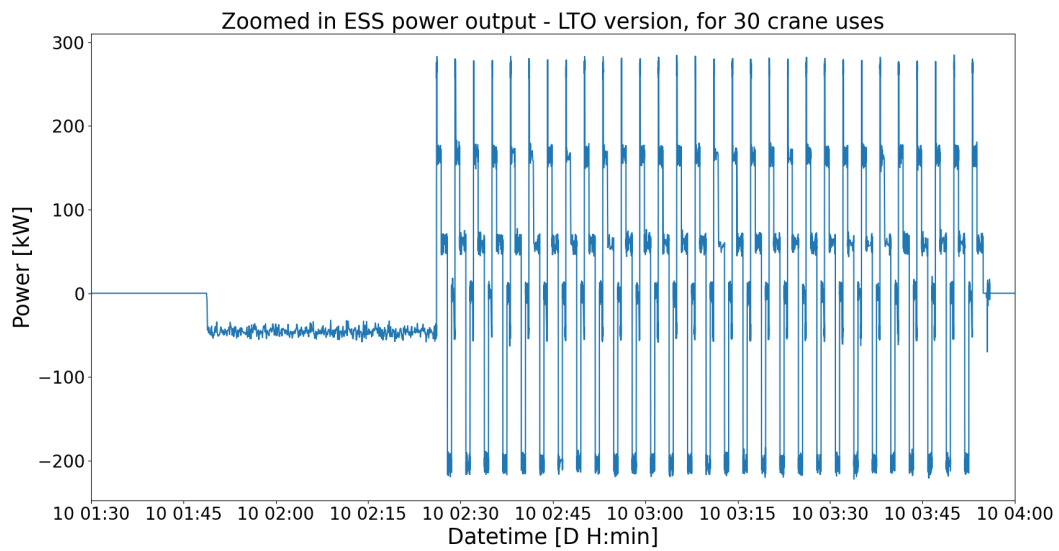
Figure A.51: Figure of the LTO battery power output of the LTO version of the HP ESS shore power configuration, zoomed in on the crane uses. The LTO battery peak shaves the crane uses of the vessel power profile of Figure A.42.
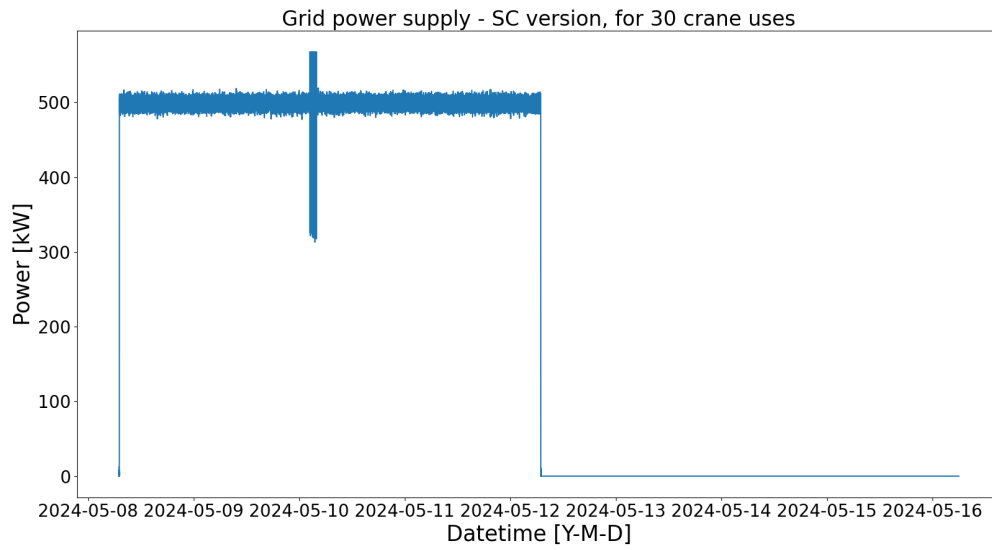
Figure A.52: Figure of the grid power supply by the SC version of the HP ESS shore power configuration. The crane uses of the vessel power profile of Figure A.42 are peak shaven by the SC.
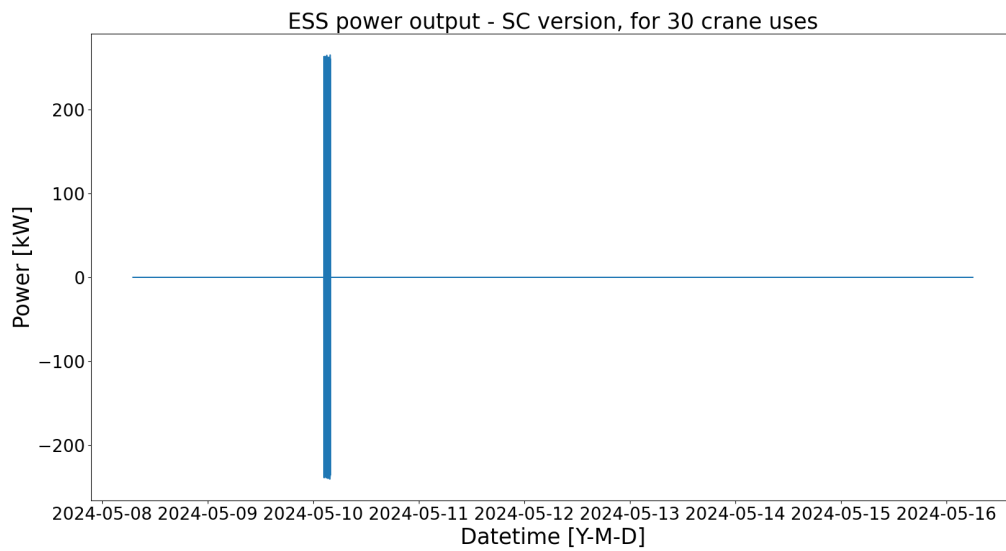
Figure A.53: Figure of the SC power output of the SC version of the HP ESS shore power configuration. The SC peak shaves the crane uses of the vessel power profile of Figure A.42.
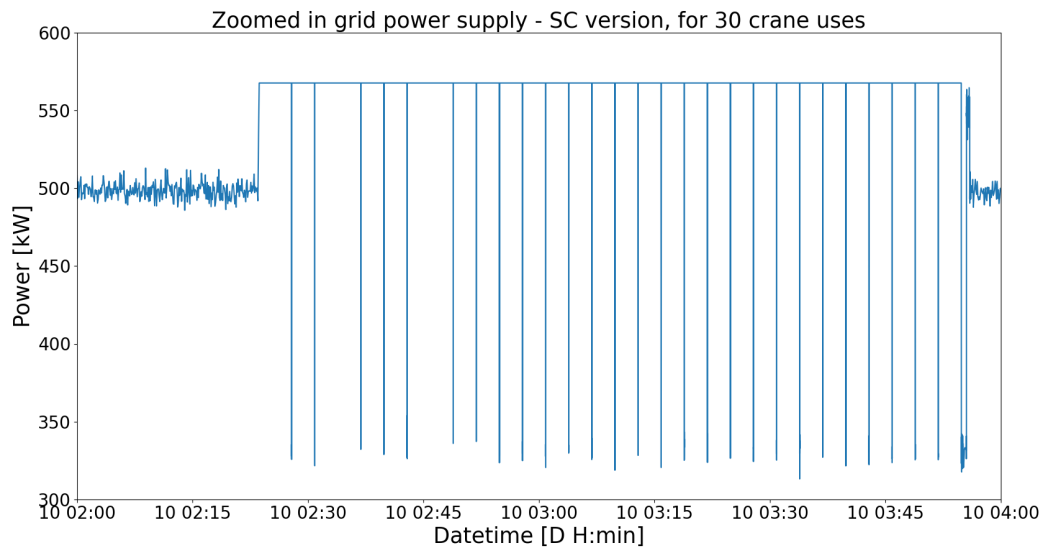
Figure A.54: Figure of the grid power supply by the SC version of the HP ESS shore power configuration, zoomed in on the crane uses. The crane uses of the vessel power profile of Figure A.42 are peak shaven by the SC.
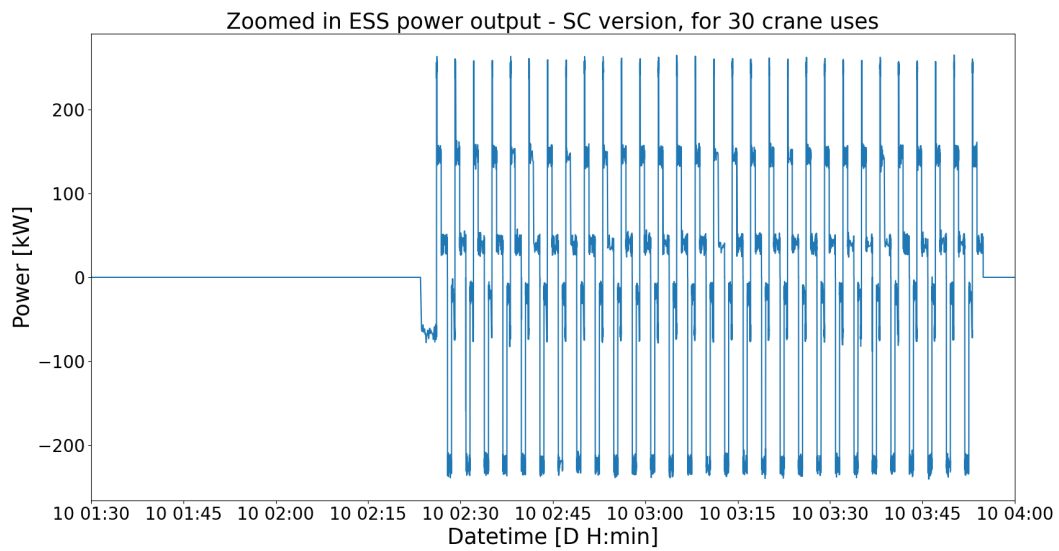
Figure A.55: Figure of the SC power output of the SC version of the HP ESS shore power configuration, zoomed in on the crane uses. The SC peak shaves the crane uses of the vessel power profile of Figure A.42.
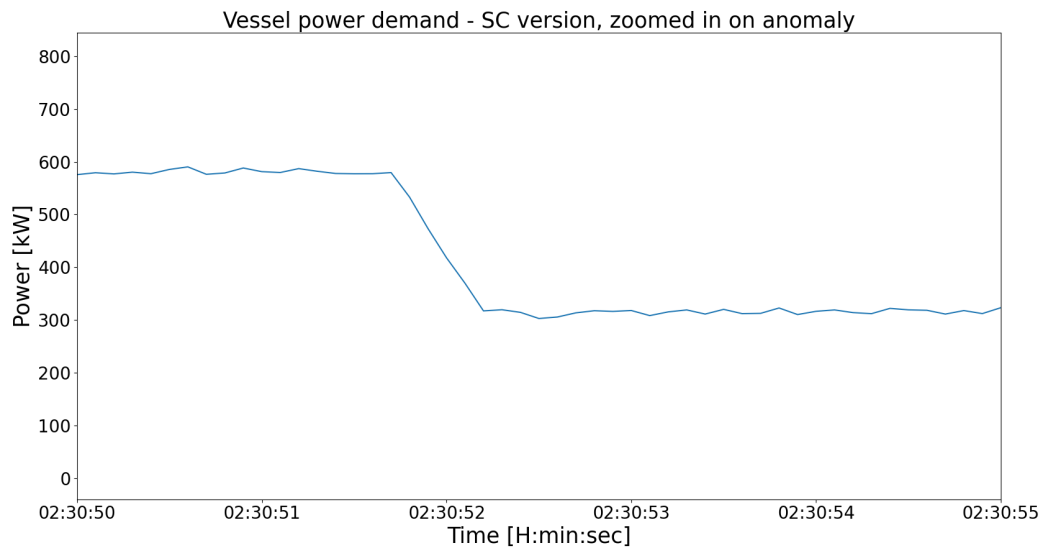
Figure A.56: Figure of the zoomed in version of the vessel power profile of Figure A.42. It is zoomed in on the same time of an anomaly in Figure A.54. The figure shows the transition from the swinging around of the crane use to the dropping of the load.
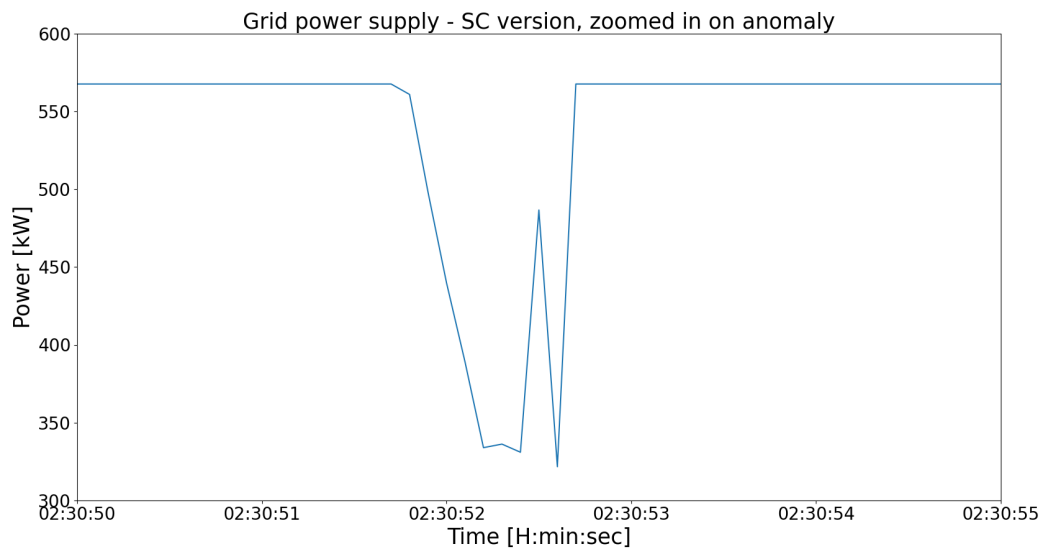
Figure A.57: Figure of the zoomed in version of the grid power supply of Figure A.54. It is zoomed in on an anomaly where the grid power supply drops for a very short amount of time. The figure shows this short drop of only a few seconds.
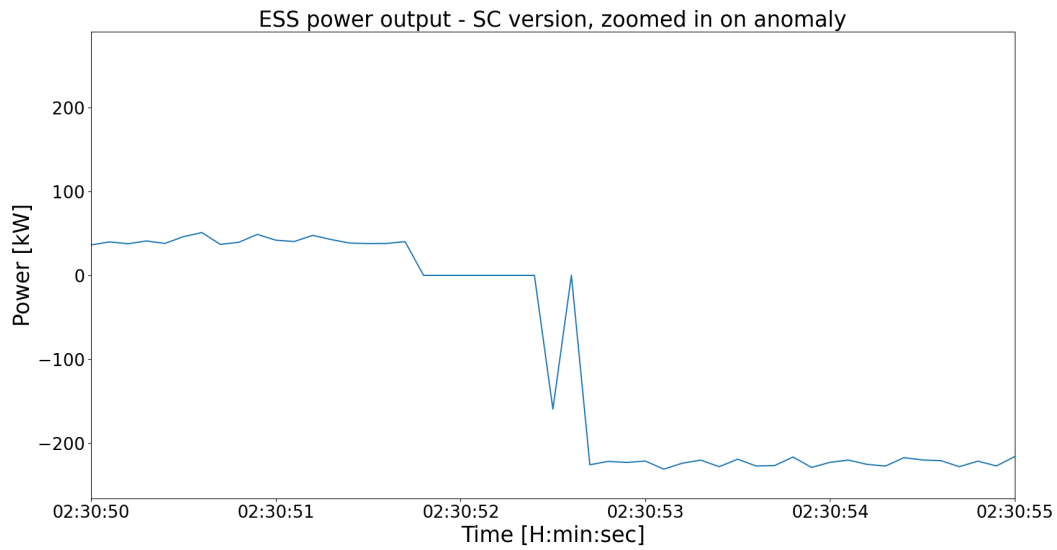
Figure A.58: Figure of the zoomed in version of the SC output power of Figure A.55. It is zoomed in on the same time of an anomaly in Figure A.54. The figure shows the inverse of the spike shown in Figure A.57 just after the transition in Figure A.56 is complete.
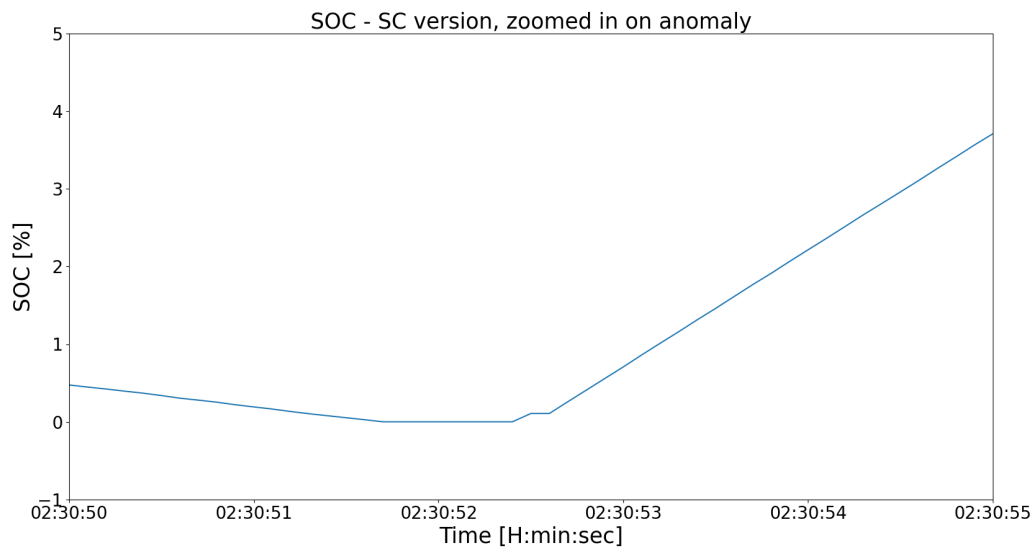
Figure A.59: Figure of the zoomed in version of the SC SOC, zoomed in on the same time of an anomaly in Figure A.54. The figure shows the SC SOC becoming zero just before the transition in Figure A.56 starts. So, the drop in the grid power supply shown in Figure A.57 has to happen, because the SC does not need to be charged just yet. The charging happens a few seconds later instead.
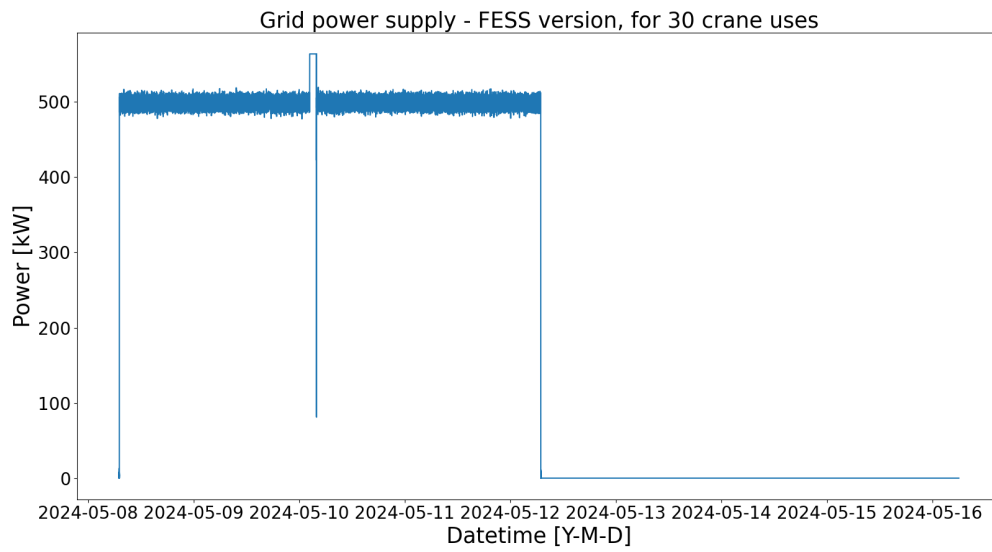
Figure A.60: Figure of the grid power supply by the FESS version of the HP ESS shore power configuration. The crane uses of the vessel power profile of Figure A.42 are peak shaven by the FESS.
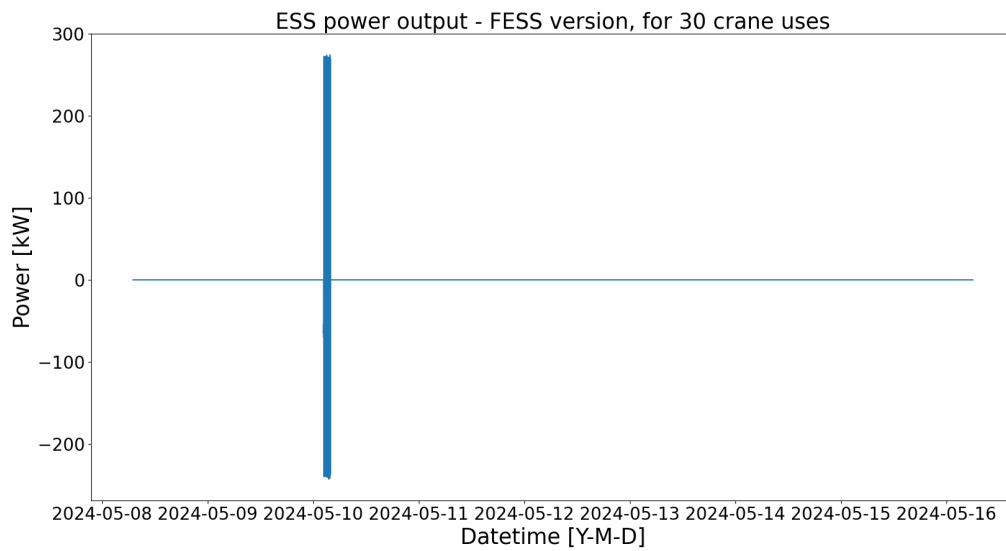
Figure A.61: Figure of the FESS power output of the FESS version of the HP ESS shore power configuration. The FESS peak shaves the crane uses of the vessel power profile of Figure A.42.
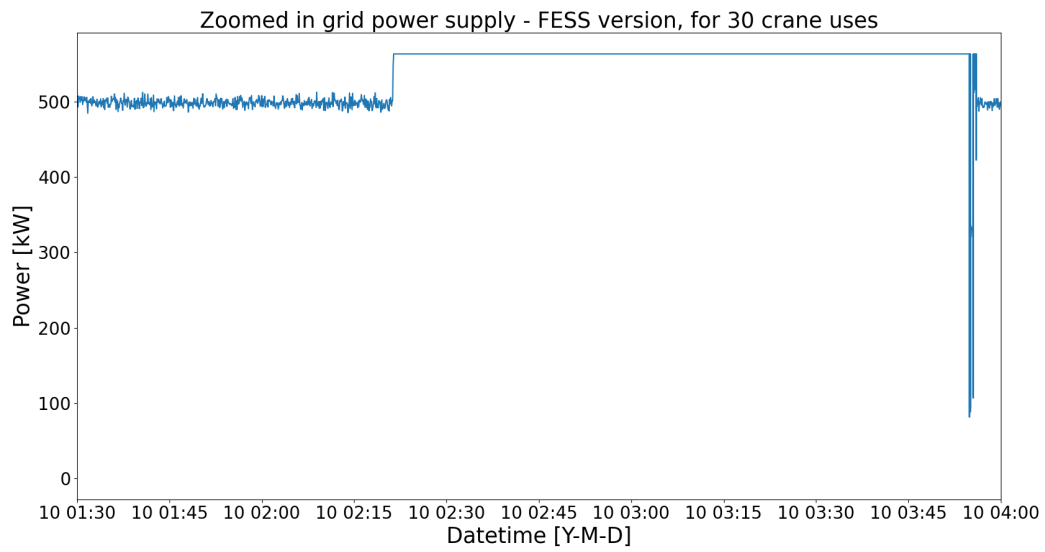
Figure A.62: Figure of the grid power supply by the FESS version of the HP ESS shore power configuration, zoomed in on the crane uses. The crane uses of the vessel power profile of Figure A.42 are peak shaven by the FESS.
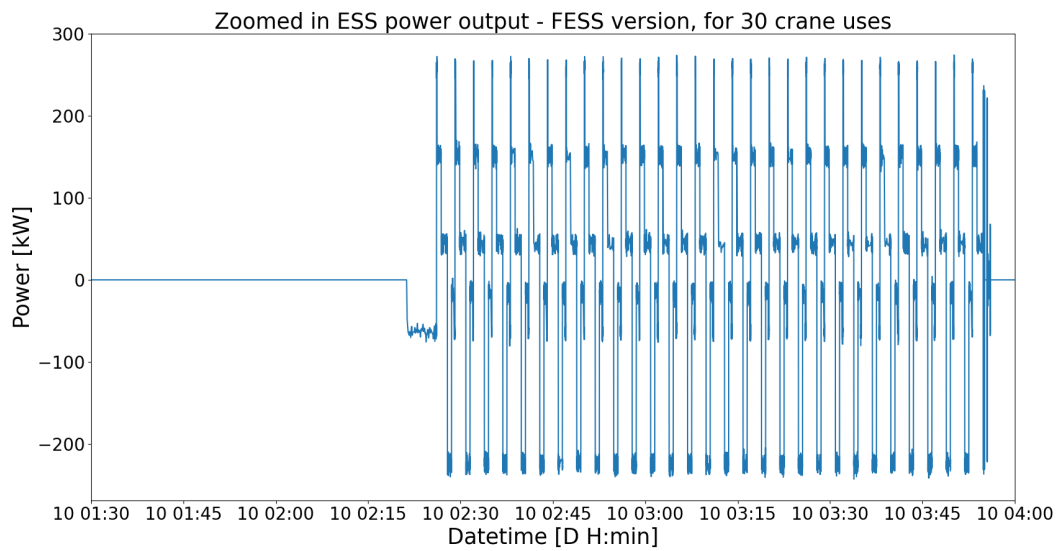
Figure A.63: Figure of the FESS power output of the FESS version of the HP ESS shore power configuration, zoomed in on the crane uses. The FESS peak shaves the crane uses of the vessel power profile of Figure A.42.
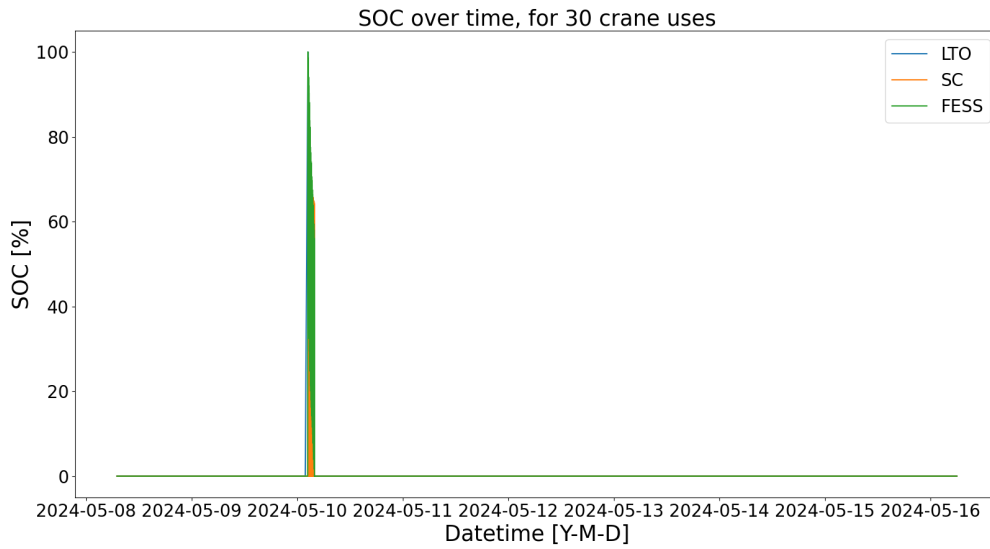
Figure A.64: Figure of the SOC of the different versions of the HP ESS shore power configuration. All the ESS are only used for the crane uses in the vessel power profile of Figure A.42.
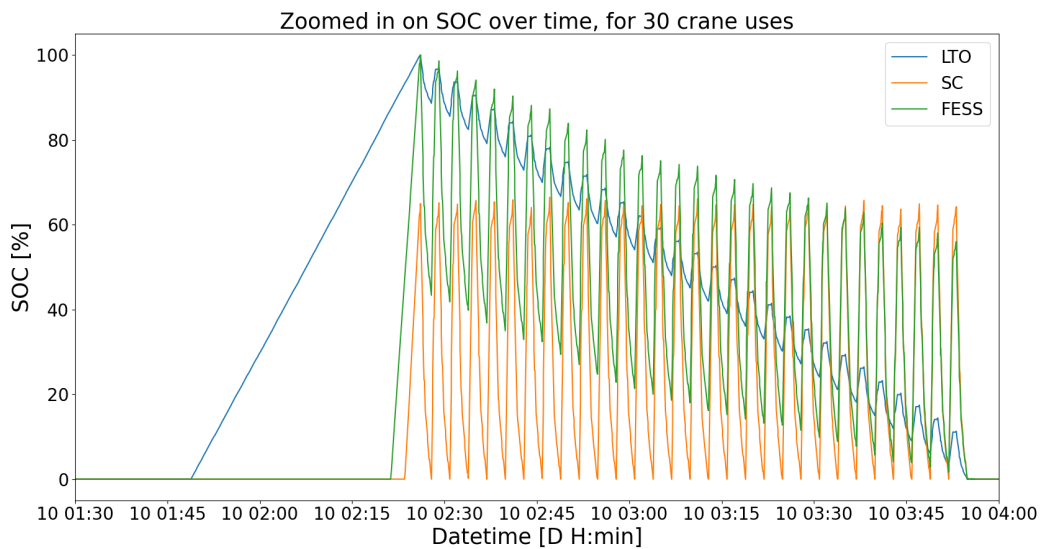
Figure A.65: Figure of the zoomed in version of the SOC of the different versions of the HP ESS shore power configuration. The figure is zoomed in on the crane uses. The swings in SOC that are synchronized for each of the ESS are when the crane uses happen. The ESS are charged up just before the crane uses start. The LTO version and the FESS version are charged up fully, while the SC is only charged to about 60% and fully discharged each crane use.
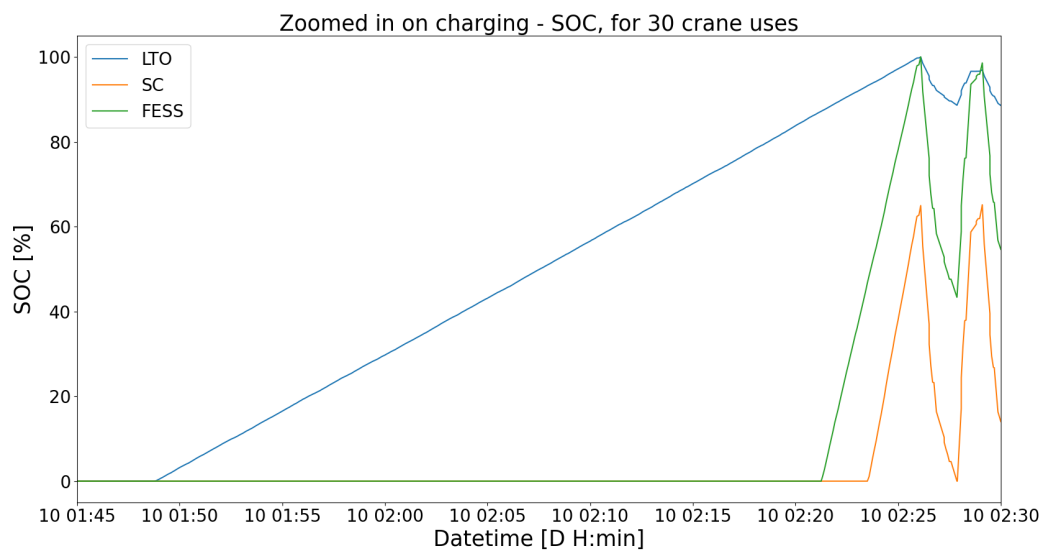
Figure A.66: Figure of the zoomed in version of the SOC of the different versions of the HP ESS shore power configuration. The figure is zoomed in on the charging up of the ESS just before the crane uses start. The FESS and SC are charged up in under 5 minutes, while the LTO takes longer at around 35 minutes.

A.3.2. 50 crane uses
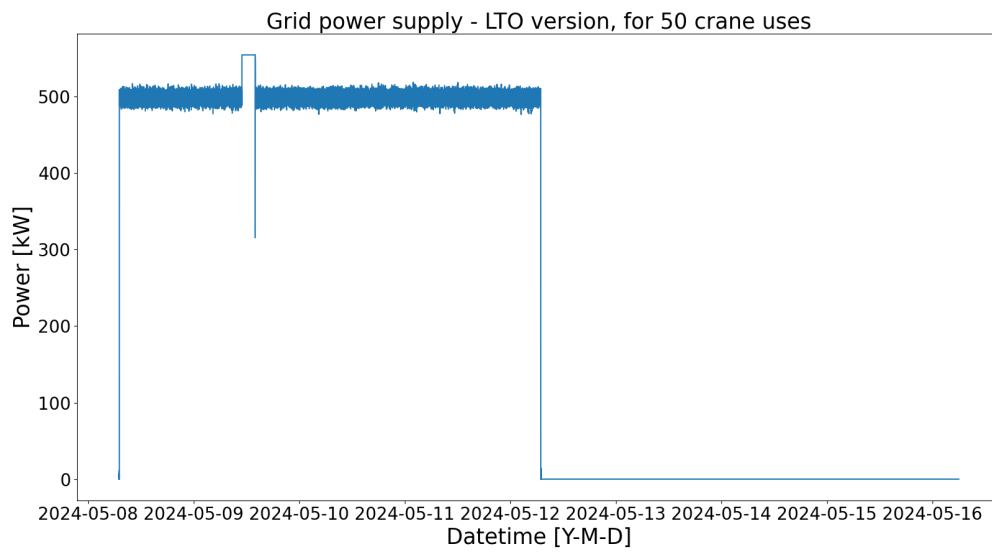
Figure A.67: Figure of the grid power supply by the LTO version of the HP ESS shore power configuration. The crane uses of the vessel power profile of Figure A.44 are peak shaven by the LTO battery.
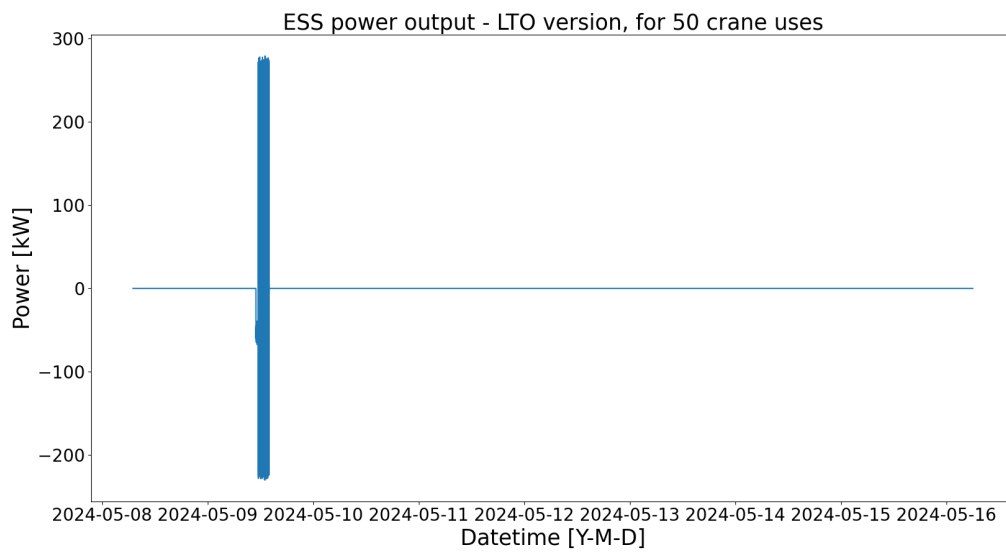
Figure A.68: Figure of the LTO battery power output of the LTO version of the HP ESS shore power configuration. The LTO battery peak shaves the crane uses of the vessel power profile of Figure A.44.
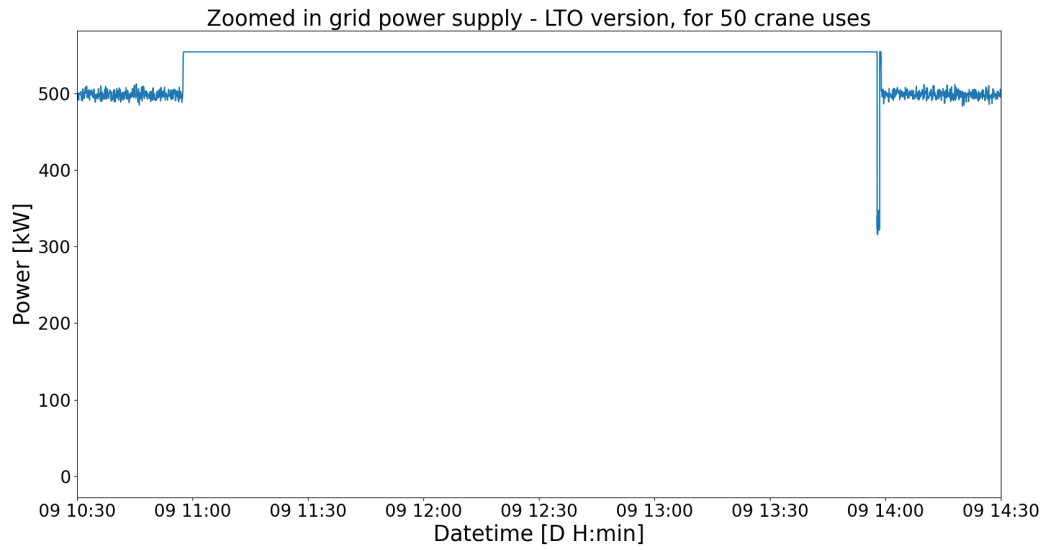
Figure A.69: Figure of the grid power supply by the LTO version of the HP ESS shore power configuration, zoomed in on the crane uses. The crane uses of the vessel power profile of Figure A.44 are peak shaven by the LTO battery.
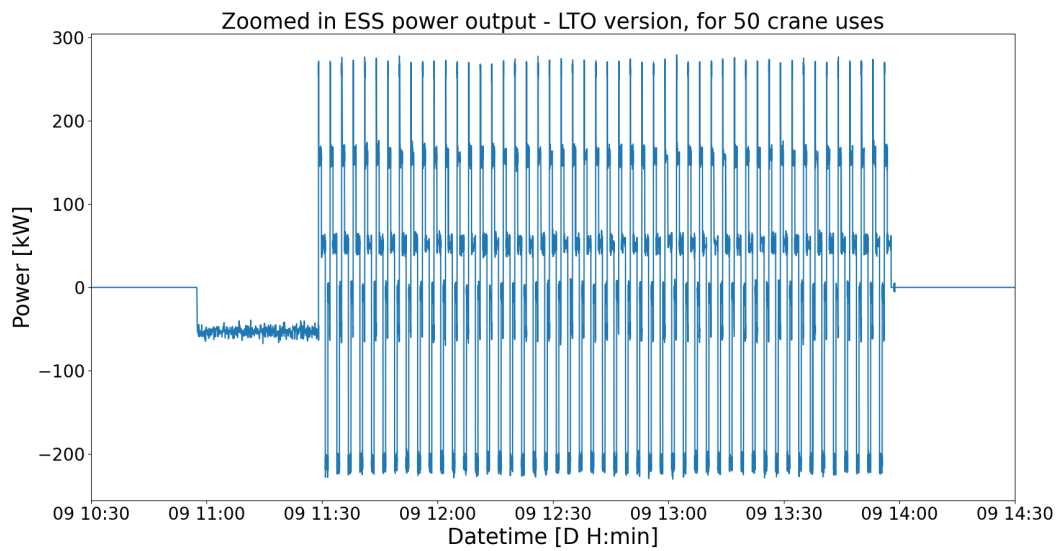
Figure A.70: Figure of the LTO battery power output of the LTO version of the HP ESS shore power configuration, zoomed in on the crane uses. The LTO battery peak shaves the crane uses of the vessel power profile of Figure A.44.
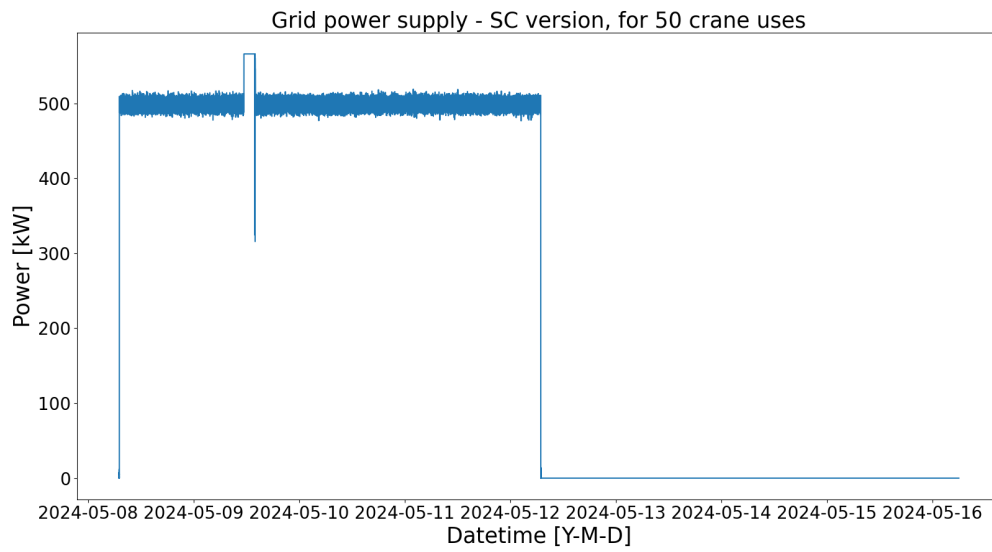
Figure A.71: Figure of the grid power supply by the SC version of the HP ESS shore power configuration. The crane uses of the vessel power profile of Figure A.44 are peak shaven by the SC.
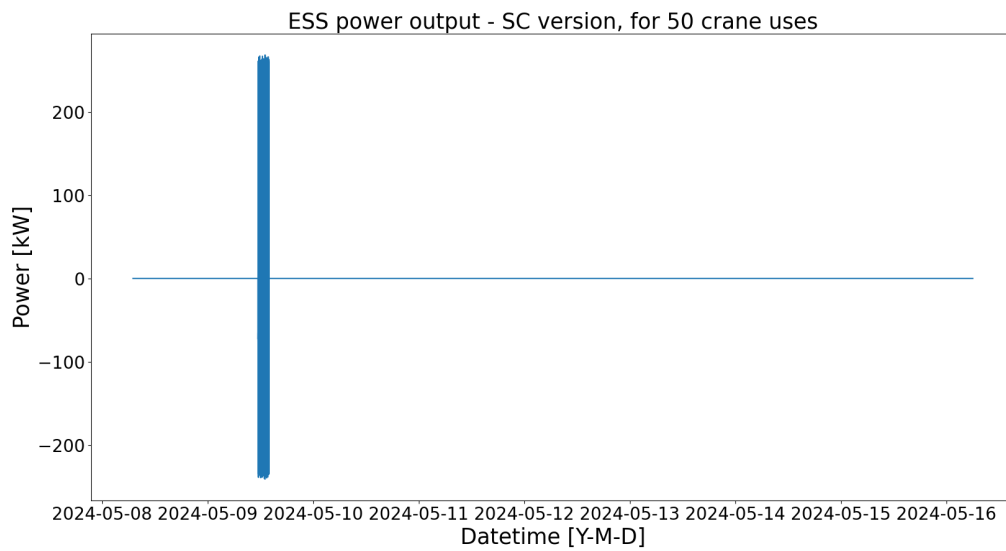
Figure A.72: Figure of the SC power output of the SC version of the HP ESS shore power configuration. The SC peak shaves the crane uses of the vessel power profile of Figure A.44.
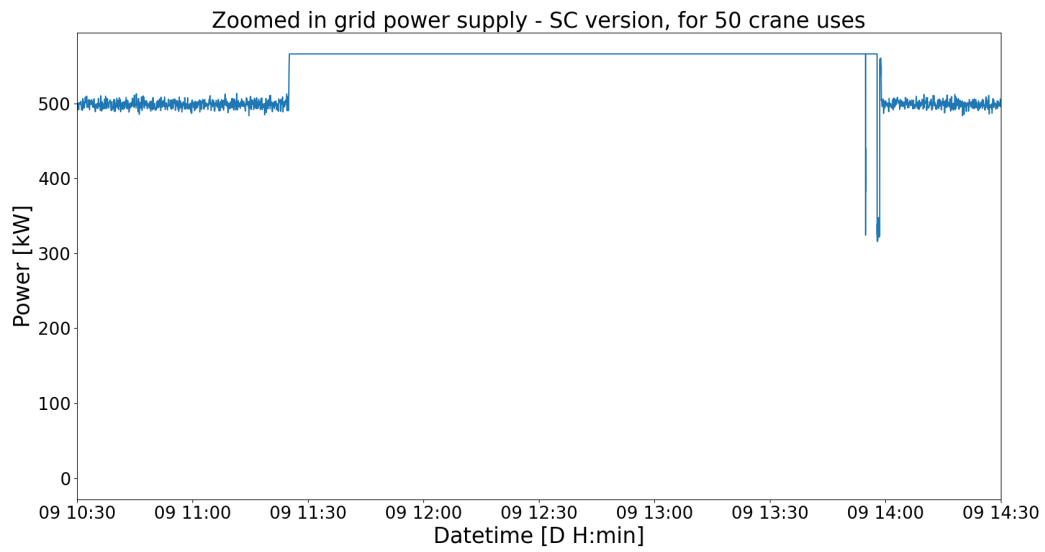
Figure A.73: Figure of the grid power supply by the SC version of the HP ESS shore power configuration, zoomed in on the crane uses. The crane uses of the vessel power profile of Figure A.44 are peak shaven by the SC.
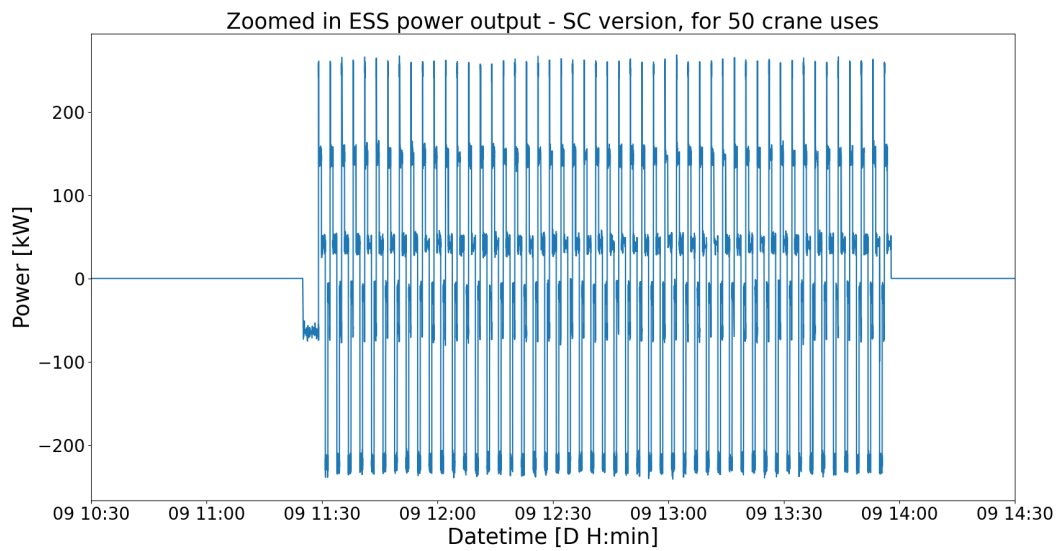
Figure A.74: Figure of the SC power output of the SC version of the HP ESS shore power configuration, zoomed in on the crane uses. The SC peak shaves the crane uses of the vessel power profile of Figure A.44.
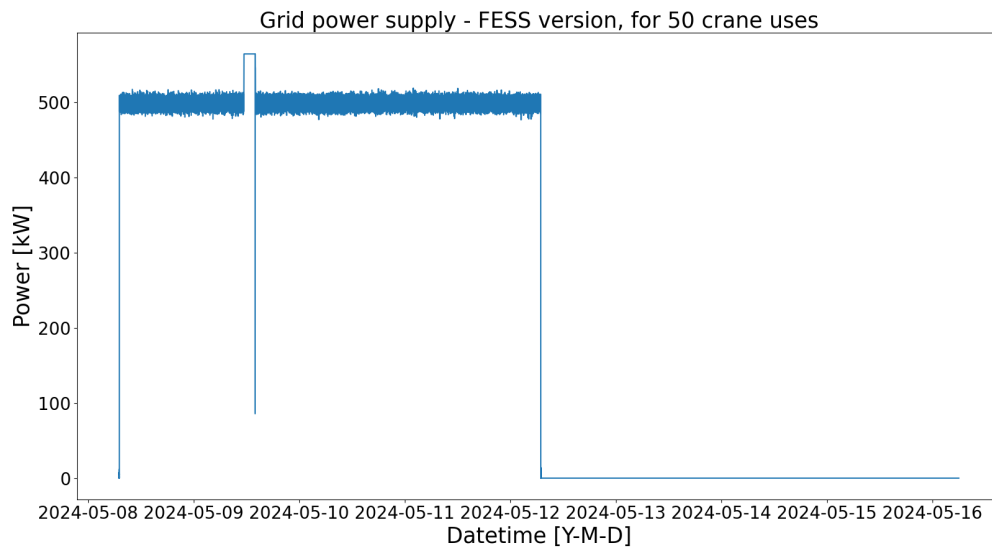
Figure A.75: Figure of the grid power supply by the FESS version of the HP ESS shore power configuration. The crane uses of the vessel power profile of Figure A.44 are peak shaven by the FESS.
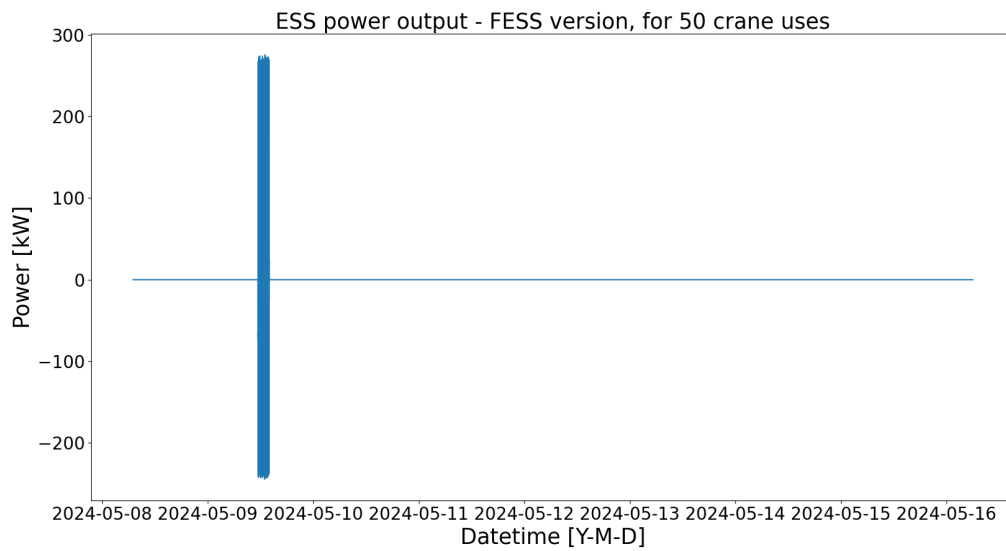
Figure A.76: Figure of the FESS power output of the FESS version of the HP ESS shore power configuration. The FESS peak shaves the crane uses of the vessel power profile of Figure A.44.
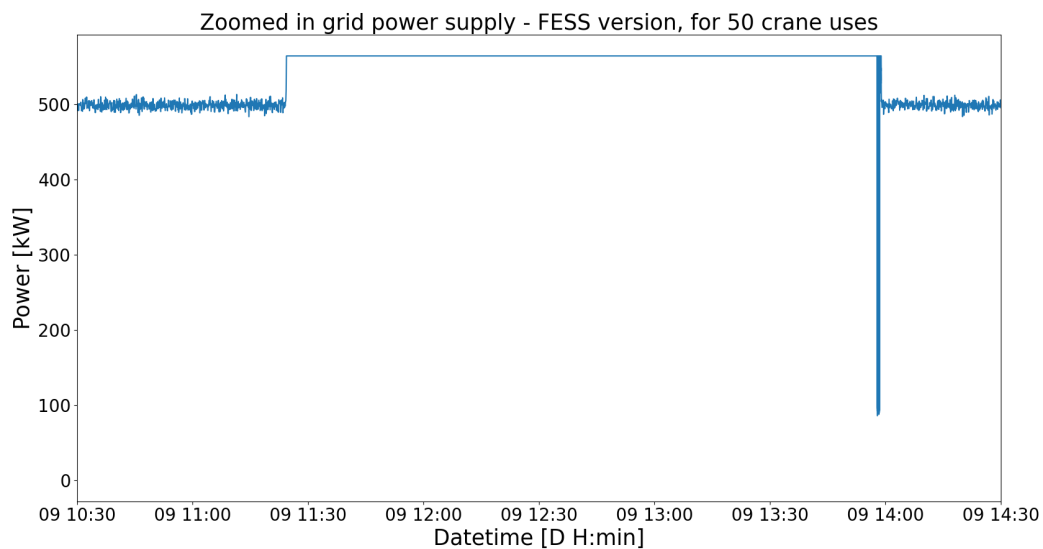
Figure A.77: Figure of the grid power supply by the FESS version of the HP ESS shore power configuration, zoomed in on the crane uses. The crane uses of the vessel power profile of Figure A.44 are peak shaven by the FESS.
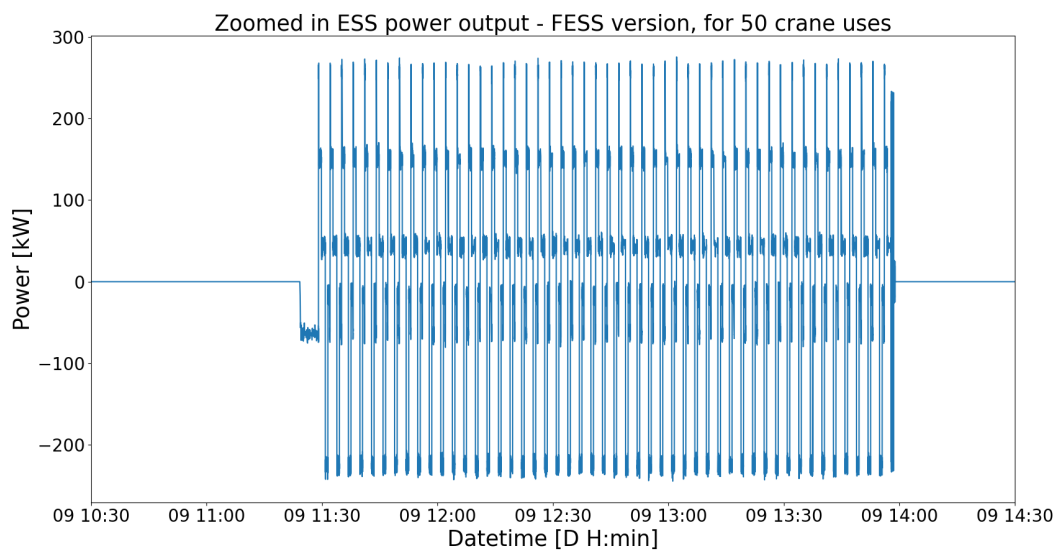
Figure A.78: Figure of the FESS power output of the FESS version of the HP ESS shore power configuration, zoomed in on the crane uses. The FESS peak shaves the crane uses of the vessel power profile of Figure A.44.
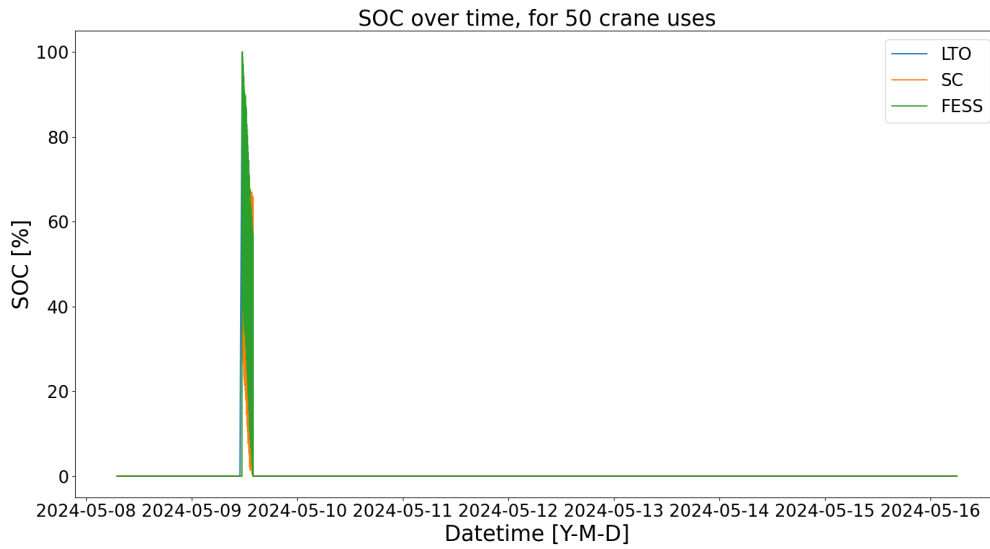
Figure A.79: Figure of the SOC of the different versions of the HP ESS shore power configuration. All the ESS are only used for the crane uses in the vessel power profile of Figure A.44.
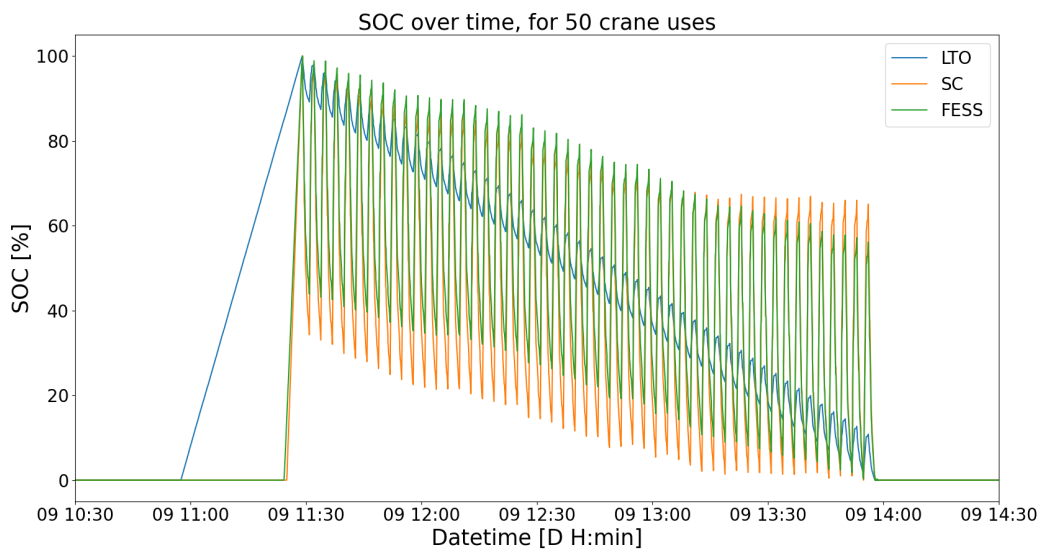
Figure A.80: Figure of the zoomed in version of the SOC of the different versions of the HP ESS shore power configuration. The figure is zoomed in on the crane uses. The swings in SOC that are synchronized for each of the ESS are when the crane uses happen. The ESS are charged up just before the crane uses start and they are fully discharged at the final crane use.

A.3.3. 100 crane uses
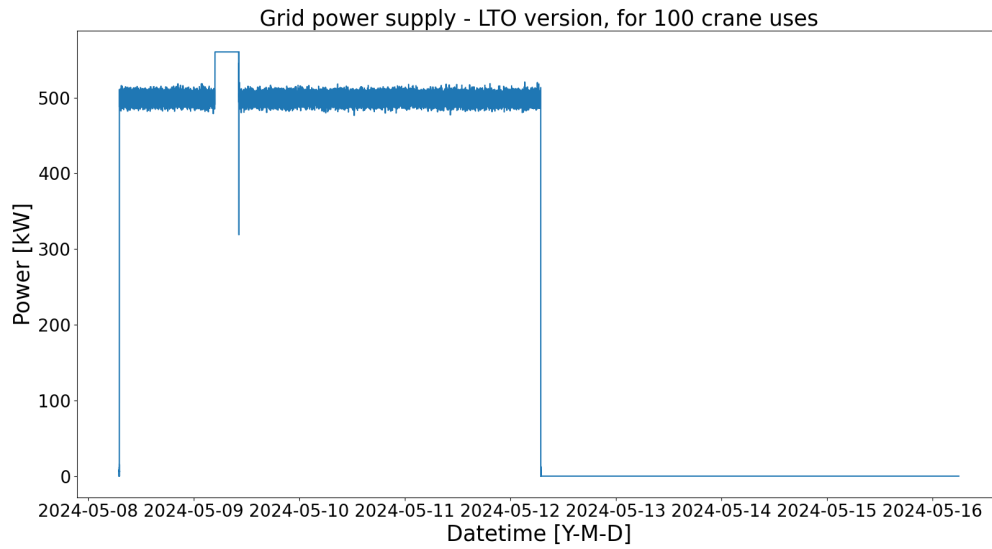
Figure A.81: Figure of the grid power supply by the LTO version of the HP ESS shore power configuration. The crane uses of the vessel power profile of Figure A.46 are peak shaven by the LTO battery.
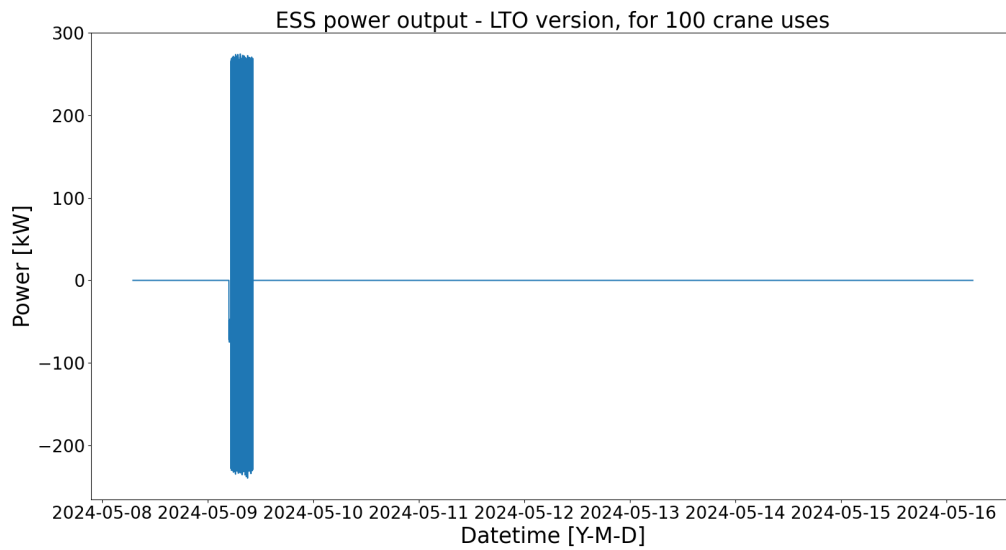
Figure A.82: Figure of the LTO battery power output of the LTO version of the HP ESS shore power configuration. The LTO battery peak shaves the crane uses of the vessel power profile of Figure A.46.
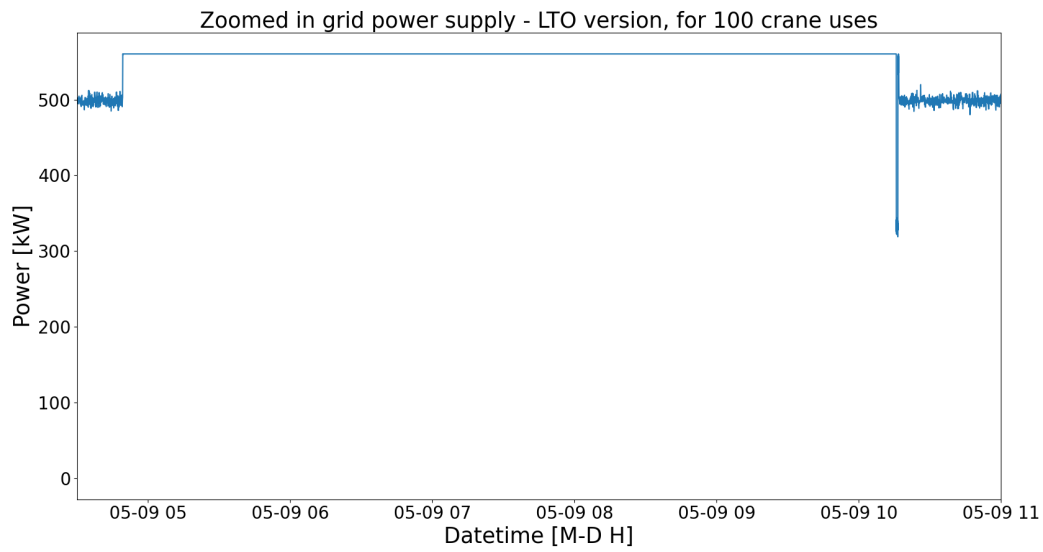
Figure A.83: Figure of the grid power supply by the LTO version of the HP ESS shore power configuration, zoomed in on the crane uses. The crane uses of the vessel power profile of Figure A.46 are peak shaven by the LTO battery.
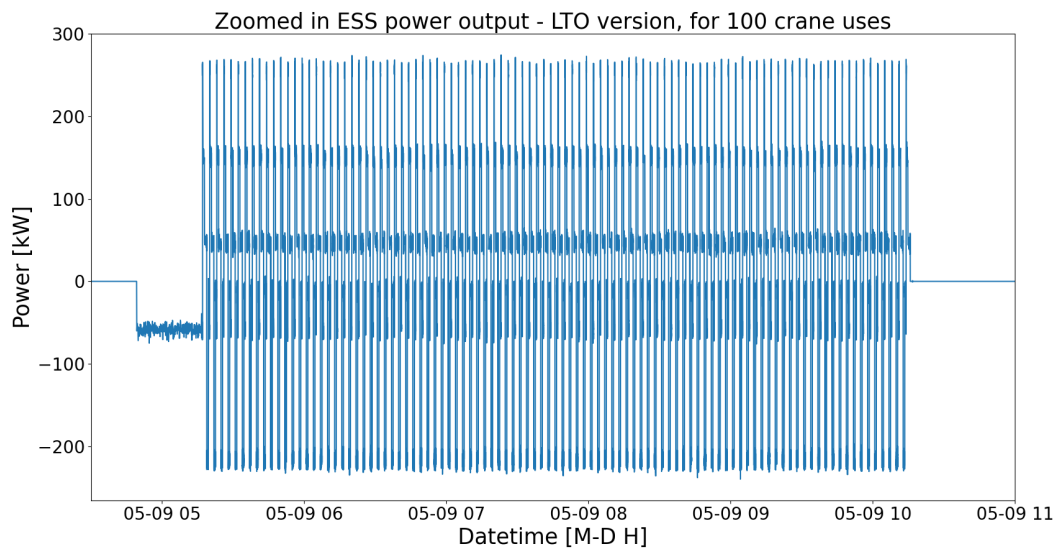
Figure A.84: Figure of the LTO battery power output of the LTO version of the HP ESS shore power configuration, zoomed in on the crane uses. The LTO battery peak shaves the crane uses of the vessel power profile of Figure A.46.
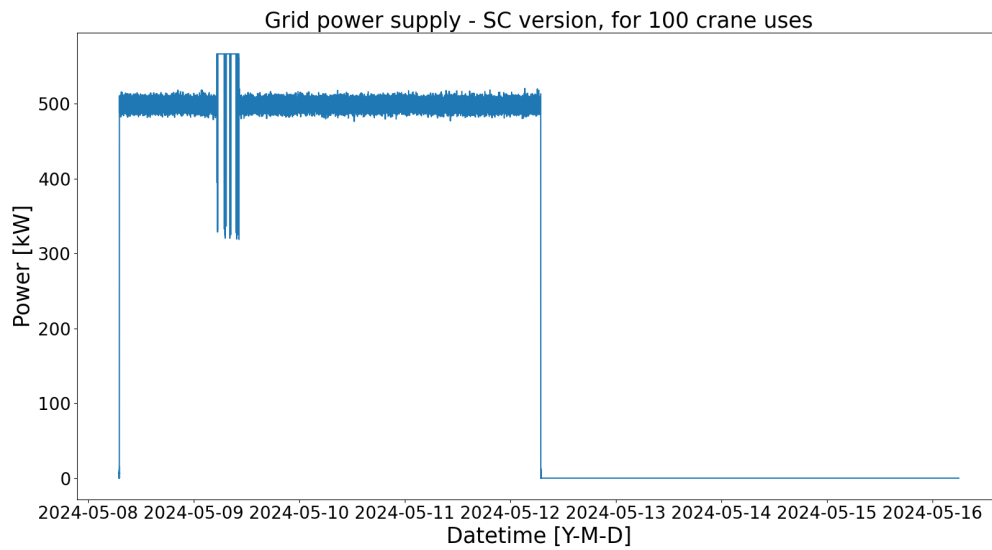
Figure A.85: Figure of the grid power supply by the SC version of the HP ESS shore power configuration. The crane uses of the vessel power profile of Figure A.46 are peak shaven by the SC.
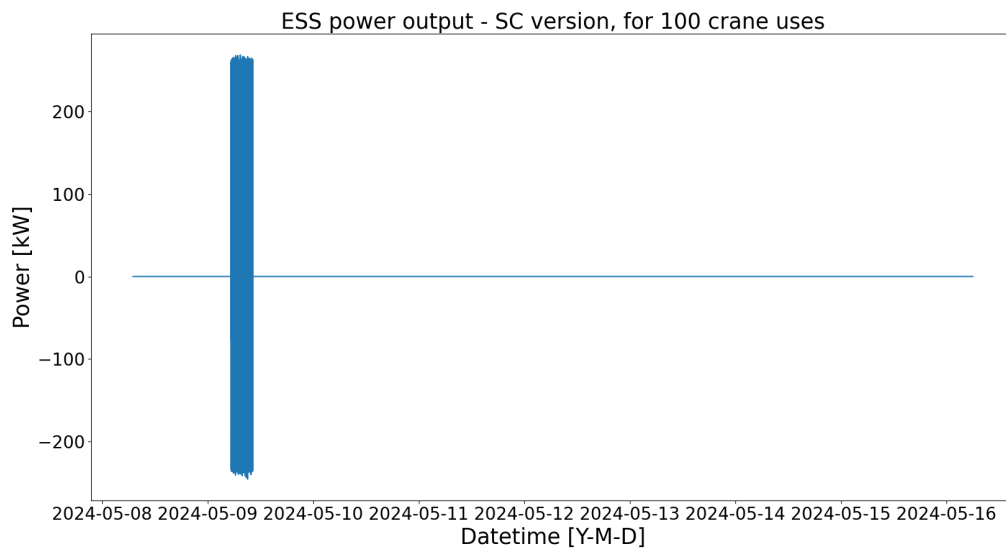
Figure A.86: Figure of the SC power output of the SC version of the HP ESS shore power configuration. The SC peak shaves the crane uses of the vessel power profile of Figure A.46.
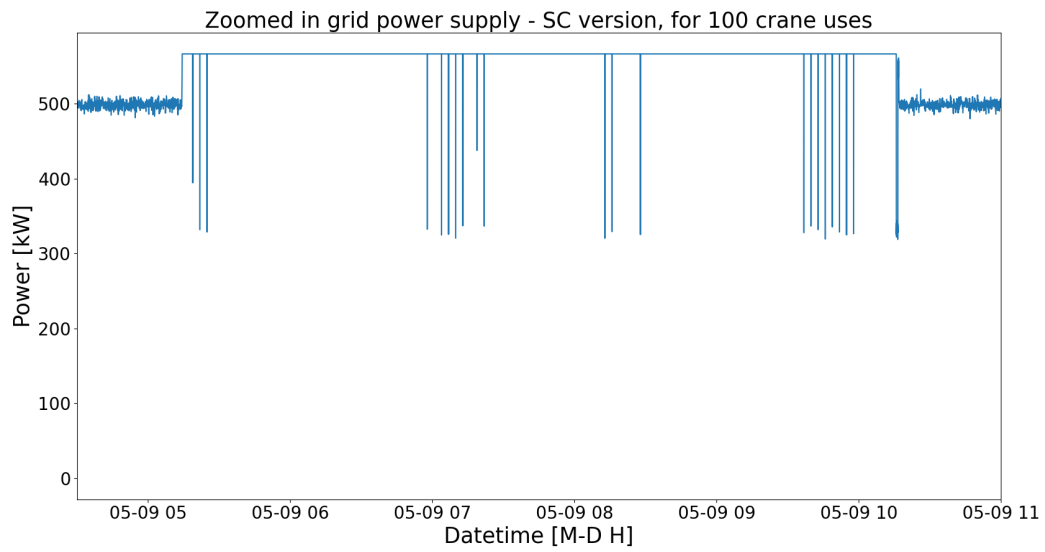
Figure A.87: Figure of the grid power supply by the SC version of the HP ESS shore power configuration, zoomed in on the crane uses. The crane uses of the vessel power profile of Figure A.46 are peak shaven by the SC.
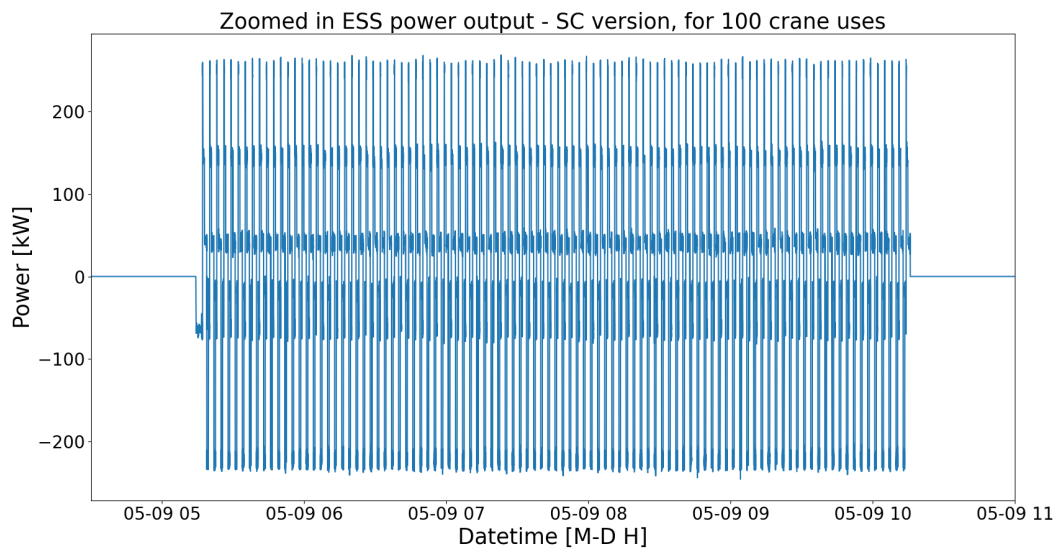
Figure A.88: Figure of the SC power output of the SC version of the HP ESS shore power configuration, zoomed in on the crane uses. The SC peak shaves the crane uses of the vessel power profile of Figure A.46.
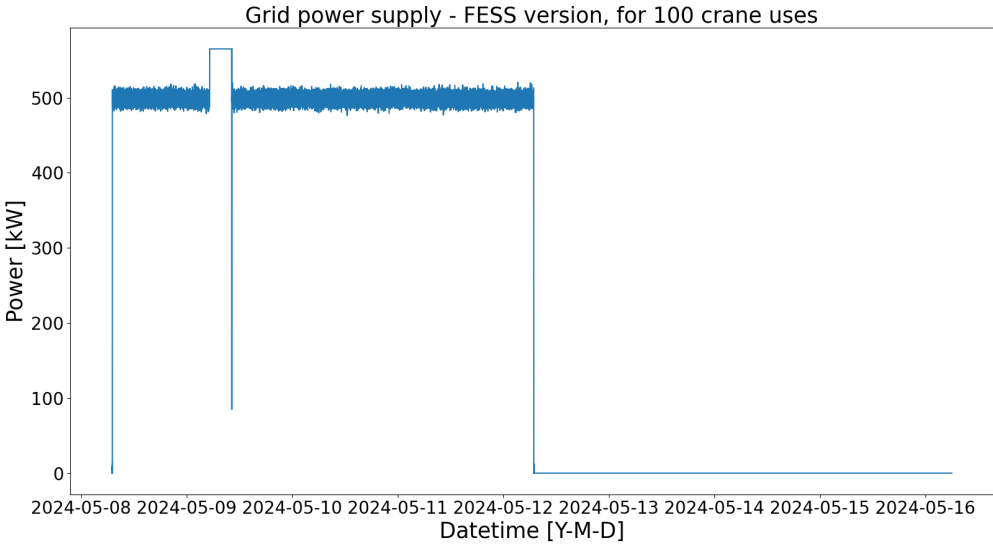
Figure A.89: Figure of the grid power supply by the FESS version of the HP ESS shore power configuration. The crane uses of the vessel power profile of Figure A.46 are peak shaven by the FESS.
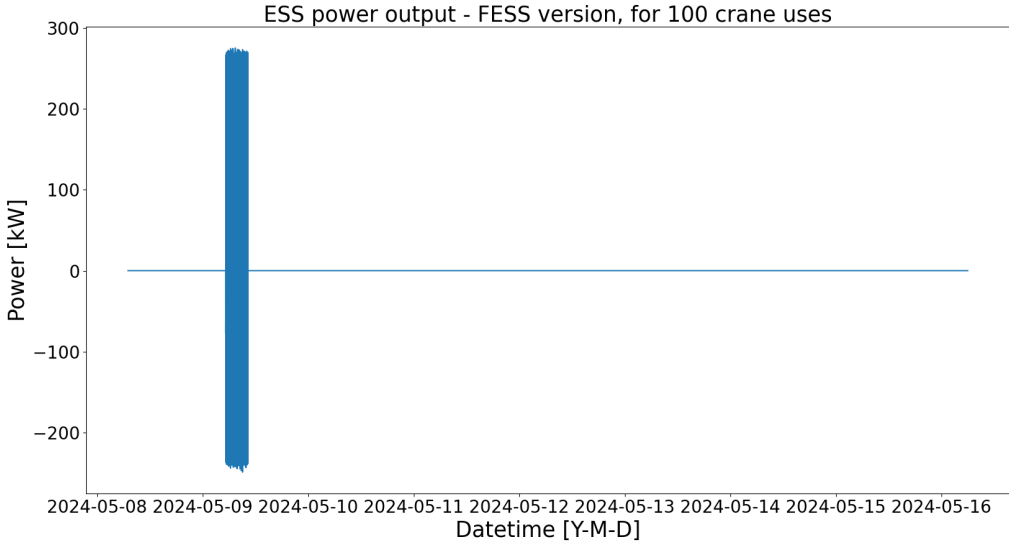
Figure A.90: Figure of the FESS power output of the FESS version of the HP ESS shore power configuration. The FESS peak shaves the crane uses of the vessel power profile of Figure A.46.
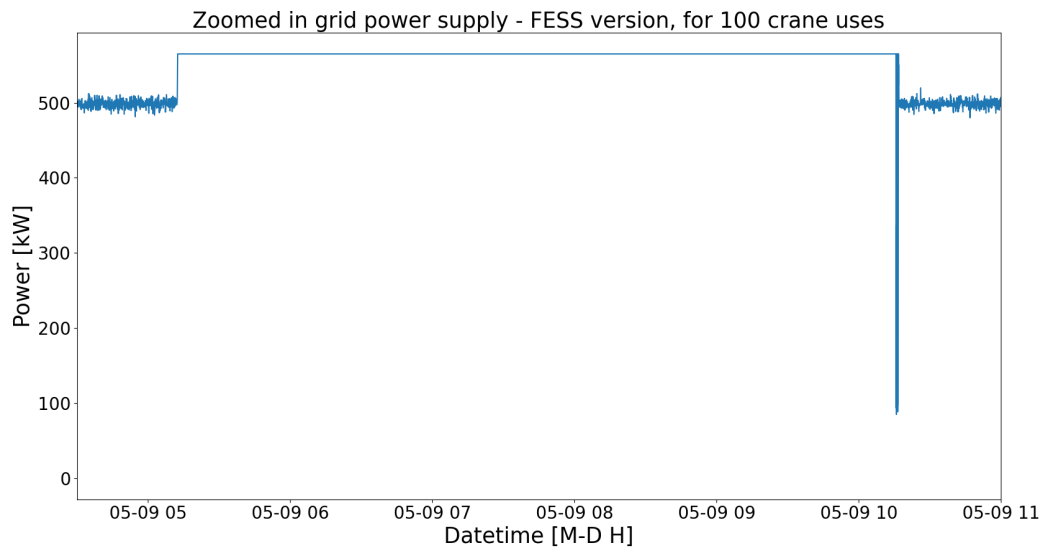
Figure A.91: Figure of the grid power supply by the FESS version of the HP ESS shore power configuration, zoomed in on the crane uses. The crane uses of the vessel power profile of Figure A.46 are peak shaven by the FESS.
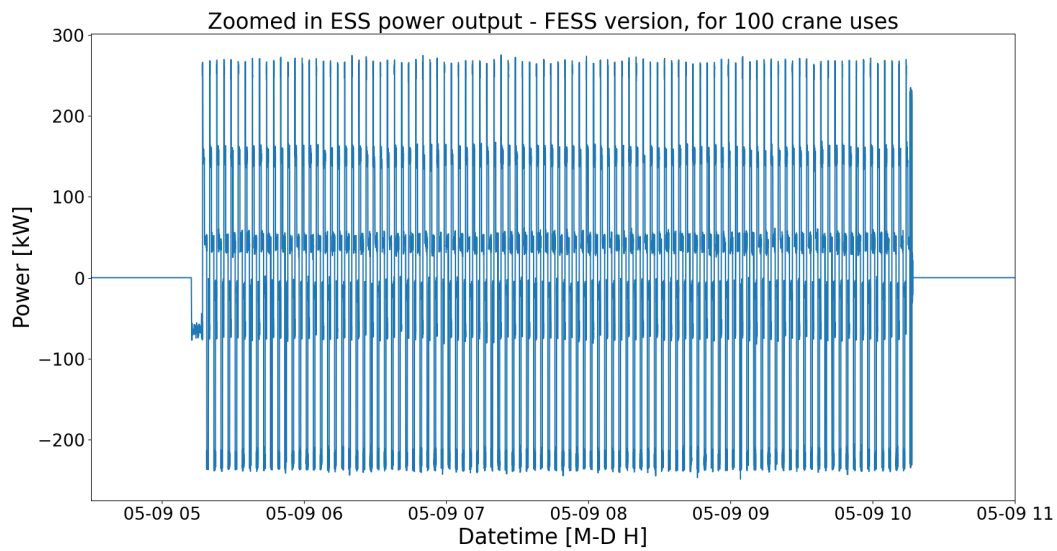
Figure A.92: Figure of the FESS power output of the FESS version of the HP ESS shore power configuration, zoomed in on the crane uses. The FESS peak shaves the crane uses of the vessel power profile of Figure A.46.
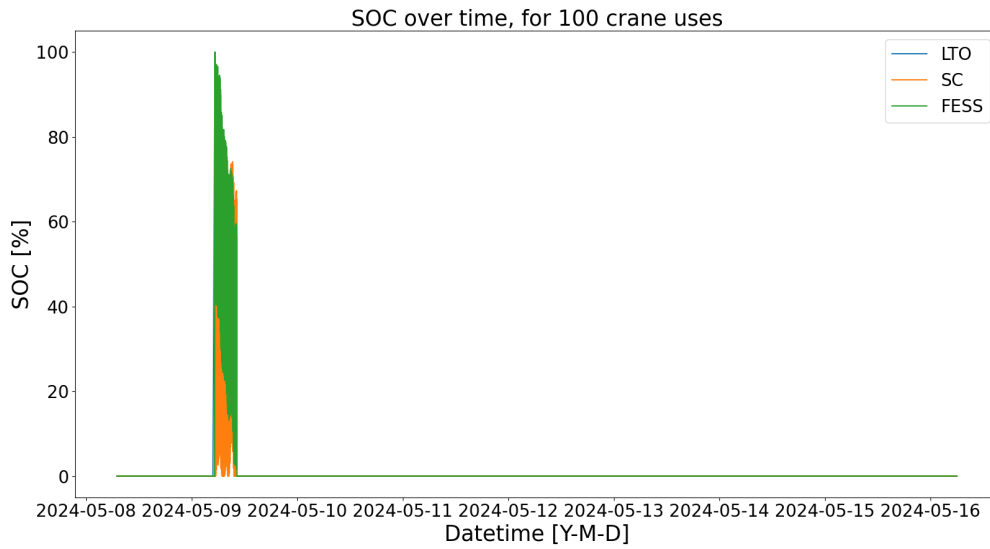
Figure A.93: Figure of the SOC of the different versions of the HP ESS shore power configuration. All the ESS are only used for the crane uses in the vessel power profile of Figure A.46.
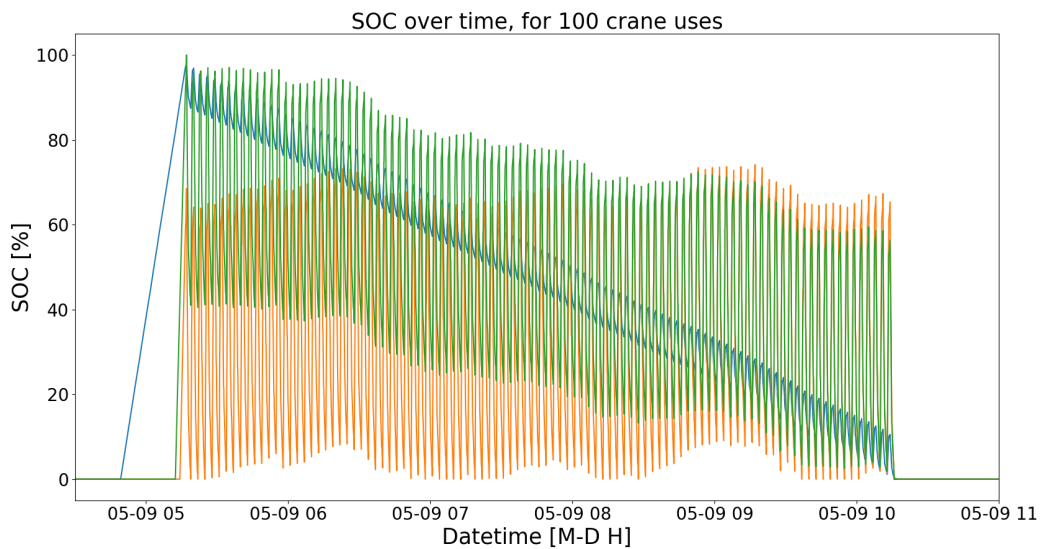
Figure A.94: Figure of the zoomed in version of the SOC of the different versions of the HP ESS shore power configuration. The figure is zoomed in on the crane uses. The swings in SOC that are synchronized for each of the ESS are when the crane uses happen. The ESS are charged up just before the crane uses start. The LTO version and FESS version are fully charged at the start, and SC is charged up to around 60%. All the version are fully discharged at the final crane use.

A.4. P_{nom} **of crane**
A.4.1. **20 kW P_{nom} of crane**
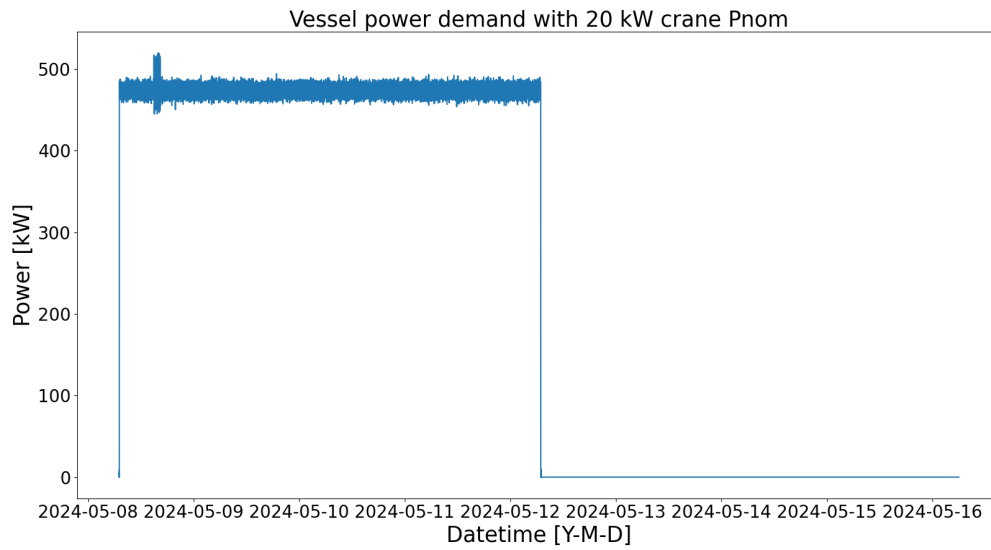
Figure A.95: Figure of the power profile of 4 days and 4 days of downtime. The power demand includes 30 consecutive crane uses, with the P_{nom} of the crane being 20 kW. The vessel power profile was used for the HP ESS shore power configuration. The x-axis is in datetime meaning that each data point is fixed to a particular date and time.

Figure A.96: Figure of the grid power supply by the LTO version of the HP ESS shore power configuration. The crane uses and some minor fluctuations of the vessel power profile of Figure A.95 are peak shaven by the LTO battery.
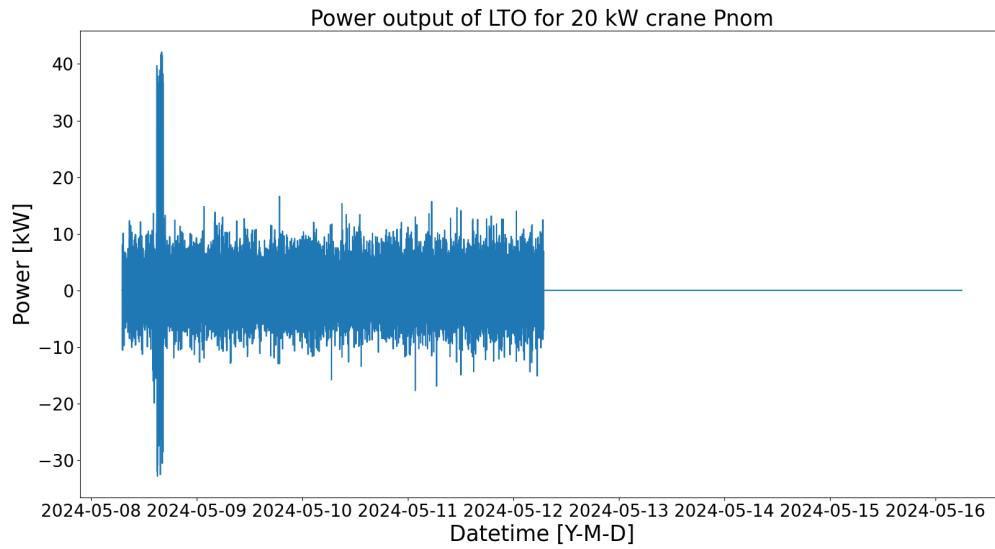
Figure A.97: Figure of the LTO battery power output of the LTO version of the HP ESS shore power configuration. The LTO battery peak shaves the crane uses and some of the minor fluctuations of the vessel power profile of Figure A.95. The peak of the crane use has an overshoot.
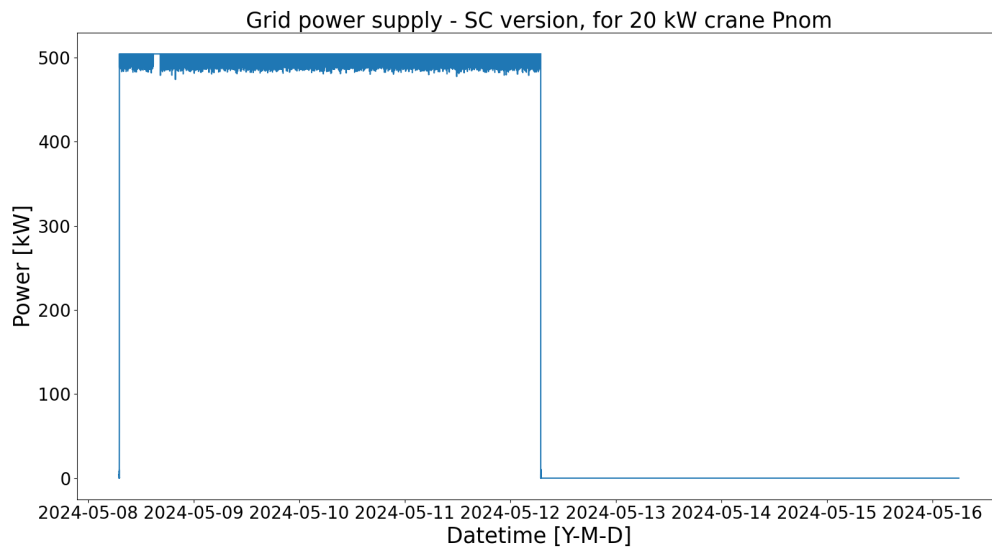
Figure A.98: Figure of the grid power supply by the SC version of the HP ESS shore power configuration. The crane uses and some minor fluctuations of the vessel power profile of Figure A.95 are peak shaven by the SC.
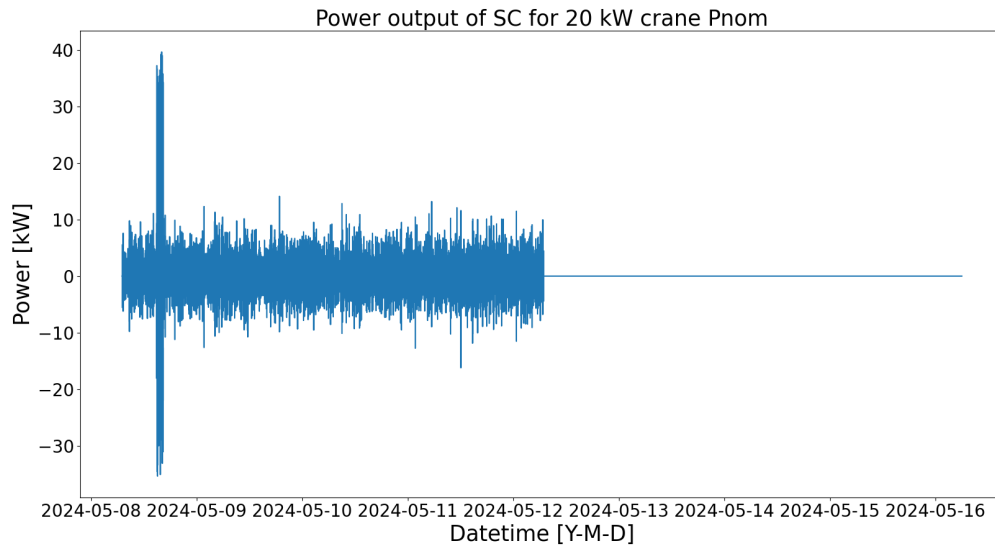
Figure A.99: Figure of the SC power output of the SC version of the HP ESS shore power configuration. The SC peak shaves the crane uses and some of the minor fluctuations of the vessel power profile of Figure A.95. The peak of the crane use has an overshoot.
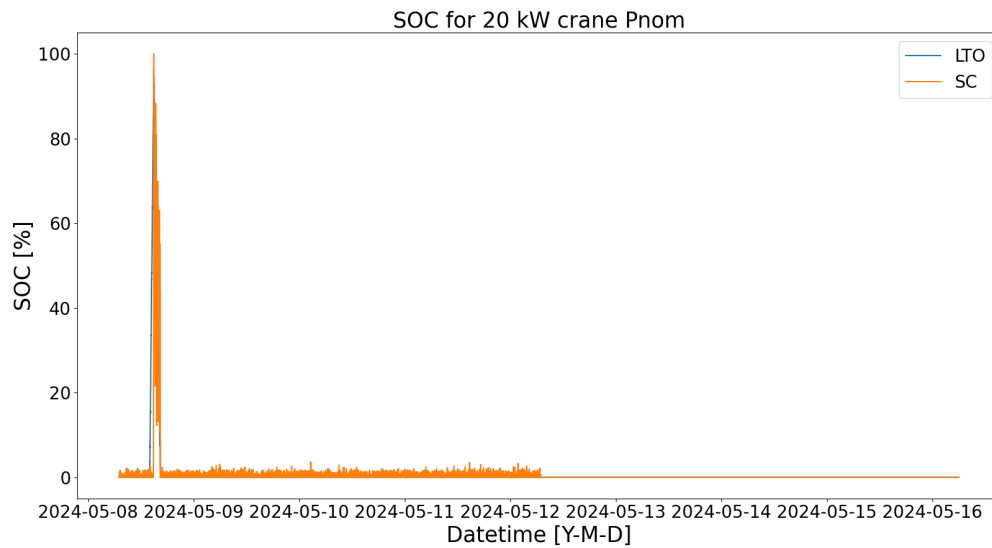
Figure A.100: Figure of the SOC of the LTO and SC versions of the HP ESS shore power configuration. The FESS is excluded because the crane P_{nom} is too small for it to be cost-effective. The ESS are used for the crane uses and the minor fluctuations in the vessel power profile of Figure A.95.
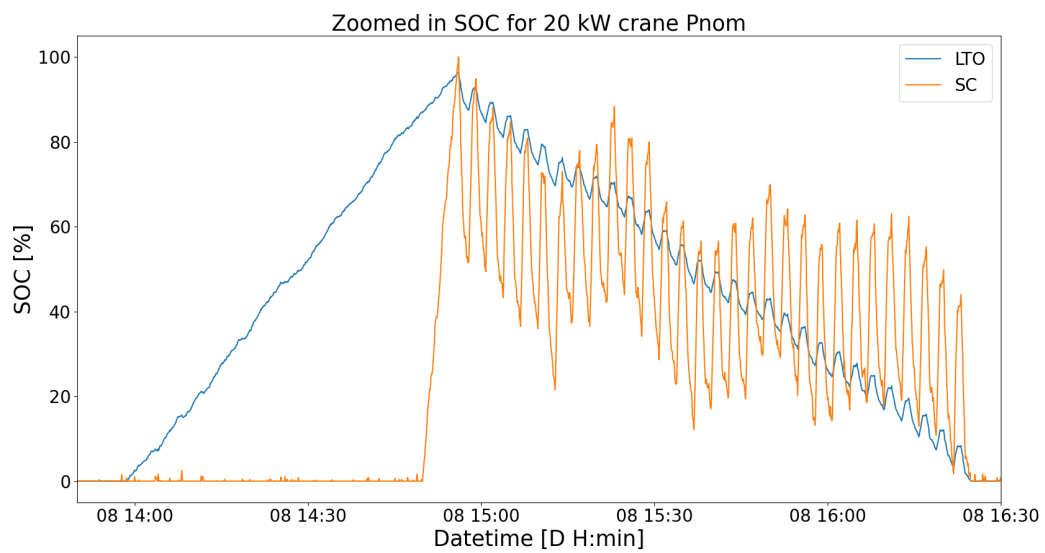
Figure A.101: Figure of the zoomed in SOC of the LTO and SC versions of the HP ESS shore power configuration. The FESS is excluded because the crane P_{nom} is too small for it to be cost-effective. The figure is zoomed in on the crane uses. The swings of the SOC correspond to the crane uses. The ESS are charged up fully just before the crane uses start.

A.4.2. 40 kW P_{nom} of crane
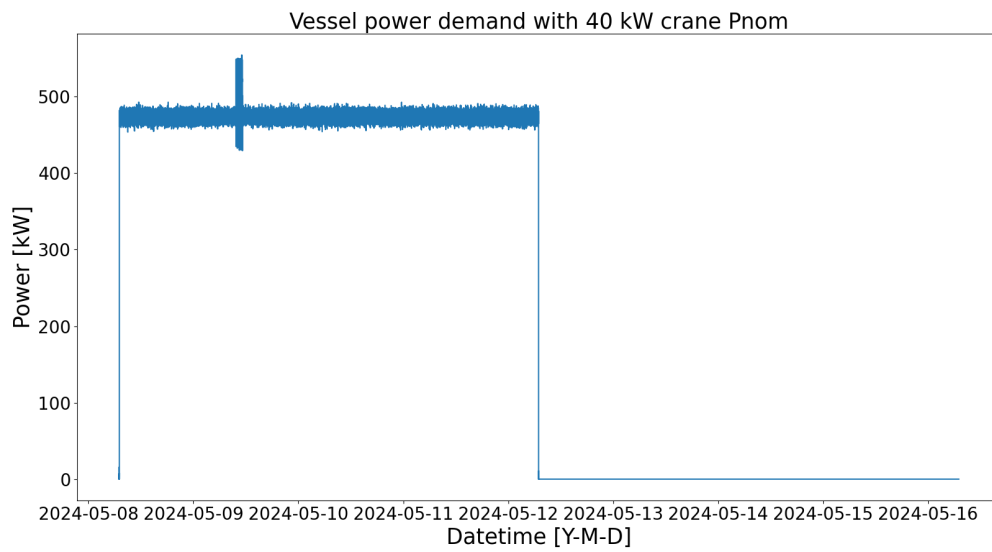
Figure A.102: Figure of the power profile of 4 days and 4 days of downtime. The power demand includes 30 consecutive crane uses, with the P_{nom} of the crane being 40 kW. The vessel power profile was used for the HP ESS shore power configuration. The x-axis is in datetime meaning that each data point is fixed to a particular date and time.

Figure A.103: Figure of the grid power supply by the LTO version of the HP ESS shore power configuration. The crane uses and some minor fluctuations of the vessel power profile of Figure A.102 are peak shaven by the LTO battery.

Figure A.104: Figure of the LTO battery power output of the LTO version of the HP ESS shore power configuration. The LTO battery peak shaves the crane uses and some of the minor fluctuations of the vessel power profile of Figure A.102. The peak of the crane use has an overshoot.

Figure A.105: Figure of the grid power supply by the SC version of the HP ESS shore power configuration. The crane uses and some minor fluctuations of the vessel power profile of Figure A.102 are peak shaven by the SC.
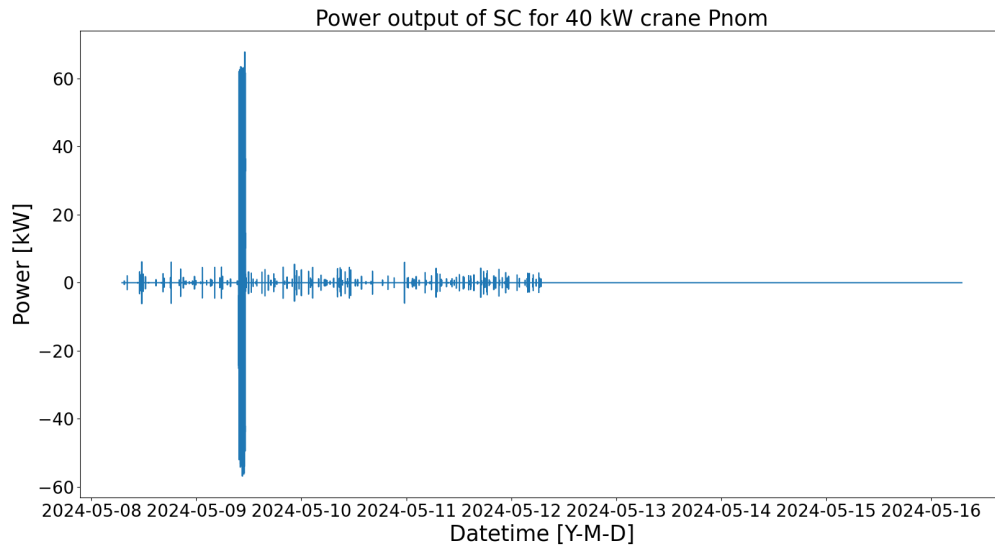
Figure A.106: Figure of the SC power output of the SC version of the HP ESS shore power configuration. The SC peak shaves the crane uses and some of the minor fluctuations of the vessel power profile of Figure A.102. The peak of the crane use has an overshoot.
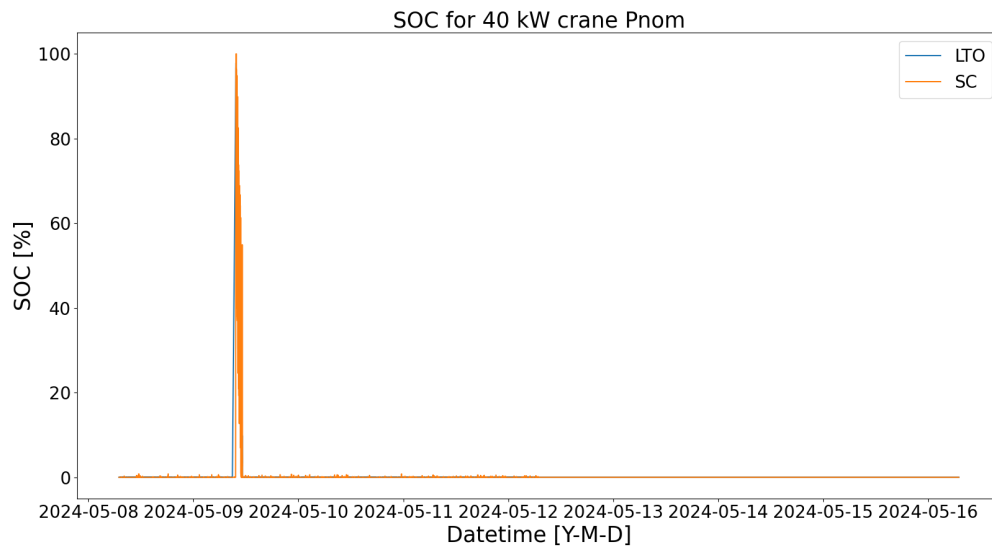
Figure A.107: Figure of the SOC of the LTO and SC versions of the HP ESS shore power configuration. The FESS is excluded because the crane P_{nom} is too small for it to be cost-effective. The ESS are used for the crane uses and the minor fluctuations in the vessel power profile of Figure A.102.
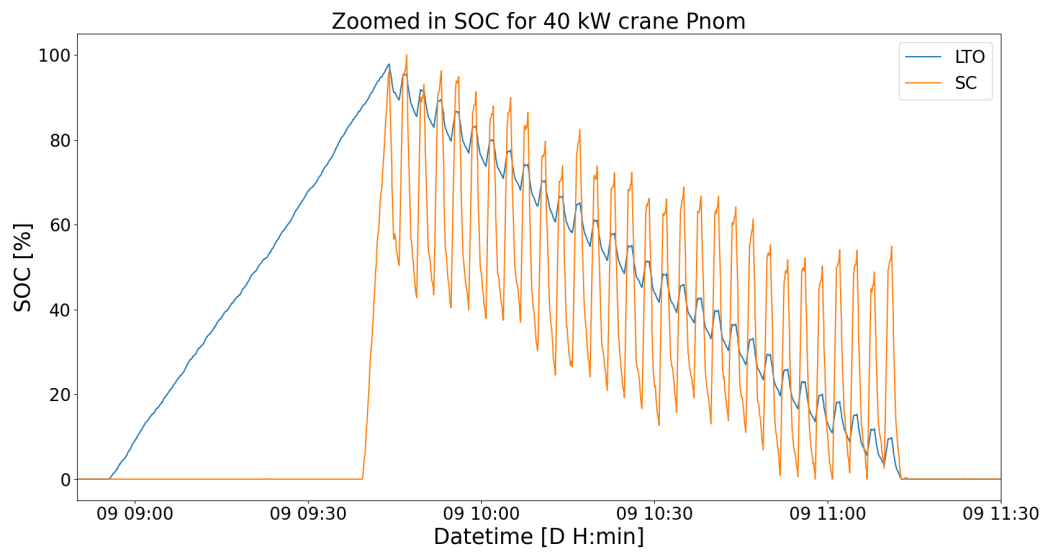
Figure A.108: Figure of the zoomed in SOC of the LTO and SC versions of the HP ESS shore power configuration. The FESS is excluded because the crane P_{nom} is too small for it to be cost-effective. The figure is zoomed in on the crane uses. The swings of the SOC correspond to the crane uses. The ESS are charged up fully just before the crane uses start.

A.4.3. 60 kW P_{nom} of crane
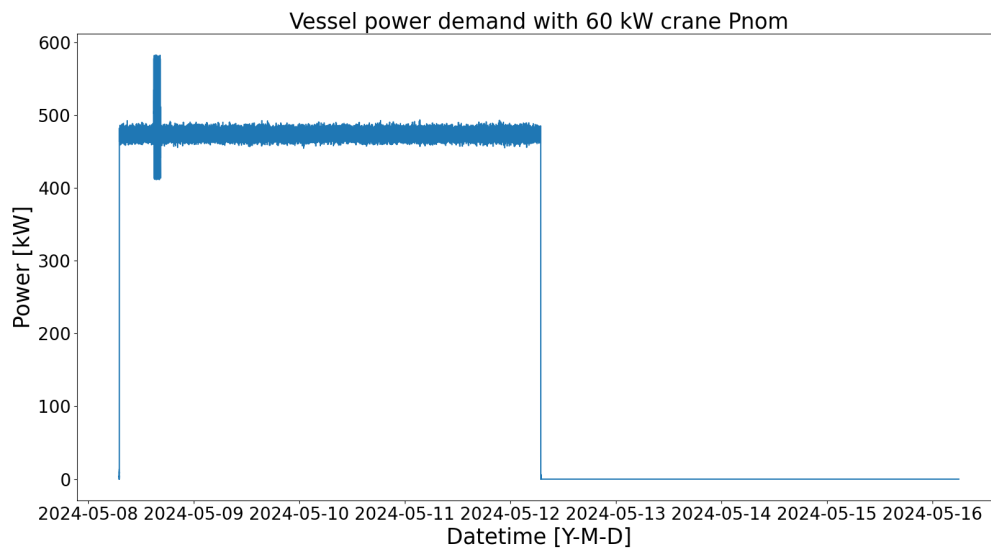
Figure A.109: Figure of the power profile of 4 days and 4 days of downtime. The power demand includes 30 consecutive crane uses, with the P_{nom} of the crane being 60 kW. The vessel power profile was used for the HP ESS shore power configuration. The x-axis is in datetime meaning that each data point is fixed to a particular date and time.
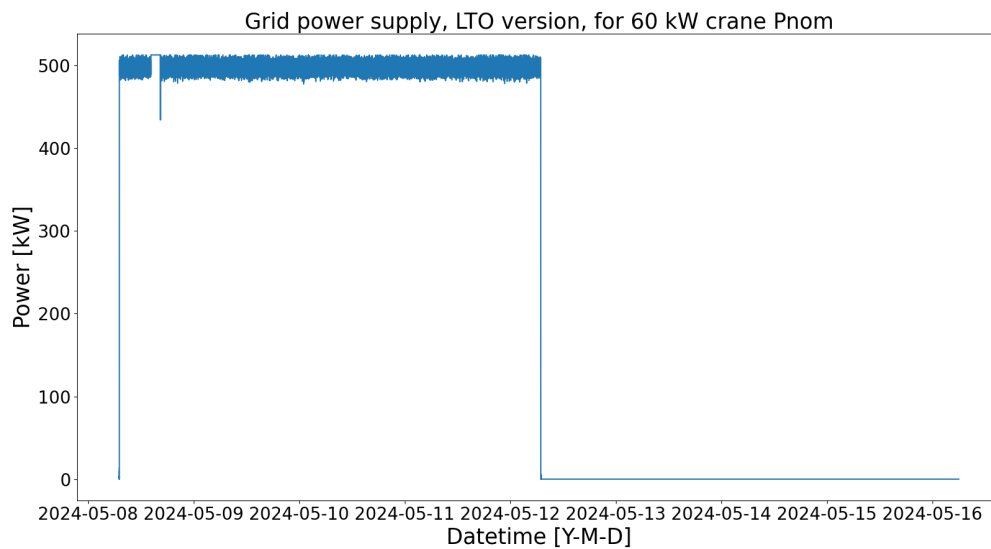
Figure A.110: Figure of the grid power supply by the LTO version of the HP ESS shore power configuration. The crane uses and some minor fluctuations of the vessel power profile of Figure A.109 are peak shaven by the LTO battery.

**Figure A.111:** Figure of the LTO battery power output of the LTO version of the HP ESS shore power configuration. The LTO battery peak shaves the crane uses and some of the minor fluctuations of the vessel power profile of Figure A.109. The peak of the crane use has an overshoot.
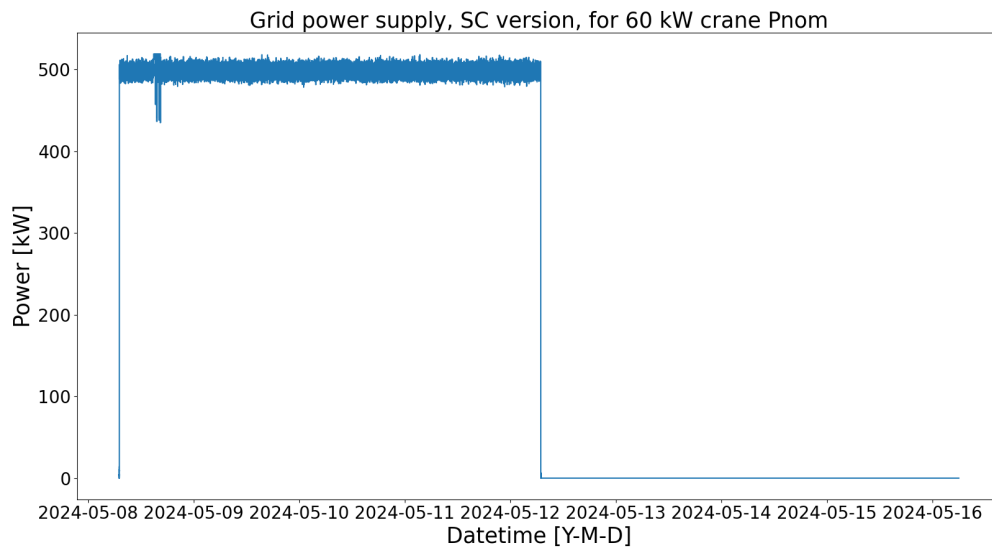
Figure A.112: Figure of the grid power supply by the SC version of the HP ESS shore power configuration. The crane uses of the vessel power profile of Figure A.109 are peak shaven by the SC.
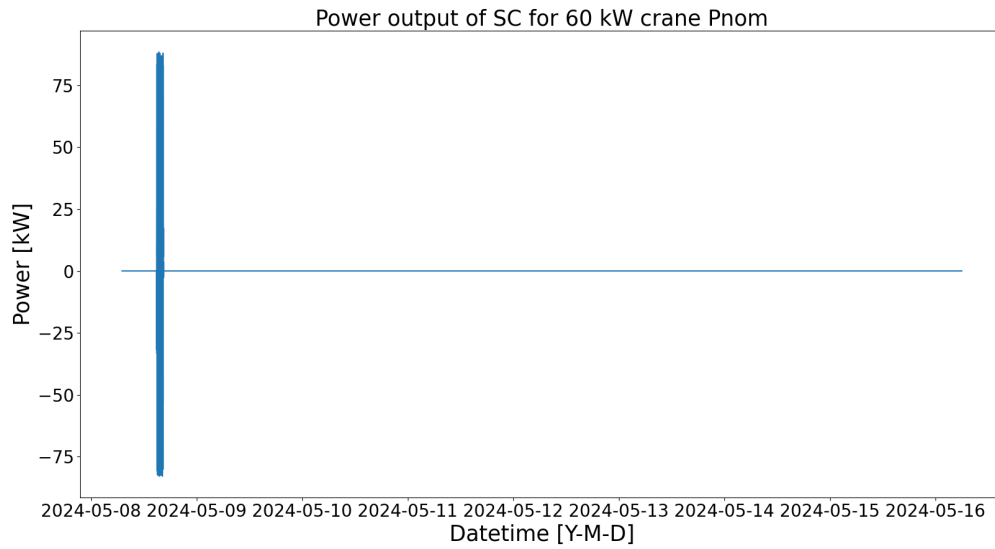
Figure A.113: Figure of the SC power output of the SC version of the HP ESS shore power configuration. The SC peak shaves the crane uses of the vessel power profile of Figure A.109. The peak of the crane use has an overshoot.
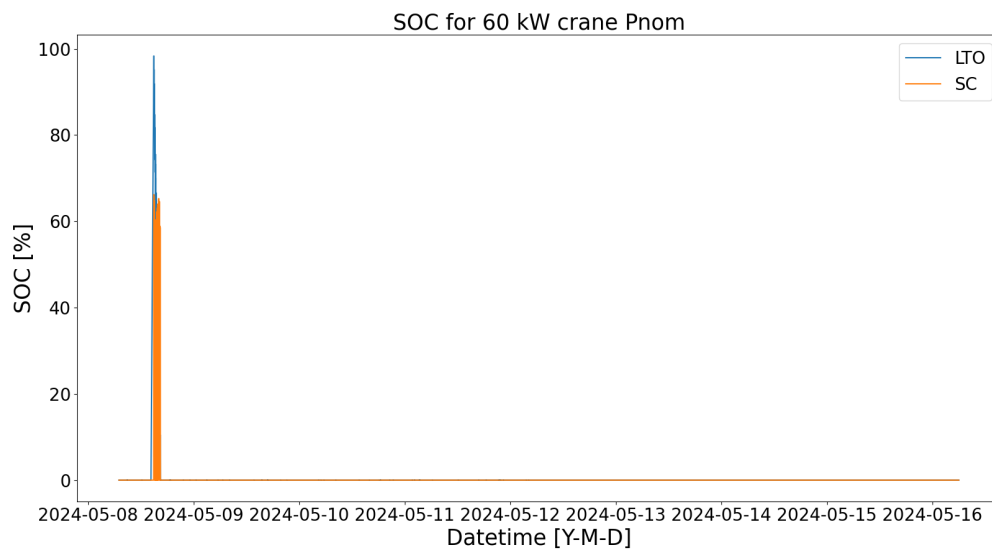
Figure A.114: Figure of the SOC of the LTO and SC versions of the HP ESS shore power configuration. The FESS is excluded because the crane P_{nom} is too small for it to be cost-effective. The ESS are used for the crane uses and the LTO version is also used for minor fluctuations in the vessel power profile of Figure A.109.
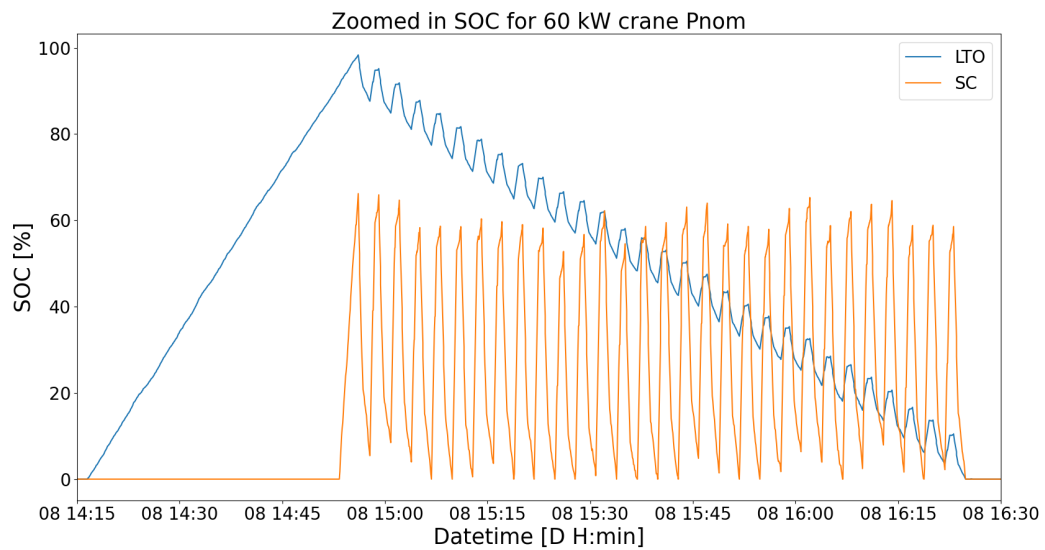
Figure A.115: Figure of the zoomed in SOC of the LTO and SC versions of the HP ESS shore power configuration. The FESS is excluded because the crane P_{nom} is too small for it to be cost-effective. The figure is zoomed in on the crane uses. The swings of the SOC correspond to the crane uses. The LTO version is charged up fully just before the crane uses start and the SC version is charged up to 60% and both are fully discharged at the last crane use.

A.4.4. 80 kW P_{nom} of crane
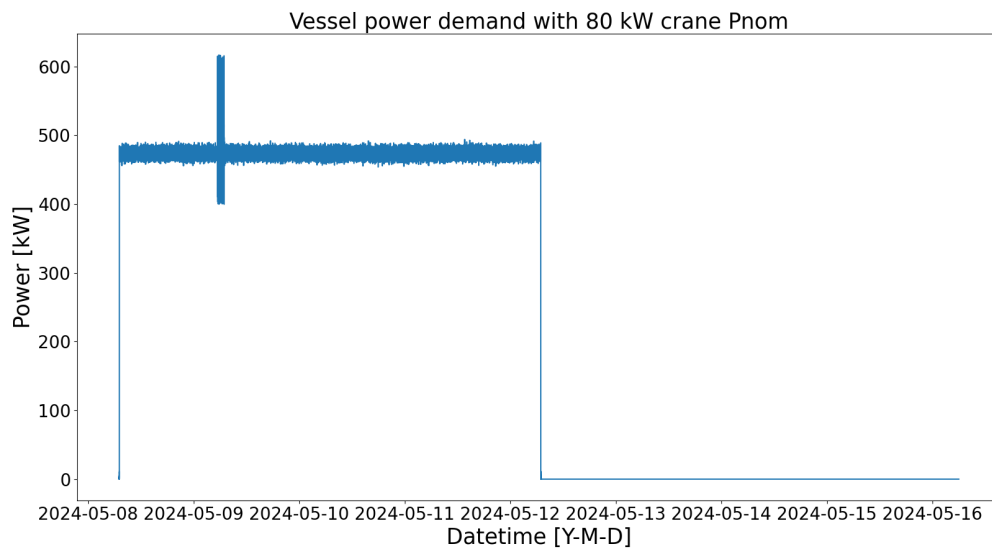
Figure A.116: Figure of the power profile of 4 days and 4 days of downtime. The power demand includes 30 consecutive crane uses, with the P_{nom} of the crane being 80 kW. The vessel power profile was used for the HP ESS shore power configuration. The x-axis is in datetime meaning that each data point is fixed to a particular date and time.
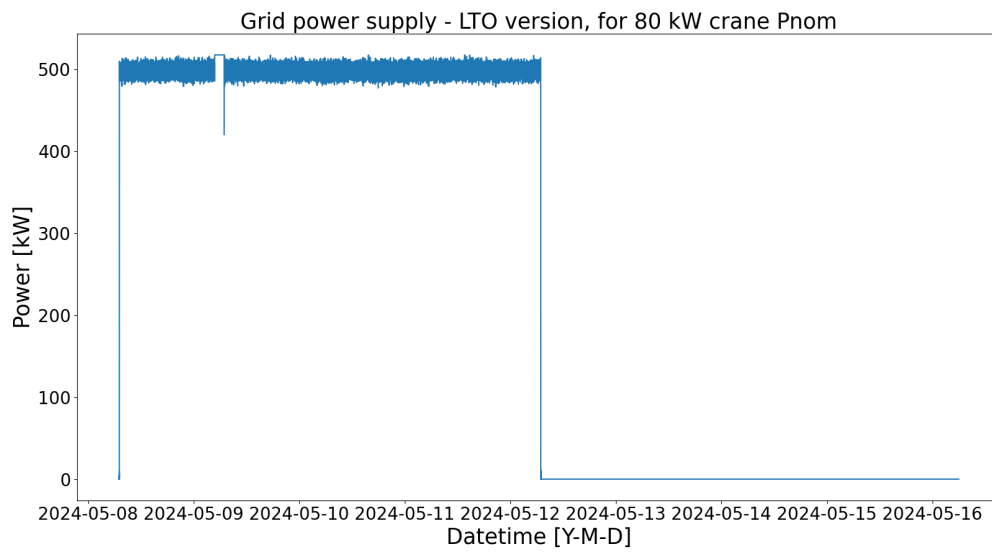
Figure A.117: Figure of the grid power supply by the LTO version of the HP ESS shore power configuration. The crane uses of the vessel power profile of Figure A.116 are peak shaven by the LTO battery.

Power output of LTO for 80 kW crane Pnom
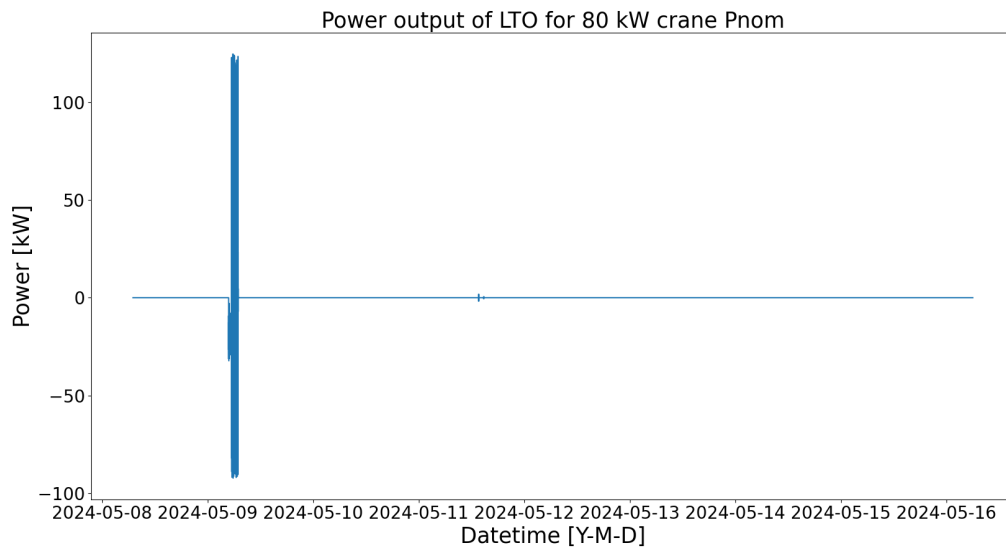
Figure A.118: Figure of the LTO battery power output of the LTO version of the HP ESS shore power configuration. The LTO battery peak shaves the crane uses of the vessel power profile of Figure A.116. The peak of the crane use has an overshoot.

Grid power supply - SC version, for 80 kW crane Pnom
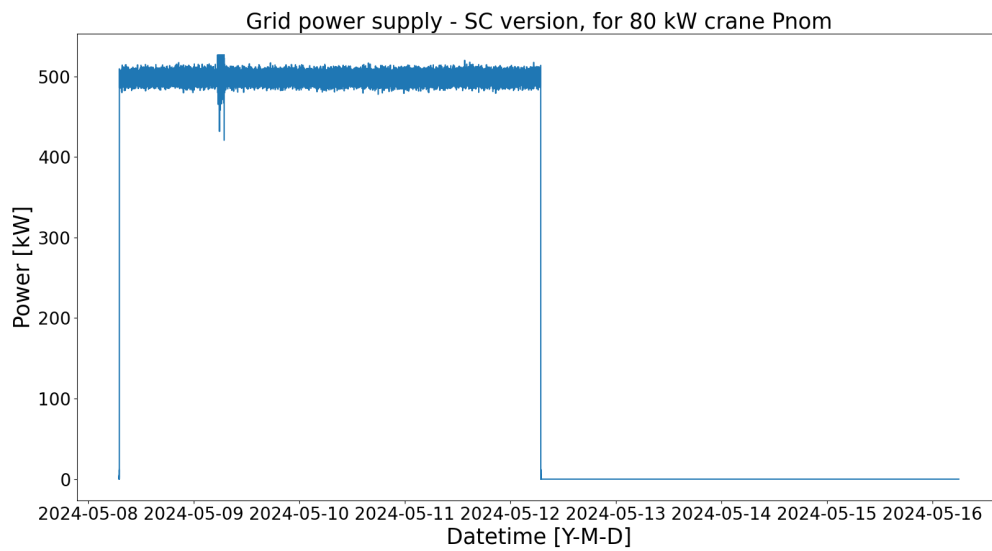
Figure A.119: Figure of the grid power supply by the SC version of the HP ESS shore power configuration. The crane uses of the vessel power profile of Figure A.116 are peak shaven by the SC.
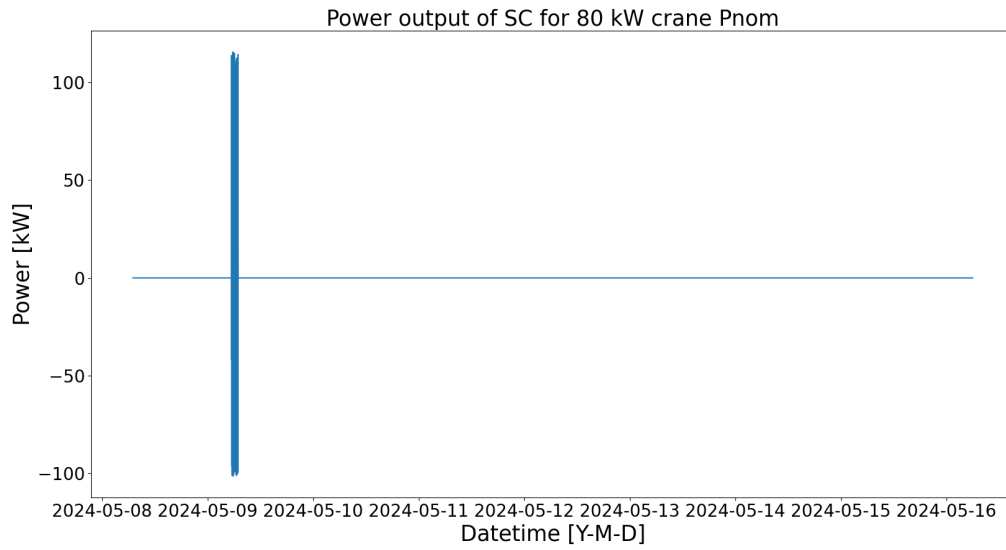
Figure A.120: Figure of the SC power output of the SC version of the HP ESS shore power configuration. The SC peak shaves the crane uses of the vessel power profile of Figure A.116. The peak of the crane use has an overshoot.
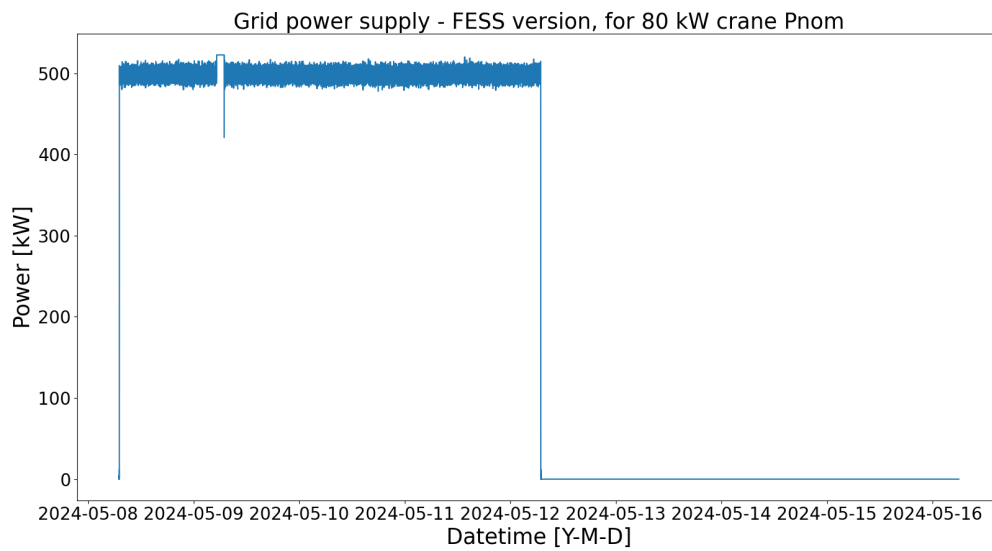
Figure A.121: Figure of the grid power supply by the FESS version of the HP ESS shore power configuration. The crane uses of the vessel power profile of Figure A.116 are peak shaven by the FESS.
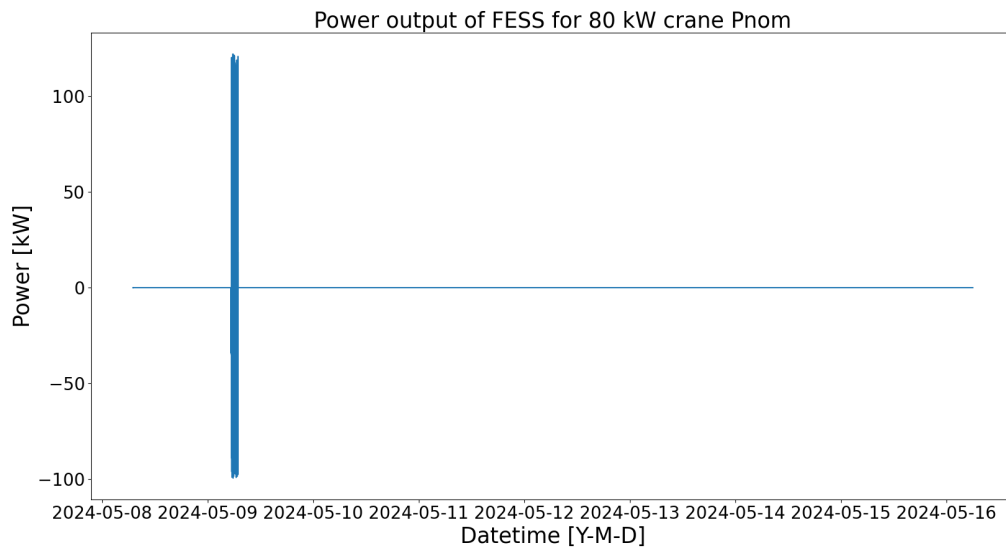
Figure A.122: Figure of the FESS power output of the FESS version of the HP ESS shore power configuration. The FESS peak shaves the crane uses of the vessel power profile of Figure A.116. The peak of the crane use has an overshoot.
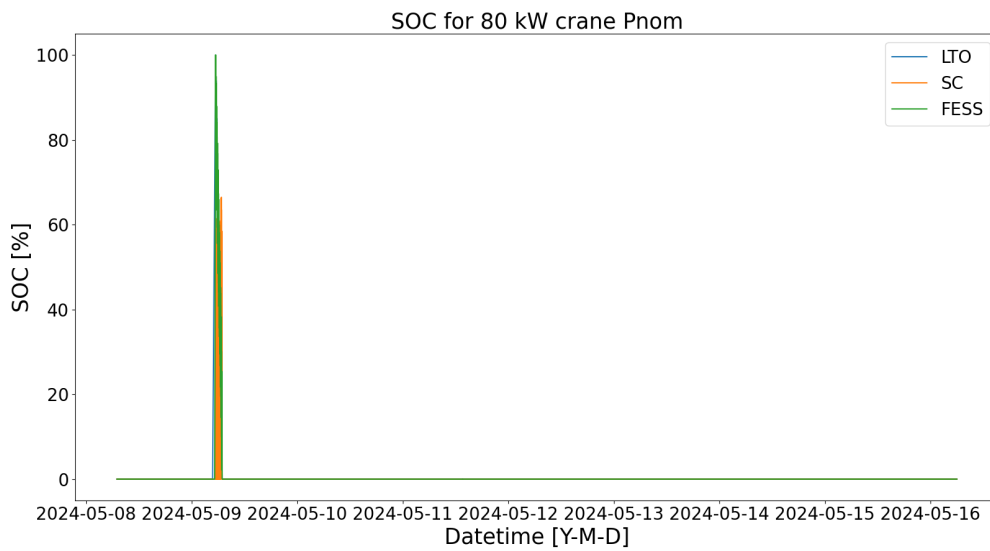
Figure A.123: Figure of the SOC of the different versions of the HP ESS shore power configuration. The ESS are used for the crane uses of the vessel power profile of Figure A.116.
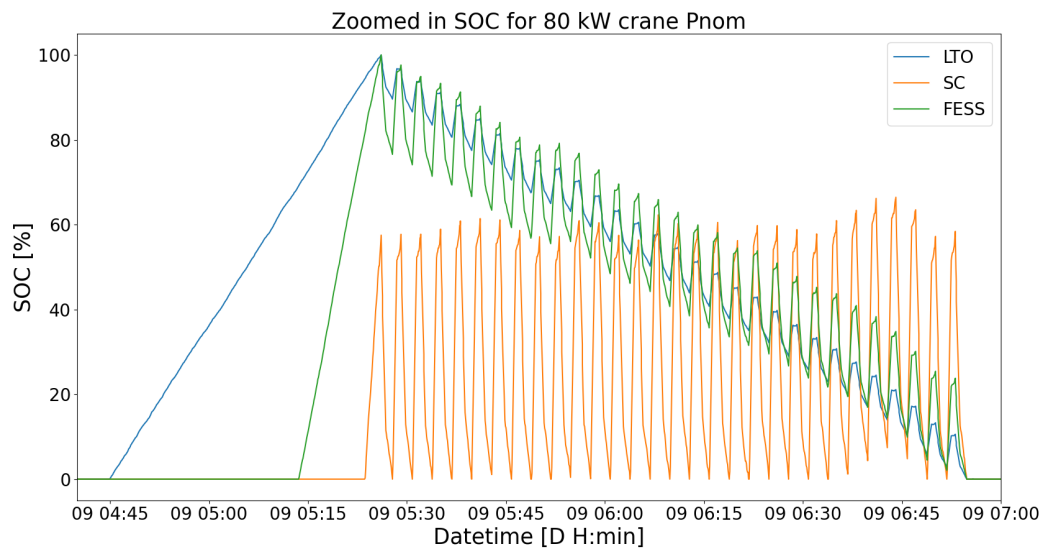
Figure A.124: Figure of the zoomed in SOC of the different versions of the HP ESS shore power configuration. The figure is zoomed in on the crane uses. The swings of the SOC correspond to the crane uses. The LTO version and the FESS version are charged up fully just before the crane uses start and the SC version is charged up to 60% and all are fully discharged at the last crane use.

A.4.5. 100 kW P_{nom} of crane
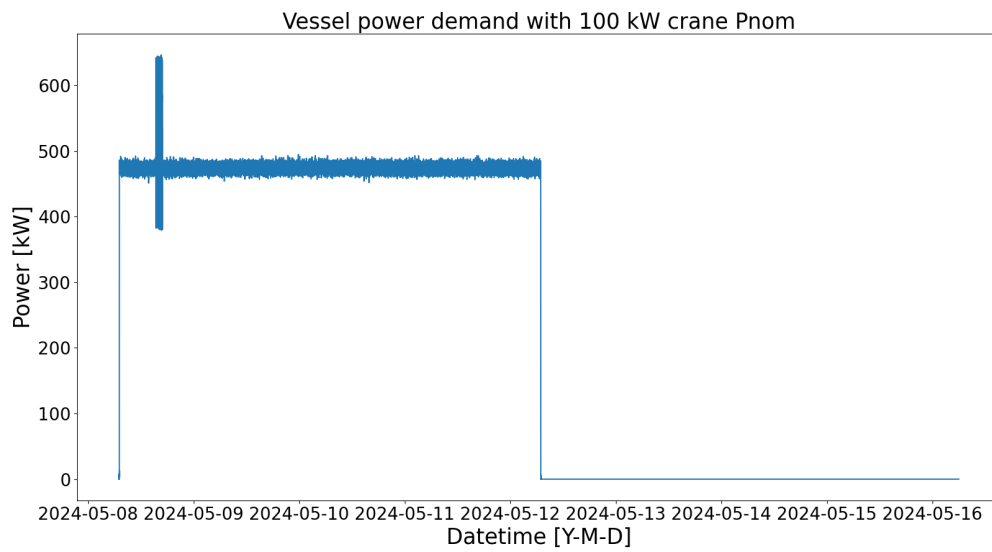
Figure A.125: Figure of the power profile of 4 days and 4 days of downtime. The power demand includes 30 consecutive crane uses, with the P_{nom} of the crane being 100 kW. The vessel power profile was used for the HP ESS shore power configuration. The x-axis is in datetime meaning that each data point is fixed to a particular date and time.
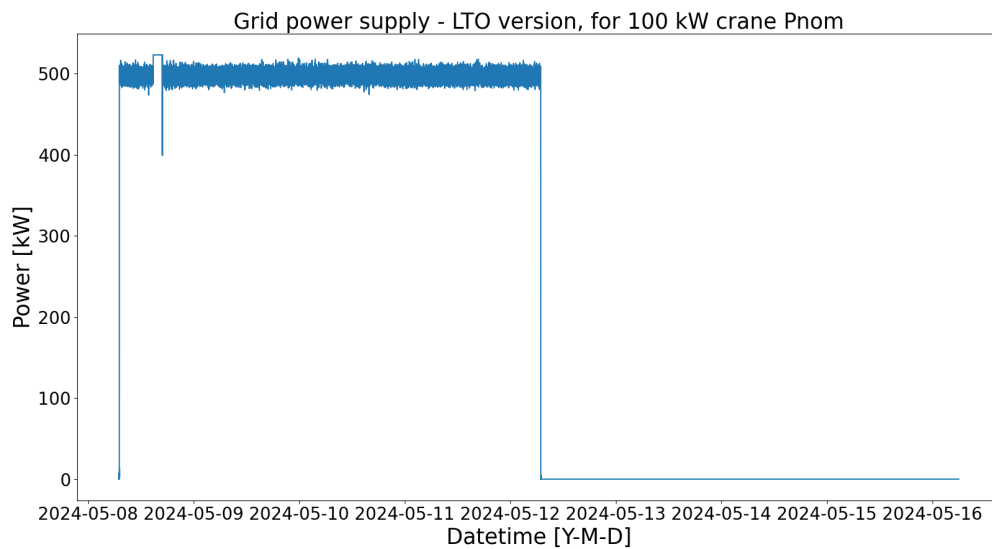
Figure A.126: Figure of the grid power supply by the LTO version of the HP ESS shore power configuration. The crane uses of the vessel power profile of Figure A.125 are peak shaven by the LTO battery.
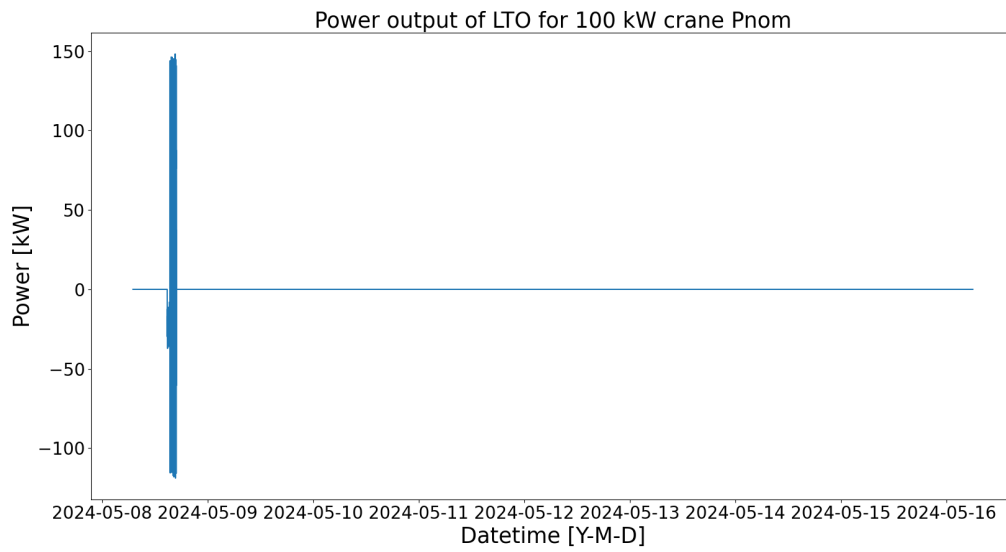
Figure A.127: Figure of the LTO battery power output of the LTO version of the HP ESS shore power configuration. The LTO battery peak shaves the crane uses of the vessel power profile of Figure A.125. The peak of the crane use has an overshoot.
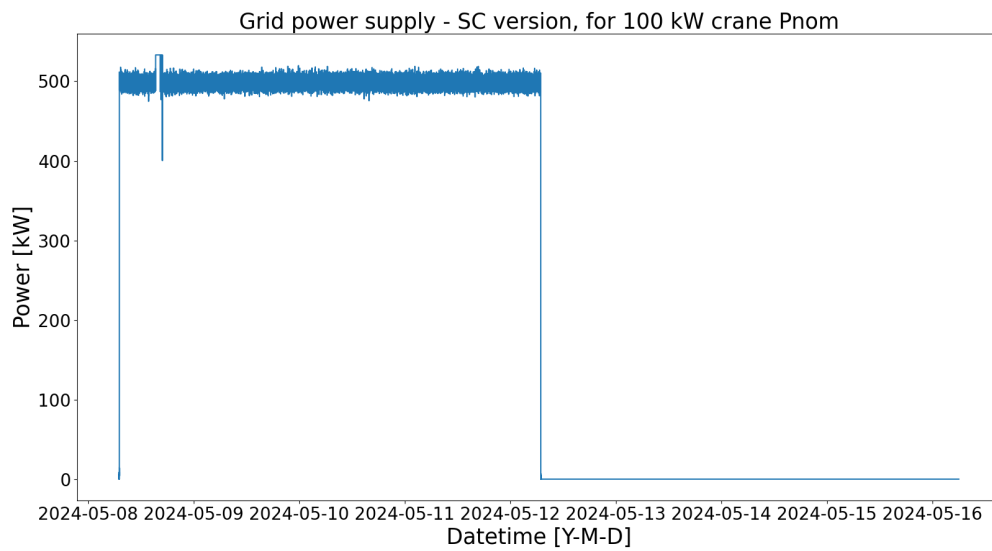
Figure A.128: Figure of the grid power supply by the SC version of the HP ESS shore power configuration. The crane uses of the vessel power profile of Figure A.125 are peak shaven by the SC.

Power output of SC for 100 kW crane Pnom
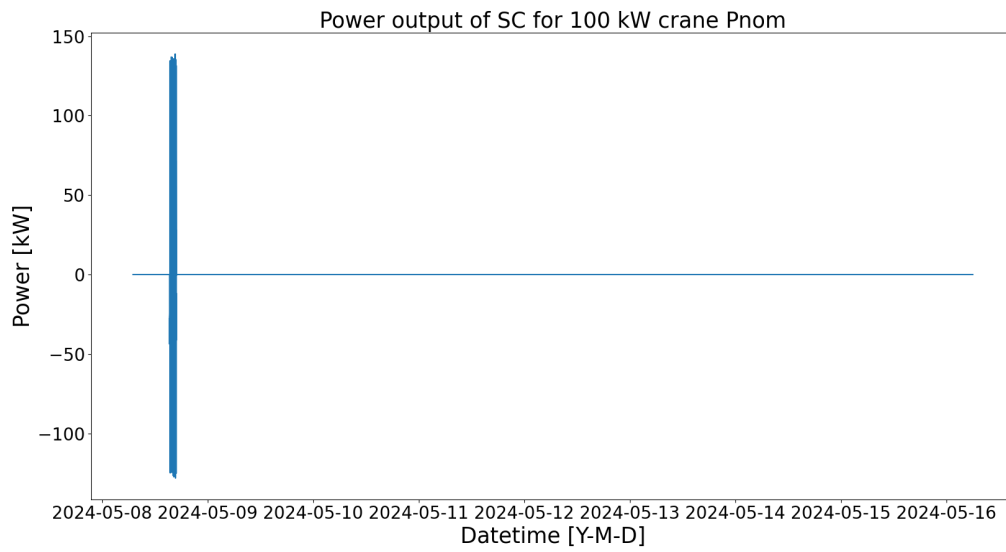
Figure A.129: Figure of the SC power output of the SC version of the HP ESS shore power configuration. The SC peak shaves the crane uses of the vessel power profile of Figure A.125. The peak of the crane use has an overshoot.

Grid power supply - FESS version, for 100 kW crane Pnom
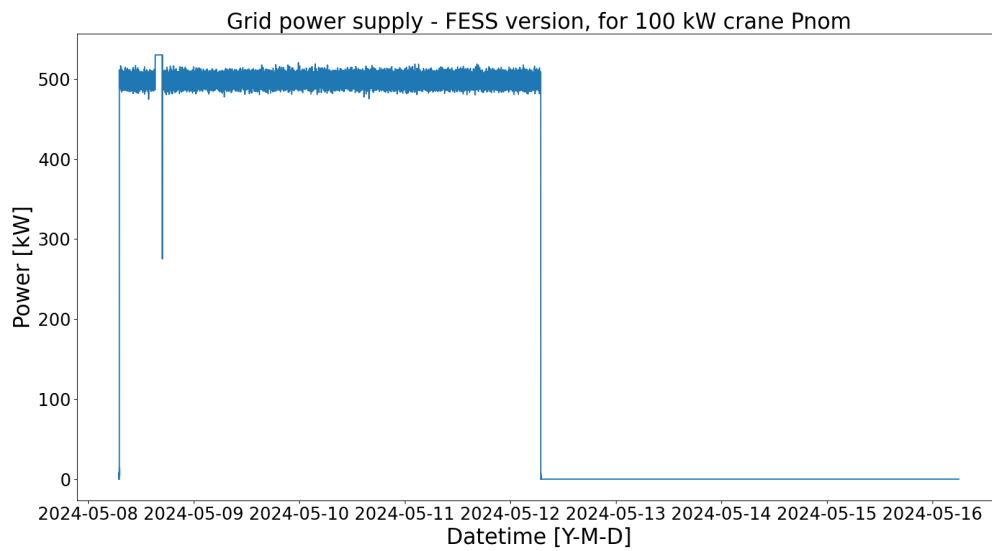
Figure A.130: Figure of the grid power supply by the FESS version of the HP ESS shore power configuration. The crane uses of the vessel power profile of Figure A.125 are peak shaven by the FESS.

Figure A.131: Figure of the FESS power output of the FESS version of the HP ESS shore power configuration. The FESS peak shaves the crane uses of the vessel power profile of Figure A.125. The peak of the crane use has an overshoot.
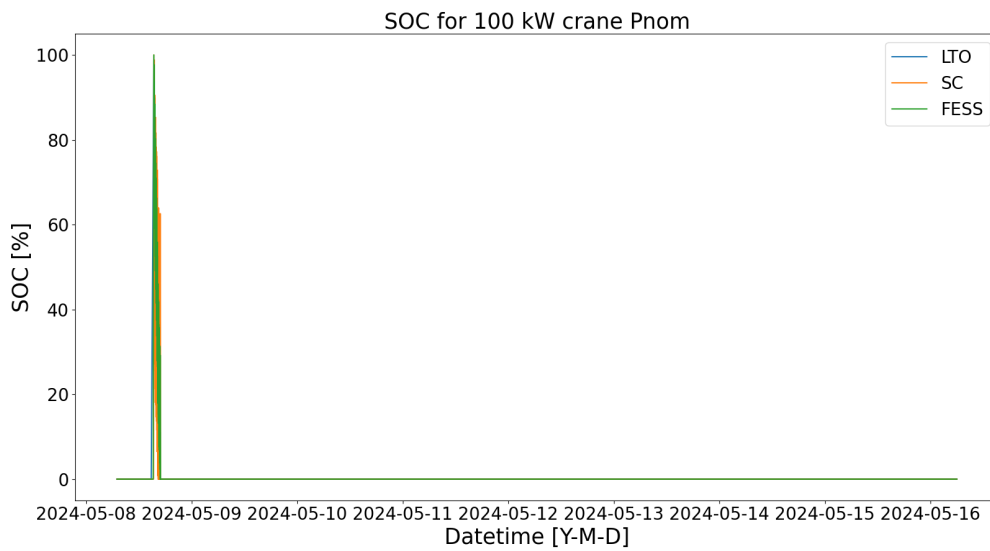
Figure A.132: Figure of the SOC of the different versions of the HP ESS shore power configuration. The ESS are used for the crane uses of the vessel power profile of Figure A.125.

Figure A.133: Figure of the zoomed in SOC of the different versions of the HP ESS shore power configuration. The figure is zoomed in on the crane uses. The swings of the SOC correspond to the crane uses. The ESS are charged up fully just before the crane uses start and all are fully discharged at the last crane use.

A.5. PV
A.5.1. Basic PV
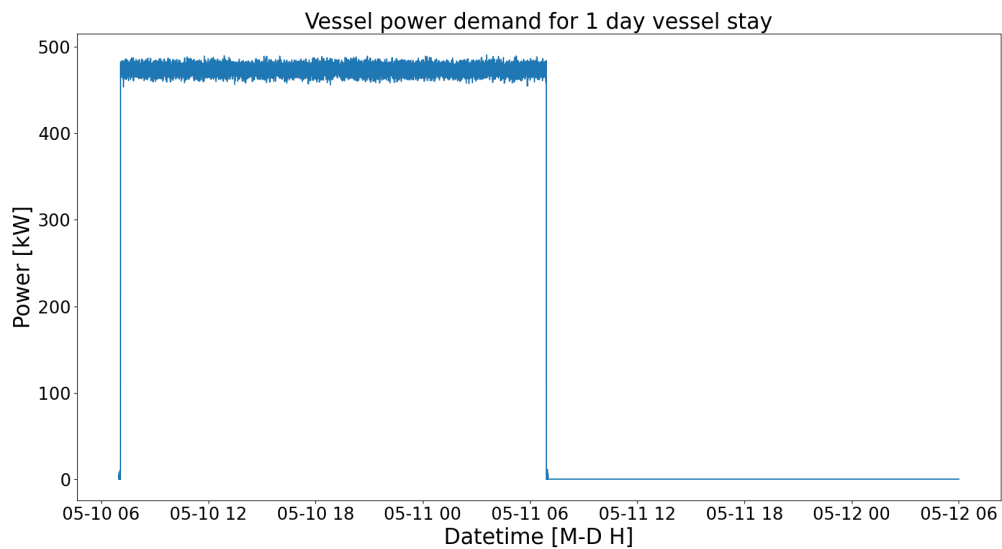
Figure A.134: Figure of the vessel power profile of 1 day and 1 day of downtime. The power demand has no crane uses. The vessel power profile was used for the Basic PV shore power configuration. The x-axis is in datetime, meaning that every data point is fixed to a date and time.
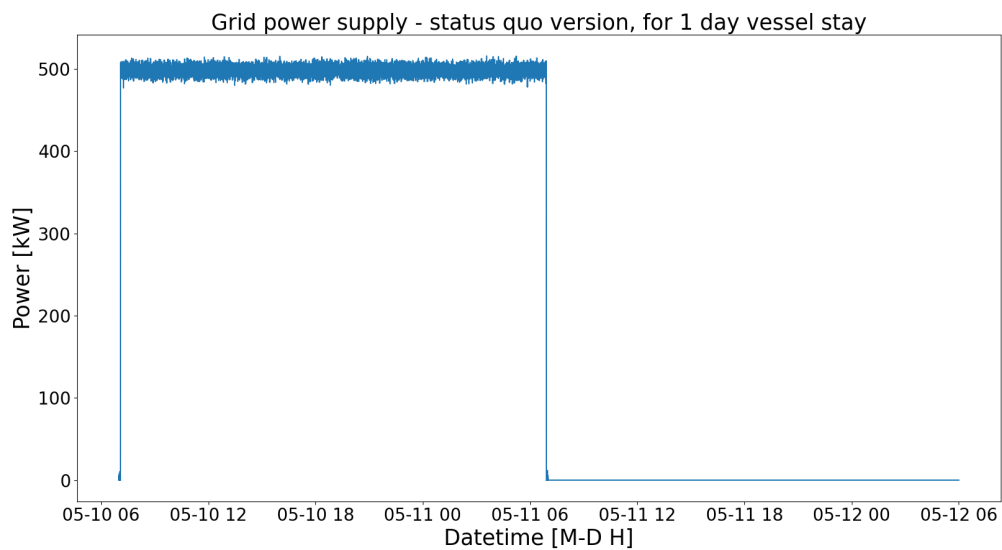
Figure A.135: Figure of the grid power supply by the status quo shore power configuration. The grid supplies the power that the power demand of Figure A.134. This figure is used to compare to the Basic PV shore power configuration.
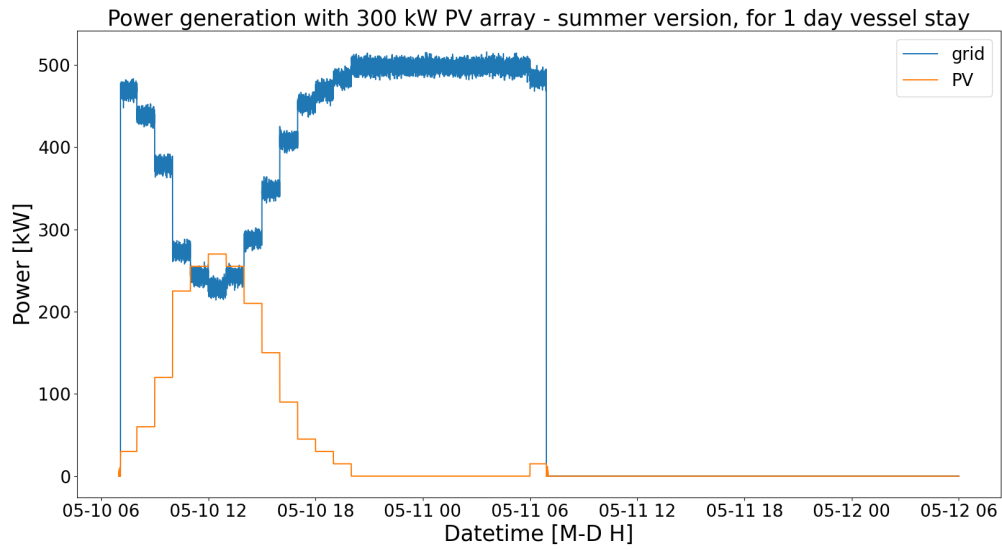
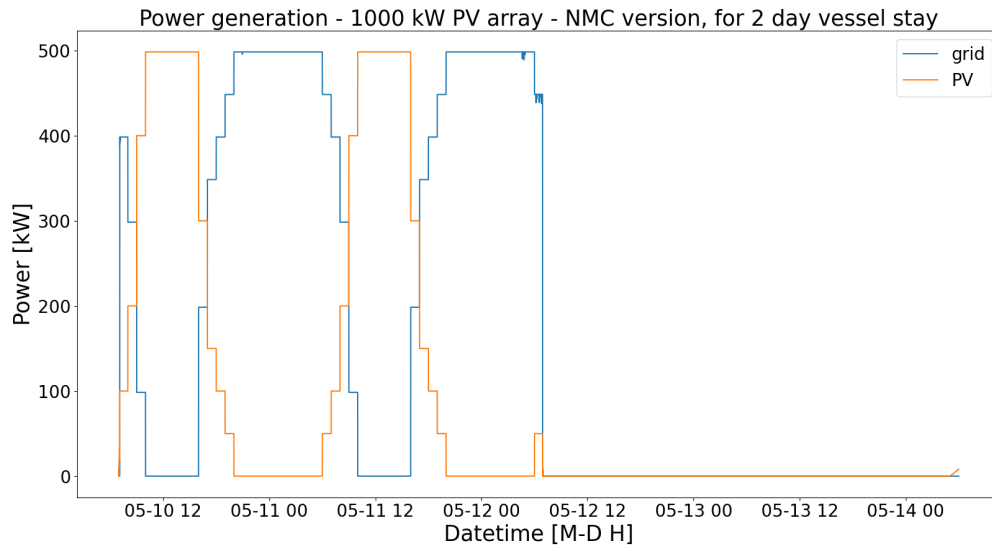**Figure A.136:** Figure of the power generation of the Basic PV shore power configuration with a 300 kW PV array. The solar generation is from an average summer day. The power generation is for the power demand from Figure A.134.
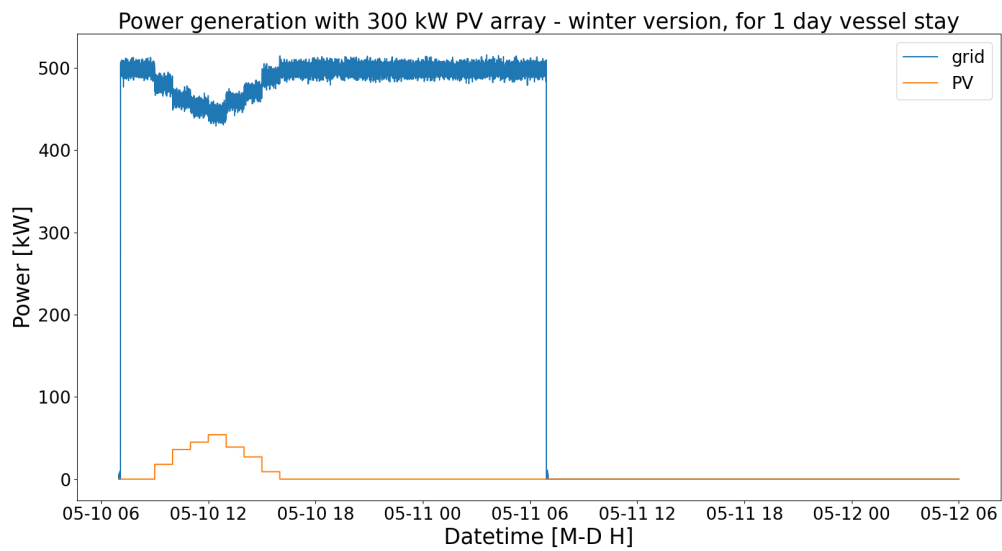
Figure A.137: Figure of the power generation of the Basic PV shore power configuration with a 300 kW PV array. The solar generation is from an average winter day. The power generation is for the power demand from Figure A.134.
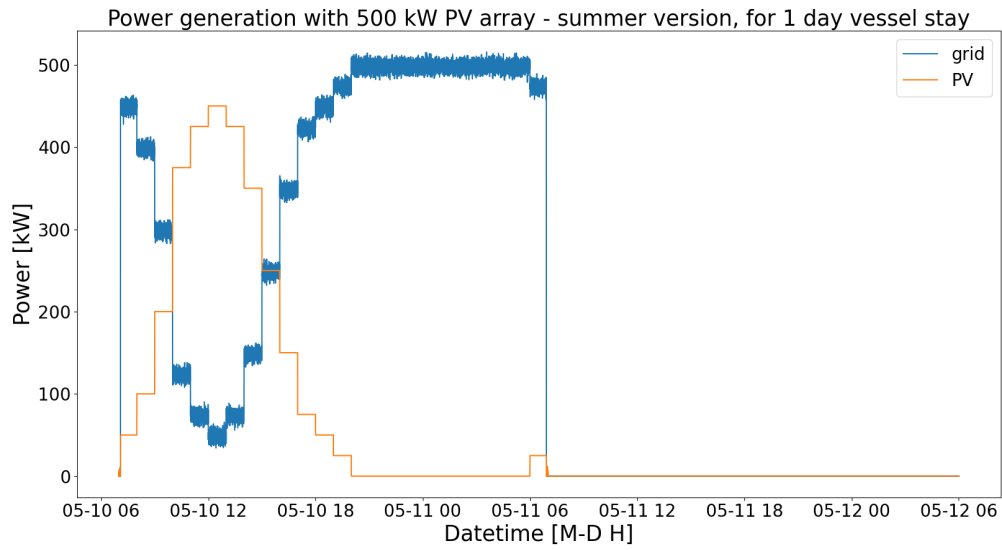
Figure A.138: Figure of the power generation of the Basic PV shore power configuration with a 500 kW PV array. The solar generation is from an average summer day. The power generation is for the power demand from Figure A.134.
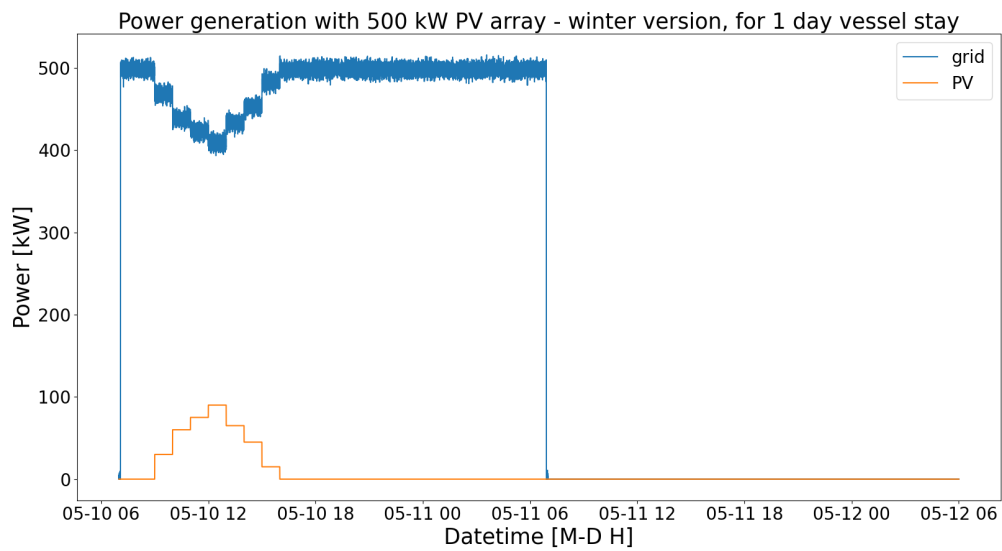
Figure A.139: Figure of the power generation of the Basic PV shore power configuration with a 500 kW PV array. The solar generation is from an average winter day. The power generation is for the power demand from Figure A.134.
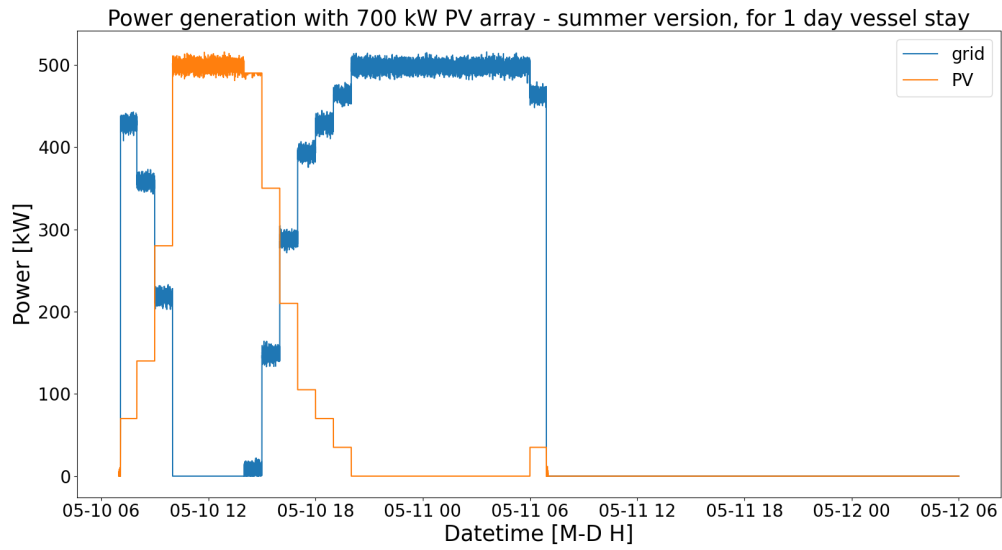
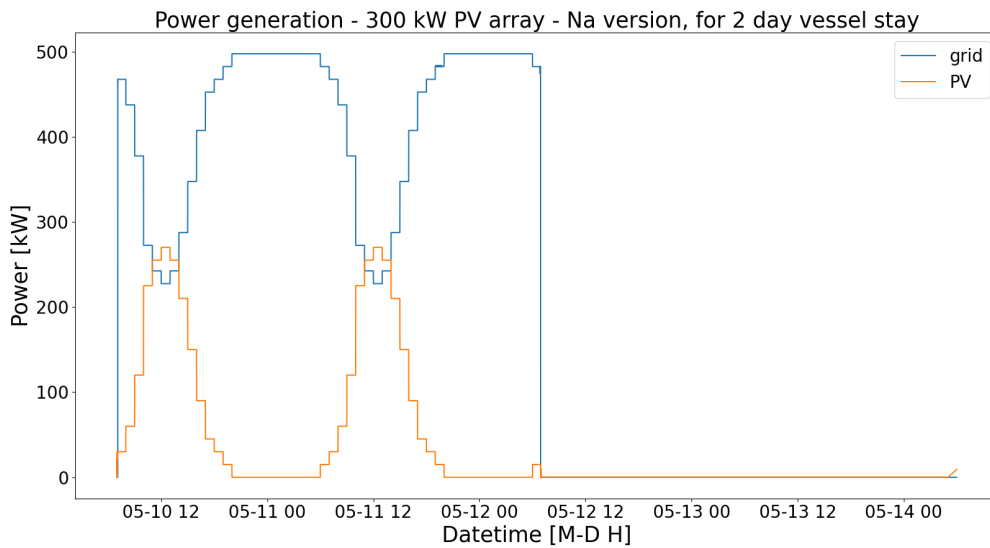**Figure A.140:** Figure of the power generation of the Basic PV shore power configuration with a 700 kW PV array. The solar generation is from an average summer day. The power generation is for the power demand from Figure A.134.
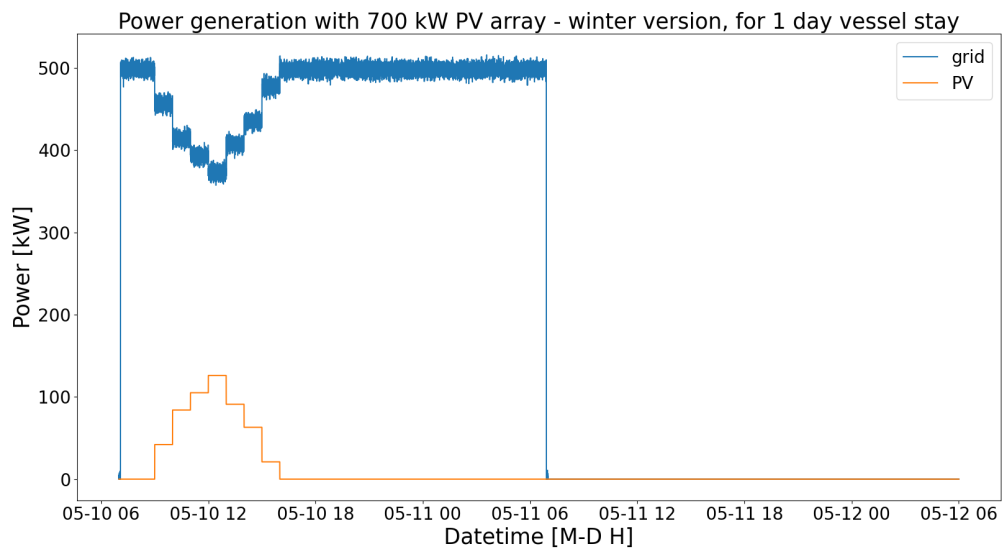
Figure A.141: Figure of the power generation of the Basic PV shore power configuration with a 700 kW PV array. The solar generation is from an average winter day. The power generation is for the power demand from Figure A.134.
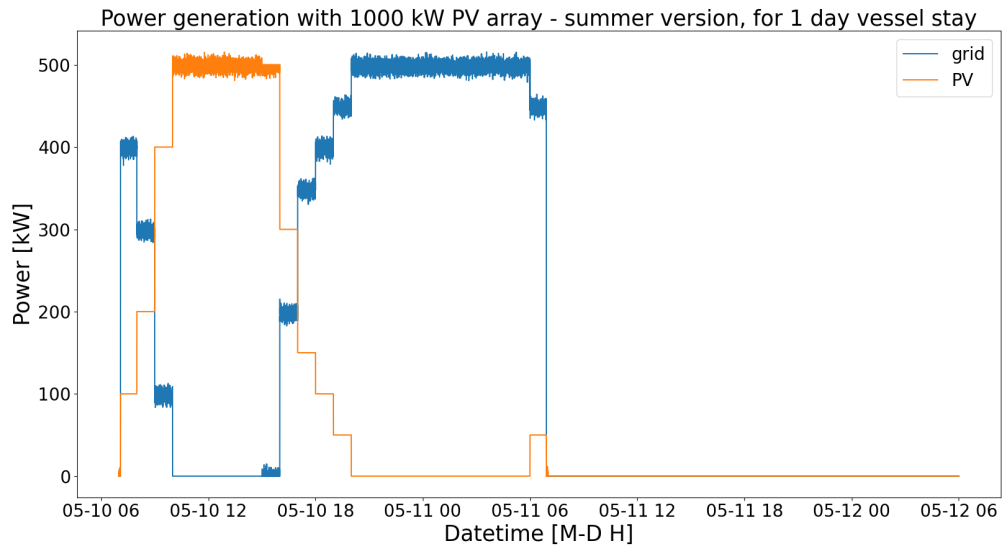
Figure A.142: Figure of the power generation of the Basic PV shore power configuration with a 1000 kW PV array. The solar generation is from an average summer day. The power generation is for the power demand from Figure A.134.
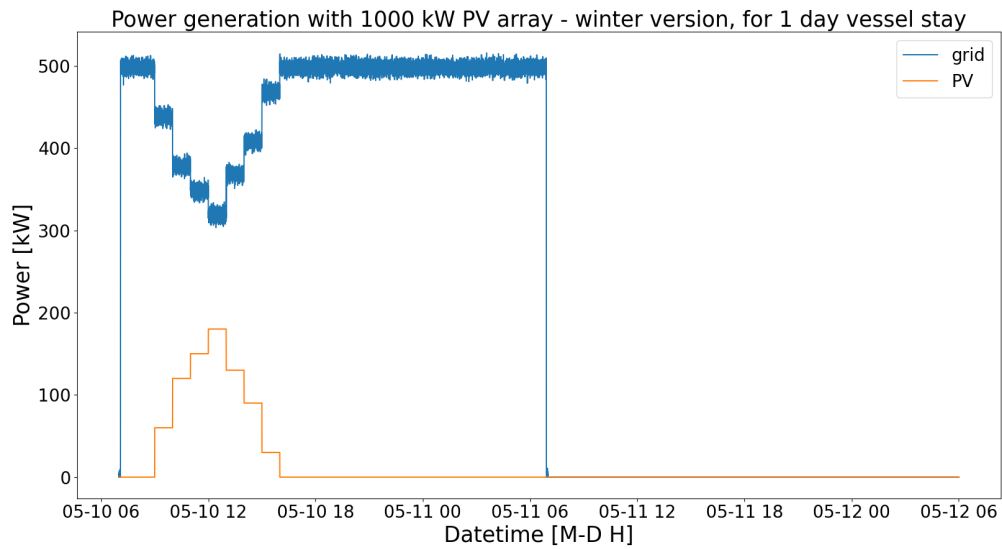
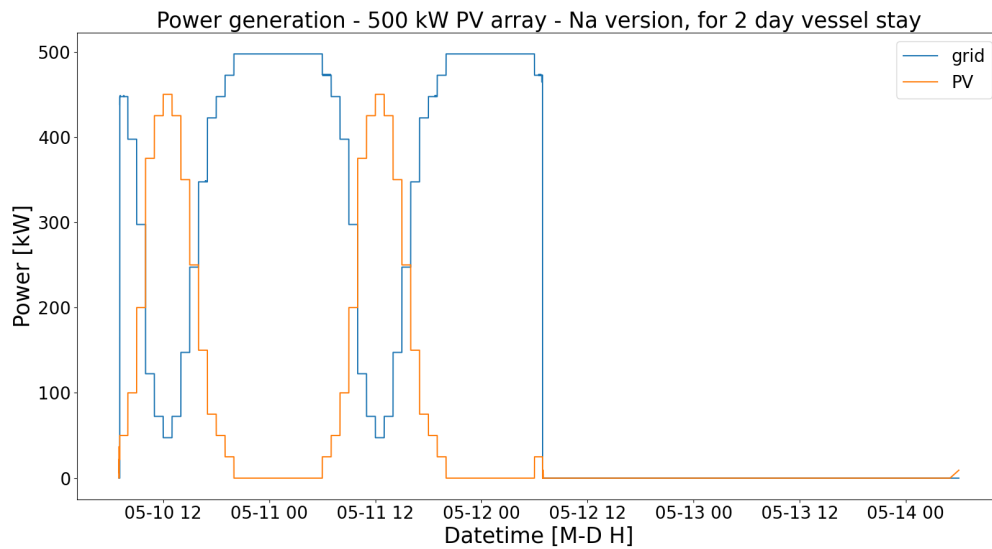**Figure A.143:** Figure of the power generation of the Basic PV shore power configuration with a 1000 kW PV array. The solar generation is from an average winter day. The power generation is for the power demand from Figure A.134.

A.5.2. HE PV for 1 day vessel stay
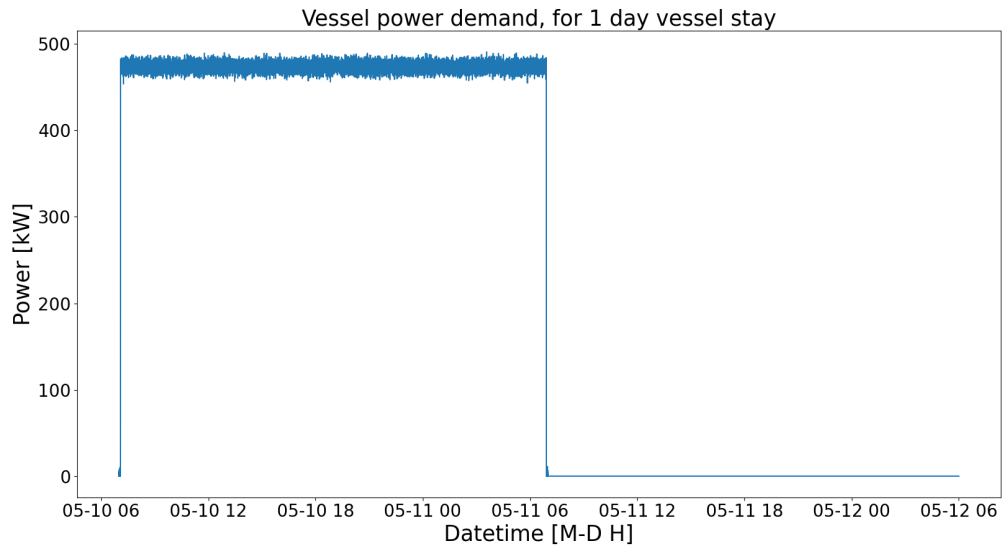
Figure A.144: Figure of the vessel power profile of 1 day and 1 day of downtime. The power demand has no crane uses. The vessel power profile was used for the HE PV shore power configuration. The x-axis is in datetime, meaning that every data point is fixed to a date and time.
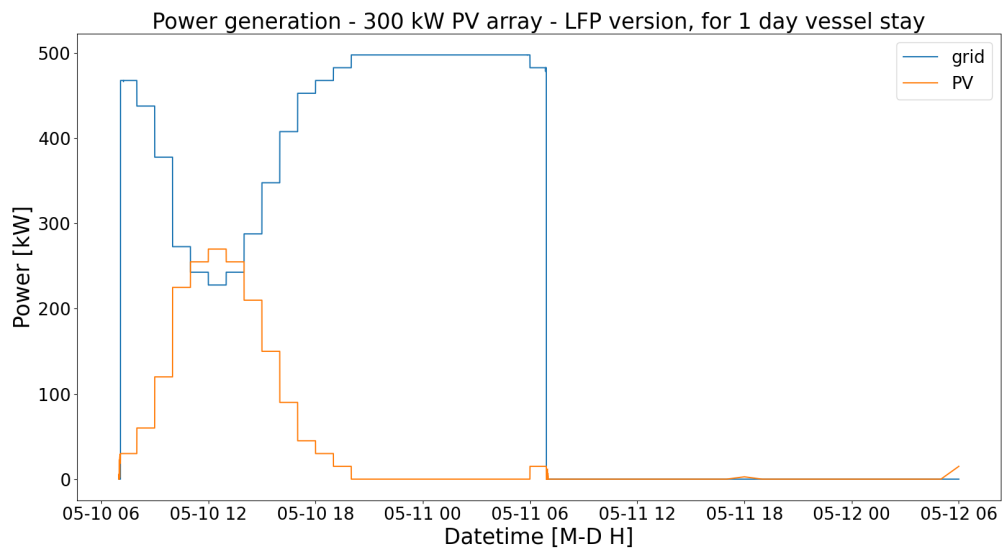
Figure A.145: Figure of the power generation of the LFP version of the HE PV shore power configuration with a 300 kW PV array. The solar generation is from an average summer day. The power generation is for the power demand from Figure A.144. The minor fluctuations of the power profile are being peak shaven by the LFP battery.
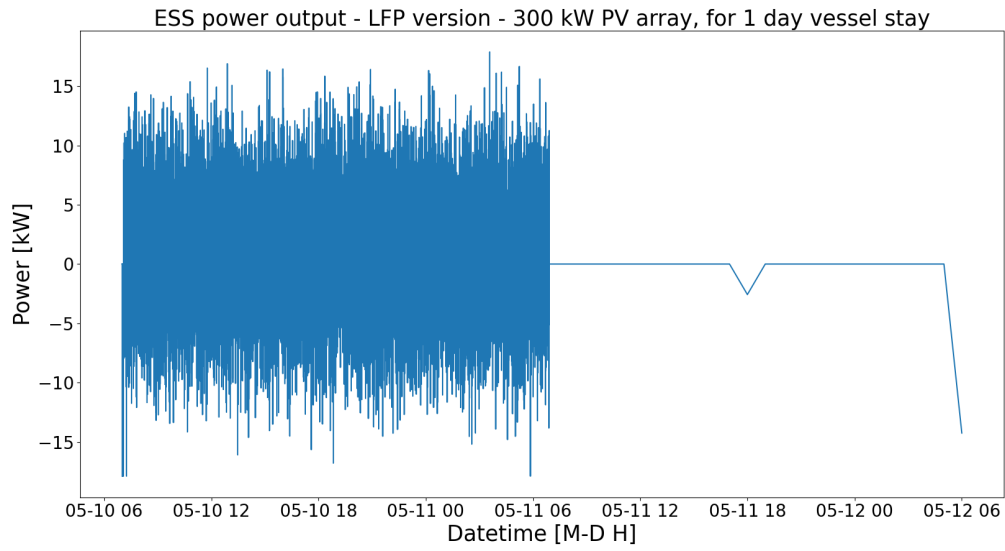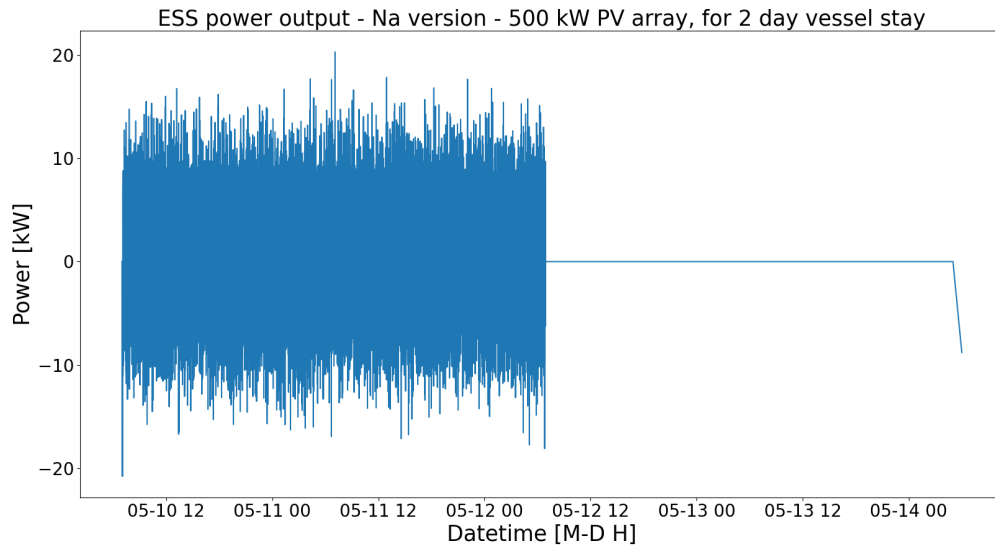
Figure A.146: Figure of the LFP battery output power of the LFP version of the HE PV shore power configuration with 300 kW PV array. The LFP battery peak shaves the minor fluctuations of the power demand of Figure A.144.
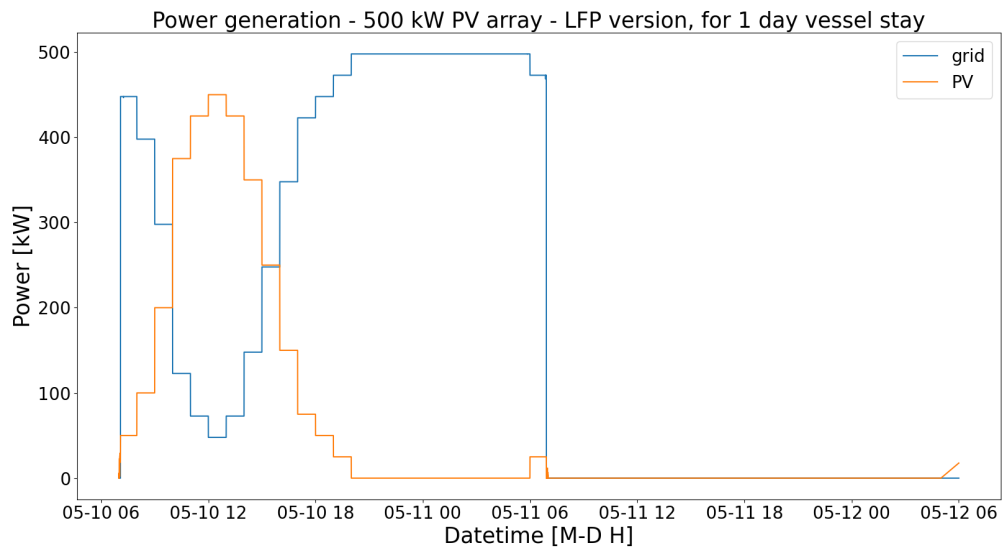
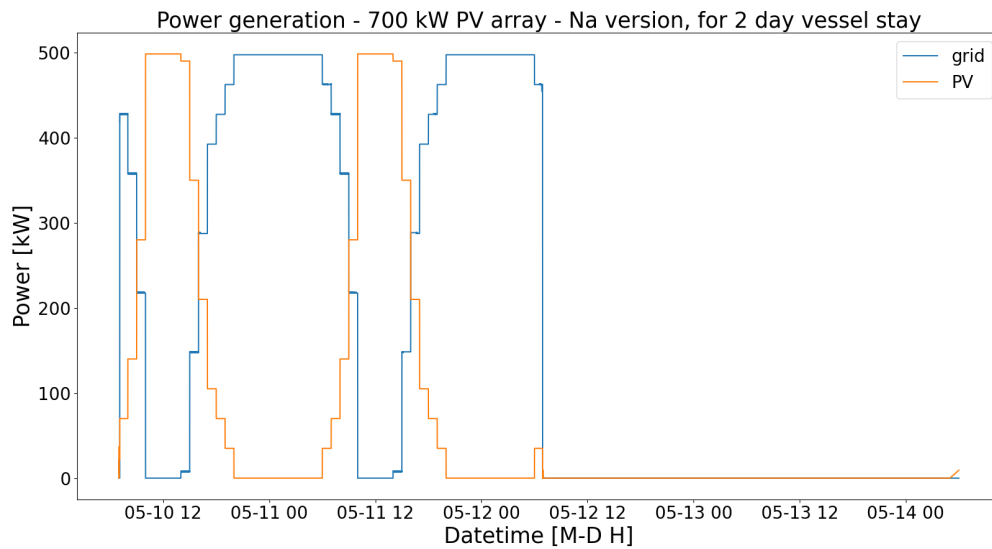**Figure A.147:** Figure of the power generation of the LFP version of the HE PV shore power configuration with a 500 kW PV array. The solar generation is from an average summer day. The power generation is for the power demand from Figure A.144. The minor fluctuations of the power profile are being peak shaven by the LFP battery.
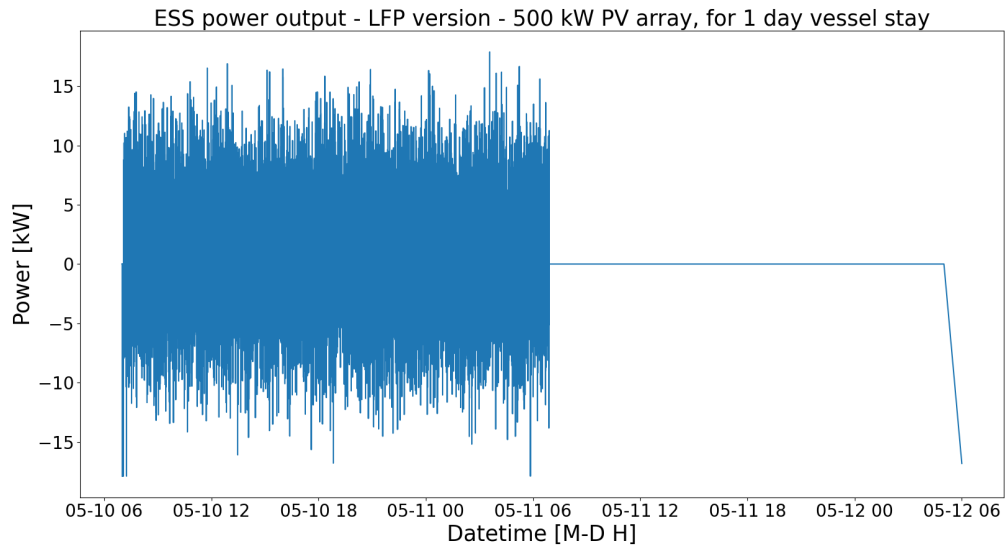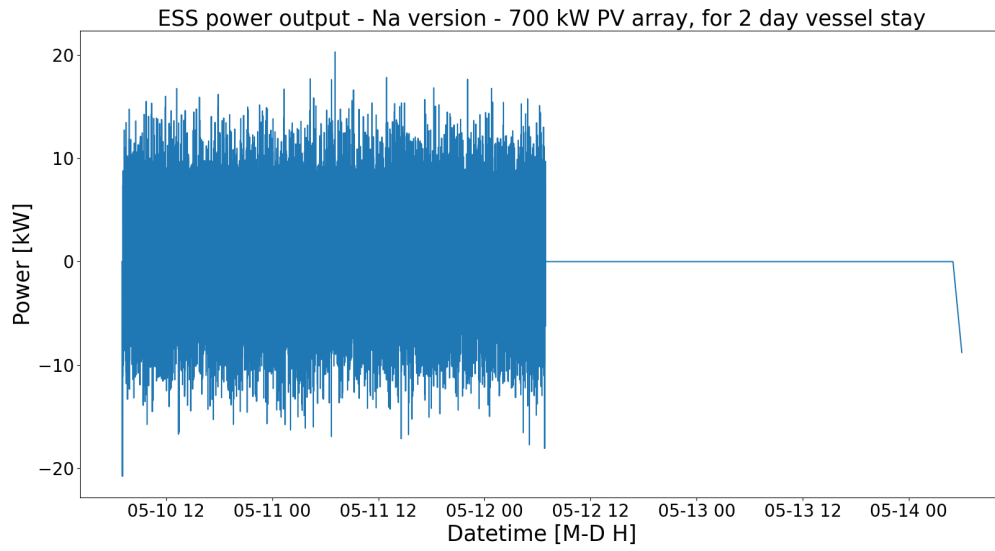
Figure A.148: Figure of the LFP battery output power of the LFP version of the HE PV shore power configuration with 500 kW PV array. The LFP battery peak shaves the minor fluctuations of the power demand of Figure A.144.
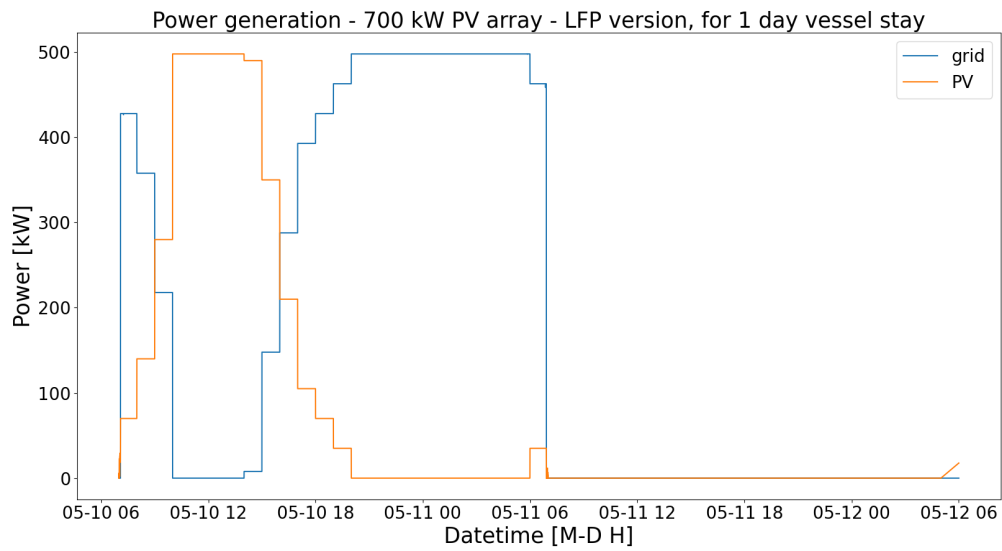
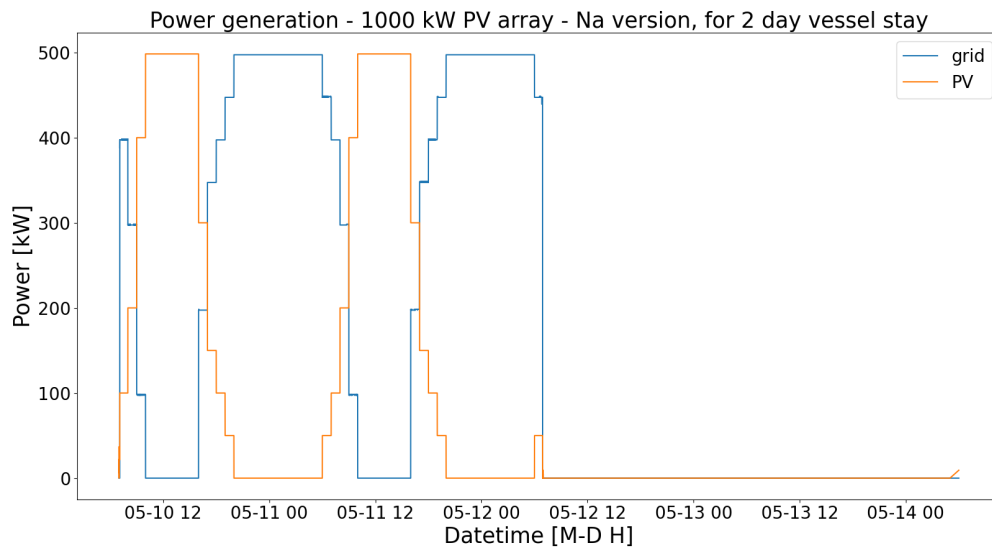**Figure A.149:** Figure of the power generation of the LFP version of the HE PV shore power configuration with a 700 kW PV array. The solar generation is from an average summer day. The power generation is for the power demand from Figure A.144. The minor fluctuations of the power profile are being peak shaven by the LFP battery.
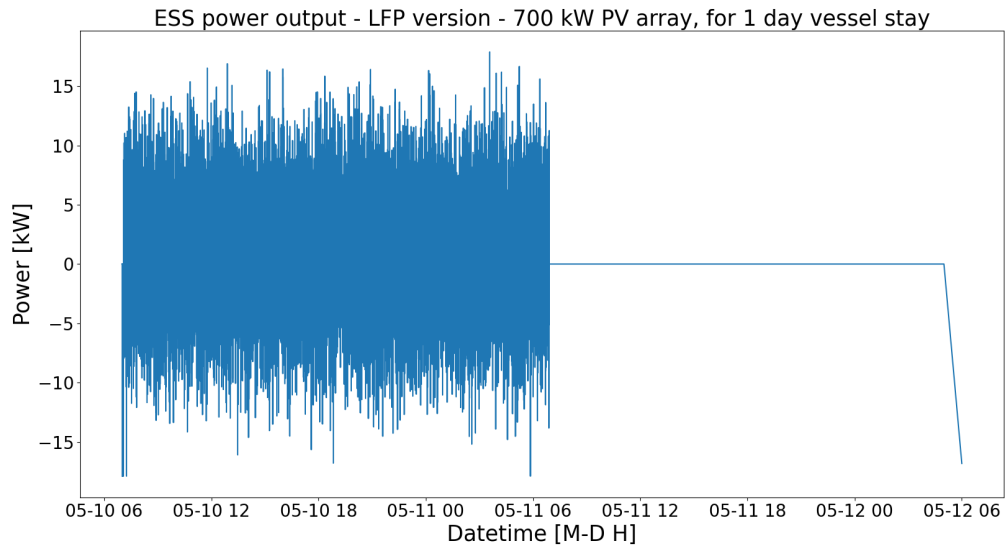
Figure A.150: Figure of the LFP battery output power of the LFP version of the HE PV shore power configuration with 700 kW PV array. The LFP battery peak shaves the minor fluctuations of the power demand of Figure A.144.
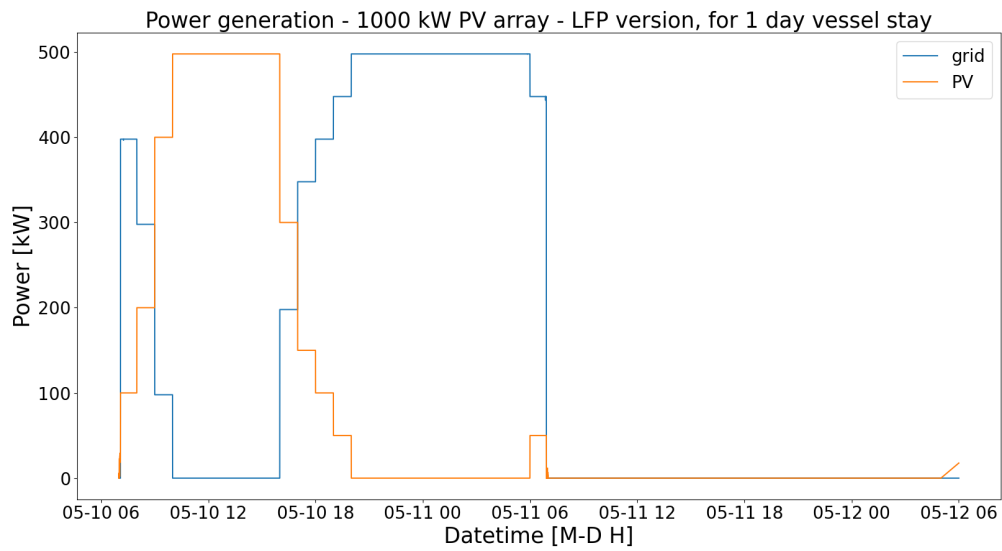
Figure A.151: Figure of the power generation of the LFP version of the HE PV shore power configuration with a 1000 kW PV array. The solar generation is from an average summer day. The power generation is for the power demand from Figure A.144. The minor fluctuations of the power profile are being peak shaven by the LFP battery.
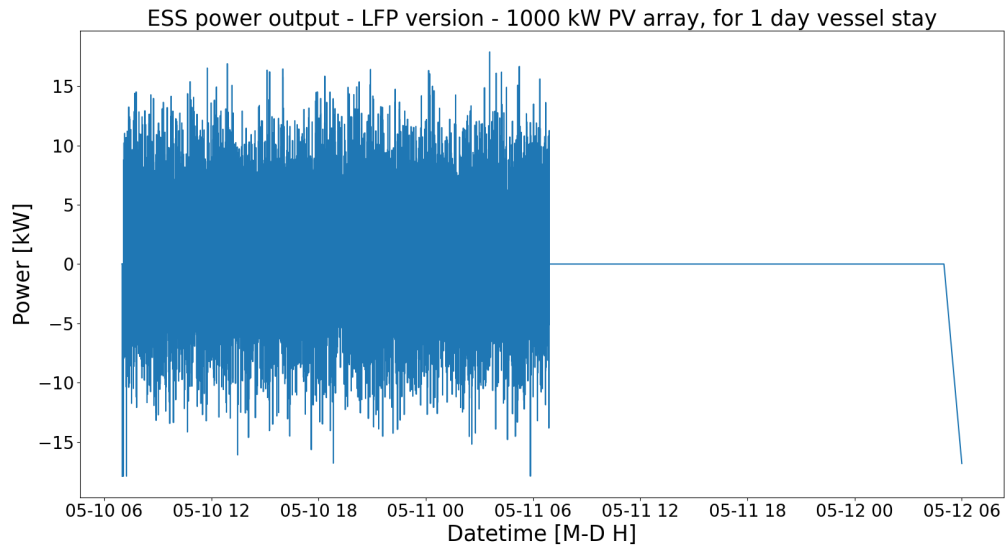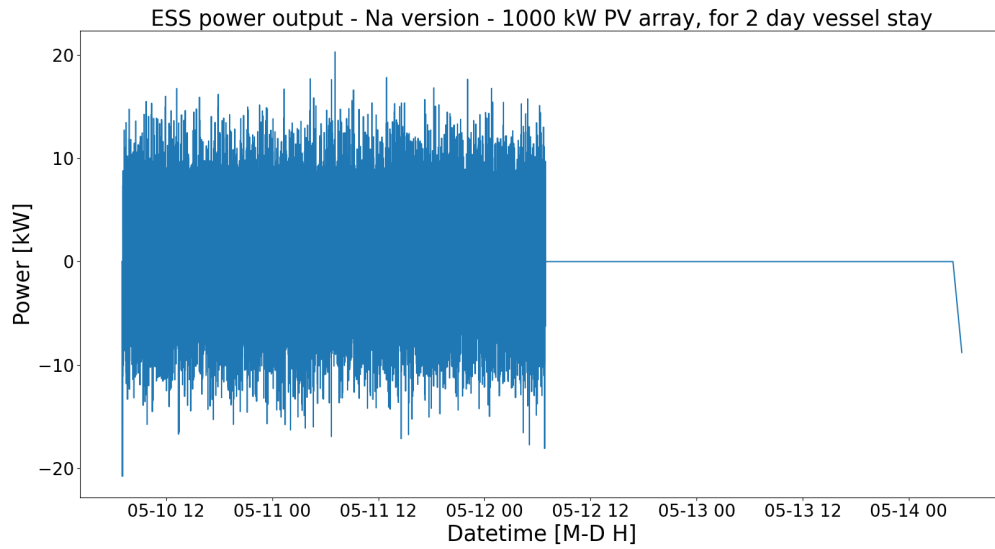
Figure A.152: Figure of the LFP battery output power of the LFP version of the HE PV shore power configuration with 1000 kW PV array. The LFP battery peak shaves the minor fluctuations of the power demand of Figure A.144.
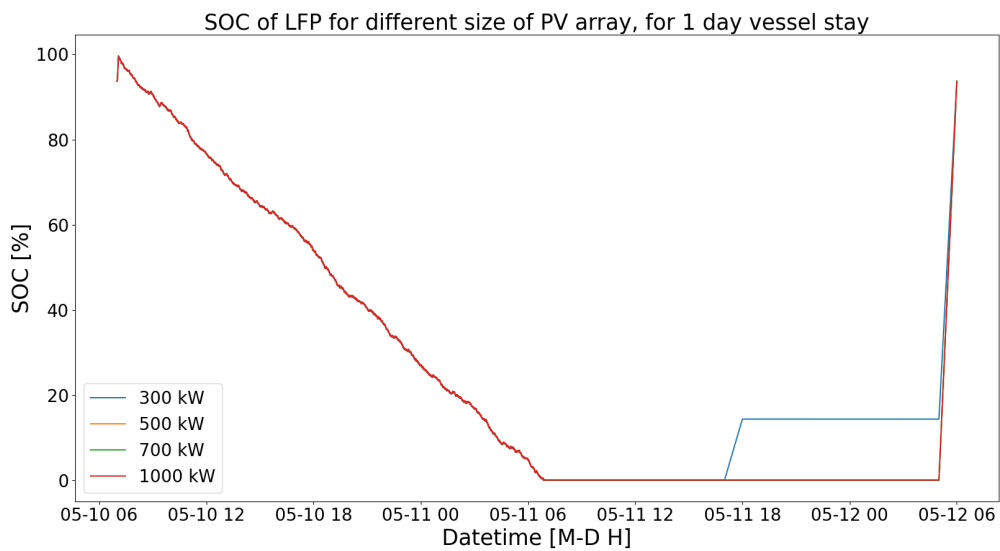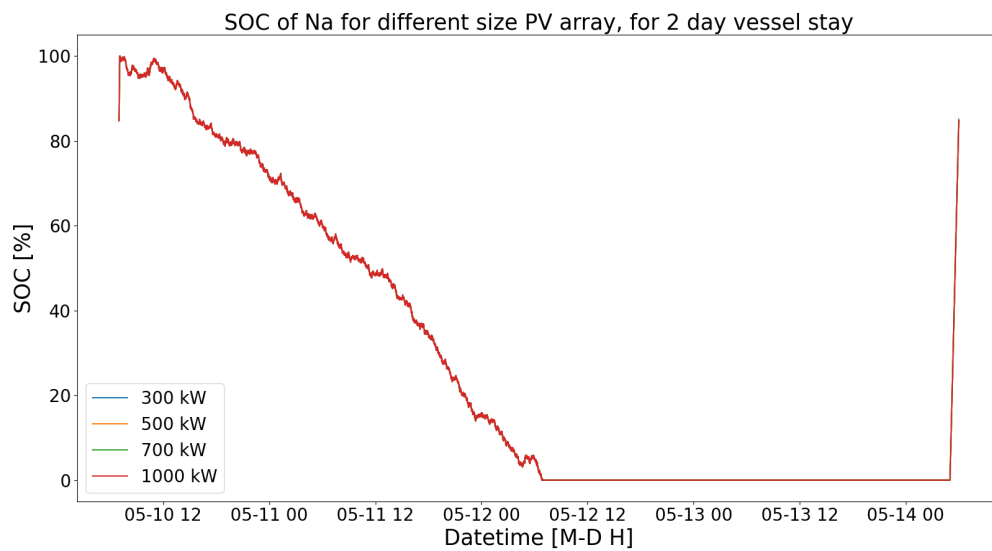

Figure A.153: Figure of the SOC of the LFP battery of the LFP version of the HE PV shore power configuration. The plot includes different implementations using different sizes of PV array. All the different implementations discharge in the same exact way.
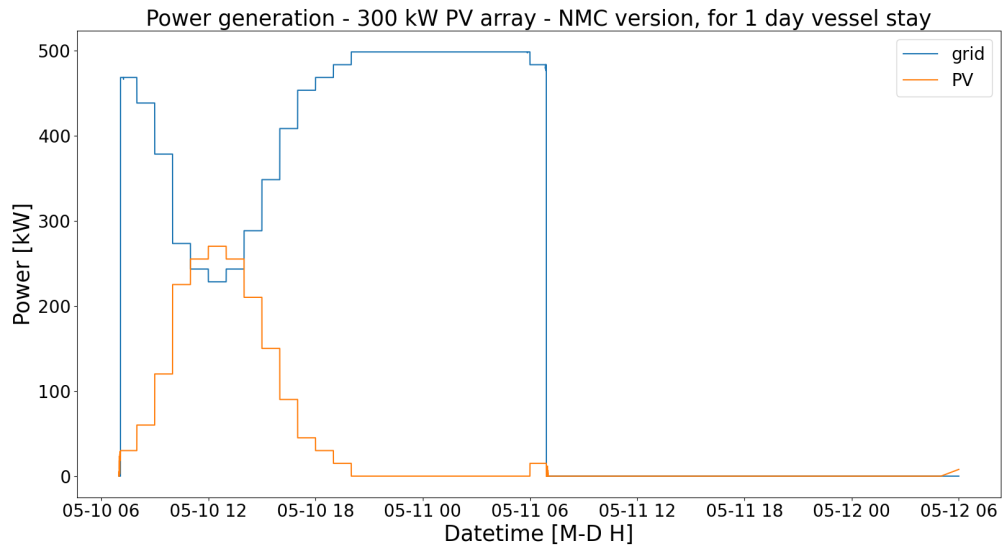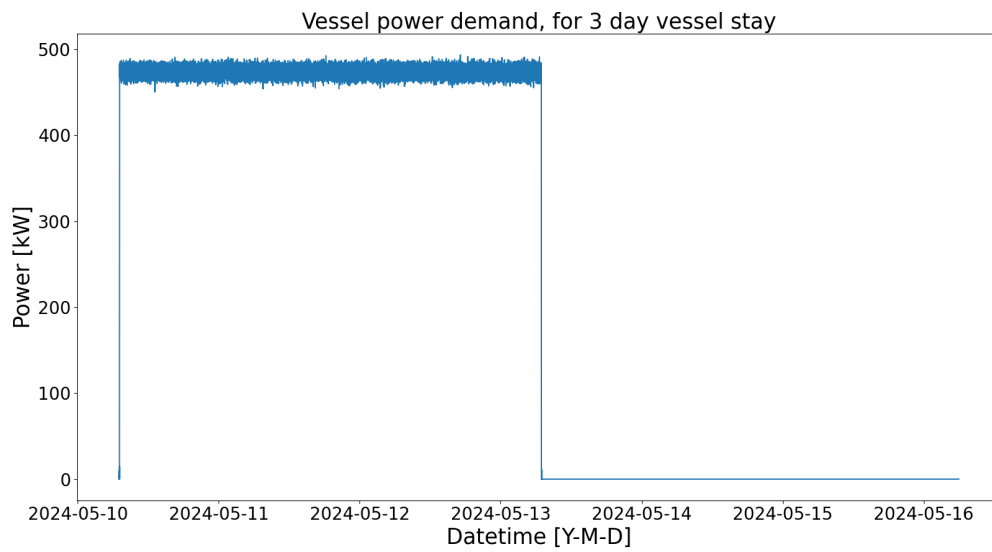
Figure A.154: Figure of the power generation of the NMC version of the HE PV shore power configuration with a 300 kW PV array. The solar generation is from an average summer day. The power generation is for the power demand from Figure A.144. The minor fluctuations of the power profile are being peak shaven by the NMC battery.
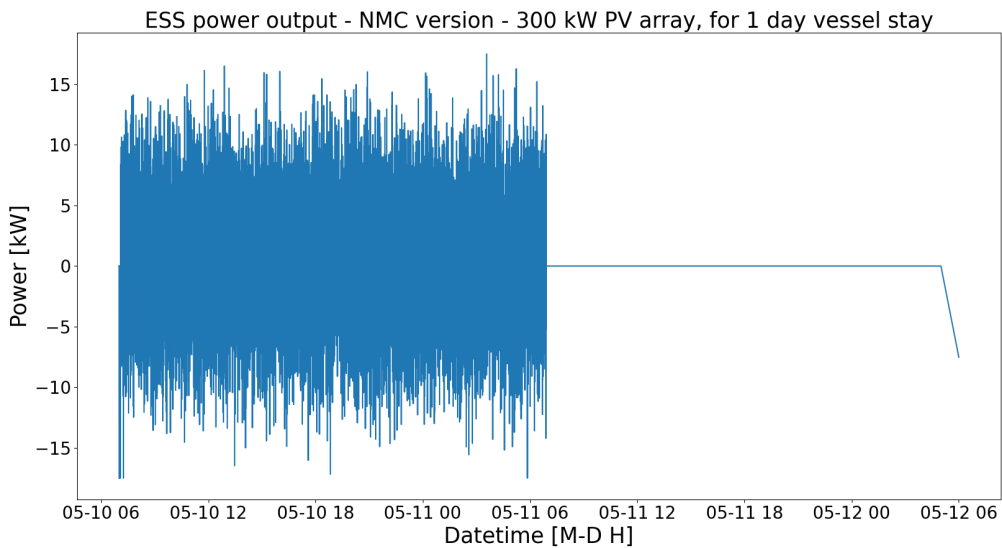
Figure A.155: Figure of the NMC battery output power of the NMC version of the HE PV shore power configuration with 300 kW PV array. The NMC battery peak shaves the minor fluctuations of the power demand of Figure A.144.
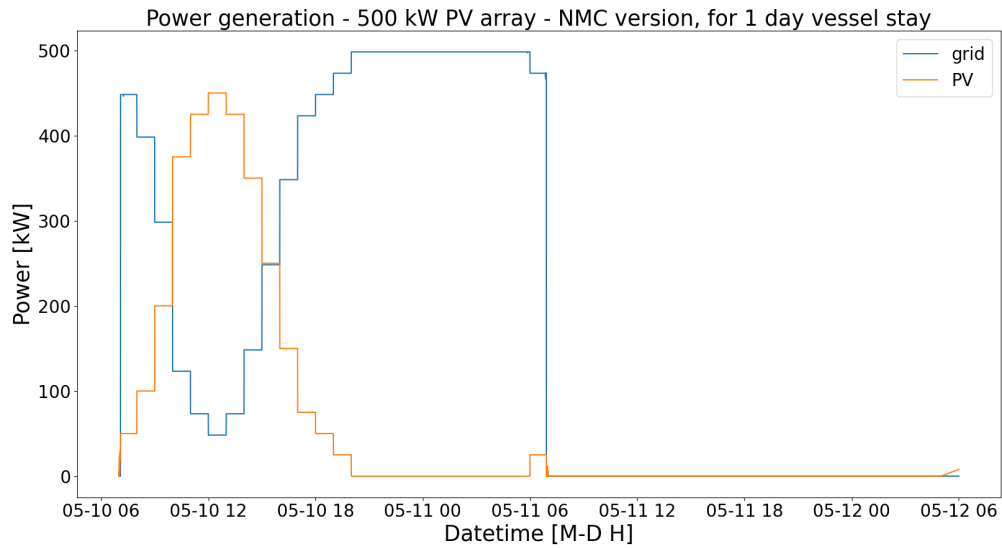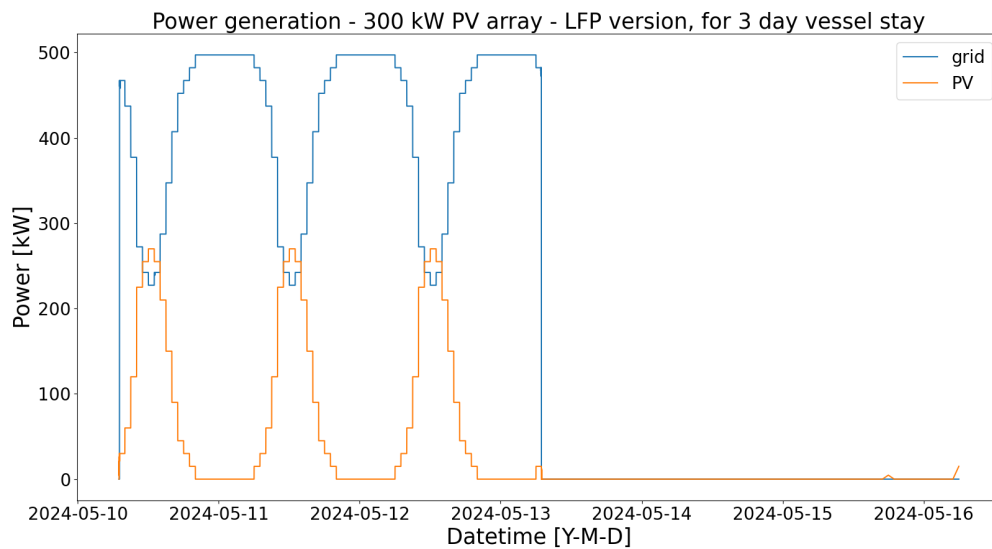
Figure A.156: Figure of the power generation of the NMC version of the HE PV shore power configuration with a 500 kW PV array. The solar generation is from an average summer day. The power generation is for the power demand from Figure A.144. The minor fluctuations of the power profile are being peak shaven by the NMC battery.
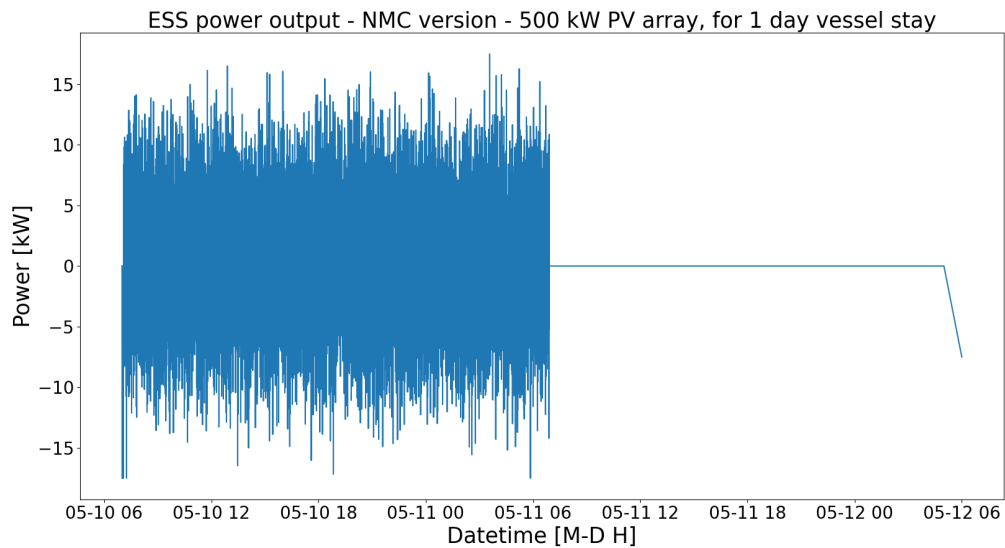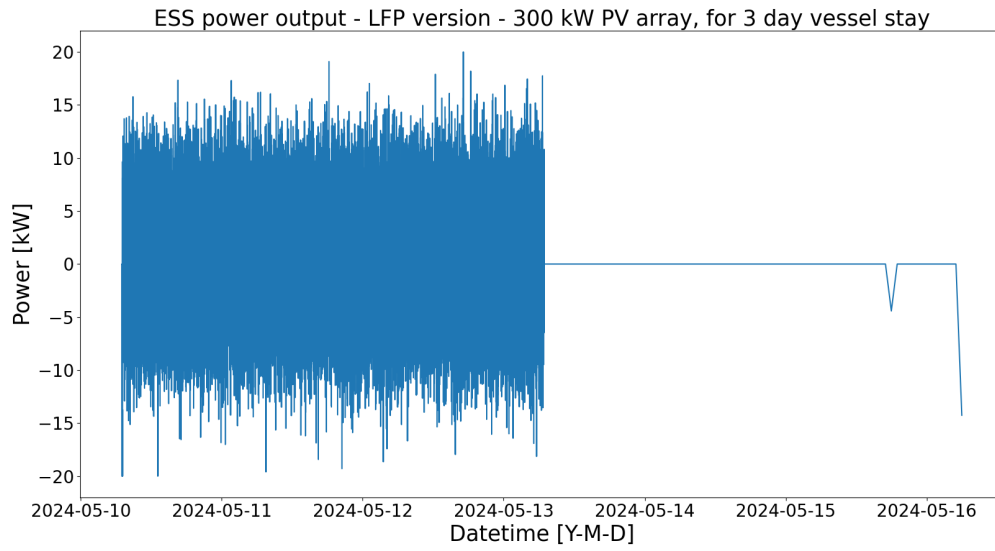

Figure A.157: Figure of the NMC battery output power of the NMC version of the HE PV shore power configuration with 500 kW PV array. The NMC battery peak shaves the minor fluctuations of the power demand of Figure A.144.
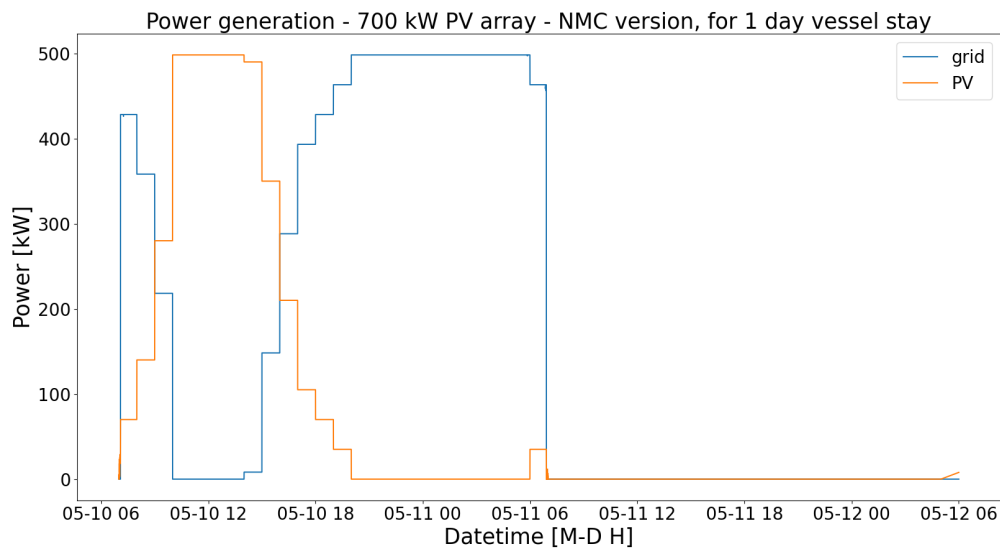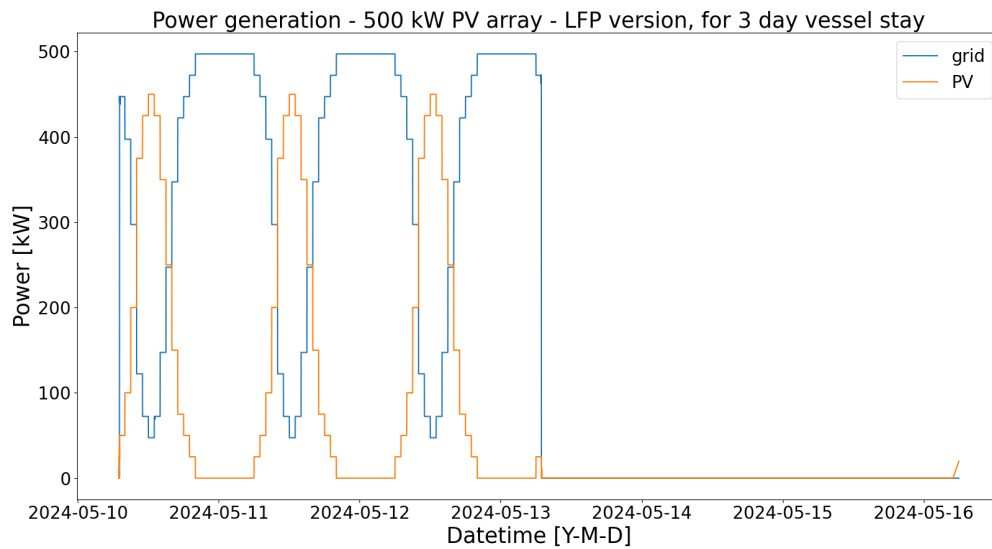
Figure A.158: Figure of the power generation of the NMC version of the HE PV shore power configuration with a 700 kW PV array. The solar generation is from an average summer day. The power generation is for the power demand from Figure A.144. The minor fluctuations of the power profile are being peak shaven by the NMC battery.
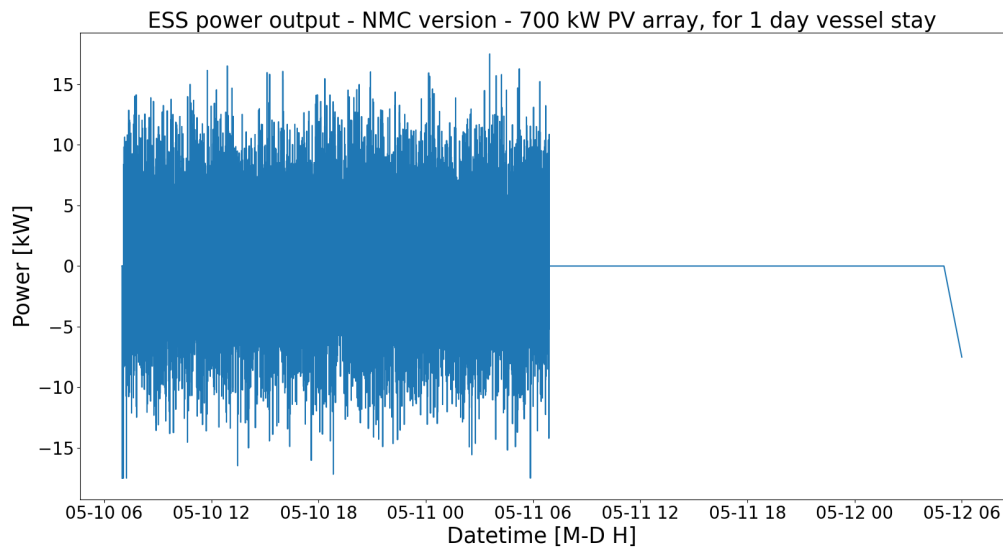
Figure A.159: Figure of the NMC battery output power of the NMC version of the HE PV shore power configuration with 700 kW PV array. The NMC battery peak shaves the minor fluctuations of the power demand of Figure A.144.
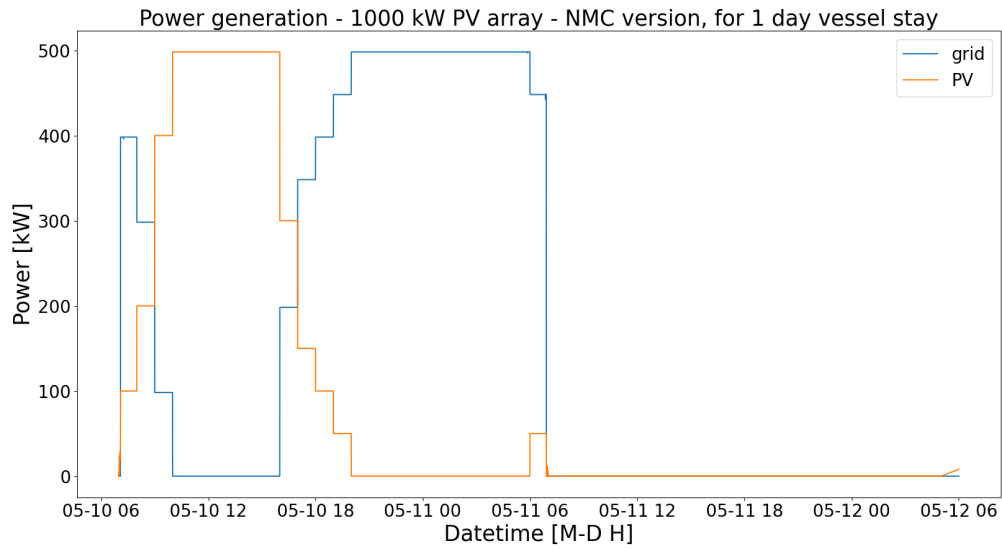
Figure A.160: Figure of the power generation of the NMC version of the HE PV shore power configuration with a 1000 kW PV array. The solar generation is from an average summer day. The power generation is for the power demand from Figure A.144. The minor fluctuations of the power profile are being peak shaven by the NMC battery.
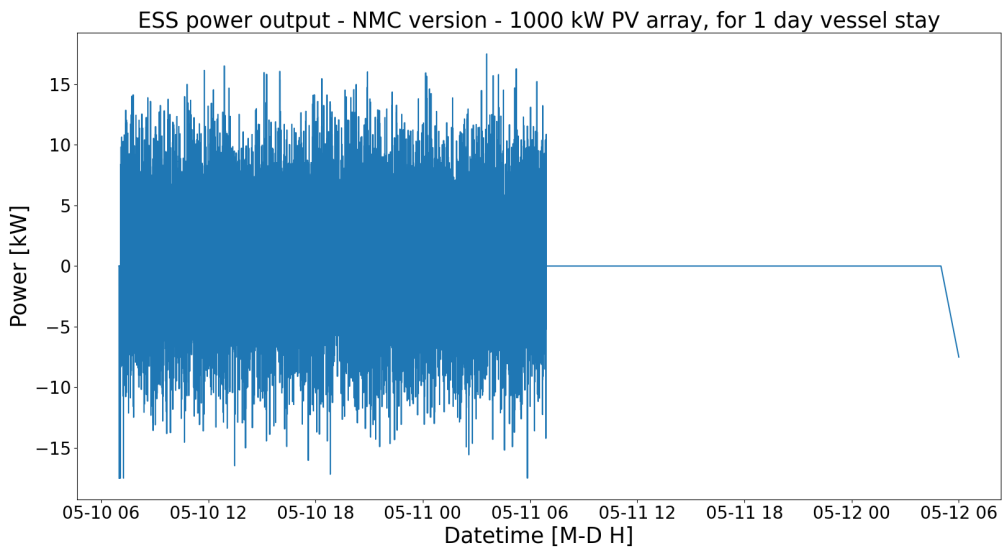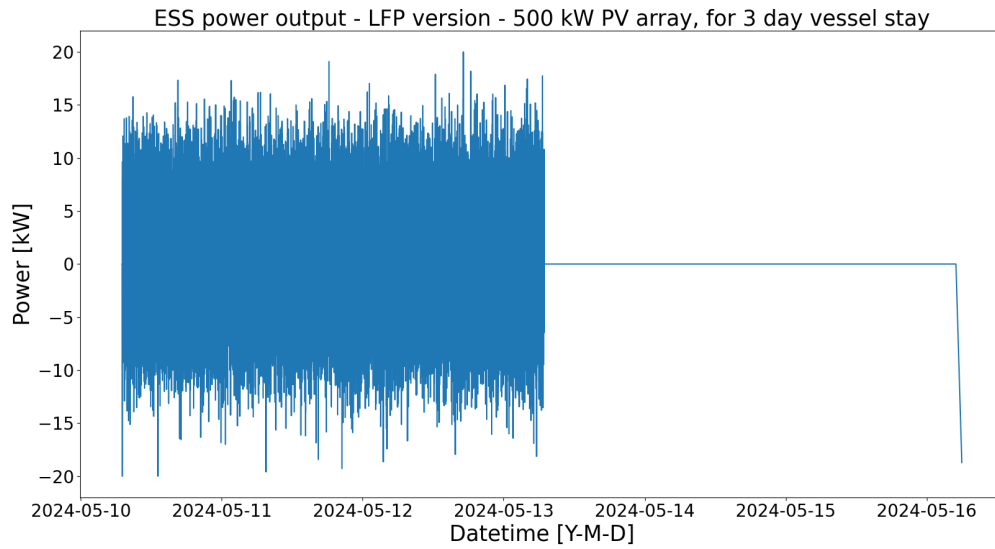

Figure A.161: Figure of the NMC battery output power of the NMC version of the HE PV shore power configuration with 1000 kW PV array. The NMC battery peak shaves the minor fluctuations of the power demand of Figure A.144.
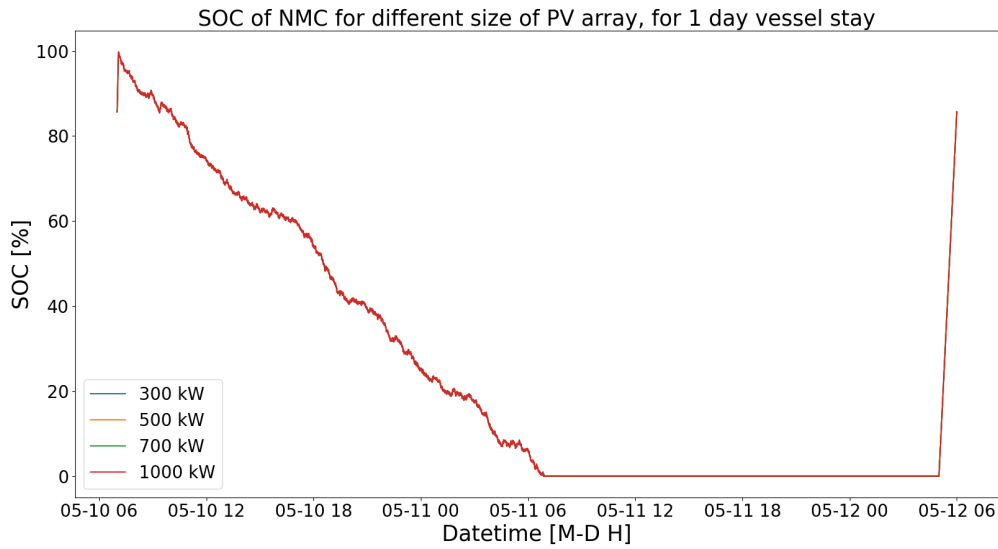
Figure A.162: Figure of the SOC of the NMC battery of the NMC version of the HE PV shore power configuration. The plot includes different implementations using different sizes of PV array. All the different implementations discharge in the same exact way.
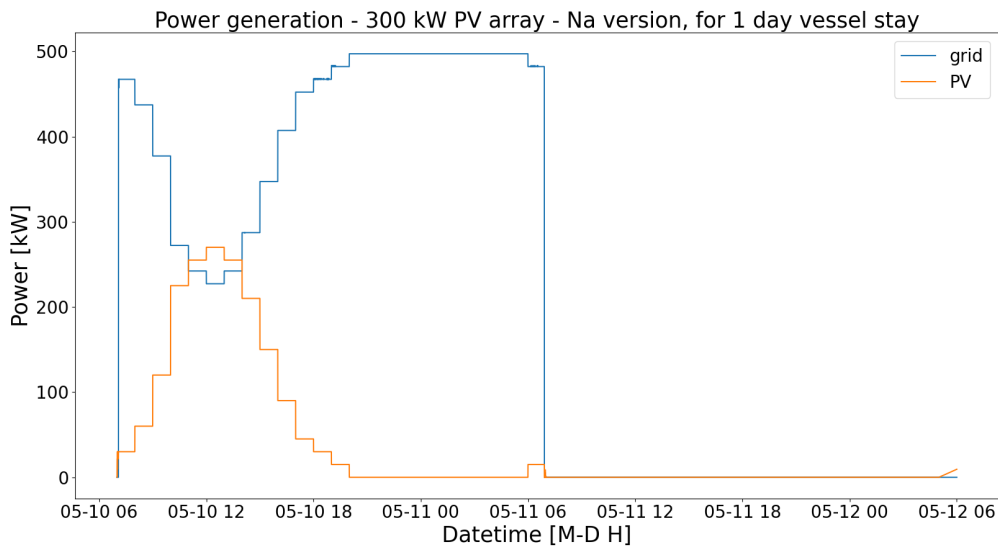
Figure A.163: Figure of the power generation of the Na-ion version of the HE PV shore power configuration with a 300 kW PV array. The solar generation is from an average summer day. The power generation is for the power demand from Figure A.144. The minor fluctuations of the power profile are being peak shaven by the Na-ion battery.
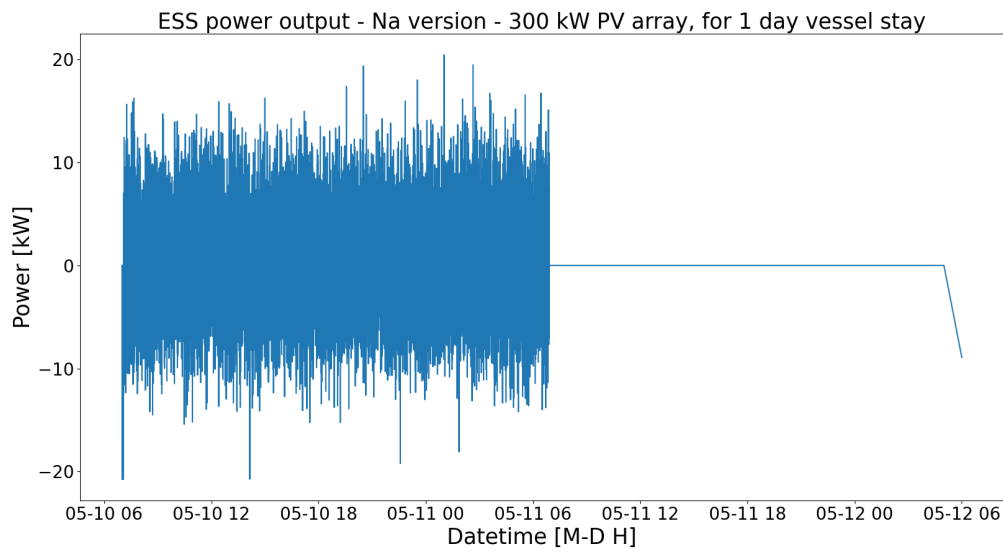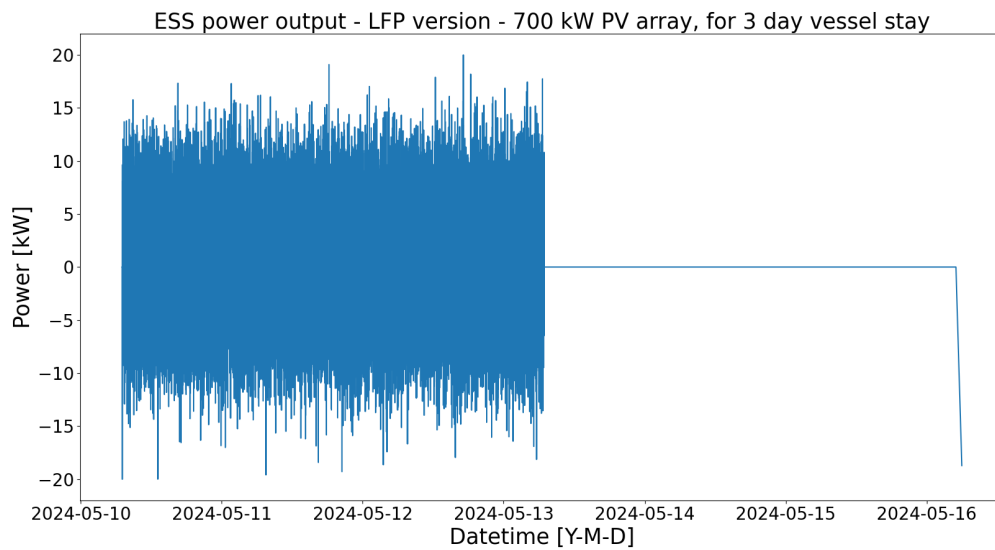
Figure A.164: Figure of the Na-ion battery output power of the Na-ion version of the HE PV shore power configuration with 300 kW PV array. The Na-ion battery peak shaves the minor fluctuations of the power demand of Figure A.144.
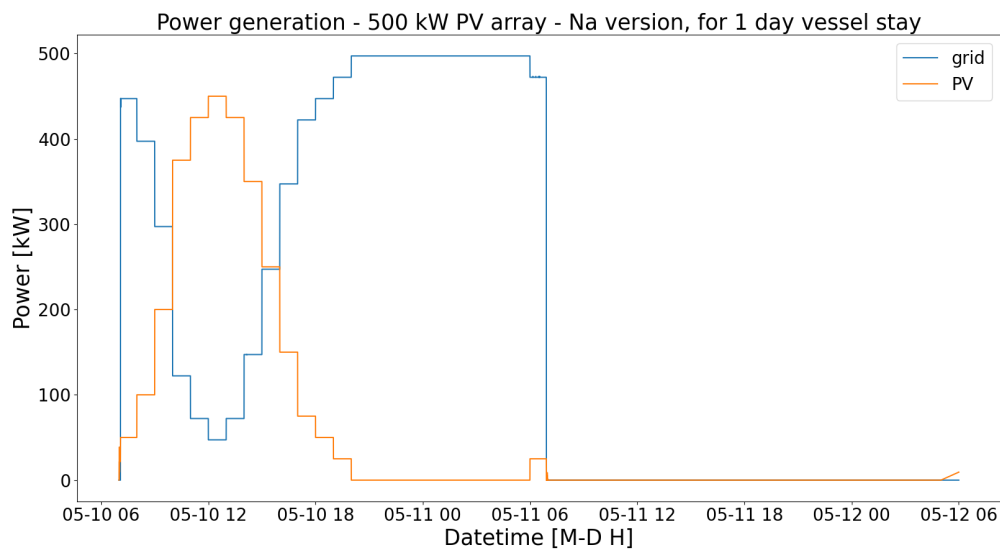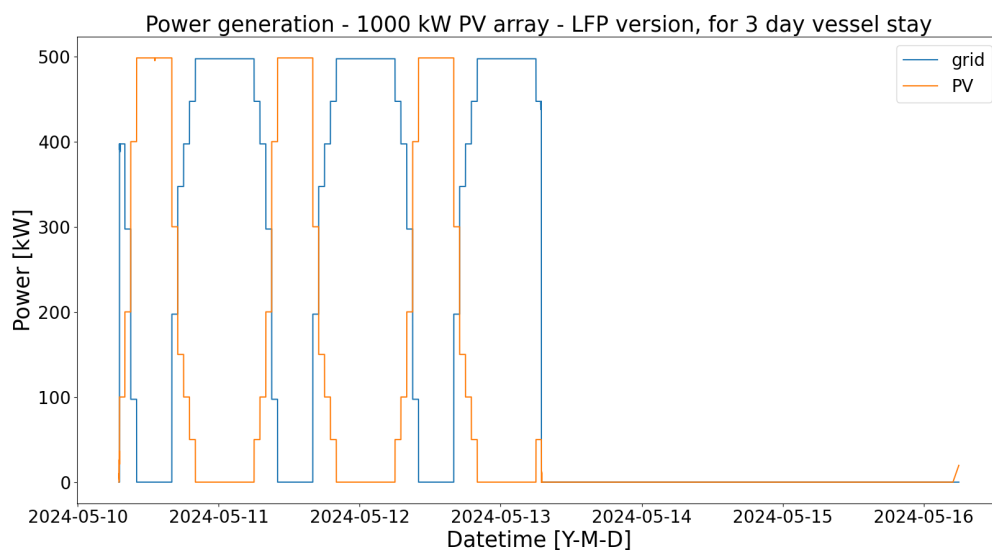

Figure A.165: Figure of the power generation of the Na-ion version of the HE PV shore power configuration with a 500 kW PV array. The solar generation is from an average summer day. The power generation is for the power demand from Figure A.144. The minor fluctuations of the power profile are being peak shaven by the Na-ion battery.
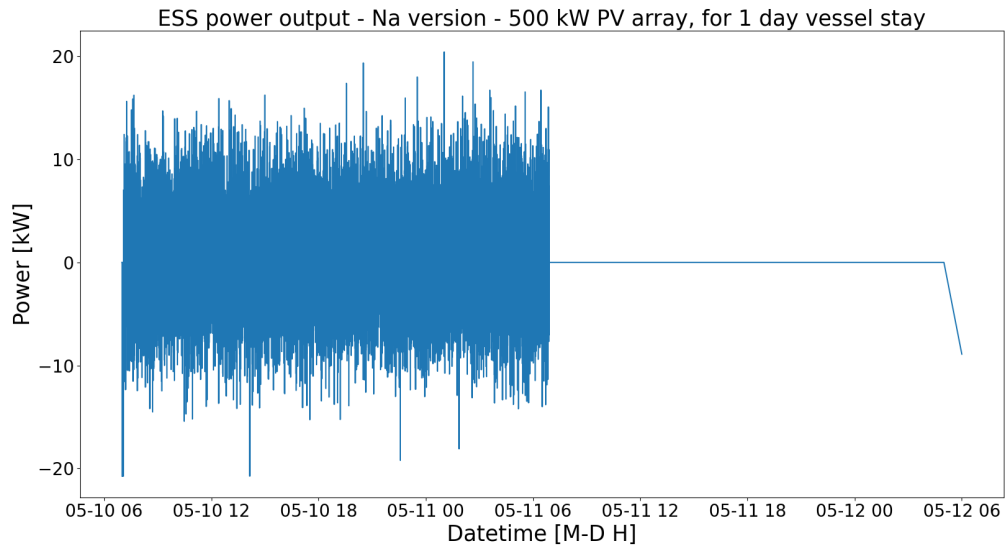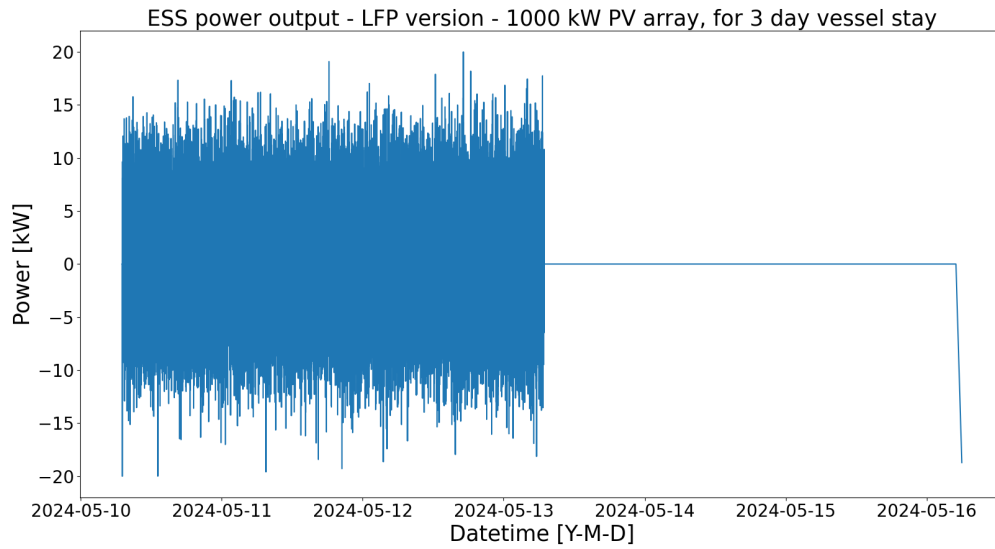
Figure A.166: Figure of the Na-ion battery output power of the Na-ion version of the HE PV shore power configuration with 500 kW PV array. The Na-ion battery peak shaves the minor fluctuations of the power demand of Figure A.144.
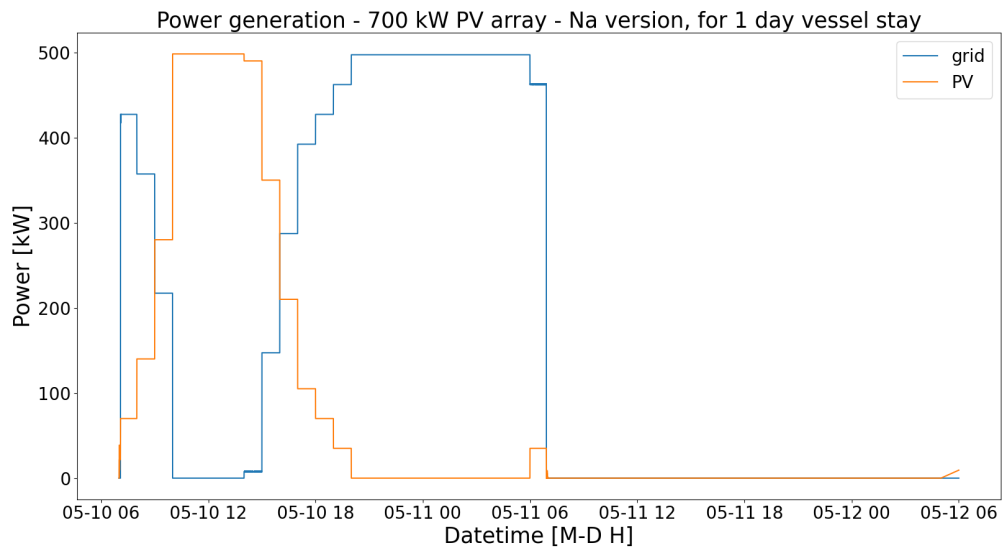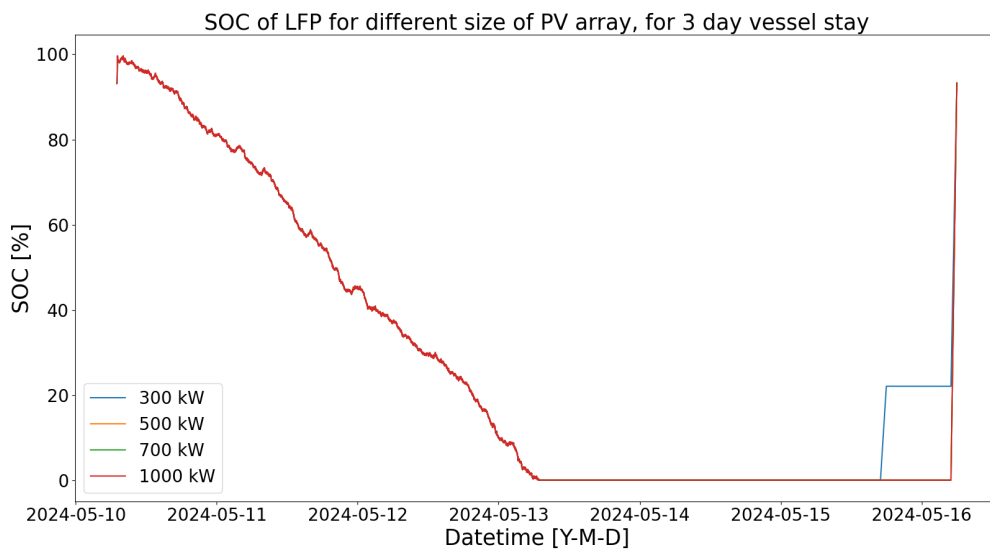

Figure A.167: Figure of the power generation of the Na-ion version of the HE PV shore power configuration with a 700 kW PV array. The solar generation is from an average summer day. The power generation is for the power demand from Figure A.144. The minor fluctuations of the power profile are being peak shaven by the Na-ion battery.
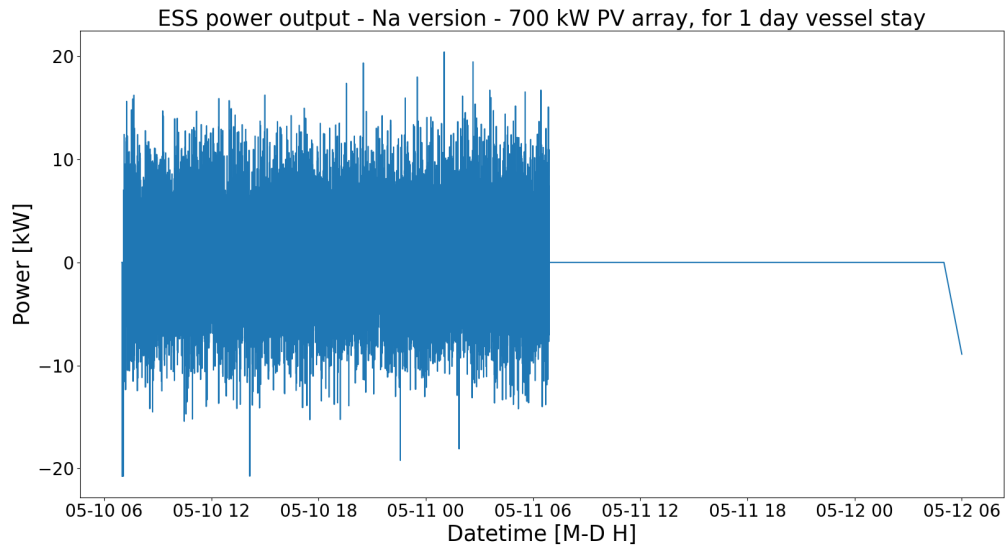
Figure A.168: Figure of the Na-ion battery output power of the Na-ion version of the HE PV shore power configuration with 700 kW PV array. The Na-ion battery peak shaves the minor fluctuations of the power demand of Figure A.144.
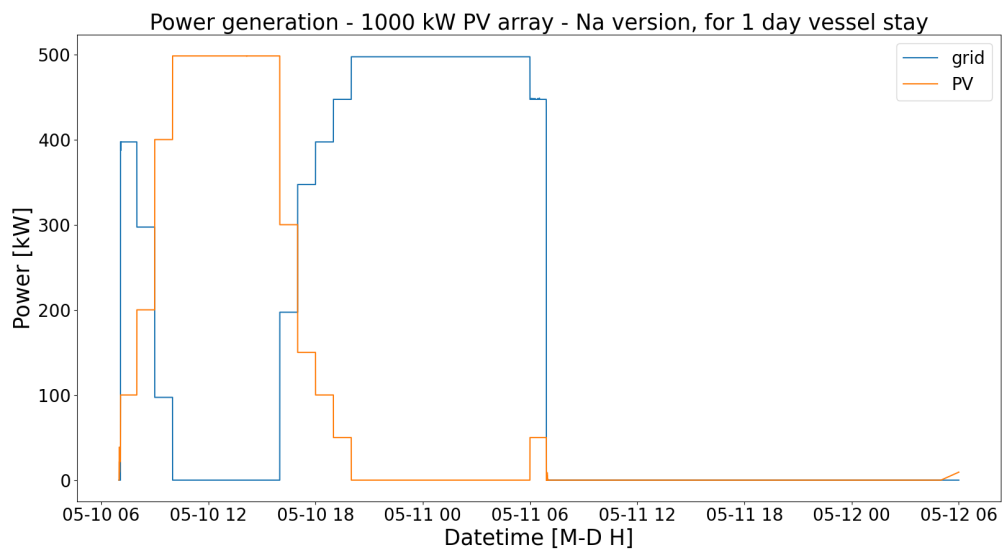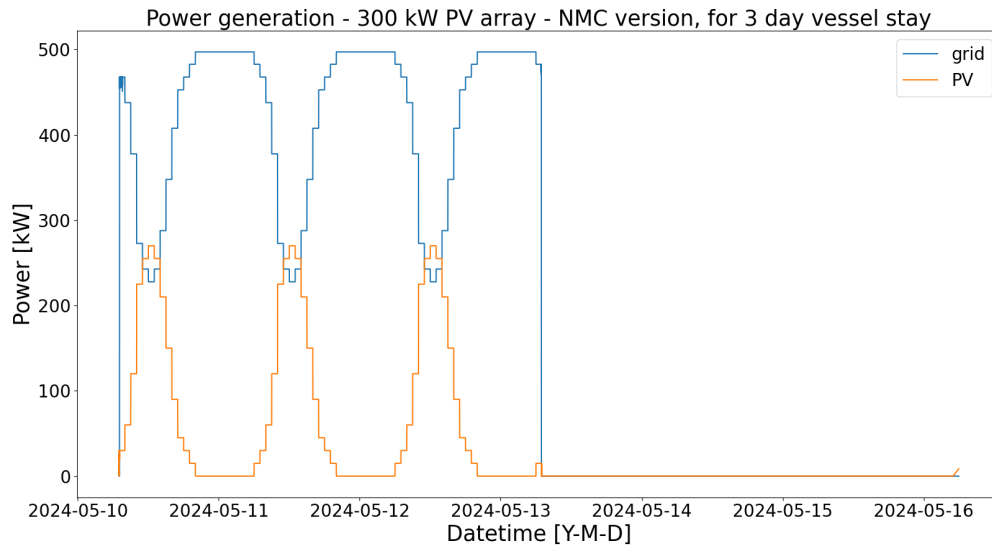

Figure A.169: Figure of the power generation of the Na-ion version of the HE PV shore power configuration with a 1000 kW PV array. The solar generation is from an average summer day. The power generation is for the power demand from Figure A.144. The minor fluctuations of the power profile are being peak shaven by the Na-ion battery.
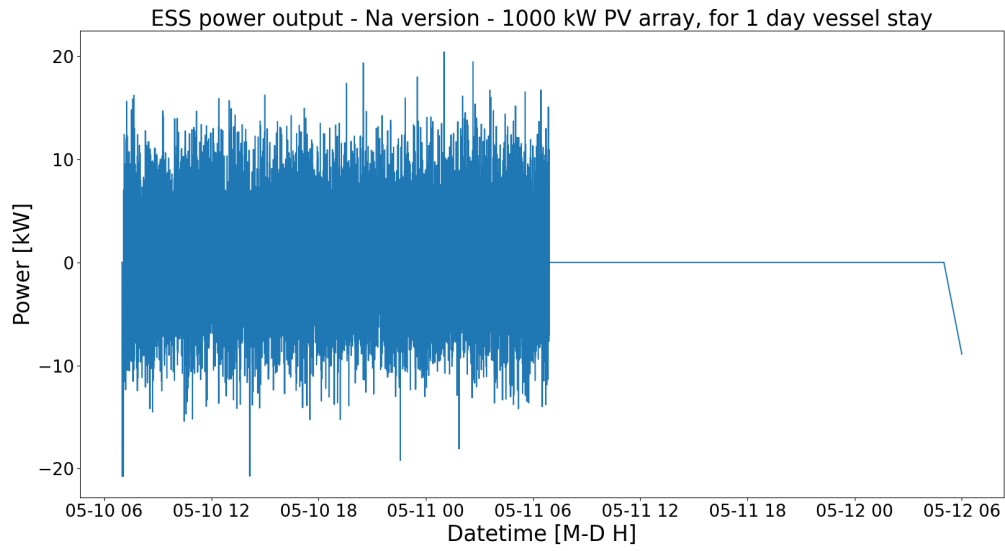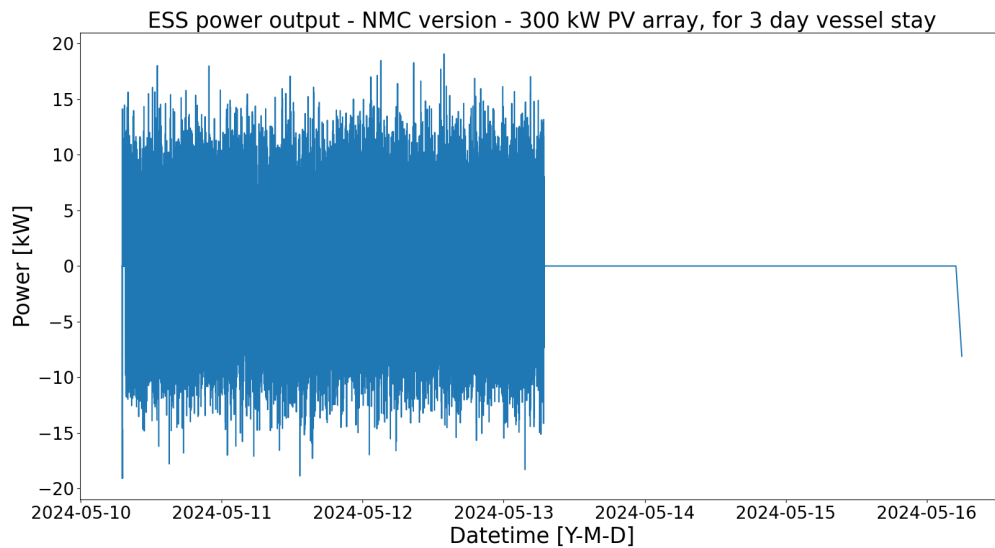
Figure A.170: Figure of the Na-ion battery output power of the Na-ion version of the HE PV shore power configuration with 1000 kW PV array. The Na-ion battery peak shaves the minor fluctuations of the power demand of Figure A.144.
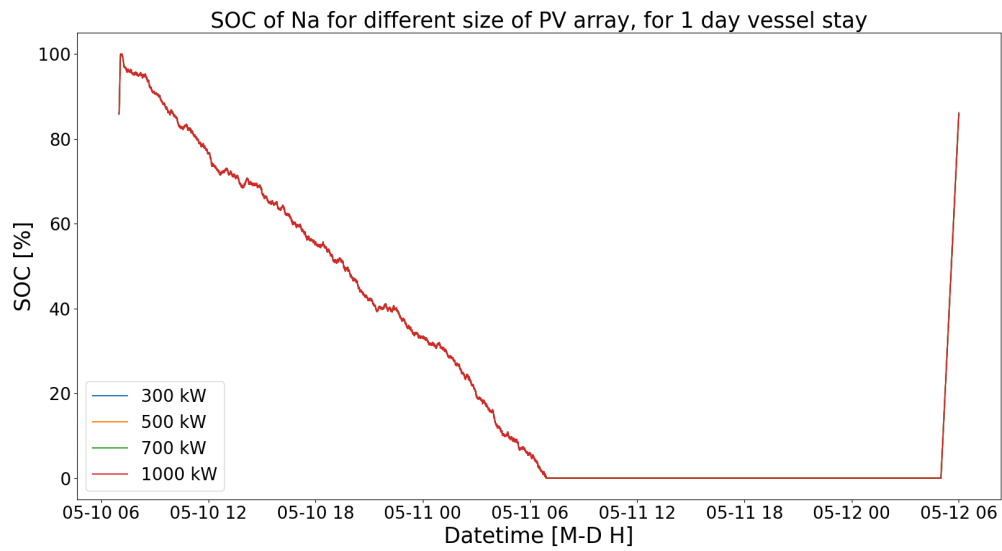

Figure A.171: Figure of the SOC of the Na-ion battery of the Na-ion version of the HE PV shore power configuration. The plot includes different implementations using different sizes of PV array. All the different implementations discharge in the same exact way.

A.5.3. HE PV for 2 day vessel stay
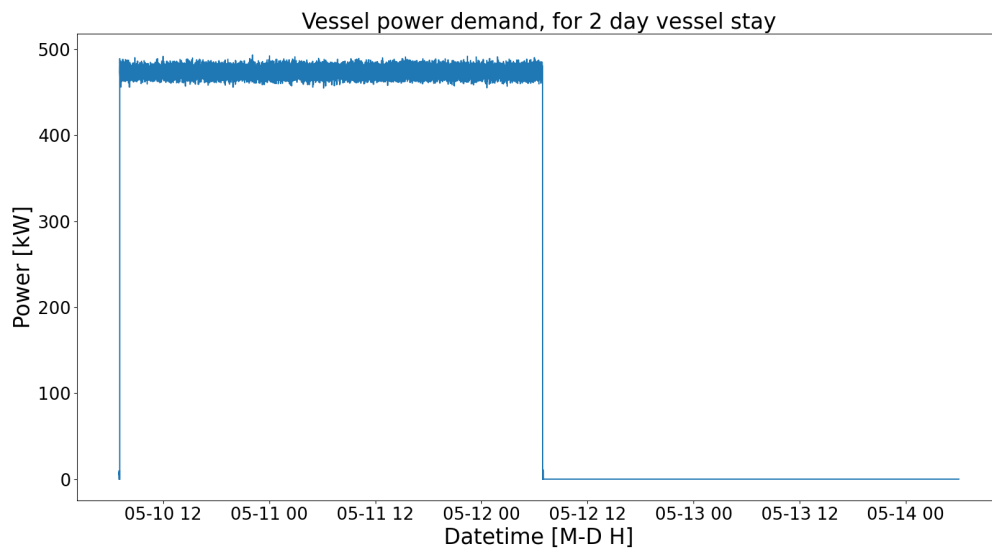
Figure A.172: Figure of the vessel power profile of 2 days and 2 days of downtime. The power demand has no crane uses. The vessel power profile was used for the HE PV shore power configuration. The x-axis is in datetime, meaning that every data point is fixed to a date and time.
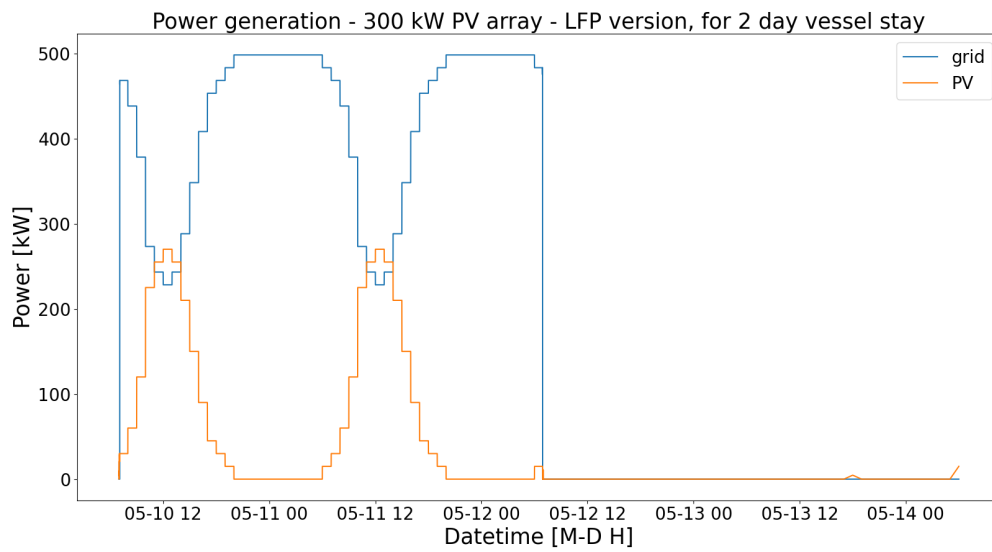
Figure A.173: Figure of the power generation of the LFP version of the HE PV shore power configuration with a 300 kW PV array. The solar generation is from an average summer day. The power generation is for the power demand from Figure A.172. The minor fluctuations of the power profile are being peak shaven by the LFP battery.
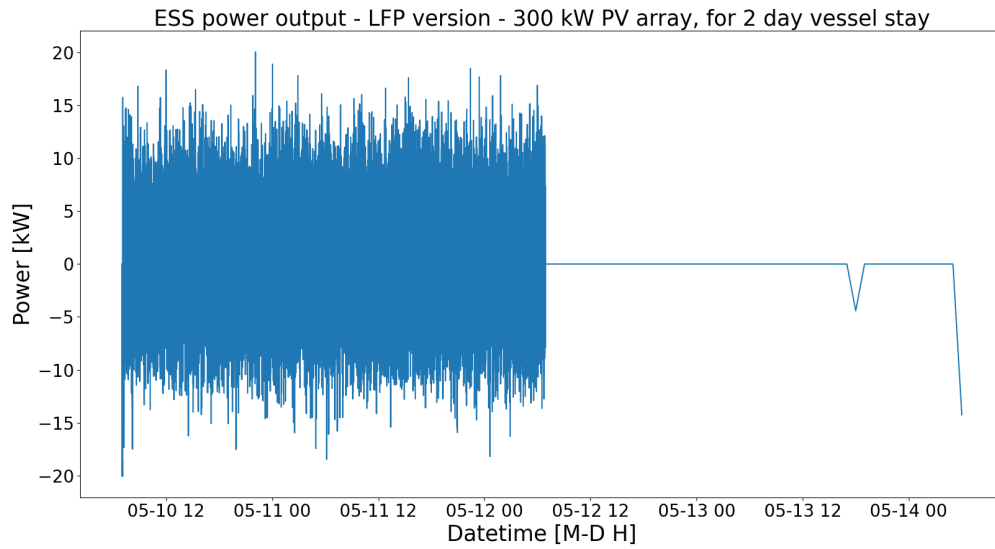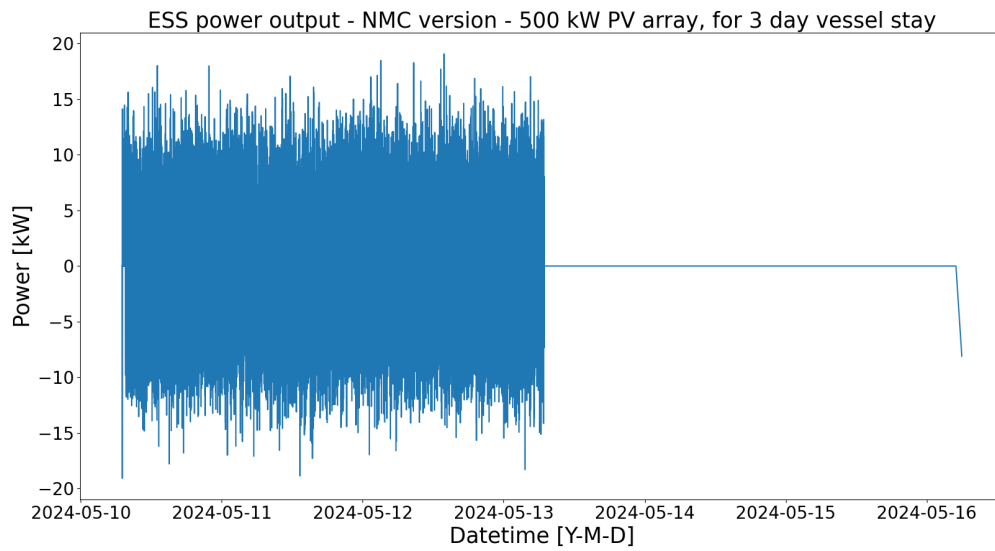
Figure A.174: Figure of the LFP battery output power of the LFP version of the HE PV shore power configuration with 300 kW PV array. The LFP battery peak shaves the minor fluctuations of the power demand of Figure A.172.
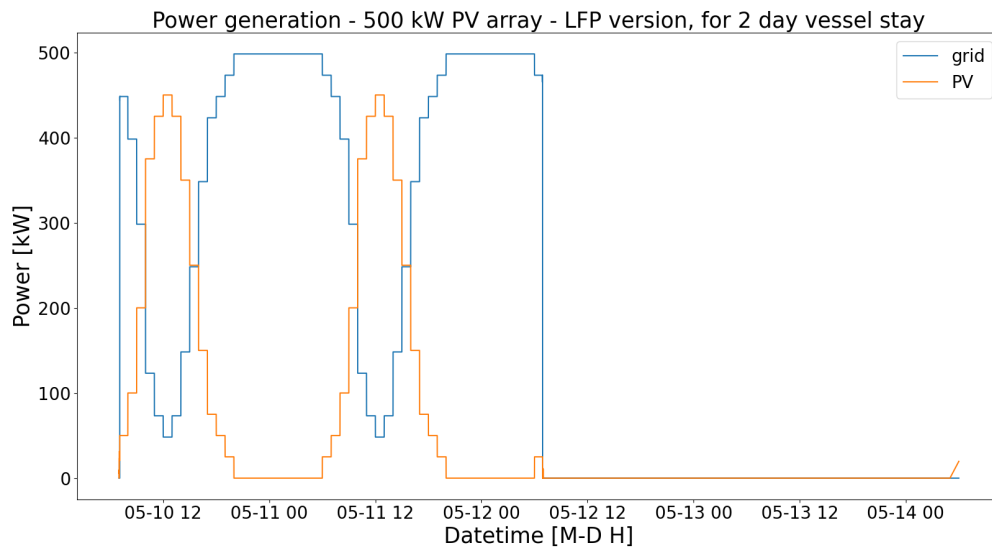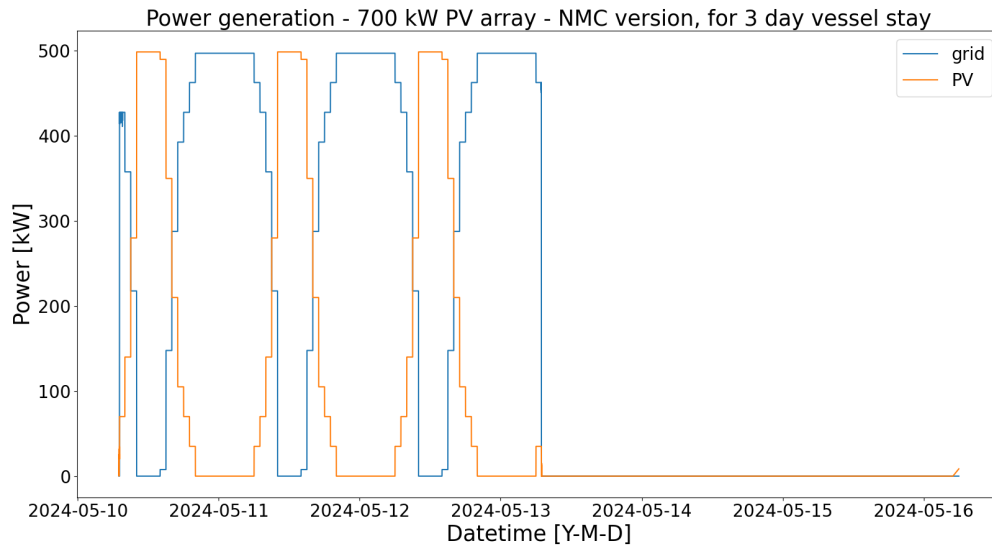

Figure A.175: Figure of the power generation of the LFP version of the HE PV shore power configuration with a 500 kW PV array. The solar generation is from an average summer day. The power generation is for the power demand from Figure A.172. The minor fluctuations of the power profile are being peak shaven by the LFP battery.
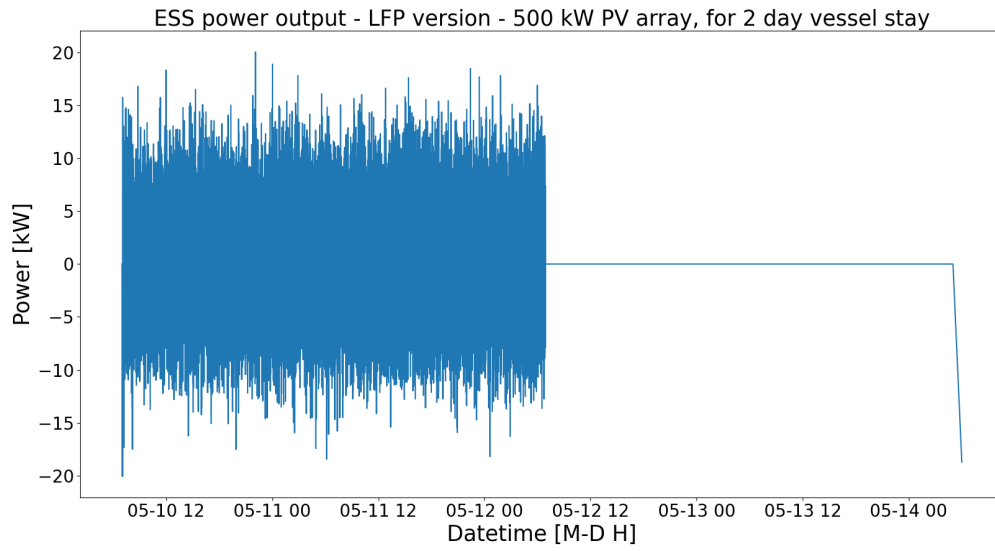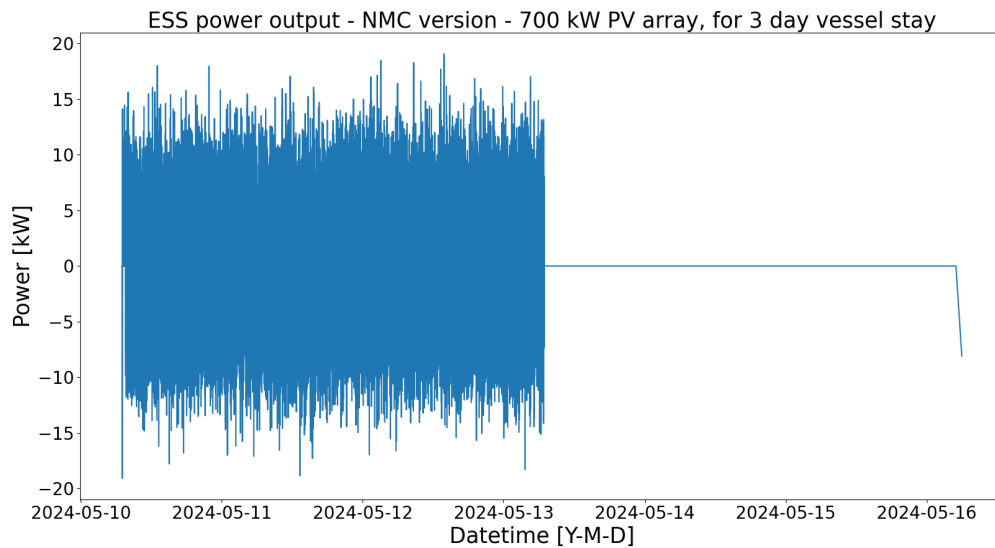
Figure A.176: Figure of the LFP battery output power of the LFP version of the HE PV shore power configuration with 500 kW PV array. The LFP battery peak shaves the minor fluctuations of the power demand of Figure A.172.
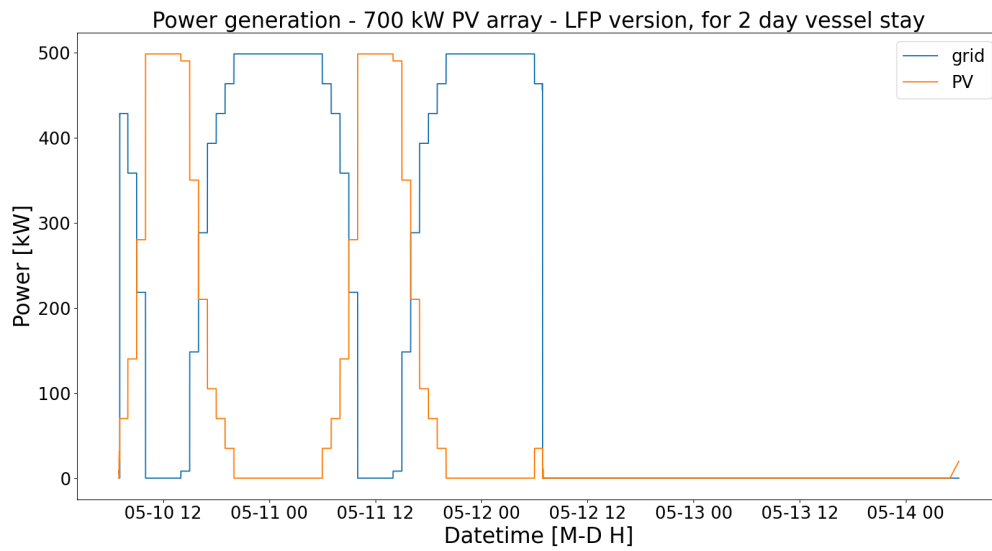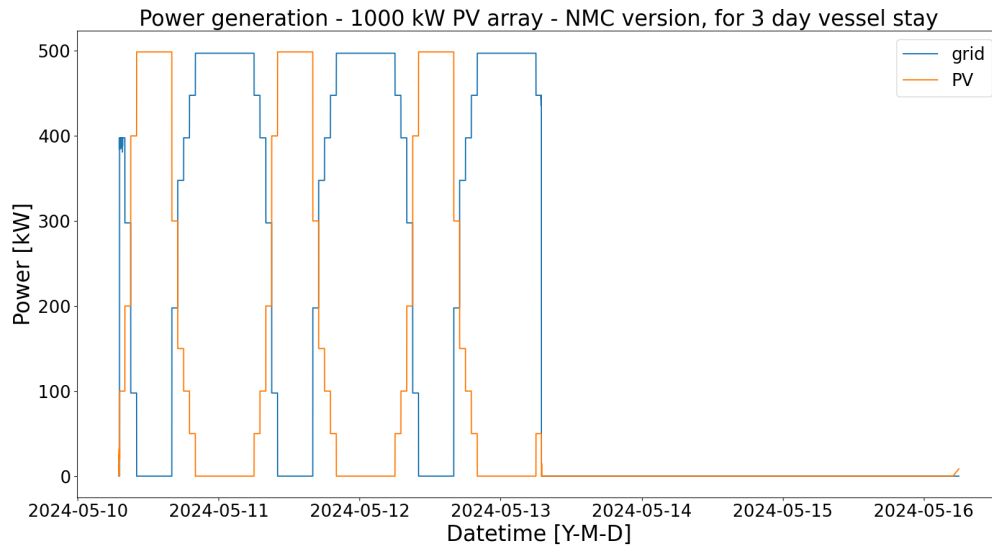

Figure A.177: Figure of the power generation of the LFP version of the HE PV shore power configuration with a 700 kW PV array. The solar generation is from an average summer day. The power generation is for the power demand from Figure A.172. The minor fluctuations of the power profile are being peak shaven by the LFP battery.
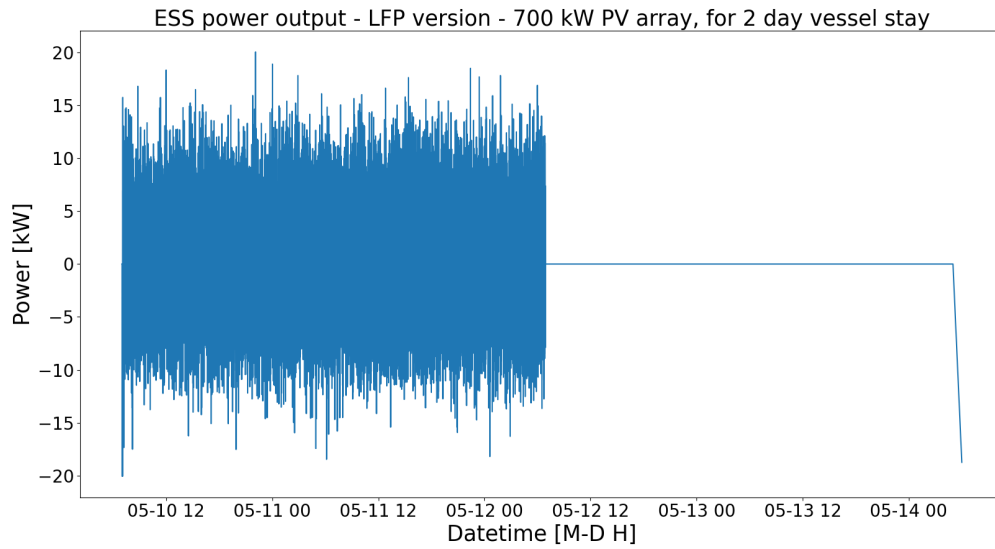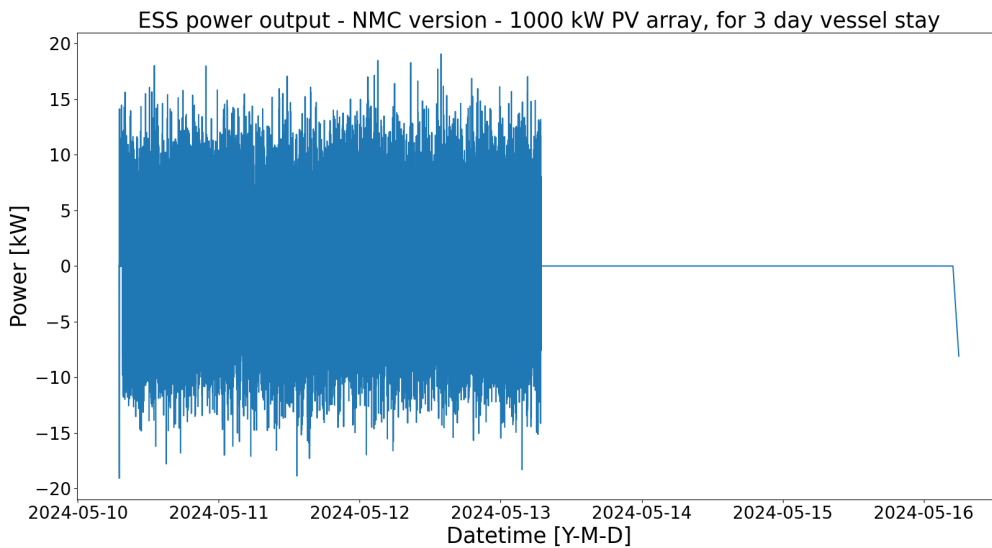
Figure A.178: Figure of the LFP battery output power of the LFP version of the HE PV shore power configuration with 700 kW PV array. The LFP battery peak shaves the minor fluctuations of the power demand of Figure A.172.
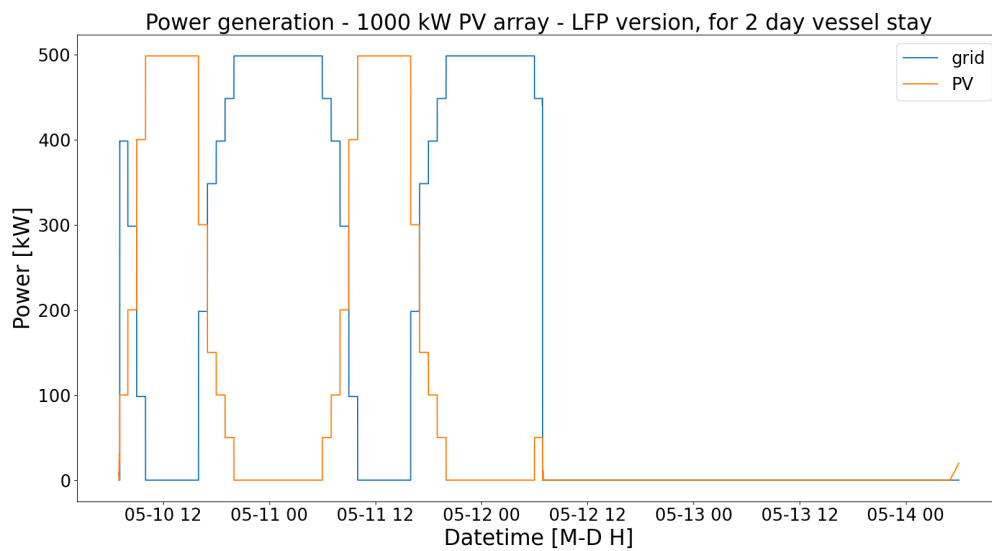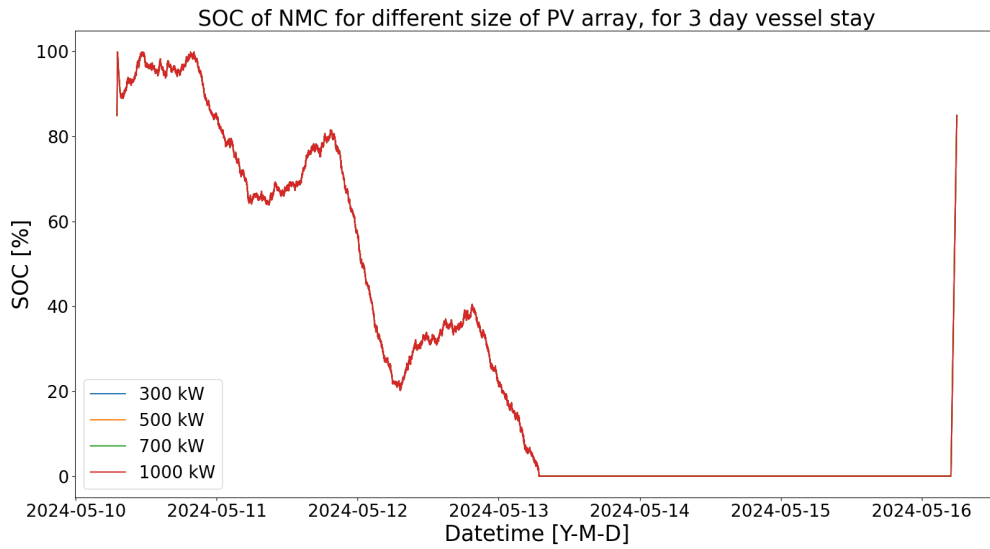

Figure A.179: Figure of the power generation of the LFP version of the HE PV shore power configuration with a 1000 kW PV array. The solar generation is from an average summer day. The power generation is for the power demand from Figure A.172. The minor fluctuations of the power profile are being peak shaven by the LFP battery.
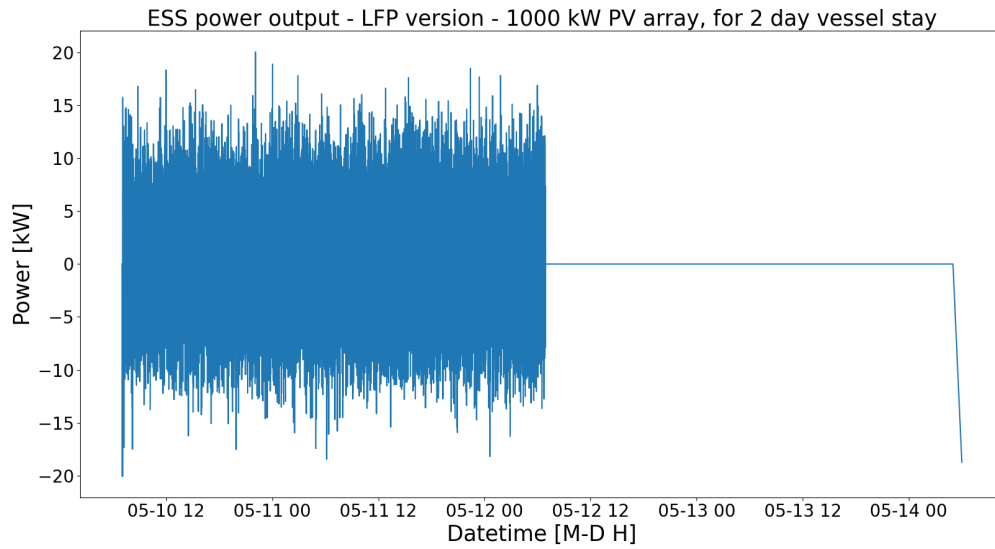
Figure A.180: Figure of the LFP battery output power of the LFP version of the HE PV shore power configuration with 1000 kW PV array. The LFP battery peak shaves the minor fluctuations of the power demand of Figure A.172.
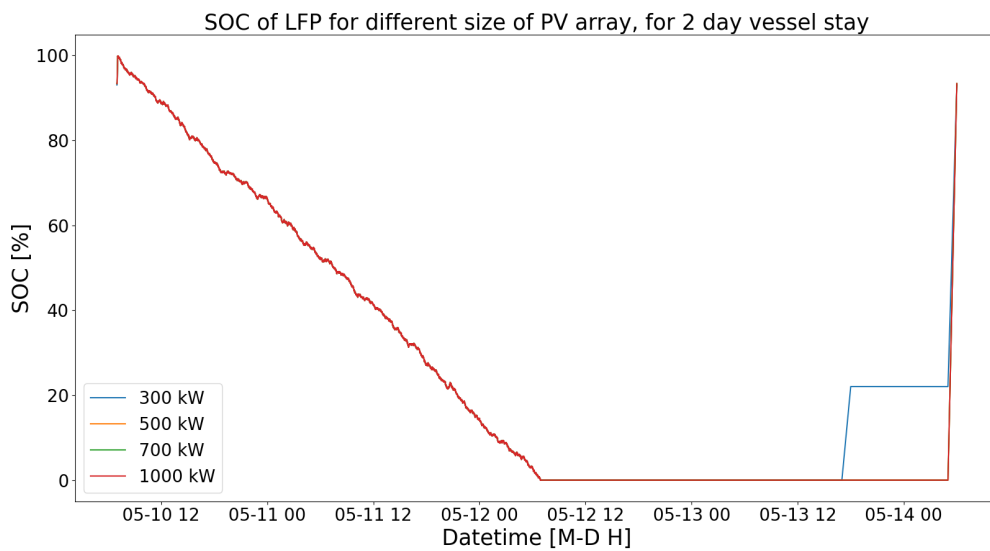
Figure A.181: Figure of the SOC of the LFP battery of the LFP version of the HE PV shore power configuration. The plot includes different implementations using different sizes of PV array. All the different implementations discharge in the same exact way.
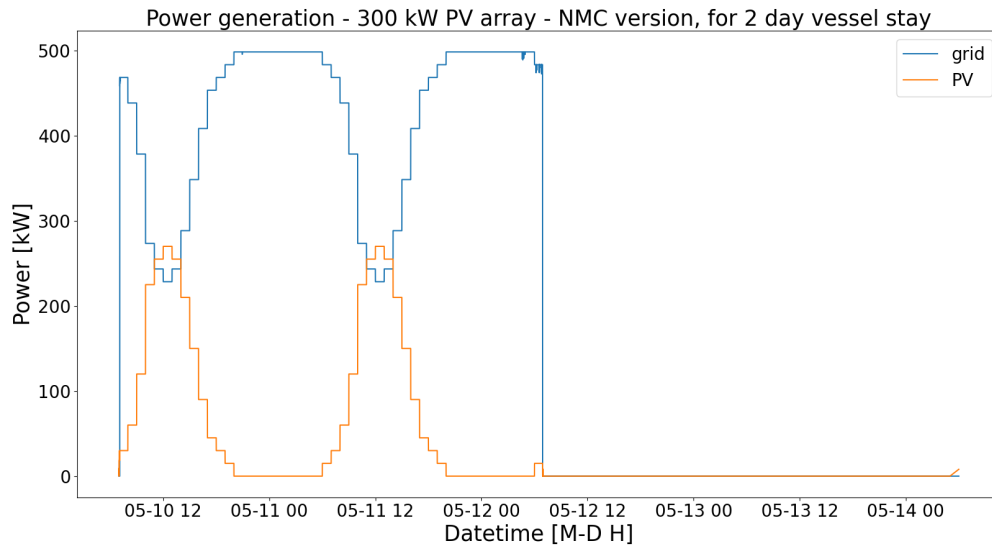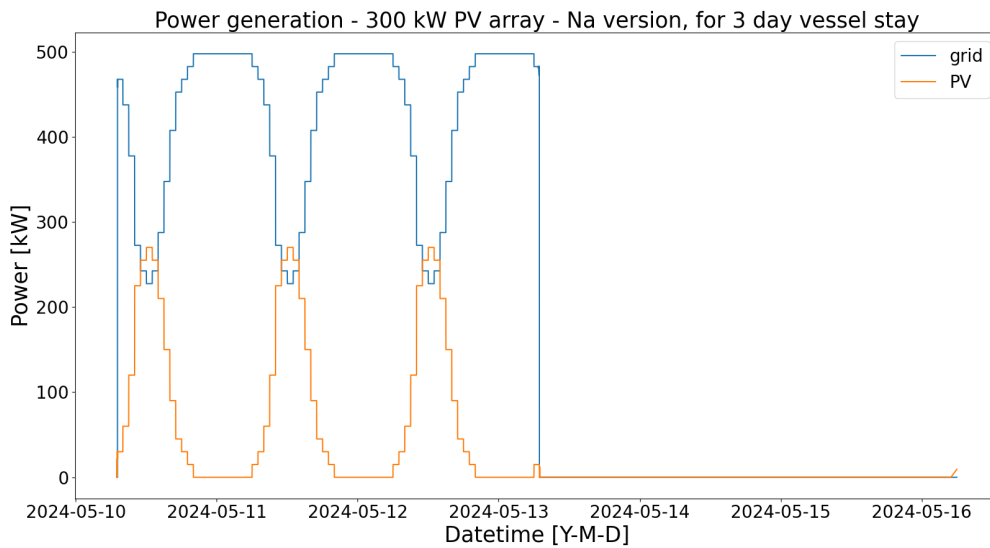
Figure A.182: Figure of the power generation of the NMC version of the HE PV shore power configuration with a 300 kW PV array. The solar generation is from an average summer day. The power generation is for the power demand from Figure A.172. The minor fluctuations of the power profile are being peak shaven by the NMC battery.
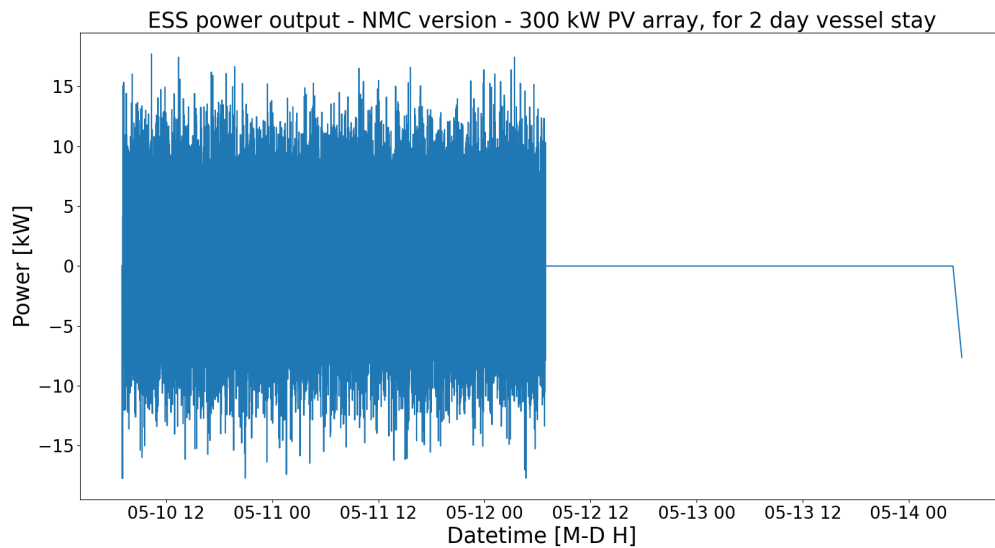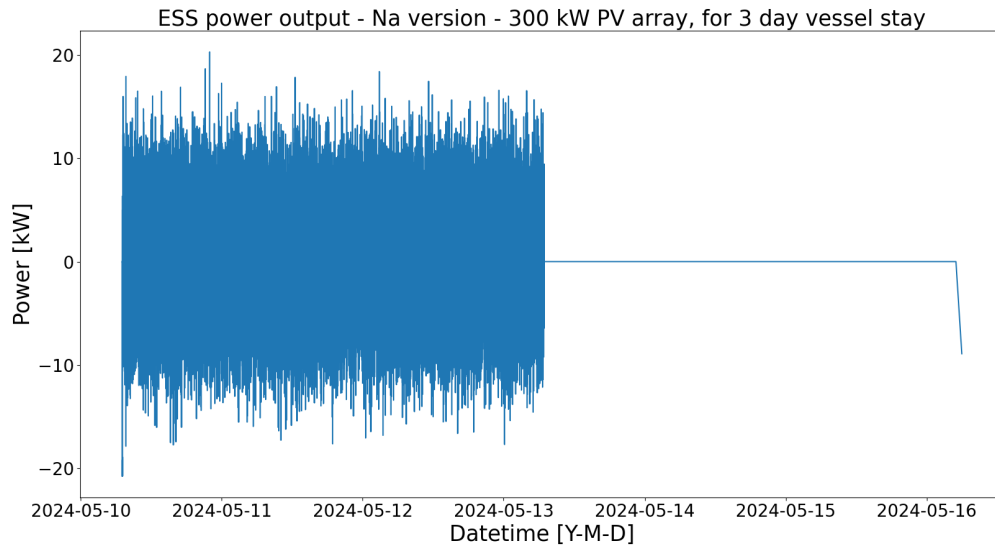

Figure A.183: Figure of the NMC battery output power of the NMC version of the HE PV shore power configuration with 300 kW PV array. The NMC battery peak shaves the minor fluctuations of the power demand of Figure A.172.
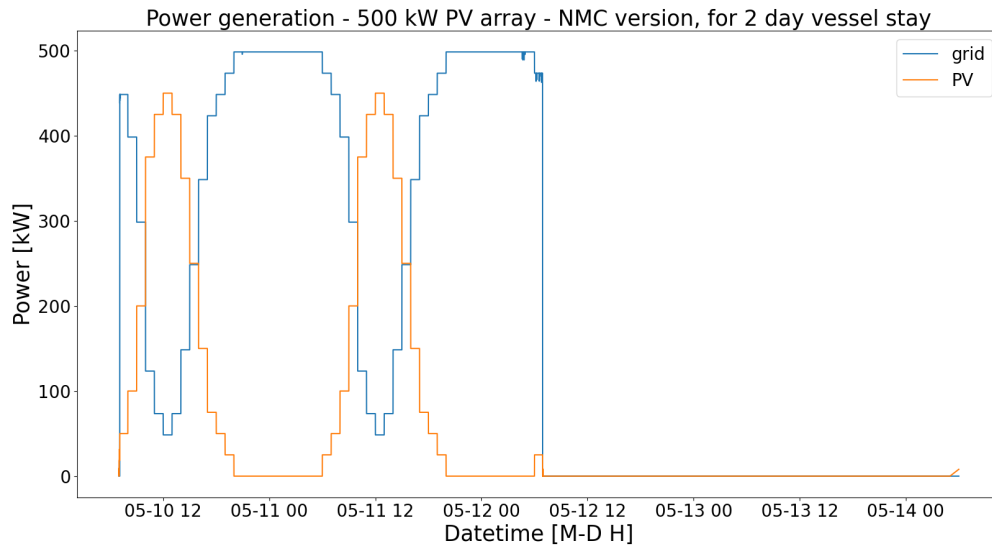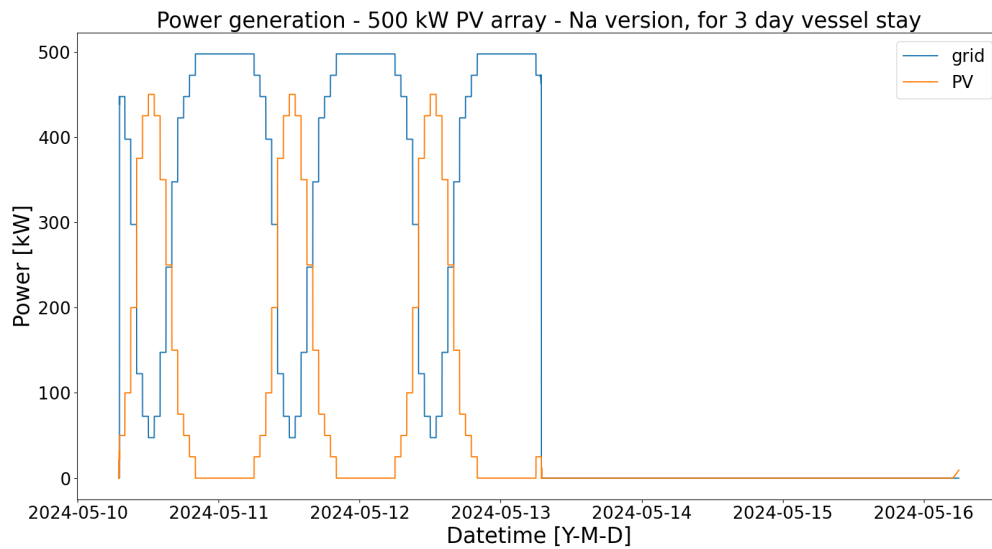
Figure A.184: Figure of the power generation of the NMC version of the HE PV shore power configuration with a 500 kW PV array. The solar generation is from an average summer day. The power generation is for the power demand from Figure A.172. The minor fluctuations of the power profile are being peak shaven by the NMC battery.
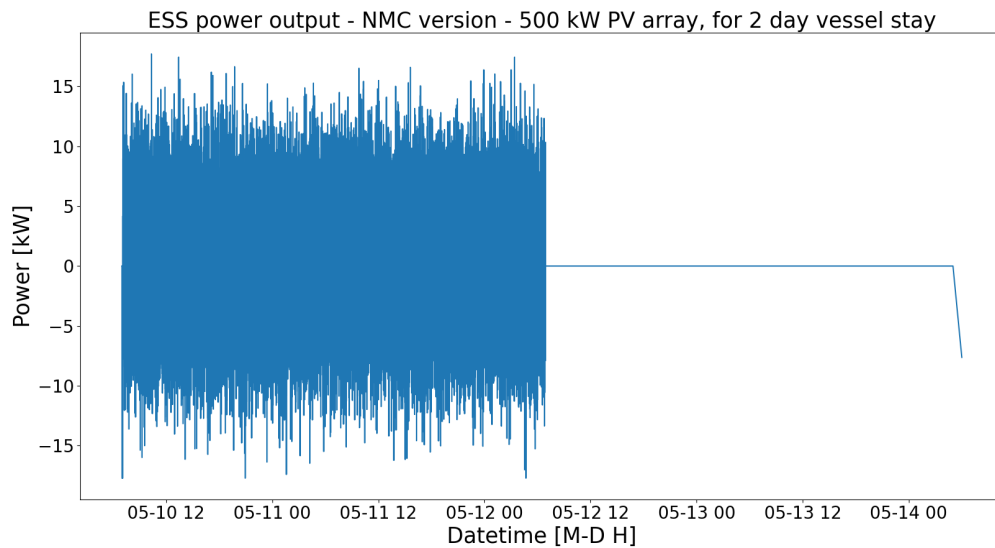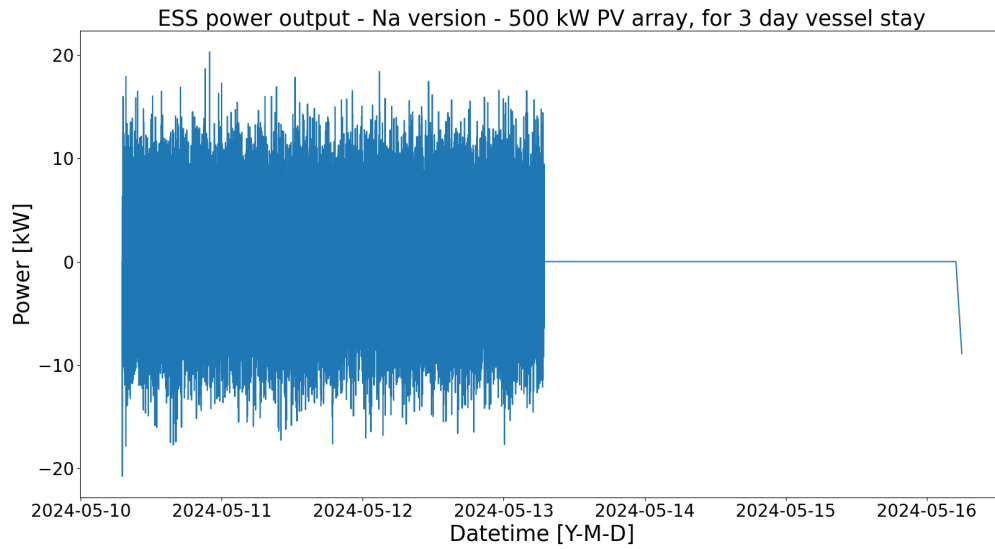

Figure A.185: Figure of the NMC battery output power of the NMC version of the HE PV shore power configuration with 500 kW PV array. The NMC battery peak shaves the minor fluctuations of the power demand of Figure A.172.
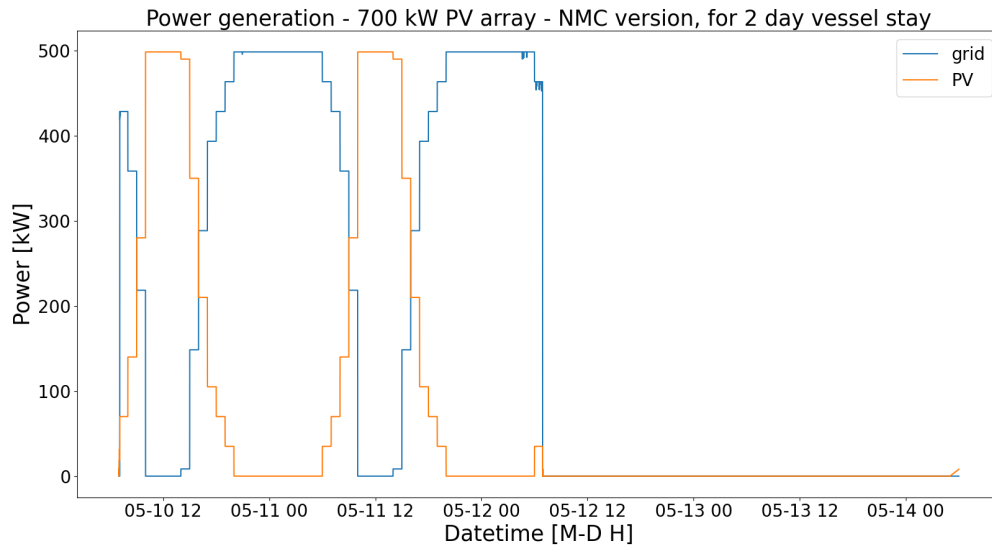
Figure A.186: Figure of the power generation of the NMC version of the HE PV shore power configuration with a 700 kW PV array. The solar generation is from an average summer day. The power generation is for the power demand from Figure A.172. The minor fluctuations of the power profile are being peak shaven by the NMC battery.
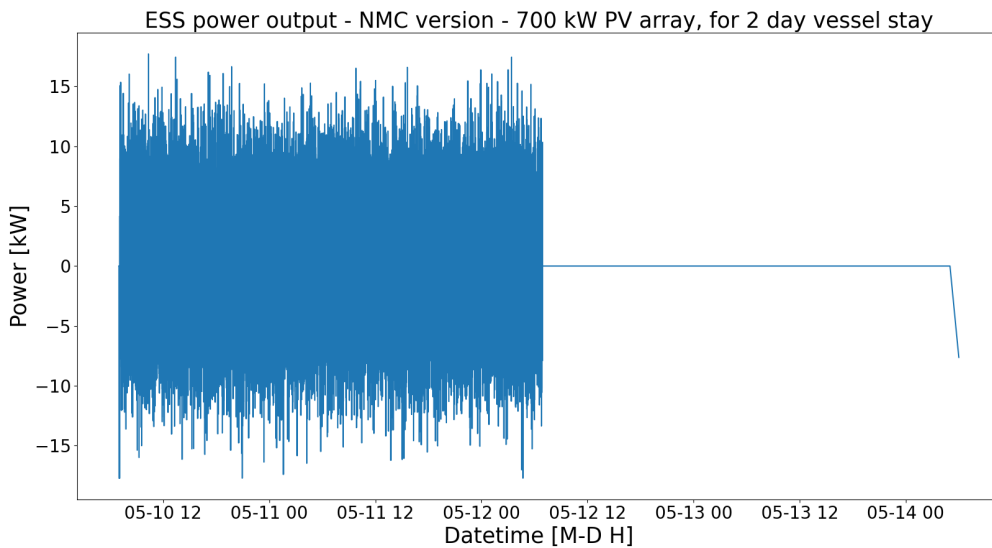
Figure A.187: Figure of the NMC battery output power of the NMC version of the HE PV shore power configuration with 700 kW PV array. The NMC battery peak shaves the minor fluctuations of the power demand of Figure A.172.
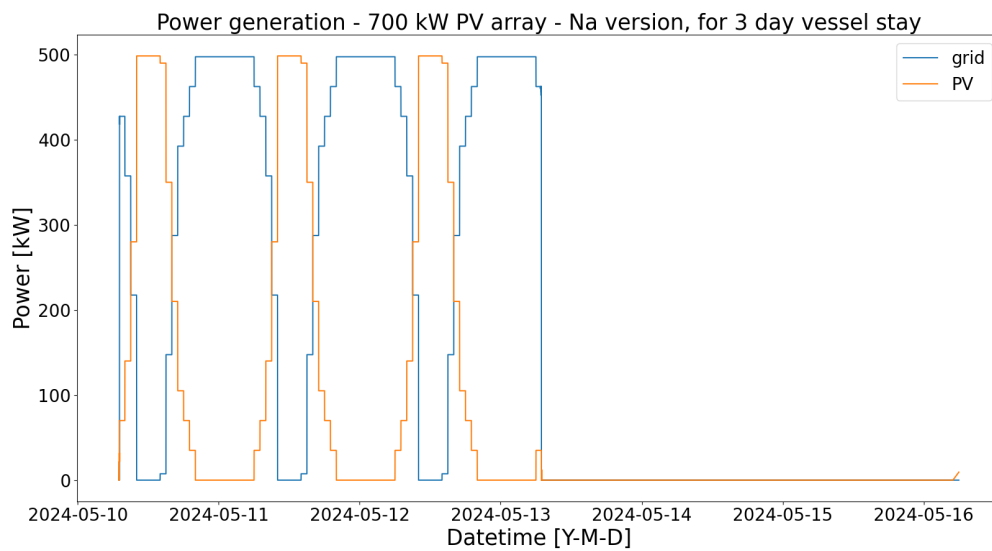
Figure A.188: Figure of the power generation of the NMC version of the HE PV shore power configuration with a 1000 kW PV array. The solar generation is from an average summer day. The power generation is for the power demand from Figure A.172. The minor fluctuations of the power profile are being peak shaven by the NMC battery.
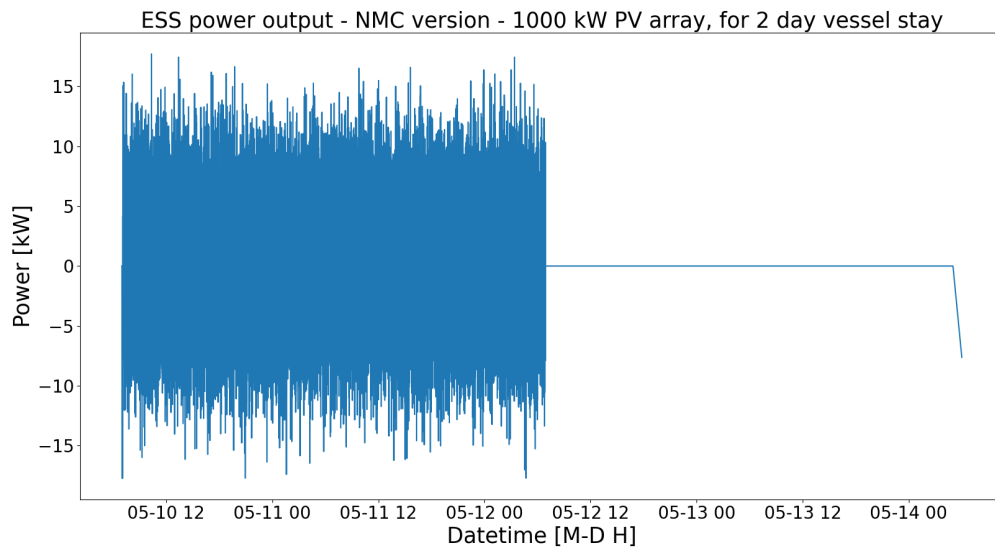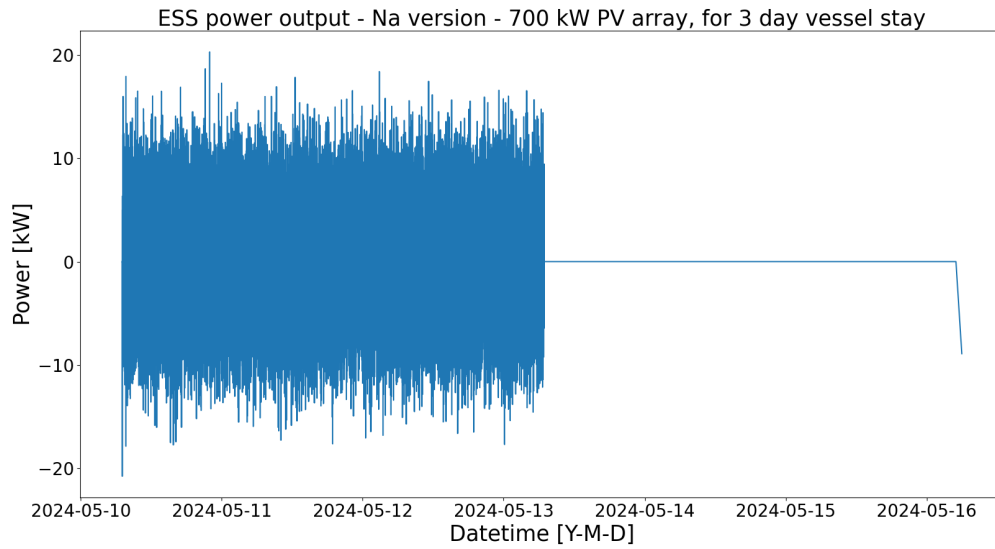

Figure A.189: Figure of the NMC battery output power of the NMC version of the HE PV shore power configuration with 1000 kW PV array. The NMC battery peak shaves the minor fluctuations of the power demand of Figure A.172.
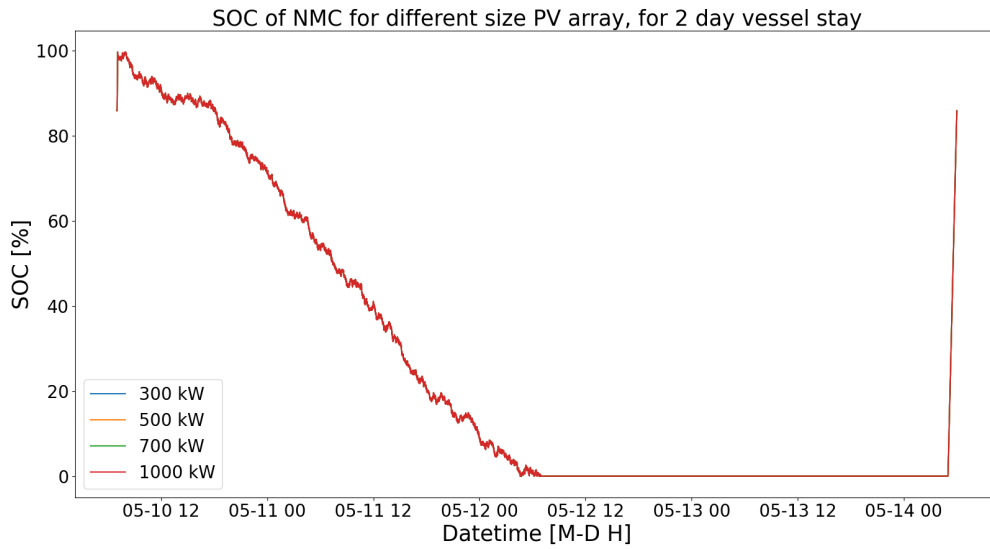
Figure A.190: Figure of the SOC of the NMC battery of the NMC version of the HE PV shore power configuration. The plot includes different implementations using different sizes of PV array. All the different implementations discharge in the same exact way.
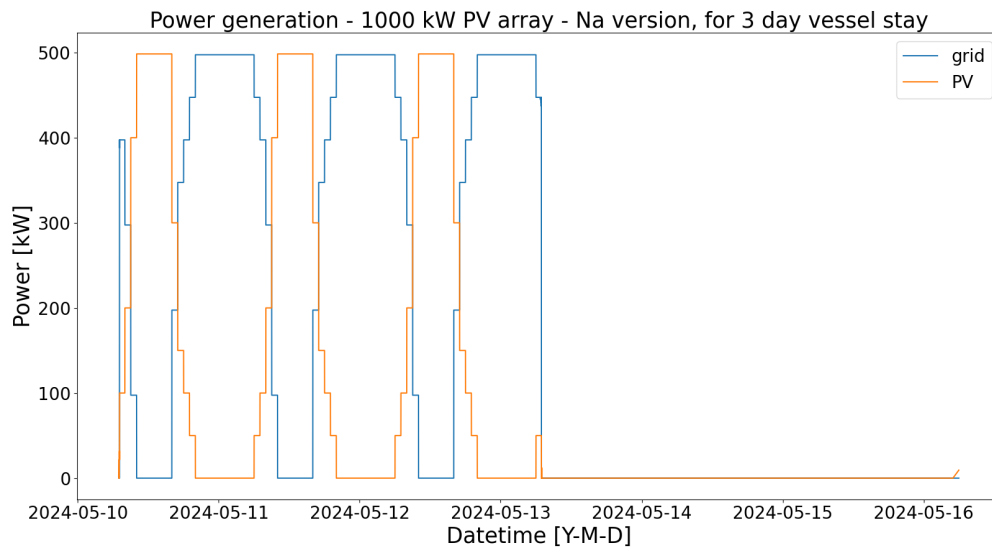

Figure A.191: Figure of the power generation of the Na-ion version of the HE PV shore power configuration with a 300 kW PV array. The solar generation is from an average summer day. The power generation is for the power demand from Figure A.172. The minor fluctuations of the power profile are being peak shaven by the Na-ion battery.
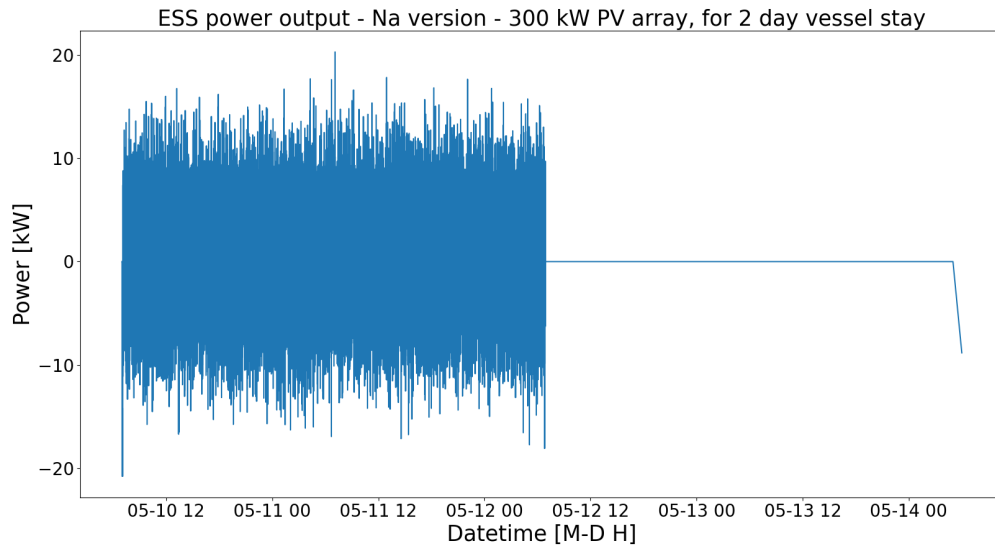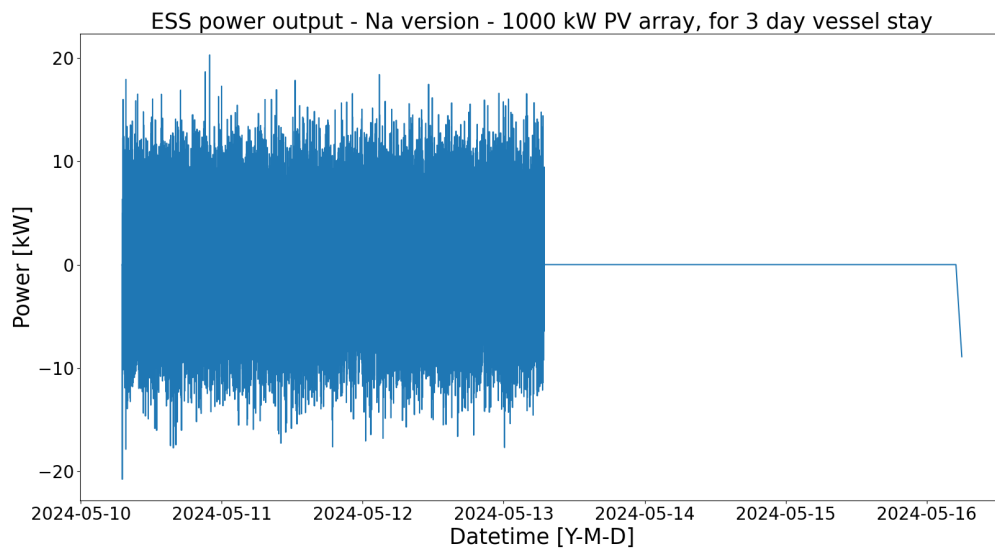
Figure A.192: Figure of the Na-ion battery output power of the Na-ion version of the HE PV shore power configuration with 300 kW PV array. The Na-ion battery peak shaves the minor fluctuations of the power demand of Figure A.172.
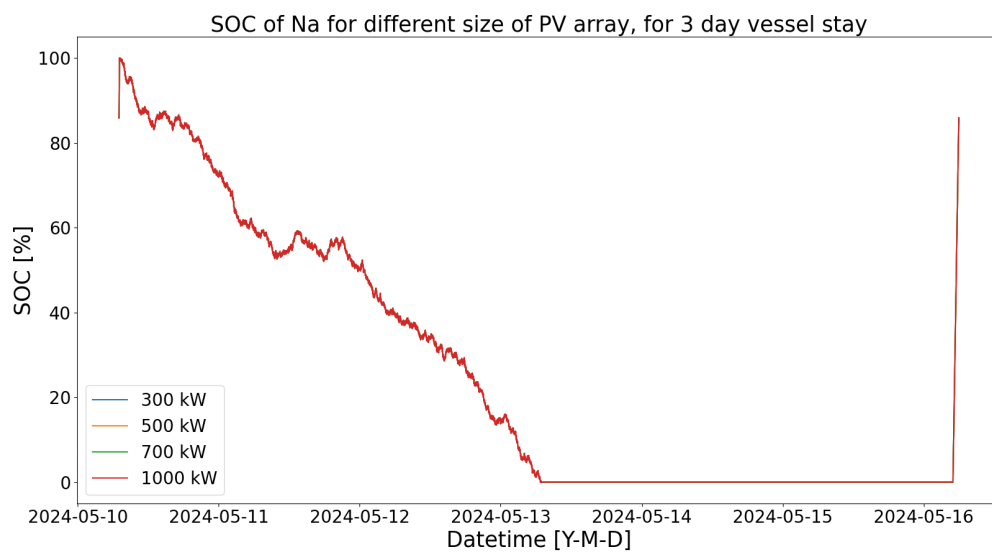

Figure A.193: Figure of the power generation of the Na-ion version of the HE PV shore power configuration with a 500 kW PV array. The solar generation is from an average summer day. The power generation is for the power demand from Figure A.172. The minor fluctuations of the power profile are being peak shaven by the Na-ion battery.

Figure A.194: Figure of the Na-ion battery output power of the Na-ion version of the HE PV shore power configuration with 500 kW PV array. The Na-ion battery peak shaves the minor fluctuations of the power demand of Figure A.172.
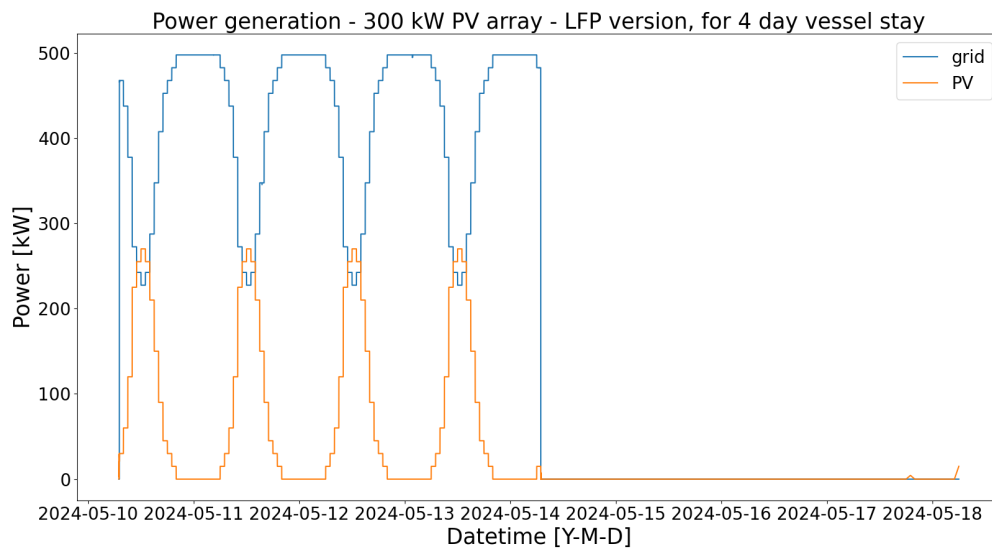

Figure A.195: Figure of the power generation of the Na-ion version of the HE PV shore power configuration with a 700 kW PV array. The solar generation is from an average summer day. The power generation is for the power demand from Figure A.172. The minor fluctuations of the power profile are being peak shaven by the Na-ion battery.

Figure A.196: Figure of the Na-ion battery output power of the Na-ion version of the HE PV shore power configuration with 700 kW PV array. The Na-ion battery peak shaves the minor fluctuations of the power demand of Figure A.172.

Figure A.197: Figure of the power generation of the Na-ion version of the HE PV shore power configuration with a 1000 kW PV array. The solar generation is from an average summer day. The power generation is for the power demand from Figure A.172. The minor fluctuations of the power profile are being peak shaven by the Na-ion battery.
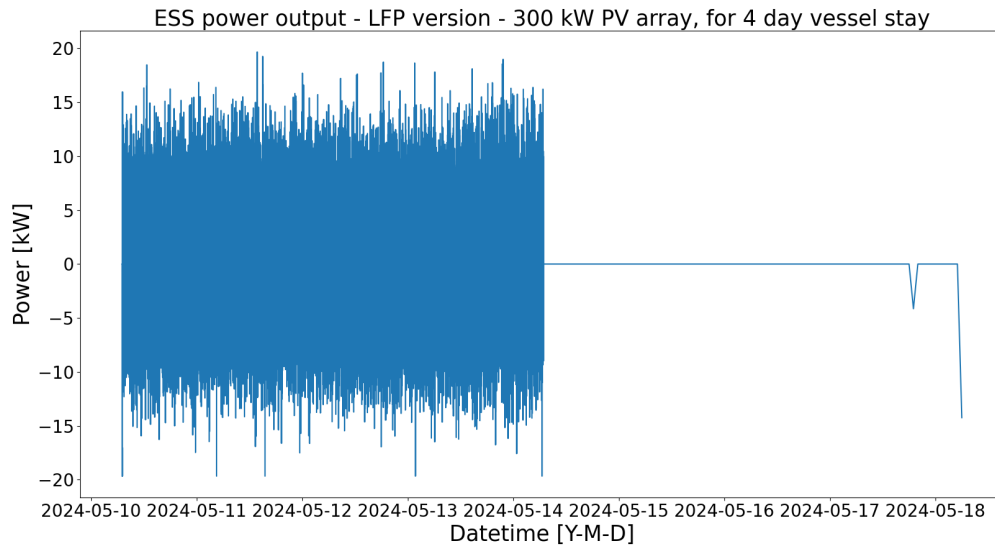
Figure A.198: Figure of the Na-ion battery output power of the Na-ion version of the HE PV shore power configuration with 1000 kW PV array. The Na-ion battery peak shaves the minor fluctuations of the power demand of Figure A.172.


Figure A.199: Figure of the SOC of the Na-ion battery of the Na-ion version of the HE PV shore power configuration. The plot includes different implementations using different sizes of PV array. All the different implementations discharge in the same exact way.

A.5.4. HE PV for 3 day vessel stay

Figure A.200: Figure of the vessel power profile of 3 days and 3 days of downtime. The power demand has no crane uses. The vessel power profile was used for the HE PV shore power configuration. The x-axis is in datetime, meaning that every data point is fixed to a date and time.

Figure A.201: Figure of the power generation of the LFP version of the HE PV shore power configuration with a 300 kW PV array. The solar generation is from an average summer day. The power generation is for the power demand from Figure A.200. The minor fluctuations of the power profile are being peak shaven by the LFP battery.

Figure A.202: Figure of the LFP battery output power of the LFP version of the HE PV shore power configuration with 300 kW PV array. The LFP battery peak shaves the minor fluctuations of the power demand of Figure A.200.
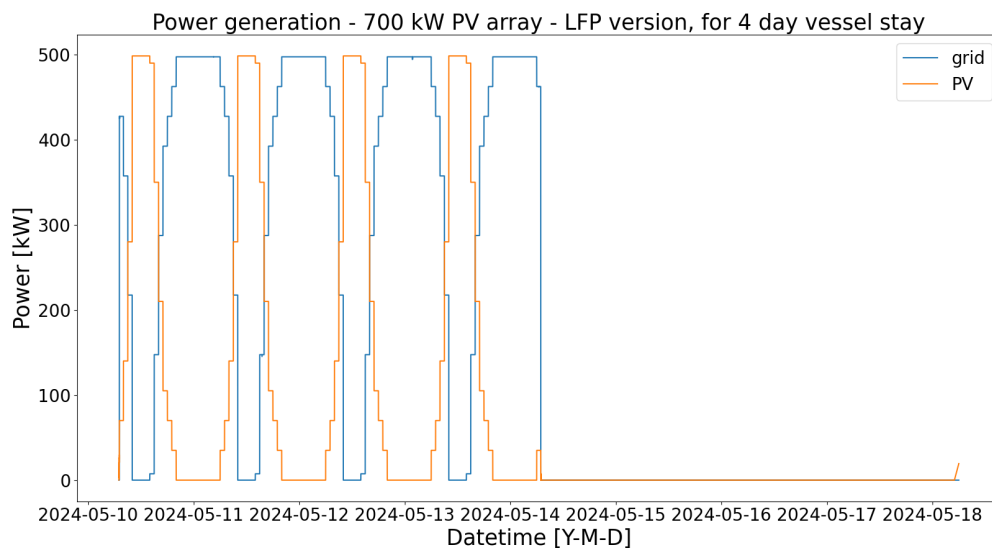

Figure A.203: Figure of the power generation of the LFP version of the HE PV shore power configuration with a 500 kW PV array. The solar generation is from an average summer day. The power generation is for the power demand from Figure A.200. The minor fluctuations of the power profile are being peak shaven by the LFP battery.
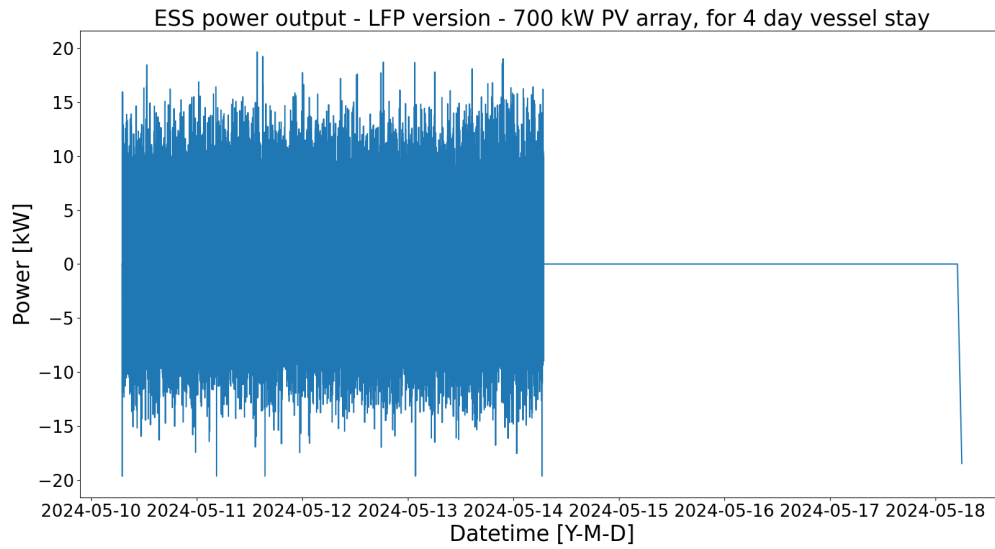
Figure A.204: Figure of the LFP battery output power of the LFP version of the HE PV shore power configuration with 500 kW PV array. The LFP battery peak shaves the minor fluctuations of the power demand of Figure A.200.
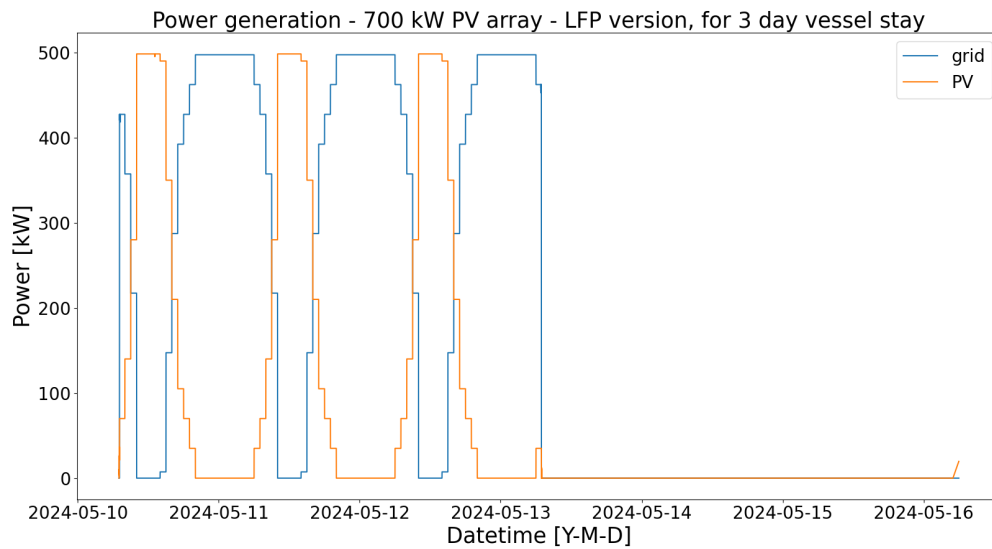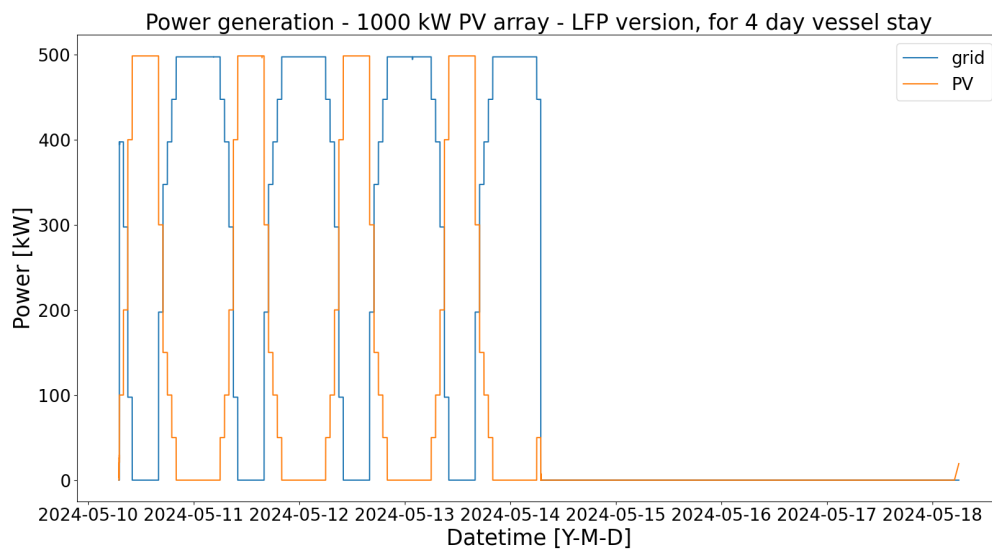

Figure A.205: Figure of the power generation of the LFP version of the HE PV shore power configuration with a 700 kW PV array. The solar generation is from an average summer day. The power generation is for the power demand from Figure A.200. The minor fluctuations of the power profile are being peak shaven by the LFP battery.
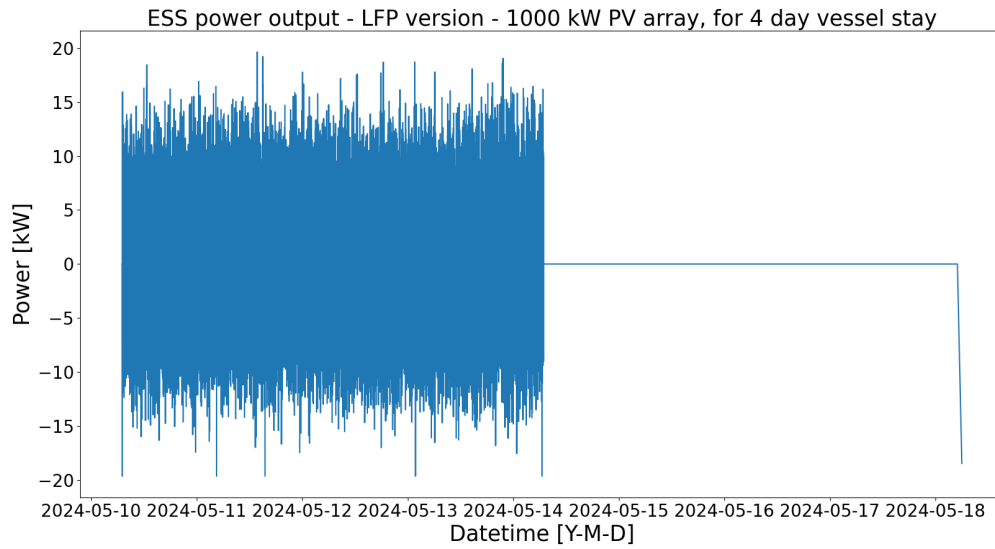
Figure A.206: Figure of the LFP battery output power of the LFP version of the HE PV shore power configuration with 700 kW PV array. The LFP battery peak shaves the minor fluctuations of the power demand of Figure A.200.
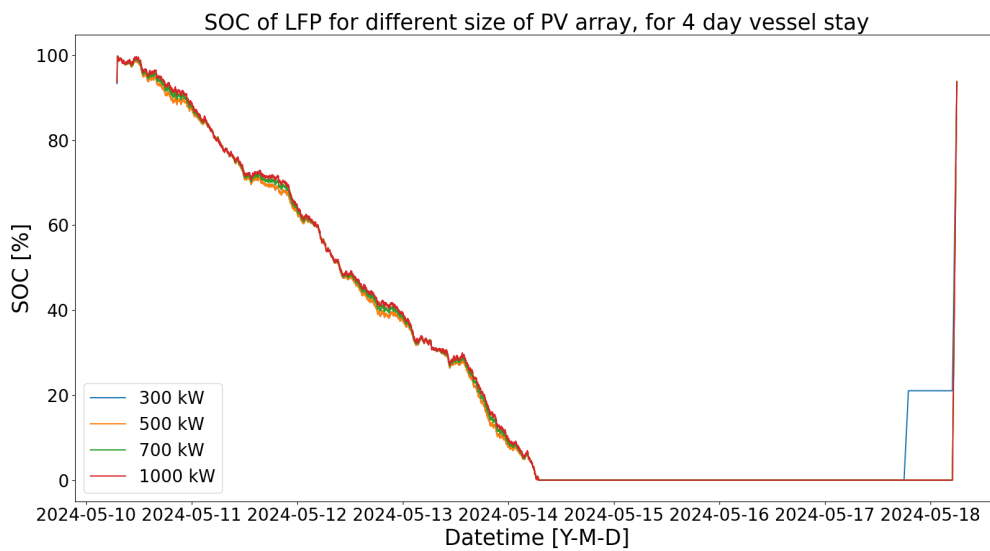

Figure A.207: Figure of the power generation of the LFP version of the HE PV shore power configuration with a 1000 kW PV array. The solar generation is from an average summer day. The power generation is for the power demand from Figure A.200. The minor fluctuations of the power profile are being peak shaven by the LFP battery.

Figure A.208: Figure of the LFP battery output power of the LFP version of the HE PV shore power configuration with 1000 kW PV array. The LFP battery peak shaves the minor fluctuations of the power demand of Figure A.200.

Figure A.209: Figure of the SOC of the LFP battery of the LFP version of the HE PV shore power configuration. The plot includes different implementations using different sizes of PV array. All the different implementations discharge in the same exact way.
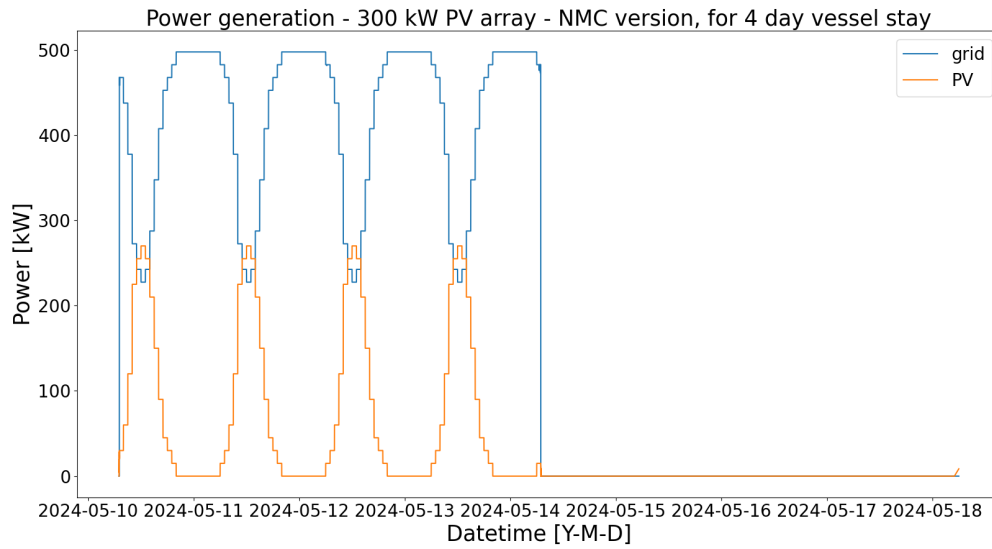
Figure A.210: Figure of the power generation of the NMC version of the HE PV shore power configuration with a 300 kW PV array. The solar generation is from an average summer day. The power generation is for the power demand from Figure A.200. The minor fluctuations of the power profile are being peak shaven by the NMC battery.
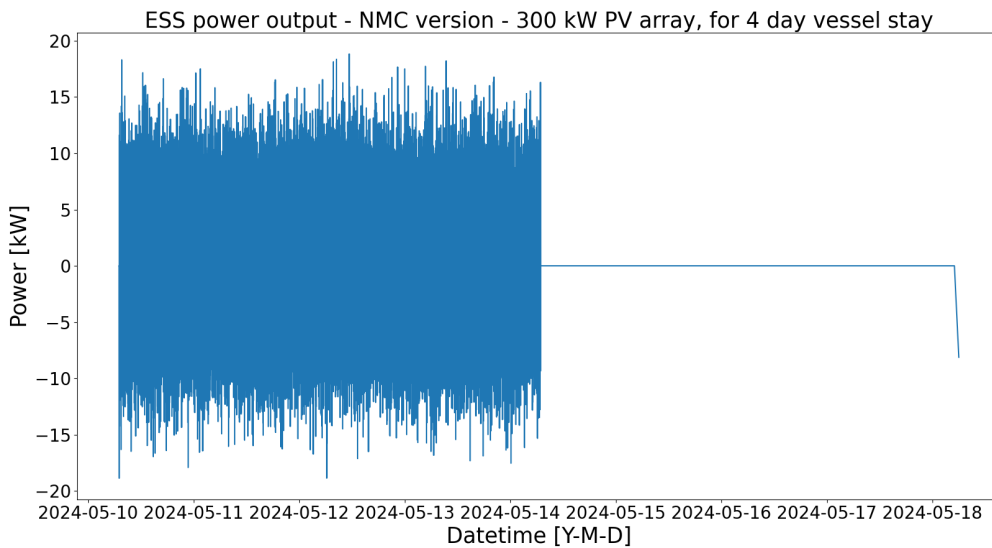

Figure A.211: Figure of the NMC battery output power of the NMC version of the HE PV shore power configuration with 300 kW PV array. The NMC battery peak shaves the minor fluctuations of the power demand of Figure A.200.
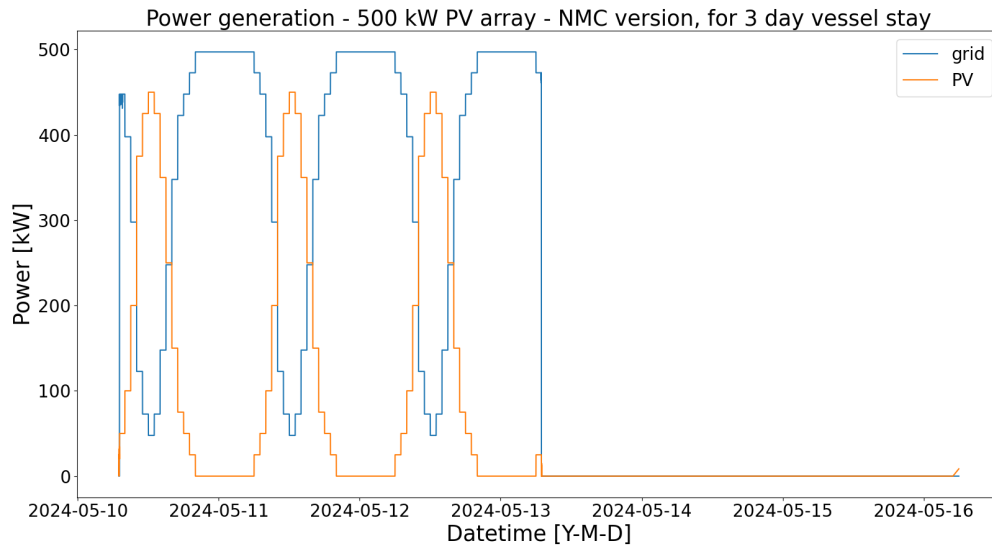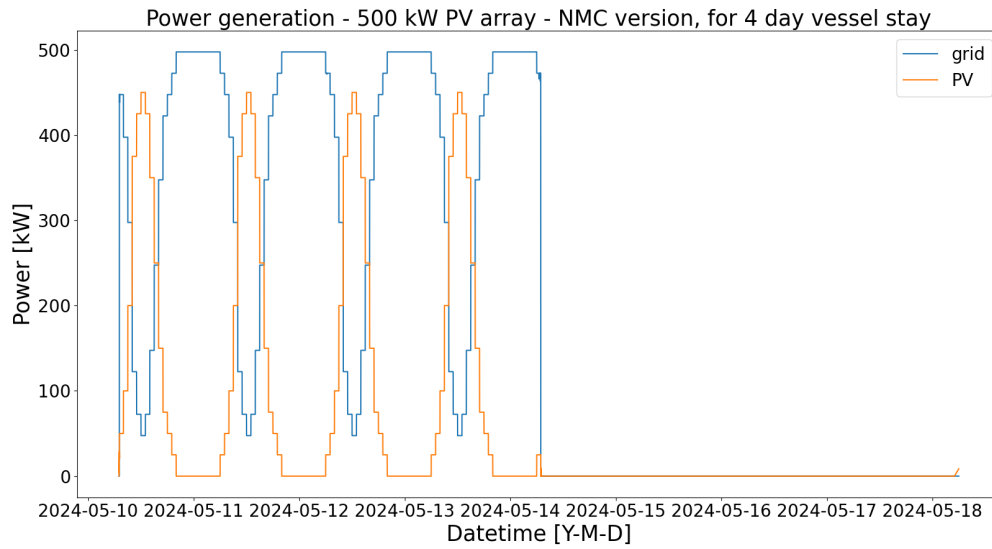
Figure A.212: Figure of the power generation of the NMC version of the HE PV shore power configuration with a 500 kW PV array. The solar generation is from an average summer day. The power generation is for the power demand from Figure A.200. The minor fluctuations of the power profile are being peak shaven by the NMC battery.
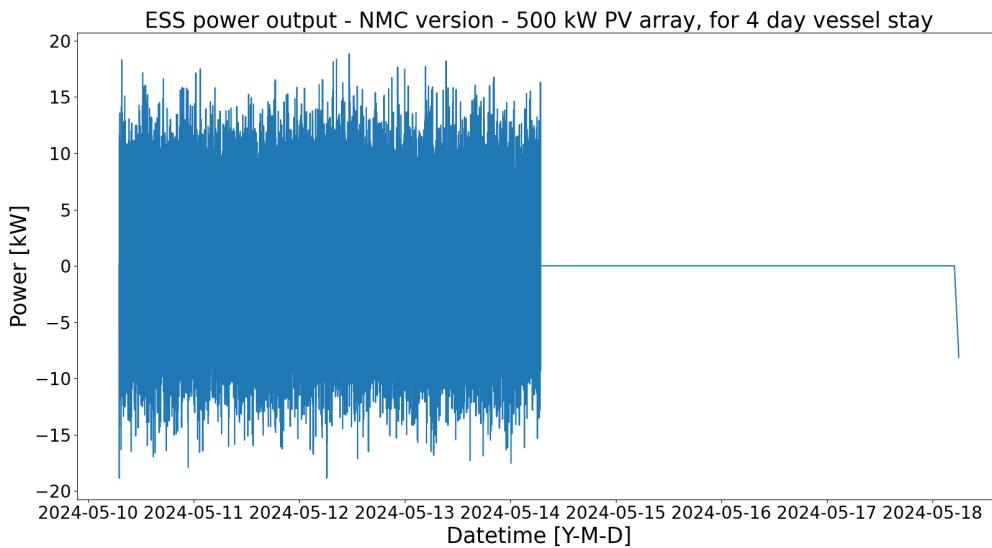

Figure A.213: Figure of the NMC battery output power of the NMC version of the HE PV shore power configuration with 500 kW PV array. The NMC battery peak shaves the minor fluctuations of the power demand of Figure A.200.
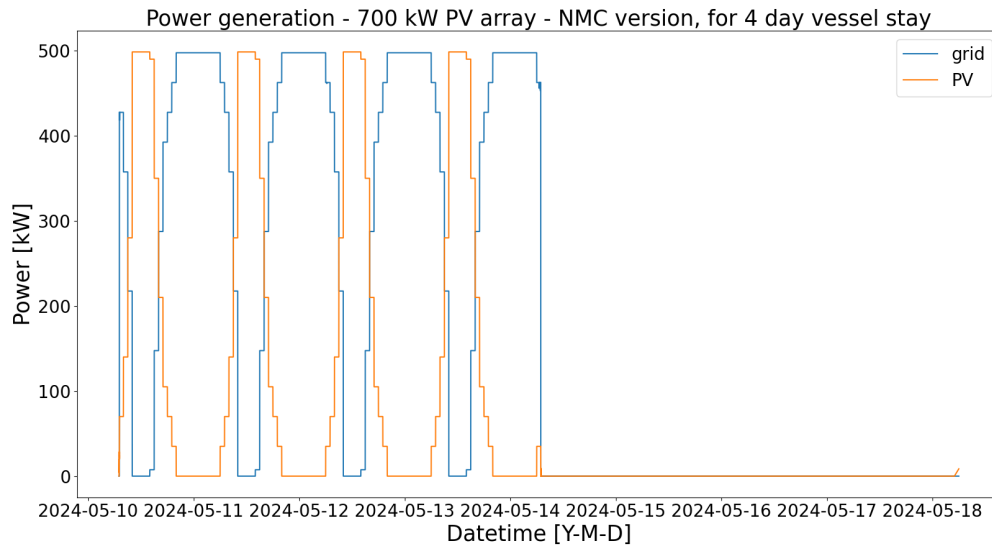
Figure A.214: Figure of the power generation of the NMC version of the HE PV shore power configuration with a 700 kW PV array. The solar generation is from an average summer day. The power generation is for the power demand from Figure A.200. The minor fluctuations of the power profile are being peak shaven by the NMC battery.
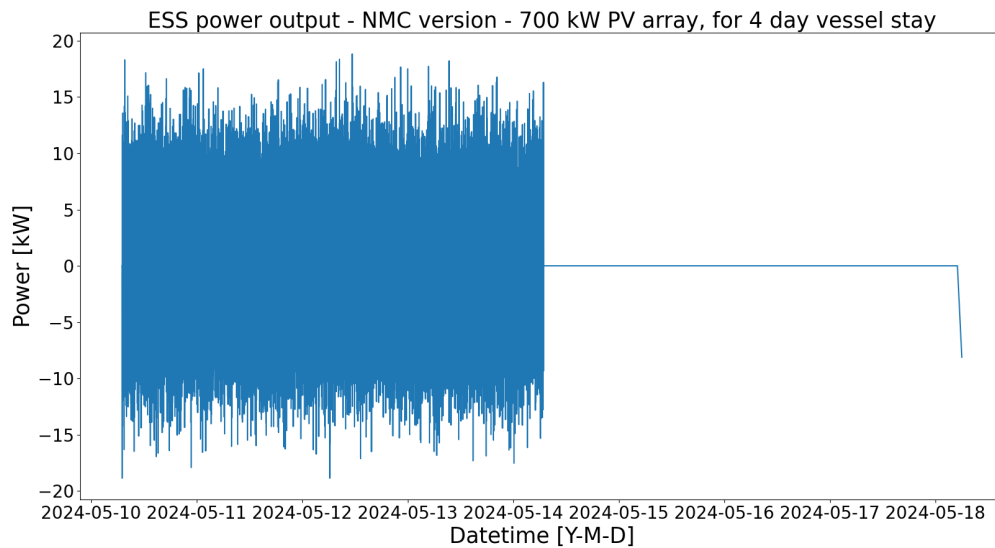

Figure A.215: Figure of the NMC battery output power of the NMC version of the HE PV shore power configuration with 700 kW PV array. The NMC battery peak shaves the minor fluctuations of the power demand of Figure A.200.

Figure A.216: Figure of the power generation of the NMC version of the HE PV shore power configuration with a 1000 kW PV array. The solar generation is from an average summer day. The power generation is for the power demand from Figure A.200. The minor fluctuations of the power profile are being peak shaven by the NMC battery.

Figure A.217: Figure of the NMC battery output power of the NMC version of the HE PV shore power configuration with 1000 kW PV array. The NMC battery peak shaves the minor fluctuations of the power demand of Figure A.200.
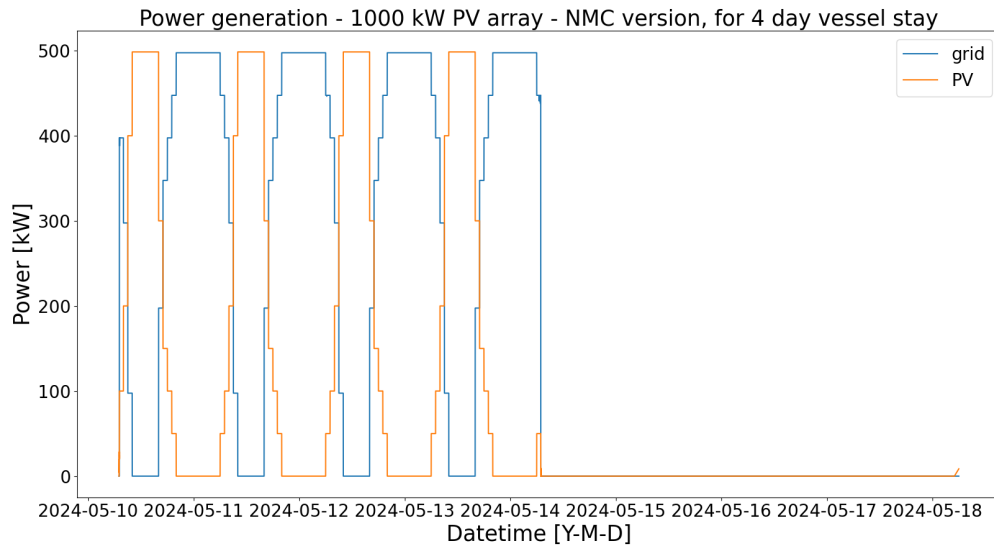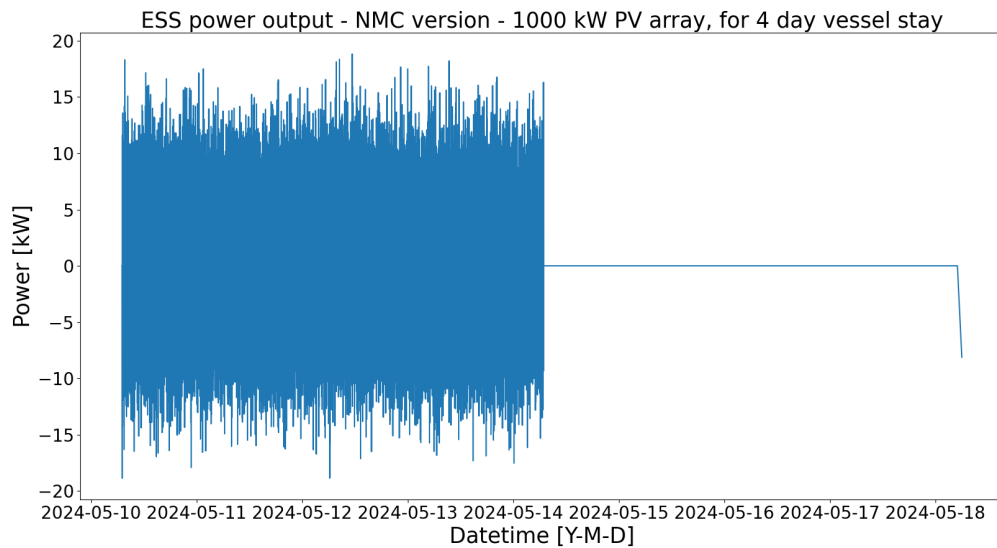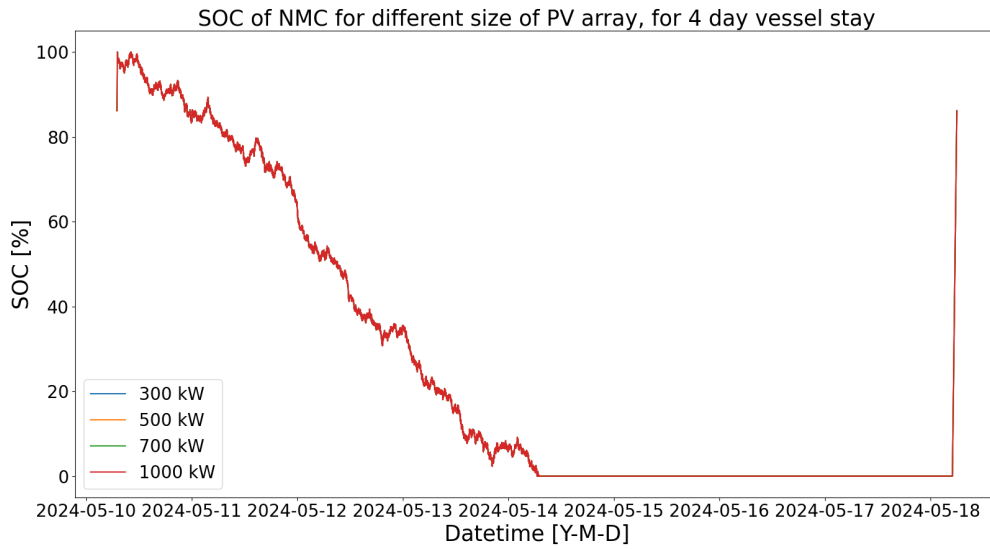
Figure A.218: Figure of the SOC of the NMC battery of the NMC version of the HE PV shore power configuration. The plot includes different implementations using different sizes of PV array. All the different implementations discharge in the same exact way.

Figure A.219: Figure of the power generation of the Na-ion version of the HE PV shore power configuration with a 300 kW PV array. The solar generation is from an average summer day. The power generation is for the power demand from Figure A.200. The minor fluctuations of the power profile are being peak shaven by the Na-ion battery.

Figure A.220: Figure of the Na-ion battery output power of the Na-ion version of the HE PV shore power configuration with 300 kW PV array. The Na-ion battery peak shaves the minor fluctuations of the power demand of Figure A.200.
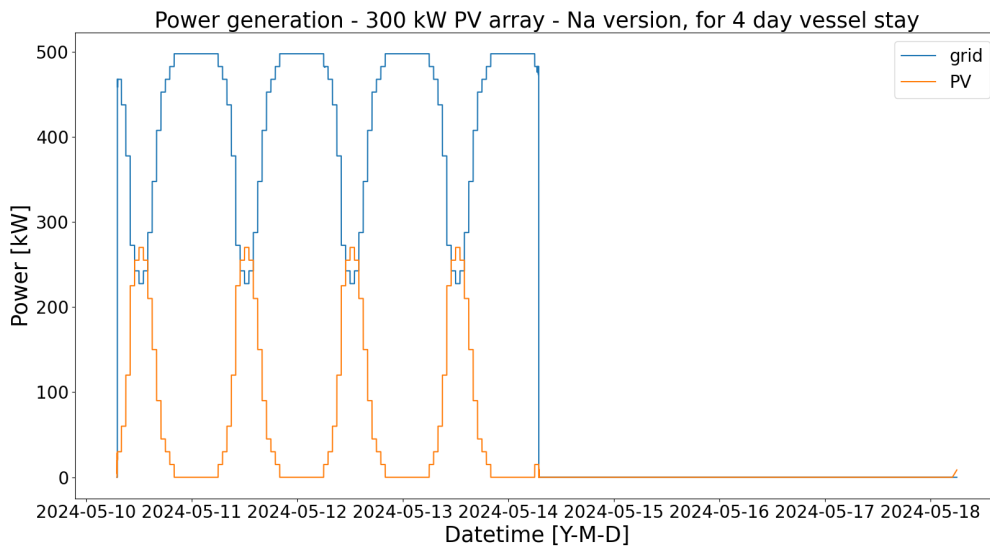

Figure A.221: Figure of the power generation of the Na-ion version of the HE PV shore power configuration with a 500 kW PV array. The solar generation is from an average summer day. The power generation is for the power demand from Figure A.200. The minor fluctuations of the power profile are being peak shaven by the Na-ion battery.

Figure A.222: Figure of the Na-ion battery output power of the Na-ion version of the HE PV shore power configuration with 500 kW PV array. The Na-ion battery peak shaves the minor fluctuations of the power demand of Figure A.200.

Figure A.223: Figure of the power generation of the Na-ion version of the HE PV shore power configuration with a 700 kW PV array. The solar generation is from an average summer day. The power generation is for the power demand from Figure A.200. The minor fluctuations of the power profile are being peak shaven by the Na-ion battery.
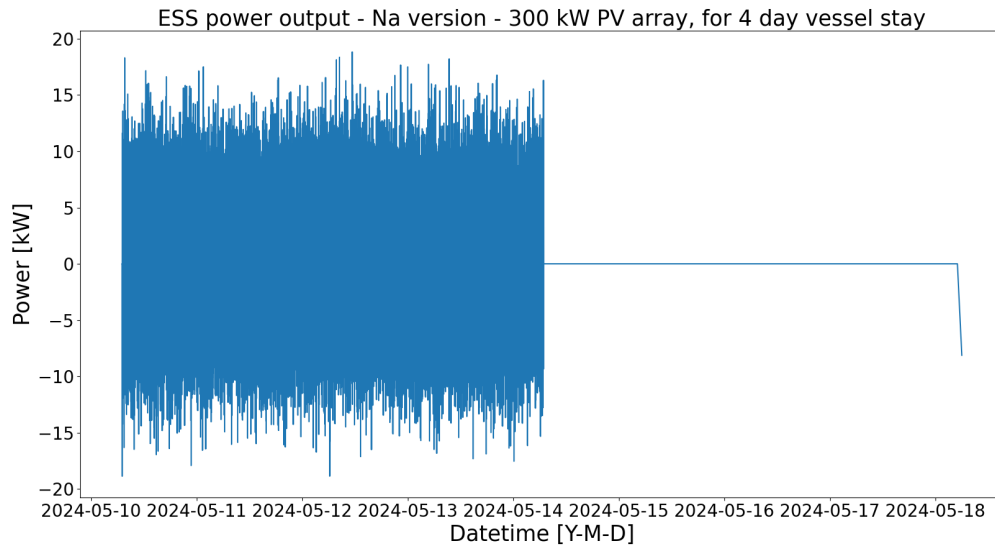
Figure A.224: Figure of the Na-ion battery output power of the Na-ion version of the HE PV shore power configuration with 700 kW PV array. The Na-ion battery peak shaves the minor fluctuations of the power demand of Figure A.200.
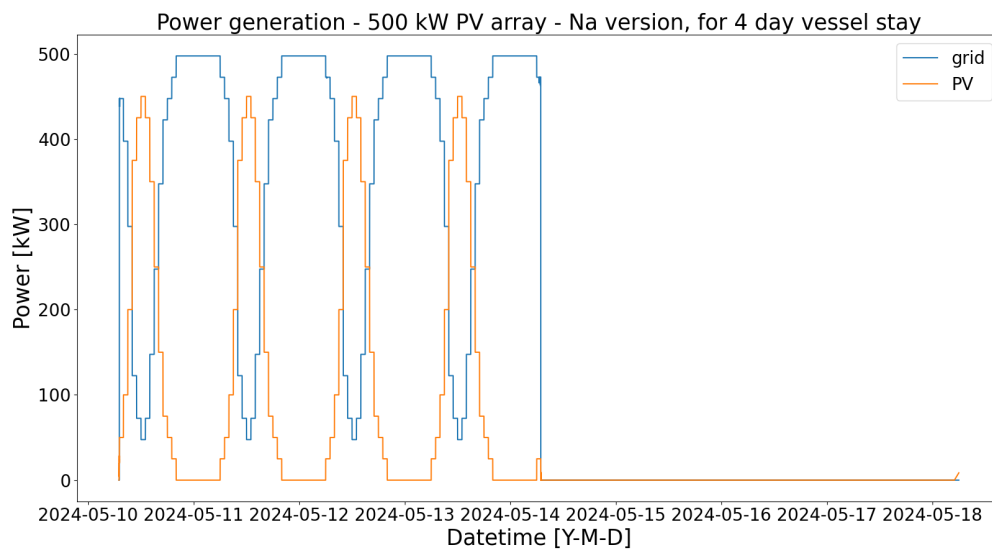

Figure A.225: Figure of the power generation of the Na-ion version of the HE PV shore power configuration with a 1000 kW PV array. The solar generation is from an average summer day. The power generation is for the power demand from Figure A.200. The minor fluctuations of the power profile are being peak shaven by the Na-ion battery.
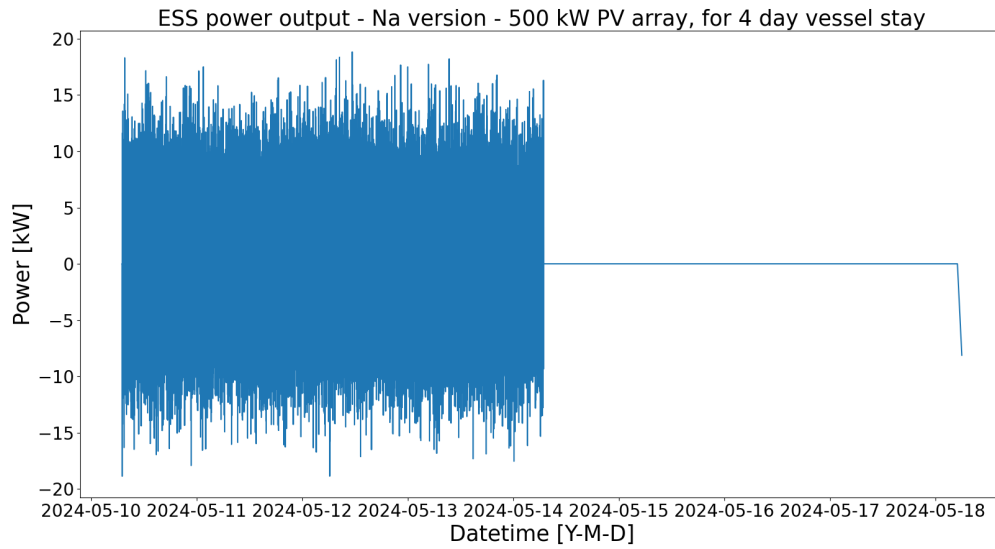
Figure A.226: Figure of the Na-ion battery output power of the Na-ion version of the HE PV shore power configuration with 1000 kW PV array. The Na-ion battery peak shaves the minor fluctuations of the power demand of Figure A.200.
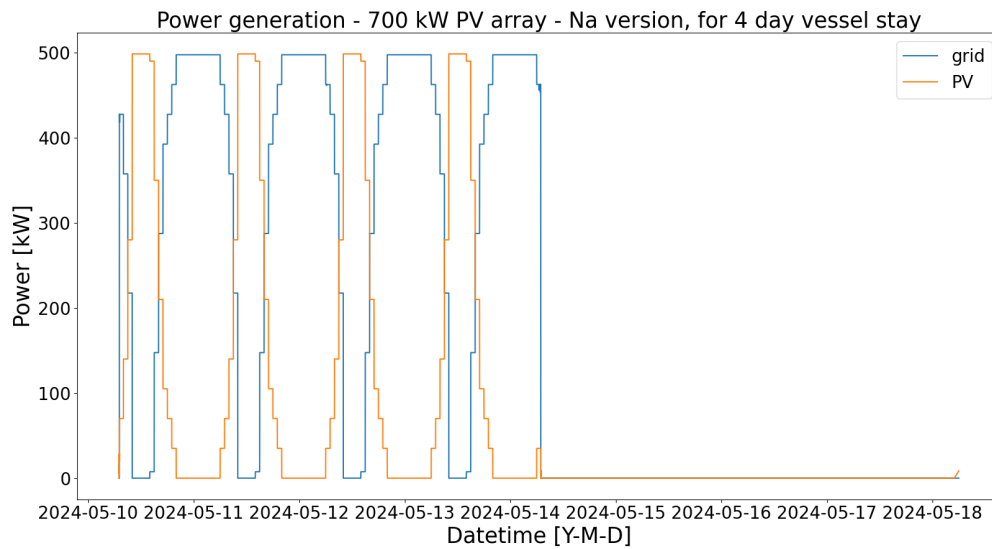

Figure A.227: Figure of the SOC of the Na-ion battery of the Na-ion version of the HE PV shore power configuration. The plot includes different implementations using different sizes of PV array. All the different implementations discharge in the same exact way.

A.5.5. HE PV for 4 day vessel stay
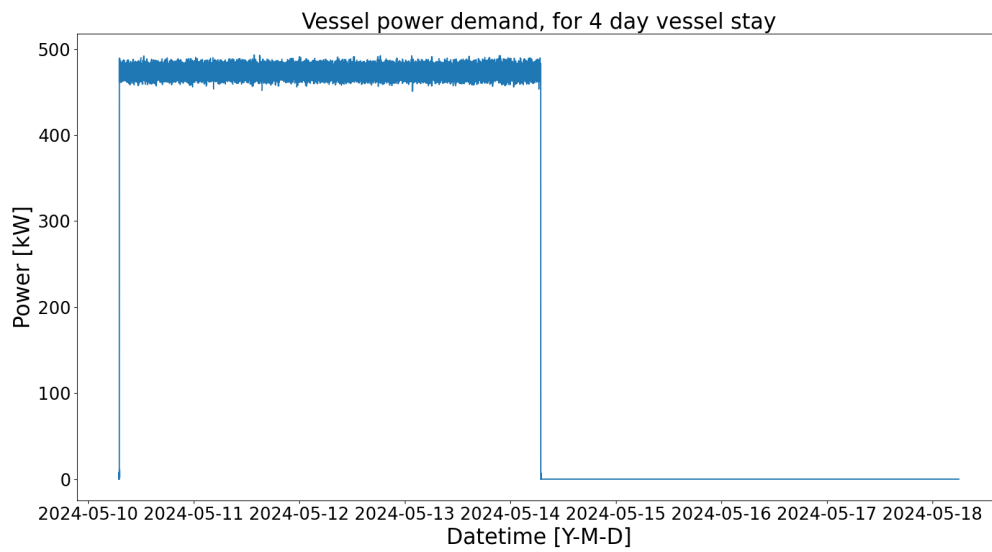
Figure A.228: Figure of the vessel power profile of 4 days and 4 days of downtime. The power demand has no crane uses. The vessel power profile was used for the HE PV shore power configuration. The x-axis is in datetime, meaning that every data point is fixed to a date and time.

Figure A.229: Figure of the power generation of the LFP version of the HE PV shore power configuration with a 300 kW PV array. The solar generation is from an average summer day. The power generation is for the power demand from Figure A.228. The minor fluctuations of the power profile are being peak shaven by the LFP battery.
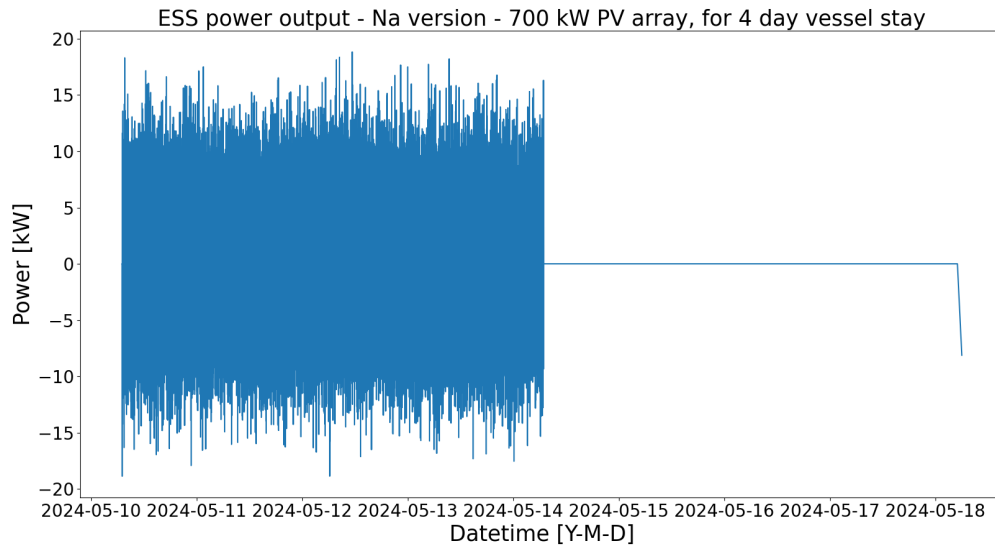
Figure A.230: Figure of the LFP battery output power of the LFP version of the HE PV shore power configuration with 300 kW PV array. The LFP battery peak shaves the minor fluctuations of the power demand of Figure A.228.
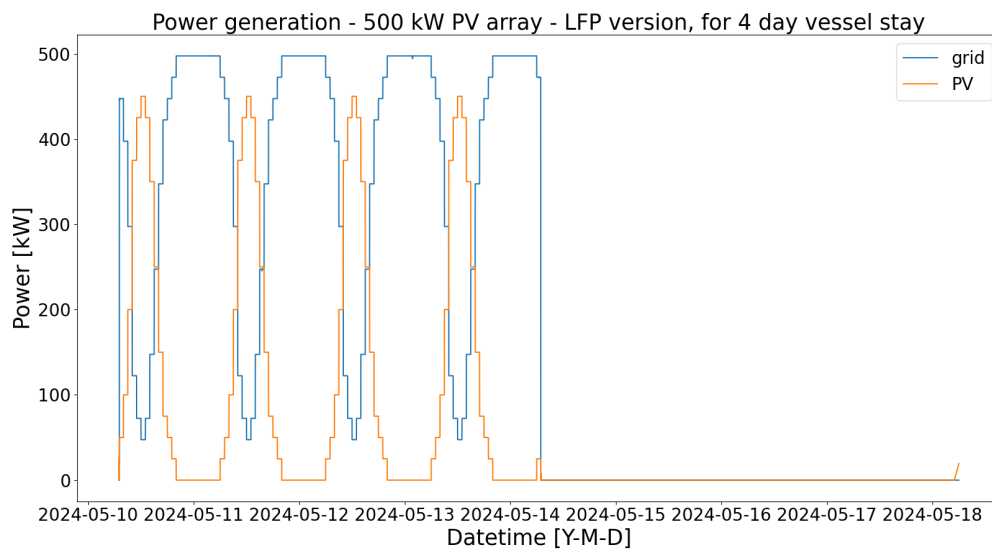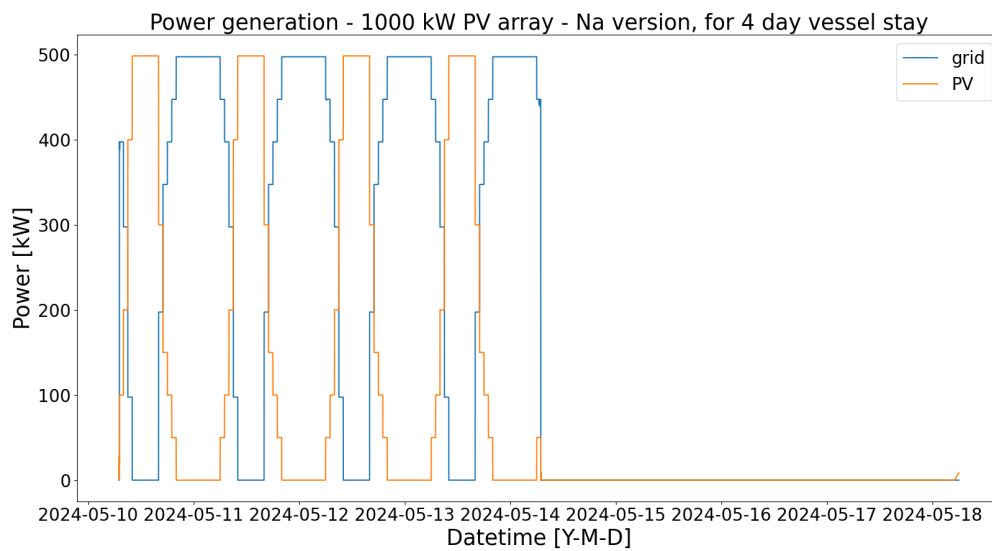

Figure A.231: Figure of the power generation of the LFP version of the HE PV shore power configuration with a 500 kW PV array. The solar generation is from an average summer day. The power generation is for the power demand from Figure A.228. The minor fluctuations of the power profile are being peak shaven by the LFP battery.
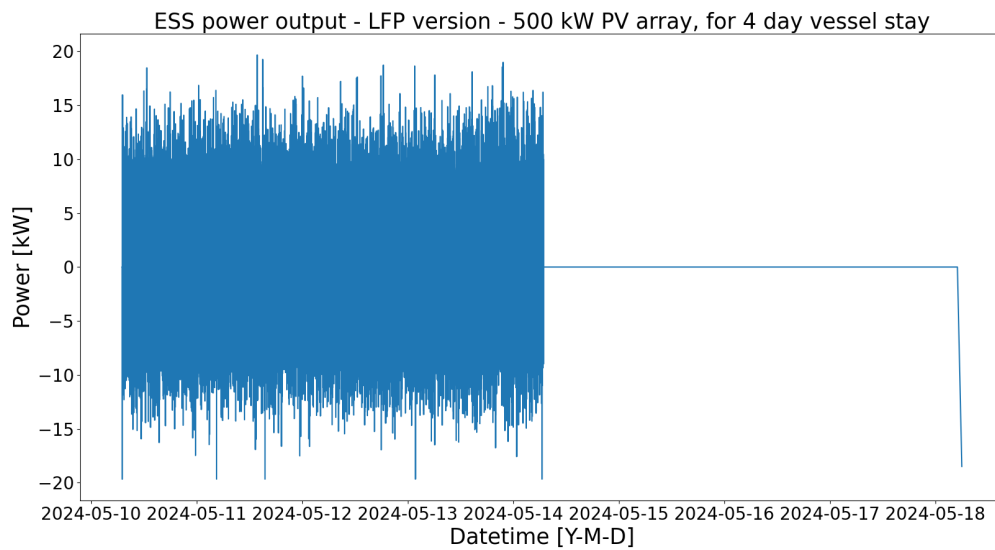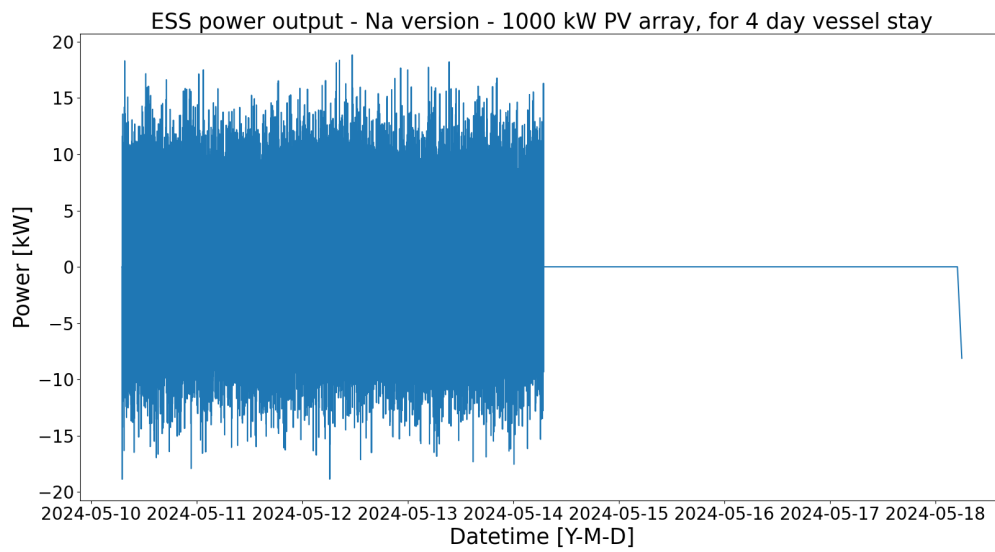
Figure A.232: Figure of the LFP battery output power of the LFP version of the HE PV shore power configuration with 500 kW PV array. The LFP battery peak shaves the minor fluctuations of the power demand of Figure A.228.

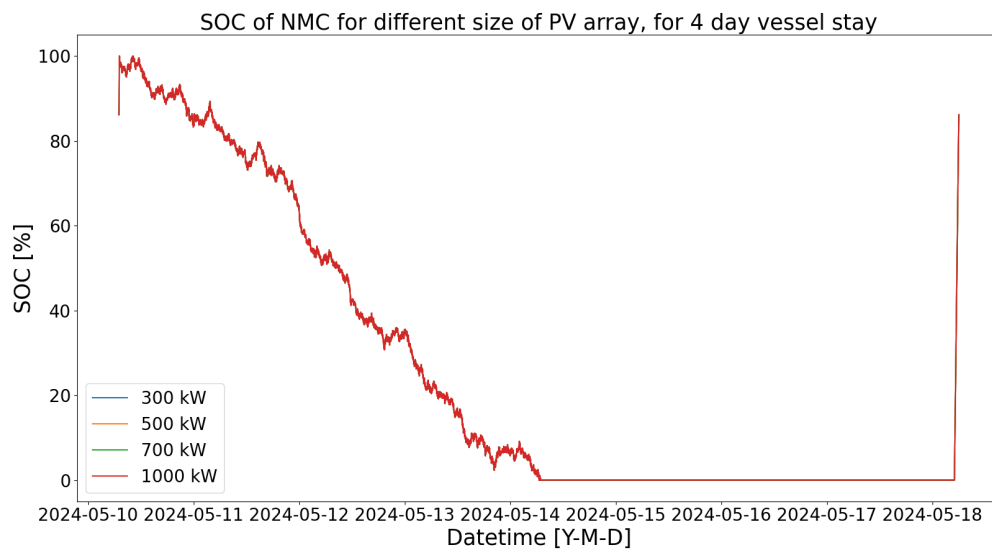**Figure A.233:** Figure of the power generation of the LFP version of the HE PV shore power configuration with a 700 kW PV array. The solar generation is from an average summer day. The power generation is for the power demand from Figure A.228. The minor fluctuations of the power profile are being peak shaven by the LFP battery.

Figure A.234: Figure of the LFP battery output power of the LFP version of the HE PV shore power configuration with 700 kW PV array. The LFP battery peak shaves the minor fluctuations of the power demand of Figure A.228.

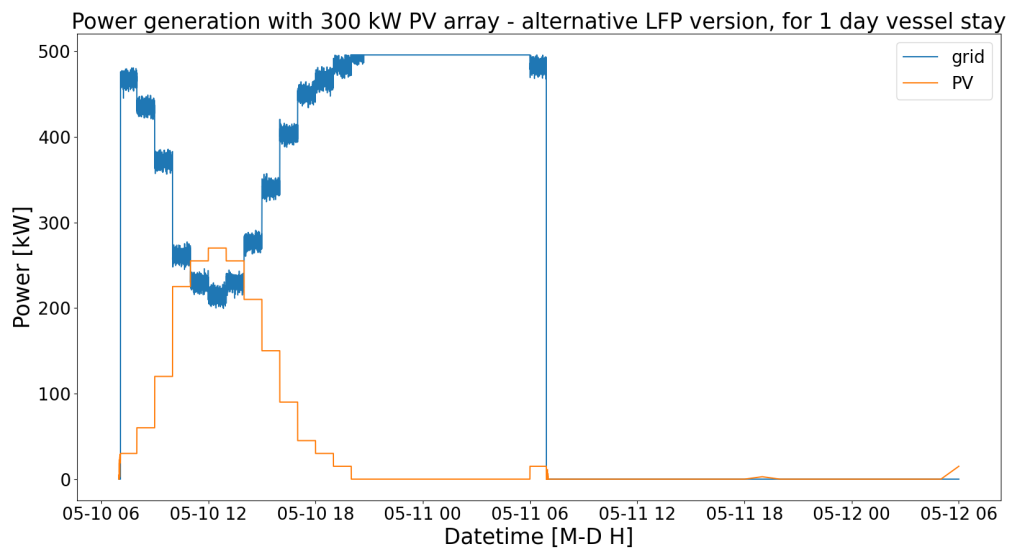**Figure A.235:** Figure of the power generation of the LFP version of the HE PV shore power configuration with a 1000 kW PV array. The solar generation is from an average summer day. The power generation is for the power demand from Figure A.228. The minor fluctuations of the power profile are being peak shaven by the LFP battery.
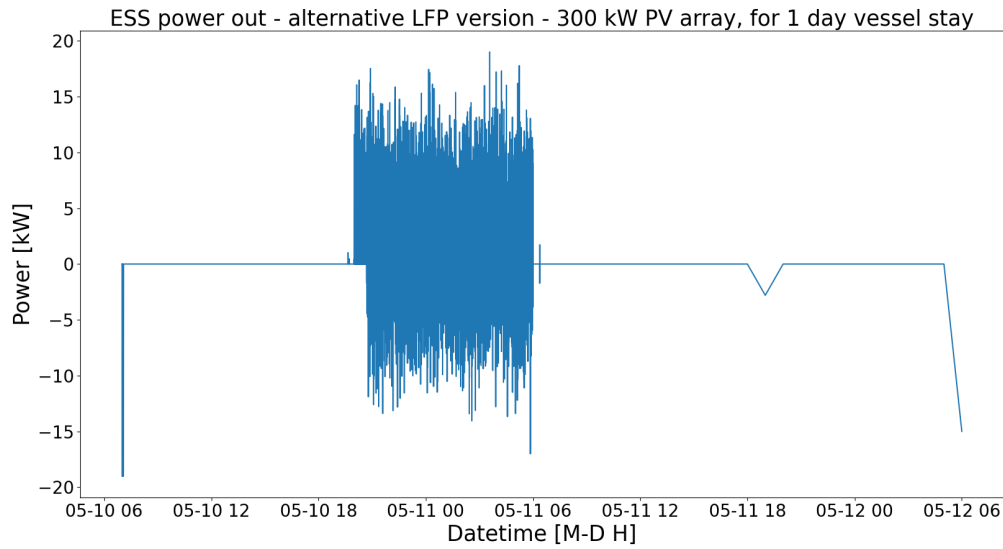
Figure A.236: Figure of the LFP battery output power of the LFP version of the HE PV shore power configuration with 1000 kW PV array. The LFP battery peak shaves the minor fluctuations of the power demand of Figure A.228.

Figure A.237: Figure of the SOC of the LFP battery of the LFP version of the HE PV shore power configuration. The plot includes different implementations using different sizes of PV array. All the different implementations discharge in the same exact way.
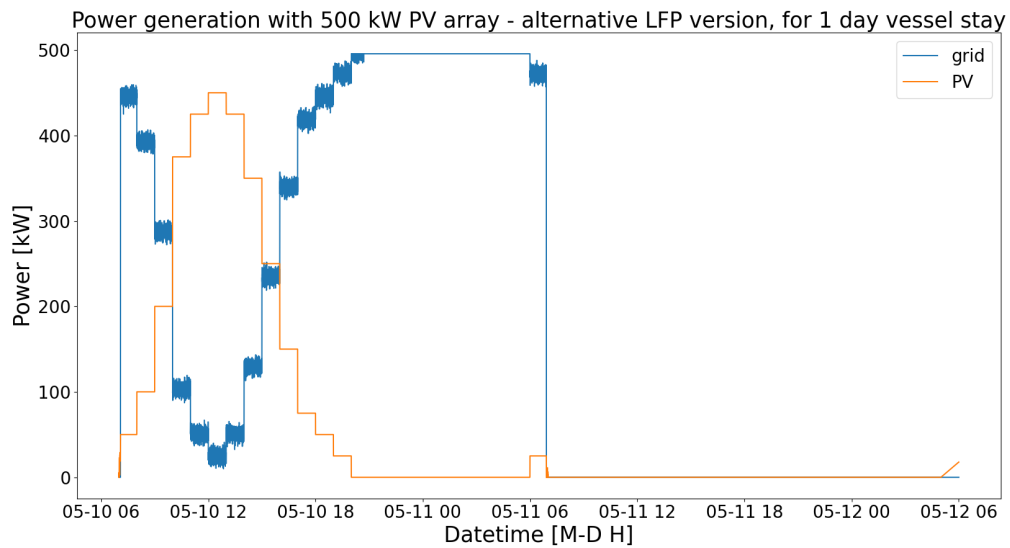
Figure A.238: Figure of the power generation of the NMC version of the HE PV shore power configuration with a 300 kW PV array. The solar generation is from an average summer day. The power generation is for the power demand from Figure A.228. The minor fluctuations of the power profile are being peak shaven by the NMC battery.

Figure A.239: Figure of the NMC battery output power of the NMC version of the HE PV shore power configuration with 300 kW PV array. The NMC battery peak shaves the minor fluctuations of the power demand of Figure A.228.

Figure A.240: Figure of the power generation of the NMC version of the HE PV shore power configuration with a 500 kW PV array. The solar generation is from an average summer day. The power generation is for the power demand from Figure A.228. The minor fluctuations of the power profile are being peak shaven by the NMC battery.
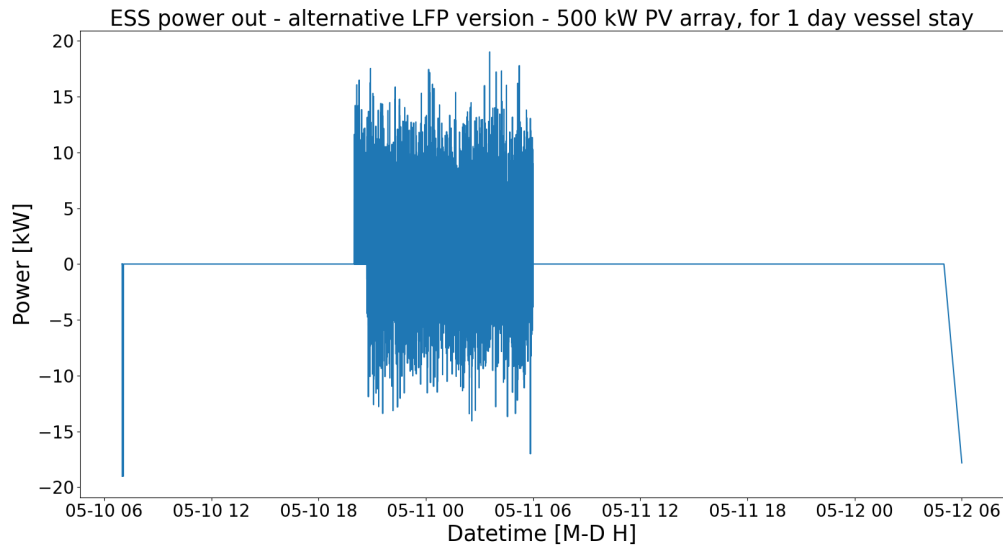

Figure A.241: Figure of the NMC battery output power of the NMC version of the HE PV shore power configuration with 500 kW PV array. The NMC battery peak shaves the minor fluctuations of the power demand of Figure A.228.

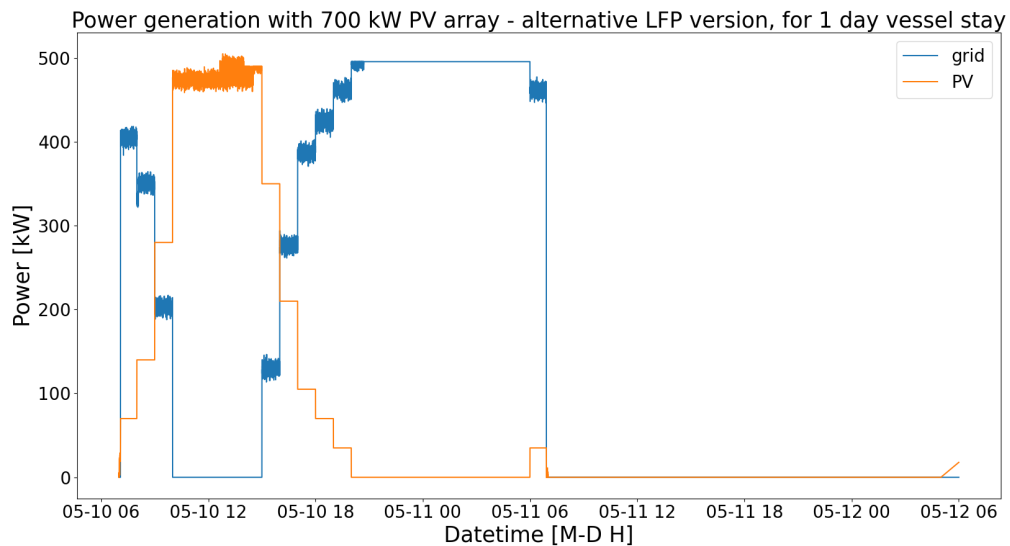**Figure A.242:** Figure of the power generation of the NMC version of the HE PV shore power configuration with a 700 kW PV array. The solar generation is from an average summer day. The power generation is for the power demand from Figure A.228. The minor fluctuations of the power profile are being peak shaven by the NMC battery.
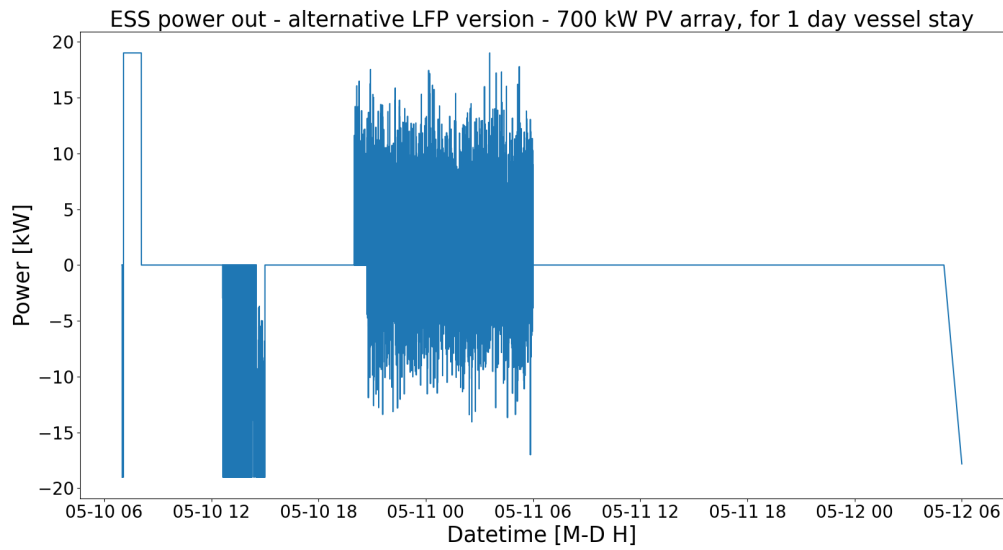

Figure A.243: Figure of the NMC battery output power of the NMC version of the HE PV shore power configuration with 700 kW PV array. The NMC battery peak shaves the minor fluctuations of the power demand of Figure A.228.
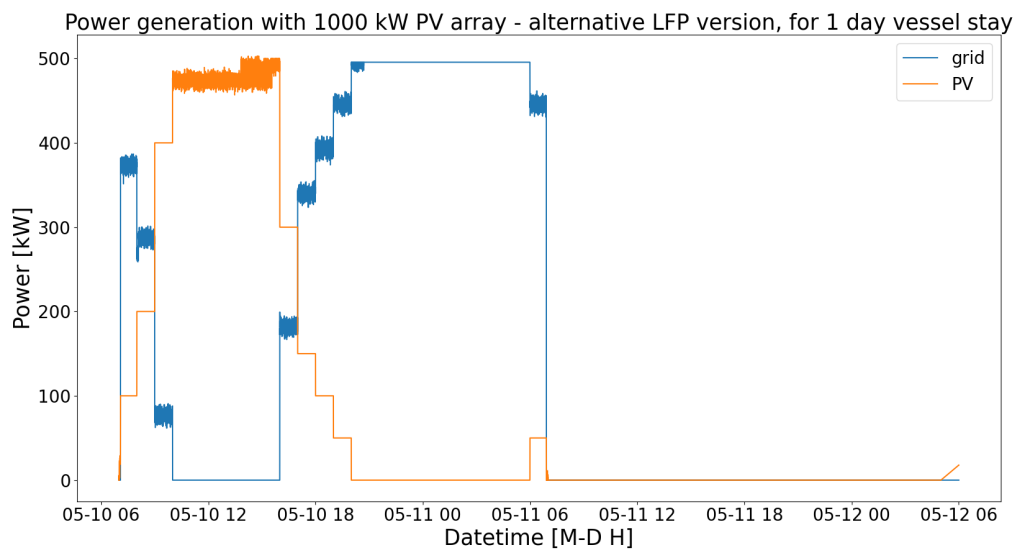
Figure A.244: Figure of the power generation of the NMC version of the HE PV shore power configuration with a 1000 kW PV array. The solar generation is from an average summer day. The power generation is for the power demand from Figure A.228. The minor fluctuations of the power profile are being peak shaven by the NMC battery.

Figure A.245: Figure of the NMC battery output power of the NMC version of the HE PV shore power configuration with 1000 kW PV array. The NMC battery peak shaves the minor fluctuations of the power demand of Figure A.228.

Figure A.246: Figure of the SOC of the NMC battery of the NMC version of the HE PV shore power configuration. The plot includes different implementations using different sizes of PV array. All the different implementations discharge in the same exact way.

Figure A.247: Figure of the power generation of the Na-ion version of the HE PV shore power configuration with a 300 kW PV array. The solar generation is from an average summer day. The power generation is for the power demand from Figure A.228. The minor fluctuations of the power profile are being peak shaven by the Na-ion battery.

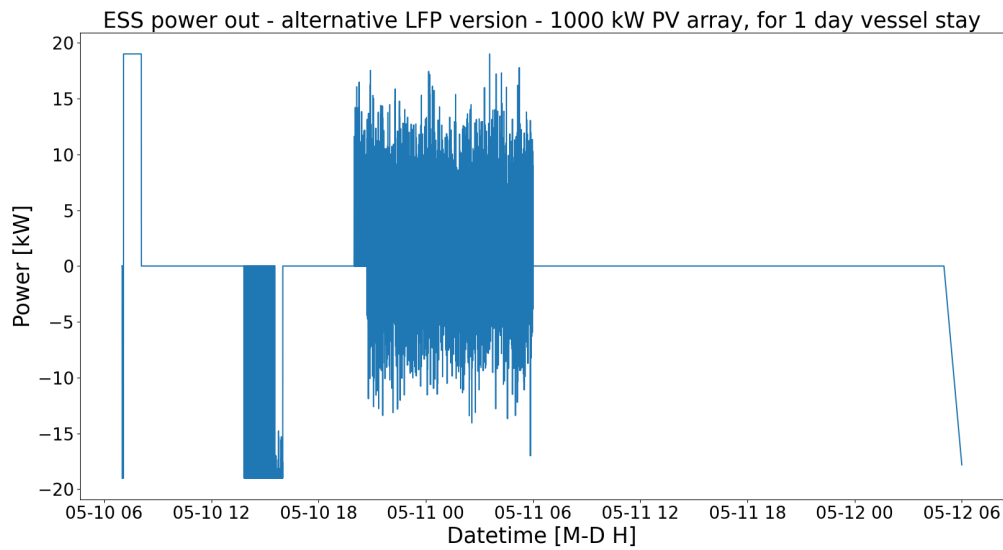**Figure A.248:** Figure of the Na-ion battery output power of the Na-ion version of the HE PV shore power configuration with 300 kW PV array. The Na-ion battery peak shaves the minor fluctuations of the power demand of Figure A.228.

Figure A.249: Figure of the power generation of the Na-ion version of the HE PV shore power configuration with a 500 kW PV array. The solar generation is from an average summer day. The power generation is for the power demand from Figure A.228. The minor fluctuations of the power profile are being peak shaven by the Na-ion battery.

Figure A.250: Figure of the Na-ion battery output power of the Na-ion version of the HE PV shore power configuration with 500 kW PV array. The Na-ion battery peak shaves the minor fluctuations of the power demand of Figure A.228.
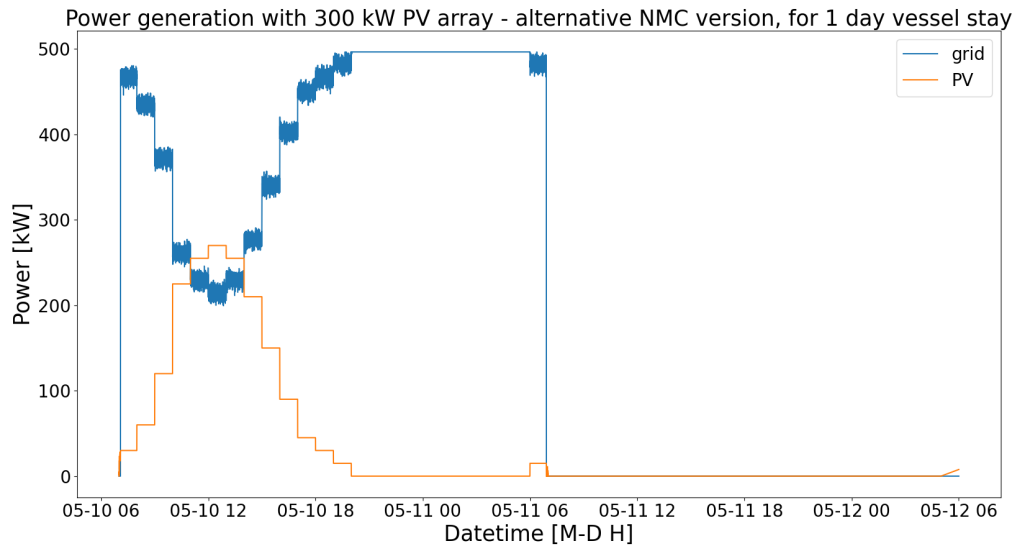

Figure A.251: Figure of the power generation of the Na-ion version of the HE PV shore power configuration with a 700 kW PV array. The solar generation is from an average summer day. The power generation is for the power demand from Figure A.228. The minor fluctuations of the power profile are being peak shaven by the Na-ion battery.

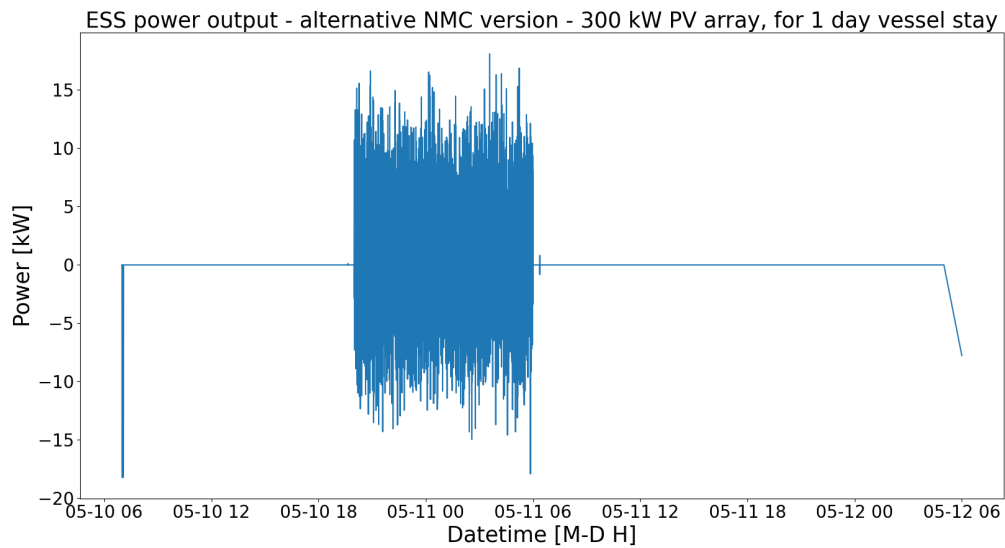**Figure A.252:** Figure of the Na-ion battery output power of the Na-ion version of the HE PV shore power configuration with 700 kW PV array. The Na-ion battery peak shaves the minor fluctuations of the power demand of Figure A.228.
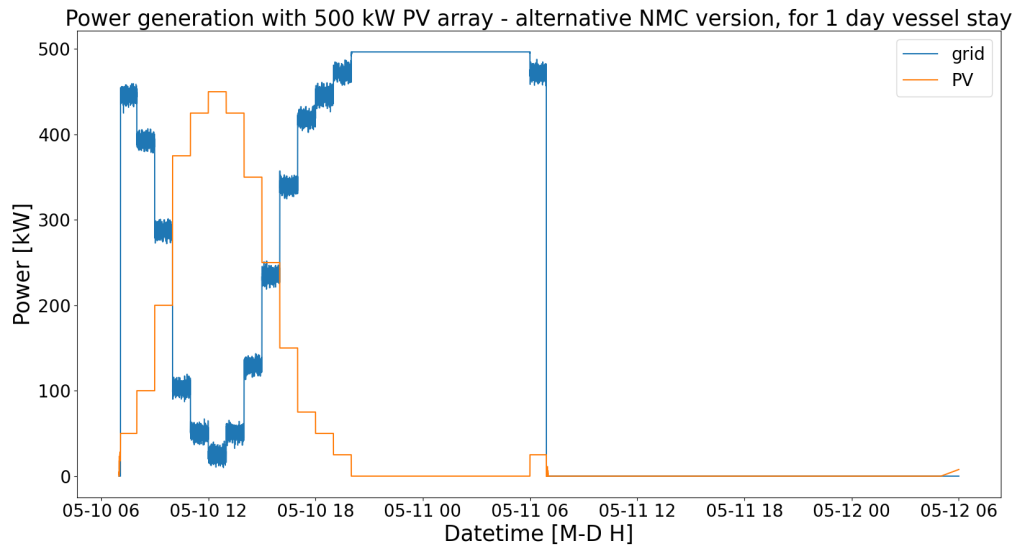

Figure A.253: Figure of the power generation of the Na-ion version of the HE PV shore power configuration with a 1000 kW PV array. The solar generation is from an average summer day. The power generation is for the power demand from Figure A.228. The minor fluctuations of the power profile are being peak shaven by the Na-ion battery.
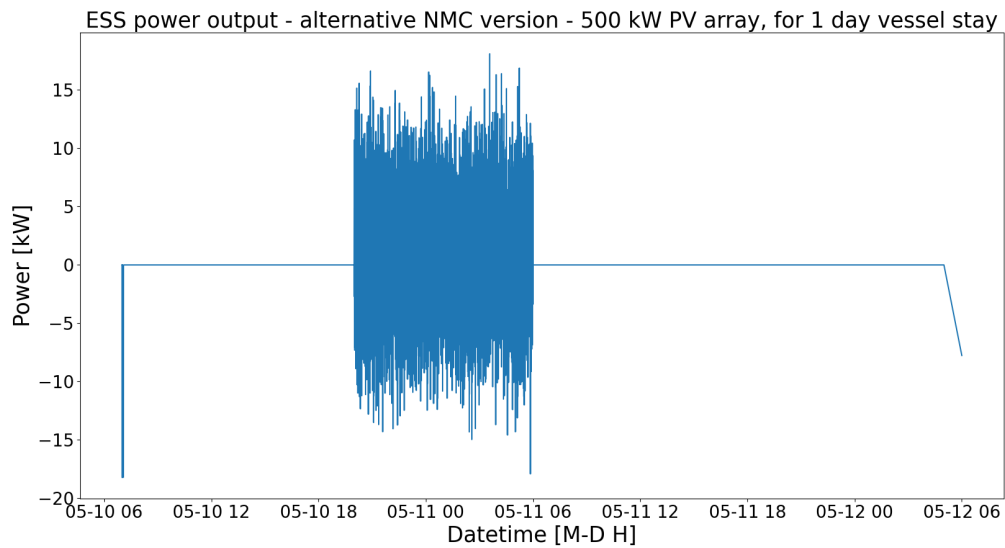
Figure A.254: Figure of the Na-ion battery output power of the Na-ion version of the HE PV shore power configuration with 1000 kW PV array. The Na-ion battery peak shaves the minor fluctuations of the power demand of Figure A.228.

Figure A.255: Figure of the SOC of the Na-ion battery of the Na-ion version of the HE PV shore power configuration. The plot includes different implementations using different sizes of PV array. All the different implementations discharge in the same exact way.

A.5.6. Alternative HE PV
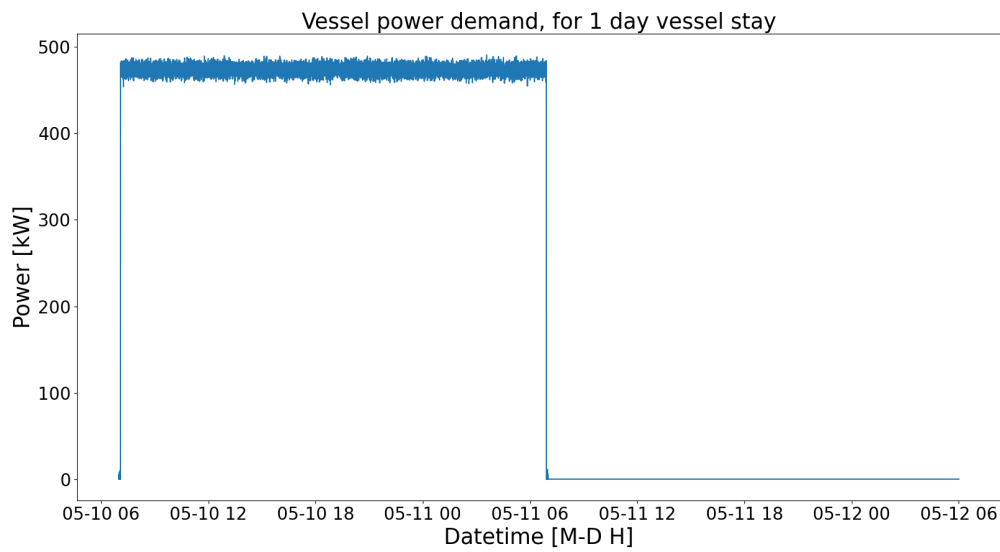
Figure A.256: Figure of the vessel power profile of 1 day and 1 day of downtime. The power demand has no crane uses. The vessel power profile was used for the alternative HE PV shore power configuration. The x-axis is in datetime, meaning that every data point is fixed to a date and time.

Figure A.257: Figure of the power generation of the LFP version of the alternative HE PV shore power configuration with a 300 kW PV array. The solar generation is from an average summer day. The power generation is for the power demand from Figure A.256. The minor fluctuations of the power profile are being peak shaven by the LFP battery when the sun is down.

Figure A.258: Figure of the LFP battery output power of the LFP version of the alternative HE PV shore power configuration with 300 kW PV array. The LFP battery peak shaves the minor fluctuations of the power demand of Figure A.256 when the sun is down.
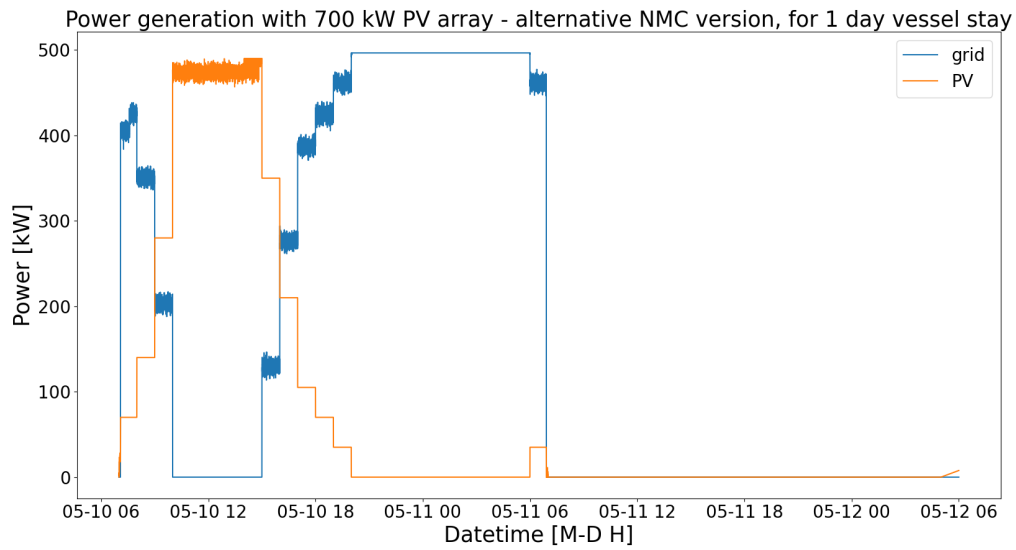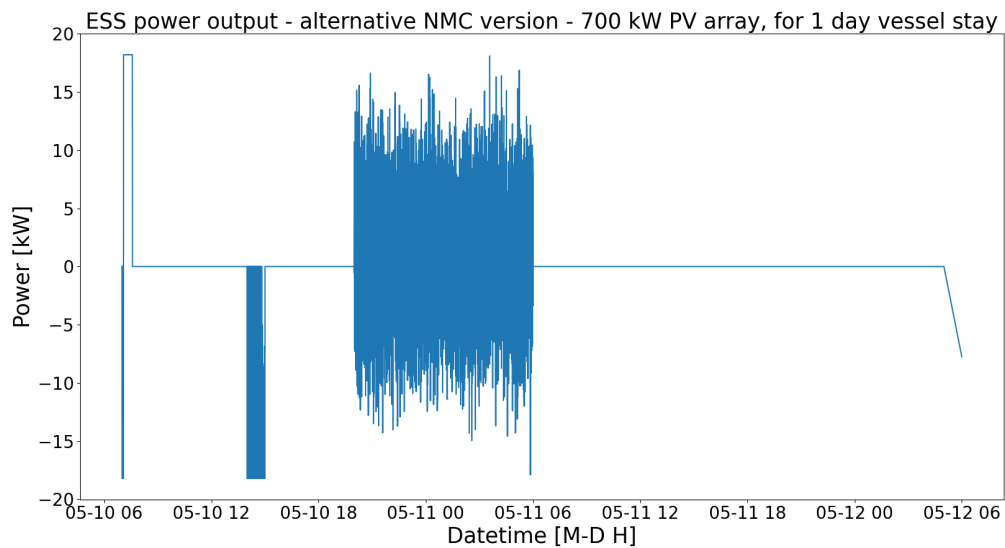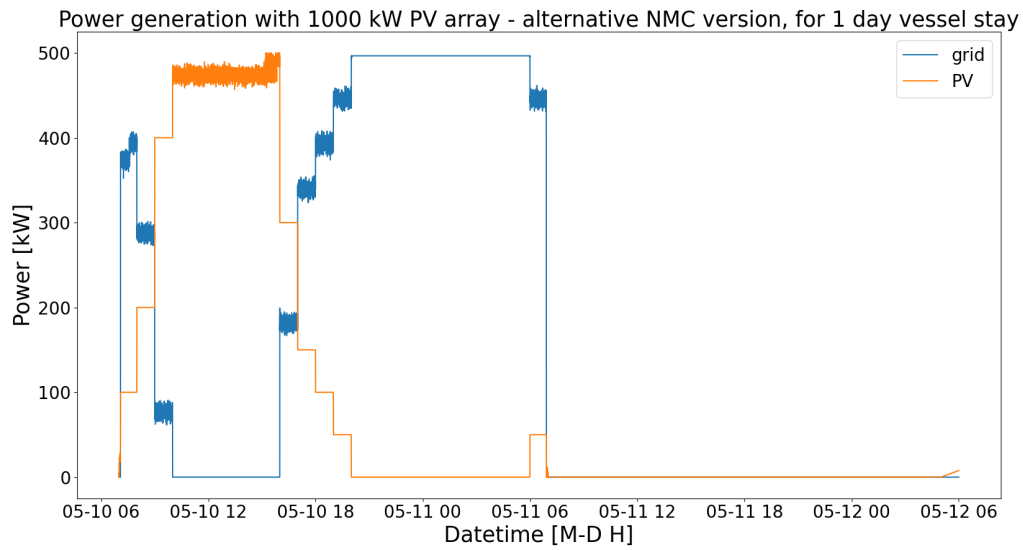

Figure A.259: Figure of the power generation of the LFP version of the alternative HE PV shore power configuration with a 500 kW PV array. The solar generation is from an average summer day. The power generation is for the power demand from Figure A.256. The minor fluctuations of the power profile are being peak shaven by the LFP battery when the sun is down.

Figure A.260: Figure of the LFP battery output power of the LFP version of the alternative HE PV shore power configuration with 500 kW PV array. The LFP battery peak shaves the minor fluctuations of the power demand of Figure A.256 when the sun is down.

Figure A.261: Figure of the power generation of the LFP version of the alternative HE PV shore power configuration with a 700 kW PV array. The solar generation is from an average summer day. The power generation is for the power demand from Figure A.256. The minor fluctuations of the power profile are being peak shaven by the LFP battery when the sun is down.
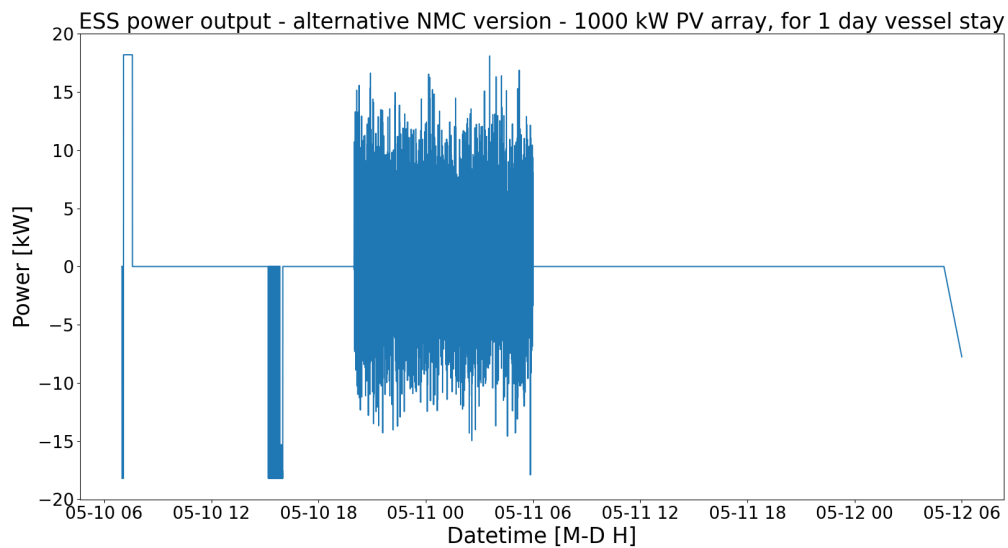
Figure A.262: Figure of the LFP battery output power of the LFP version of the alternative HE PV shore power configuration with 700 kW PV array. The LFP battery peak shaves the minor fluctuations of the power demand of Figure A.256 when the sun is down. And the ESS is charged up during the day, just before the solar generation starts to dip below the power demand of the vessel.
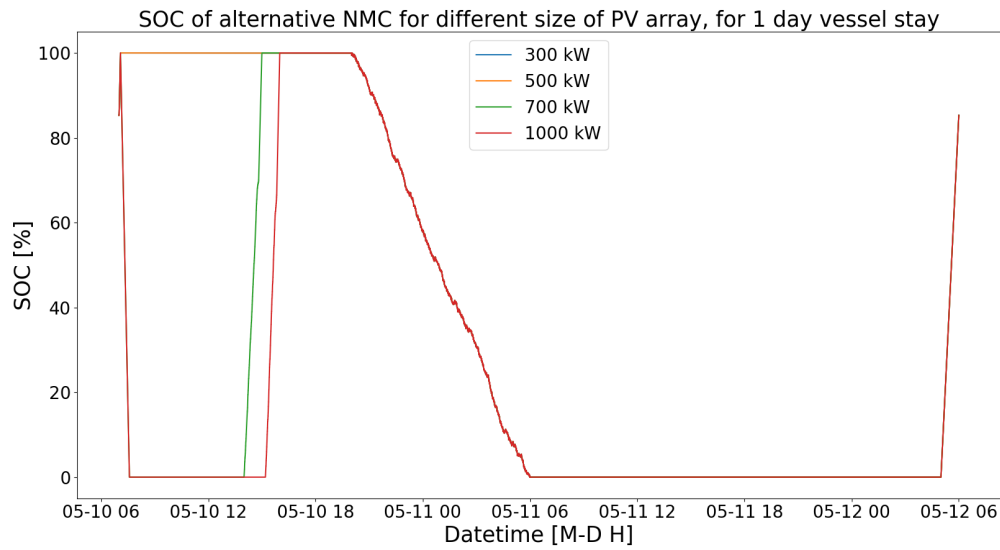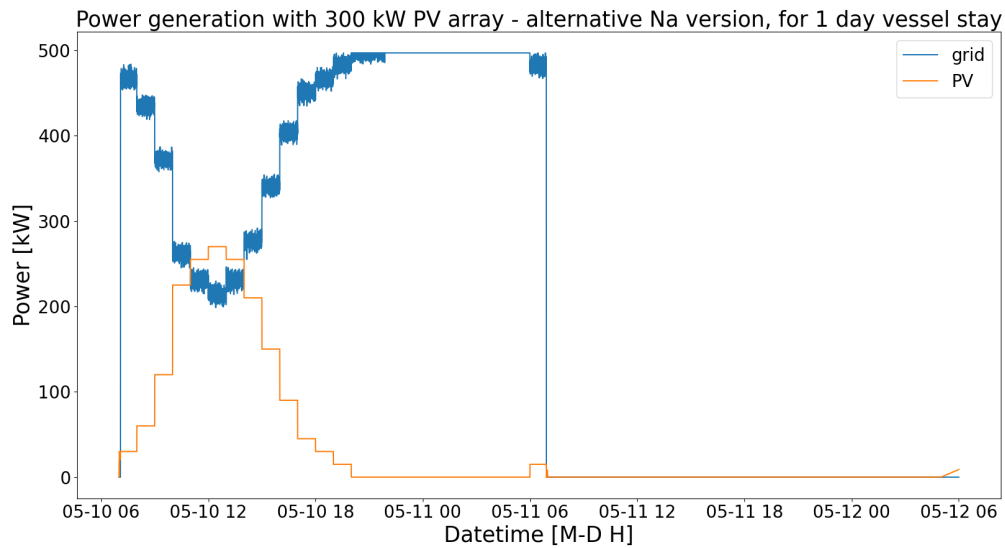

Figure A.263: Figure of the power generation of the LFP version of the alternative HE PV shore power configuration with a 1000 kW PV array. The solar generation is from an average summer day. The power generation is for the power demand from Figure A.256. The minor fluctuations of the power profile are being peak shaven by the LFP battery when the sun is down.

Figure A.264: Figure of the LFP battery output power of the LFP version of the alternative HE PV shore power configuration with 1000 kW PV array. The LFP battery peak shaves the minor fluctuations of the power demand of Figure A.256 when the sun is down. And the ESS is charged up during the day, just before the solar generation starts to dip below the power demand of the vessel.
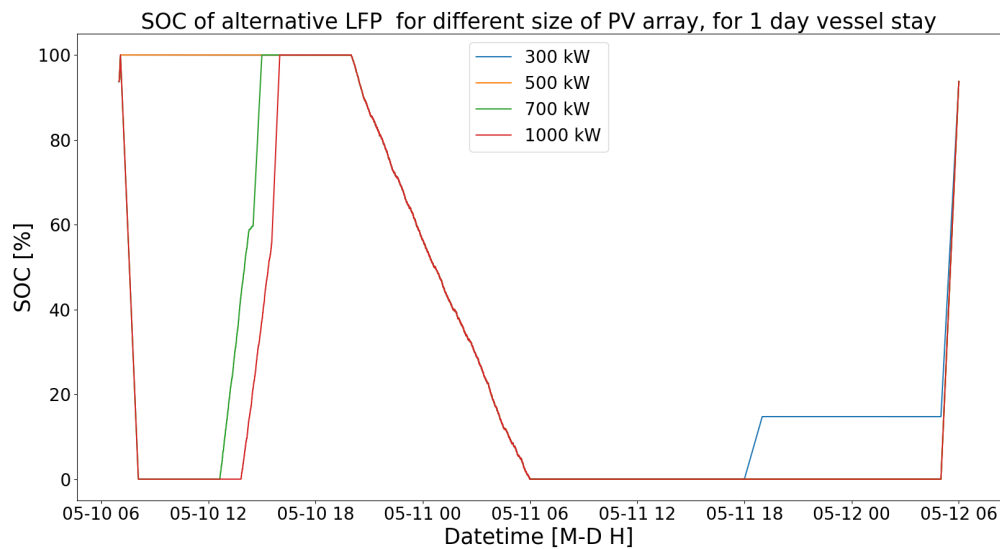
Figure A.265: Figure of the SOC of the LFP battery of the LFP version of the alternative HE PV shore power configuration. The plot includes different implementations using different sizes of PV array. If the solar generation is higher than the demand of the vessel, the ESS can be charged just before the solar generation dips below the power demand of the vessel. Otherwise, the ESS is charged beforehand.

Power generation with 300 kW PV array - alternative NMC version, for 1 day vessel stay

Figure A.266: Figure of the power generation of the NMC version of the alternative HE PV shore power configuration with a 300 kW PV array. The solar generation is from an average summer day. The power generation is for the power demand from Figure A.256. The minor fluctuations of the power profile are being peak shaven by the NMC battery when the sun is down.

ESS power output - alternative NMC version - 300 kW PV array, for 1 day vessel stay

Figure A.267: Figure of the NMC battery output power of the NMC version of the alternative HE PV shore power configuration with 300 kW PV array. The NMC battery peak shaves the minor fluctuations of the power demand of Figure A.256 when the sun is down.

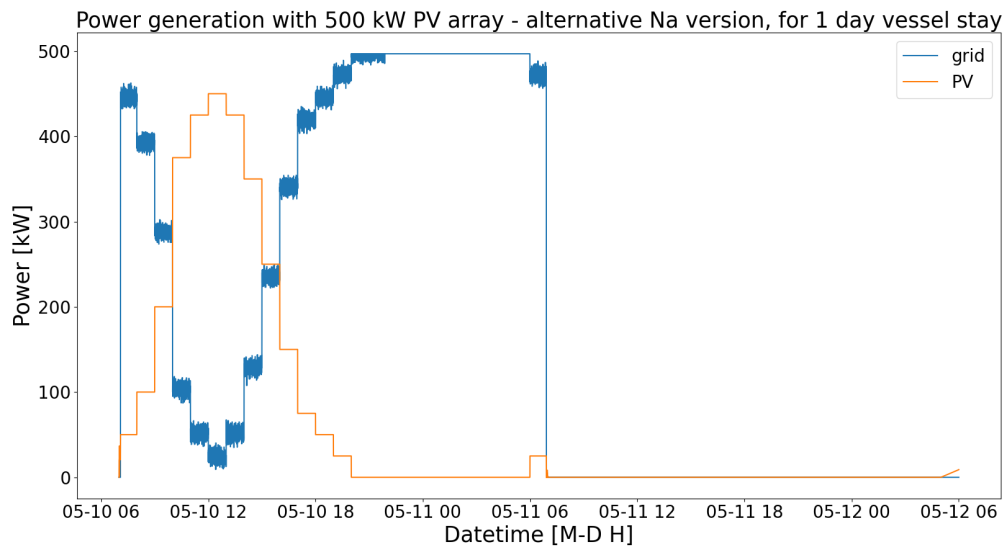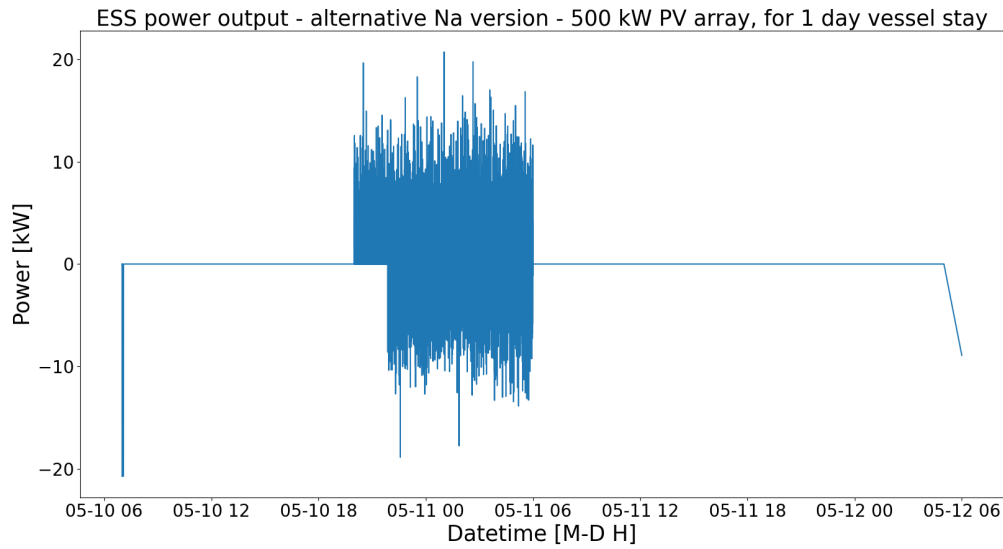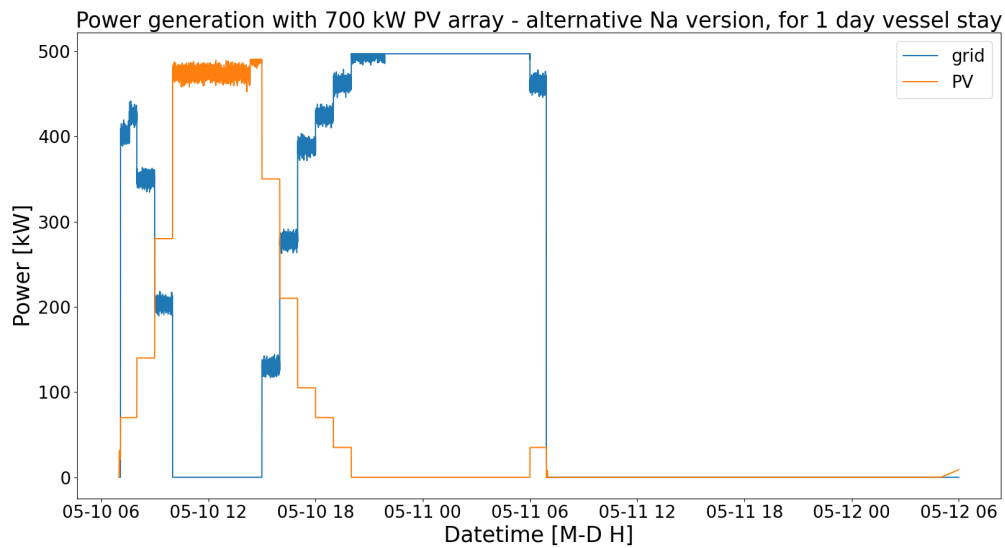**Figure A.268:** Figure of the power generation of the NMC version of the alternative HE PV shore power configuration with a 500 kW PV array. The solar generation is from an average summer day. The power generation is for the power demand from Figure A.256. The minor fluctuations of the power profile are being peak shaven by the NMC battery when the sun is down.

Figure A.269: Figure of the NMC battery output power of the NMC version of the alternative HE PV shore power configuration with 500 kW PV array. The NMC battery peak shaves the minor fluctuations of the power demand of Figure A.256 when the sun is down.

Figure A.270: Figure of the power generation of the NMC version of the alternative HE PV shore power configuration with a 700 kW PV array. The solar generation is from an average summer day. The power generation is for the power demand from Figure A.256. The minor fluctuations of the power profile are being peak shaven by the NMC battery when the sun is down.
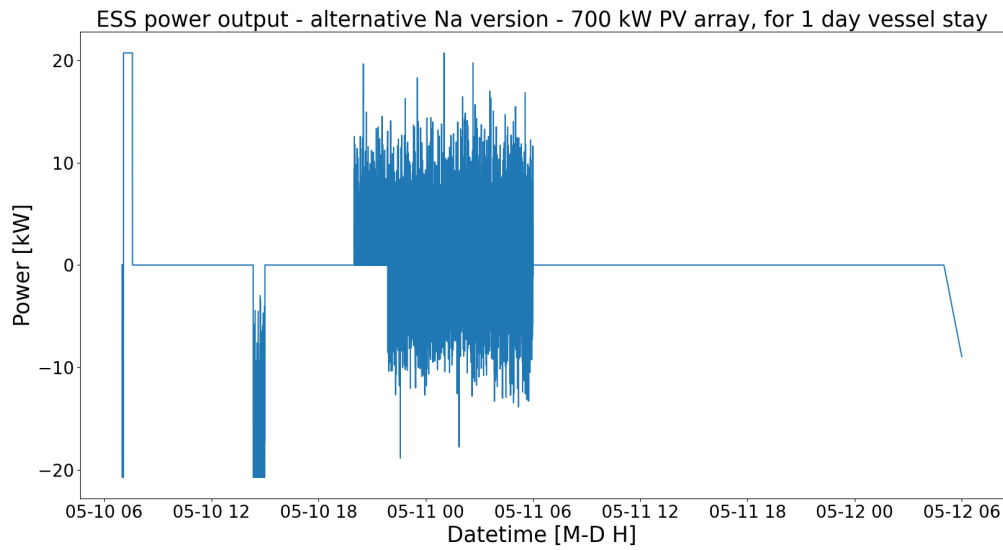

Figure A.271: Figure of the NMC battery output power of the NMC version of the alternative HE PV shore power configuration with 700 kW PV array. The NMC battery peak shaves the minor fluctuations of the power demand of Figure A.256 when the sun is down. And the ESS is charged up during the day, just before the solar generation starts to dip below the power demand of the vessel.
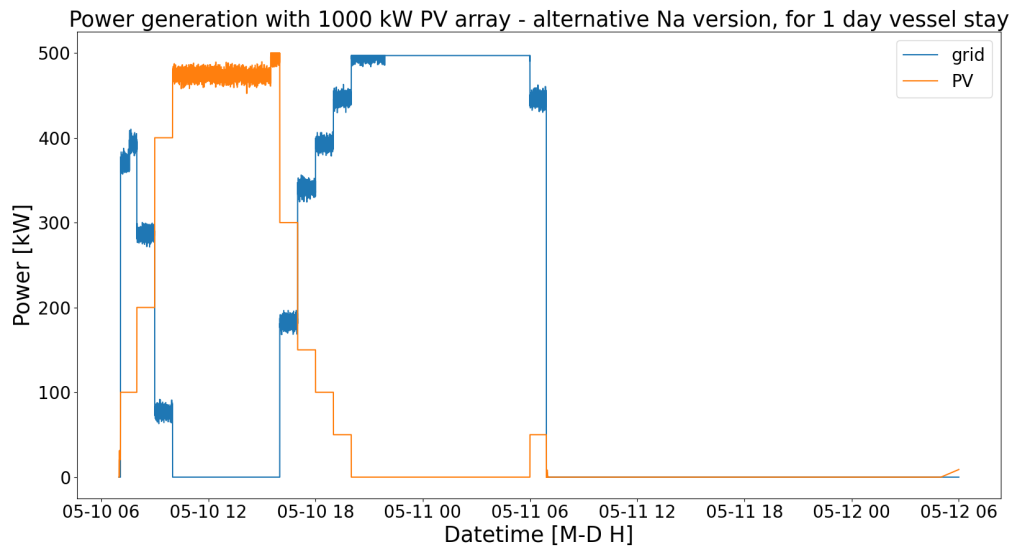
Figure A.272: Figure of the power generation of the NMC version of the alternative HE PV shore power configuration with a 1000 kW PV array. The solar generation is from an average summer day. The power generation is for the power demand from Figure A.256. The minor fluctuations of the power profile are being peak shaven by the NMC battery when the sun is down.
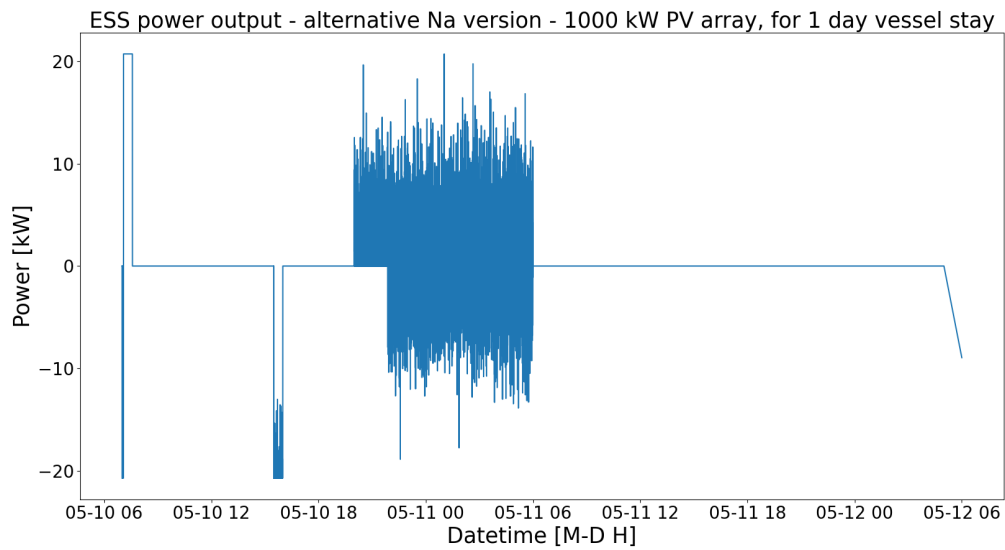

Figure A.273: Figure of the NMC battery output power of the NMC version of the alternative HE PV shore power configuration with 1000 kW PV array. The NMC battery peak shaves the minor fluctuations of the power demand of Figure A.256 when the sun is down. And the ESS is charged up during the day, just before the solar generation starts to dip below the power demand of the vessel.
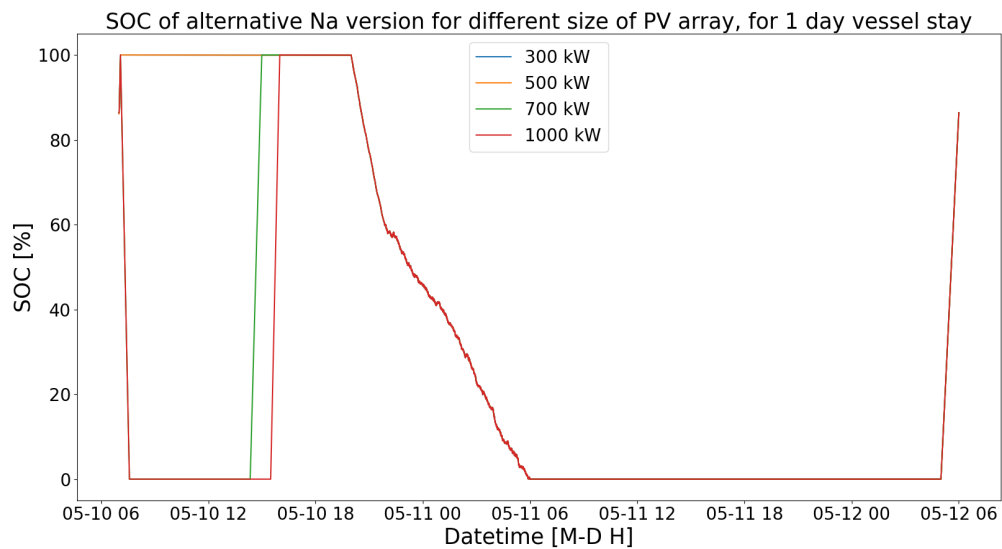
Figure A.274: Figure of the SOC of the NMC battery of the NMC version of the alternative HE PV shore power configuration. The plot includes different implementations using different sizes of PV array. If the solar generation is higher than the demand of the vessel, the ESS can be charged just before the solar generation dips below the power demand of the vessel. Otherwise, the ESS is charged beforehand.
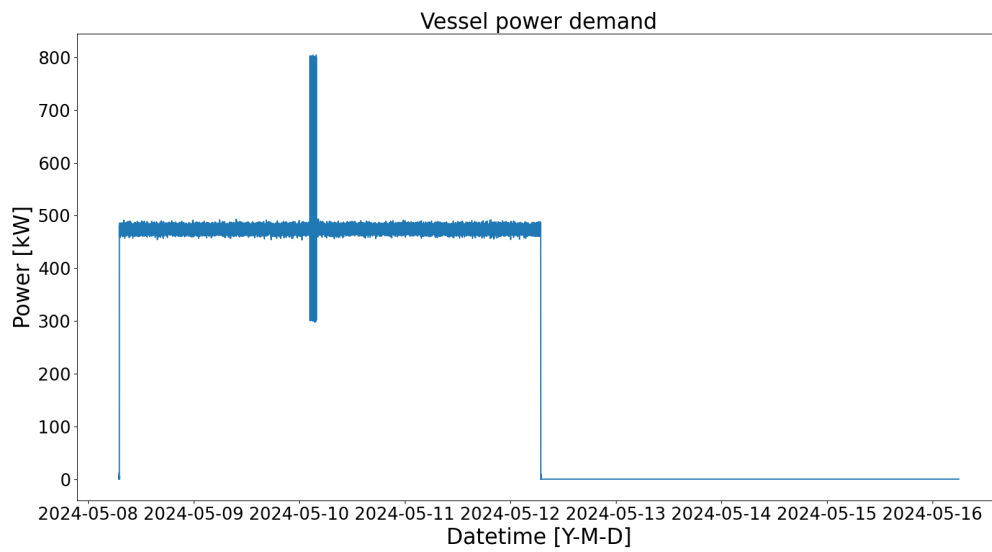

Figure A.275: Figure of the power generation of the Na-ion version of the alternative HE PV shore power configuration with a 300 kW PV array. The solar generation is from an average summer day. The power generation is for the power demand from Figure A.256. The minor fluctuations of the power profile are being peak shaven by the Na-ion battery when the sun is down.
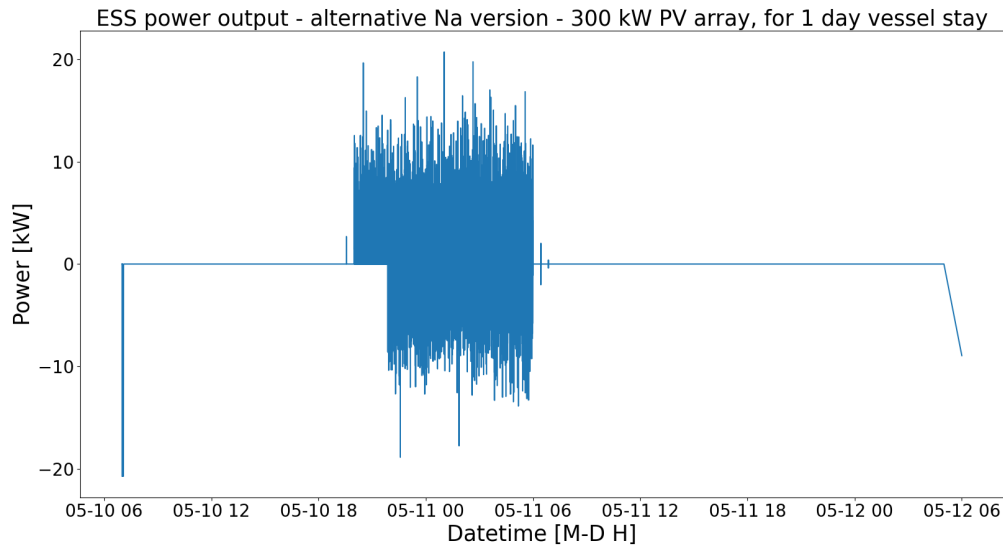
Figure A.276: Figure of the Na-ion battery output power of the Na-ion version of the alternative HE PV shore power configuration with 300 kW PV array. The Na-ion battery peak shaves the minor fluctuations of the power demand of Figure A.256 when the sun is down.
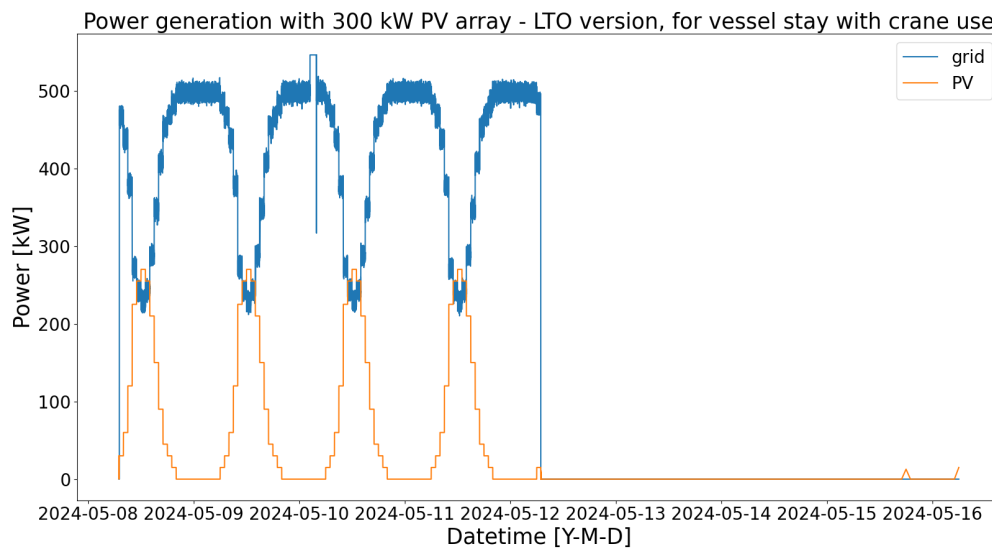

Figure A.277: Figure of the power generation of the Na-ion version of the alternative HE PV shore power configuration with a 500 kW PV array. The solar generation is from an average summer day. The power generation is for the power demand from Figure A.256. The minor fluctuations of the power profile are being peak shaven by the Na-ion battery when the sun is down.

Figure A.278: Figure of the Na-ion battery output power of the Na-ion version of the alternative HE PV shore power configuration with 500 kW PV array. The Na-ion battery peak shaves the minor fluctuations of the power demand of Figure A.256 when the sun is down.
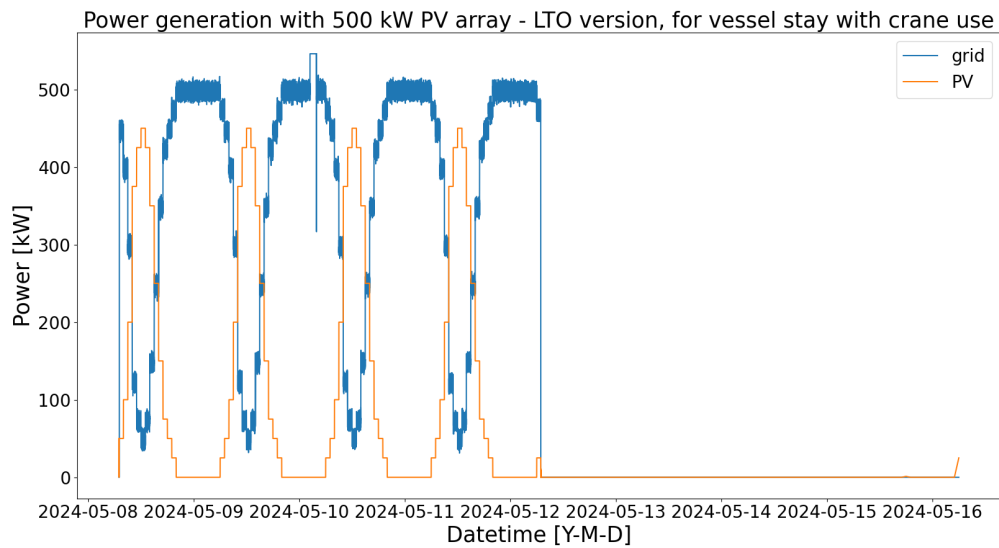

Figure A.279: Figure of the power generation of the Na-ion version of the alternative HE PV shore power configuration with a 700 kW PV array. The solar generation is from an average summer day. The power generation is for the power demand from Figure A.256. The minor fluctuations of the power profile are being peak shaven by the Na-ion battery when the sun is down.

Figure A.280: Figure of the Na-ion battery output power of the Na-ion version of the alternative HE PV shore power configuration with 700 kW PV array. The Na-ion battery peak shaves the minor fluctuations of the power demand of Figure A.256 when the sun is down. And the ESS is charged up during the day, just before the solar generation starts to dip below the power demand of the vessel.
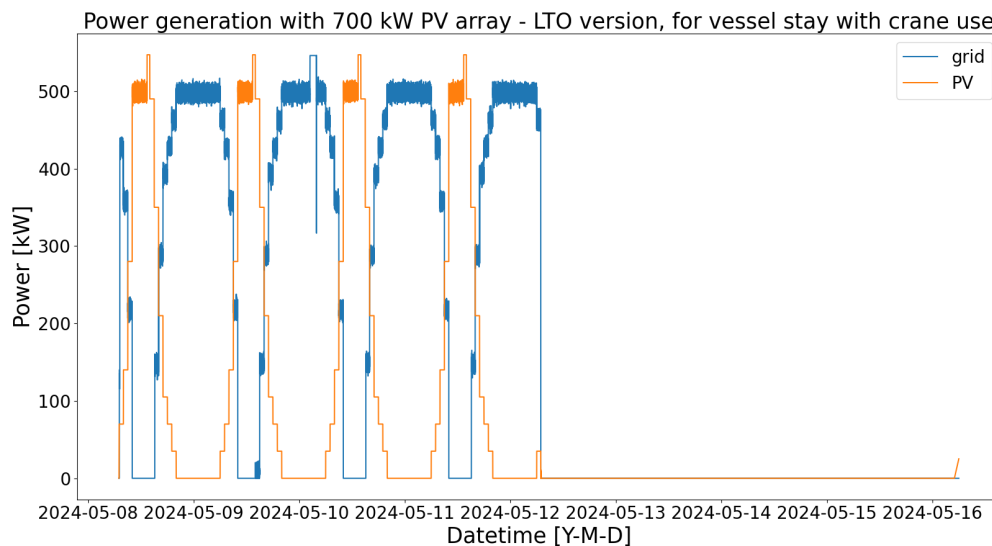

Figure A.281: Figure of the power generation of the Na-ion version of the alternative HE PV shore power configuration with a 1000 kW PV array. The solar generation is from an average summer day. The power generation is for the power demand from Figure A.256. The minor fluctuations of the power profile are being peak shaven by the Na-ion battery when the sun is down.

Figure A.282: Figure of the Na-ion battery output power of the Na-ion version of the alternative HE PV shore power configuration with 1000 kW PV array. The Na-ion battery peak shaves the minor fluctuations of the power demand of Figure A.256 when the sun is down. And the ESS is charged up during the day, just before the solar generation starts to dip below the power demand of the vessel.

Figure A.283: Figure of the SOC of the Na-ion battery of the Na-ion version of the alternative HE PV shore power configuration. The plot includes different implementations using different sizes of PV array. If the solar generation is higher than the demand of the vessel, the ESS can be charged just before the solar generation dips below the power demand of the vessel. Otherwise, the ESS is charged beforehand.

A.5.7. HP PV

Figure A.284: Figure of the vessel power profile of 4 days and 4 days of downtime. The power demand includes 30 consecutive crane uses. The vessel power profile was used for the HP PV shore power configuration. The x-axis is in datetime, meaning that every data point is fixed to a date and time.
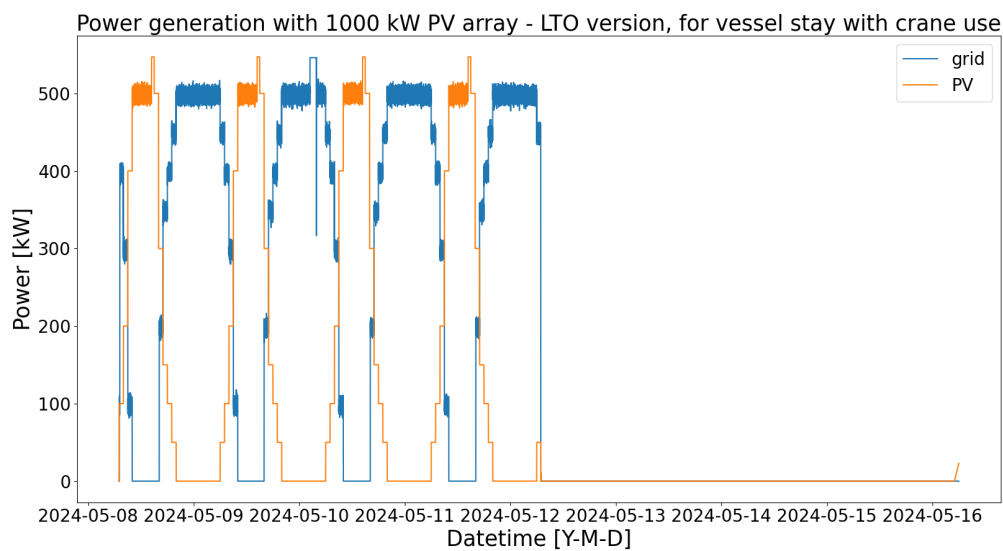

Figure A.285: Figure of the power generation of the LTO version of the HP PV shore power configuration with a 300 kW PV array. The solar generation is from an average summer day. The power generation is for the power demand from Figure A.284. The crane uses of the power profile are peak shaven by the LTO battery.
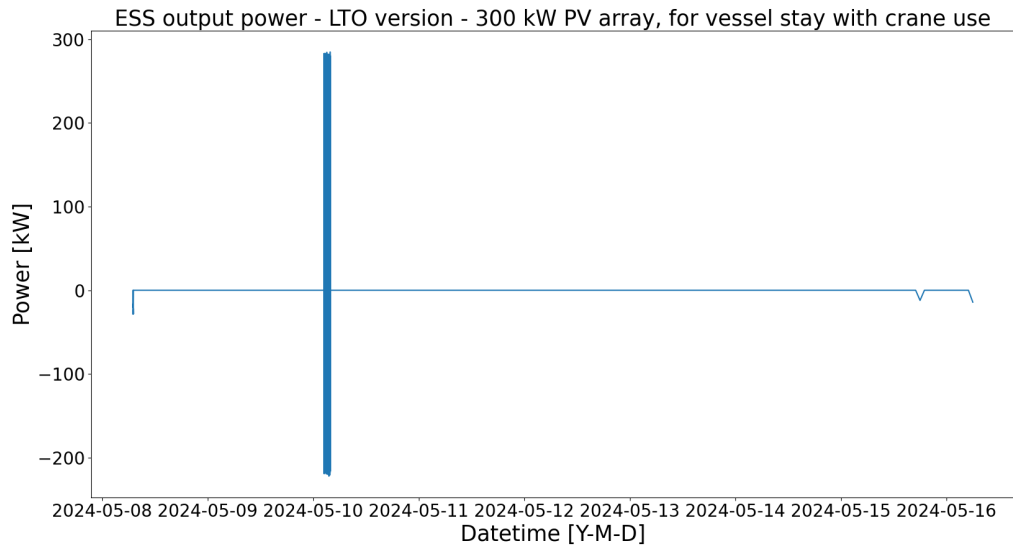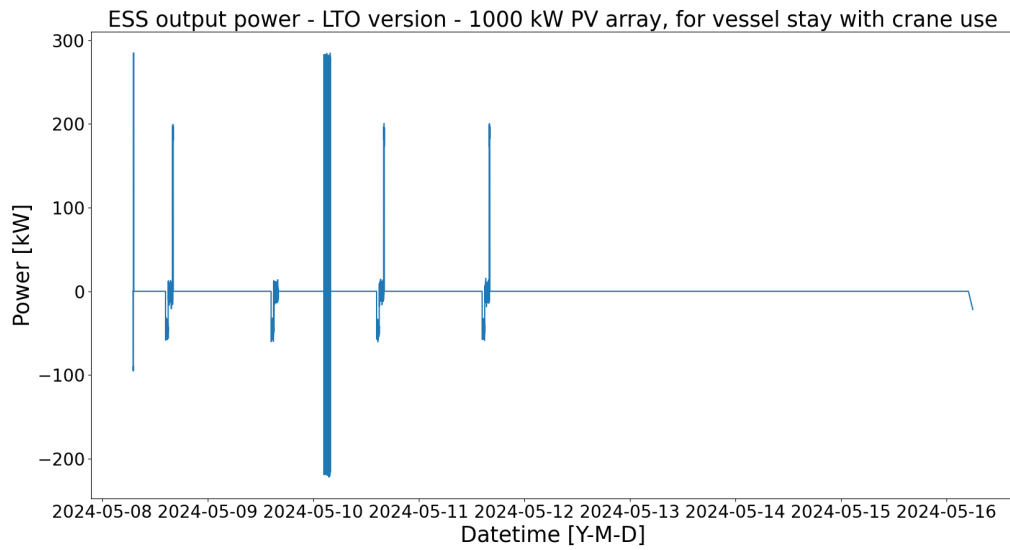
Figure A.286: Figure of the power output of the LTO battery from the LTO version of the HP ESS shore power configuration with a 300 kW PV array. The solar generation is from an average summer day. The LTO battery peak shaves the crane uses of the power demand from Figure A.284.

Figure A.287: Figure of the power generation of the LTO version of the HP PV shore power configuration with a 500 kW PV array. The solar generation is from an average summer day. The power generation is for the power demand from Figure A.284. The crane uses of the power profile are peak shaven by the LTO battery.
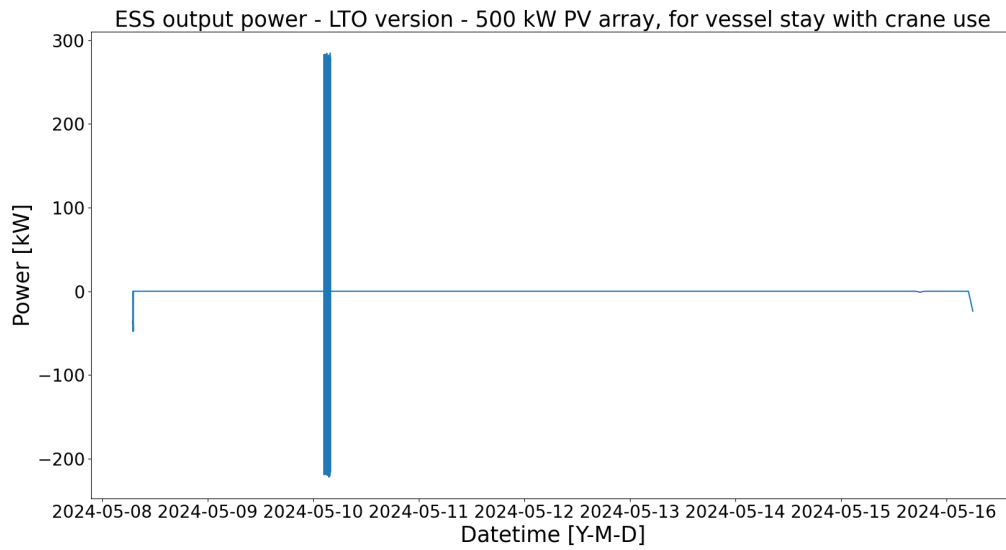
Figure A.288: Figure of the power output of the LTO battery from the LTO version of the HP ESS shore power configuration with a 500 kW PV array. The solar generation is from an average summer day. The LTO battery peak shaves the crane uses of the power demand from Figure A.284.

Figure A.289: Figure of the power generation of the LTO version of the HP PV shore power configuration with a 700 kW PV array. The solar generation is from an average summer day. The power generation is for the power demand from Figure A.284. The crane uses of the power profile are peak shaven by the LTO battery and the LTO battery is used to soften the transition of the solar generation dipping below the power demand of the vessel.
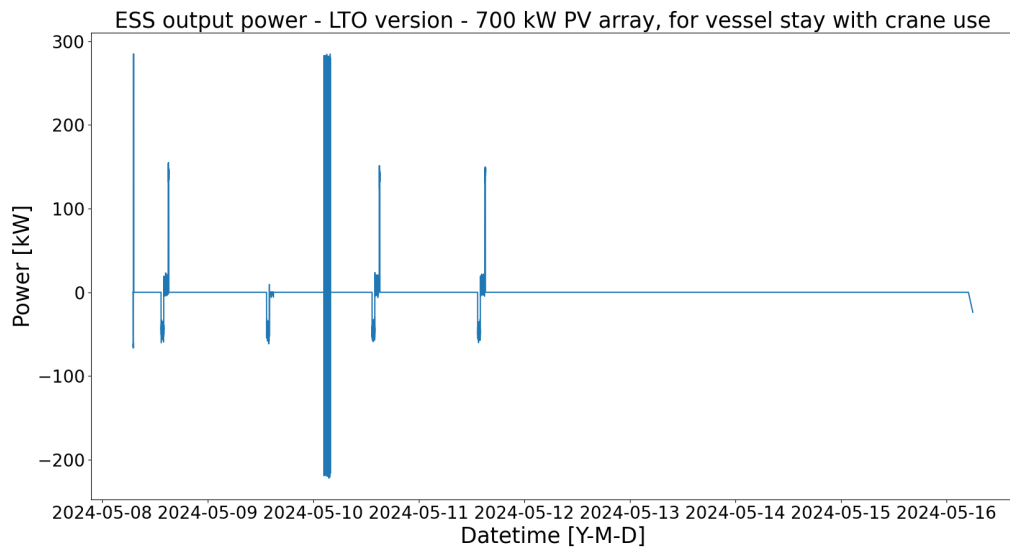
Figure A.290: Figure of the power output of the LTO battery from the LTO version of the HP ESS shore power configuration with a 700 kW PV array. The solar generation is from an average summer day. The LTO battery peak shaves the crane uses of the power demand from Figure A.284 and the LTO battery is used to soften the transition of the solar generation dipping below the power demand of the vessel.
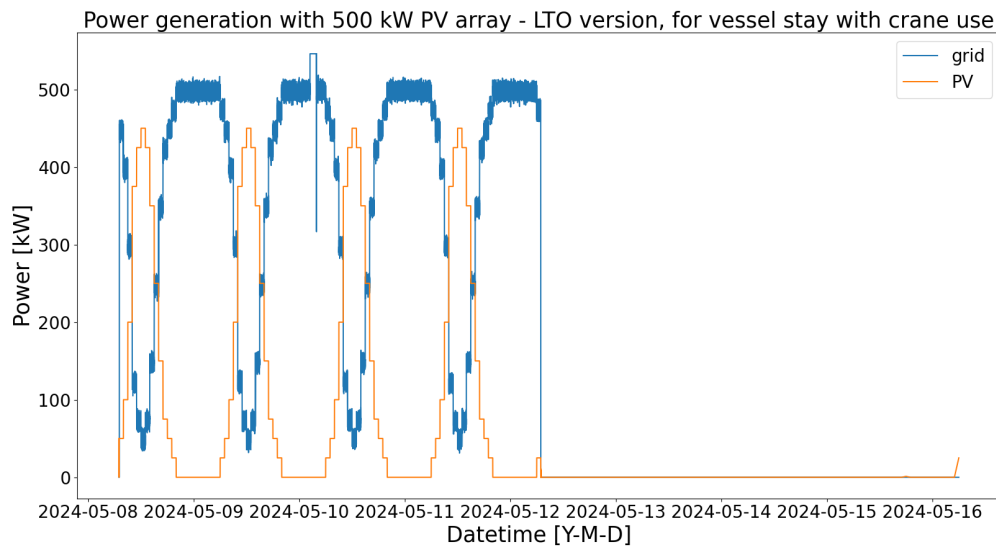

Figure A.291: Figure of the power generation of the LTO version of the HP PV shore power configuration with a 1000 kW PV array. The solar generation is from an average summer day. The power generation is for the power demand from Figure A.284. 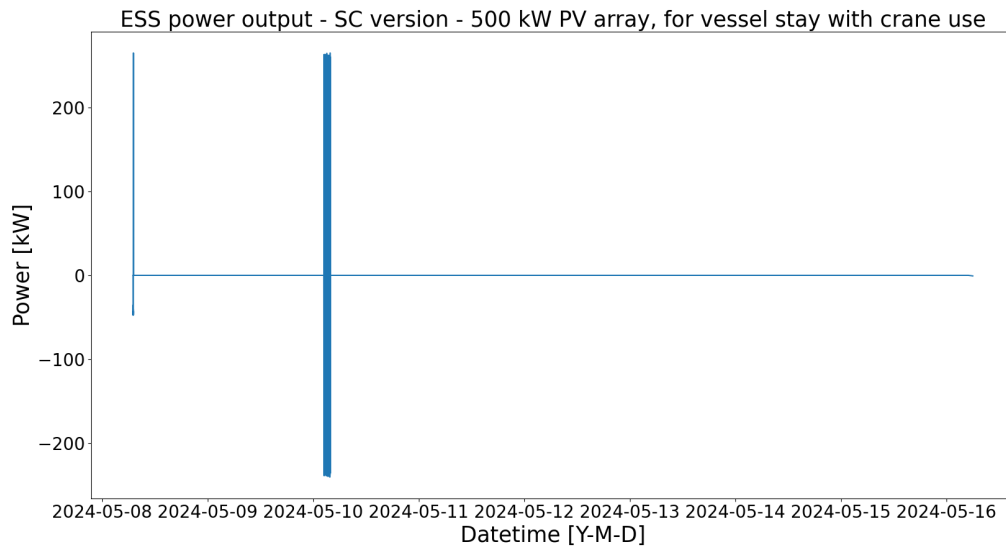The crane uses of the power profile are peak shaven by the LTO battery and the LTO battery is used to soften the transition of the solar generation dipping below the power demand of the vessel.

Figure A.292: Figure of the power output of the LTO battery from the LTO version of the HP ESS shore power configuration with a 1000 kW PV array. The solar generation is from an average summer day. The LTO battery peak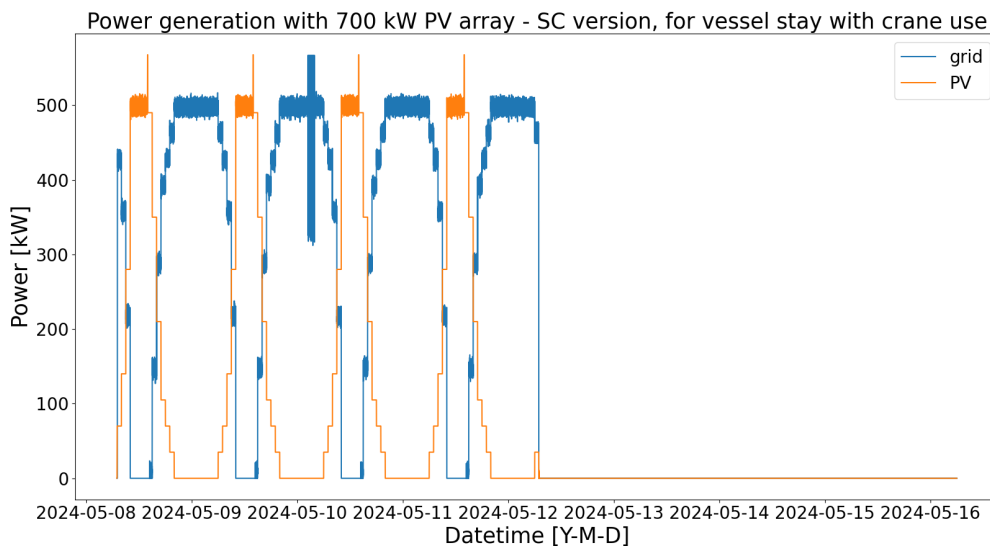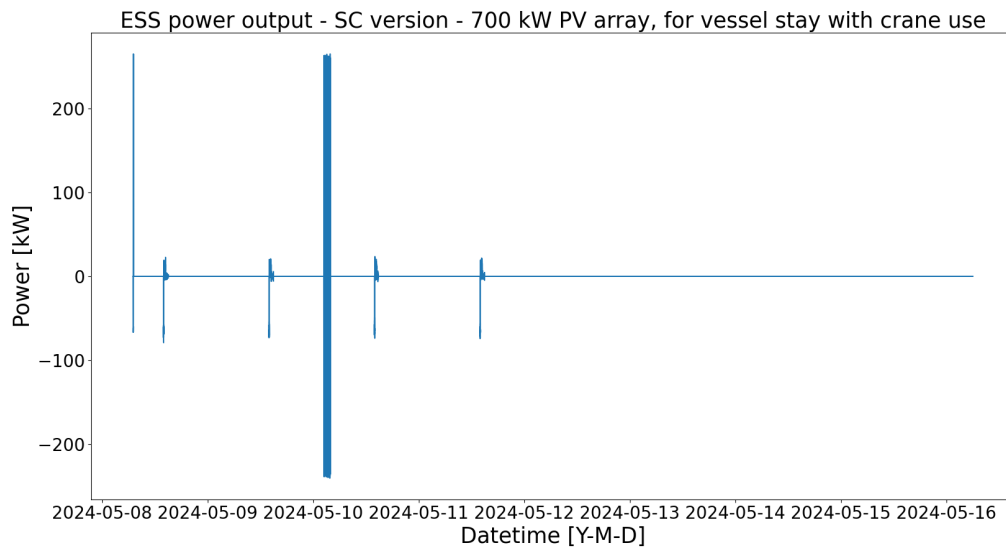 shaves the crane uses of the power demand from Figure A.284 and the LTO battery is used to soften the transition of the solar generation dipping below the power demand of the vessel.
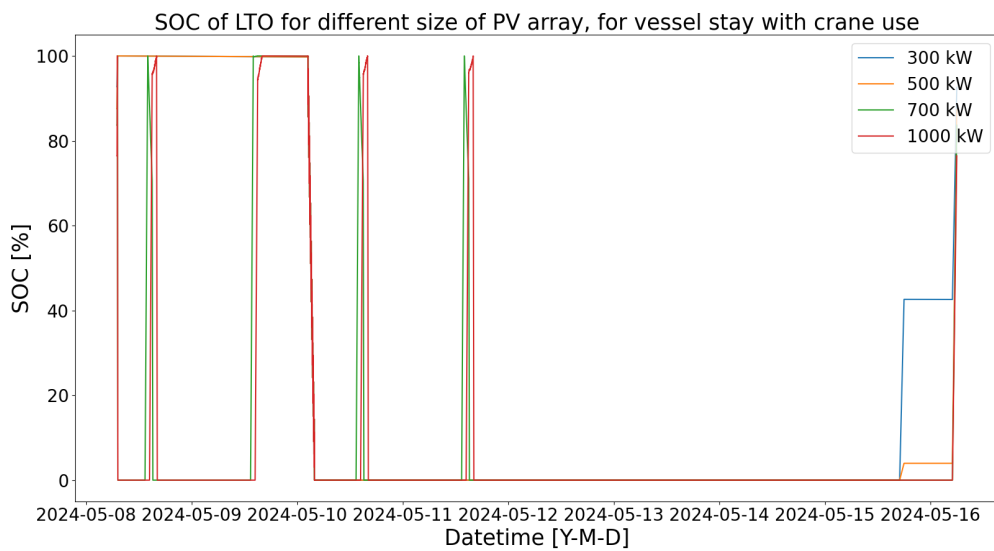
Figure A.293: Figure of the SOC of the LTO version of the HP PV shore power configuration. The different plots correspond to the different sizes of PV array. If the solar generation is higher than the power demand of the vessel, then the ESS is used charged by the free electricity and the ESS discharges where optimal. Otherwise, the ESS is charged just for the crane uses.
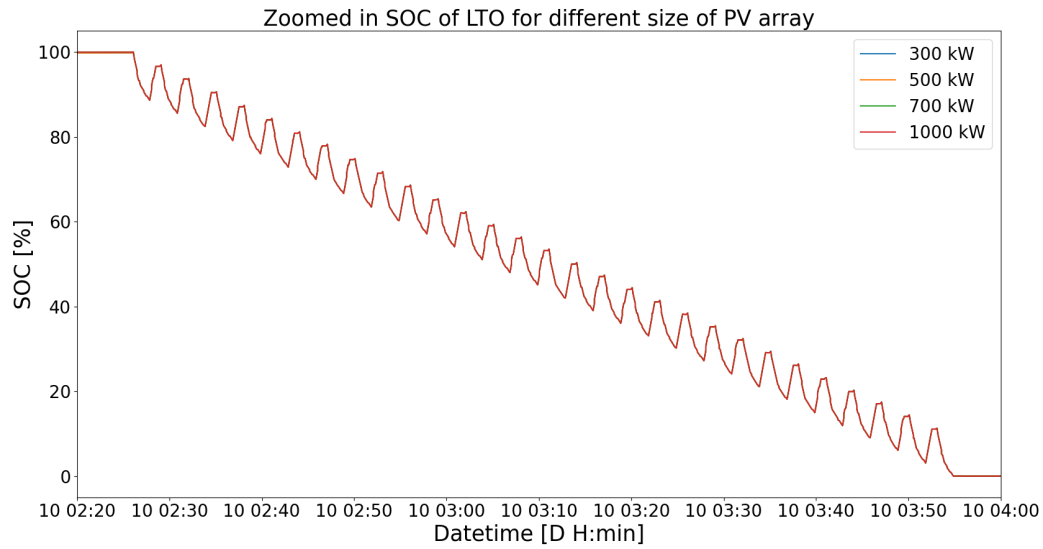
Figure A.294: Figure of the zoomed in SOC of the LTO version of the HP PV shore power configuration. The SOC is zoomed in on the consecutive crane uses. The swings in SOC correspond to the crane uses. The different plots correspond to the different sizes of the PV array. They overlap exactly to peak shave the crane uses.
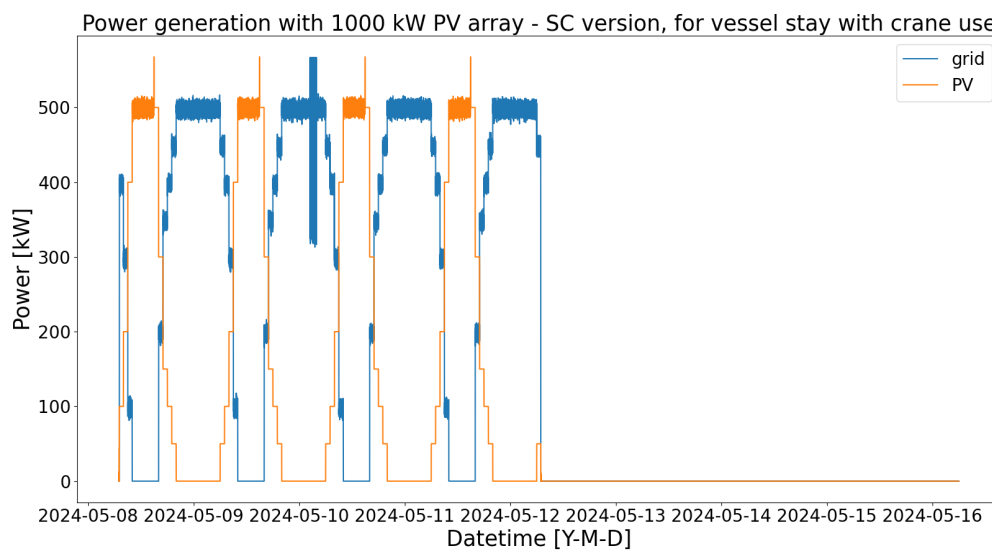

Figure A.295: Figure of the power generation of the SC version of the HP PV shore power configuration with a 500 kW PV array. The solar generation is from an average summer day. The power generation is for the power demand from Figure A.284. The crane uses of the power profile are peak shaven by the SC.

Figure A.296: Figure of the power output of the SC from the SC version of the HP ESS shore power configuration with a 500 kW PV array. The solar generation is from an average summer day. The SC peak shaves the crane uses of the power demand from Figure A.284.

Figure A.297: Figure of the power generation of the SC version of the HP PV shore power configuration with a 700 kW PV array. The solar generation is from an average summer day. The power generation is for the power demand from Figure A.284. The crane uses of the power profile are peak shaven by the SC and the SC is used to soften the transition of the solar generation dipping below the power demand of the vessel.
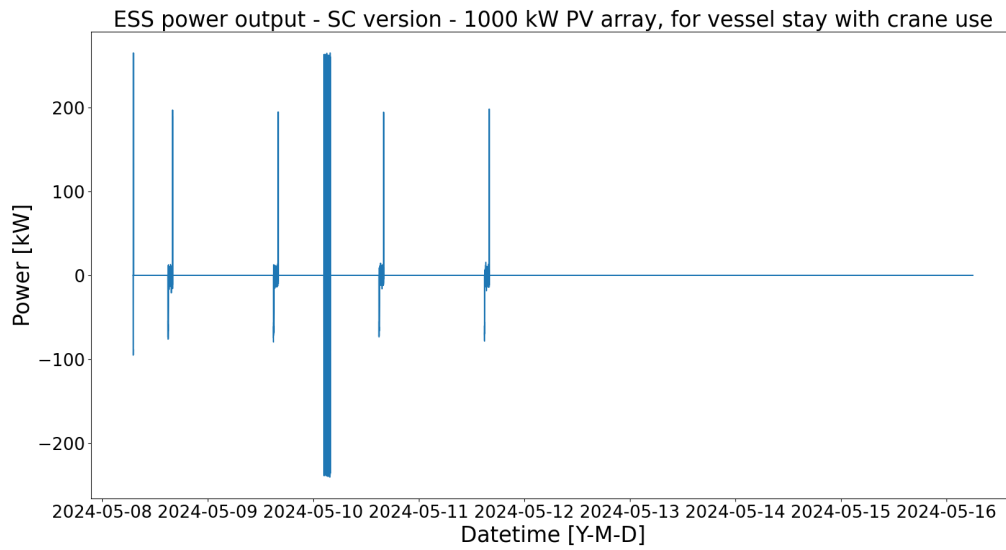
Figure A.298: Figure of the power output of the SC from the SC version of the HP ESS shore power configuration with a 700 kW PV array. The solar generation is from an average summer day. The SC peak shaves the crane uses of the power demand from Figure A.284 and the SC is used to soften the transition of the solar generation dipping below the power demand of the vessel.
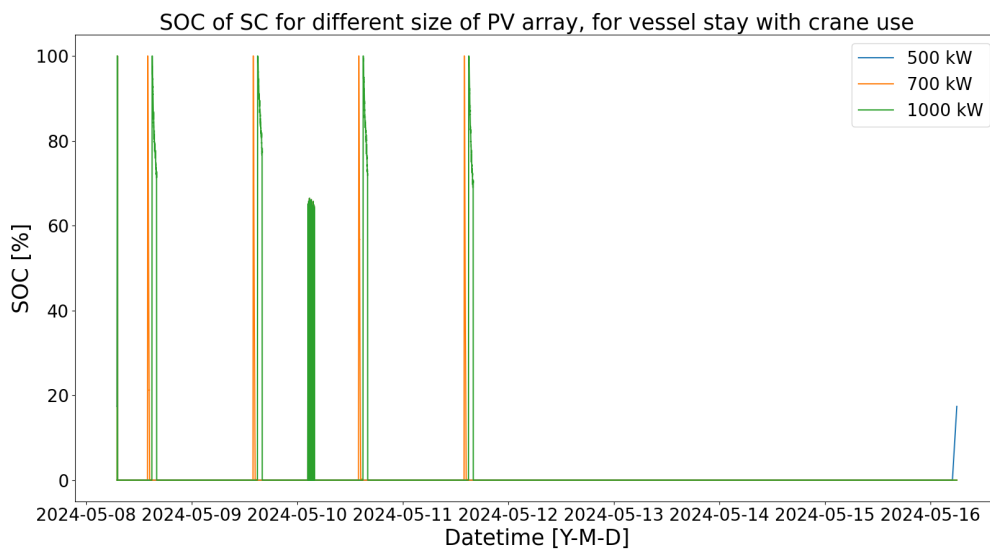

Figure A.299: Figure of the power generation of the SC version of the HP PV shore power configuration with a 1000 kW PV array. The solar generation is from an average summer day. The power generation is for the power demand from Figure A.284. The crane uses of the power profile are peak shaven by the SC and the SC is used to soften the transition of the solar generation dipping below the power demand of the vessel.

Figure A.300: Figure of the power output of the SC from the SC version of the HP ESS shore power configuration with a 1000 kW PV array. The solar generation is from an average summer day. The SC peak shaves the crane uses of the power demand from Figure A.284 and the SC is used to soften the transition of the solar generation dipping below the power demand of the vessel.

Figure A.301: Figure of the SOC of the SC version of the HP PV shore power configuration. The different plots correspond to the different sizes of PV array. If the solar generation is higher than the power demand of the vessel, then the ESS is used charged by the free electricity and the ESS discharges where optimal. Otherwise, the ESS is charged just for the crane uses.
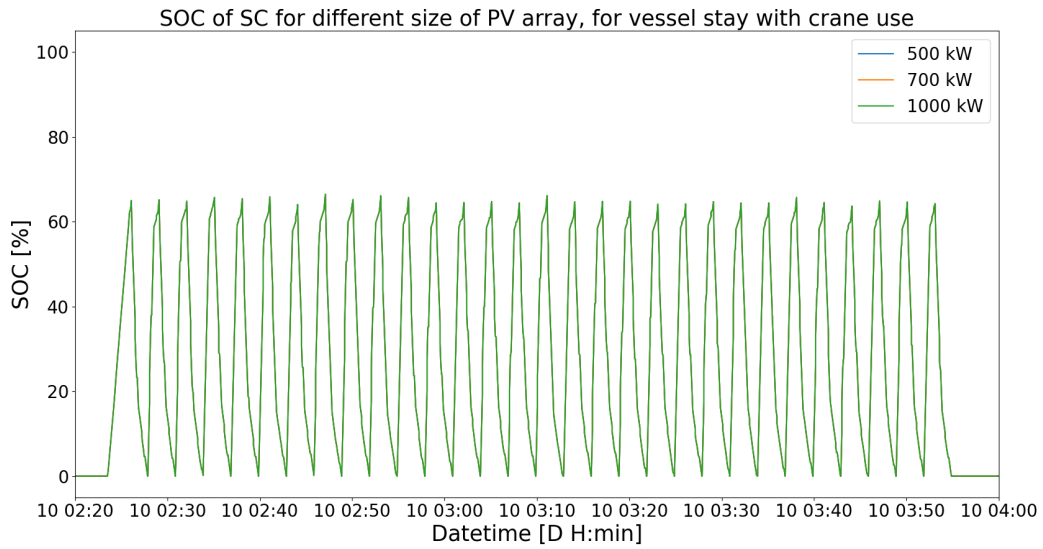
Figure A.302: Figure of the zoomed in SOC of the SC version of the HP PV shore power configuration. The SOC is zoomed in on the consecutive crane uses. The swings in SOC correspond to the crane uses. The different plots correspond to the different sizes of the PV array. They overlap exactly to peak shave the crane uses.
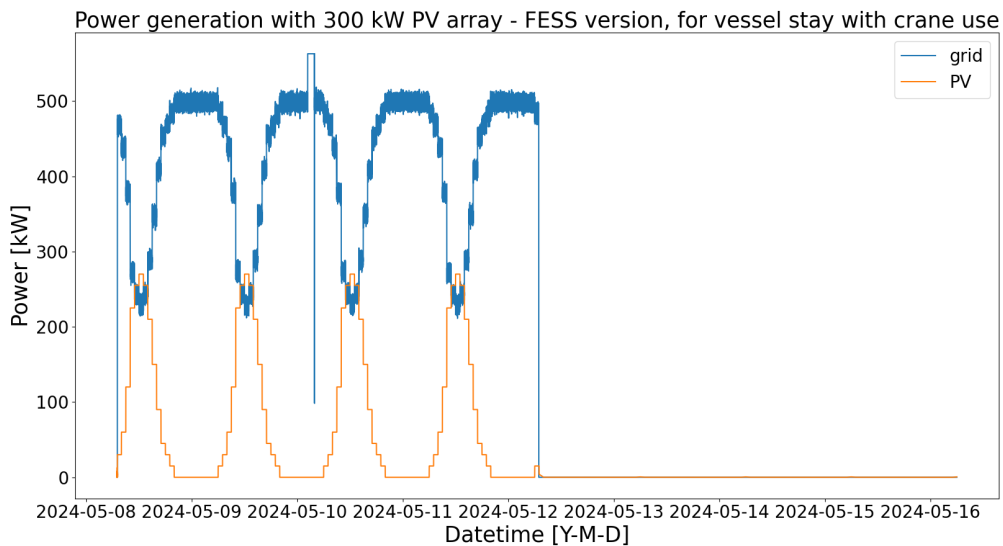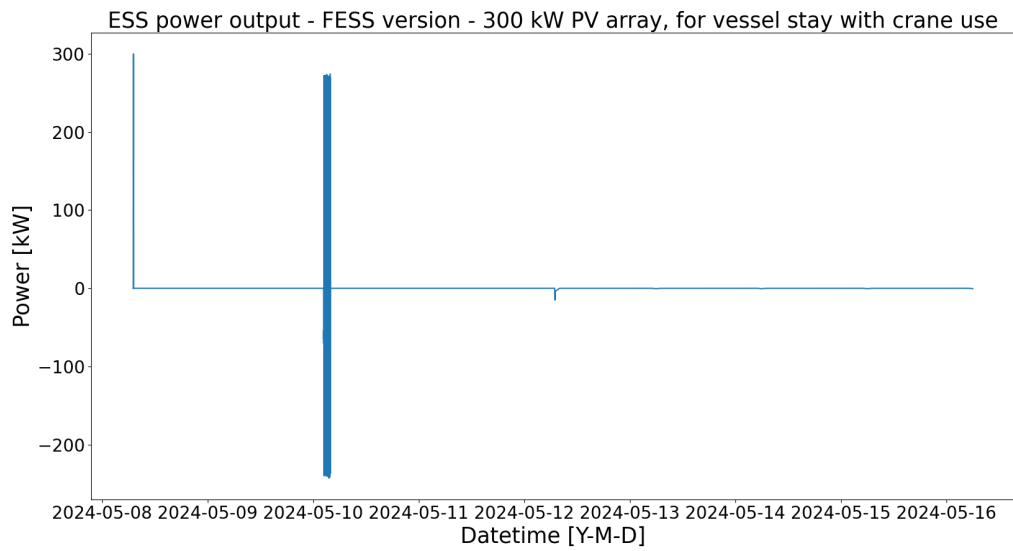

Figure A.303: Figure of the power generation of the FESS version of the HP PV shore power configuration with a 300 kW PV array. The solar generation is from an average summer day. The power generation is for the power demand from Figure A.284. The crane uses of the power profile are peak shaven by the FESS.

Figure A.304: Figure of the power output of the FESS from the FESS version of the HP ESS shore power configuration with a 300 kW PV array. The solar generation is from an average summer day. The FESS peak shaves the crane uses of the power demand from Figure A.284.
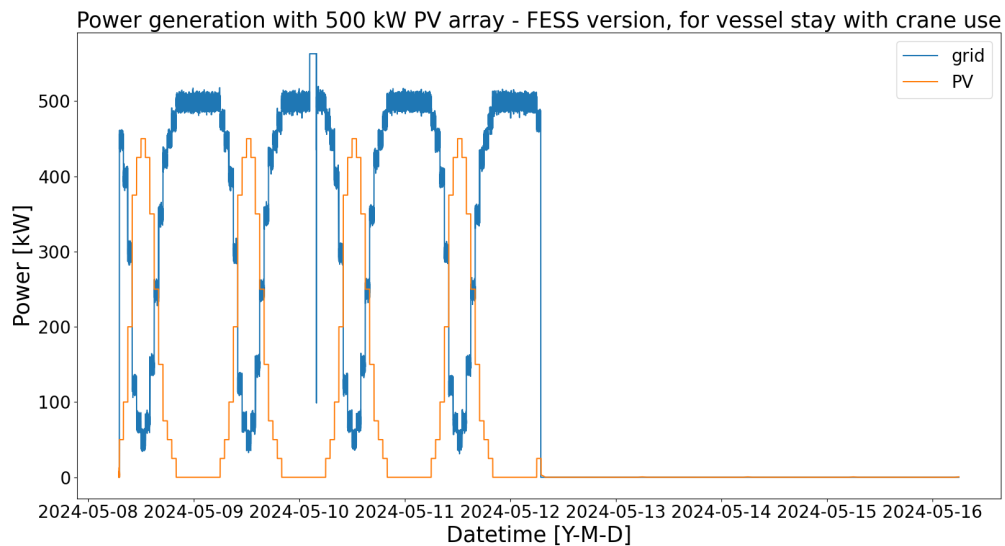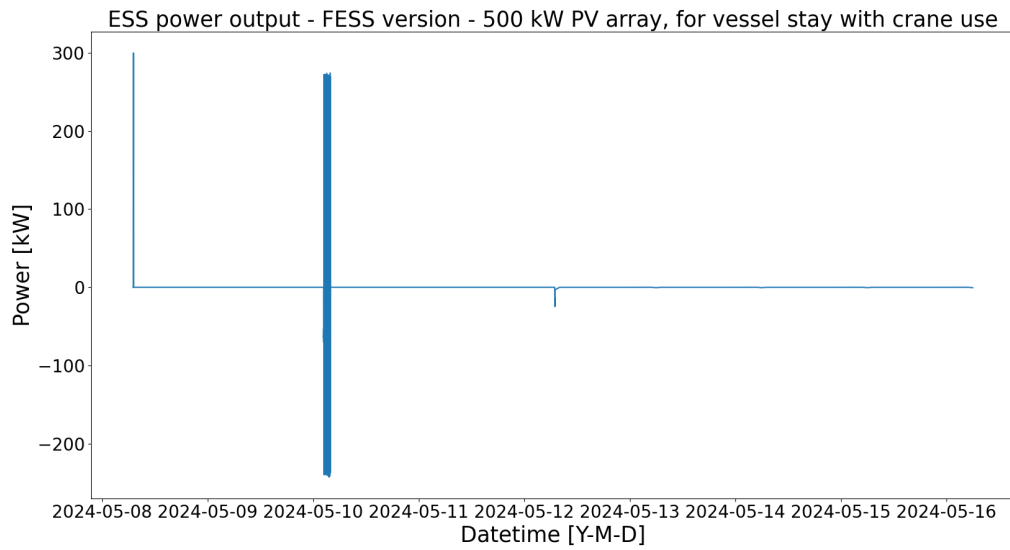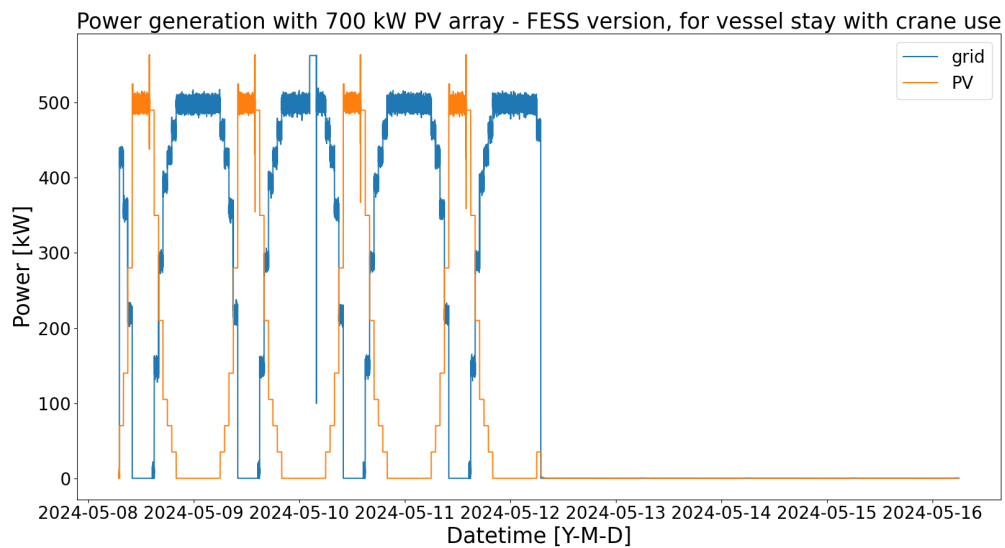

Figure A.305: Figure of the power generation of the FESS version of the HP PV shore power configuration with a 500 kW PV array. The solar generation is from an average summer day. The power generation is for the power demand from Figure A.284. The crane uses of the power profile are peak shaven by the FESS.

Figure A.306: Figure of the power output of the FESS from the FESS version of the HP ESS shore power configuration with a 500 kW PV array. The solar generation is from an average summer day. The FESS peak shaves the crane uses of the power demand from Figure A.284.

Figure A.307: Figure of the power generation of the FESS version of the HP PV shore power configuration with a 700 kW PV array. The solar generation is from an average summer day. The power generation is for the power demand from Figure A.284. The crane uses of the power profile are peak shaven by the FESS and the FESS is used to soften the transition of the solar generation dipping below the power demand of the vessel.
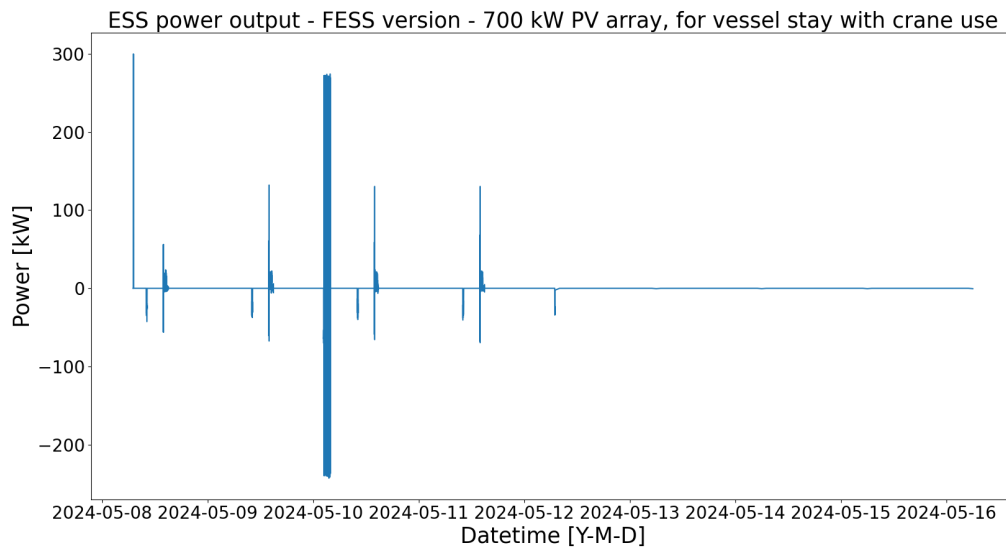
ESS power output - FESS version - 700 kW PV array, for vessel stay with crane use

Figure A.308: Figure of the power output of the FESS from the FESS version of the HP ESS shore power configuration with a 700 kW PV array. The solar generation is from an average summer day. The FESS peak shaves the crane uses of the power demand from Figure A.284 and the FESS is used to soften the transition of the solar generation dipping below the power demand of the vessel.
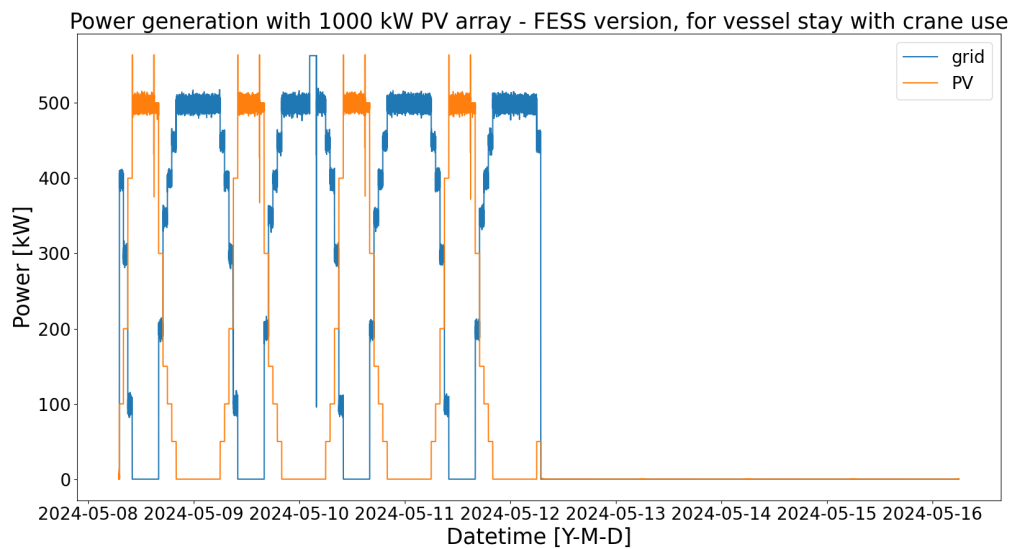
Power generation with 1000 kW PV array - FESS version, for vessel stay with crane use

Figure A.309: Figure of the power generation of the FESS version of the HP PV shore power configuration with a 1000 kW PV array. The solar generation is from an average summer day. The power generation is for the power demand from Figure A.284. The crane uses of the power profile are peak shaven by the FESS and the FESS is used to soften the transition of the solar generation dipping below the power demand of the vessel.
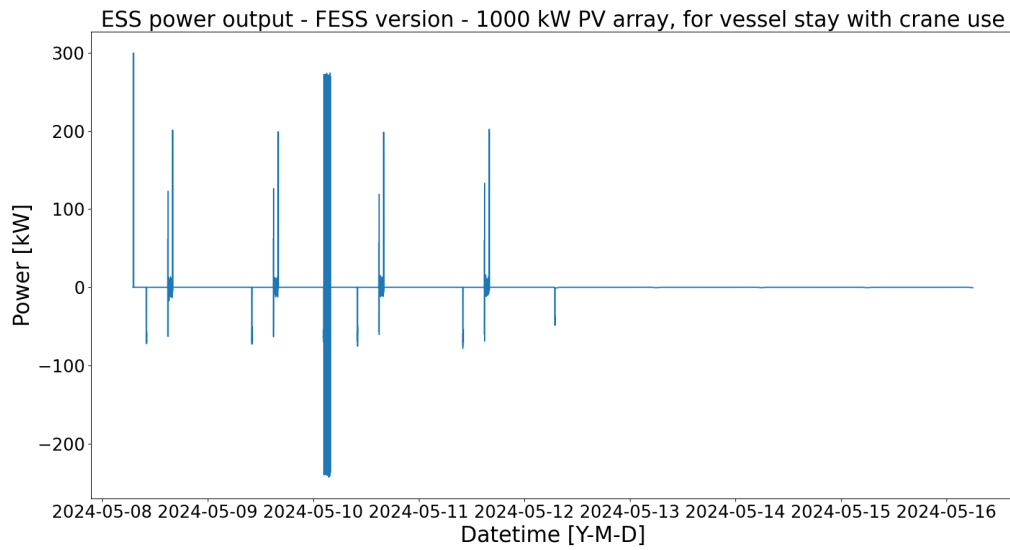
Figure A.310: Figure of the power output of the FESS from the FESS version of the HP ESS shore power configuration with a 1000 kW PV array. The solar generation is from an average summer day. The FESS peak shaves the crane uses of the power demand from Figure A.284 and the FESS is used to soften the transition of the solar generation dipping below the power demand of the vessel.
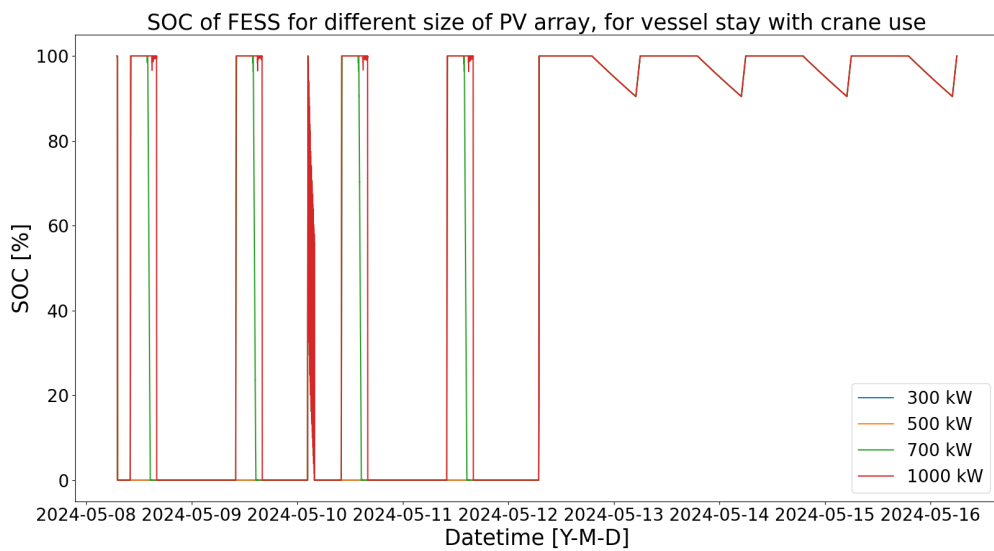

Figure A.311: Figure of the SOC of the FESS version of the HP PV shore power configuration. The different plots correspond to the different sizes of PV array. If the solar generation is higher than the power demand of the vessel, then the ESS is used charged by the free electricity and the ESS discharges where optimal. Otherwise, the ESS is charged just for the crane uses.
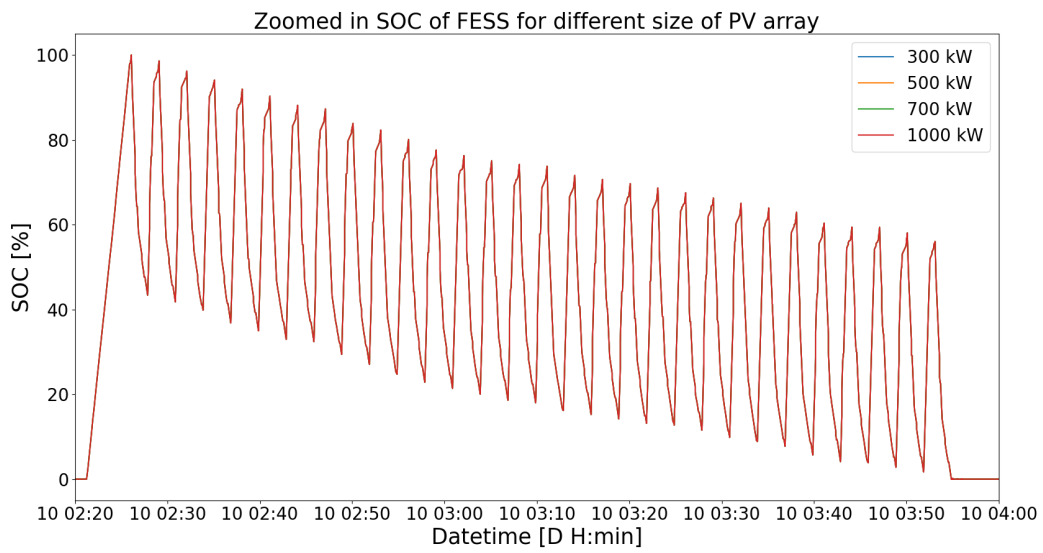
Figure A.312: Figure of the zoomed in SOC of the FESS version of the HP PV shore power configuration. The SOC is zoomed in on the consecutive crane uses. The swings in SOC correspond to the crane uses. The different plots correspond to the different sizes of the PV array. They overlap exactly to peak shave the crane uses.